

Lecture Notes in Mechanical Engineering

B. B. V. L. Deepak

D. R. K. Parhi

B. B. Biswal *Editors*

Advanced Manufacturing Systems and Innovative Product Design

Select Proceedings of IPDIMS 2020

 Springer

Lecture Notes in Mechanical Engineering

Series Editors

Francisco Cavas-Martínez, Departamento de Estructuras, Universidad Politécnica de Cartagena, Cartagena, Murcia, Spain

Fakher Chaari, National School of Engineers, University of Sfax, Sfax, Tunisia

Francesco Gherardini, Dipartimento di Ingegneria, Università di Modena e Reggio Emilia, Modena, Italy

Mohamed Haddar, National School of Engineers of Sfax (ENIS), Sfax, Tunisia

Vitalii Ivanov, Department of Manufacturing Engineering Machine and Tools, Sumy State University, Sumy, Ukraine

Young W. Kwon, Department of Manufacturing Engineering and Aerospace Engineering, Graduate School of Engineering and Applied Science, Monterey, CA, USA

Justyna Trojanowska, Poznan University of Technology, Poznan, Poland

Lecture Notes in Mechanical Engineering (LNME) publishes the latest developments in Mechanical Engineering—quickly, informally and with high quality. Original research reported in proceedings and post-proceedings represents the core of LNME. Volumes published in LNME embrace all aspects, subfields and new challenges of mechanical engineering. Topics in the series include:

- Engineering Design
- Machinery and Machine Elements
- Mechanical Structures and Stress Analysis
- Automotive Engineering
- Engine Technology
- Aerospace Technology and Astronautics
- Nanotechnology and Microengineering
- Control, Robotics, Mechatronics
- MEMS
- Theoretical and Applied Mechanics
- Dynamical Systems, Control
- Fluid Mechanics
- Engineering Thermodynamics, Heat and Mass Transfer
- Manufacturing
- Precision Engineering, Instrumentation, Measurement
- Materials Engineering
- Tribology and Surface Technology

To submit a proposal or request further information, please contact the Springer Editor of your location:

China: Dr. Mengchu Huang at mengchu.huang@springer.com

India: Priya Vyas at priya.vyas@springer.com

Rest of Asia, Australia, New Zealand: Swati Meherishi
at swati.meherishi@springer.com

All other countries: Dr. Leontina Di Cecco at Leontina.dicecco@springer.com

To submit a proposal for a monograph, please check our Springer Tracts in Mechanical Engineering at <http://www.springer.com/series/11693> or contact Leontina.dicecco@springer.com

Indexed by SCOPUS. All books published in the series are submitted for consideration in Web of Science.

More information about this series at <http://www.springer.com/series/11236>

B. B. V. L. Deepak · D. R. K. Parhi ·
B. B. Biswal
Editors

Advanced Manufacturing Systems and Innovative Product Design

Select Proceedings of IPDIMS 2020

 Springer

Editors

B. B. V. L. Deepak
Department of Industrial Design
National Institute of Technology
Rourkela, Odisha, India

D. R. K. Parhi
Department of Mechanical Engineering
National Institute of Technology
Rourkela, Odisha, India

B. B. Biswal
Department of Industrial Design
National Institute of Technology Rourkel
Rourkela, Odisha, India

ISSN 2195-4356

ISSN 2195-4364 (electronic)

Lecture Notes in Mechanical Engineering

ISBN 978-981-15-9852-4

ISBN 978-981-15-9853-1 (eBook)

<https://doi.org/10.1007/978-981-15-9853-1>

© The Editor(s) (if applicable) and The Author(s), under exclusive license to Springer Nature Singapore Pte Ltd. 2021

This work is subject to copyright. All rights are solely and exclusively licensed by the Publisher, whether the whole or part of the material is concerned, specifically the rights of translation, reprinting, reuse of illustrations, recitation, broadcasting, reproduction on microfilms or in any other physical way, and transmission or information storage and retrieval, electronic adaptation, computer software, or by similar or dissimilar methodology now known or hereafter developed.

The use of general descriptive names, registered names, trademarks, service marks, etc. in this publication does not imply, even in the absence of a specific statement, that such names are exempt from the relevant protective laws and regulations and therefore free for general use.

The publisher, the authors and the editors are safe to assume that the advice and information in this book are believed to be true and accurate at the date of publication. Neither the publisher nor the authors or the editors give a warranty, expressed or implied, with respect to the material contained herein or for any errors or omissions that may have been made. The publisher remains neutral with regard to jurisdictional claims in published maps and institutional affiliations.

This Springer imprint is published by the registered company Springer Nature Singapore Pte Ltd. The registered company address is: 152 Beach Road, #21-01/04 Gateway East, Singapore 189721, Singapore

Contents

Design for Aesthetics, Ergonomics and Sustainability	
Strategies of Affective Instructional Design for Elderly	3
Anirban Chowdhury and Prachi Karkun	
Design of an Awareness Model to Develop Proper Sanitary Habit Among the Rural People of Jharkhand	11
Pallavi Rani and Amrita Bhattacharjee	
Design and Evaluation of Speed Forms for Design of an Amphibious Vehicle	21
Debashis Majumder and Anirban Chowdhury	
Design and Analysis with Optimization of Car Radiators Using Nanofluids	33
S. Deepankumar, B. Saravanan, V. Sudhirkumar, N. Boopalan, A. Sundaramahalingam, and S. Dhayaneethi	
Design and Cost Analysis of Mini Tiller-Cum-Basin-Maker for Coconut Trees	47
Abi Varghese and Jippu Jacob	
Computer-Aided Ergonomic Analysis for Rubber Tapping Workers	57
Abi Varghese and Vinay V. Panicker	
Participatory Approach for Ergonomics Intervention: A Review	69
Yogesh Mishra, M. L. Meena, and G. S. Dangayach	
Creating Products from Textile Waste Generated During Fabric Cutting Stage in the Garment Production Process	79
Jharna Joshi and Anirban Chowdhury	

Forced Draft and Superheated Steam for Design and Development of Community Smoke Less Chulha to Help Women in Rural Areas . . .	93
Ramesh Chandra Nayak, Manmatha K. Roul, Saroj Kumar Sarangi, Abhisek Sarangi, and Asish Sarangi	
Lightweight Materials for Engine Cylinder Blocks/Liners—A Critical Review	103
B. Pavani Srikavya, P. Srinivasa Rao, and Syed Kamaluddin	
Selection of Suppliers by Weighted Aggregated Sum Product Assessment (WASPAS) Method	117
Shankha Shubhra Goswami and Dhiren Kumar Behera	
Design of an Impact Attenuator for a Formula Type Race Car	131
Shivam Mahajan, Neeraj Dokania, Akshay Kumar, and Sujeet Kumar Mishra	
Design Optimization and Static Force Analysis of L-Type Rotary Tiller Blade	147
Deepanshu Pandey, Dheeraj Rangera, Divyansh Bhatia, Ghanvir Singh, and Rajiv Chaudhary	
Influence of Vegetable Oil Based Lubricants with Nano Particles on Surface Roughness of AISI 1020 and AA 2024 Alloy	163
T. Ramya, M. Venu, K. T. Sunil Kumar, and K. Anupama Francy	
Experimental Investigation, Parametric Optimization, and Cost Analysis in EDM of Aluminium-Silicon Carbide Metal Matrix Composite	175
Subhashree Naik, Soumyashree Sabat, Sudhansu Ranjan Das, Debabrata Dhupal, and Bijoy Kumar Nanda	
Optimum Design and Analysis of Bell Crank Lever for an Automobile	189
Ch. Sowjanya, V. Nagabhushana Rao, and B. Pavani Sri Kavya	
Evaluation of Compressive Strength of Thermoplastic Materials Prepared Using 3D Printer with Different in-Fill Structures	209
Srinivas Kona, K. Ch. Sekhar, A. Lakshumu Naidu, and V. V. Rama Reddy	
Fabrication of Low Temperature Stage for Atomic Force Microscope	217
P. H. J. Venkatesh, M. S. R. Viswanath, Asit Kumar Meher, and Rohan Shilwant	
Fabrication and Testing of Magnetic Plate Handling Truck	241
P. H. J. Venkatesh, Sai Kumar Amda, B. Taraji Naik, Kandukuri Srinivas, and D. Thulasi Ram	

Design of Pico Hydro Power Plant Using an Impulse Turbine 251
 P. H. J. Venkatesh, Vivek Viswanadha, K. Sravan Kumar,
 and Koyyana Ramesh

**Experimental Analysis of Performance and Emission Characteristics
 of Four Stroke Single Cylinder VCR Diesel Engine Using Palm
 Biodiesel and Diesel Along with Comparison** 261
 Savadana Venkataramana and N. Ramanaiah

**Scoping Review on Composition of Non Asbestos Organic Friction
 Materials for Automotive Brake Pad** 271
 S. S. Shirsath and R. N. Yerrawar

**Investigation of Solid Particle Erosion Wear Behavior of Activated
 Carbon Polymer Composites** 283
 M. Sivaji Ganesh, G. Raghavendra, S. Ojha, and M. Om Prakash

**Computer-Aided Ergonomic Analysis for Rubber Tapping
 Workers** 293
 Abi Varghese and Vinay V. Panicker

**User Interface/User Experience (UI/UX), Human Computer
 Interface (HCI)**

**Redesign and Assessment of Two Passenger Car Dashboard Warning
 Icons in India** 305
 Sourav Bhattacharya and Dhananjay Singh Bisht

**Designing Interface for an Online Bike Rental Service for Personified
 Tourism** 315
 Arvind Kumar Nishad and Anirban Chowdhury

**Creating Awareness About Health and Hygiene During Menstrual
 Cycle Among Indian Adolescent Girls Using Virtual Reality** 327
 Shakti Banerjee, Anirban Chowdhury, and Anmol Srivastava

**Real-Time Obstacle Proximity Warning Through Human Machine
 Interface and Quadrature Interpretation of a Two-Axis Robotic
 Inspection System** 341
 P. M. Aishwarya Priya, N. Swetha, S. Rajesh Kannan, Saji Jacob George,
 Joel Jose, and S. Joseph Winston

A New Finite Automata Approach of Right State Machine 351
 Sarat K. Parhi

Gleaming of Lights by Pedaling Using Arduino 359
 T. Thirumala Rao, B. Venkateswara Rao, K. V. V. R. S. Vishnu,
 and Y. Jaswanth

A Vision-Based Unstructured Road Detection Algorithm for Self-driving Cars	369
R. Rajesh and P. V. Manivannan	
Experimental Investigation of Automatic Aeration Process and Condition of Aqua Ponds Monitoring System with the Help of Internet of Things	381
Mummina Vinod, M. Raghuraman, and V. Mahesh Chakravarthi	
Modeling and Designing of Plug-in Electric Vehicle Under V2G Compatability	391
K. Kiran Kumar and B. Srinivasa Rao	
Influence of Drone Rotors Over Droplet Distribution in Precision Agriculture	401
Umamaheswara Rao Mogili and B. B. V. L. Deepak	
CAD/CAM/CIM and Robotics	
Effect of Porosity and Thermal Medium on the Vibration Characteristics of Two-Dimensional FGM Plates	413
I. Ramu, M. Raghuraman, and M. Venu	
FEA Approach for Modal Analysis of an Electric Motor in Electric Vehicle Drive	425
Tushar Amale, Prajwal Badwaik, Sumedh Durge, Ajay Dube, and Amit Belveker	
Analysis of Interference-Fit Orbital Motor Using Finite Element Analysis in ANSYS Workbench	435
Dinesh Kumar Ramesh, Avinash Ramakrishnan Rao, Sai Tharun Reddy Garlapati, and Abhijit Nag	
Comparison of Mechanical Performance of the Various Stent Materials: A Finite Element Analysis (FEA) Approach	449
M. Raghuraman, I. Ramu, and V. Chaithanya Vinay	
Applicability of Empirical Correlations for Critical Heat Flux in Transfer Line Cool-Down Boiling	457
Asit Kumar Meher, P. H. J. Venkatesh, M. S. R. Viswanath, J. Naga Raju, and Ankit Kumar	
Virtual Design Optimization of Motorbike Rear Sprocket Based on ANSYS and Hybrid MOORA-Fuzzy Inference System	481
Abhishek Barua, Dilip Kumar Bagal, Siddharth Jeet, Swastik Pradhan, Dulu Patnaik, and Ajit Kumar Pattanaik	

Fused Filament Fabrication (FFF) Based 3D Printer and Its Design: A Review 497
 Krishnanand and Mohammad Taufik

Determination of Optimal Ordering Policy Using Genetic Algorithm for a Multi-stage Serial Supply Chain 507
 Rachit Kumar, Richard Johnson, Ritvik Mohandas, Pranav Pramod, Dony S. Kurian, and V. Madhusudanan Pillai

Comparative Investigation of CNC Turning of Nickel-Chromoly Steel Under Different Cutting Environment with a Fabricated Portable Mist Lubricator: A Super Hybrid Taguchi-WASPAS-GA-SA-PSO Approach 515
 Siddharth Jeet, Abhishek Barua, Dilip Kumar Bagal, Swastik Pradhan, Dulu Patnaik, and Ajit Kumar Pattanaik

Computational Analysis of Composite MoS₂-TiO₂-ZrO₂ Soft Coating on Tribological Performance in Dry Sliding Contact 533
 Avinash Borgaonkar and Ismail Syed

Optimal Path Planning of Steam Generator Tube Inspection System’s Robotic Manipulator Using Genetic Algorithm 541
 S. Joseph Winston and P. V. Manivannan

Kinematic Simulation of Dual Arm Agricultural Mobile Robot 551
 A. Sridhar Reddy, V. V. S. Kesava Rao, and B. B. V. L. Deepak

About the Editors

Dr. B. B. V. L. Deepak is currently working at National Institute of Technology, Rourkela, as Head of the Department of Industrial Design. He received his Master's and Ph.D. degrees from the National Institute of Technology, Rourkela in 2010 and 2015, respectively. He has 9 years of research and teaching experience in Manufacturing and Product Design fields. He produced 3 Ph.D. theses and is supervising 4 Ph.D. scholars. He published more than 100 papers in various peer-reviewed journals and conferences along with 1 patent. He is also currently handling two sponsored research projects in the field of robotics. He received several national and international awards such as Ganesh Mishra Memorial Award-2019, IEI Young Engineer Award-2018, Early Career Research Award-2017, etc.

Prof. D. R. K. Parhi is working in NIT Rourkela as a Professor (HAG). He is currently heading the Department of Mechanical Engineering. He has received his Ph.D. in Mobile Robotics field from Cardiff School of Engineering, UK. He has 26 years of research and teaching experience in Robotics and Artificial Intelligence fields. He has guided more than 20 Ph.D. theses and published more than 300 papers in various journals and conferences along with 3 patents. He has also completed and is currently handling several sponsored research projects in the field of robotics.

Prof. B. B. Biswal is currently acting as Director of National Institute of Technology, Meghalaya. He is also a Professor (HAG) in the Department of Industrial Design of NIT Rourkela. He has 33 years of research and teaching experience in FMS, CAD/CAM, and Robotics fields. He has guided more than 15 Ph.D. theses and published more than 200 papers in various journals and conferences along with 3 patents/copyrights. He has international collaboration with Loughborough University and Slovak University of Technology in Bratislava. He has also completed and is currently handling several sponsored research projects in his research field.

Design for Aesthetics, Ergonomics and Sustainability

Strategies of Affective Instructional Design for Elderly



Anirban Chowdhury and Prachi Karkun

Abstract Aging poses limitations in motor skills and cognitive abilities, due to which the elderly face problems while interacting with new technology. On the contrary elderly are said to have better control of their emotion due to the self-regulation process. The learning needs of the elderly differ from young due to changes in the information processing system and the role played by affective system during the learning process. There is selective cognitive processing due to which the elderly focus only on emotionally relevant information. Therefore, the current paper proposes a framework for instructional design solution in the light of the positive affect resulting from the perception of characteristics of the instructions. The suggested framework can act as a guideline for planning and executing instructional strategies targeting the elderly.

Keywords Affect · Cognition · Emotion · Ergonomics · Instructional design · UX

1 Introduction

Advanced technologies have become an inseparable part of our daily lives. Every advancement comes with an inherent condition of learning and new ways of interaction. Ignorance or inability to learn newly introduced product or technology may pose many challenges as one being dependent on others for completion of simple tasks. In order to gain independence and efficiency in work, it becomes imperative, for people of all ages to interact with technology. Specially in order to assist and aid older adults, products specifically targeting elderly user group have been introduced in the market. However, their adoption by elderly has not been very promising

A. Chowdhury (✉)

School of Design (SoD), University of Petroleum and Energy Studies (UPES), Dehradun 248007, Uttarakhand, India

e-mail: chowdhuryanirban14@gmail.com

P. Karkun

Department of User Experience Design, MIT-Institute of Design, Pune 412201, India

© The Author(s), under exclusive license to Springer Nature Singapore Pte Ltd. 2021
B. Deepak et al. (eds.), *Advanced Manufacturing Systems and Innovative Product Design*,
Lecture Notes in Mechanical Engineering,
https://doi.org/10.1007/978-981-15-9853-1_1

[1]. Therefore, there is a need to have an understanding that why older adults have difficulty adapting to new technologies? Related studies have suggested that elderly attitude toward a technology is based on the product's features, convenience of its usage and learning support provided along with it [2]. Age-related declines affect this attitude toward new technology or product, as it is an established fact that aging has effect on cognition learning needs of elderly different from younger counterparts [2, 3]. Deficits on attention and memory, difficulties in recalling items encountered recently, are some of the reasons affecting the ability to learn [3]. However, due to aging better emotional regulation is observed which in turn is resultant of changes in cognitive abilities. Therefore, there is need to understand human cognitive and emotional processes in order to address learning needs of elderly. This paper aims to develop a theoretical framework on existing theories of affect and cognition of elderly people to develop effective instructional strategies which could be applied for interface design of different products and software.

2 Methodology

Initially a secondary research was conducted and data collected from online resources such as Google Scholar, Science Direct, etc. A systematic literature review has been performed to filter out important resources and data as per objectives of this study. Then the Schema Construction Method (SCM) has been applied on collected data to derive a framework which allows designers to relate their design and to develop affective instructional design strategies for elderly people.

3 Effect of Aging on Human Cognition

Cognition is the set of mental processes that take place between sensation and perception and the response [4, 5]. A human cognitive system is primarily composed of working memory and long-term memory [6, 7]. Working memory (sometimes known as short-term memory) is considered to be limited while long-term memory is comparatively unlimited [7]. Working memory is primarily used while performing tasks. However, working memory is limited to seven new elements of information at a time where only two or three items of information can be processed simultaneously [8–10]. Due to this limited working memory there is a risk to have a cognitive overload if instructions are represented as unstructured, unplanned or complex [11]. Since long time, it is established that cognitive abilities decline with age [3]. These declines are observed in the storage capacity of working memory, cognitive control, attention and information processing speed [12–14]. Decline in working memory elevates the difficulty level to perform tasks. Therefore, as compared to young elderly face more issues in performing tasks. Although, long-term memory is unaffected due to aging, recalling information existing from previous experience is not an issue for

older adults. Therefore, ability to learn instructions may be dependent on the mental models/schemata or how information is organized structured in long-term memory [10]. It is difficult to recall new information, but if information due to previous knowledge resting in long-term memory (LTM) can be accessed and utilized while performing tasks, elderly may feel motivated to adopt new technologies.

4 Effect of Aging on Human Emotion

The affective system and cognitive system tend to work parallel to each other as depicted in Fig. 1 [15]. As experience of learning a new interface can only be explained in terms of human emotions. Studies suggest that affect is a quick, automatic natural phenomenon, occurring even unconsciously on exposure to stimulus [16]. This affect resulting due to interaction with a learning medium can be positive, negative. For example, a complex interface causing difficulty to interpret may lead to frustration disappointment, distress, anger, contempt, disgust, guilt, fear, nervousness [17], etc., which are characteristics of negative emotion. On the contrary familiarity due to similar past experience may lead to feeling of confidence, satisfaction and enthusiasm which are characteristics of a positive emotion.

Aging leads to better emotional regulation, the self-regulation of emotion, is caused due to selective cognitive processing [3]. In selective cognitive processing, most of cognitive resources are allocated to emotionally relevant information only.

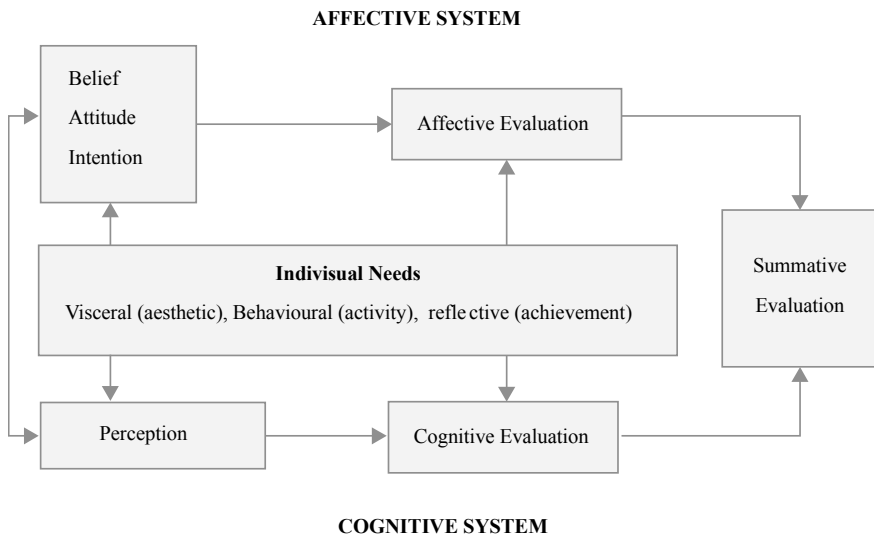


Fig. 1 Affective system and cognitive system as parallel processes (Adopted from [15])

Although which information is relevant and which is not is typically individualistic in nature. These are resultant of a person's belief, attitude, previous knowledge, intention, etc. Studies suggest that attention bias exists toward certain specific piece of information. Elderly tend to ignore information which is highly negative. It was observed that affect plays an important role in driving the elderly attention, motivation, and decision-making, e.g. a highly positive affect results in a state of high energy, full concentration, leading to engagement [15]. Therefore, the paper proposes that instructional design characteristics should reflect positivity in order to have prolonged engagement by the elderly.

5 Design Needs for Elderly

To enable affective matching of instructional designs with elderly, instructions should appear to be minimalistic in nature, as complexity may desist elderly to interact with it. Hence, the instruction environment should appear to be positive and supportive. Proposed design guidelines for elderly are that figurative representations, simple or cartoon-like characters grab the attention of elderly [18]. Visual impairment due to aging makes it difficult to read texts with small font sizes. Therefore, it is recommended that large fonts with typefaces such as 'Futura', 'Helvetica' and 'Frutiger' be utilized for improving readability under low vision conditions [19]. All Textual representations should be well organized, preferably into blocks of paragraphs of five lines or less [20] in order to enhance the readability. The differentiation between relevant/important information, a strong contrast can be used. A smooth transition between gray to white or different shades of color helps in comprehending image and text [20]. The above guidelines suggest that the tone, presentation, composition and typography are those characteristics of instructions that reflect positivity. The attention toward such instruction will allow elderly to make the first move toward interacting with the instructions.

6 Framework for Affective Instructional Design for Elderly

As already stated, that affective state on exposure to stimulus drives the motivation for engagement with product or software; therefore, it becomes essential to consider how instruction through the medium is represented? The characteristics of the instructions, i.e. its presentation style should match the needs of elderly. To enable affective matching of instructional designs with elderly the following framework (please see Fig. 2) can be considered. The framework suggests that affective matching of needs of elderly is primarily dependent on the characteristics of the instructions and its suitability which leads to the motivation to initiate interaction with the design. However, the perception for the instruction is highly individualistic in nature. It is generally depending on how it is interpreted based on previous knowledge. Therefore, while

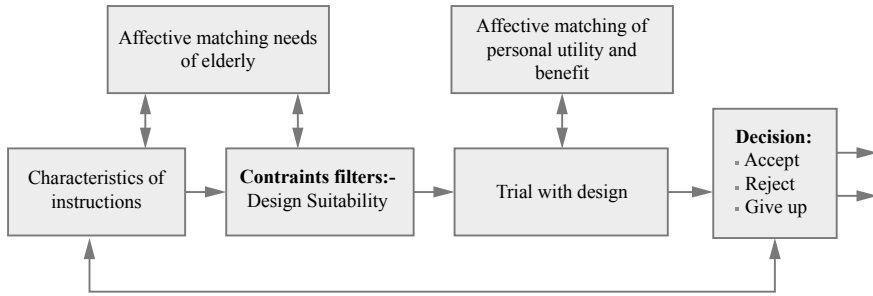


Fig. 2 Evaluation process of instructions for product/software/service use

interacting with instructions if elderly perceive it to be of use then the medium may be accepted by the elderly for future use. On the contrary if the medium is perceived to provide no benefits to the elderly then it may be rejected. The experience after interacting with instructions determines the fate of the product that is why it becomes imperative to design instructions considering the needs of elderly.

7 Practical Implications

Products like Automated Teller Machine (ATM) machines, Microwave ovens, television, etc., are used on daily basis. Most of the elderly refrain themselves to perform tasks on these products as they perceive it to be complex. Simplicity in appearance may cause elderly to have a trial with the product. The present article presented ways to get positive affect of elderly using few innovative instructional designs.

7.1 Touch-Based Interactive Interfaces

Considering the case of microwave as an example, presently all functionalities are performed using its control panel (please see Fig. 3). The instructions to use the product are explained in a separate instruction manual. The technical language and mode of representation used in manuals causes elderly to often refrain from reading them.

Therefore, it is recommended that the concept of control panel can be replaced by an interactive touch screen microwave interface, with minimal functions (please see Fig. 4). A step-by-step instruction to perform a task using functionality of microwave can be given on the screen; and thus, the complexity on the screen can be avoided. Support messages can be displayed on the screen to guide the navigation while choosing the options of these support messages requiring immediate actions can be interactive.



Fig. 3 A regular microwave with control panel

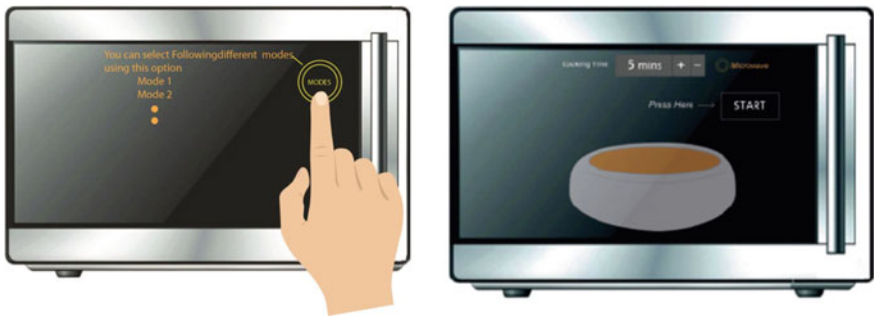


Fig. 4 Proposed microwave designs with touch-based control panel

7.2 Instruction with Emoticons

As elderly tend to show attention bias toward positive emotions; the instructions that are childlike (cartoonish) and appear to be funny can be used as instructions for guiding users for products like ATM machines or services like online payment through mobile devices/websites, etc. In this context, emoticons (please see Fig. 5)



To have a successfull transaction you need to Select 'ENTER' and thats it you are done !!

Fig. 5 Proposed emoticon-based instructions



Fig. 6 Video-based model for training elderly (Adopted from [21])

can be displayed upfront in such interfaces in order to motivate elderly to perform tasks.

7.3 Video-Based Training for Elderly

A study reported [21] that video-based training that conveys step-by-step instructions has proven to be very effective to train elderly (please see Fig. 6), as it led to a lower cognitive load. Similarly, agent-based or avatar-based virtual systems may also be employed to train elderly that explain instructions in a sequential manner.

8 Conclusion

The problem to remember and recall new information makes it difficult for elderly to adapt to new technology. This paper highlighted that there is a need to keep these limitations into consideration while designing instructional designs for elderly. The role played by the affective and cognitive systems are crucial in determining instructional design strategies. Therefore, the paper suggested a framework that highlights factors for affective matching in elderly. As the framework suggested that affective matching is dependent on the characteristics of instructions, it is recommended that the attention bias of elderly toward positively valenced emotional stimulus should

be considered as an important element for designing the instructions. Taking examples of the product used on daily basis, this paper also presented ways that can be utilized for designing instructions for elderly to use products/software fruitfully. The framework may be useful for instructional designers and human factor experts for designing strategies that motivate elderly to adopt new technologies. However, the subjective analysis can be done in future to validate the effectiveness of the affective instructions for elderly in different contexts of product and software design.

References

1. Czaja, S.J., Lee, C.C.: The impact of aging on access to technology. *Univ. Access Inf. Soc* **5**(4), 341–349 (2007)
2. Mitzner, T.L., Boron, J.B., Fausset, C.B., et al.: Older adults talk technology: technology usage and attitudes. *Comp. Hum. Behav.* **26**(6), 1710–1721 (2010)
3. Mather, M., Carstensen, L.L.: Aging and motivated cognition: the positivity effect in attention and memory. *Trend Cogni. Sci.* **9**(10), 496–502 (2005)
4. Chowdhury, A., Reddy, S.M., Chakrabarti, D. et al.: Cognitive theories of product emotion and their applications in emotional product design. In: Chakraborty, A. (ed.) *Proceedings of ICoRD'15—Research into Design Across Boundaries, India* (2015)
5. Leventhal, H., Scherer, K.: The relationship of emotion to cognition: a functional approach to a semantic controversy. *Cogni. Emo.* **1**(1), 3–28 (1987)
6. Cowan, N.: What are the differences between long-term, short-term, and working memory? *Prog. Brain Res.* **169**, 323–338 (2008)
7. Kirschner, P.A.: Cognitive load theory: Implications of cognitive load theory on the design of learning. *Learn. Instr.* **12**(1), 1–10 (2002)
8. Miller, G.A.: The magical number seven, plus or minus two: some limits on our capacity for processing information. *Psychol. Rev.* **63**, 81–97 (1956)
9. Baddeley, A.: Working memory. *Science* **255**(5044), 556–559 (1992)
10. Cowan, N.: *Working Memory Capacity*. Psychology Press, United Kingdom (2012)
11. Sweller, J., Van Merriënboer, J.J., Paas, F.G.: Cognitive architecture and instructional design. *Educ. Psychol. Rev.* **10**(3), 251–296 (1998)
12. Braver, T.S., Barch, D.M.: A theory of cognitive control, aging cognition, and neuromodulation. *Neuro. Biobehav. Rev.* **26**(7), 809–817 (2002)
13. Johnson, M.K., Raye, C.L.: Cognitive and brain mechanisms of false memories and beliefs. *Memory Brain Belief*, 35–86 (2000)
14. Bunge, S.A.: Age-Related Changes in Memory: A Cognitive Neuroscience Perspective
15. Cacioppo, J.T., Berntson, G.G.: The affect system architecture and operating characteristics. *Curr. Direct Psychol. Sci.* **8**(5), 133–137 (1999)
16. Martin, L.L., Tesser, A.: *Striving and Feeling: Interactions Among Goals, Affect, and Self-Regulation*. Psychology Press, United Kingdom (1996)
17. Watson, D., Clark, L.A., Tellegen, A.: Development and validation of brief measures of positive and negative affect: the PANAS scales. *J. Pers. Soc. Psychol.* **54**(6), 1063 (1988)
18. Mansoor, L.E., Dowse, R.: Effect of pictograms on readability of patient information materials. *Ann. Pharmacother.* **37**(7/8), 1003–1009 (2003)
19. Kline, D.W., Lynk, L.: Printed material for older readers. In: *Calgary: Report Prepared for the Senior Services Division of Calgary Parks and Recreation* (1993)
20. Strickler, Z., Neafsey, P.: Visual design of interactive software for older adults. *Vis. Lang.* **36**(1), 4 (2000)
21. Struve, D.: Process-oriented versus product-oriented worked examples for training older adults to use interactive systems. *Gerontechnology* **7**(2), 216–216 (2008)

Design of an Awareness Model to Develop Proper Sanitary Habit Among the Rural People of Jharkhand



Pallavi Rani and Amrita Bhattacharjee

Abstract Rural areas of India represent most of the population of this country. As per the census report of India 2011, about 70% Indians live in rural areas. Jharkhand is a newly formed state (2000) in eastern India that belongs to EAG. It has 24 districts among which an ethnographic study has been done in three districts, namely Saraikela-Kharsawan, Dhanbad and Godda. More precisely, the study has been conducted to understand the sanitary system in these areas. The research data has been gathered through observation and interviews with village people. It has been noticed that people of these villages are using open areas such as field, river-bank, forest and mountain areas for sanitary purpose. Though there are different schemes from Government of India for clean and healthy sanitisation (e.g. Swachh Bharat Abhiyan) however, the people of these villages are not changing their sanitary habit because they are traditionally used to it. Also, they have many cultural and social notions behind it. According to their perspective sanitisation in open area is water saving, time saving and as a whole money saving. So, they are not willing to change their habit. Eventually it has been found that though there is toilet but they are reluctant to use it for sanitisation. Therefore, a lack of awareness on hygiene and health is prevailing in these areas in spite of government initiatives. According to the Ministry of Rural Development of India, rural development implies both the economic betterment of people as well as greater social transformation. So, it can be said that there is a need to create awareness among rural people of India to socially transform India. Motivation needs to be spread among the people of rural villages to use proper sanitisation system, which is lacking in the present scenario. As the existing awareness programme arranged by the government is not effective in these villages a new model of awareness programme needs to be designed. The design

P. Rani (✉)
NIFT, Mumbai, India
e-mail: pallavi.rani.bhu@gmail.com

A. Bhattacharjee
IIITDM, Jabalpur, India
e-mail: bhattacharjee.amrita1@gmail.com

model must be more communicative as well as interactive with the rural people of India.

Keywords Sanitation · Rural development · Jharkhand

1 Introduction

Rural areas of India represent most of the population of this country. As per the Census 2011 [1], 70% Indians live in rural areas and among them 69.3% households do not have a latrine. In rural areas of Jharkhand open defecation prevails highest among all other Indian states. UNICEF has highlighted that 92.4% of the people in rural areas of Jharkhand do not have a latrine and they practise open defecation in the field, near the riverbank and other open places. To combat with the open defecation problem, in 1990, WHO and UNICEF [2] started the Joint Monitoring Programme (JMP) 2 for Water Supply, Sanitation and Hygiene that is collectively termed as 'WASH'. The term 'open defecation' became widely used in the WASH sector from 2008 onwards. For sanitation two categories were created, improved and unimproved sanitation. Open defecation belongs to the unimproved sanitation. It has been observed by UNICEF that, in between 2000 and 2015, the number of people practising open defecation has been reduced globally from 1229 to 892 million, i.e. an average decrease of 22 million people per year. In 2015, United Nations set 17 global goals named as Sustainable Development Goals (SDGs) which is driven by WASH mission. According to SDGs Agenda, open defecation has to be shortened within 2030.

The Indian government has started to promote rural sanitation since 1986. Under the Central Rural Sanitation Programme (CRSP), subsidized hardware was given to households for building latrines [3]. Later, CRSP (Department of drinking water supply Ministry of rural development GOI) was reframed as the Total Sanitation Campaign (TSC) with the target to end open defecation [4]. To inspire communities to reach full sanitation coverage, Clean Village Awards (Nirmal Gram Puraskar) [3] were announced in 2003 which offers cash prizes to villages that attained open-defecation free status. The Indian Government has been continuously providing a massive budgetary allocation and priority to the issue. In 2012, the GoI started Nirmal Bharat Abhiyan (NBA, 'Clean India Campaign') to succeed the TSC with an aim to achieve 100% sanitation access to all rural households by 2022. This new campaign aimed to quicken rural sanitation coverage by continuing the 'community-led' and 'people-centred' strategies of the TSC, with amplified importance on community mobilization, collective and sustainable behaviour change, information, education and communication (IEC) activities. Financial incentives continued for building latrines and were offered to more households belonging from BPL as well as above poverty line (IAPL) [5, 6]. In October 2014, GoI introduced NBA as Swachh Bharat Mission (SBM) [7] that targets to eradicate open defecation by 2019. The SBM has got unprecedented support from Government, the private sector and civil society. The

rural programme endorses pour-flush twin-pit toilets; those are intended to contain wastes in situ until they are safe to handle. The programme targets behaviour change and community approaches to sanitation are being adopted throughout the country. However, after all these efforts also, through field study conducted in 2018–19 in rural Jharkhand area it has been observed that there is lack of awareness regarding open defecation problem and the practice is still going on. Therefore, there is need for modifying existing strategies to eradicate the problem of open defecation. The present study aims to develop a feedback-based awareness model that will help to improve the existing scenario by digging up to the root of the problem. The novelty of the study is not to come up with a new strategy, but to understand the cause of the failure of the existing strategies by incorporating the behavioural activities of people into the model. It is expected that the proposed awareness model will augment the process of abolition of open defecation from rural India through the continuous modification of the strategies by analysing the feedback received from the local people.

2 Ethnography Study

An ethnography study has been conducted in three administrative divisions of Jharkhand named as Santhal Pargana (Godda district), North Chotanagpur (Dhanbad district) and Kolhan (Saraikela-Kharsawan district). In these areas, the field study has been done in rural villages like Raghunathpur and Mansa, of Godda district; Baghmara, Lawadih and Bandhdih of Dhanbad district and Govindpur, Bagarasai and Murumdih, of Saraikela-Kharsawan district. Unstructured interview (Fig. 1) has been conducted among children, women, men and elderly of these rural villages. From the interview, it has been found that there are many reasons, which is hindering the government initiatives to eliminate open defecation. The findings of interviews are as discussed below.

- **LACK OF INFRASTRUCTURE:** Most of the households in rural villages of Jharkhand do not have the concept to construct a latrine in the house. The standard house infrastructure of these households consists of bedroom, kitchen and courtyard. There is no concept of bathroom and toilet within the house premises. Eventually there are lack of toilets in their houses, or in nearby localities where they live. Toilets situated at far places from houses (e.g. schools or in the farms) lead people to defecate in the open space. Absence of water supply inside or next to toilets is also a reason to defecate in open area near riverbanks. It is tedious for them to collect water from a distance place before using the toilet. So, the whole architectural infrastructure needs to be revised to mitigate the problem.
- **MONETARY ISSUE:** Most of the people in these areas are afraid of cost-effectiveness of latrine system. According to them, latrines are too expensive to purchase and instal. So, this in turn forces them to defecate in open spaces.



Fig. 1 Interview with village people

- **HABITUAL PREFERENCE:** In rural areas, early in the morning people go outside to defecate in the fields or bushes. They prefer to defecate in nature than in a closed space like toilet. There is habitual preference for defecating ‘in the open air’. Even, in some villages, toilets are found to be used for other purposes, such as storing household items, animals, farm products or used as kitchens.
- **SOCIAL PREFERENCE:** Some people especially women in rural villages consider open defecation as a social activity. In the conservative societal norms, this is the time when they can go out of their home and can take some time to interact with the neighbour women. Also, they can take care of their animals and farms on their way to the fields for open defecation.
- **SOCIAL TABOOS:** Open defecation is an ancient practice and a part of social norms. In some cultures, there are social taboos for daughters-in-law to not to use the same toilet with the other male in-laws.
- **SOCIAL STIGMA:** People are scared of cleaning their toilet pits as cleaning garbage may stigmatized as impure or ‘untouchable’. In the society, where casteism is still an alarming issue, people do not like to be stigmatized because of pits cleaning. Therefore, they prefer to go out to delay the toilet pit filling up.
- **CONSERVATIVE BELIEVES:** According to some age-old scripture valued by the societies, people should not defecate in their household area. It encourages people to defecate away from their locality to maintain ritual purity. Due to lack

of educational enlighten people still obey this age-old misconception and practice accordingly.

- **LACK OF AWARENESS:** In some areas of Dhanbad and Godda it is observed that people of some communities have no idea about the health benefits of using toilets. They are not even aware of the government policies and initiatives in this regard. The government campaigns to spread awareness are not reaching them properly. Some villages still do not have electricity, so, they are not able to view awareness advertisements broadcasted through televisions or any other e-media. Due to lack of literacy rate, they are not able to read awareness posters. Therefore, awareness through print media is also not effectively communicating with them. In addition, they are not aware of the harmful effect of open defecation on health. In 2015 WHO [8] has pointed open defecation as a leading cause of diarrheal death. An average of 2000 children under the age of five die every day from diarrhoea. So, a proper awareness model needs to be designed to develop proper sanitary habit among the rural people of Jharkhand.

Therefore, through the ethnography study it is understood that there is a communication gap between the existing awareness programme arranged by the government and the behaviour of people. In addition, lack of awareness among them is not forcing to change their habitual practices. Therefore, a model needs to be designed to motivate people of rural villages to use proper sanitisation system that is lacking in the present scenario. The design model must be more communicative as well as interactive with the rural people of India.

3 Literature Survey for Designing Awareness Model

To change the practice of open defecation it is needed to focus on three major segments: effective communication, awareness creation and behavioural modification. All these three segments are interlinked and intersecting with each other. So, to design the proposed model it is necessary to understand the methodologies which already exist in these segments.

- **EFFECTIVE COMMUNICATION:** A well-developed communications strategy [9] must be comprised of a communications objective, the audience's current attitude towards the issue, and the best ways to reach the target audience. The most effective communications approach will consist of face-to-face contacts of strategic organizations with target audience. Food and Agriculture Organization of the United Nations (FAO) [10] produced a document concerning the Communication for Development (ComDev). ComDev is a communication approach based on the systematic use of participatory methods and tools. In this approach, stakeholders are integrated with the system to make all the strategic decisions communicative and effective for the target people. This will engage and empower target people and rural stakeholders by ensuring equitable access to information, knowledge sharing and inclusive decision-making. The integration of local knowledge

and communication systems with the media (e.g. rural radio, mobile phones) will help to give rural stakeholders, more power to take initiative to change their lives for betterment.

- **AWARENESS CREATION:** A study has been conducted by earlier researchers [11], in village of Haryana to find out the most effective method for creating awareness among the rural population regarding sanitation. The study has mentioned that there is lack of electricity in most of the villages whereas most of the awareness campaigns are done through electronic media. The study suggested that the agencies associated with any sanitation programme should create awareness for sanitation among the rural people through street play, folk shows, etc. which will communicate with them in their own way.
- **BEHAVIOURAL MODIFICATION:** Behaviour change is a process of modification of human behaviour. For changing behaviour, many processes have been adopted. To make an ODF (Open Defecation Free) community a community-mobilization model named as Community-Led Total Sanitation (CLTS) [12], which works as community mapping tool. It encourages communities to come up with their own solutions to their sanitation problems through a facilitated discussion.

Water and Sanitation Program (WSP) [13] of the World Bank has done research studies among households, which informed the development of behaviour change communication (BCC) and other demand-creation strategies and tools. Conceptual framework called SaniFOAM (Sanitation Focus, Opportunity, Ability, and Motivation) has been developed to design formative surveys to understand barriers and drivers of improved sanitation and monitor progress of the effectiveness of its behaviour change programme [14].

At the community level participatory approaches have found to be an effective method in shifting sanitation behaviours by encouraging latrine adoption in many areas of different countries. In 2000, Bangladesh developed Community-Led Total Sanitation (CLTS) [15] to transform sanitation behaviours in communities explicitly to end open defecation. The success of this participatory approach led to its implementation in other communities of Asia and Africa. It underlines that an understanding of behaviour alone provides insufficient clues on which to base effective processes for changing behaviour. Therefore, for effective behaviour change proper communication and awareness creation is needed at a time.

4 Proposed Design for Awareness Model

From the above discussion, it can be said that there is a lack of connection among effective communication, awareness creation and behavioural modification. As per knowledge, none of the awareness strategies has considered all these factors at a time. Therefore, an awareness model (Fig. 2) has been designed to conglomerate all the factors for developing a proper sanitary habit among the rural people of Jharkhand.

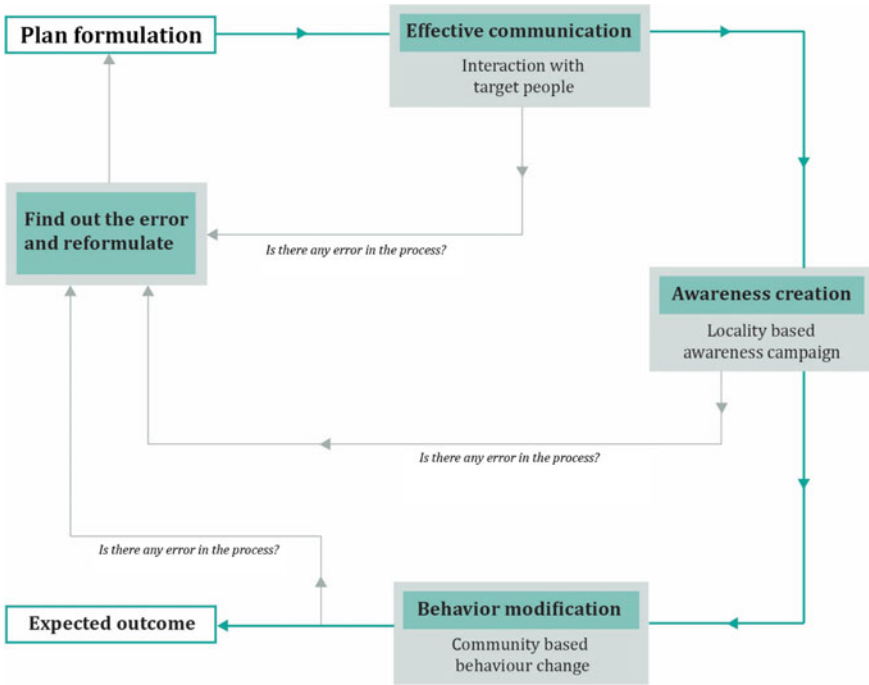


Fig. 2 Awareness model

The awareness model is a self-feedback system where in each step the system can verify the error of the system and can modify the plan accordingly. The system has broadly three steps named as effective communication, awareness creation and behaviour modification. The effective communication can be done by face-to-face interaction with the target people. Also, local communication systems such as TV, radio, mobile can help to be communicated with the local people. In rural village areas panchayat-based meeting and discussion can be a useful communication tool to propagate formulated plan. If all these communication methods are effective then only the system will proceed to the next step, else, error needs to be found out and the plan has to be reformulated accordingly. If the communication method is effective then through its locality-based awareness campaign can be generated with the help of cultural activities by engaging target people in the campaign process and by influencing them through local leaders/dignified persons. If in these ways, awareness can be generated properly then the process will move to the next step, else, again by finding out the error of the plan it has to be modified accordingly. If the awareness process is successful then it is mandatory to sustain the changed habit of target people. Therefore, the process should be recursive to make behaviour change of the whole community.

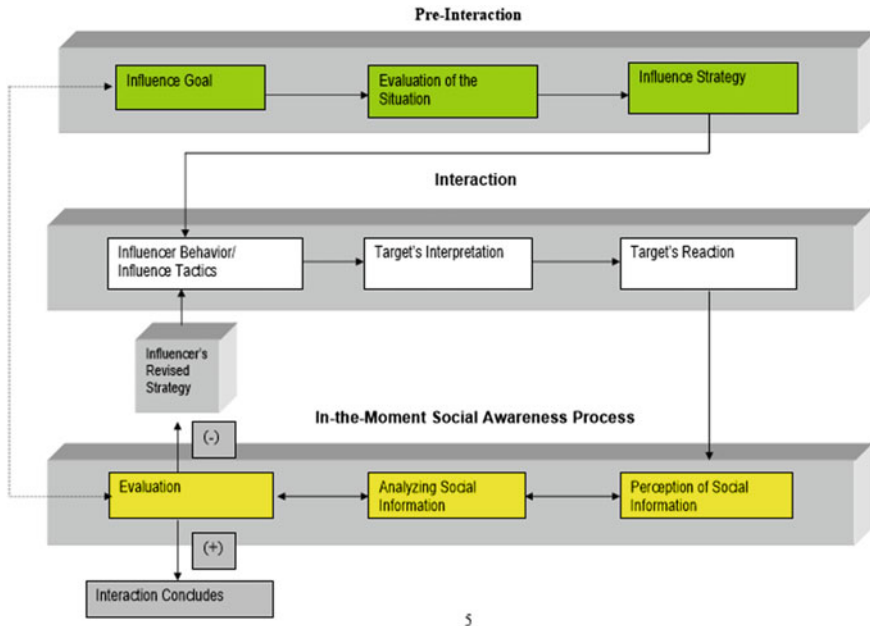
To make behavioural change there should be intervention of both external and internal bodies in the system. External body consists of government officers/staffs

who can motivate and monitor the expected outcome by economically supporting the process. Whereas internal body consists of local people (who have already adopted habit of proper sanitation through awareness creation) need to make strategies towards behaviour modification by understanding their own community mindset and act accordingly. In India, each community has different cultural and ritual beliefs and strategies for behaviour change must be built by understanding their notions. Consequently, people belong to that particular community can only make proper strategy for modifying any cultural and ritual beliefs. However, external and internal body must be two-way interactive and will give continuous feedback to each other while making any strategical movement. After monitoring for a long-term period if it is found that behaviour of target people is not modified towards proper sanitary habit, then error of the process needs to be found out and plan has to be formulated accordingly, else, the process can be terminated. In the whole process, each step is recursive based on feedback of the expected outcome. Therefore, to develop proper sanitary habit among the rural people of Jharkhand it is necessary to have an awareness model, which will continuously reformulate its planning based on positive or negative feedback of the whole system.

5 Discussion

An awareness model has been designed to develop proper sanitary habit among the rural people of Jharkhand. The designed model is an attempt to fill up the lacuna of the existing awareness model found through literature survey. Different fruitful awareness processes have been integrated in this design. For example, participatory approaches like CLTS has been recommended in a more interactive way so that people can make strategies for themselves to end open defecation. As per knowledge, none of the existing awareness process has tried to incorporate the feedback-based modification system to generate awareness in a proper way. As an example, the concepts of influence and leadership is shown in Fig. 3. In this figure, social awareness and influence process in the context of leadership interactions with a wide range of other individuals has been explained. In the context of an influence attempt, the social awareness process described below would occur during the interaction between the influencer and the target of the influence which is lacking feedback system [16].

It is found in literature that an understanding of behaviour alone provides insufficient clues on which to base effective processes for changing behaviour. Thus, a feedback-based model has been designed to find out the error in each step and modify the whole process accordingly. Therefore, there is no provision for modification of planning within the process. It is expected that this proposed model will fulfill the existing lacuna and will help to develop a proper sanitary habit among the rural people of Jharkhand.



5

Fig. 3 A model of social awareness and influence

6 Conclusion

It has been found that lack of sanitation is statistically linked with extreme poverty. Therefore, elimination of poverty will certainly help to eliminate open defecation. Also, the lack of safe, private toilets makes women and girls vulnerable to violence and is a hindrance to girls' education. All these issues need to be considered while making planning to develop healthy sanitation habit. According to the SBM Gramin (2018–19) [17], among 35 states and union territory, 18 states had reported themselves to be open-defecation free. According to report, Jharkhand has achieved 62.51% ODF status. It is expected that the proposed design model will help to formulate the planning in the right way so that a healthy sanitation habit can be generated not only in rural Jharkhand but also for the rest of India. In addition, it can be said that the proposed design model might be applicable for other social awareness programmes as well.

References

1. Ministry of Home Affairs, India, Government of "Census of India 2011 Availability and Type of Latrine Facility : 2001-2011."Ministry of Home Affairs, Government of India (2011)

2. WHO, and UNICEF: Progress on Drinking Water, Sanitation and Hygiene. World Health Organization (2017). <https://doi.org/10.1111/tmi.12329>
3. Water and Sanitation Program: A Decade of the Total Sanitation Campaign, vol. 1. World Bank (2011)
4. India, Planning Commission Government of. Evaluation Study on Total Sanitation Campaign Evaluation Study on Total Sanitation Campaign. 2013.
5. Department of Drinking Water Supply Ministry of Rural Development GOI: Central Rural Sanitation Programme Total Sanitation Campaign (2007)
6. UNICEF: Sanitation and Hygiene Advocacy and Communication Strategy Framework 2012–2017 (2012)
7. Tarraf, A.: Social and Behaviour Change Communication Insights and Strategy Case Study: Open Defecation in India (2016)
8. United Nations: Fast Facts (2015). https://sanitationdrive2015.org/wp-content/uploads/2013/03/DSG_Sanitation_Fast-Facts_final.pdf
9. Lane, R., We, R.: Communication, Public Awareness and Outreach (2009)
10. Food and Agriculture Organization of the United Nations: Communication for Rural Edevelopment (2014)
11. Amin, W.: Effective awareness generation methods for rural sanitation campaign: a study from a village in Haryana. *Int. J. Sociol. Anthropol.* **5**(3), 78–83 (2013). <https://doi.org/10.5897/IJSA12.079><https://doi.org/10.5897/IJSA12.079>
12. Kar, K., Chambers, R.: Handbook on Community-Led Total Sanitation. *Inst. Od Develop. Stud. Brighton***44** (2008). <https://www.communityledtotalsanitation.org/sites/communityledtotal sanitation.org/files/cltshandbook.pdf>
13. Connell, K.O., et al.: What influences open defecation and latrine ownership in rural households? *Find. Glob. Rev.* (2014)
14. Action, National, and Committee For Government of Zimbabwe National Action Committee for Water, Sanitation and Hygiene National Sanitation and Hygiene (2016)
15. Chambers, R.: Going to scale with community-led total sanitation: reflections on experience, issues and ways forward. *IDS Pract. Pap.* **1** (2009). https://doi.org/10.1111/j.2040-0225.2009.00001_2.x
16. Mueller-Hanson, R.A., et al.: Social awareness and leader influence: a proposed model and training intervention. In: Research report. Arlington, Virginia : U.S. Army Research Institute for the Behavioral and Social Sciences 2511 Jefferson Davis Highway, Arlington, Virginia (2007)
17. Ministry of Drinking Water and Sanitation, GOI: Swachh Bharat Mission Gramin. GOI (2018). <https://sbm.gov.in/sbmdashboard/>

Design and Evaluation of Speed Forms for Design of an Amphibious Vehicle



Debashis Majumder and Anirban Chowdhury

Abstract Amphibious vehicles (AV) are vehicles that can operate on land as well as on water. Historical evidences of different models of amphibious vehicles show that it has been lacking aesthetic and styling aspects in its design. An effort has been made in this paper to derive bio-inspired speed forms considering aesthetic and dynamism characteristics to design the AV for amusement purpose. Aesthetics based on visual characteristics or expressions that are created in 2D and 3D by taking inspirations from biological organisms are called speed forms. Speed Forms for AV are evaluated to know the user choices. User survey was conducted for understanding aesthetic preferences, perception of dynamism and their selection criteria. A total of 22 users participated (age range: 18–35 years; 70% males, 30% females) in this study and they like to explore AV for amusement purpose. The data was analyzed by using SPSS software using descriptive and inferential statistics (Friedman ANOVA and Wilcoxon signed test). It was observed that speed form 1 (inspired from frog) was most preferable among three speed forms explored in this study. The speed form 1 was aesthetically better than other speed forms; however, all the selected speed forms had dynamic characteristics. Hence, speed form 1 has the potential to be considered for designing amphibious vehicles used for amusement purpose.

1 Introduction

Automotive design and styling play a crucial role in designing vehicle exteriors [1]. Designer uses intuitive methods to come out with interesting forms which can be used for vehicle design. There are numerous researches happening in this field to come out with genuine and interesting forms for vehicle design which includes market experience, user choices, sales, etc. [2].

D. Majumder · A. Chowdhury (✉)
School of Design (SoD), University of Petroleum and Energy Studies (UPES), Dehradun 248007,
Uttarakhand, India
e-mail: chowdhuryanirban14@gmail.com

Automotive design extends to all areas of the vehicle readily visible to the customer. This may be metal, glass, wheels, lamps, mirrors, grilles, badges, etc. Some parts of interiors like soft trim, seats, door trims, instrument panel, controls, steering wheel, switches, radio, console, etc. [3]. The aim of this paper is to design and evaluate the speed form for design of amphibious vehicles. The objective is to improve aesthetic and styling aspects of amphibious vehicles for amusement purpose. To quantify the various ingredients of aesthetics and do user survey to measure user feedback on their choices. Use statistical method to come out with best user choice.

2 Literature Review

Various literature on amphibious vehicle and vehicle form generation principles are studied. The case studies are described below.

2.1 *Vehicle Form Generation Strategies*

Vehicle styling and design strategy is an important activity in the modern vehicle industry. It acts well for future automotive designs and special areas of mobility design. Appearance of the vehicle is very important for selling of the vehicle also. It's a powerful tool for communication. Vehicle Shape, Proportion, surfaces are to be designed as per users' choices and psychosocial considerations. This contributes to user interface and user experience of the product. These aspects are covered and known as emotional design [4]. Engineering Vehicle design do consider styling as one of the specialized areas of vehicle development and without which it is incomplete [5]. The importance of styling was mentioned as important activity by many authors. Styling is an intuitive process that mostly depends on designer's individual perception. It mostly consists of form development and graphic language [2]. The usage of semantic aspects and pragmatic aspects are dealt with in developing form and graphic language. This depends on facts and usage of products. This intern comes out as character. The debate is on whether it is a planned process in contrast to structured problem-solving process or it is a reflective process within certain context. The form development contributes to visual appearance of product, so various research is happening in this field to establish vehicle design methods [6]. In current design practice, it is hard to standardize an all-inclusive manner. However, there is a lot of application of gestalt in developing character and interpretation of character [7]. Abstractions of 3 types. They are abstract, semi concrete and concrete [8]. The methodology followed here is mostly with pencil and paper. Often physical clay, industrial clay, foam are used to make physical models. This is a reflective process where designer checks to and fro with situation, materials, cost and production methods. Cad and morphing is proved to be a very useful tool in this [6].



Fig. 1 Speed forms in nature adapted for aerodynamics

2.2 *Speed Form and Aerodynamics*

When we talk of vehicle design, aerodynamics comes into play as an integral part of design process. In engineering language, it can be said that automotive aerodynamics is the study of the aerodynamic properties of vehicle design reducing drag and wind noise and prevent undesired lift forces causing instability at high speed. Aerodynamic forms are generated by designers by mimicking high-speed animals, birds or objects in nature. Lot of similarity can be found in design of an airplane with that of a flying bird. Many a time aerodynamic forms and shapes of leopard are mimicked in designing a vehicle or bike [1, 5].

Recent research shows that speed form generation based on certain high-speed animals or creatures (Fig. 1) has much better aerodynamic properties than conventional shapes. This also brings new aesthetics language and newness in design.

2.3 *Speed Form and Vehicle Design*

Speed forms are generated by designers in a way to generate one idea from another idea. Transformation through sketches and understanding the design are followed. Process of lateral and vertical transformation of sketches are followed [9]. Lateral transformation converts one idea into a different idea, while vertical transformations manipulate one idea into a version of the same idea [10]. Generally sketching is the starting of generation of speed form to form an idea of attributes or properties [11].

The design and styling of automobiles are dominated by newness and innovation in terms of form design. The newness in form can be brought by imbibing character into the form. The character is studied by incorporating inspiration board. Inspiration

board is a collage of similar character objects or entities. Initially the 2D sketches are drawn by incorporating character lines from mood board. From 2D sketches 3D entities are sketched. Often 3D model is created from the sketches. Vehicle exterior and interior designs are heavily influenced by speed form process.

3 Methodology

Even though speed forms are developed to show character and innovation in form but it is designer's own interpretation. The accuracy and perfection come from experience in the similar exercise over many years. This requires understanding of user psychology, market condition, sales condition and understanding of the product also. There is no formula or quantitative method to do this. That is why it is a creative process and designers are trained to use this process. This is used in product design and vehicle design also. The effectiveness of this process can be done by having a user survey.

3.1 Participants

In this case we used user survey method to rate the various attributes in the clay models. We used 1–7 scale for rating. 1 being “minimum characteristic is found in model” and 7 is “very high characteristics are found”. A group of 22 users were interviewed which is a good sample size. The users were from 18–35 age which included male (70%) and female (30%). They were shown the 3 Clay models one by one and were asked to rate different characters like Bionic, Dynamic, Fluid, attractive, beautiful, visual delight and cute. The points were noted and analyzed by statistical method [12, 13].

3.2 Speed Form Development for Amphibious Vehicle and Clay Modeling

Amphibious vehicle is the type of vehicle which can run on roads and on water also. The look of the AV should be different from that of the land vehicle and water vehicle. In order to find a new form suitable keywords were selected to design 3 speed forms. After approval of sketches 3 forms were selected as final. The clay models were made in 1:10 scale. Models are not related with one or other. They look completely different from one and other. The first step in speed form generation is to create mood board generation. Identify Bio object or inert material to signify the



Fig. 2 Bio-inspired form transition for AV

character. Identify the significant visual character and draw sketches to arrive at an acceptable form which is good for design of amphibious vehicle (Please refer Fig. 2) [14].

The following attributes are considered for creating a speed form for design of amphibious vehicle.

Speed Form 1: This experiment shows the visual characteristics of speed form in combination of aesthetics and dynamism. This form resembles with elements like “Frog”. It is also “Dynamic”. Certain aspect of movement is indicated. The other aspects of speed form like attractive and Fluidic property are also indicated in a varying scale.

Speed Form 2: Here this reveals the characteristics of Dolphin with speed form. The attribute like “Fluidic” is present in a wave-like structure which resemble the fin-like structure of dolphin. The other aspect of amphibious vehicle is fluidic which is represented in the second model.

Speed Form 3: This speed form is inspired from “Eagle” like structure. Eagle flies high, smooth and with high speed. Body structure is balanced with wing-like structure. The amphibious vehicle character like high speed and smooth running resembles Eagle. It can also be taken as dynamic.

3.3 Aesthetics and Perceptual Evaluation of Speed Form

The sources of inspiration for these 7 attributes cannot be one. There are various objects in nature which are responsible for invoking a particular type of perceptual language. Design of a speed form is a mix and match of all these attributes in a single form. There are various options to come out with different forms which invoke varying amount of these attributes in a single model. Design of speed form depends on designer as how to combine different perceptual language in way that is most efficient in communication. The effect of cross-culture, gender and age gives varying result for the same perceptual form. Therefore, it is essential to go for survey of user perceptual mapping on these speed forms [15–18]. Please refer Fig. 3 for speed forms.

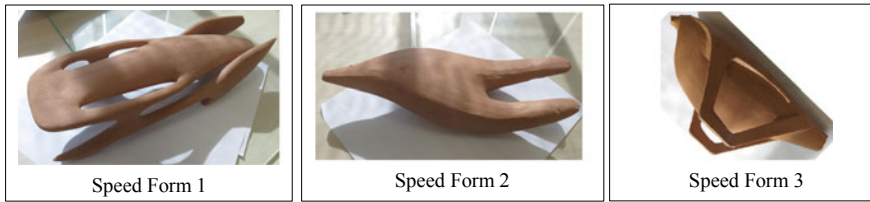


Fig. 3 Clay models of speed form used for amphibious vehicle design

3.4 *Expected Attributes of Speed Form*

In this paper, concepts of aesthetic abstraction connected with specific features and contexts are used [15, 16].

- (a) *Dynamic*: This character is very much applicable for design of AV as it moves on water and land with equal performance. People like to have speed and dynamism in the design of AV. Visual representation of dynamic properties can come from various birds in nature or animals which has great speed like “Cheetah”, “Deere”, etc. They can be sources of inspiration.
- (b) *Fluid*: This is appropriate in the design of AV as it runs on water and creates ripples. The shapes which are having streamlined body have more performance in water while moving. For example, the body structure of a fish which has great performance in water. Fluid as a character is considered as an attribute in the design of AV.
- (c) *Attractive*: Since the AV is going to be an object of desire, being attractive is a necessary attribute of the metaphor of speed form. This is an important point for purchase also.
- (d) *Beautiful*: This is a generic terminology generally used to include all kinds of people with open choices. Since this is an inclusive design, being beautiful is a necessary attribute in designing the metaphorical speed form for AV.

The speed forms are evaluated for the purpose of converting the form into an Amphibious Vehicle. When the user evaluates the form, the aspect of technicalities comes into his mind. They start relating Form with Function [17, 18]. User also judges the aesthetics of form by comparing it with other AVs in market. They imagine it in mind whether it will look superior to existing AV, etc. The acceptance criteria in mind is a mix of all the parameters and dominance of one with other. It depends on person to person depending on the background of person [19].

3.5 *Questionnaire for User Survey*

The questionnaire for the survey is based on the objective to access the physical model and judge their acceptance criteria. A google survey form was created and

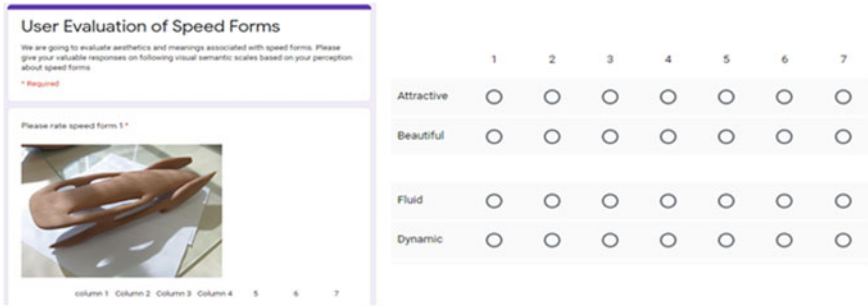


Fig. 4 Tools for questionnaire survey

users were asked to rate the 3 speed forms. They were individually shown the speed form physical models made by using automotive clay. At the end they were asked to give selection of their best choice out of 3 speed forms (Please refer Fig. 4).

3.6 Statistical Analysis of Speed Form Data

The data was analyzed in software named SPSS (Statistical package for social sciences). It was decided to go for nonparametric statistics as the sample data distribution is not following normal distribution pattern (bell curve). The Friedman ANOVA and Wilcoxon test were conducted as within-subjects study was designed (where same group of participants responded for various parameters to three different speed forms).

4 Results and Discussion

4.1 Aesthetic Perception

There were 4 different attributes given in the Model survey. The words were Attractive, Beautiful, Dynamic and Fluidic. The average responses for keywords of “Attractive” and “Visual Delight” is considered as “Attractiveness Scale”. The average responses for keywords “Dynamic” and “Fluidic” are considered as “Dynamic Scale”. From the above analysis we can find that form 1 is having “Dynamic” characteristics and “Aesthetic Characteristics” which is given by all (Please refer Fig. 5 for speed form evaluation). Results of other researches also supporting the current result [6, 20, 21].

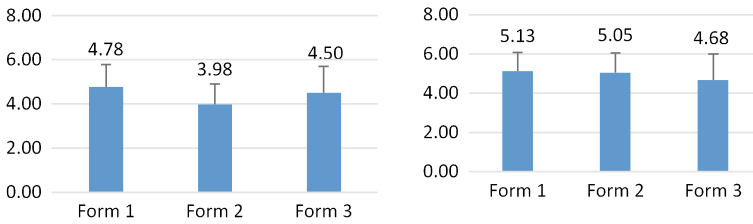


Fig. 5 Variations of aesthetics (left) and dynamism (right) perception

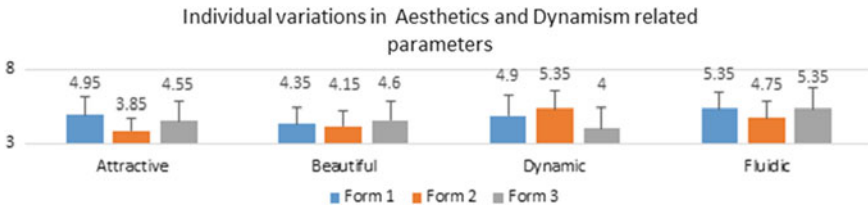


Fig. 6 Speed form evaluation for performance

4.1.1 Statistical Interpretation for Aesthetic Variations

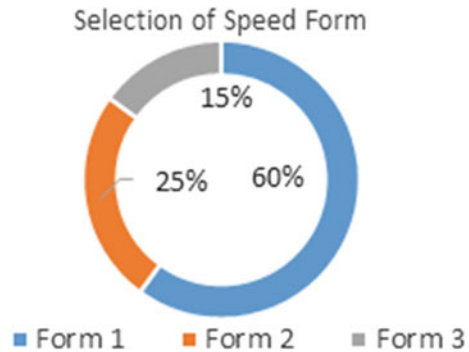
In Friedman test, p value is less than 0.05 hence there is significant variation in aesthetic value of speed form [$\chi^2(2) = 8.720$; $p = 0.01$]. In multiple comparison test, no significant difference was observed except in case of mean values of aesthetic for different speed forms as P values are above 0.05, except when aesthetic values were compared between speed form 1 and speed form 2 [$Z(2) = -2.567$; $p = 0.01$].

4.2 Dynamism Perception

All the forms are having dynamic characteristics. “Dynamic” character is more in form 2 as compared to form 1 and form 3. Form 3 is second highest in all characters except “Dynamism”. Please refer Fig. 6.

4.2.1 Statistical Interpretation for Variation of Dynamism Value

In Friedman test, p value is more than 0.05 hence there is no significant variation in dynamism value of speed form [$\chi^2(2) = 2.564$; $p = 0.28$]. In multiple comparison test, no significant difference was observed in case of mean values of dynamism for different speed forms as p values are above 0.05, when compared the dynamism

Fig. 7 Form selection rates

values in different combinations for three variations of speed forms. The above analysis by SPSS software also shows that the user preferences on “Aesthetics” and “Dynamic” characteristics of the speed form decided their choice of final preferred model.

4.2.2 Speed Form Selection Based on Perception of Users

The individual variation of attributes between all three models are shown in Fig. 7. The Chi Square Test value for the three models 0.035 which is less than 0.05, it proves the null hypothesis. There is a significant difference between two characters. While the dynamic character is not responsible for final selection of form by users, the aesthetic character is responsible for final selection of final form by users. The user survey data also shows that the majority of users select form 1 as their best choice of form. The selection of model as per user choice is shown above. The form 1 is selected by majority as final choice. Please see Fig. 7.

5 Conclusion

This was an exercise where aesthetic languages of a speed form were analyzed. The speed forms had varying attributes of “attractive”, “dynamic”, “beautiful” and “fluidic” characteristics. The user survey shows that due to high aesthetic ratings, users select the speed forms. Their preferences for aesthetics dominate their selection criteria. Form 1 was having highest preference by users over other two forms. The statistical analysis shows that there was no significant difference in score of “Dynamic”, “Beautiful” and “Fluid” form character. But there was significant difference found in “Aesthetic” character. This has resulted in final selection of form by users. We can infer that people do select speed forms based on their rating on aesthetic character.

The form 1 can be taken forward for development of exterior shape of AV. Here the detail mechanism and ergonomics are not considered as it is initial exploration. In future detail design can be made considering Ergonomics and actual mechanics for development of AV. This approach can be made useful for innovative form design of AV. Currently in AV design, this aspect is missing. It is useful for creating form based on its function which will be unique to its application.

References

1. Kozlov, A., Chowdhury, H., Mustary, I., Loganathan, B., Alam, F.: Bio-inspired design: aerodynamics of boxfish. *Proc. Eng.* **1**(105), 323–328 (2015)
2. Tovey, M., Porter, S., Newman, R.: Sketching, concept development and automotive design. *Des. Stud.* **24**(2), 135–153 (2003)
3. Clements, C., Porter, S.: *Automotive Design*. Design Council (2008)
4. Stamov, T.: On some principles of vehicle design and styling: character of the forms. *Int. J. Eng. Appl. Sci.* **4**(3)
5. Colton, J.S., Ouellette, M.P.: A form verification system for the conceptual design of complex mechanical systems. *Eng. Comput.* **10**(1), 33–44 (1994)
6. Abidin, S.B.: Practice-Based Design Thinking for Form Development and Detailing
7. Taylor, J.F.: The psychology of perception: a philosophical examination of gestalt theory and derivative theories of perception. *J. Philos.* **55**(2), 77–81 (1958)
8. Andreasen, T.: An approach to knowledge-based query evaluation. *Fuzzy Sets Syst.* **140**(1), 75–91 (2003)
9. Goel, V.: *Sketches of Thought*. MIT Press (1995)
10. Zhang, W., Zhao, J., Zou, F.: Semantic analysis of Chinese adjectives: a new approach to mapping the form-based metaphors in automobile styling. *Des. Rigor Relev.* 59–60 (2009)
11. Mezghani, M., Zayani, C.A., Amous, I., Gargouri, F.: A user profile modelling using social annotations: a survey. In: *Proceedings of the 21st International Conference on World Wide Web 2012 Apr 16*, pp. 969–976
12. Babapour, M., Rehammar, B., Rahe, U.: A comparison of diary method variations for enlightening form generation in the design process. *Des. Technol. Educ. Int. J.* **17**(3)
13. Liem, A., Abidin, S., Warell, A.: Designers' perceptions of typical characteristics of form treatment in automobile styling. In: *5th International Workshop on Design and Semantics of Form and Movement, DesForm 2009 Oct 26*
14. Abidin, S.Z., Sigurjonsson, J., Liem, A., Keitsch, M.: On the role of form giving in design. In: *DS 46: Proceedings of E & PDE 2008, the 10th International Conference on Engineering and Product Design Education, Barcelona, Spain, 04–05 Sep 2008*, pp. 365–370
15. Bouchard, C., Kim, J., Aoussat, A.: Kansei information processing in design. In: *Proceedings of IASDR Conference 2009*, pp. 3327–3337
16. Akner-Koler, C.: *Form and Formlessness*. Chalmers University of Technology, Gothenburg (2007)
17. Chen, L.L., Kang, H.C., Hung, W.K.: Effects of Design Features on Automobile Styling Perceptions
18. Krause, F.L., Bock, Y., Dreher, S.: Design evaluation of virtual clay models using selective laser sintering. In: *Machining Impossible Shapes 1999*, pp. 201–207. Springer, Boston, MA
19. Hamid, A., Hanifa, A., Zainal Abidin, S., Abdullah, M.H.: The interaction of product noise and form design in evoking users' responses. In: *DS 76: Proceedings of E & PDE 2013, the 15th International Conference on Engineering and Product Design Education, Dublin, Ireland, 05–06 Sep 2013*

20. Kyffin, S.D., Feijs, L., Young, B.: Design and Semantics of Form and Movement. Lucerne, Suíça (2010)
21. Hekkert, P.: Design aesthetics: principles of pleasure in design. Psychol. Sci. **48**(2), 157 (2006)

Design and Analysis with Optimization of Car Radiators Using Nanofluids



S. Deepankumar, B. Saravanan, V. Sudhirkumar, N. Boopalan,
A. Sundaramahalingam, and S. Dhayaneethi

Abstract In the present automobile sector, a computational fluid dynamics analysis helps in optimizing the radiator size. Cooling performances of nanofluid over the tubes of a radiator are to be observed. The dominance of nanofluid over the base fluid, water has to be evaluated. Governing the continuity, energy and momentum equations for laminar flow helps in a numerical simulation. In this phase, Maruti Suzuki 800 radiator is taken as a model that has to be optimized. Based on the existing dimensions the modeling is carried out. The test liquid will flow over the radiator which consists of 57 tubes with circular section while air makes a constant cross flow inside the banks of tubes. Nanofluids could enhance engine heat dissipating capacity. The main motto of our project is to optimize the size of the radiator and the heat dissipating capacity is to be increased. The modeling is created using SolidWorks. The optimization of Nanofluids is to be analyzed using Computational Fluid Dynamics.

Keywords Radiators · Nanofluids · Heat transfer · CFD analysis

S. Deepankumar (✉) · B. Saravanan · V. Sudhirkumar · A. Sundaramahalingam · S. Dhayaneethi
Department of Automobile Engineering, Bannari Amman Institute of Technology,
Sathyamangalam 638401, India
e-mail: deepankumar@bitsathy.ac.in

B. Saravanan
e-mail: saravananb@bitsathy.ac.in

V. Sudhirkumar
e-mail: sudhirkumar@bitsathy.ac.in

A. Sundaramahalingam
e-mail: sundaramahalingama@bitsathy.ac.in

S. Dhayaneethi
e-mail: dhayaneethi@bitsathy.ac.in

N. Boopalan
Department of Automobile Engineering, Kongu Engineering College, Perundurai 638060, India
e-mail: boopalan.auto@kongu.ac.in

1 Introduction

The internal combustion engine is where occurs the fuel combustion (like fossil fuel) with an oxidizer in a combustion chamber, the essential part of the fluid flow circuit. For a few parts of an engine direct force is provided through the amplification of the temperature and pressurized gases fabricated by combustion process carried out in the Internal Combustion Engine (ICE). Turbine blades, a nozzle or pistons, typically gets the pressure applied. This transformation of chemical energy into mechanical energy produces a force that helps in moving the component to a specific distance. Etienne Lenoir was the creator of the first successful Internal Combustion Engine commercially. The term internal combustion engines are usually found in components such as two-stroke, four-stroke piston engines, along with alternatives, including the Wankel rotary engine and six-stroke piston engine, which is referred to as an engine in which combustion is spasmodic. Continuous combustion is used in a second class of internal combustion engines, such as jet engines, most rocket engines and gas turbines [1–6].

1.1 Cooling System

The parts of the engine need to be cooled, to prevent them from overheating. Ambient air is the only fluid that can help absorb the heat. In an engine operation, it has to be ignited soon, rising up to the required temperature and has to be maintained at the same narrow level. Meanwhile the load of the engine can vary from a minimum to maximum, and fluctuation is allowed in these load ranges. While the ambient air temperature can vary, between -20 and $+40$ °C. Cooling system has to operate appropriately, at that wide range of circumstances [7, 8].

1.1.1 Radiators

The transfer of heat energy from one medium to another for cooling and heating purpose is carried out by the radiators. Radiators are especially mounted on the Internal Combustion Engines for cooling, mainly found in automobiles but also in locomotives of railway, piston engine, plants that generate stationary, motorcycles and where these IC engines are used. A coolant is sent via the engine block, to absorb thermal energy from the engine and to chill it down. The coolant that is hot now passed through the inlet tank of the radiator, where it gets distributed around the radiator core. On its way to the opposite tank, it gets cooled down. The cold coolant then flows back to the engine and the cycle is repeated [9, 10].

Mostly, water-based coolants are used, which leads to freezing, erosion, cavitation and corrosion. To prevent this, the coolant is mixed with glycols. Sometimes, the coolant might also be oil-based. Thermo siphons were used in the coolant to

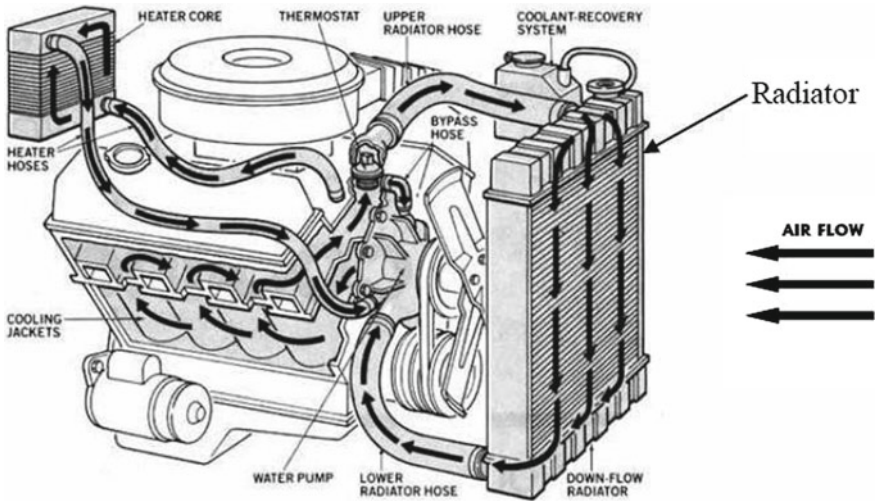


Fig. 1 IC engine cooling system

circulate in the first engines; while now, almost all the smallest engines use pumps. As circulating via tubes, the coolant transfers its heat to the fins laying between each row of tubes. The ambient air gets heated up by the fins. Fins significantly increase the contact surface of the tubes with the ambient air, thus escalating the exchange capability. Fig. 1 shows the coolant flow inside the radiator, radiator hoses and coolant jackets. Comparatively a large volume of air flow has to be given, to capture heat from the coolant, since liquid coolants are denser and have higher heat capacity than air. Hence radiators are provided with one or more fans to help adequate air flow. Radiators are often mounted behind the grill framework that is placed in the front of a vehicle, to save fan power consumption in vehicles [11, 12] (Fig. 2).

1.1.2 Nanofluids

Suspensions of nanoparticles, with dimensions smaller than 100 nm, in fluid state, with that of significantly enhanced properties, are called as nanofluids. Nanofluids have wide range of applications in every field, from automobile to medical fields. Nanofluids, containing nanoparticles which are usually composed of metals, carbides, carbon nanotubes or oxides, with common base fluids as oil, water and ethylene glycol [13].

1.1.3 CFD

Computational fluid dynamics (CFD), is a branch of fluid mechanics that resolve and analyze problems that involve fluid flows using mathematics and algorithms.



Fig. 2 Radiator—cooling system

Computers help in performing the calculations needed to vitalize the liquids and gases interactions with surfaces that are determined by boundary conditions. Better solutions can be achieved, with highly efficient computers. Researches are carried out to yield a software that could improve the precision and complex simulation scenarios speed, as of turbulent or transonic flows. Validation of such software experimentally is performed with a wind tunnel, and finally with the full-scale testing, e.g. flight tests [14].

2 Modeling Methodology

Parameters refer to restrictions that define the geometry or shape of the assembly or model. Parameters can be either geometric or numeric. Numeric parameters are correlated with each other, which aid them for design capture. Design is the respond expected by the creator to the changes and updates made. For an instant, if you would like to have a hole on the top of a beverage can, on its top surface, despite the dimension of the can, SolidWorks will allow the consumer to mention the hole as a feature on the top surface, and will carry out the design intent, letting them assign the

desired can size. Features refer to the elementary units of the part, which regulates the shapes and operations of the part. 2D or 3D sketch of shapes such as holes, bosses, slots are usually the beginning of the shape-based features. This shape is then cut to include or exclude material from the part. While the operation-based features are not based on sketches, and include other features such as shells, chamfers, fillets, applying outline to the sides of a part, etc.

2D sketch is the first and foremost step in building a solid work model. This sketch that is usually composed of geometrical aspects such as points, arcs, lines and conics, is added with dimensions to mark the location and size of geometry. Attributes like tangency, parallelism, perpendicularity and concentricity are defined by relations with respect to sketch geometry. Dimensions and relations are the key features that drive the parametric nature of SolidWorks. The sketch dimensions can be independent, or related to others. The analog to sketch relations are the assembly mates. The assembly mates with respect to the individual parts or components, define equivalent relations which in turn makes the construction of assemblies easier. Additional advanced mating features are included in SolidWorks such as cam follower mates and gear. These let gear assemblies to repeat the rotational movement more relatively. The optimum coolant temperature for Maruti Suzuki 800 radiator is around 92 °C. The temperature at which the thermostat valve begins to open is 82 °C. The temperature at which valve becomes completely open is 95 °C. Radiator modeling is done using SolidWorks. The design parameters are taken from a Maruti Suzuki 800 radiator [15, 16].

3 Design and Analysis

3.1 CAD Model

Material of tubes: Aluminum.

Number of tubes: 57.

Inner diameter of tube: 3 mm.

Outer diameter of tube: 3.3 mm.

Material of fin: Aluminum.

Thickness of fin: 0.1 mm (Figs. 3, 4, 5 and 6).

3.2 Meshing

The meshing of one of the tubes from the radiator is fine meshed using ANSYS workbench 14.0. One of the fin is also fine meshed. The statistics of the meshed objects are obtained as following [17].

Statistics of tubes Nodes—415,902.

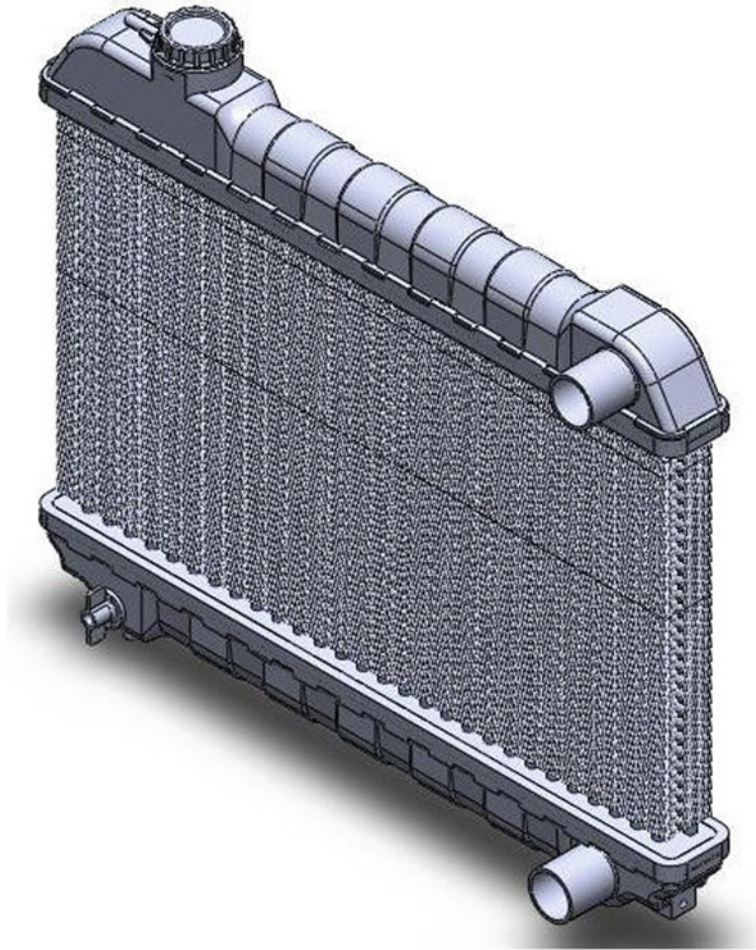


Fig. 3 CAD model of the radiator done using SolidWorks

Elements—1,776.

Statistics of fins Nodes—26,161.

Elements—9956 (Fig. 7).

3.3 Heat Transfer Calculations

3.3.1 Parameters

Inner diameter of tubes, $d_i = 0.0056$ m.

Length of tubes, $l = 0.275$ m.

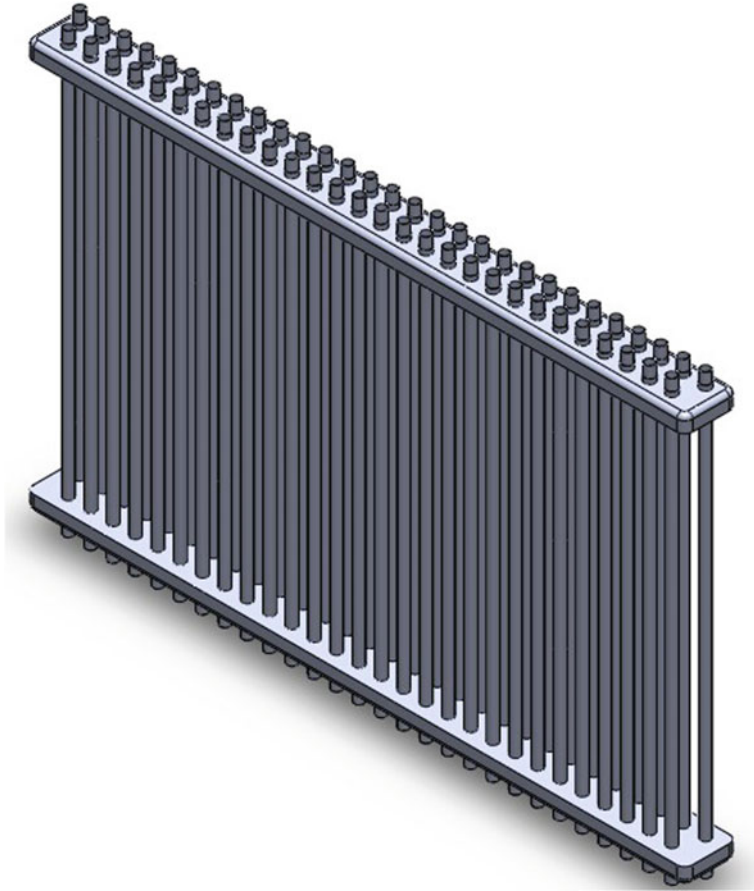


Fig. 4 CAD model of the radiator tubes done using SolidWorks

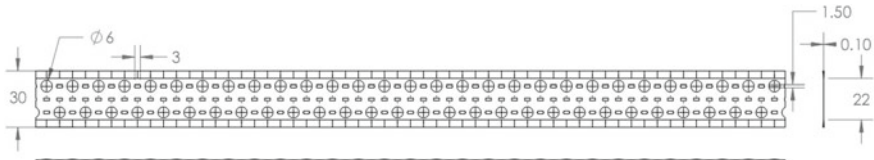


Fig. 5 2D sketch of a fin of the radiator from SolidWorks

Inlet temperature, $t_i = 90\text{ }^\circ\text{C} = 363\text{ K}$.
Tube wall temperature, $t_w = 55\text{ }^\circ\text{C} = 328$.
Number of tubes, $N = 57$.

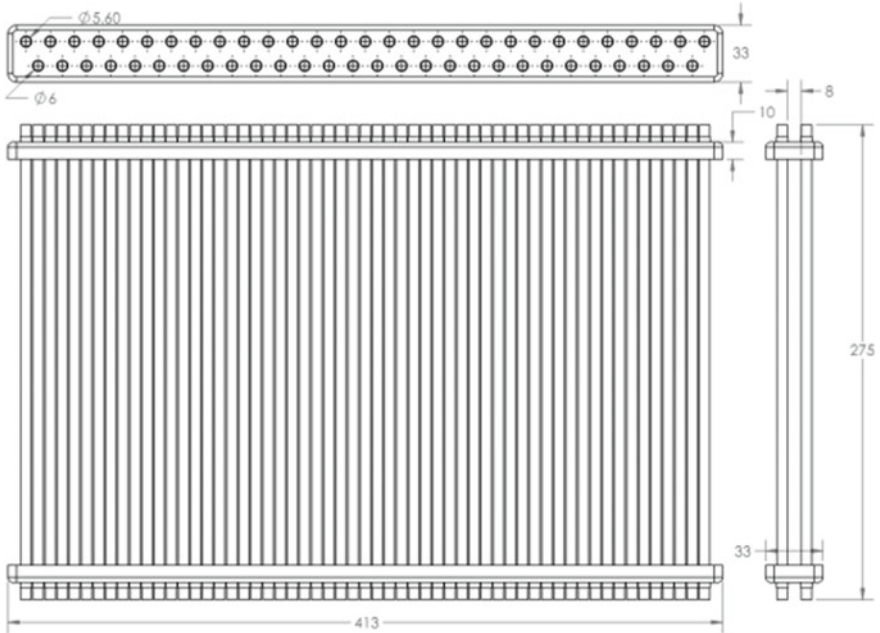


Fig. 6 2D sketch of bank of tubes of the radiator from SolidWorks

3.3.2 Formulae Used

Total flow area, $A_f = N \times (\pi/4) \times d_i^2$ $A_f = \dot{m}/v\rho$.

Reynolds number, $Re = vd/\nu$.

Nusselt number, $Nu = hd/k$.

Mass flow rate, $\dot{m} = \rho Av$.

Heat transfer, $Q = \dot{m} C_p(t_i - t_o)$ $Q = hA(t_m - t_w)$.

3.3.3 Boundary Conditions

Inlet condition. Inlet temperature as 80 °C (Fig. 8).

Material—Aluminum alloy

See Fig. 9.

Outlet

See Fig. 10.

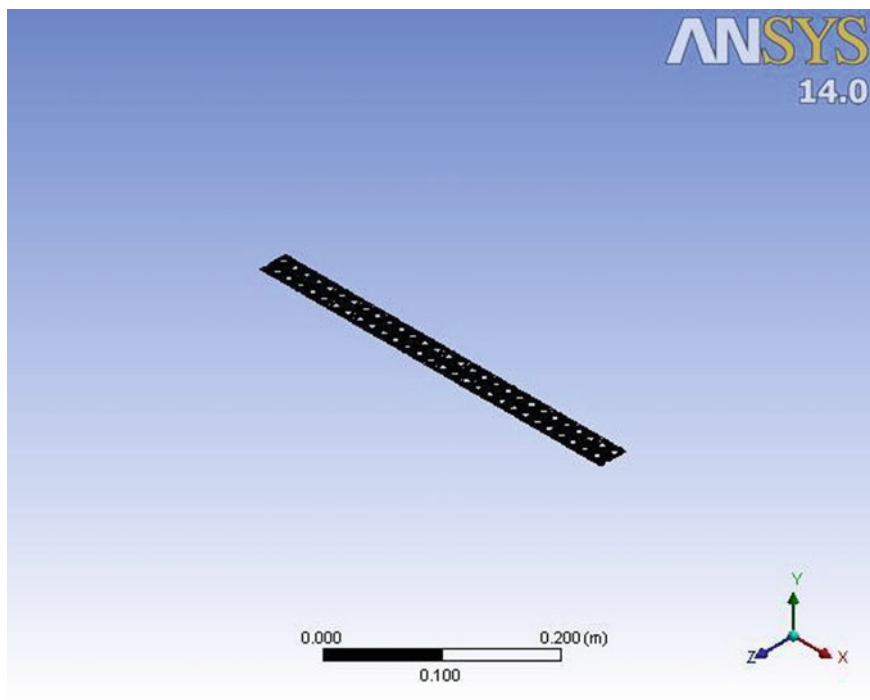


Fig. 7 Meshed fin of radiator from ANSYS

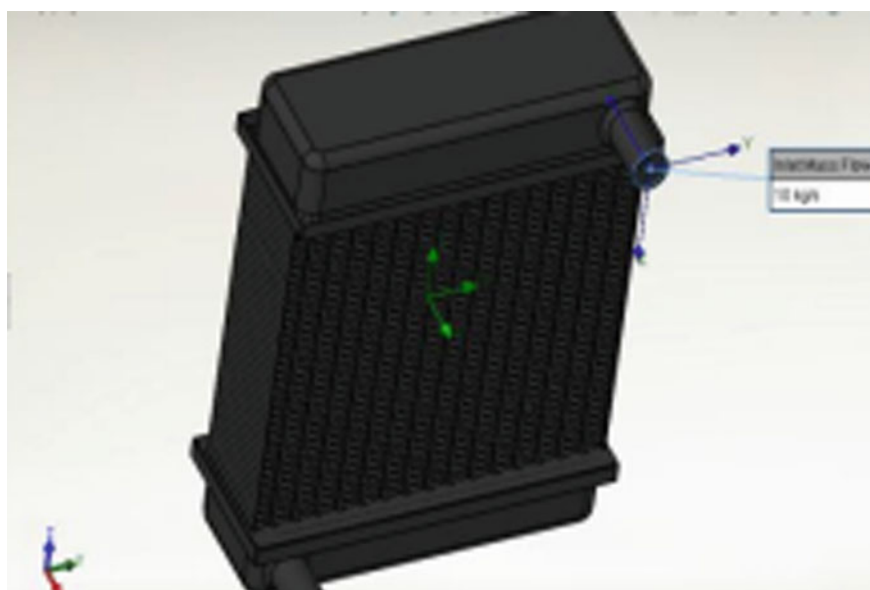


Fig. 8 Inlet temperature as 80 °C

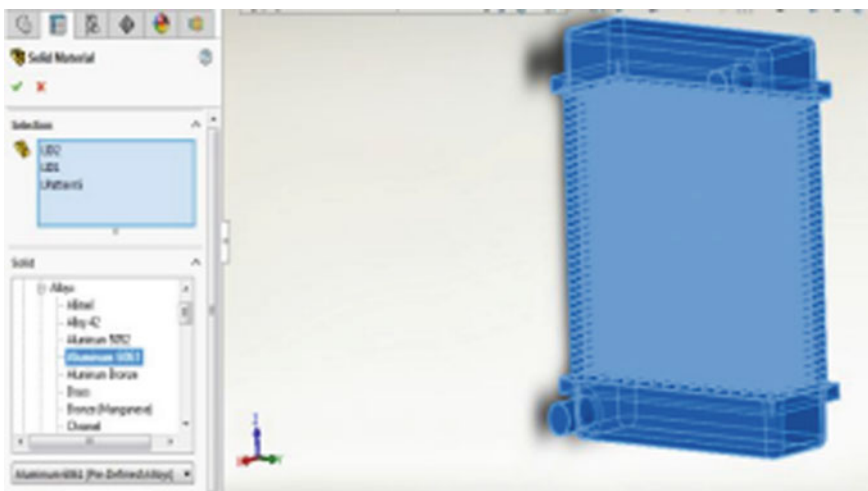


Fig. 9 Material—aluminum alloy

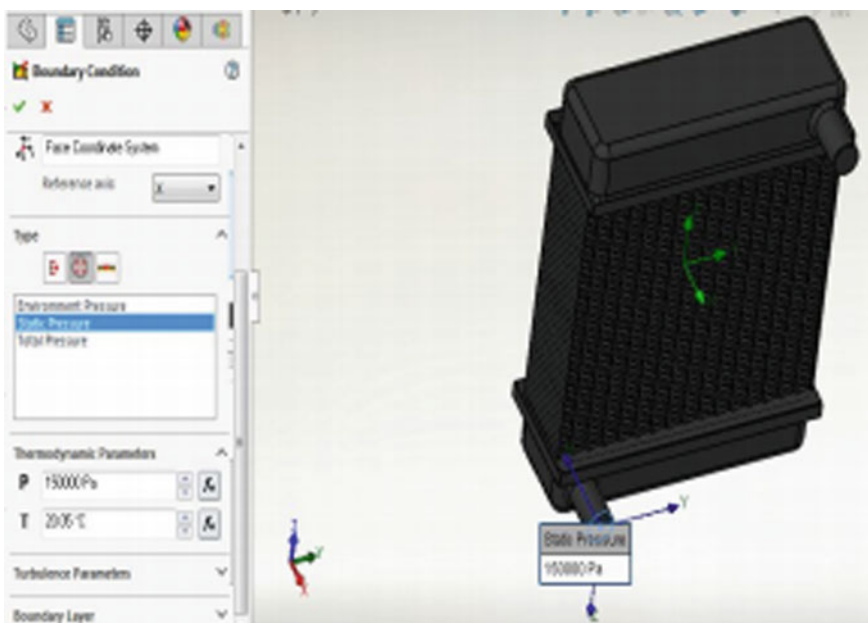


Fig. 10 Outlet temperature

4 Results

Total flow area, $A_f = 1.4039 \times 10^{-3}$ m Velocity of water, $v = 71.229$ m/h $v = 0.0198$ m/s.

From Heat transfer Data book, water at 90 °C Density, $\rho = 967.5$ kg/m³.

Prandtl number, $Pr = 1.98$ Kinematic viscosity, $\nu = 0.3285$ m²/s.

Thermal Conductivity, $k = 0.67455$ W/mK Specific heat, $C_p = 4205.5$ J/kgK.

Reynolds number, $Re = 337.53 < 2300$. Therefore, it is a laminar flow.

For laminar flow, Nusselt number, $Nu = 3.66$.

Heat transfer coefficient, $h = 440.866$ W/mK.

Mass flow rate, $\dot{m} = 0.029$ kg/s.

Outlet temperature, $t_o = 66.748$ °C.

Temperature

See Fig. 11.

Pressure

See Fig. 12.

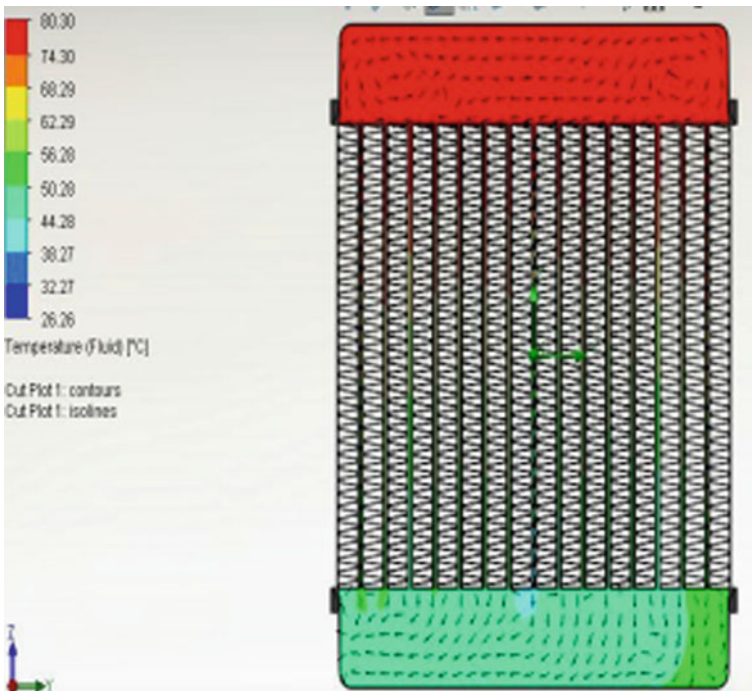


Fig. 11 Temperature result

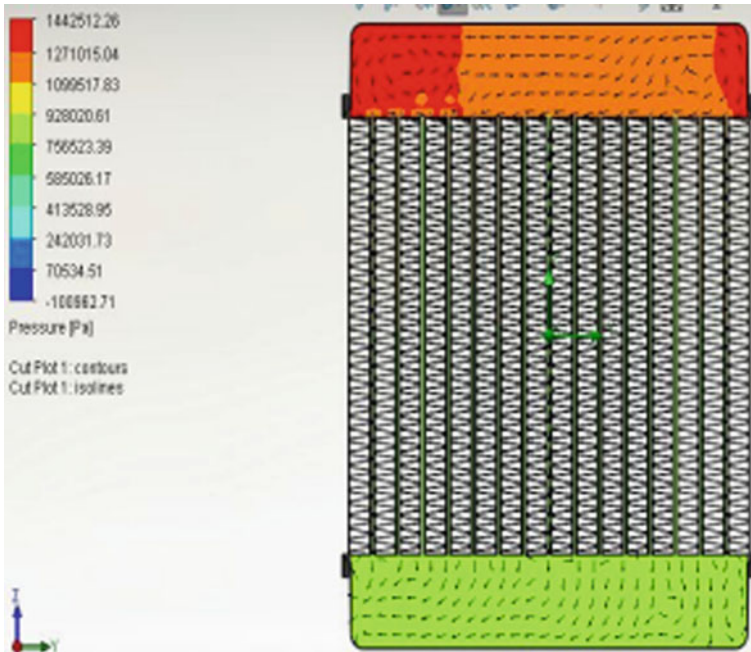


Fig. 12 Pressure result

Velocity

See Fig. 13.

Fluid	Inlet temperature (°C)	Outlet temperature (°C)
Water	80	29.49
Nanofluid	80	26.26

5 Conclusion

Thermal analysis of cooling system is carried out using analysis software. First CFD thermal analysis is carried out simulation approach and theoretically according to the operating condition. The presence of nanofluid can improve the heat transfer rate of the automobile radiator. Fluid flow rates, core dimensions, temperatures, fins and tubes details like thermal conductivities, thickness and number of tubes are given as inputs. Accuracy of this analysis can be increased by embodying CFD. ANSYS CFX is a CFD program that helps increase fluid flow in tubes of radiator. The amount of the heat transfer improvement hangs on the quantity of nanofluid added. From



Fig. 13 Velocity result

the result, we conclude that nanofluids provide improved convection i.e. provides superior cooling to engine compared to water.

References

1. Mehta, A., Tantia, D.K.: Heat exchanger using nano fluid. *Int. J. Adv. Eng. Technol.*
2. Bhatt, R.J., Patel, H.F., et al.: Nano fluid a new generation coolant. *IJRMT* **4**
3. Tirupathi Rao, D., Ravibabu, S. et al.: Experimental investigation of cooling performance of an Automobile radiator using Al_2O_3 -Water + Ethylene glycol nano fluid. *Int. J. Eng. Res. Develop.*
4. Chavan, D.K., Tasgaonkar, G.: Study, analysis and design of automobile radiator (heat exchanger) proposed with cad drawings and geometrical model. In: *Heat Exchangers Selection Rating and Thermal Design*. CRC Press LLC (2002)
5. Amrutkar, P.S., Patil, S.R.: Automotive radiator sizing and rating—simulation approach. *IOSR J. Mech. Civil Eng. (IOSR-JMCE)*
6. Golakiya et al.: Analysis of radiator with different types of nanofluids. *J. Eng. Res. Stud.*
7. Wang, X.-Q., Mujumdar, A.S.: Heat transfer characteristics of nanofluids: a review. *Int. J. Therm. Sci.* (2007)
8. Yadav, J.P., Singh, B.R.: Study on performance evaluation of automotive radiator. *S-JPSET* **2**(2). ISSN: 2229-7111
9. Yoo, D.-H., Hong, K.S., Hong, T.E., Eastman, J.A., Yang, H.-S.: Thermal conductivity of Al_2O_3 /water nanofluids. *J. Korean Phys. Soc.* **51** (2007)

10. Deepankumar, S.: Experimental analysis of performance and emission characteristics of single cylinder direct injection diesel engine using algae as a biodiesel and barium oxide as a nanofuel. *Int. J. Mech. Prod. Eng. Res. Develop. (IJMPERD)* **9**(1), 35–42
11. Deepankumar, S.: Enhancing the four stroke ci engine performance and reducing emission by preheating and oxidation process using biodiesel. *Int. J. Mech. Prod. Eng. Res. Develop. (IJMPERD)* **8**(7), 230–240
12. Deepankumar, S.: Experimental investigation on emission analysis of multi-cylinder direct injection diesel engine using manifold injection of ethanol. *Int. J. Mech. Prod. Eng. Res. Develop. (IJMPERD)* **8**(7), 704–710
13. Deepankumar, S.: Experimental investigation of performance and emission characteristics of diesel-bio diesel (CSOME) with nano additive blends in CI engine. *Adv. Automob. Eng.* **7**(176), 2
14. Deepankumar, S.: Experimental investigation of performance and emission characteristics of diesel-bio diesel (CSOME)-ethanol-diethyl ether blends in CI engine. *J. Therm. Energy Syst.* **2**(3), 148–155
15. Deepankumar, S.: Experimental investigation of performance and emission characteristics of diesel-bio diesel (CSOME)—ethanol diethyl ether blends in CI engine. *J. Therm. Energy Syst.* **2**(3), 148–155
16. Deepankumar, S.: Experimental investigation of performance and emission characteristics of diesel-bio diesel (CSOME) with nano additive blends in CI engine. *Mater. Sci. Eng.* **764**(1), 1–10
17. Deepankumar, S.: Corrosion characteristics on friction stir welding of dissimilar AA2014/AA6061 alloy for automobile application, 2019-28-0063

Design and Cost Analysis of Mini Tiller-Cum-Basin-Maker for Coconut Trees



Abi Varghese  and Jippu Jacob

Abstract Mini Tiller-cum-Basin-Maker is a miniature machine which helps in loosening soil and trimming roots around the coconut tree. It helps the coconut tree in storing water during monsoon, regulating infiltration and percolation, stimulating root growth, manuring, applying of fertilizer, to aerating it, including controlling or destroying of weeds, insects, pests and worms. The machine consists of a petrol engine, chassis, belt and chain drive, tie-rod member, openable loop, scraper blade and a rotavator shaft with 32 blades. The openable loop is connected at the end of tie-rod member which is attached to the trunk of a tree. Motion is then imparted to the mini tiller and the blades, which cause the machine to move around the tree trunk. The engine is connected to the blades through belt and chain drive which helps to plough the land. A scraper blade is fastened behind the rotavator shaft, which is inclined to the axis of shaft help to gather the soil radially outward. It also helps to deposit the soil behind the scraper attachment to form a circular bund. The scraping and shifting of the soil cause to form a basin of some depth around the tree. The extendable tie-rod member helps in varying the radial distance of the basin from the tree trunk. Cost analysis of the machine is calculated and the operating cost of machine for making per basin is Rs. 31.40 which is more promising when compared to traditional manual basin making method which is Rs. 39.

Keywords Coconut · Coconut tree · Mini tiller · Basin-maker

A. Varghese (✉)

Department of Mechanical Engineering, National Institute of Technology Calicut, Calicut, Kerala, India

e-mail: abivarghese777@gmail.com

A. Varghese · J. Jacob

Department of Mechanical Engineering, Amal Jyothi College of Engineering, Kottayam, India

1 Introduction

Coconuts are essential to the traditional lifestyle and also one of the major income sources of the people of India, which is one of the largest producers of coconut [1, 2]. The major by-product from coconut trees are (i) Coconut which includes Coconut water, Coconut meat, Copra, Coconut oil, Coconut Cake (ii) Coconut Toddy (iii) Coconut shell-based product (iv) Coconut Coir-based product (v) Coconut leaves (vi) Coconut wood-based product [3, 4]. Coconut trees are hard to grow in drought climate and frequent irrigation is required to grow new leaves [5]. Therefore, before monsoon season, circular deep groove is dug around the coconut tree. It provides maximum rain water available during monsoon season and removes the old roots and replaces it with the new ones. It helps to provide good humus fertile soil around the tree and penetration of the new roots also becomes easy. It also helps in aerating it, storing water, regulating infiltration and percolation, stimulating root growth, manuring, applying fertilizer, including controlling or destroying of weeds, insects, pests, and worms. Generally, soil manipulation of this sort is done manually using spades, pickaxe, or soil tilling tools. Manual digging of a groove up to 2 m radius and 220 mm in depth, it takes around 15–25 min, depends on soil condition, physical strength of the worker, and size of the tree. Thereby making work much more tedious and time-consuming. It affects productivity and increasing demand of labour and labour cost.

Mini Tiller-cum-Basin-Maker [6] is a miniature machine which helps in loosening soil and trimming roots, which leads to aerating it, storing water, regulating infiltration and percolation, stimulating root growth, manuring, applying of fertilizer, including controlling or destroying of weeds, insects, pests, and worms. Other than traditional methods, an attachment is developed to the tiller for making basins around trees [7]. It consists of a horizontal ‘L-shaped’ member, one end which is attached to the tree trunk and other end is connected to the tiller. The movement of the tiller in forward direction and the influence of the ‘L-Shaped’ member aids the tiller to plough in a circular path. In 2015, Kerala Agriculture University has developed coconut basin digger which is an attachment to power tiller [8]. While digging, the attachment is connected around the coconut tree and helps to move around. But it is very time-consuming, because of complex connecting mechanism and very hard to till the soil near the tree, due to minimum turning radius. Power weeders developed by many companies are also used for making coconut basin in many areas. Though a mini tiller, garden tiller, power tiller, or tractor is used to till around the tree, its limitations in steering close to the tree; may be due to drooping branches, short turning radius, etc.; impose restrictions in making the operation easier or effective. It is under these circumstances that the machine under invention becomes useful. The machine is applied for Indian Patent with the application of 1025/CHE/2013 shows the novelty of the product.

2 Materials and Method

2.1 Design

Figure 1 provides the schematic drawing of Mini Tiller-cum-Basin-Maker [6]. The mini tiller and its tilling unit consists of a petrol engine, transmission unit, scraper blade, rotavator shaft, openable loop, and tie-rod member.

Engine

Petrol engine is the main power source of the machine, which is separably fixed to the chassis. The power from the engine is transmitted to the rotavator shaft through a belt drive and a chain drive.

Power Transmission Unit

The power from the engine is transmitted with a belt drive to a chain drive. Appropriate shields and covers protect the transmission systems. Driven pulley of the belt drive and driver sprocket of the chain drive is fixed on the same intermediate shaft. Driven sprocket of the chain drive is fixed on the rotavator shaft carrying a plurality of blades.

Scraper Blade

Scraper blade separable attached to the mini tiller, but behind the rotavator shaft shown in Fig. 2. It is set at an appropriate angle inclined to the longitudinal centre line of the mini tiller so as to (i) gather the soil, weeds, trash, etc., (ii) displace them

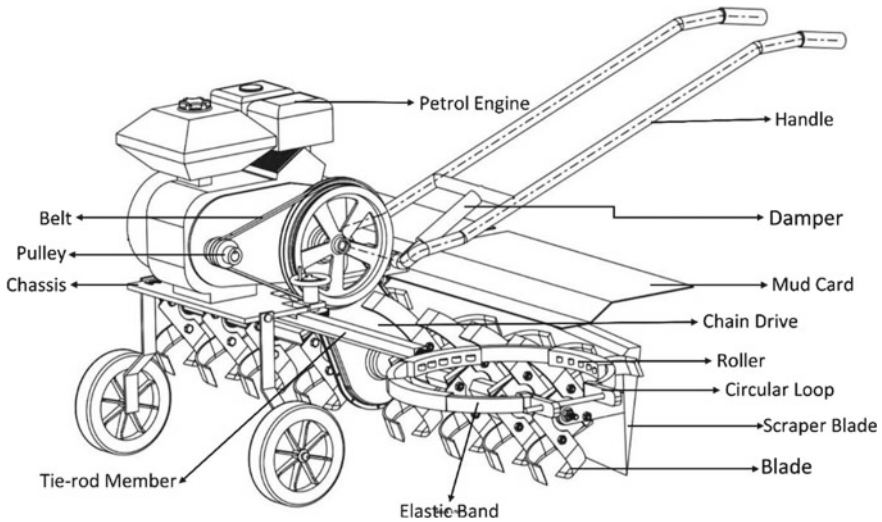


Fig. 1 Schematic diagram of mini tiller-cum-basin-maker [6]

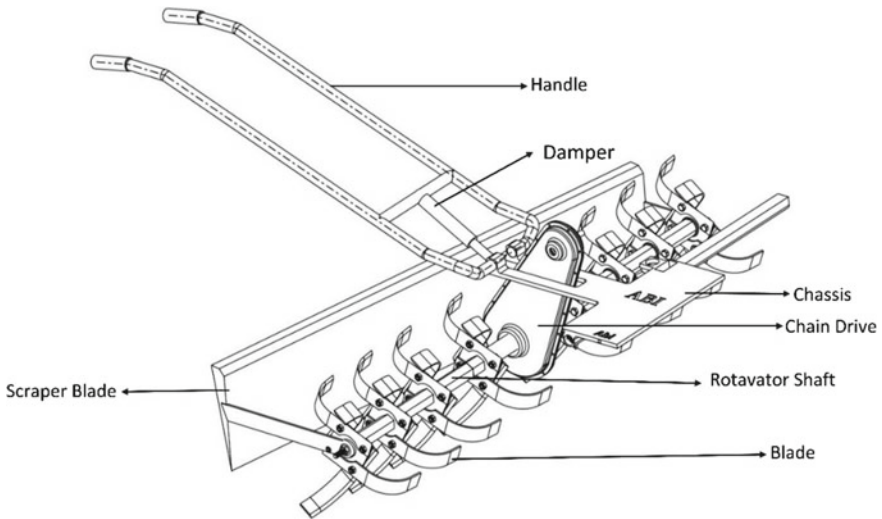


Fig. 2 Schematic diagram of rotavator shaft and its associated parts

outwardly towards the periphery of the scraper blade, and (iii) deposit them there, but outer to the scraper blade, forming a circular or near-circular ridge or bund around the post or tree trunk.

Rotavator Shaft

Driven sprocket of the chain drive is fixed on the rotavator shaft carrying 32 blades and depth of the tilling can be adjusted with a handle which is connected by a damper shown in Fig. 2. Mud card is provided on the top of the rotavator shaft.

Tie-Rod Member

Tie-rod member shown in Fig. 3 is separable and extendable, fixed on the chassis through an assembly of a rack and pinion to facilitate the varying of the length of the extended portion of the said tie-rod member to one side of the mini tiller in any incremental length. The assembly of rack and pinion helps in varying the radial distance of operation of the mini tiller from the respective tree trunk.

Openable Circular Loop

Openable circular loop shown in Fig. 3 carried at the free end of the tie-rod member, with a provision for loosely, but sufficiently, wrapping it around the respective tree trunk. It helps to serve as a boss as in a hinge or pivot. The circular loop helps in pivoting the mini tiller to a tree trunk through the nut and bolt assembly. Its inner surface carries a plurality of roller, as in a roller bearing, to facilitate easy rotation of the loop about the tree trunk and to prevent or reduce damage to bark of the tree. It has a plurality of elastic bands so arranged as to vary its diameter to suit various diameters of the tree trunk.

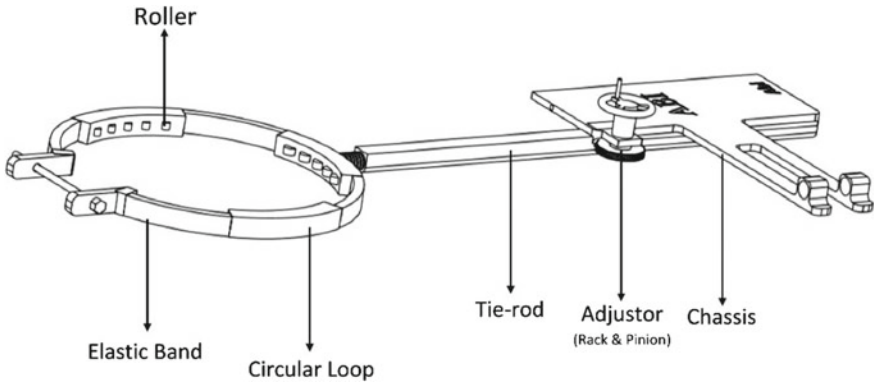


Fig. 3 Schematic diagram of Tie-rod member and its associated parts

2.2 Operation

The mini tiller and its tilling unit consist of major separable parts like an engine, transmission unit, a chassis, and a blade attached rotavator shaft. It has facilities to vary the tilling depth by adjusting the handle. Its soil gathering and guiding attachment shall comprise of major separable parts like a scraper blade, and its fastening members. Its restraining attachment comprises of major separable parts like an extendable tie-rod member having an openable circular loop on its free end and the former being separably attached to one side of the mini tiller, but extending from there. The circular loop has facilities to loosely tie and hinge the tie-rod member together with the mini tiller to the respective tree trunk to facilitate the mini tiller’s motion in a more or less circular path around the trunk of a tree.

In operation, the mini tiller is connected to the tree trunk using the tie-rod member with help of an openable loop. Motion is imparted to the mini tiller and the rotavator shaft causes the mini tiller to move along the circular path. The extendable tie-rod member helps in varying the radial distance of the basin from the tree trunk using rack and pinion (adjuster). The movement of the blade helps the tiller to plough the land.

The scraper blade fastened behind the rotavator shaft with some inclination to its axis helps to gather the soil and guides it radially outwardly. It also helps to deposit soil outer to the scraping attachment to form a circular bund. The scraping and shifting of the soil cause to form a basin of some depth around the tree. Figure 4 shows the isometric view and Fig. 5 shows the exploded view of the Mini Tiller-cum-Basin-Maker. The bill of materials is included in Table 1.

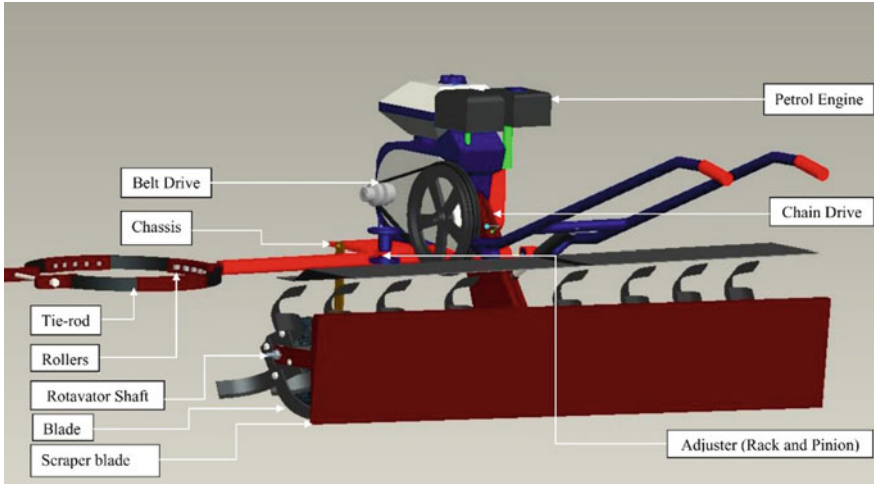


Fig. 4 Isometric view of the mini tiller-cum-basin-maker

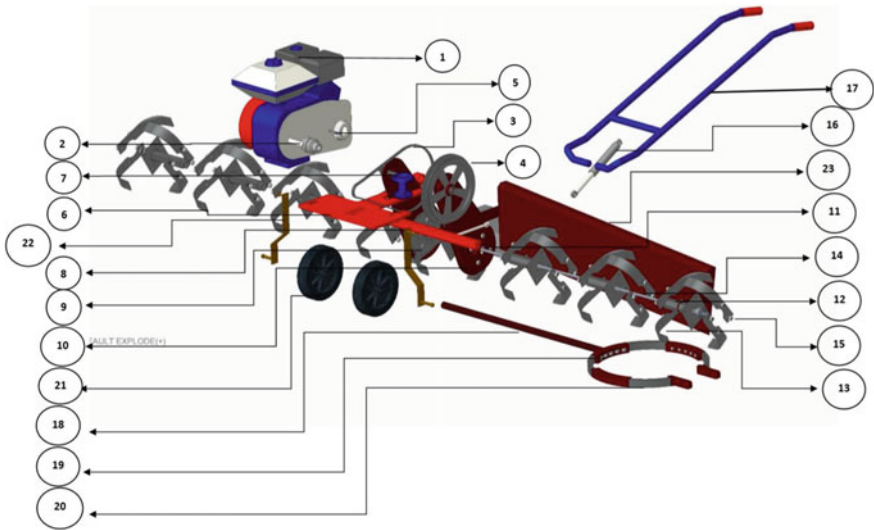


Fig. 5 Exploded view of the mini tiller-cum-basin-maker

2.3 Cost Economics and Its Comparison

The operation cost of the Mini Tiller-cum-Basin-Maker was calculated. The remuneration for manual basin making around coconut tree and the labour charges were based on the data published by the government of Kerala [9]. The operation cost

Table 1 Bill of materials

Part No.	Description	Quantity	Materials
1	Petrol engine	1	
2	Small pulley	1	Cast iron
3	V-Belt	1	Rubber
4	Large pulley	1	Plastic
5	Key	2	Cast iron
6	Chassis	1	Cast iron
7	Small sprocket	1	Cast iron
8	Chain	1	Alloy steel
9	Large sprocket	1	Cast iron
10	Chain cover	2	Mild steel
11	Bearings	2	Chrome steel
12	Blade plate	8	High carbon steel
13	Blade	32	High carbon steel
14	Blade shaft	1	Mild steel
15	Nut and bolt	32	Stainless steel
16	Damper	1	
17	Handle	1	Mild steel
18	Tie-rod member	1	Cast iron
19	Roller	15	Mild steel
20	Elastic member	1	Rubber
21	Wheel	2	Nylon
22	Wheel holder	2	Mild steel
23	Scraper blade	1	Mild steel

with Mini Tiller-cum-Basin-Maker was compared with the manual method of basin making around coconut tree.

- i. Machine Fabrication cost (including the cost of material, C)
- ii. Average life of the machine, $L = 10$ years
- iii. Working hours (60 days per year), $H = 360$ h
- iv. Salvage Cost (10% of cost of machine), S
- v. Interest (Initial Capital), $i = 12\%$ per year
- vi. Worker Required = 1
- vii. Remuneration per day of 6 h = Rs. 660
- viii. Maintenance cost = 5% (machine cost)
- ix. Insurance = 1.5% (average cost of machine per year).

3 Result and Discussion

3.1 Cost Analysis of Mini Tiller-cum-Basin-Maker

Machine Fabrication cost (including the cost of material, C)

- Honda GX200 Petrol Engine—Rs. 19,300/-
- Sprocket + Chain (Pair)—Rs. 810/-
- V-Belt + Pulley (Pair)—Rs. 750/-
- Bearing (4 Nos.)—Rs. 1600/-
- Materials Cost (including labour charge)—Rs. 10,500/-

Therefore, $C = 19,300 + 810 + 750 + 1600 + 10,500 = \text{Rs. } 32,960/-$

3.2 Cost Calculation

Fixed cost per year

$$\begin{aligned} \text{(i) Depreciation cost, } A &= \frac{C - S}{L} \\ &= \frac{32960 - 3296}{10} \\ &= \text{Rs. } 2966.4 \end{aligned}$$

$$\begin{aligned} \text{(ii) Interest on investment, } B &= \frac{C + S}{2} \times \frac{i}{100} \\ &= \frac{32960 + 3296}{2} \times \frac{12}{100} \\ &= \text{Rs. } 2175.36 \end{aligned}$$

$$\begin{aligned} \text{(iii) Insurance, shelter etc., } C &= \frac{32960 + 3296}{2} \times \frac{1.5}{100} \\ &= \text{Rs. } 271.92 \end{aligned}$$

$$\begin{aligned} \text{Total fixed cost per year} &= A + B + C \\ &= 2966.4 + 2175.36 + 271.92 \\ &= \text{Rs. } 5413.68 \end{aligned}$$

$$\begin{aligned} \text{Total fixed cost per hour} &= 5413.68 \div 800 \\ &= \text{Rs. } 7.76 \end{aligned}$$

Variable cost per hour

$$(i) \text{ Labour cost, } D = 660 \div 6 \\ = \text{Rs. } 110 = \text{Rs. } 110$$

$$(ii) \text{ Repair and maintenance, } E = 32960 \times \frac{5}{100} \times \frac{1}{800} \\ = \text{Rs. } 2.06$$

$$(iii) \text{ Fuel Cost}(1.251/\text{hr})@80 \text{ Rs.} = 80 \times 1.25 = \text{Rs. } 1000/-$$

$$\text{Total variable cost per hour} = D + E + F \\ = 110 + 2.06 + 100 \\ = \text{Rs. } 212.06$$

$$\text{Total operating cost of machine} = \text{Fixed cost} + \text{Variable cost} \\ = 7.76 + 212.06 \\ = \text{Rs. } 219.82$$

$$\text{Basin created per hour} = 7 \\ \text{Cost per basin} = 219.82 \div 7 \\ = \text{Rs. } 31.40$$

3.3 Cost Analysis by Manual basin Making

$$\text{Workers Required} = 1 \\ \text{Working hours(per day)} = 6 \\ \text{Remuneration per day} = \text{Rs. } 700/- \\ \text{Remuneration per hour} = \text{Rs. } 117/- \\ \text{No. of basin per hour} = 3 \\ \text{Cost of making per basin} = \text{Rs. } 39$$

The operating cost of the Mini Tiller-cum-Basin-Maker is 226.82 Rs. per hour and cost of making per basin is 31.40 Rs. The operating cost of the traditional manual basin making method is 117 Rs. per hour and cost of making per basin is 39 Rs.

3.4 Comparative Study

A comparative study has been conducted between the Mini Tiller-cum-Basin-Maker and the manual basin making method (Table 2).

Table 2 Comparative study

	Manual basin making method	Mini tiller-cum-basin-maker
Cost per basin (Rs.)	39	31.40
Time (basin per hour)	3	7
Physical work load	High	Low

4 Conclusion

Mini Tiller-cum-Basin-Maker is a machine that helps to dig grooves around the coconut tree with uniform radius. It is designed and the cost analysis with the manual method is completed. Time required for completing is 8–9 min per basin with Mini Tiller-cum-Basin-Maker, which is far better than the manual method which required 15–25 min depending on the size of the tree. The operating cost of the Mini Tiller-cum-Basin-Maker was found to be the most promising. Though the machine improves the production, the basin making is a seasonal work. So, there is a scope of implementing the same machine in different agricultural crops apart from coconut cultivation.

References

1. Arulandoo, X., Sritharan, K., Subramaniam, M.: The coconut palm. Ref. Mod. Life Sci. Encycl. Appl. Plant Sci. **2**(3), 426–430 (2017)
2. Varghese, A., Jacob, J.: A study on the KAU coconut husking tool. In: Annual International Conference on Emerging Research Area: Magnetics, Machine and Drives (AICERA/iCMMMD), pp. 1–6 (2014)
3. DebMandal, M., Mandal, S.: Coconut (*Cocos nucifera* L.: Areaceae): in health promotion and disease prevention. Asian Pac. J. Trop. Med. **4**(3), 241–247 (2011)
4. Varghese, A., Francis, K., Jacob, J.: A study of physical and mechanical properties of the Indian coconut for efficient de-husking. J. Nat. Fibers **14**(3), 390–399 (2016)
5. Nair, K.: The Coconut Palm (*Cocos nucifera* L.): The Agronomy and Economy of Important Tree Crops of the Developing World, pp. 67–109 (2010)
6. Varghese, A.: Mini-Tiller Cum-Basin-Maker (1025/CHE/2013), Indian Patent Office (2013)
7. Muhammad, C.P., Jacob, J., Ramachandran, V.R.: An attachment for making basins around trees, Patent No. IN 236544 (2009)
8. Kerala Agriculture University: Coconut basin digger. The Hindu daily, 8th May 2015
9. Kerala Gazette: Labour and skill. Government Kerala **6**(6) (2017)

Computer-Aided Ergonomic Analysis for Rubber Tapping Workers



Abi Varghese  and Vinay V. Panicker 

Abstract The work-related musculoskeletal disorders (MSDs) among the rubber tapping workers are high due to awkward tapping postures and tapping at different gutter heights. In this context, a study has been carried out to conduct a posture analysis of rubber tappers using CATIA V5. For this work, three tapping heights or gutter heights of 500, 1000, and 1500 mm are considered, and the virtual environment is developed. The digital human models are created based on the Anthropometric and strength data of Indian agricultural workers. The study shows that rubber workers tapping at the gutter height of 500 and 1500 mm having the maximum impact on the posture due to forward bending and stretching during tapping. The gutter height of 1000 mm between waist level and shoulder level shows the minimum impact. It is concluded that there is a correlation between the gutter height and the tapping postures among the rubber tappers.

Keywords Posture analysis · Rubber tapping · Musculoskeletal disorders · Rapid upper limb assessment (RULA)

1 Introduction

Rubber cultivation is one of the major income sources of the people in Asia. Asia produces 90% of the global natural rubber production [11]. Rubber tapping is the first and foremost step in natural rubber processing. In tapping, worker scores the bark in the downward spiral half of the trunk of the rubber tree as shown in Fig. 1, with the aid of a rubber tapping knife. In general, tapping starts on rubber trees at 1 metre

A. Varghese · V. V. Panicker (✉)

Department of Mechanical Engineering, National Institute of Technology Calicut, Kozhikode, Kerala, India

e-mail: vinay@nitc.ac.in

A. Varghese

Department of Mechanical Engineering, Amal Jyothi College of Engineering, Kottayam, Kerala, India



Fig. 1 Rubber tree and its tapping method

above the ground level, when the circumference of the tree trunk is about 50 cm in length. The lactiferous vessel situated between the cambium and the wood is used for collecting latex, incision of this vessel at an angle of 30° to the horizontal makes the latex flow properly [3]. For tapping, two types of knives are generally used (i) Michie Golledge (ii) Jebong Knife [2]. Every worker has to tap 300–1000 rubber trees per day [1]. Due to the repetitive operation, postures like forward bending and lateral twisting, and manual workload during rubber tapping may cause musculoskeletal disorders among the rubber tappers.

The work-related musculoskeletal disorders (MSDs) among the farmworkers are very high due to heavy workload, repetitive movement during various agricultural operations, awkward posture, and the manual handling of load [4, 8]. A study conducted among the Thai rubber tapping workers reports that half of the workers (52%) have lower back pain followed by pain in legs (14.8%), upper arms (8.9%), neck (3.0%), wrists (2.3%), and lower arms (2.1%) due to awkward tapping posture and different tapping level [7]. Few researchers have found that the prevalence of low back pain among Thai rubber farmers was 55.7%, and the major factors identified as body mass index, education level, and tapping level [13]. Another study was conducted among the Srilankan rubber tappers revealed that 66% of the rubber tappers experience MSDs and the prevalence are varying in the shoulder (96.7%), back (94.4%), and neck (83.3%). The major factor associated with MSDs is a gender difference, cultural difference, age, supplementary job, and alternative hands during tapping [12]. An exploratory study was conducted among rubber tappers from Colombia reveals that tapping height, squatting, bending, and sporadic trunk

rotation during tapping are the major reason for MSDs [14]. A study conducted using the Boston Carpal Tunnel Syndrome Questionnaire to evaluate Carpal Tunnel Syndrome (CTS) among Thai rubber tappers identified 133 CTS cases. The major reason was found to be the number of trees tapping per day, tapping height, hand postures during tapping, and hand dominance [9]. In-line with the previous study, ergonomically designed rubber tapping knife (Jebong Knife) has been designed to improve the wrist posture of CTS tapping workers. The result shows that there is a significant improvement in CTS symptoms and also compare the improvement with traditional knife users [10].

The review of the literature shows that most of the rubber tappers experience MSDs due to awkward tapping postures and tapping height. Therefore, it is essential to correlate the tapping height and its impact on tapping postures among the rubber tappers. In fact, this is the novelty of the present work. The objectives of this work are as follows:

- Identify the various tapping heights which are commonly used
- Apply Computer-aided Ergonomic Analysis to correlate the tapping height and its impact among the rubber tappers
- Explore the possible ergonomic intervention to improve the tapping posture.

2 Materials and Methods

2.1 Digital Human Modelling

The digital human models ‘Manikin’ are inserted from the library in CATIA. The Anthropometric data and strength data of Indian agricultural workers are adopted from [6] to design human models. As rubber tapping is predominantly seen in the state of Kerala, the anthropometric data of workers from the Southern region is applied. The various parameters considered in this work are gender, stature, weight, hip height, hip breadth, chest breadth, and waist breadth, for 95th and 5th percentile population. The dimensions applied for digital human models are given in Table 1.

2.2 Work Environment Model

The rubber tapping working environment is created using CATIA V5 based on the following three types of tapping height or Gutter height, data collected during the field study.

- Tapping height below waist level (Gutter height—500 mm)
- Tapping height between waist level and shoulder level (Gutter height—1000 mm)
- Tapping height above shoulder level (Gutter height—1500 mm)

Table 1 Dimensions adopted for digital human modelling [6]

	Male					Female				
	Mean	Standard deviation	Range	5th percentile	95th percentile	Mean	Standard deviation	Range	5th percentile	95th percentile
Weight (kg)	56.1	9.7	34.0–94.0	40.2	72.1	47.2	8.3	30.0–79.0	33.5	60.9
Stature (mm)	1649	64	1490–1815	1522	1735	1508	60	1334–1676	1409	1606
Hip height (mm)	869	51	635–1030	785	954	842	42	734–939	773	911
Hip breadth (mm)	291	24	202–393	251	330	264	19	205–312	232	295
Chest breadth (mm)	278	26	191–380	234	321	241	21	204–352	206	275
Waist breadth (mm)	255	29	175–356	206	303	222	20	187–285	189	256

2.3 Body Posture Analysis

As an initial analysis, a posture analysis is conducted. Rapid upper limb analysis (RULA) [5] is one of the major tools to evaluate body posture analysis. It assesses the muscle strain that occurs during each operation and provides the score from 1 to 7. A score value of 1 and 2, means the posture is acceptable. The score value of 3 and 4 indicates an alteration in posture. The value of 5 and 6 is poor posture and alterations are required at the earliest. Score 7 reveals a higher risk and an urgent alteration is needed.

3 Result and Discussion

3.1 Digital Human Modelling

The digital human model has been created based on the anthropometric data of the south Indian population using 'Human Measurements Editor' and the proposed model is shown in Fig. 2a, b.

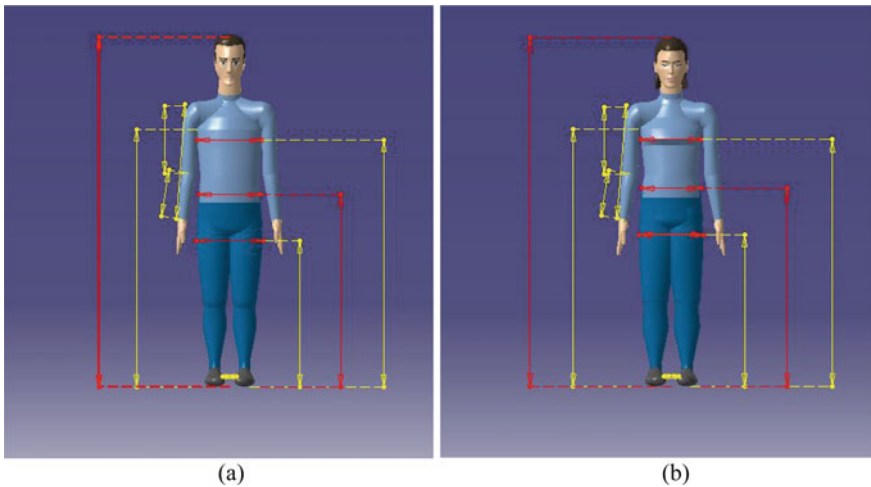


Fig. 2 a CATIA digital human model (male), b CATIA digital human model (female)

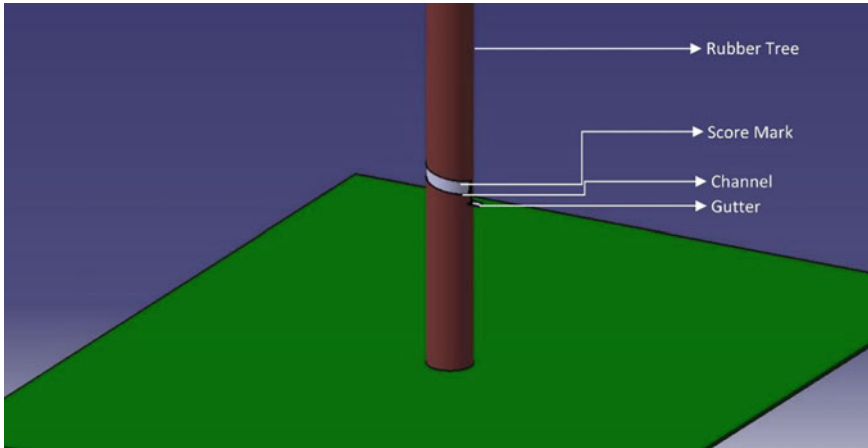


Fig. 3 Rubber tree and its tapping method (CATIA virtual model)

3.2 Work Environment Model

The working environment of rubber tapping workers has been developed in CATIA V5 using the sample dimension collected from the field and is shown in Fig. 3.

As a general practice, there are three sections in tapping with three levels of tapping height or gutter height. The initial tapping height is from 1 m from the ground level, and the score moves down nearly to the ground level. When the initial tapping area has been completed, the tapping height again starts from 1.5 m from the ground as the second section. Similarly, in the third section also consider the same procedure used as that of the second section. The three levels of gutter height are depicted in Fig. 4.

3.3 Body Posture Analysis

The RULA analysis of the male and female rubber tappers using CATIA v5 has been completed. Figure 5 shows the digital human models of rubber workers developed using CATIA.

Table 2a–d formulates the scores that are obtained from the various body parts associated with rubber tappers.

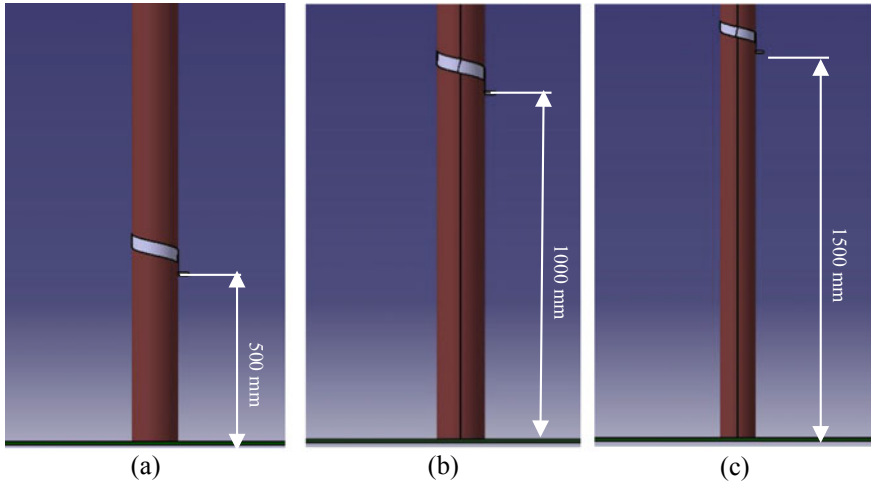


Fig. 4 Tapping height (CATIA model) **a** below waist level, **b** between waist and shoulder level, **c** above shoulder level

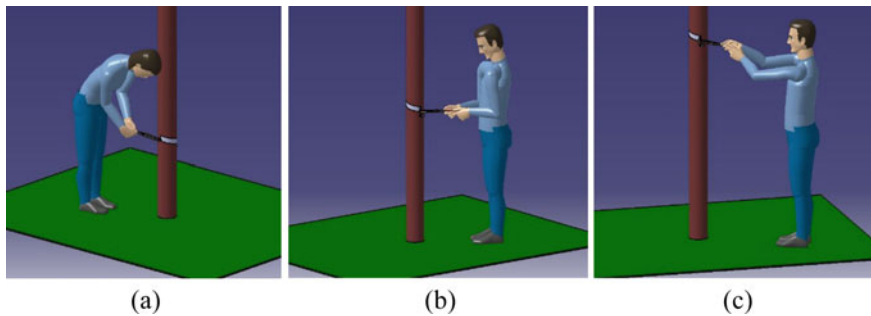


Fig. 5 RULA analysis for rubber tappers **a** gutter height 500 mm (female), **b** gutter height 1000 mm (male), **c** gutter height 1500 mm (male)

3.4 Statistical Analysis of RULA Score

Kruskal–Wallis Test is a non-parametric test used to determine the significant difference between more than one dependent or independent variable. The summary of the Independent sample Kruskal–Wallis tests is tabulated in Table 3.

The statistical analysis reveals that the various body parts like the upper arm, forearm, neck, and trunk associated with rubber tapping operations, have a significant difference in terms of various gutter height. However, it is to be noted that the score for the wrist is found to be the same at various gutter heights.

Moreover, post-hoc analyses have been carried out and are tabulated in Table 4. The post-hoc analyses conclude that the posture with a gutter height of 1000 mm is

Table 2 **a** RULA score for Male rubber tappers at 95th percentile obtained from CATIA. **b** RULA score for female rubber tappers at 95th percentile obtained from CATIA. **c** RULA score for Male rubber tappers at 5th percentile obtained from CATIA. **d** RULA score for female rubber tappers at 5th percentile obtained from CATIA

	Gutter height (500 mm)		Gutter height (1000 mm)		Gutter height (1500 mm)	
	Left	Right	Left	Right	Left	Right
<i>(a) Male at 95th percentile</i>						
Upper arm	3	3	1	1	3	4
Fore arm	2	2	1	1	3	2
Wrist	4	3	3	4	3	4
Neck	1	1	2	2	1	1
Trunk	3	3	2	2	1	1
Leg	1	1	1	1	1	1
RULA score	6	5	3	3	4	4
<i>(b) Female at 95th percentile</i>						
Upper arm	2	3	2	2	5	5
Fore arm	2	2	2	2	3	3
Wrist	3	3	4	3	4	3
Neck	1	1	2	2	1	1
Trunk	4	4	1	1	1	1
Leg	1	1	1	1	1	1
RULA score	6	7	4	3	5	5
<i>(c) Male at 5th percentile</i>						
Upper arm	2	3	1	1	4	4
Fore arm	3	3	1	1	3	3
Wrist	3	3	3	3	3	4
Neck	1	1	2	2	1	2
Trunk	3	3	2	2	1	1
Leg	1	1	1	1	1	1
RULA score	5	5	3	3	4	5
<i>(d) Female at 5th percentile</i>						
Upper arm	2	3	2	2	5	5
Fore arm	2	2	2	2	3	3
Wrist	3	3	3	3	5	4
Neck	1	1	2	2	1	1
Trunk	3	3	1	1	1	2
Leg	1	1	1	1	1	1
RULA score	6	6	3	3	5	6

Table 3 Summary of independent value of Kruskal–Wallis Test

S. No.	Null hypothesis	Significance value	Decision
1	The distribution of upper arm is the same across the gutter height	0.000	Reject the null hypothesis
2	The distribution of forearm is the same across the gutter height	0.080	Fail to reject the null hypothesis
3	The distribution of wrist is the same across the gutter height	0.000	Reject the null hypothesis
4	The distribution of neck is the same across the gutter height	0.000	Reject the null hypothesis
5	The distribution of Trunk is the same across the gutter height	0.000	Reject the null hypothesis
6	The distribution of RULA Score is the same across the gutter height	0.000	Reject the null hypothesis

Table 4 Post-hoc analysis of RULA score

Gutter height (mm)	Adjacent significance
500–1000	0.00
1000–1500	0.026
1500–500	0.337

found to have a minimum impact on the muscles due to the minimum body bending and trunk rotation.

Further, a frequency distribution of the RULA scores is done as depicted in Table 5. The results show that about 54.2% of the RULA score is in the range between 5 and 7, which indicates that the body posture is under risk, and appropriate alterations are needed to avoid MSDs.

Table 5 Frequency distribution of RULA score

RULA score	Percent	Cumulative percent
4.00	16.7	45.8
5.00	29.2	75.0
6.00	20.8	95.8
7.00	4.2	100.0
Total	100.0	

4 Conclusion

The work-related musculoskeletal disorders among the rubber tapping workers are reported to be high due to the awkward tapping postures such as bending and twisting of the body during tapping and at different tapping or gutter height. The present study focuses on the computer-aided posture analysis of the rubber tapping workers subjected to three tapping heights using RULA method. Digital human models are created using the anthropometric data of Indian agricultural workers in CATIA V5. Appropriate statistical analyses of the RULA scores have been carried out SPSS software. It is observed that the tapping or gutter height of 1000 mm has a minimum impact on postures. This may be due to the minimum body bending and trunk rotation. The scores for other body parts like the upper arm, forearm, neck, and trunk associated with rubber tapping operations have a significant difference in terms of various gutter height. The score for the wrist is found to be the same at various gutter heights. Though RULA can be used to identify risk for musculoskeletal disorders, the limitation of this method is that the duration of exposures has not been considered.

References

1. Boonphadh, P.: The Perceived Effects of Work on Health of Rubber Farmers in Southern Thailand. Massey University, New Zealand (2008)
2. Centre for E-learning KAU Agriculture University: Plantation Crops-Rubber: KAU Agri-Infotech Portal. <https://www.celkau.in>
3. FAO Economic and Social Development Series: The Rubber Tree: Better Farming Series. ISBN 92-5-100156-1 (1977)
4. Kirkhorn, S.R., Earle-Richardson, G., Banks, R.J.: Ergonomic risks and musculoskeletal disorders in production agriculture: recommendations for effective research to practice. *J. Agromed.* **15**(3), 281–299 (2010)
5. Lynn, M., Corlett, E.N.: RULA: a survey method for the investigation of world-related upper limb disorders. *Appl. Ergon.* **24**(2), 91–99 (1993)
6. Majumder, J., Mehta, C.R., Khadatkar, A.: Anthropometric and strength data of Indian agricultural workers for farm equipment design. In: Gite, L.P. (ed.) Bhopal, India: Central Institute of Agricultural Engineering. ISBN 978-81-909305-0-5 (2009)
7. Meksawi, S., Tangtrakulwanich, B., Chongsuvivatwong, V.: Musculoskeletal problems and ergonomic risk assessment in rubber tappers: a community-based study in southern Thailand. *Int. J. Ind. Ergon.* **42**(1), 129–135 (2012)
8. Momeni, Z., Choobineh, A., Razeghi, M., Ghaem, H., Azadian, F., Daneshmandi, H.: Work-related musculoskeletal symptoms among agricultural workers: a cross-sectional study in Iran. *J. Agromed.* 1–10 (2020)
9. Pramchoo, W., Geater, A.F., Tangtrakulwanich, B.: Physical ergonomic risk factors of carpal tunnel syndrome among rubber tappers. *Arch. Environ. Occup. Health* **75**(1), 1–9 (2020)
10. Pramchoo, W., Geater, A.F., Harris-Adamson, C., Tangtrakulwanich, B.: Ergonomic rubber tapping knife relieves symptoms of carpal tunnel syndrome among rubber tappers. *Int. J. Ind. Ergon.* **68**, 65–72 (2018)
11. Report of Association of Natural Rubber Producing Countries (ANRPC) (2017). www.anrpc.org

12. Stankevitz, K., Schoenfisch, A., de Silva, V., Tharindra, H., Stroo, M., Ostbye, T.: Prevalence and risk factors of musculoskeletal disorders among Sri Lankan rubber tappers. *Int. J. Occup. Environ. Health* **22**(2), 91–98 (2016)
13. Udom, C., Janwantanakul, P., Kanlayanaphotporn, R.: The prevalence of low back pain and its associated factors in Thai rubber farmers. *J. Occup. Health* **58**(6), 534–542 (2016)
14. Velásquez, S., Valderrama, S., Giraldo, D.: Ergonomic assessment of natural rubber processing in plantations and small enterprises. *Ingeniería Y Competitividad* **18**(2), 233–246 (2016)

Participatory Approach for Ergonomics Intervention: A Review



Yogesh Mishra, M. L. Meena, and G. S. Dangayach

Abstract Recently, Participatory Ergonomics (PE) approach has been broadly accepted as a system to minimize musculoskeletal disorders (MSDs) and associated injuries among the workers. This review emphasizes on specific topics such as critical success factors of PE approach, conceptual framework for implementation of PE programs, effectiveness and measure elements for successful implementation of PE programs. The literature is preferred from reputed ergonomics journals by refining abstracts and titles utilizing selected words such as ‘intervention’, ‘ergonomic’, and ‘participatory’, and by analyzing the abstracts and findings the 62 articles have been preferred for this review. The review aims to analyze the usual elements and obstructions associated with PE intervention program, thereby giving the recommendations for future research.

Keywords Participatory ergonomics (PE) · Intervention · Musculoskeletal disorders (MSDs)

1 Introduction

Participatory Ergonomics (PE) approach is emerging from various trends such as Community involvement, coordination of production activities as per principles of sociotechnical aspect, and ergonomics evolution from ‘micro-level’ to ‘macro-level’. The meaning of the participatory approach includes intervention at a broad extent (macro), e.g., organizational and system levels, and additionally small extent (micro),

Y. Mishra (✉) · M. L. Meena · G. S. Dangayach
Malaviya National Institute of Technology, Jaipur, Rajasthan, India
e-mail: Yogeshmishranhr@gmail.com

M. L. Meena
e-mail: Mlmeenamnit@gmail.com

G. S. Dangayach
e-mail: dangayach@gmail.com

e.g., personal, where employees are accustomed with the freedom and strength to apply their understanding to hold ergonomic issues associated with the work activities they perform [1]. PE could be interpreted as an approach that involves the use of participative methods and different modes of workplace participation [2]. As per Wilson [3], PE is the participation of employees' in planning as well as in controlling a considerable proportion of their individual tasks, accompanying adequate understanding and ability to control both activities and results to attain preferable targets. Participatory techniques are gradually used in the improvement of ergonomics at workplaces. The advantages of such techniques are broadly anticipated as methods for advocating initiatives of individuals and achieving required workplace solutions [4].

A PE program usually engages one or more teams to bring together intending to improve the designing of the task, and the usual aspect is to make sure the use of specialist's ability such employees acquire of their tasks by associating the employees, and others likely concerned with recommended changes [5]. PE programs have been generally concentrated on musculoskeletal injuries though such approaches have focused to build better human-oriented task [6]. Maciel [7] mentioned that PE programs have been used to enhance organizational conditions while Punnett et al. [8] suggested the use of such a framework for health promotion. PE can be treated as an approach related to design a work system and so, basically, an approach of macro-ergonomics [9–13]. The advantages of PE methods are generally acknowledged by encouraging individual's initiatives and attaining desired feasible results [14–20]. Nowadays, PE methods have acquired global attention in developing ergonomics and avoiding workplace injuries. Additionally, such participatory methods were initiated usually to minimize risks related to an individual's experience at the workplace, accidents, and ailment like musculoskeletal disorders.

PE projects have been executed over a wide extent of organizations as well as in industries too [1]. Though, the majority of implementation areas of PE projects have been mentioned by Burgess-Limerick [5]. It includes implementation in construction [21–28], healthcare [29–34], office domains [14, 35–38], mining [39–42] and in various manufacturing concerns [13, 43–53].

There have been plenty of publications (either peer-reviewed or grey literature) that advocated numerous aspects of PE approach such as implementation areas, critical success factors, conceptual framework, effectiveness, and implementation of PE programs. So this review is an attempt to provide significant pieces of information regarding the PE approach on a single platform.

2 Critical Success Factors for Participatory Approach

Critical Success Factors (CSF) is required for any organization to attain the desired goals. These factors help the team members or workers to know the exact requirements or important aspects of ongoing work. As stated by Zink et al. [54], in the case of a participatory approach, the earlier focus was on individual issues like reduction

of cost, process refinement which results in slight success. There are various elements for the failures of such projects that may be detected in the consideration of a few critical factors which are liable for successful implementation of the project:

- Preference of long-term strategy for the deployment of resources along with the availability of required resources;
- Participation of the workers and teams more concerned with the changes;
- The impact of organizational culture must be considered;
- Integrity among various initiatives and conduction of such initiatives with the integral process;
- More priority on an individual's behavior and structures and seeing the reliance among them;
- Initiatives must not be limited to time-bounded program and it should be a transformative process.

Critical Success Factors are firmly associated with the objectives of the ongoing project/project. These facilitate to trace and compute the progress of the running projects and provide a unique platform of references where an individual or team can access the significant requirements of the project. As per Zink et al. [54], at a brief look, the critical success factors can appear to be extremely distinctive, but on a further conceptual level, it found more challenging to integrate every initiative with subjective and objective dimensions which is shown in Fig. 1. In the logical (or objective) dimension, a crucial adjustment of all actions has to be executed as per the overall integrated concept. In most of the cases, production systems merely targeting manufacturing only and other organizational subsystems are not considered in their long-term strategy. Hence, models based on international merit can provide an additional appropriate framework that has to be implemented as per the specific requirement of the organization.

The prerequisite of subjective dimension is to develop an understanding among the workers about the association between the strategic goals of the organization and projected change actions which leads to certain changes into the routine practice. Further, the employees should be aware of the incorporation of individual actions into an overall approach. So, the participatory approach can develop a better flow of information and promote an advanced understanding of the system. Adequate cooperation of the workers leads to the success of the expert-driven techniques. The participation of the employees is required in expert-driven techniques because the measure focus of such approaches is on logical dimensions only and it neglects the issues of subjective incorporation against the worker's perspective. In this manner, there is a requirement of an administrative approach which aims particularly on the responsibility of administrators to control innovative changes and on effective participation employees at different organizational levels.

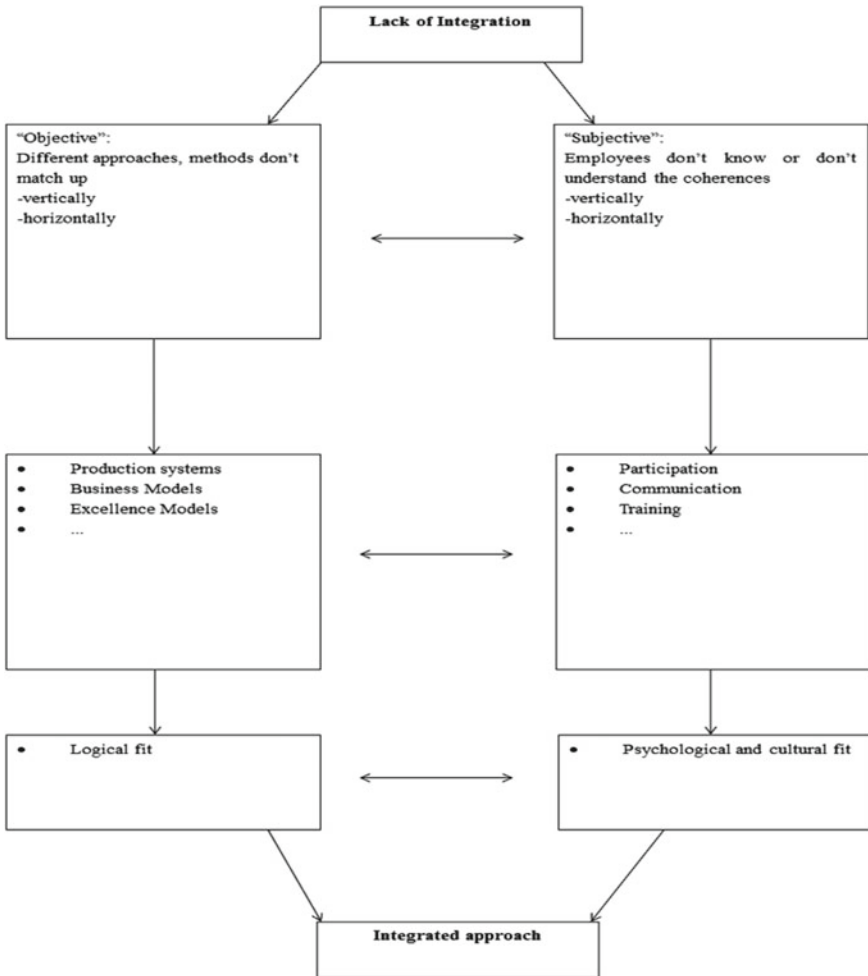


Fig. 1 Dimensions of integration [54]

3 A Conceptual Framework for Execution of PE Programs

A conceptual framework is required to recognize and evaluate the mentioned changes in the creative activities of organizations. Haines et al. [55] proposed a theoretical framework for PE programs. The importance of workers' involvement is highlighted by the ranked dimensions. The top two dimensions imply the workers' involvement in decision-making as well as at every level of an organization. The stability of the input related to ergonomics is given as the low rank which indicates that such addition is project-specific. Hignett et al. [1] also stated that this framework defines the range of

variations while implementing a PE program. Further, Burgess-Limerick [5] defined these dimensions as per their importance stated as:

1. Position of decision-making capability—either maintained at management level and directed to specific employees or their teams;
2. A combination of participating candidates—the inclusion of staff from every level of organization;
3. Remit—involvement of the participants in the PE process, problem identification, interpretation, and suggestions for effective implementation;
4. Responsibility of ergonomics consultant—recognized as dynamic and developing over some time, extensive scope, i.e., as an organizer, instructor, specialist, or consultant;
5. Type of task involvement—involvement of all concerned workers or selected individual workers;
6. Focus—either intended to task design or issues related to the organization of work;
7. Level of influence—change in the organizational level where the intervention occurs, either department level, or across the entire organization;
8. Requirement—entirely depends upon the kind of participation, observing that it may change as per the members of the group;
9. Permanence—scope for both temporary and permanent problem-solving programs, entirely depends on the kind of task which is to be performed.

The capability of a PE intervention can vary due to the various combinations of the above-stated dimensions. Nature and commitment level of the organizations plays a significant role in the success of PE programs and it also impacts the results of such programs. PE programs may vary in connection with the involvement of the designs with which the tasks are fixed.

4 Effectiveness and Implementation of PE Approach

Rivilis et al. [56] stated such a decent implementation of PE programs results in the improvement of specific health issues, also associated with depletion of symptoms related to musculoskeletal disorders (MSDs), injuries, and claims related to compensation of workers. Tompa et al. [18] identified further confirmation that PE programs are productive and are related to the health and work-related outcomes along with their economic effect. Successful implementation of PE programs follows the reduction in cases related to first aid and modified duty, reduction in the unusual absence of workers, and increment in financial and economic benefits. Van Eerd et al. [57] suggested nine elements for successful implementation of PE programs as:

1. Obtain assistance and support in-favor-of the program from every level of organization

2. Formation of a panel for mentoring the process by including people from different levels of the organization.
3. Make management liable for maintaining sufficient resources.
4. Build small groups of devoted people to conduct intervention by including ergonomists, supervisors, and workers.
5. Aware team members about the organizational culture.
6. Provide ergonomics instructions and training to the team members for the assessment of risks related to the workplace.
7. Set up definite roles and responsibilities for the workers.
8. Preference for group decisions instead of individual decisions.
9. Promote effective communication between all the team members during the whole intervention period.

The recent study of Cuny-Guerrier et al. [58] has described the required procedure and strategies which led to the commitment of senior managers during the implementation of PE intervention in the context of subcontractors. The focus was on prevention of MSDs in the meat processing sector by using the reflexive practice approach and obtained the results which emphasize the significance of stakeholder during the commitment of strategies in PE. Mahdavi et al. [59] conducted a study in a resin manufacturing company of Iran and stated the implementation steps of the PE program to manage factors related to ergonomic risks of human work. The emphasis was on to minimize the risks of human-work related injuries within the organization. Similarly, Capodaglio [60] implemented a PE project in an Italian wool processing company for the improvement of strategies related to the prevention of MSDs in maintenance workers and identified that PE program can be helpful in the management of crucial maintenance activities by the worker's empowerment and recognition of suitable solutions related to MSDs problems of maintenance environment. Narsia and Raj [61] executed a PE program in Indian cashew nut factories to avoid occurrence of Work-Related Musculoskeletal Disorders (WRMSD) in workers and determined that PE programs can also be beneficial to lessen the amount of worker's leaves which leads to productivity improvement. Bernardes et al. [62] conducted a PE intervention in a Brazilian garment company and stated the feasibility and effectiveness of PE intervention approach to minimize the risk of WRMSDs in industries. Hence, for the effective execution of PE programs, the analysis about risk and the control of information must be easily accessible throughout all levels of the organization.

5 Result and Discussion

Most of the studies concerning effectiveness of PE approach emphasized only on outcomes related to health of workers which comprised of assessment of symptoms related to MSDs, severity of injury, or pain along with the spot of manifestation through body part [8, 12–14, 19, 20, 24, 31, 32, 38, 40, 43, 48, 56, 60–62]. The

effectiveness of PE programs is also assessed by economic evaluation of PE interventions that leads to quality and productivity improvement [17, 18, 50]. So, for the assessment of the effectiveness of the PE program, this study emphasizes on further characteristics such as PE intervention process, recognition, and implementation of changes concerning ergonomic intervention along with the study of risk elements.

6 Conclusion

The review has provided significant information's regarding critical success factors of PE approach, the conceptual framework for the implementation of PE programs, effectiveness, and measure elements for the effective execution of PE programs. Attainment of these usual elements and obstructions can be helpful in the promotion of a successful PE intervention program. The measure strength of the PE approach is the flexibility to the situation and workplace requirements, project assignments, and workers. The review has also identified the following research gaps that can also be treated as directions for future research.

- Due to the variety of PE research methods; limited information is available in the studies regarding the effectiveness of PE programs in the improvement of various outcomes related to worker's health. The primary logic behind that is the availability of less number of systematically sound researches in the concerned literature.
- In most of the PE intervention studies, the measure focus was on the physical facet of the task, in spite of factors related to the psychosocial aspect.
- Still, there is a need for an effective framework for the conduction of the PE intervention program which ensures adequate involvement of workers and nurturing interest to assure sustainability.
- Due to the lack of time and unavailability of necessary resources, a more extended review can be done in future by including grey literature related to PE intervention.

References

1. Hignett, S., Wilson, J.R., Morris, W.: Finding ergonomic solutions—participatory approaches. *Occup. Med.* **55**(3), 200–207 (2016)
2. Vink, P., Wilson, J.R.: Participatory ergonomics. In: Proceedings of the XVth Triennial Congress of the International Ergonomics Association and the 7th Joint conference of the Ergonomics Society of Korea/Japan Ergonomics Society, 'Ergonomics in the Digital Age', Seoul, Korea, pp. 24–29 (2003)
3. Wilson, J.R.: Ergonomics and participation. *Eval. Hum. Work A Pract. Ergon. Methodol.* **2**, 1071–1096 (1995)
4. Kogi, K.: Advances in participatory occupational health aimed at good practices in small enterprises and the informal sector. *Ind. Health* **44**(1), 31–34 (2006)

5. Burgess-Limerick, R.: Participatory ergonomics: evidence and implementation lessons. *Appl. Ergon.* **68**, 289–293 (2018)
6. Imada, A.: Participatory Ergonomics: a strategy for creating human-centred work. *J. Sci. Labour* **76**(3), 25–31 (2000)
7. Maciel, R.: Participatory ergonomics and organisational change. *Int. J. Ind. Ergon.* **22**, 4–5 (1998)
8. Punnett, L., Warren, N., Henning, R., Nobrega, S., Cherniack, M.: Participatory ergonomics as a model for integrated programs to prevent chronic disease. *J. Occup. Environ. Med.* **55**, 19–24 (2013)
9. Hendrick, H.W.: An overview of macroergonomics. *Macroergonomics: Theory Methods Appl.* 1–23 (2002)
10. Kleiner, B.M.: Macroergonomics: analysis and design of work systems. *Appl. Ergon.* **37**(1), 81–89 (2006)
11. Kleiner, B.M.: Macroergonomics: work system analysis and design. *Hum. Factors* **50**(3), 461–467 (2008)
12. Guimarães, L.D.M., Ribeiro, J.L.D., Renner, J.S., De Oliveira, P.A.B.: Worker evaluation of a macroergonomic intervention in a Brazilian footwear company. *Appl. Ergon.* **45**(4), 923–935 (2014)
13. Guimarães, L.D.M., Anzanello, M.J., Ribeiro, J.L.D., Saurin, T.A.: Participatory ergonomics intervention for improving human and production outcomes of a Brazilian furniture company. *Int. J. Ind. Ergon.* **49**, 97–107 (2015)
14. Vink, P., Peeters, M., Gründemann, R.W.M., Smulders, P.G.W., Kompier, M.A.J., Dul, J.: A participatory ergonomics approach to reduce mental and physical workload. *Int. J. Ind. Ergon.* **15**(5), 389–396 (1995)
15. Zalk, D.M.: Grassroots ergonomics: initiating an ergonomics program utilizing participatory techniques. *Ann. Occup. Hyg.* **45**(4), 283–289 (2001)
16. Khai, T.T., Kawakami, T., Kogi, K.: Participatory action oriented training: PAOT programme trainer’s manual. Centre for Occupational Health and Environment, Cantho (2005)
17. Tompa, E., Dolinschi, R., Laing, A.: An economic evaluation of a participatory ergonomics process in an auto parts manufacturer. *J. Saf. Res.* **40**(1), 41–47 (2009)
18. Tompa, E., Dolinschi, R., Natale, J.: Economic evaluation of a participatory ergonomics intervention in a textile plant. *Appl. Ergon.* **44**(3), 480–487 (2013)
19. Hongsranagon, P., Somana, Y., Maha-Udomporn, S.O.M.K.I.E.T., Siritwong, W., Havanond, P., Deelertyueng, N., Saksri, P.: Participatory ergonomics intervention for improving work-related musculoskeletal disorders in the ‘one tambon one product’ industry in Thailand. *J. Hum. Ergol.* **40**(1_2), 11–18 (2011)
20. Tappin, D.C., Vitalis, A., Bentley, T.A.: The application of an industry level participatory ergonomics approach in developing MSD interventions. *Appl. Ergon.* **52**, 151–159 (2016)
21. Vink, P., Urlings, I.J., van der Molen, H.F.: A participatory ergonomics approach to redesign work of scaffolders. *Saf. Sci.* **26**(1–2), 75–85 (1997)
22. De Jong, A.M., Vink, P.: The adoption of technological innovations for glaziers; evaluation of a participatory ergonomics approach. *Int. J. Ind. Ergon.* **26**(1), 39–46 (2000)
23. De Jong, A.M., Vink, P.: Participatory ergonomics applied in installation work. *Appl. Ergon.* **33**(5), 439–448 (2002)
24. Dennis, G., Burgess-Limerick, R.: Participative ergonomics in civil construction handbook: reducing the risk of musculoskeletal injury in the civil construction industry. Department of Employment and Industrial Relations (2007)
25. Jaegers, L., Dale, A.M., Weaver, N., Buchholz, B., Welch, L., Evanoff, B.: Development of a program logic model and evaluation plan for a participatory ergonomics intervention in construction. *Am. J. Ind. Med.* **57**(3), 351–361 (2014)
26. Dale, A.M., Jaegers, L., Welch, L., Gardner, B.T., Buchholz, B., Weaver, N., Evanoff, B.A.: Evaluation of a participatory ergonomics intervention in small commercial construction firms. *Am. J. Ind. Med.* **59**(6), 465–475 (2016)

27. Brandt, M., Madeleine, P., Samani, A., Ajslev, J.Z., Jakobsen, M.D., Sundstrup, E., Andersen, L.L.: Effects of a participatory ergonomics intervention with wearable technical measurements of physical workload in the construction industry: cluster randomized controlled trial. *J. Med. Internet Res.* **20**(12), e10272 (2018)
28. Lowe, B.D., Albers, J., Hayden, M., Lampl, M., Naber, S., Wurzelbacher, S.: Review of construction employer case studies of safety and health equipment interventions. *J. Constr. Eng. Manag.* **146**(4), 04020012 (2020)
29. Bohr, P.C., Evanoff, B.A., Wolf, L.D.: Implementing participatory ergonomics teams among health care workers. *Am. J. Ind. Med.* **32**(3), 190–196 (1997)
30. Evanoff, B.A., Bohr, P.C., Wolf, L.D.: Effects of a participatory ergonomics team among hospital orderlies. *Am. J. Ind. Med.* **35**(4), 358–365 (1999)
31. Carrivick, P.J., Lee, A.H., Yau, K.K., Stevenson, M.R.: Evaluating the effectiveness of a participatory ergonomics approach in reducing the risk and severity of injuries from manual handling. *Ergonomics* **48**(8), 907–914 (2005)
32. Rasmussen, C.D.N., Holtermann, A., Bay, H., Sogaard, K., Jorgensen, M.B.: A multifaceted workplace intervention for low back pain in nurses' aides: a pragmatic stepped wedge cluster randomised controlled trial. *Pain* **156**(9), 1786 (2015)
33. Chin, W., Kurowski, A., Chen, G., Gore, R., Punnett, L.: Enhancing the usability of a mobile app for process evaluation in a participatory ergonomics healthcare intervention. In: Congress of the International Ergonomics Association, Springer, Cham, pp. 523–530 (2018)
34. Jakobsen, M.D., Aust, B., Kines, P., Madeleine, P., Andersen, L.L.: Participatory organizational intervention for improved use of assistive devices in patient transfer: a single-blinded cluster randomized controlled trial. *Scand. J. Work Environ. Health* **45**(2), 146–157 (2019)
35. Haims, M.C., Carayon, P.: Theory and practice for the implementation of 'in-house', continuous improvement participatory ergonomic programs. *Appl. Ergon.* **29**(6), 461–472 (1998)
36. Bohr, P.C.: Office ergonomics education: a comparison of traditional and participatory methods. *Work* **19**(2), 185–191 (2002)
37. Polanyi, M.F., Cole, D.C., Ferrier, S.E., Facey, M.: Paddling upstream: a contextual analysis of implementation of a workplace ergonomic policy at a large newspaper. *Appl. Ergon.* **36**(2), 231–239 (2005)
38. Baydur, H., Ergör, A., Demiral, Y., Akalın, E.: Effects of participatory ergonomic intervention on the development of upper extremity musculoskeletal disorders and disability in office employees using a computer. *J. Occup. Health* **16**, 3 (2016)
39. McPhee, B.: Ergonomics in mining. *Occup. Med.* **54**(5), 297–303 (2004)
40. Burgess-Limerick, R., Dennis, G., Straker, L., Pollock, C., Leveritt, S., Johnson, S.: Participative ergonomics for manual tasks in coal mining. In: Proceedings of the Queensland Mining Industry Health and Safety Conference, Townsville, Australia, pp. 14–17 (2005)
41. Torma-Krajewski, J., Hipes, C., Steiner, L., Burgess-Limerick, R.: Ergonomic interventions at vulcan materials company. *Mining Eng.* 54–58 ((2007))
42. Apud, E.: Ergonomics in mining: the Chilean experience. *Hum. Factors* **54**(6), 901–907 (2012)
43. Cantley, L.F., Taiwo, O.A., Galusha, D., Barbour, R., Slade, M.D., Tessier-Sherman, B., Cullen, M.R.: Effect of systematic ergonomic hazard identification and control implementation on musculoskeletal disorder and injury risk. *Scand. J. Work Environ. Health* **40**(1), 57–65 (2014)
44. St-Vincent, M., Chicoine, D., Beaugrand, S.: Validation of a participatory ergonomic process in two plants in the electrical sector. *Int. J. Ind. Ergon.* **21**(1), 11–21 (1998)
45. St-Vincent, M., Lortie, M., Chicoine, D.: Participatory ergonomics training in the manufacturing sector and ergonomic analysis tools. *Relat. Industrielles/Ind. Relat.* **56**(3), 491–515 (2001)
46. Nagamachi, M.: Requisites and practices of participatory ergonomics. *Int. J. Ind. Ergon.* **15**(5), 371–377 (1995)
47. Halpern, C.A., Dawson, K.D.: Design and implementation of a participatory ergonomics program for machine sewing tasks. *Int. J. Ind. Ergon.* **20**(6), 429–440 (1997)
48. Laing, A., Frazer, M., Cole, D., Kerr, M., Wells, R., Norman, R.: Study of the effectiveness of a participatory ergonomics intervention in reducing worker pain severity through physical exposure pathways. *Ergonomics* **48**(2), 150–170 (2005)

49. Liker, J.K., Nagamachi, M., Lifshitz, Y.R.: A comparative analysis of participatory ergonomics programs in US and Japan manufacturing plants. *Int. J. Ind. Ergon.* **3**(3), 185–199 (1989)
50. Motamedzade, M., Shahnnavaz, H., Kazemnejad, A., Azar, A., Karimi, H.: The impact of participatory ergonomics on working conditions, quality, and productivity. *Int. J. Occup. Saf. Ergon.* **9**(2), 135–147 (2003)
51. Moore, J.S., Garg, A.: Participatory ergonomics in a red meat packing plant, Part I: Evidence of long-term effectiveness. *Am. Ind. Hyg. Assoc. J.* **58**(2), 127–131 (1997)
52. Gjessing, C.C., Schoenborn, T.F., Cohen, A.: Participatory ergonomic interventions in meat-packing plants, US department of health and human services. Public Health Service, Centers for Disease Control and Prevention, National Institute for Occupational Safety and Health. DHHS (NIOSH) Publication, pp. 94–124 (1994)
53. Fontes, A.R.M., Braatz, D., da Silva, J.E.A.R., Ferreira, R., Menegon, N.L.: The perspective of ergonomics in the design of work situations using computational tools: case in a plastic film manufacturing plant. *Prod. Manag. Dev.* **16**(2), 114–121 (2019)
54. Zink, K.J., Steimle, U., Schröder, D.: Comprehensive change management concepts: development of a participatory approach. *Appl. Ergon.* **39**(4), 527–538 (2008)
55. Haines, H., Wilson, J.R., Vink, P., Koningsveld, E.: Validating a framework for participatory ergonomics (the PEF). *Ergonomics* **45**(4), 309–327 (2002)
56. Rivilis, I., Van Eerd, D., Cullen, K., Cole, D.C., Irvin, E., Tyson, J., Mahood, Q.: Effectiveness of participatory ergonomic interventions on health outcomes: a systematic review. *Appl. Ergon.* **39**(3), 342–358 (2008)
57. Van Eerd, D., Cole, D., Irvin, E., Mahood, Q., Keown, K., Theberge, N., Cullen, K.: Process and implementation of participatory ergonomic interventions: a systematic review. *Ergonomics* **53**(10), 1153–1166 (2010)
58. Cuny-Guerrier, A., Savescu, A., Tappin, D.: Strategies to commit senior subcontractor managers in participatory ergonomics interventions. *Appl. Ergon.* **81**, 102878 (2019)
59. Mahdavi, N., Shafiee Motlagh, M., Darvishi, E.: Implementation of ergonomic interventions using participatory program method of PERforM. *Iran. J. Ergon.* **7**(2), 19–29 (2019)
60. Capodaglio, E.M.: Participatory ergonomics for the reduction of musculoskeletal exposure of maintenance workers. *Int. J. Occup. Saf. Ergon.* 1–21 (2020). (Just-Accepted)
61. Narsia, R.H., Raj, J.O.: Participatory ergonomics: work related musculoskeletal disorders among cashew nut factory workers in Karkala Taluka. *Acta Sci. Orthop.* **3**(6) (2020). ISSN: 2581–8635
62. Bernardes, J.M., Ruiz-Frutos, C., Moro, A. R.P., Dias, A.: A low-cost and efficient participatory ergonomic intervention to reduce the burden of work-related musculoskeletal disorders in an industrially developing country: an experience report. *Int. J. Occup. Saf. Ergon.* 1–8 (2020)

Creating Products from Textile Waste Generated During Fabric Cutting Stage in the Garment Production Process



Jharna Joshi and Anirban Chowdhury

Abstract Fashion and clothing function beyond physiological requirements and satisfy many other human needs. The garment industry is one of the most widespread and interconnected businesses in the world. However, it is also the second most polluting in the world. Therefore, this industry is under lot of pressure to bring about a radical change and reduce the negative impacts on the environment. There is a lot of textile waste generation during the fabric cutting stage in the production process. In smaller manufacturing units like tailor shops and boutique the waste produced is all the more because each piece is custom made. All this waste is dumped into landfills or water bodies and also burnt. The objectives of this research are (1) To find out ways to utilize textile waste generated during the fabric cutting stage of the production stage, (2) develop miscellaneous products, and (3) validation of products based on heuristic analysis. The research was Practice based. A design process was followed to create products of common use form this waste. These products were validated for their quality by conducting Heuristic Analysis. Experts from the field of design evaluated these products for various features and the results were recorded. It was concluded that in the present scope of the study the results were satisfactory. There is a possibility of utilizing the smallest scrap of the textile waste and converting it into products, which are high on usability and pleasure index.

Keywords Clothing · Product design · Social impact · Sustainable fashion · Textile waste · Usability

J. Joshi · A. Chowdhury (✉)
School of Design (SoD), University of Petroleum and Energy Studies (UPES), Dehradun 248007,
Uttarakhand, India
e-mail: chowdhuryanirban14@gmail.com

© The Author(s), under exclusive license to Springer Nature Singapore Pte Ltd. 2021
B. Deepak et al. (eds.), *Advanced Manufacturing Systems and Innovative Product Design*,
Lecture Notes in Mechanical Engineering,
https://doi.org/10.1007/978-981-15-9853-1_8

79

1 Introduction

The clothing, being a basic human need to protect one from heat, cold, and rain has evolved to functions beyond physiological needs. In today's world, it serves the purpose of adornment, identity creation, expression of individuality, a means to communicate self-worth, economic status, and cultural expression. Over the years commercialization and globalization has changed the entire dynamics of fashion industry. The manufacturing, use, and disposal of fashion clothing creates huge environmental and social impact of [1]. The consumerist society obsessed with acquiring more and more has encouraged the 'fast fashion', which has led to a massive growth of cheap mass-produced products. Therefore, the fashion industry needs to identify the factors in the product life cycle that have a negative environmental and social impact. Many people believe the current garment business model is not sustainable at all and are looking for alternatives and solutions. A balance between three elements: economy (focus on economic viability), environment (focus on ecological stability), and social equity is the requirement of sustainability [2, 3]. The solution lies in studying the entire lifecycle of a garment and apply sustainable approaches at every stage.

According to a study in the UK, 2.35 million tons of textile waste are generated over a year. A major part of this is sent to landfill (74%) while rest is shared equally between material recovery and incineration (26%) [4]. Thus, statistic states that an enormous amount of textile waste either goes into landfills or incinerated. The purpose of this study was to find ways to utilize textile waste generated during the fabric cutting stage of the production stage.

2 Review of Literature

2.1 Sustainability

Sustainable development is an open process that requires constant change of our priorities and objectives. The World Commission on Environment and Development (WCED) [5] defines sustainable development as a model of development where the present generation can fulfil all its requirements, without compromising the environment or the needs of the future generation [6]. Although scattered and inoperative, this is the most commonly used definition of sustainable development. Sustainability is defined as having three elements: economy, environment, and social equity [1, 2]. However, other researchers [7] state that sustainability is a more complex topic and has more aspects to it than just these three elements.

2.2 *Fashion and Sustainability*

Fashion is the way in which our clothes exhibit and communicate our individual thoughts to others, linking us to time and space [8]. Fashion is a means of expression, which defines who we are and how we connect to people. Fashion trends are usually very dynamic, superficial, and transient. This reflects negatively on the business of fashion mainly due to the way it is manifested and used [9]. Inherently change can neither be positive nor negative and nature of the change is the only thing that matters. From a negative viewpoint, fashion is discarding clothes that are in perfect condition for reasons that are only metaphorical [10]. It is a known fact that production of fashion garments produces a huge amount of waste, which is a hurdle toward the goal of sustainability. The right approach would be that there should be no contradiction between fashion and sustainable principles. Fashion in fact has a greater role in the promotion and achievement of sustainable ways and principles [9]. According to another definition fashion is defined as a process which is worn and used as an expression by people and has a direct link to environment as a material object [11].

2.3 *The Supply Chain*

The textile garment and fashion industry consists of various market segments, which range from haute couture and custom-made tailoring to Ready-to-wear brands and online platforms. There is a variation in the scale of production and the garment characteristics with respect to the various levels of the market. However, there is a common set of stages that exist within all market levels of the industry (Fig. 1 and Fig. 2).

2.4 *Sustainable Design Strategies*

In order to be sustainable, one needs to think through all the stages in the life cycle of a garment and consider environmental and social impacts at every stage.

Design led approach. Understand how the end user will engage with the clothing that is developed. Designing a transformable, multifunctional, or highly durable garment that may purposefully change with age, becoming different through use. It is important for a designer to look for opportunities for materials and resources to be used wisely and efficiently. Reducing textile waste.

Production Stage. The pattern-making and toiling phase of the production process determines the final look of the garment, its appropriate construction methods and its material and labor requirements. The designer should look for Zero waste cutting methods and reducing textile waste in this stage. Ethical Fashion should be practiced by looking into human and labor rights.

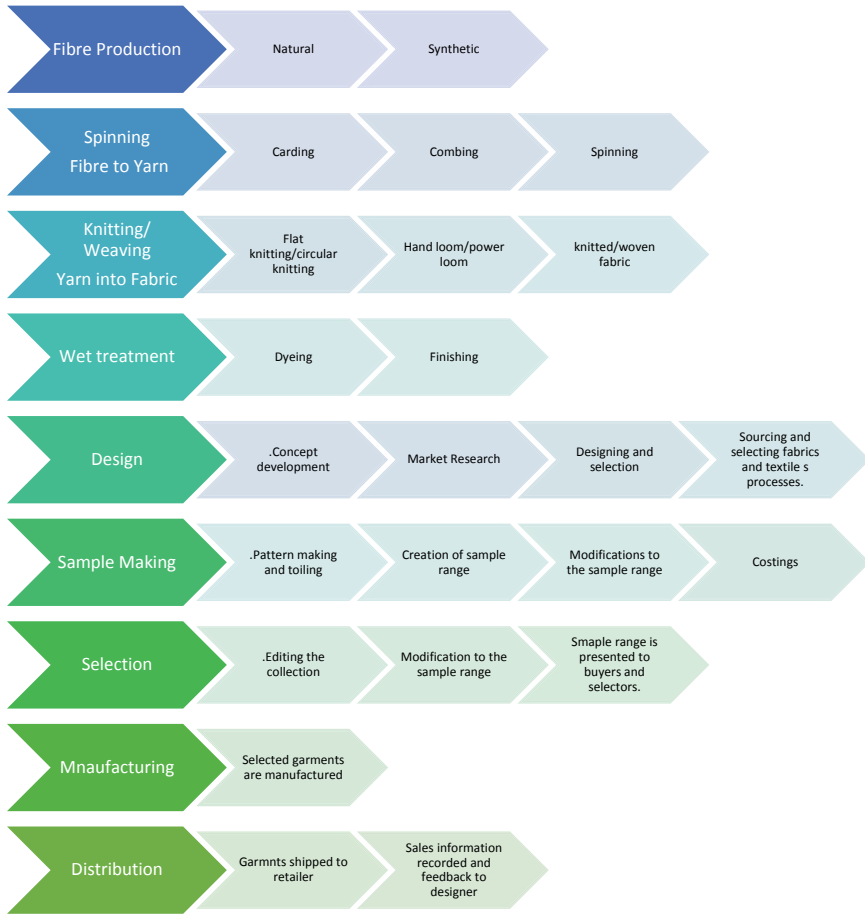


Fig. 1 Activities of the supply chain

Distribution: suppliers and producers. Reducing environmental impacts related to the shipping of materials and resources between suppliers, makers, and producers.

The user stage. Washing, Drying, and ironing and storing of garments.

The end of the life cycle. Reuse, reinvent, upcycle, recycle.

2.5 Research Gap

There are many suggested solutions and many practices that are recommended for sustainable fashion practices but lot of it lacks practical application. The research seeks to develop a sustainable design strategy to reduce specific environmental impact of textile waste generated during fabric cutting stage of the production phase.

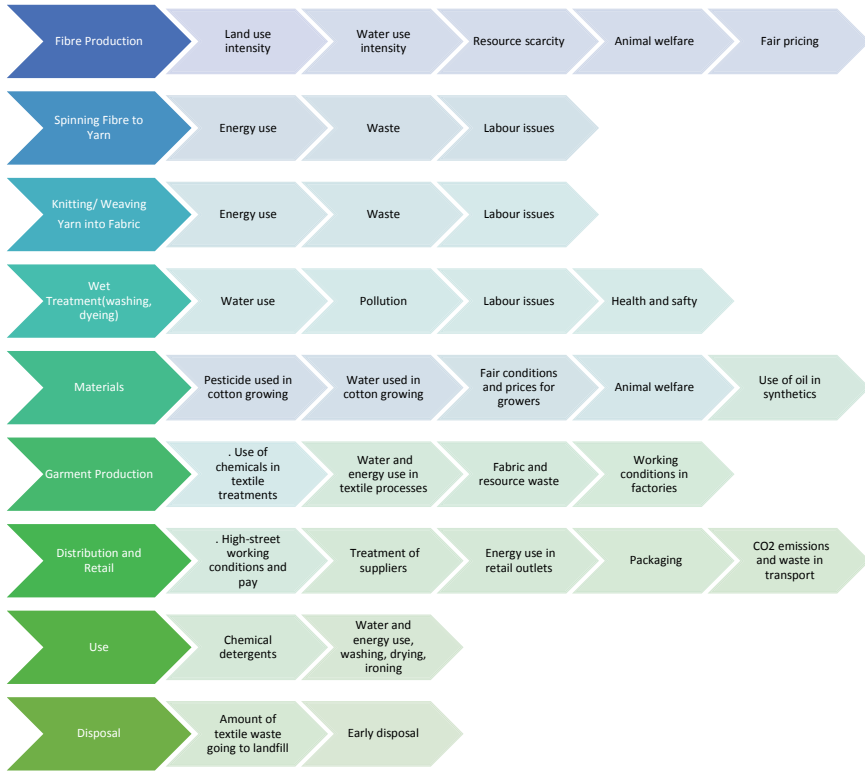


Fig. 2 Impacts of the textile and garment industry

2.6 Research Objectives

To find out ways to utilize textile waste generated during the fabric cutting stage of the production stage.

To develop miscellaneous product and further validation of products based on product quality.

3 Methods

A practice-based research approach was taken to create products from the textile waste. The experts, thus following qualitative research method, further evaluated these products for various features.

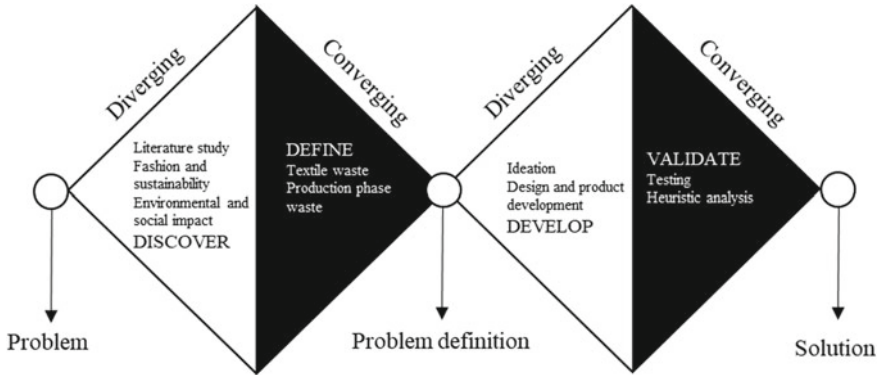


Fig. 3 Double diamond design process [5]

3.1 Design Process

Double Diamond model of design process is applied during this research, which was popularized by the British Design Council in 2005 [12]. According to this process the two diamonds represent: Divergent thinking (a process of exploring a problem) and Convergent thinking (taking a focused action) (Fig. 3).

3.2 The First Phase

A practicing designer, with an entrepreneurial experience of many years, the amount of textile waste generated in my own space always alarmed me. This waste always used to end up in landfill and sometimes burnt in my own backyard. An extensive exploratory research and years of experience led to the identification of various unethical and non-sustainable practices in the product supply chain.

The creation of unnecessary textile waste is one of the biggest problem associated with the production phase. In the ‘cut, make and trim’ (CMT) process, up to 15% of the fabric is wasted due to uncreative approaches to pattern making.

In the conventional pattern-making methods, paper pattern pieces produced are difficult to lay efficiently within the full width and length of the fabric, which then leads to the creation of textile waste during manufacture. Even with the computer aided design (CAD) pattern-cutting software programs, which produce a marker using the pattern pieces in an efficient and cost-effective way, waste is unavoidable. For this study, the formal garment industry was not explored and the waste was collected from local boutiques and tailor shops. All of these places dispose of the textile waste in landfills and water bodies and many times, they burn it adding to the air pollution

Many designers are exploring zero-waste approaches to pattern making to minimize or avoid textile waste. When we explore beyond the industry setup, in a boutique or tailor shop the waste generated is even more because each piece is custom made. In the current study, our focus was on these small manufacturing places.

3.3 The Second Phase (Production Process)

The various steps followed for the creation of the products were as follows:

Collection of material. The raw material in this case is the textile waste of the production stage collected from few boutiques and tailoring shops.

Segregation of the textile waste. The textile waste or the ‘Katrans’, as they are locally known are sorted into different lots in terms of size, quality, and color. The size sorting will determine the kind of product that can be designed out of it. The very tiny pieces of fabric, which are called ‘chindis’ in local language are difficult to incorporate in most of the designs and are also difficult to sew. Alternate methods of attaching these to create interesting products were used.

Finalizing the designs.

Making of patterns. Paper patterns were made according to the design and size of the product finalized.

Cutting of fabric. The fabric is cut using the patterns and waste generated here can again be added to the ‘chindi’ lot for further use.

Stitching the pieces together. These small cut pieces are then stitched together like the joining of a jigsaw puzzle. This completes the patched piece.

Cutting the pattern pieces. These patched pieces will be further cut using patterns to form the different parts of the product.

Sewing the various pattern pieces together to create the final product.

3.4 Heuristic Analysis

It is well established that usability and pleasure are the important factors in the acceptance of any product [13]. This was further corroborated through many research papers that were reviewed to understand the hierarchy of needs [14–16]. Therefore, an appropriate list of heuristics was established and expert evaluators from the field of design were selected. After briefing, these experts evaluated the products for the heuristics and the results were recorded. The products were evaluated by experts for the following heuristics:

User control and freedom. The user should be free to use the product in whichever way he or she wants to and this should not alter the quality or property of the

Quality and standard. The product quality should be equivalent to similar products availability in the market.

Fig. 4 Mug rug**Fig. 5** Face mask

Flexibility and efficiency of usage. The product should be high on usability and serve the purpose they are meant for.

Aesthetics and minimalistic design. It is related to visual pleasure, product or interface styling and use of minimal elements to achieve the beauty of product (Figs. 4, 5, 6, 7 and 8).

4 Results and Discussions

The aesthetics of a product plays a major role in influencing a target user [17, 18]. Further to this, usability of a product also predicts user acceptance [19]. Literature review of product acceptance research suggests that aesthetics also impacts user perception in terms of the quality of the product [20–22].

In this study, all the three design experts agreed that almost all the products created matched the heuristic standards established for the analysis.

The analysis of the various products shared in detail:

Fig. 6 The stole

4.1 Mug Rug

This product was rated high on aesthetics due to the good use of color combination and a quality finish. In terms of usage also it shows flexibility and user control (Table 1).

Fig. 7 Key ring**Fig. 8** Cushion cover

Table 1 Heuristic analysis of designed products

Heuristics	Mug Rug	Cushion cover	Keyring	Stole	Mask
User control and freedom	Y	Y	M	M	Y
Quality and standard	Y	M	N	Y	N
Flexibility and efficiency of usage	Y	Y	M	Y	N
Aesthetics and minimalistic design	Y	M	N	Y	Y
Star Ratings	*****	****	**	*****	***
Expert Comments	Finishing and quality is very good. The aesthetics are also high	Better quality of fabric can be used which is colorfast. Prints on the different fabrics should be well matched	Quality needs improvement	Very good quality silk fabric was used and an excellent finish was given.	Due to blended fabric, user might face breathing problems. The issue can be resolved with additional filter like N95 masks

*Quality Ratings, Y—Very good, M—Moderate, N—Not good

4.2 Cushion Cover

This product requires some improvement in the quality of fabric selected. It is an everyday use product; therefore, fabric should be durable and color fast. Since cotton prints were used for this sample, therefore the fabric pieces need to be tested for their color fastness and the prints should be well matched (Table 1).

4.3 Key Ring

This product needs improvement in terms of both aesthetics and quality. The textile waste material used here are the scraps (‘Chindis’) so the tassels created out of it have to be finished in a better way. This will improve the overall aesthetics of the product (Table 1).

4.4 Stole

Good quality silk fabric pieces were utilized in the construction of this product and a high quality of finish was achieved. In terms of aesthetics, finishing and quality of this product is rated very high. There is one issue in terms of flexibility of use, as this can be used only from one side (Table 1).

4.5 Mask

A good product in terms of aesthetics and user control. However, this sample was made from blended fabric hence there could be breathing issues for the end user. The issue can be resolved with additional filter (Table 1).

5 Conclusion

The outcome of the current study was very encouraging in terms of utilization of fabric waste for development of quality products. Therefore, it can be concluded that in the present scope of the study the results were satisfactory. There is a possibility of utilizing the smallest scrap of the textile waste and converting it into products, which are high on usability and pleasure index.

This study covered only a very small section of the manufacturing process of the entire industry and this could be a limiting factor of the research. A further well-planned and well-supported research initiative is something that one would look for in the future. An alternate business model, which could support this kind of manufacturing from textile waste, is an area for further research.

References

1. Gwilt, A.: A practical guide to sustainable fashion. Bloomsbury Publishing (2020)
2. Elkington, J.: Cannibals with forks: the triple bottom line of 21st century business. New Society Publishers, Gabriola Island. BC (1998)
3. Frankel, C.: In earth's company: business, environment, and the challenge of sustainability. New Society Pub (1998)
4. Allwood, J.M., Laursen, S.E., de Rodriguez, C.M., Bocken, N.M.: Well dressed?: the present and future sustainability of clothing and textiles in the United Kingdom. *J. Home Econ. Inst. Aust.* **22**(1), 42 (2015)
5. Sw, W.C.E.D.: World commission on environment and development. *Our Common Future* **29**(17), 1–91 (1987)
6. Gardetti, M.A., Torres, A.L.: A special issue on textiles, fashion and sustainability. *J. Corp. Citizenship.* 45 (2012)

7. Gilding, P.: Sustainability-doing it. Sustainability: the corporate challenge of the 21st Century. 38–52 (2000)
8. Griffiths, A.: Sustainability: the corporate challenge of the 21st Century. Allen & Unwin (2000)
9. Fletcher, K.: Sustainable fashion and textiles: design journeys, p. 13. Sterling, Earthscan. London (2008)
10. Walker, S.: Object lessons: enduring artifacts and sustainable solutions. *Des. Issues* **22**(1), 20–31 (2006)
11. Niessen, B.: OpenWear. Sustainability, OpenneSS and p 2p production in the World of fashion
12. Hethborn, J., Ulasewicz, C.: Sustainable fashion, why now? A conversation about issues, practices, and possibilities
13. Jordan, P.W.: Designing pleasurable products: an introduction to the new human factors. CRC press (2002)
14. Chowdhury, A.: Design and development of a stencil for mobile user interface (UI) design. In: *Research into Design for a Connected World 2019*, pp. 629–639. Springer, Singapore
15. Chowdhury, A.: Design and evaluation of user interface of a mobile application for aiding entrepreneurship. In: *Innovative Product Design and Intelligent Manufacturing Systems 2020*, pp. 71–79. Springer, Singapore
16. Chowdhury, A., Chakrabarti, D., Karmakar, S.: Anthropomorphic televisions are more attractive: the effect of novelty. In: *Ergonomics in Caring for People 2018*, pp. 243–249. Springer, Singapore
17. Koli, A., Chowdhury, A., Dhar, D.: Requirement of new media features for enhancing online shopping experience of smartphone users. In: *Intelligent Systems Technologies and Applications 2016*, pp. 423–435. Springer, Cham
18. Chowdhury, A., Karmakar, S., Reddy, S.M., Ghosh, S., Chakrabarti, D.: Product personality rating style for satisfaction of tactile need of online buyers—a human factors issue in the context of e-retailers’ web-design. In: *2013 International Conference on Human Computer Interactions (ICHCI) 2013 Aug 23*, pp. 1–8. IEEE
19. Chowdhury, A., Karmakar, S., Reddy, S.M., Ghosh, S., Chakrabarti, D.: Usability is more valuable predictor than product personality for product choice in human-product physical interaction. *Int. J. Ind. Ergon.* **44**(5), 697–705 (2014)
20. Karkun, P., Dhar, D., Chowdhury, A.: Usability and cognitive interference in technology adoption for elderly—a critical review of literatures in HCI context. In: *Proceedings of International Ergonomics Conference HWWE 2014*, pp. 408–411. Tata McGraw-Hill
21. Rafi-Ul-Shan, P., Perry, P., Grant, D.: Managing sustainability in the fashion supply chain Operationalization and challenges at a UK textile company. (2016) e- www.koganpage.com
22. Council, B.D.: Eleven lessons. A study of the design process, British Design Council (2016)

Forced Draft and Superheated Steam for Design and Development of Community Smoke Less Chulha to Help Women in Rural Areas



Ramesh Chandra Nayak, Manmatha K. Roul, Saroj Kumar Sarangi, Abhisek Sarangi, and Asish Sarangi

Abstract Kitchen smoke is the leading cause of infections in the respiratory system in developing countries. The World Health Organization estimates that indoor pollution causes one million premature deaths every year in India. Despite the growth in utilization of LPG, still 40% of Indian family continue to use traditional fuels for food preparation. Although there are many solutions available for the poor people in urban areas but people living in rural areas have no other option than to use traditional fuels like wood in chulhas. Thus, the problem of indoor air contamination is a major public health hazard for the country, which accounted for more than 1.6 million premature deaths in the year 2019. In this work an attempt has been made to overcome this problem by designing and developing a smokeless chulha, which is operated by force draft and superheated steam as secondary fuel. This innovative smokeless stove/Chula is very fuel efficient which needs less biomass for its operation. It offers a harmless home environment to the occupants and decreases the menace of respiratory diseases. The thermal efficiency of our modified Chulha is about 16% more than that of the traditional Chulhas due to the creation of forced draft and supply of superheated steam. The result from this work indicates that the calorific value of biomass fuel is increased as a result of which less fuel is required

R. C. Nayak (✉)

Department of Mechanical Engineering, Synergy Institute of Engineering and Technology, Dhenkanal, Odisha, India
e-mail: rameshnayak23@gmail.com

M. K. Roul

Department of Mechanical Engineering, GITA, Bhubaneswar, Odisha, India

S. K. Sarangi

Department of Mechanical Engineering, NIT, Patna, Bihar, India

A. Sarangi

Mechanical Engineering Department, IGIT, Sarang, Dhenkanal, Odisha, India

A. Sarangi

Mechanical Engineering Department, CET, Bhubaneswar, Odisha, India

for cooking and it produces very negligible smoke and hence it can be used as a cost effective and environmental friendly replacement for the traditional chulha.

Keywords Smokeless chulha · Superheated steam · Secondary fuel · LPG · Air pollution · Calorific value

Nomenclature

L	Length of inner vertical tube (m)
D_o	Outer Diameter of tubes (m)
D_i	Inner Diameter of tubes (m)
t	Thickness of tubes (m)
A	Surface area of vertical tubes (m^2)
T	Temperature (K)
K	Thermal conductivity
CV	Calorific value

1 Introduction

Chulha (Cooking Furnace) is a conventional Indian cooking wood stove used for food preparation. The process of cooking by conventional chulha is done by using cow dung, wood, crop waste, dry leaves, etc. During operation of chulha it is required to supply air manually by blowing air through mouth, which is a very dangerous process. It is found that 90% of women using this traditional chulha are suffering from throat problem, maximum of them also suffer from throat cancer. It is also the main cause of indoor air pollution.

In Odisha, 85% of rural women are using this type of traditional chulha. Generally, in village areas of Odisha, people are cooking 3 times a day as breakfast, lunch, and dinner by using this traditional chulha. In India, PradhanMantriUjjwalaYojana (PMUY) was started on May 1, 2016 by Prime Minister of India Sri Narendra Modi to distribute LPG connections to women of BPL families. But the sad part of it is that a number of families are there who don't have any BPL cards, and also the family having BPL card and availing the LPG connection, they don't have sufficient money for next time LPG filling, which is a major cause of concern. And also due to less number of LPG distributors there is some problem of filling LPG in time.

The main objective of this work is to design and fabricate a community smokeless chulha, which is operated by force draft and superheated steam as secondary fuel. It consists of three cylinders (inner, middle, and outer), superheater, water tank, blower, insulating material such as glass wool. The studies are also carried out on experimental setup, design calculation, calorific value, thermal efficiency, and measurement

of pollution index. Although extensive work has been done on the study of smokeless chulha and its design but utilization of superheated steam is a unique initiative of this work.

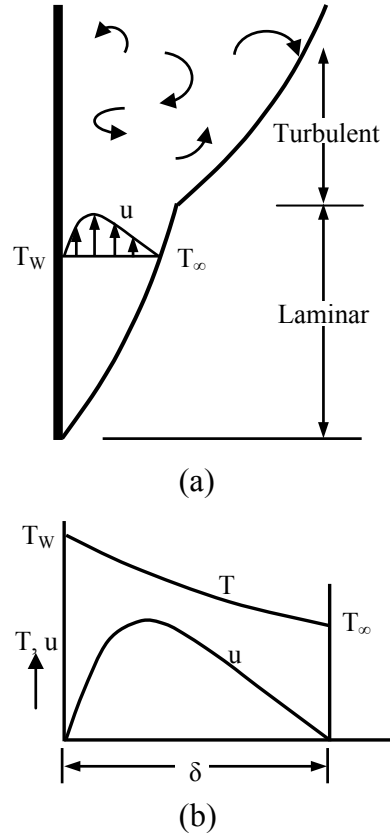
Mitchell et al. [1] studied on emissions from domestic stove by combustion of biomass and solid fuels. They observed that NO_x formation was directly proportional to the Nitrogen content of the fuel for all types of fuels. Winijkul and Bond [2] studied on emissions by housing combustion and its diminution method and found that diminution in definite area depends on the existing fuel blend and the inhabitants' distribution along with land nature. Fachinger et al. [3] studied on emission aspect for altered fuels and found that handling of surplus air or burning of wood that is totally dehydrated or in very miniature form, effect in powerfully prominent emission aspect. Sharma and Batra [4] studied on smokeless kitchen in rural India and suggested that innovations are required for reducing smoke and improving the health of people living in rural areas.

Someswararao et al. [5] evaluated the performance of improved stoves and found that enhanced Udairaj cook stoves are improved over the conventional stove as regard to its specific fuel consumption, power rating, and thermal efficiency. Udairaj product is very popular as it is very simple to build owing to its easy assemble for its installation. Singh et al. [6] studied on importance of smokeless chulha for farm women. They observed that conventional chulha offer dangerous and harmful atmosphere to the farm women. So it is required to provide more knowledge regarding smokeless chulha to farm women. Das and Panda [7] studied the importance of smokeless chulha for improving quality of life and found that the improvement technique, planning to develop a smokeless chulha is very important, and also mentioned that financial support from government is required to implement this technique. Sharma et al. [8] investigated on eco efficiency and low emission of smokeless chulha and its application in rural areas. They found that smokeless chulha provides better efficiency and is suitable for healthier, cleaner, and faster cooking.

Takemitsu et al. [9] observed that the unwanted aroma of barley can be reduced by food preparation with superheated steam. They initiated steam cooking system functional to barley preparation for the first time using inclusive study and found the suitability and deliciousness of this first-class food affluent in nutritional thread. Johnson et al. [10] studied about the emission from in home cook stoves used in Asia and Africa and found that the traditional chulha causes maximum pollution and in order to overcome such problem it is required to develop technology and laboratory facility for testing purpose.

Chantrabose et al. [11] investigated on improvement of energy competent wood stove for rural purpose and found that proper initiative from government is required to encourage for the design and development of smokeless chulha for betterment of the rural people and also the environment. Kuptniratsaikul et al. [12] studied about the benefit of chulha knot where they found that the tensile strength could be increased to make it easier to tie. Roul and Nayak [13] studied natural convection heat transfer in heated tubes, in which they explained about the heat transfer characteristics by taking various parameters like varying length of tubes with provision of internal obstacles to improve the natural convection heat transfer. Nayak et al. [14–16] studied on their

Fig. 1 a Boundary layer on a vertical wall b temperature and velocity distribution



another work to explain the heat transfer behavior experimentally and theoretically, where they found that heat transfer behavior is affected by provision of internal obstacles as rings. Sahoo et al. [17–19] applied computational fluid dynamics methods to analyze heat transfer from pin finned vertical and horizontal plates.

The objective of this work is to setup a model stove for prevention of diseases or to restore the good health by some means by creating awareness for the use of zero emission cook stove. For this we conducted a randomized controlled study of 66 households in one villages at Cuttack districts in Odisha to analyze improved cook stove adoption. Figure 1 shows the boundary layer on vertical tube, temperature, and velocity distribution.

2 Experimental Setup and Procedure

Figure 2 demonstrates the investigational setup, which consists of the entire equipment and the main mechanism. The experimental arrangement comprises of a test

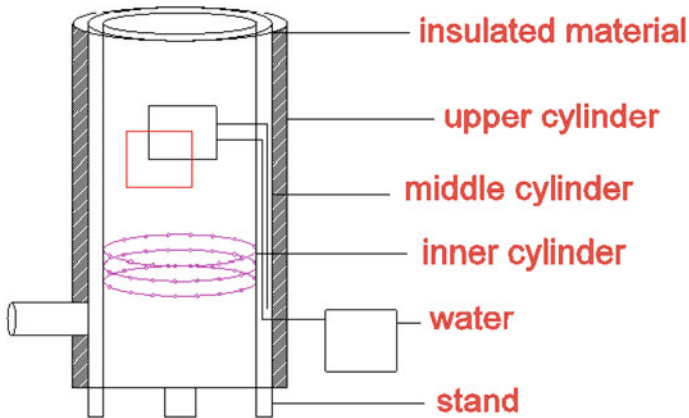


Fig. 2 Experimental set-up

section, which consists of three cylinders, a superheater connected with water tank, blower and glass wool as insulated material.

The isometric view, sectional view, front view, and the top view of the experimental arrangement is presented in Fig. 3a–d. In this study, three cylindrical tubes are made of mild steel sheet which is 1.29 mm in thickness. The inner cylinder is having 10 in. inner diameter, middle cylinder is 12 in. inner diameter, and outer cylinder is having 14 in. inner diameter. All cylinders are of 24 in. vertical height. Super heater is provided in the middle cylinder which is 2 in. in diameter and 3 in. in height. Water is supplied from the external chamber to the super heater through the pipe connected with the super heater at its bottom. The external chamber is made up of galvanized iron tube having 4 in. diameter and 12 in. length. It is just like a container in conventional stove to carry kerosene but here it contains water and the bottom part of the cylinders is fixed with a base. For less heat loss from the system, insulated material such as glass wool is provided in between middle and external cylinder. All three cylinders are placed on the same base. The passage for supplying of wood to internal cylinder is provided at a distance of 4 in. from top of test section. Another passage is provided at a distance of 4 in. from the bottom of the section up to the middle cylinder for provision of blower to supply air. There are some holes which are provided on periphery of inner cylinder to supply air from blower to the inner cylinder. This supply of air to inner cylinder is done to create forced draft.

Initially water is placed in the external chamber and the valves of that chamber are initially kept in closed condition. Small pieces of wood are placed in the internal chamber and they are fired. At the time of initial fire, the blower is kept at off condition. After 2–3 min the blower is allowed to start to supply air to the internal chamber. At this time continuous supply of small pieces of wood to internal chamber is done. After 3–4 min it is found that the flame starts to increase. At this time pumping of water from the external chamber is done in order to spray superheated

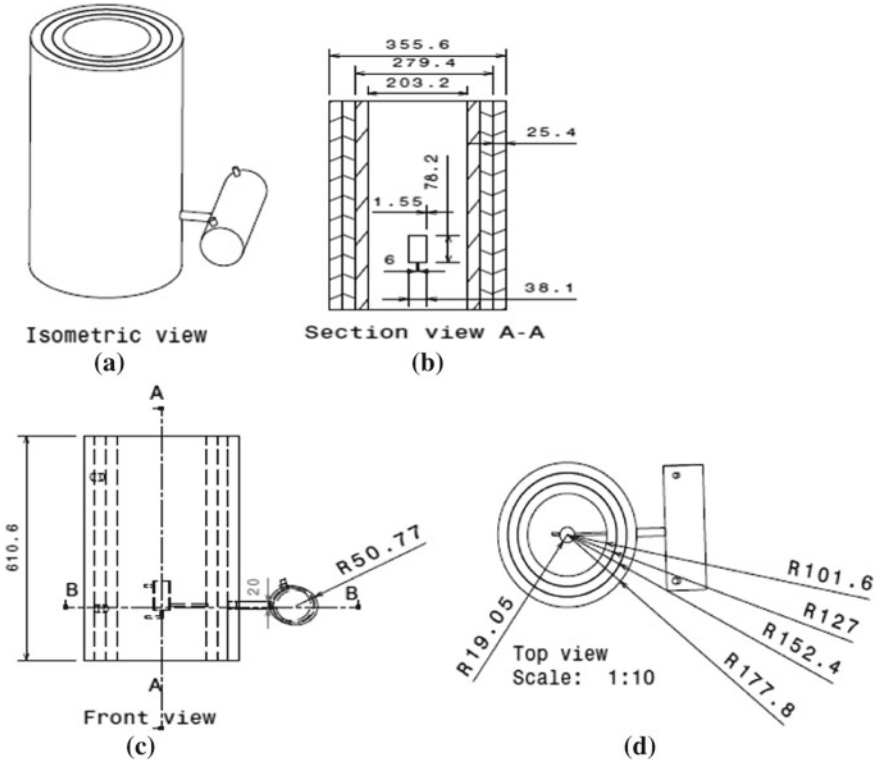


Fig. 3 a Isometric view of test section b sectional view c front view d top view

steam inside the internal cylinder. After spraying of superheated steam it is found that the flame temperature increases, and smoke quantity rapidly reduces. In this work the superheated steam act as secondary fuel.

The sequence of operation of Smokeless Stove/Chulha in step wise is mentioned.

- Step 1: Connection of blower to electric supply.
- Step 2: Loading of biomass.
- Step 3: Igniting by putting paper or small amount of kerosene.
- Step 4: Starting of blower.
- Step 5: Final burning.
- Step 6: Pumping of water to supply super-heated steam.

In this work a blower is provided for producing forced draft but in place of blower a fan just at the bottom of the cylinder can be placed which can also run by small rechargeable battery to save electricity or to overcome the problem of unavailability

of electricity supply. To avoid heat loss from the system a layer of glass wool is provided in between external cylinder and middle cylinder.

3 Results and Discussion

There is major encumber of environmental impact linked with cooking using conventional chulha and biomass fuels. In this work an attempt has been made to recognize various factors to speed up development in the design and fabrication of chulha with improvement in technology. The main objective of this work is to reduce emission and improve thermal efficiency so that harmful effect on the environment and public health can be reduced.

Table 1 shows the results of thermal efficiency, power output, calorific value, and CO formation. It is evident from Table 1 that the average thermal efficiency of this modified chulha is 26.41% whereas the thermal efficiency of the conventional chulha is generally less than 10%. So the thermal efficiency of our modified chulha is about 16% more than that of the traditional chulhas due to the creation of forced draft and supply of superheated steam. Thus the cooking time as well as the fuel consumption decreases. The CO level decreases as compared with traditional chulha. It was also observed that the ash as well as smoke formation decreases as compared to the traditional chulha. The caloric value of fuel increases due to provision of superheated steam and forced draft.

Table 2 shows the flow volume, power output, dilution ratio, flame temperature, and body temperature in various positions. It can be seen from this table that when flow volume increases power output increases. It is also observed that with increase in flow volume, the flame temperature also increases due to complete combustion of fuel. The power output is very high as compared with traditional chulhas. Flame temperature also increases due to the increase in flow volume. When the flow volume reaches to 1.12 m³ the flame temperature increases to 634 °C.

Figure 4 shows the modified innovative chulha during its operation. The experimental arrangement comprises of a test section, which consists of three concentric cylinders, a superheater connected with water tank, a blower. Glass wools are provided as insulating material between exterior and middle cylinder in order to reduce heat loss to the surrounding from the wall of the cooking furnace.

4 Conclusions

The improved smokeless chulha has been designed and developed experimentally, where superheated steam is taken as secondary fuel and air from fan or blower is used for producing forced draft. Glass wool is used as insulating material. The conclusions drawn by the design, development, and experimentation of this smokeless chulha can be enumerated as follows.

Table 1 Experimental Results of efficiency, CV, CO

Stove	Thermal efficiency in (%)	CO (ppm)	Velocity (m/s)	Fuel B. R (kg/h)	M.C. D.B (%)	CV of Fuel (kcal/kg)	CO (≤ 5)	TPM (mg/m ²)	TPM (≤ 150 mg/Mjd)	CO: CO ₂
Expt -1	25.89	289.18	2.20	3.00	6.0	4450.00	3.16	15.35	158.20	0.018
Expt -2	27.36	462.38	2.70	3.50	5.80	4403.85	5.09	12.82	133.20	0.063
Expt -3	25.57	562.10	2.70	3.50	5.70	4408.53	6.61	13.49	149.79	0.087
Expt -4	26.20	270.53	2.60	3.50	6.00	4450.00	2.69	14.49	143.89	0.024
Expt -5	26.36	305.92	2.70	3.50	5.90	4422.70	3.48	14.36	154.11	0.030
Expt -6	27.08	373.60	2.90	3.50	4.00	4450.00	4.42	15.07	168.18	0.048
Average	26.41	372.28	2.63	3.42	5.57	4430.85	4.24	14.27	152.23	0.05

Table 2 Experimental results of flow volume, body temperature, flame temperature

Stove	Flow volume (m ³)	Power output (kW)	Dilution ratio	Body temp (°C)	Flame temp (°C)	Handle temp (°C)
Expt -1	0.62	4.02	53.99	50.00	550	70
Expt -2	0.98	4.90	56.80	62.00	576	71
Expt -3	0.96	4.59	56.80	46.00	569	68
Expt -4	1.02	5.01	54.69	56.00	612	73
Expt -5	1.12	5.75	56.80	48.00	634	72
Expt -6	0.96	4.90	61.00	47.00	531	71
Average	0.94	4.65	56.68	51.50	537	70.83

**Fig. 4** Modified chulha during operation

- (1) It offers a harmless home environment to the occupants and decreases the menace of respiratory diseases.
- (2) This innovative smokeless stove/chulha is very fuel efficient which needs less biomass for its operation.
- (3) Superheated steam is taken as secondary fuel, which helps in reducing smoke and increasing calorific value of biomass.

References

1. Mitchell, E.J.S., Lea-Langton, A.R., Jones, J.M., Williams, A., Layden, P., Johnson, R.: The impact of fuel properties on the emissions from the combustion of biomass and other solid fuels in a fixed bed domestic stove. *Fuel Process. Technol.* **142**, 115–123 (2016)
2. Winijkul, E., Bond, T.C.: Emissions from residential combustion considering end-uses and spatial constraints: part II emission reduction scenarios. *Atmos. Environ.* **124**, 1–11 (2016)
3. Fachinger, F., Drewnick, F., Gieré, R., Borrmann, S.: How the user can influence particulate emissions from residential wood and pellet stoves: emission factors for different fuels and burning conditions. *Atmos. Environ.* **158**, 216–226 (2017)
4. Sharma, P., Batra, S.: Smokeless kitchens in rural India—an overview. *Int. J. Eng. Sci. Invention Res. Dev.* **3**, 377–380 (2017)
5. Someswararao, C., Kumar, G.P., Satyanarayana, C.V.V.: Performance evaluation of improved cook stoves. *Nat Environ. Pollut. Technol.* **11**, 621–624 (2012). ISSN: 0972-6268
6. Singh, R., Chaudhary, R.P., Choudhary, G.K., Gautam, U.S.: Impact of smokeless Chulha for farm women to improve quality of life: on farm trial. *Int. J. Current Microbiol. Appl. Sci. Spec. Issue* **7**, 3614–3618 (2018)
7. Das, S.S., Panda, H.: Smokeless Chulha—a way for enhancing quality of life. *Int. J. Res. Sci. Innov. (IJRSI)* **4**, 70–78 (2017)
8. Sharma, M.K., Shrivastava, R.N., Sharma, N.: Smokeless cook stove an advancement of the combustion technology and innovative approach towards eco-efficiency and low emissions in rural areas. *Am. J. Eng. Res. (AJER)* **4**, 171–177 (2015)
9. Takemitsu, H., Amako, M., Sako, Y., Kita, K., Ozeki, T., Inui, H., Kitamura, S.: Reducing the undesirable odor of barley by cooking with superheated steam. *J. Food Sci. Technol.* **56**, 4732–4741 (2019)
10. Johnson, M.A., Garland, C.R., Jagoe, K., Edwards, R., Ndemere, J., Weyant, C., Patel, A., Kithinji, J., Wasirwa, E., Nguyen, T., Khoi, D.D., Kay, E., Scott, P., Nguyen, R., Yagnaraman, M., Mitchell, J., Derby, E., Chiang, R.A., Pennise, D.: In-home emissions performance of cookstoves in Asia and Africa. *Atmosphere* **10**, 290 (2019)
11. Chantrabose, R., Kayalvizhi, S., Murugan, V., Karpagavalli, B., Kirubakaran, V.: Development of energy efficient wood stove for rural application. In: *International Conference on Energy Efficient Technologies for Sustainability, ICEETS 2016*, pp. 792–795 (2016). Art. No. 7583855
12. Kuptniratsaikul, S., Promsang, T., Kongrukgratit, K.: The Chula knot: a new sliding locking knot with a special property. *Arthroscopy Tech.* **3**, 465–467 (2014)
13. Roul, M.K., Nayak, R.C.: Experimental investigation of natural convection heat transfer through heated vertical tubes. *Int. J. Eng. Res. Appl.* **2**, 1088–1096 (2012)
14. Nayak, R.C., Roul, M.K., Sarangi, S.K.: Experimental investigation of natural convection heat transfer in heated vertical tubes with discrete rings. *Exp. Tech.* **41**, 585–603 (2017)
15. Nayak, R.C., Roul, M.K., Sarangi, S.K.: Experimental investigation of natural convection heat transfer in heated vertical tubes. *Int. J. Appl. Eng. Res.* **12**, 2538–2550 (2017)
16. Nayak, R.C., Roul, M.K., Sarangi, S.K.: Natural convection heat transfer in heated vertical tubes with internal rings. *Arch. Thermodyn.* **39**, 85–111 (2018)
17. Sahoo, L.K., Roul, M.K., Swain, R.K.: CFD analysis of steady laminar natural convection heat transfer from a pin finned isothermal vertical plate. *Heat Transfer Asian Res.* **46**, 840–862 (2017)
18. Sahoo, L.K., Roul, M.K., Swain, R.K.: Natural convection heat transfer augmentation factor with square conductive pin fin arrays. *J. Appl. Mech. Tech. Phys.* **58**, 1115–1122 (2017)
19. Sahoo, L.K., Roul, M.K., Swain, R.K.: CFD analysis of natural convection heat transfer augmentation from square conductive horizontal and inclined pin fin arrays. *Int. J. Ambient Energy* **39**, 840–851 (2018)

Lightweight Materials for Engine Cylinder Blocks/Liners—A Critical Review



B. Pavani Srikavya, P. Srinivasa Rao, and Syed Kamaluddin

Abstract Lightweight Materials have become a choice for many industries like automobile and aerospace due to its tunable mechanical properties like extremely high strength to weight ratio. Aluminum is the best lightweight material. Al metal/alloy matrix composites improve the mechanical properties but lack wear resistance. By applying proper coatings will improve wear resistance. These Al MMCs are used to make engine parts like piston, connecting rod, engine cylinders, drum brakes, disc and cylinder liners. The present review is mainly about the properties of Aluminum Alloys in combination with different reinforcements produced by stir casting method and ultrasonic assisted stir casting method. And survey on the results of different reinforcements on the mechanical and tribological properties. In the present paper the use of composite materials and hard coatings explored so far are reviewed.

Keywords Al alloy MMCs · Tribological coatings · Engine applications

1 Introduction

Lightweight materials can carry the goods at cheaper cost especially in aerospace payloads. Carrying each 1 kg of additional payload will cost in millions of dollars. Application of lightweight materials in automobile and aerospace industry has always a challenging task as they need to satisfy high performance characteristics and pass through several tests. Still people are making large efforts to bring them into their ever since the application of Al-Cu alloys used by Wright Brothers in the manufacture of

B. Pavani Srikavya (✉) · P. Srinivasa Rao
Department of Mechanical Engineering, Centurion University of Technology and Management,
Parlakhemundi, India
e-mail: pavs.kavya@gmail.com

B. Pavani Srikavya · S. Kamaluddin
Department of Mechanical Engineering, Vignan's Institute of Information Technology (A),
Visakhapatnam, India

the first flights in 1903. Use of those alloys was limited to the structural components of aircraft like wings and flooring.

But use of these alloys in the heavy engine parts is started recently and still under study. The following basic properties are to be satisfied by engine materials.

1. Thermal properties: High thermal conductivity and low thermal expansion.
2. Mechanical Properties: High strength, wear resistance, and scuffing resistance.
3. Physical Property: Low density
4. Chemical Property: High corrosion resistance
5. Structural Properties: Good vibration dampening and high modulus of elasticity
6. Manufacturing properties: Good castability and machinability.

As monolithic materials cannot satisfy all above properties composite aluminum alloy-based metal matrix composites have been extensively tried and experimented by many researchers in the recent past. These MMCs may satisfy many of these properties. But they lack wear resistance. To enhance the wear resistance chrome/nickel chromium electroplating or thermal spraying with hard coatings are applied on the bore. Electroplating is restricted due to environmental restrictions imposed on handling of toxic Cr^{+6} ions. In the present paper the use of composite materials and hard coatings explored so far are reviewed and scope of new base alloys/reinforcements materials are discussed.

Composites are materials in which the popular properties of separate materials are united by mechanically binding them together. They have advanced properties from individual materials and their alloys as well. Expansion of metal matrix composite materials consists of mixture of pleasing attributes of metals as matrix and any appropriate reinforcement. The addition of high strength, high modulus refractory particles to a ductile metal matrix create a material whose mechanical properties are transitional between the matrix alloy and ceramic reinforcement.

Long ago, a range of studies have been carried out on metal matrix composites. SiC, TiC, TiB_2 , WC, and B_4C are the most frequently used particulates to reinforce metal or alloy matrix of aluminum or iron. Effort on MMCs began in the 1950s since then researchers made an effort on numerous combinations of matrices and reinforcements which led to the expansion of product for aerospace, but resultant profitable applications were limited. The introduction of ceramic whiskers as reinforcement and the progress of in situ eutectics in the 1960s aided high temperature applications in aircraft engines. In the late 1970s the automobile industries ongoing took MMCs seriously. In the last 20 years, MMCs evolved from laboratories to a group of materials with numerous applications and commercial markets.

2 Previous Work

Raghavendra et al., investigated on the wear behavior Al7075 with reinforcement is Al_2O_3 . In this paper the particle size and volume fraction varied to analyze the wear behavior. The hardness is decreased with increasing the size of particle from 100 to

200 μm . The increment of the volume fraction 3–12% wt. reduced the coefficient of friction and wear [1].

K. C. Mohan kumara et al., done research on Al 1100 5% Mg alloy with SiC is prepared by stir casting technique. Al 1100 is one of the common aluminum alloys and it is soft and low strength. The addition of Mg particles improved the strength. In this paper they studied the variation of percentage of SiC. Increasing the percentage of SiC gives the gradual improvement of Hardness and tensile strength and ductility. The best results are noticed in 12% of SiC addition in composite material [2].

Amol Mali et al., studied about Al365. Al365 have incredibly good casting and machining characteristics. The alumina improves the thermal and mechanical properties, i.e., high heat resistance, high thermal conductivity, and high strength, high hardness. They chose combination of Al365 with Alumina and reinforcement is fly ash. The combination of specimen is prepared in stir casting method. And the analyses are done to find the mechanical properties like compressive strength, tensile strength, Hardness. The % of weight reinforcement and alumina shows different results. The increasing weight of reinforcement increases the tensile strength, hardness, and compressive strength [3].

Prashant Kumar Suragimath et al., had done an investigation on Aluminum alloy (LM6) metal matrix composites. LM6 Aluminum Alloy having good resistance to corrosion and outstanding castability. In this paper the aluminum is base metal and SiC, fly ash are the reinforcing materials. The Addition of reinforcing materials made the results better by increasing mechanical properties, impact strength, and reducing percentage of elongation [4].

Johny James et al., studied about machining and mechanical properties of hybrid composite. In this paper analyses the best result of % SiC and % TiB₂. The reinforcement TiB₂ gives the high strength and durability. The maximum limited percentage of TiB₂ is 2.5% for 10% SiC. The addition of TiB₂ behind the limit is to cause porosity which effected on the mechanical property, i.e., hardness. The results proved that TiB₂ % improves the wear resistance. The result 10% SiC and 2.5% TiB₂ gives less wear compared to 10% SiC and 0% TiB₂ [5].

R. S. Ravendra et al., had prepared Nano ceramics to use synthesis method. In this paper studied the phase formation, size of Nano ceramics and Characterization of aluminum 6061. The morphological test (SEM) shows the constant allocation of the ceramic particles in the matrix. Addition of $\alpha\text{-Al}_2\text{O}_3$ Nano ceramics exhibits the superior properties, i.e., increase the hardness compressive strength and tensile strength [6].

S. M. Russel Kabir Roomey et al., done research on fly ash, base metal A356.2. The fly ash is produced from industrial. The industrial waste is used as reinforcement in manufacturing of composite material. Increasing % of fly ash it develops the hardness, compressive strength, and ultimate strength. But increasing the fly ash content reduces the elongation [7].

Amal E. Nassar et al., done research on PM technique is used to fabricate the aluminum Nano titanium dioxide (TiO₂) composites. The TiO₂ tiny particles mixed with pure aluminum powder. The range of TiO₂ vol.% is 0.5, 1.5, 2.5, 3.5, and 4.5. The addition of TiO₂ particles to enhance the ultimate tensile and yield strength and

hardness of composites. The Nano composites are used to defend the surface so wear resistance also is improved [8].

M. N. Ervina Efzan et al., had reported on Al Alloy LM6 composite with fly ash is fabricated by compo-casting method. In this paper fly ash particles were integrated into semi-solid state of LM6 melt. The semi-solid particles improved the wettability. Addition of 6% wt. of fly ash enhances the 50% of hardness and 30% tensile strength compared to unreinforced LM6 alloy [9].

Vipin K. Sharma et al., studied about mechanical properties and tribological properties of AMMC. Tribological properties investigated by using a Pin-on-disc setup. The fly ash content in composite material is limited up to 4% beyond the limit the maximum average coefficient of friction (COF) is increased. i.e. 4% of fly ash shows COF is 0.12 and 6% of fly ash shows COF is 0.16 [10].

Blaza Stojanovic et al., evaluated new materials, coatings, and high-tech machining processes that were formerly considered to be too costly due to which they are used in complex applications and are now reasonably priced. Presently, owing to the growth in processing of materials, development of new materials to suit different applications has become feasible. Manufacturing of new materials for diesel engine application with tremendously high thermal resistance is vital so the heat losses are reduced and recovered to be partly altered into useful work. Ceramic whiskers or particulates are frequently used as reinforcement in Al-based alloys because of their high modulus, high hardness, low cost, easy availability, and limited reactivity with Al. The hybrid composites containing graphite (Gr) shows better wear-resistance properties than mono reinforcement [11]. Multiple reinforcements (hybrid MMCs) were adopted as they convey improved mechanical, thermal and tribological properties, and they are finer substitutes for composites with single reinforcement.

Narender Panwar et al., reviewed on fabrication methods of aluminum metal matrix methods. The fabrication methods are broadly classified into two types, i.e., solid state and liquid state processing. In this liquid state processing, stir casting method is simple in operation and cost is less compared to other processes. The solid-state process commonly used as powder metallurgy method. This method provides the homogenous allocation of particles but expensive than liquid state processing methods [12].

Mariusz Walczak et al., studied about tribological properties of aluminum metal matrix composite. This paper presented the results of wear test of AlSi12CuNiMg/5.7 wt% Gr aluminum composite material. The wear test had executed on the Ball-On-Disc tribometer. The SEM results show that uniform distribution of graphite particles in composite material. The graphite particles reduced the coefficient of friction. Comparative analysis done to find the importance of graphite particles on wear behavior and reduction % of coefficient friction. The coefficient of friction of composite material AlSi12CuNiMg/5.7 wt% Gr is 0.440 and AlSi12CuNiMg (without graphite) is 0.483 [13].

Vinoth et al., studied about Al-Si eutectic alloy based SiC and Cenosphere reinforced hybrid MMCs. The hybrid MMC's are future materials for the aerospace and automobile industries due to their preferable mechanical properties. Pure aluminium

gives the properties like soft, corrosion resistant, ductile and high electrical conductivity. To improve the wear resistance to use the SiC, Cenosphere can be used as fillers and it is exceptionally light weight. The combination of these three reinforcements gives the superior properties used for the applications of piston, cylinder sleeve and engine blocks [14].

A. K. Kuruvilla et al., studied towards the improvement of modulus of elasticity, strength and thermal stability with respect to the precipitation behavior of reinforcement particles into Al alloys [15].

H. O. Santos et al., investigated and evaluated the microstructures of three-cylinder liners alloys, i.e., grey cast iron and two aluminum silicon alloys. The gray cast iron gave better hardness value than spray formed Al-Si alloys. The surface finish of the spray formed alloys was lesser roughness than the gray cast iron cylinder liner [16].

S. Devaganesh et al., studied and focused on the hybrid composites, Al 7075 with reinforcement is SiC 5 wt% and different solid lubricants graphite, hexagonal boron nitride, molybdenum disulfide with 5 wt% fabricated using stir casting method. Analyzed results show that Al7075 alloy with SiC and graphite ceramic particles influence the great mechanical and tribological properties [17].

Md. Bengir Ahmed Shuvho et al., investigated on the hybrid composites, the combination of composite is Al 6063 with SiC-Al₂O₃-TiO₂ particles, the effect of SiC shows the good results of wear rate and friction coefficient [18].

3 Fabrication methods

Metal matrix composites can be fabricated by different methods. Processing methods are mainly four types.

1. Liquid state process
2. Solid state process
3. In Situ processes
4. Deposition techniques

The liquid state fabrication of metal matrix composites involves incorporation of dispersed phase into a molten matrix metal. Stir casting is the simplest and the most cost-effective method of liquid state process. Content of dispersed phase is limited (usually not more than 30% volume). The main limitation of this process is distribution of dispersed phase throughout matrix is not perfectly homogenous. To overcome the limitations Ultrasonic probe is used. The combination of stir casting with ultrasonic vibration improves the mechanical properties. It gives good distribution of the reinforcement particles within the Aluminum matrix. To improve the microstructure by avoiding agglomeration and results shows the uniform distribution of particles (Fig. 1).

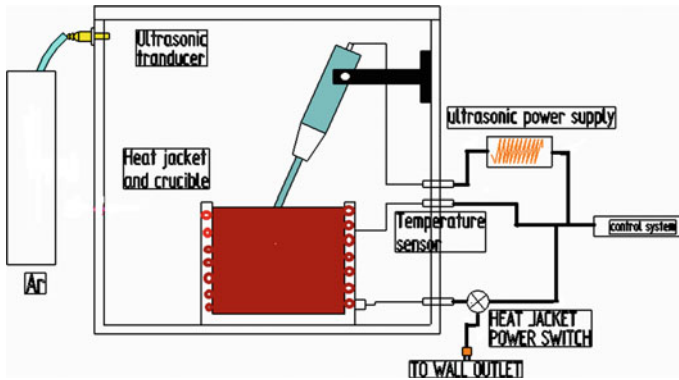


Fig. 1 Ultrasonic stir casting

The Ultrasonic stir casting is relatively simple and decreases the porosity in composites. This process improves the mechanical properties and its vibration creates the homogenous distribution of particles.

For the convenience some of the important reported works are also presented in tabular form as given Tables 1, 2 and 3; Fig. 2.

The Microstructure is seen in SEM. Figure 3 shows the microstructure of with and without Ultrasonic treatment of Al5083+ 10 wt% TiC. The range of TiC particles are 1–5 μm . In the same location Clustering of particle was also observed. Ultrasonic treatment of the alloy and composites melt led to refinement of grains size and homogenous distribution of TiC particles.

4 Coatings

The metal matrix composites satisfied the thermal, physical, chemical and mechanical properties. The wear resistance is very low. To improve the wear resistance and to increase the performance of IC engine by coating the cylinder block with antifriction and anti-wear Nano-coatings.

Some of the coatings are mostly used for improving wear resistance

1. StainlessSpray
2. Chromeboride
3. Tungstencarbide
4. Molybdenum
5. TitaniumOxide
6. Stellite
7. WC-Co-Cr
8. Cr_2O_3 (Ceramic)
9. Al_2O_3 - TiO_2 (Ceramic)

Table 1 Comparison study of different aluminum composites and results

S. No.	Composition	Elongation %	Compression strength (M Pa)	UTS (M Pa)	Hardness (BHN)	References
1	Al-7075		265	210	115	[19]
2	Al-7075 + 2%Al ₂ O ₃		270	219	117	
3	Al-7075 + 4% Al ₂ O ₃		275	226	121	
4	Al-7075 + 6% Al ₂ O ₃		283	229	124	
5	Al-7075 + 8% Al ₂ O ₃		294	236	134	
6	Al6061-1% Graphite	7.31	847.9	173.8	44.58	[20]
7	Al6061-2% Graphite	8.47	946.1	181.2	40.64	
8	Al6061-3% Graphite	8.6	1028.72	182.1	39.98	
9	Al6061-4% Graphite	9.4	1067.21	191.65	37.38	
10	Al(LM25) + 0Al ₂ O ₃ + 3%FA	7.1		136	57.2	[21]
11	Al(LM25) + 5Al ₂ O ₃ + 3%FA	5.3		162	61	
12	Al(LM25) + 10Al ₂ O ₃ + 3%FA	4		187	61.8	
13	Al(LM25) + 15Al ₂ O ₃ + 3%FA	2.4		168	62	

1. StainlessSpray:

These coatings are suitable for resistance to abrasive wear, corrosion and erosion. Stainless steel 316 and stainless steel 316 L afford the high wear resistance and corrosion resistance to form small pits on a surface. The stainless steel-II showed the lower friction coefficients compared to uncoated material.

2. Chrome boride:

The chrome boride is also known as chromium mono boride. It is very hard, high strength and conducts electricity and heat. These properties are creating the additional strength to the material and overcome the wear to increase the life of the material.

Table 2 Mechanical properties of Al 5083 (monolithic material) and Al 5083 reinforced with SiC with and without ultrasonic treatment

S. No.	Composition	Tensile strength		% Increment		Compression strength (MPa)		% Increment	References
		Without ultrasonic treatment	With ultrasonic treatment	Without ultrasonic Treatment	With ultrasonic treatment	Without ultrasonic Treatment	With ultrasonic treatment		
1	Al5083 + 0% SiC	223.4	228.6	2.32	312	324	3.84	[22]	
2	Al5083 + 3% SiC	227	236.49	4.18	319	332.8	4.14		
3	Al5083 + 5% SiC	231.8	240.75	3.86	320.8	337	5.04		
4	Al5083 + 8% SiC	234	250.64	7.11	330.8	344.8	4.23		
5	Al5083 + 10% SiC	238.4	254.9	6.92	336	350	4.16		

Table 3 Mechanical properties of Al 5083 (monolithic material) and Al 5083 reinforced with TiC with and without ultrasonic treatment

S. No.	Composition	Compression strength (MPa)		% Increment	Hardness (BHN)		% Increment	References
		Without ultrasonic treatment	With ultrasonic treatment		Without ultrasonic treatment	With ultrasonic treatment		
1	Al5083	236.82	439.4	85.5	63 ± 1.6	80 ± 2	26.9	[23]
2	Al5083 + 5 wt.% TiC	251.62	421.47	67.5	74 ± 7.1	82 ± 6	10.81	
3	Al5083 + 10 wt.% TiC	277.79	416.1	49.7	92 ± 14.2	93 ± 12	1	

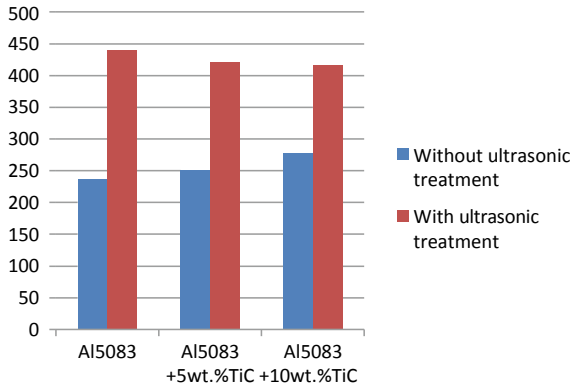


Fig. 2 Shows the compressive strength of specimen of different wt% of TiC for with and without ultrasonic treatment in bar graph

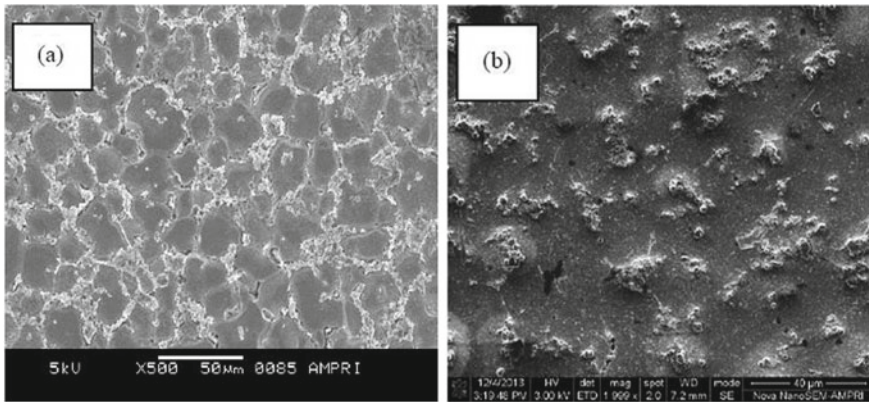


Fig. 3 Microstructure of **a** Al5083-10 wt.% TiC composite with ultrasonic and **b** aluminum 5083-10 wt.% TiC composite without ultrasonic treatment

CrB is used as candidate material for wear resistant coatings and high temperature diffusion barriers.

3. Tungsten carbide:

The chemical compound of tungsten carbide holds equal parts of tungsten and carbon atoms. The HVOF thermal spray process produces large amount of K. Einto the coated powder particles. The results of these coatings improve the low residual stress, high bond strength, high wear resistance, good corrosion resistance and low porosity.

4. **Molybdenum:**

Molybdenum cannot be used on copper, >20% Cu alloys, chromed or nitrated parts. However, Molybdenum can and is used on hardened base agents to obtain improved sealing properties. Molybdenum Coatings are not suitable due to very low micro hardness values.

5. **TitaniumOxide:**

Titania is another name of titanium oxide. The chemical formula is TiO_2 . The major part of titanium oxide consumption (80%) used as some important applications. The application areas are paints, varnishes and paper and plastics. The other applications are such as printing inks, fibers, rubber, cosmetic products and food.

6. **Stellite:**

The stellite alloys mainly consist of carbon and small amount of tungsten or molybdenum. It is designed for wear resistance. And other properties of stellite alloys are corrosion resistance and withstand high temperatures.

7. **Tungsten Carbide cobalt(WC-Co-Cr):**

The combination of WC-Co-Cr coatings improved the corrosion resistance, adhesion and wear performance. It is widely used in industry applications. The WC-Co Cr coatings are also used as an alternative to hard chromium plating.

8. **Chromium Oxide(Cr_2O_3):**

The Chromium oxide coatings are used as industrial coatings. Another name is black oxide coatings. These coatings have self-mating, anti-galling properties. The material is mostly recommended for wear resistance and corrosion resistance.

9. **Al_2O_3 - TiO_2 :**

The Aluminum oxide and titanium dioxide coatings mostly used in industry. It improves the mechanical, electrical properties and improves the wear resistance [24].

V. Rajini kanth et al., investigated on WC coating to test sliding wear behavior. Four different combinations of specimens are tested on pin on disc apparatus. In addition to the spraying parameters, the degree of decomposition of WC and the carbide size energetically affected the microstructure of the coating. Thus, HVOF sprayed coatings give the low porosity. For dry sliding conditions, WC coating is used for protection of wear resistance [25].

Ying Chun Zhu et al., The nanostructure WC coating was prepared with the vacuum plasma spraying processes. The structure of the coating was determined with SEM, TEM and XRD. The results show that particular WC grain size of 35 nm is equal to grain size of the primary powders. In some locations the grain size of WC reduced to about the 10 nm embedded in an incomplete matrix. This is formed

by the melting of the WC-CO powders. In some areas the grain size increased to 100 nm. Whereas the second recrystallization developed, strip shaped and square shaped structures are created. The minor phases of the coatings are α -W₂C, β -WC_{1-x}, and W₃Co₃C. The hardness of Nano WC-CO coating is improved compared to the conventional WC-CO coatings [26].

Aleksandar Vencl et al., done research on Atmospheric plasma spraying method (APS). This method is used to find tribological properties. In this paper two types of ferrous thermal spray coatings were investigated on pin on ring tribometer. The coatings A and B consist of iron oxides with magnetite (Fe₃O₄) and wustite (FeO). The hardness of coating A was greater than the coating B and it is also improved the tribological properties. The test results showed that both coatings had acceptable values of wear and friction. The APS process is used to solve the tribological effects of aluminum material. So the lightweight aluminum is best permutation for gray castiron [27].

Zhang Xiao-feng et al., studied microstructure and properties of HVOF sprayed Ni- based submicron WS₂/CaF₂ self-lubricating composite coating. The submicron powder is produced in a ball milling equipment. The self-lubricating composite coatings have low hardness value and low adhesive strength due to the many holes and micro cracks. The two types of coatings taken to test the friction coefficient. The compositions of coatings are Ni45-5%CaF₂-10%WS₂ and Ni45-10%CaF₂-5%WS₂ (mass fraction). Minimum friction coefficient produces the Ni45-10%CaF₂-5%WS₂ composition, i.e., 0.32–0.38 [28].

K. Włodarczyk et al., done research on Nano composite coatings. To enhance the low friction and wear resistant to use the Nano crystallite of chromium or titanium. The tests are carried out for nc-CrC/a-C(:H) and nc-TiC/a-C(:H) coatings. The coatings deposited by magnetron sputtering illustrate the superior tribological properties. The Hardness of nc- TiC/a-C and nc-TiC/a-C:H coatings is 15–20 GPa. The Hardness of nc-CrC/a-C and nc-CrC/a-C:H coatings is 15–17 GPa [29].

Ankit Tyagiet al., studied about that deposition of DLC/CNTs coatings on the substrate materials improves wear, corrosion and mechanical properties of the substrate. Selection of substrate material is very important role on the coatings [30].

5 Conclusion

From the study it is concluded that best results are noticed in 12% of SiC addition in composite material [2] it improved the mechanical properties. The most economical fabrication method of metal matrix composites are stir casting but it gives some limitations .i.e., distribution of dispersed phase throughout matrix is not perfectly homogenous. The combination of stir casting with ultrasonic vibration improves the mechanical properties. It gives good dispersion of the reinforcement particles within the Aluminum matrix [23].

The anti-friction and anti-wear Nano-coatings improved the wear resistance. Based on the survey these coatings improved the tribological properties. The High

Velocity Oxy-Fuel (HVOF) Tungsten Carbide cobalt (WC-Co) coatings give best results and create the high dense, zero porosity and wear resistant surfaces [26].

References

1. Raghavendra, N., Ramamurthy, V.S.: Effect of particle size and weight fraction of alumina reinforcement on wear behavior of aluminum metal matrix composites. *Int. J. Innov. Res. Sci. Eng. Technol.* **3**(4) (2014)
2. Mohanakumara, K.C., Rajeshkar, H., Ghanaraja, S., Ajitprasad, S.L.: Development and mechanical properties of SiC reinforced cast and extruded Al based metal matrix composite. In: *International Conference on Advances in Manufacturing and Materials Engineering*, pp. 934–943 (2014)
3. Mali, A., Sonawane, S.A., Dombale, S.: Effect of hybrid reinforcement on mechanical behavior of aluminum matrix composite. *J. Eng. Res. Technol. (IJERT)* **4**(1) (2015)
4. Suragimath, P.K., Purohit, G.K.: A study on mechanical properties of aluminum alloy (LM6) reinforced with SiC and Fly Ash. *8*(5):13–18 (2013)
5. James, S.J., Venkatesan, K., Kupan, P., Ramanujam, R.: Hybrid aluminum metal matrix composite reinforced with SiC and TiB₂. In: *12th Global Congress on Manufacturing and Management, Procedia Engineering vol. 97*, pp. 1018–1026 (2014)
6. Raveendra, R.S., Krupakara, P.V., Prashanth, P.A., Nagabhushana, B.M.: Enhanced mechanical properties of Al-6061 metal matrix composites reinforced with α -Al₂O₃ nanoceramics. *J. Mater. Sci. Surface Eng.* **4**(7), 483–487 (2016)
7. Roomey, R.K.S.M., Haque, M.E., Sabiha Akhter: Development and analysis of Fly Ash reinforced aluminum alloy matrix composites. *Am. J. Eng. Res. (AJER)* **6**(12), 334–339
8. Nassar, A.E., Nassar, E.E.: Properties of aluminum matrix Nano composites prepared by powder metallurgy processing. *J. King Saud Univ. Eng. Sci.* **29**, 295–299 (2017)
9. ErvinaEftzan, M.N., SitiSyazwani, N., Abdullah, M.M.A.B.: Microstructure and mechanical properties of Fly Ash particulate reinforced in LM6 for energy enhancement in automotive applications. *Mater. Sci. Eng.* **133**, 012046 (2016)
10. Sharma, V.K., Singh, R.C., Chaudhary, R.: Effect of fly ash particles with aluminum melt on the wear of aluminum metal matrix composites. *Eng. Sci. Technol. Int. J* **20**, 1318–1323 (2017)
11. Stojanovic, B., Ivanovic, L.: Application of aluminum hybrid composites. In: *Automotive Industry, Research gate*. <https://doi.org/10.17559/tv-20130905094303>
12. Panwara, N., Chauhan, A.: Fabrication methods of particulate reinforced aluminum metal matrix composite-a review. *Mater. Today Proc.* **5**, 5933–5939 (2018)
13. Walczak, M., Zwierzchowski, M., Bienias, J., Caban, J.: The tribological characteristics of Al-Si/Graphite composite. *Tribologia* **1**(207), 97–104
14. Vinoth, M.A., Arun, L.R., Patil, B.: The fabrication process and mechanical characterization of pure Al-Si MMC's for engine applications. *Int. J. Innov. Res. Sci. Eng. Technol.* **3**(6), (2014)
15. Kuruvilla, A.K., Bhanuprasad, V.V., Prasad, K.S., Mahajan, Y.R.: Effect of different reinforcements on composite strengthening in aluminum. *Mater. Sci.* **12**(5) 495–505 (1989)
16. Santos, H.O., Costa, I., Rossi, J.L.: Mechanical and microstructural characterization of cylinder liners. *Powder Processing Centre - CPPP. O. Box 11049-CEP05422-970*
17. Devaganesh, S., Dinesh Kumar, P.K., Venkatesh, N., Balaji, R.: Study on the mechanical and tribological performances of hybrid SiC-Al7075 metal matrix composites, *J. Mater. Res. Technol.* **9**(3):3759–3766 (2020)
18. Shuvho, M.B.A., Chowdhury, M.A., Hossain, N., Roy, B.K., Kowser, M.A., Islam, A.: Tribological study of Al-6063-based metal matrix embedded with SiC–Al₂O₃–TiO₂ particles. *SN Appl. Sci.* (2020)
19. Hariharan, V., Mohankumar, P., Gnaneswaran, A Review on Tribological And Mechanical Behaviors of Aluminium Metal Matrix Composites, *Int. J. Mech. Eng. Rob. (IJMER)* **2**(6), (2014). ISSN (Print): 2321–5747

20. Ramesh, A., Prakash, J.N., Gowda, A.S.S., Appaiah, S.: Comparison of the mechanical properties of AL6061/albite and AL6061/graphite metal matrix composites. *J. Minerals Mater. Charact. Eng.* **8**(2):93–106 (2009)
21. Patil, S.R., Motgi, B.S.: Study on mechanical properties of Fly Ash and alumina reinforced aluminium alloy (LM25) composites. **7**(6):PP41–46 (2013)
22. Idrisi, A.H., Singh, V.D., Saxena, V.: Development and testing of Al5083 alloy reinforced by SiC particles. *Int. J. Sci. Res. Eng. Technol. (IJSRET)* **2**(11):697–704 (2014). www.ijret.org ISSN 2278 – 0882
23. Patela, K.K., Kumarb, V., Purohitb, R., Guptaa, G.K.: Effect of ultrasonic stirring on changes in microstructure and mechanical properties of cast insitu Al 5083 alloy composites containing 5wt.% and 10wt.% TiC particles. *Mater. Today Proc.* **4**, 3494–3500 (2017)
24. Malyshev, V.N., Volkhin, A.M., Gantimirov, B.M.: Tribological characteristics improvement of wear resistant MAO-coatings. *J. Coat.* **5** (2013). Article ID 262310
25. Rajinikanth, V., Venkateswarlu, K.: An investigation of sliding wear behavior of WC–Co coating. *Tribol. Int.* **44**, 1711–1719 (2011)
26. Zhua, Y.C., Dingb, C.X., Yukimurac, K., Xiao, T.D., Strutt, P.R.: Deposition and characterization of nanostructured WC–Co coating. *Ceram. Int.* **27**, 669–674 (2001)
27. Venci, A., Mrdak, M., Cvijović, I.: Microstructures and tribological properties of ferrous coatings deposited by APS (atmospheric plasma spraying) on Al-alloy substrate. *FME Trans.* **34**, 151–157 (2006)
28. Zhang, X.-F., Zhang, X.-L., Wang A.-H., Huang Z.-W.: Microstructure and properties of HVOF sprayed Ni-based submicron WS₂/CaF₂ self-lubricating composite coating. *Trans. Nonferrous Meter. Soc. China* **19**, 85–92 (2009)
29. Włodarczyk, K., Makówka, M., Nolbrzak, P., Wendler, B.: Low friction and wear resistant nanocomposite nc-MeC/a-C and nc-MeC/a-C:H coatings. *J. Achievements Mater. Manufact. Eng.* **37**(2) (2009)
30. Tyagi, A., Walia, R.S., Murtaza, Q., Pandey, S.M., Tyagi, P.K., Bajaj, B.: Critical review of diamond like carbon coating for wear resistance applications. *Int. J. Refract Metals Hard Mater. Rmhm* (2018). <https://doi.org/10.1016/j.ijrmhm.2018.09.006>

Selection of Suppliers by Weighted Aggregated Sum Product Assessment (WASPAS) Method



Shankha Shubhra Goswami  and Dhiren Kumar Behera 

Abstract Selection of an efficient supplier has always been a tough task in the arena of logistics management. The performance of a supplier depends on several factors that enables the researchers to consider this as a multi-criteria decision making (MCDM) problem. The goal of this research paper is to propose the most efficient supplier among 18 available alternatives on the basis of 5 performance criteria namely, price, distance, quality, supply variety and delivery performance by implementing analytic hierarchy process (AHP) to evaluate the criteria weights and weighted aggregated sum product assessment (WASPAS) to rank the alternatives. The results obtained shows that, supplier 10 and supplier 7 is the best and the worst choice, respectively among these 18 suppliers. On comparing with the previous researchers existing results executed by COPRAS and TOPSIS, it is observed that there are differences in the preference order of the alternatives, but the best and worst choice of suppliers remains same in all methods.

Keywords MCDM · AHP · Supplier selection · WAPAS

1 Introduction

Supplier selection problem now a days has become one of the core areas of interest for the decision maker (DM) to execute with the help of MCDM tools, as it involves several conflicting criteria for its efficient selection. Proper selection of a supplier is very much crucial for an engineering firm, as it is equally important with respect to other factors for the success of every industrial concern [1]. Lots of researchers successfully implemented different MCDM tools for the supplier selection in the last few years and some of the applications are stated as follows.

S. S. Goswami (✉) · D. K. Behera
Indira Gandhi Institute of Technology, Sarang, Dhenkanal 759146, Odisha, India
e-mail: ssg.mech.official@gmail.com

D. K. Behera
e-mail: dkb_igit@rediffmail.com

© The Author(s), under exclusive license to Springer Nature Singapore Pte Ltd. 2021
B. Deepak et al. (eds.), *Advanced Manufacturing Systems and Innovative Product Design*,
Lecture Notes in Mechanical Engineering,
https://doi.org/10.1007/978-981-15-9853-1_11

117

Liu et al. [2] applied DEA for the supplier selection in a manufacturing firm. Shyur and Shih [3] developed a hybrid MCDM model of TOPSIS and ANP for deliberate vendor selection. Onut et al. [4] developed a supplier estimation approach in the GSM sector based on TOPSIS and ANP methods to help a Turkish telecommunication company under the fuzzy environment. Singh [5] evaluated and selected the most efficient supplier in fuzzy environment for television manufacturing organization using TOPSIS MCDM approach. Kilic [6] proposed an integrated approach of fuzzy-TOPSIS for choosing appropriate supplier in multi-supplier environment. Madic et al. [1] applied COPRAS method for estimating the performances of the suppliers. Murali et al. [7] analyzed a supplier selection problem by PROMETHEE and TOPSIS.

Nallusamy et al. [8] studied the applications of AHP, fuzzy logic and ANN for efficient supplier selection in manufacturing industries. Adali et al. [9] applied an alternative version of fuzzy-PROMETHEE for the selection of best supplier. Yazdani et al. [10] delivered a combined model for solving supplier selection problem using WASPAS, SWARA and QFD. Guchhait [11] solved a supplier evaluation problem by MOORA, SAW and TOPSIS method. Assellaou et al. [12] investigated a supplier selection problem of an African well-known refining company using a hybrid DEMATEL-ANP-TOPSIS methodology. Stojic et al. [13] implemented rough AHP to determine the weight coefficients of the criteria and rough WASPAS to rank the suppliers in a PVC producing company.

Bhakat and Raja [14] considered a case study of a Turkish textile company, where grey-AHP model is used for weighting the set of conflicting criteria and grey-WASPAS model for ordering the suppliers. Jayant et al. [15] presented a hybrid combination of WASPAS and MOORA MCDM procedures for vendor assessment and SWARA to evaluate the criteria weights in a battery manufacturing industry. Koganti et al. [16] proposed a MCDM model for supplier selection using GRA to pick out the proper criterions from existing options, AHP to determine the criteria weights and TOPSIS for the final selection process.

Apart from these, WASPAS technique is also applied in other areas like, Zavadskas et al. [17] presented a case study to rank the facades for commercial and public buildings by WPM, WSM, WASPAS and later it was examined by comparing to MOORA. Zavadskas et al. [18] applied WASPAS method for the assessment of alternative building designs and the robustness of the method is validated by applying MOORA and MULTIMOORA. Chakraborty and Zavadskas [19] explored eight manufacturing problems using WASPAS technique.

Karande et al. [20] investigated the ranking efficiency of six MCDM methods i.e. WASPAS, MOORA, MULTIMOORA, WPM and WSM using two industrial robot selection problems. Mathew and Sahu [21] solved two material handling equipment selection problem using 4 MCDM techniques i.e. WASPAS, EDAS, MOORA and CODAS. Badalpur and Nurbakhsh [22] considered an Iranian road construction project, where WASPAS is utilized for the risk assessment. Vinchurkar and Samtani [23] evaluated the performance of four different hydro-powerhouses by integrating SWARA for determining the criteria weights and WASPAS, TOPSIS, PROMETHEE to access the performance score of the alternatives.

From the above-mentioned literatures, it is clear that WASPAS method is very less utilized MCDM tool in the area of supplier selection and therefore needs to be explored more in-depth. Hence, WASPAS is adopted and applied to an existing supplier selection problem first presented by Liu et al. [2]. Later, it was further considered by Madic et al. [1] and evaluated using COPRAS method. In this paper, the criteria weights [1] and the decision matrix [1, 2] are taken from [1] and WASPAS is applied to fulfill the research gap. The output results are also compared with the previous researcher’s outcomes which shows very minor differences among the ranking orders. Overall, solving a supplier selection problem with the help of WASPAS method for the first presents the novelty of this research work.

2 Materials and Methods

To start with the calculation procedure, firstly, it is required to determine the criteria weights which is done by using AHP [24]. The weights of the 5 criteria are taken from the article presented by Madic et al. [1] through AHP is as follows: $w_{price} = 0.1361$, $w_{distance} = 0.0438$, $w_{quality} = 0.4829$, $w_{supply\ variety} = 0.0782$, $w_{delivery\ performance} = 0.2591$. Now, starting with the WASPAS [25] method which is included under the Sect 2.1.

2.1 Weighted Aggregated Sum Product Assessment (WASPAS)

In WASPAS method, a joint generalized criterion shown by Eq. 7 was proposed by Zavadskas et al. [25] which combines WSM [26–28] and WPM [28, 29] together. According to Karande et al. (pp. 402–403) [20] ‘it is applied for increasing ranking accuracy and it has the capability to reach the highest accuracy of estimation’. The WASPAS method steps are as follows.

Step 1: Create a performance evaluation matrix (decision matrix) having ‘m’ alternatives and ‘n’ criteria according to Eq. 1. The decision matrix as originally proposed by Liu et al. [2] is shown in Table 1.

$$D(m_i \times n_j) \begin{bmatrix} d_{11} & d_{12} & \dots & d_{1n} \\ d_{21} & d_{22} & \dots & d_{2n} \\ \dots & \dots & \dots & \dots \\ d_{m1} & d_{m2} & \dots & d_{mn} \end{bmatrix} \tag{1}$$

where, $i = 1, 2, \dots, m; j = 1, 2, \dots, n$.

Step 2: Normalize the decision matrix by using Eqs. 2 or 3 according to the nature of the criteria.

Table 1 Performance matrix

Types	Min	Min	Max	Max	Max
	Price (\$)	Distance (miles)	Quality (%)	Supply variety	Delivery performance (%)
S1	100	249	100	2	90
S2	100	643	99.79	13	80
S3	100	714	100	3	90
S4	100	1809	100	3	90
S5	100	238	99.83	24	90
S6	100	241	96.59	28	90
S7	100	1404	100	1	85
S8	100	984	100	24	97
S9	100	641	99.91	11	90
S10	100	588	97.54	53	100
S11	100	241	99.95	10	95
S12	100	567	99.85	7	98
S13	100	567	99.97	19	90
S14	100	967	91.89	12	90
S15	80	635	99.99	33	95
S16	100	795	100	2	95
S17	80	689	99.99	34	95
S18	100	913	99.36	9	85
Ideal value	80	238	100	53	100

Source Liu et al. [2]; Madic et al. [1]

$$\text{Maximum criteria, } N_{ij} = \frac{d_{ij}}{d_i^{\max}} \tag{2}$$

$$\text{Minimum criteria, } N_{ij} = \frac{d_i^{\min}}{d_{ij}} \tag{3}$$

where, $i = 1, 2, \dots, m; j = 1, 2, \dots, n$.

' d_i^{\max} ' and ' d_i^{\min} ' are the maximum and the minimum values of the i th criteria respectively. Table 2 shows the normalized decision matrix.

Step 3: Now calculate the weighted sum (WS_i) of each alternative using Eq. 4. The weighted sum is determined for all the alternatives and shown in Table 3.

$$WS_i = \sum_{j=1}^n N_{ij}w_j \tag{4}$$

where, $i = 1, 2, \dots, m; j = 1, 2, \dots, n$.

Table 2 Normalized matrix

	Price (\$)	Distance (miles)	Quality (%)	Supply variety	Delivery performance (%)
Weights	0.1361	0.0438	0.4829	0.0782	0.2591
S1	0.8	0.9558	1	0.0377	0.9
S2	0.8	0.3701	0.9979	0.2453	0.8
S3	0.8	0.3333	1	0.0566	0.9
S4	0.8	0.1316	1	0.0566	0.9
S5	0.8	1	0.9983	0.4528	0.9
S6	0.8	0.9876	0.9659	0.5283	0.9
S7	0.8	0.1695	1	0.0189	0.85
S8	0.8	0.2419	1	0.4528	0.97
S9	0.8	0.3713	0.9991	0.2075	0.9
S10	0.8	0.4048	0.9754	1	1
S11	0.8	0.9876	0.9995	0.1887	0.95
S12	0.8	0.4198	0.9985	0.1321	0.98
S13	0.8	0.4198	0.9997	0.3585	0.9
S14	0.8	0.2461	0.9189	0.2264	0.9
S15	1	0.3748	0.9999	0.6226	0.95
S16	0.8	0.2994	1	0.0377	0.95
S17	1	0.3454	0.9999	0.6415	0.95
S18	0.8	0.2607	0.9936	0.1698	0.85

Source Author himself

' N_{ij} ' is the normalized value of the i th alternative and j th criteria, ' w_j ' is the weight of the j th criteria and ' WS_i ' is the weighted sum of the i th alternative.

Step 4: Now calculate the weighted product (WP_i) of each alternative using Eq. 5. The weighted product is determined for all the alternatives and shown in Table 4.

$$WP_i = \prod_{j=1}^n N_{ij}^{w_j} \tag{5}$$

where, $i = 1, 2, \dots, m; j = 1, 2, \dots, n$.

' N_{ij} ' is the normalized value of the i th alternative and j th criteria, ' w_j ' is the weight of the j th criteria and ' WP_i ' is the weighted product of the i th alternative.

Step 5: Now determine the joint generalized criterion (Q_i) of each alternative by using Eq. 6 [17, 18].

Table 3 Weighted sum of the alternatives

	Price (\$)	Distance (miles)	Quality (%)	Supply variety	Delivery performance (%)	Weighted sum (WS _i)
S1	0.1089	0.0419	0.4829	0.0030	0.2332	0.8698
S2	0.1089	0.0162	0.4819	0.0192	0.2073	0.8334
S3	0.1089	0.0146	0.4829	0.0044	0.2332	0.8440
S4	0.1089	0.0058	0.4829	0.0044	0.2332	0.8352
S5	0.1089	0.0438	0.4821	0.0354	0.2332	0.9034
S6	0.1089	0.0433	0.4664	0.0413	0.2332	0.8931
S7	0.1089	0.0074	0.4829	0.0015	0.2202	0.8209
S8	0.1089	0.0106	0.4829	0.0354	0.2513	0.8891
S9	0.1089	0.0163	0.4825	0.0162	0.2332	0.8570
S10	0.1089	0.0177	0.4710	0.0782	0.2591	0.9349
S11	0.1089	0.0433	0.4827	0.0148	0.2461	0.8957
S12	0.1089	0.0184	0.4822	0.0103	0.2539	0.8737
S13	0.1089	0.0184	0.4828	0.0280	0.2332	0.8712
S14	0.1089	0.0108	0.4437	0.0177	0.2332	0.8143
S15	0.1361	0.0164	0.4829	0.0487	0.2461	0.9302
S16	0.1089	0.0131	0.4829	0.0030	0.2461	0.8540
S17	0.1361	0.0151	0.4829	0.0502	0.2461	0.9304
S18	0.1089	0.0114	0.4798	0.0133	0.2202	0.8336

Source Author himself

$$\begin{aligned}
 Q_i &= 0.5(WS_i) + 0.5(WP_i) \\
 &= 0.5 \sum_{j=1}^n N_{ij}w_j + 0.5 \prod_{j=1}^n N_{ij}^{w_j}
 \end{aligned}
 \tag{6}$$

where, $i = 1, 2, \dots, m; j = 1, 2, \dots, n$ and ‘ Q_i ’ is the joint criterion of the i th alternatives.

Saparauskas et al. [30] and Zavadskas et al. [25] proposed a more generalized formula to increase the effectiveness and the ranking accuracy of the method [19] which is shown by Eq. 7.

$$\begin{aligned}
 Q_i &= \lambda(WS_i) + (1 - \lambda)(WP_i) \\
 &= \lambda \sum_{j=1}^n N_{ij}w_j + (1 - \lambda) \prod_{j=1}^n N_{ij}^{w_j}
 \end{aligned}
 \tag{7}$$

where, $i = 1, 2, \dots, m; j = 1, 2, \dots, n$.

‘ λ ’ is a constant and its values ranges from 0 to 1. $\lambda = 0, 0.1, 0.2, 0.3, \dots, 1$.

Table 4 Weighted product of the alternatives

	Price (\$)	Distance (miles)	Quality (%)	Supply variety	Delivery performance (%)	Weighted product (WP _i)
S1	0.9701	0.9980	1	0.7739	0.9731	0.7291
S2	0.9701	0.9574	0.9990	0.8959	0.9438	0.7846
S3	0.9701	0.9530	1	0.7989	0.9731	0.7187
S4	0.9701	0.9150	1	0.7989	0.9731	0.6900
S5	0.9701	1	0.9992	0.9399	0.9731	0.8865
S6	0.9701	0.9995	0.9834	0.9513	0.9731	0.8826
S7	0.9701	0.9252	1	0.7331	0.9588	0.6308
S8	0.9701	0.9397	1	0.9399	0.9921	0.8501
S9	0.9701	0.9575	0.9996	0.8843	0.9731	0.7989
S10	0.9701	0.9612	0.9880	1	1	0.9213
S11	0.9701	0.9995	0.9998	0.8777	0.9868	0.8396
S12	0.9701	0.9627	0.9993	0.8536	0.9948	0.7924
S13	0.9701	0.9627	0.9999	0.9229	0.9731	0.8386
S14	0.9701	0.9404	0.9600	0.8903	0.9731	0.7588
S15	1	0.9579	1	0.9636	0.9868	0.9109
S16	0.9701	0.9485	1	0.7739	0.9868	0.7027
S17	1	0.9545	1	0.9659	0.9868	0.9097
S18	0.9701	0.9428	0.9969	0.8705	0.9588	0.7610

Source Author himself

From the Eqs. 6 and 7 it can be observed that, if the value of λ is 0 then the first part gets eliminated and it is converted into WPM and if λ is 1 then it is converted into WSM [19, 20].

The joint generalized criterion (Q_i) of each alternative is calculated for every λ values using Eq. 7 and shown in Table 5.

3 Results and Discussion

This section includes the outcome results and ranking of the supplier. Table 5 shows the joint generalized criteria of the 18 alternatives for every λ values. Now the supplier with the highest Q_i value is termed as the best one and the ranking is proposed according to the decreasing Q_i values. However, 11 alternative rankings can be made for the eleven individual cases which are depicted in Table 6.

From Table 6, the variations in the rankings can be observed for different λ values and it can also be noted that the best choice supplier is same for all the λ values. However, it is recommended to consider the ranking for $\lambda = 0.5$ as the final ranking by

Table 5 Joint criterion of each alternative for different ‘λ’ values

	λ = 0	λ = 0.1	λ = 0.2	λ = 0.3	λ = 0.4	λ = 0.5	λ = 0.6	λ = 0.7	λ = 0.8	λ = 0.9	λ = 1
S1	0.7291	0.7432	0.7573	0.7713	0.7854	0.7995	0.8135	0.8276	0.8417	0.8557	0.8698
S2	0.7846	0.7894	0.7943	0.7992	0.8041	0.8090	0.8139	0.8188	0.8237	0.8286	0.8334
S3	0.7187	0.7312	0.7437	0.7563	0.7688	0.7813	0.7939	0.8064	0.8189	0.8315	0.8440
S4	0.6900	0.7045	0.7190	0.7335	0.7481	0.7626	0.7771	0.7916	0.8061	0.8206	0.8352
S5	0.8865	0.8882	0.8899	0.8916	0.8933	0.8949	0.8966	0.8983	0.9000	0.9017	0.9034
S6	0.8826	0.8837	0.8847	0.8857	0.8868	0.8878	0.8889	0.8899	0.8910	0.8920	0.8931
S7	0.6308	0.6499	0.6689	0.6879	0.7069	0.7259	0.7449	0.7639	0.7829	0.8019	0.8209
S8	0.8501	0.8540	0.8579	0.8618	0.8657	0.8696	0.8735	0.8774	0.8813	0.8852	0.8891
S9	0.7989	0.8048	0.8106	0.8164	0.8222	0.8280	0.8338	0.8396	0.8454	0.8512	0.8570
S10	0.9213	0.9226	0.9240	0.9254	0.9267	0.9281	0.9295	0.9308	0.9322	0.9336	0.9349
S11	0.8396	0.8452	0.8508	0.8564	0.8620	0.8676	0.8732	0.8789	0.8845	0.8901	0.8957
S12	0.7924	0.8006	0.8087	0.8168	0.8249	0.8331	0.8412	0.8493	0.8574	0.8656	0.8737
S13	0.8386	0.8418	0.8451	0.8484	0.8516	0.8549	0.8582	0.8614	0.8647	0.8680	0.8712
S14	0.7588	0.7643	0.7699	0.7754	0.7810	0.7865	0.7921	0.7976	0.8032	0.8087	0.8143
S15	0.9109	0.9128	0.9147	0.9167	0.9186	0.9205	0.9225	0.9244	0.9263	0.9283	0.9302
S16	0.7027	0.7179	0.7330	0.7481	0.7632	0.7784	0.7935	0.8086	0.8237	0.8389	0.8540
S17	0.9097	0.9118	0.9139	0.9159	0.9180	0.9201	0.9221	0.9242	0.9263	0.9283	0.9304
S18	0.7610	0.7683	0.7755	0.7828	0.7900	0.7973	0.8046	0.8118	0.8191	0.8264	0.8336

Source Author himself

WASPAS [19] since, equal priority should be given to both WSM and WPM methods. Table 7 shows the ranking comparisons of the suppliers by COPRAS, TOPSIS and WASPAS method and Fig. 1 represents the ranking comparisons graphically. A final ranking of the suppliers is also proposed following Copeland voting method which is also provided in Table 7. Spearman rank correlation coefficient among the three rankings obtained from three different methods are also given in Table 8. The final ranking obtained from this analysis is as follows.

S10 > S17 > S15 > S6 > S5 > S8 > S13 > S11 > S12 > S9 > S2 > S1 > S18 > S16 > S14 > S3 > S4 > S7

From Table 8, it can be observed that the proposed rankings hold a good Spearman rank correlation coefficient among each other and there are not many differences in the ranking orders as depicted in Table 7. So, it is quite tough to judge and give opinion about the best one among them. But, if we notice the rank coefficient between the final ranking and the other methods, then it is clear that TOPSIS and WASPAS are coming out with the highest coefficient, i.e., 0.98762, which is enough to consider these two methods as the most robust and gives more accurate results compared to COPRAS.

Table 6 Ranking of the alternatives for different λ values

	$\lambda = 0$	$\lambda = 0.1$	$\lambda = 0.2$	$\lambda = 0.3$	$\lambda = 0.4$	$\lambda = 0.5$	$\lambda = 0.6$	$\lambda = 0.7$	$\lambda = 0.8$	$\lambda = 0.9$	$\lambda = 1$
S1	14	14	14	14	13	12	12	11	11	10	10
S2	11	11	11	11	11	11	11	12	13	14	16
S3	15	15	15	15	15	15	14	15	15	13	13
S4	17	17	17	17	17	17	17	17	16	16	14
S5	4	4	4	4	4	4	4	4	4	4	4
S6	5	5	5	5	5	5	5	5	5	5	6
S7	18	18	18	18	18	18	18	18	18	18	17
S8	6	6	6	6	6	6	6	7	7	7	7
S9	9	9	9	10	10	10	10	10	10	11	11
S10	1	1	1	1	1	1	1	1	1	1	1
S11	7	7	7	7	7	7	7	6	6	6	5
S12	10	10	10	9	9	9	9	9	9	9	8
S13	8	8	8	8	8	8	8	8	8	8	9
S14	13	13	13	13	14	14	16	16	17	17	18
S15	2	2	2	2	2	2	2	2	2	3	3
S16	16	16	16	16	16	16	15	14	12	12	12
S17	3	3	3	3	3	3	3	3	3	2	2
S18	12	12	12	12	12	13	13	13	14	15	15

Source Author himself

4 Conclusion

It can be concluded from the above analysis that supplier 10 is the best option and supplier 7 is the worst choice among these 18 available alternatives. WASPAS is more effective method than WPM and WSM alone, as it gives priority and combines the advantages of both methods and provides more accurate results when $\lambda = 0.5$. Although, the best and the worst supplier choices are exactly same for all the three methods but there are some variations in the preference ranking order which are justified by the rank coefficient. However, the three rankings show very minor differences in their order. Although, TOPSIS and WASPAS proved to be the most robust techniques, but COPRAS also competed equally and lags behind by an inch.

The same analysis can also be carried out by employing other MCDM tools like PROMETHEE, VIKOR, ELECTRE, etc., and the rankings can be compared to these. For solving supplier selection problems, there are others factors like, past experiences, service and warranty, transportation cost, behavior, etc., can also be considered along with these to make the selection process more precise and accurate.

Table 7 Ranking comparisons by TOPSIS, COPRAS and WASPAS

	TOPSIS	COPRAS	WASPAS	Final rank
S1	12	17	12	12
S2	11	11	11	11
S3	15	15	15	16
S4	17	16	17	17
S5	5	6	4	5
S6	4	5	5	4
S7	18	18	18	18
S8	6	4	6	6
S9	10	10	10	10
S10	1	1	1	1
S11	8	8	7	8
S12	9	9	9	9
S13	7	7	8	7
S14	14	14	14	15
S15	3	3	2	3
S16	13	13	16	14
S17	2	2	3	2
S18	16	12	13	13

Source Madic et al. [1]; Author himself

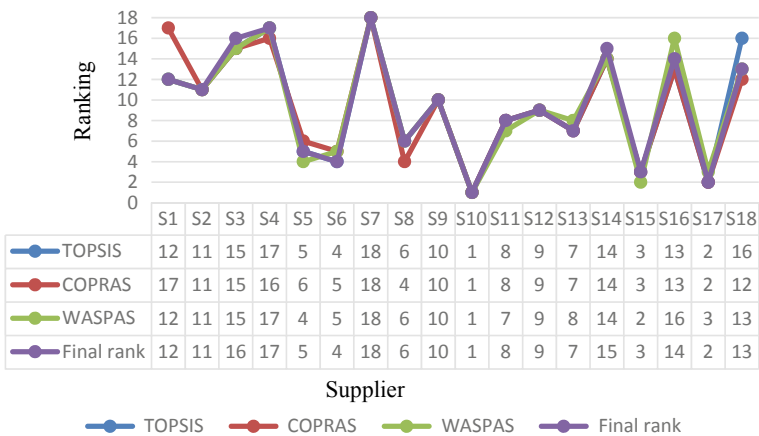


Fig. 1 Graphical comparison of different proposed rankings. Source Madic et al. [1]; Author himself; Created by Microsoft chart option

Table 8 Spearman rank correlation co-efficient among different proposed rankings

	WASPAS	TOPSIS	COPRAS	Final rank
WASPAS	–	0.97523	0.95046	0.98762
TOPSIS		–	0.95046	0.98762
COPRAS			–	0.96285
Final rank				–

Source Author himself

References

1. Madic, M., Markovic, D., Petrovic, G., Radovanovic, M.: Application of COPRAS method for supplier selection. In: 5th International conference transport and logistics, til (2014). <http://til2014.masfak.ni.ac.rs/elementi/15.pdf>
2. Liu, F., Ding, F.Y., Lall, V.: Using data envelopment analysis to compare suppliers for supplier selection and performance improvement. *Supply Chain Manag.* **5**(3), 143–150 (2000). <https://doi.org/10.1108/13598540010338893>
3. Shyur, H.J., Shih, H.S.: A hybrid MCDM model for strategic vendor selection. *Math. Comput. Model.* **44**(7–8), 749–761 (2006). <https://reader.elsevier.com/reader/sd/pii/S0895717706000549?token=29E072C1744697C6961DEB0F5B4C97C25732440536F51EE8E90859086727BDF38403CF84FC419D06EEE2C85DA61387F9>
4. Önüt, S., Kara, S.S., Işık, E.: Long term supplier selection using a combined fuzzy MCDM approach: a case study for a telecommunication company. *Expert Syst. Appl.* **36**(2), 3887–3895 (2009). <https://doi.org/10.1016/j.eswa.2008.02.045>
5. Singh, A.P.: Supplier selection using MCDM method in TV manufacturing organization. *Ind. Eng. Global J. Res. Eng.* **12**(1), (2012). https://globaljournals.org/GJRE_Volume12/1-Supplier-Selection-Using-MCDM-Method-in-TV.pdf
6. Kilic, H.S.: An integrated approach for supplier selection in multi-item/multi-supplier environment. *Appl. Math. Model.* **37**, 7752–7763 (2013). <https://reader.elsevier.com/reader/sd/pii/S0307904X13001650?token=5EB01D48B168E40E045894034A6C2BF11453A43DFA5A3CB266F002A106A2FEEA16B53EFD6343C9FE16F143E6C2BA2854>
7. Murali, P., Reddy, V.D., Phaneendra, A.N.: Supplier selection by using multi criteria decision making methods. *Int. J. Eng. Res. Gen. Sci.* **2**(6), 533–539 (2014). <http://ijergs.org.manageweb.siteportal.com/files/documents/SUPPLIER-69.pdf>
8. Nallusamy, S., Kumar, D.S.L., Balakannan, K., Chakraborty, P.S.: MCDM tools application for selection of suppliers in manufacturing industries using AHP, fuzzy logic and ANN. *Int. J. Eng. Res. Afr.* **19**, 130–137 (2015). <https://doi.org/10.4028/www.scientific.net/JERA.19.130>
9. Adalı, E., Işık, A., Kundakçı, K.: An alternative approach based on fuzzy PROMETHEE method for the supplier selection problem. *Uncertain Supply Chain Manag.* **4**(3), 183–194 (2016). http://www.growing-science.com/uscm/Vol4/uscm_2016_5.pdf
10. Yazdani, M., Zolfani, S.H., Zavadskas, E.K.: New integration of MCDM methods and QFD in the selection of green suppliers. *J. Bus. Econ. Manag.* **17**(6), 1097–1113 (2016). <https://doi.org/10.3846/16111699.2016.1165282>
11. Guchhait, A.: Supplier selection in a supply chain using multi-criteria decision making methods. *Am. J. Eng. Res.* **6**(10), 338–345 (2017). [http://www.ajer.org/papers/v6\(10\)/ZS0610338345.pdf](http://www.ajer.org/papers/v6(10)/ZS0610338345.pdf)
12. Assellaou, H., Ouhbi, B., Frikh, B.: A hybrid MCDM approach for supplier selection with a case study. In: Amodeo, L., Talbi, E.G., Yalaoui F. (eds.) *Recent Developments in Metaheuristics, Operations Research/Computer Science Interfaces Series*, vol. 62, pp. 179–197. Springer, Cham (2018). https://doi.org/10.1007/978-3-319-58253-5_12

13. Stojic, G., Stevic, Z., Antucheviciene, J., Pamucar, D., Vasiljevic, M.: A novel rough WASPAS approach for supplier selection in a company manufacturing PVC carpentry products. *Information* **9**(5), (2018). <https://www.mdpi.com/2078-2489/9/5/121/htm>
14. Bakhat, R., Rajaa, M.: Developing a novel Grey integrated multi-criteria approach for enhancing the supplier selection procedure: a real-world case of textile company. *Decis. Sci. Lett.* **8**(3), 211–224 (2019). http://www.growingscience.com/dsl/Vol8/dsl_2019_6.pdf
15. Jayant, A., Chandan, A.K., Singh, S.: Sustainable supplier selection for battery manufacturing industry: A MOORA and WASPAS based approach. In: 2nd International Conference on New Frontiers in Engineering, Science & Technology (NFEST), vol. 1240. IOP Conference Series: Journal of Physics, Kurukshetra, Haryana, India (2019). <https://iopscience.iop.org/article/10.1088/1742-6596/1240/1/012015/pdf>
16. Koganti, V., Menikonda, N., Anbuudayasankar, S., Krishnaraj, T., Athhukuri, R., Vastav, M.: GRAHP TOP model for supplier selection in supply chain: A hybrid MCDM approach. *Decis. Sci. Lett.* **8**(1), 65–80 (2019). http://www.growingscience.com/dsl/Vol8/dsl_2018_16.pdf
17. Zavadskas, E.K., Antucheviciene, J., Šaparauskas, J., Turskis, Z.: Multi-criteria assessment of facades' alternatives: Peculiarities of ranking methodology. *Procedia Eng.* **57**, 107–112 (2013). <https://reader.elsevier.com/reader/sd/pii/S1877705813007467?token=89DE453756B861A51AC21F75E4188E9853647DF1AA7B1FCC60B869A746784642E84616B3CDD0ABB5F379339C98227301>
18. Zavadskas, E.K., Antucheviciene, J., Šaparauskas, J., Turskis, Z.: MCDM methods WASPAS and MULTIMOORA: Verification of robustness of methods when assessing alternative solutions. *Econo. Comput, Econ. Cybern. Stud. Res.* **47**(2), 5–20 (2013). https://www.researchgate.net/publication/287762606_MCDM_methods_WASPAS_and_MULTIMOORA_Verification_of_robustness_of_methods_when_assessing_alternative_solutions
19. Chakraborty, S., Zavadskas, E.K.: Applications of WASPAS method in manufacturing decision making. *Informatica* **25**(1), 1–20 (2014). <https://pdfs.semanticscholar.org/ebdd/06f34eb3a0409ba23497faf6e2a52d70c525.pdf>
20. Karande, P., Zavadskas, E.K., Chakraborty, S.: A study on the ranking performance of some MCDM methods for industrial robot selection problems. *Int. J. Ind. Eng. Comput.* **7**(3), 399–422 (2016). http://www.growingscience.com/ijiec/Vol7/IJIEC_2016_1.pdf
21. Mathew, M., Sahu, S.: Comparison of new multi-criteria decision making methods for material handling equipment selection. *Manag. Sci. Lett.* **8**(3), 139–150 (2018). http://www.growingscience.com/msl/Vol8/msl_2018_4.pdf
22. Badalpur, M., Nurbakhsh, E.: An application of WASPAS method in risk qualitative analysis: a case study of a road construction project in Iran. *Int. J. Constr. Manag.* (2019). <https://doi.org/10.1080/15623599.2019.1595354>
23. Vinchurkar, S.H., Samtani, B.K.: Performance evaluation of the hydropower plants using various multi-criteria decision making techniques. *Int. J. Eng. Adv. Technol.* **8**(6), 2131–2138 (2019). <https://www.ijeat.org/wp-content/uploads/papers/v8i6/F8490088619.pdf>
24. Saaty, T.L.: *The analytic hierarchy process*. McGraw-Hill, New York (1980)
25. Zavadskas, E.K., Turskis, Z., Antucheviciene, J., Zakarevicius, A.: Optimization of weighted aggregated sum product assessment. *Electron. Electr. Eng.* **122**(6), 3–6 (2012). <https://doi.org/10.5755/j01.eee.122.6.1810>
26. Fishburn, P.C.: Additive utilities with incomplete product set: applications to priorities and assignments. *Oper. Res. Inf.* **15**(3), 537–542 (1967). <https://www.jstor.org/stable/168461>
27. MacCrimon, K.R.: Decision making among multiple attribute alternatives: a survey and consolidated approach. Rand Corporation, (1968). https://www.rand.org/pubs/research_memoranda/RM4823.html
28. Triantaphyllou, E., Mann, S.H.: An examination of the effectiveness of multi-dimensional decision-making methods: a decision-making paradox. *Decis. Support Syst.* **5**(3), 303–312 (1989). [https://doi.org/10.1016/0167-9236\(89\)90037-7](https://doi.org/10.1016/0167-9236(89)90037-7)
29. Miller, D.W., Starr, M.K.: *Executive decisions and operations research*. 2nd edn. Prentice-Hall, Englewood Cliffs, New Jersey (1969)

30. Šaparauskas, J., Zavadskas, E.K., Turskis, Z.: Selection of facade's alternatives of commercial and public buildings based on multiple criteria. *Int. J. Strateg. Property Manag.* **15**(2), 189–203 (2011). <https://journals.vgtu.lt/index.php/IJSPM/article/view/5469/4726>

Design of an Impact Attenuator for a Formula Type Race Car



Shivam Mahajan, Neeraj Dokania, Akshay Kumar,
and Sujeet Kumar Mishra

Abstract In the present paper, the design of a crashworthy impact attenuator has been carried out. Vehicle safety is a major problem and having a good energy absorbing impact attenuator improves the safety of the vehicle. It was decided to design an impact attenuator for a formula type race car because of its reduced complications and set of rules which govern the car. After consideration of various materials and evaluating them based on various parameters, aluminium honeycomb was selected for the impact attenuator. Drop test simulation in SolidWorks was carried out to evaluate the performance of the impact attenuator. Calculations abiding the rules of a formula type race car were done to calculate the energy and force, the impact attenuator will be subjected against. These calculations were also the basis for the drop height used in the drop test simulations. The sheet metal impact attenuator was rejected as it failed the drop test, so dynamic simulations were carried out on honeycomb impact attenuator in Ansys Explicit Dynamics. Several problems were faced while running the dynamic simulation and rigorous theoretical study was done to rectify the problems. Simulations were run on a limited number of cells rather than the whole structure and interpolation method was used to find the results for the whole structure. It was finally decided to go with the two layered honeycomb structure.

Keywords Impact attenuator · FEA · Dynamic analysis · Honeycomb

S. Mahajan (✉) · N. Dokania · A. Kumar · S. K. Mishra
Department of Mechanical Engineering, Birla Institute of Technology,
Mesra, Ranchi 835215, India
e-mail: shivam91198@gmail.com

N. Dokania
e-mail: dokanianeeraj@gmail.com

A. Kumar
e-mail: akshaykumar66250@gmail.com

S. K. Mishra
e-mail: sujeetmishra@bitmesra.ac.in

1 Introduction

An impact attenuator, additionally called a crash cushion, is a structure that is meant to lower the harm to the vehicle structure throughout collision of the vehicle. It is meant to soak up the vehicle kinetic energy by intensive crushing and crumbling of the structure. It provides a load path for frontal impacts in the event of off-centered and off-axis impact. The crashworthiness of impact attenuator is assessed for total energy absorbed as well as specific absorbed energy. Its unique characteristic is that rate of energy dissipation is targeted over a narrow area, whereas the rest of the structure experiences a rigid body motion.

One of the leading causes of deaths is vehicular crashes. This calls for continuous improvements and new developments in the field of vehicle safety. The impact attenuator is usually attached to the front of the car and absorbs a major part of the impact energy. Often it is included in the side road barriers to cushion the crashing vehicle in case of an accident.

The objective is to design and fabricate a crashworthy impact attenuator for a formula type race car, that is capable of taking up most of the impact energy during an event of a crash and reduce the amount of energy being transferred to the driver. It was decided to work on an impact attenuator of a formula type race car. This decision was made keeping in mind the simplicity of the car when compared to road cars. The set of rules that govern these cars also make the designing and development of different types of impact attenuators a standard process. The impact attenuator is supposed to absorb at least 7350 J of energy (considering a vehicle with mass 300 kg and impacting a solid, non-yielding impact barrier with a velocity 7 m/s).

A novel procedure is used for the research with regard to the simulation performed. An interpolation method is used to simulate the structure. Because of the number of cells, it was not possible to simulate the entire structure in one go owing to the computational constraints. However, there might be some factors which would have been unaccounted for due to the adopted method, so to incorporate those factors, a suitable factor of safety was selected.

2 Relevant Past Work

Numerous investigations have been done to determine the crashworthiness of an Impact attenuator. Raguraman and David [1] performed experimental and numerical simulations of hollow and those stuffed with honeycomb tubes. The axial quasi-static and dynamic crushing of the aluminium (6063 T6 alloy) tubes filled with Nomex RHRH-10 honeycomb was done. It was found out that honeycomb filled tubes were around 10% more efficient in terms of energy absorption. The experimental failure modes were very compatible with the predicted ones under both quasi-static and dynamic axial loading.

Abrahamson et al. [2] performed drop weight test experiment on two specimens of varying dimensions built of Plascore aluminium honeycomb. The impact mass weighing 661 lb was dropped from height of 8.3 ft with an impact velocity of above 23 ft/s.

Kumar et al. [3] performed experimental test on impact attenuator built up of Al-6063-T6 material. LS-DYNA software was used for simulation while the method of physically impacting the attenuator was used for practical tests. Both the average acceleration and deceleration were under 20 g which also complied with the SAE rule.

Sharavan Lalith et al. [4] performed Finite element analysis, drop and compression test for impact attenuators made up of three different materials: Al foils of 6083T6, wood, long fiber reinforced thermoplastic composite. The paper proposed the use of aluminium as it showed the maximum amount of energy absorption.

Williams et al. [5] studied the crash characteristics of the front of Caterham 7. Multiple simulations using finite element vehicle model to replicate a rigid barrier test in FEA code Oasys LS-DYNA3D were performed. Overall impact events and the individual component's contribution was also understood by this. Relationship between simulation and practical results was also found.

Obrovčić et al. [6] demonstrated the effective performance of carbon fiber. They studied the crash behavior of the brittle composite material using FEA model on LS-DYNA. The crash tests were performed using a drop test machine, measuring the deceleration-time diagram and after integration processes load-shortening trend and energy absorbed by the structure.

The crash behavior of the nose cone of F1 racing car impact structure was investigated by Heimbs et al. [7] by striking it against a rigid wall and validating against experimental crash test data. Different designs were analyzed in this study to evaluate the robustness of the models.

Jain and Kalia [8] used cuboidal shaped impact attenuators for passenger vehicles. The models used galvanized iron sheets and aluminium 2024 sheet with thickness 1 mm as materials. The maximum magnitude of decelerations and velocity of impact were well under acceptable limits.

Sengupta et al. [9] conducted compressive testing on truncated trapezoidal shaped impact attenuator which was fabricated using aluminium sheets of thickness 2 mm. The results clearly ruled out the use of sheet metals owing to the considerable deformations.

Hiroshi et al. [10] did FEA analysis on a spaceframe structure with steel pipes, an Al monocoque and a plastic monocoque. It was concluded that out of these three, the one made from composite material was absorbing higher energy and was the best in the three tested models.

Supakit et al. [11] performed analysis on various models of varying thickness. Their research showed the relationship between energy absorption capacity of simple section and multi cells sections with different wall thickness.

3 Methodology

To meet our objective of designing a crashworthy impact attenuator, the work was systematically split into the following stages:

1. Theoretical study.
2. Material selection.
3. CAD modeling and geometry optimization.
4. Simulation and analysis.

A decision matrix approach is followed rather than conventional approach for selecting the material to fulfill the objectives. Through this method a material can be easily eliminated and the one that suits the needs can be finalized.

To get the results for the simulation, interpolation method is used since it was not known if the behavior of cells (number of cells) was a linear relation with the energy absorbed. This method also helps in saving time and the required simulations could be performed with limited computer resources.

3.1 Theoretical Study

To design an impact attenuator that is capable of decelerating a 300 kg car moving at 7 m/s at 20 g, the first step was to calculate the energy and force that the impact attenuator will be subjected to. It is assumed that the car is stationary after the impact.

Impact velocity, $V_i = 7$ m/s

Final velocity, $V_f = 0$ m/s

Acceleration due to gravity, $g = 9.81$ m/s²

Mass, $M = 300$ kg

Acceleration, $a = 20$ g = 196 m/s²

Kinetic Energy:

$$K_e = \frac{1}{2} M V_i^2 = 7350 \text{ J}$$

By conservation of energy,

$$P_e(\text{Potential energy}) = K_e = 7350 \text{ J}$$

$$P_e = Mgh$$

where h is the drop height

Therefore,

$$h = 2.5 \text{ m}$$

Time of impact (t):

$$t = \frac{Vi}{A}$$

$$t = 0.036 \text{ s}$$

Impulse and force:

Impulse:

$$I = M(V_i - V_f)$$

$$I = 2.1 \times 10^3 \text{ kgm/s}$$

Force:

$$F = \frac{I}{t}$$

$$F = 58,335 \text{ N}$$

3.2 Material Selection

The selection of material was done keeping in mind the various material properties like density, yield strength, shear modulus, cost and feasibility (Tables 1, 2).

Out of various available materials, few of them were chosen which best suited our requirements:

1. Aluminium sheet
2. Aluminium honeycomb
3. Rohacell 110IG Foam
4. Mild steel sheet
5. Carbon fiber reinforced polymer.

Table 1 Material properties

Property	Aluminium sheet	Aluminium honeycomb	Rohacell 110IG foam	Mild steel sheet
Density (gm/cm ³)	2.78	0.054	0.11	7.85
Yield strength (MPa)	280	270	3.5	318
Shear modulus (Gpa)	28	26	0.055	83

Table 2 Material decision matrix

Parameter	Weightage	Aluminium sheet	Aluminium honeycomb	Mild steel sheet
Density	3	0	3	-3
Cost	2	2	0	2
Availability	3	3	3	3
Yield strength	1	1	1	1
Manufacturing feasibility	1	1	1	1
Total score		7	8	4

Carbon fiber reinforced plastic was rejected because of fabrication problems, while Rohacell 110IG foam was taken out of consideration due to high price and unavailability.

So, to finalize the material among the remaining options, a decision matrix was made.

The weightage of each comparing parameter was primarily based on experience and the kind of impact they can have on the work. For example, the structure should be as light as possible and should be readily available. Therefore, density and availability could be concluded as the most important parameters, hence given maximum weightage. The other parameters were also treated in a similar fashion.

Hence, aluminium honeycomb was finalized for the impact attenuator.

3.3 CAD Modeling and Geometry Optimization

Various designs were taken into account to determine the best suited geometry, which were:

The first geometry decided upon was a single layered aluminium honeycomb as shown in Fig. 1a with 200 mm × 200 mm × 200 mm, with the cell thickness of 0.08 mm with the cell width being 10 mm. This was the very basic and initial geometry constructed.

The second geometry considered was the two layered honeycomb pyramid as shown in Fig. 1b. The base size was the same as the first geometry and the cell thickness and cell width also being the same. The second layer was rested on the first layer with an aluminium plate between the two.

The third geometry constructed was a three layered honeycomb pyramid as shown in Fig. 1c. The base dimensions and cell parameters remained the same.

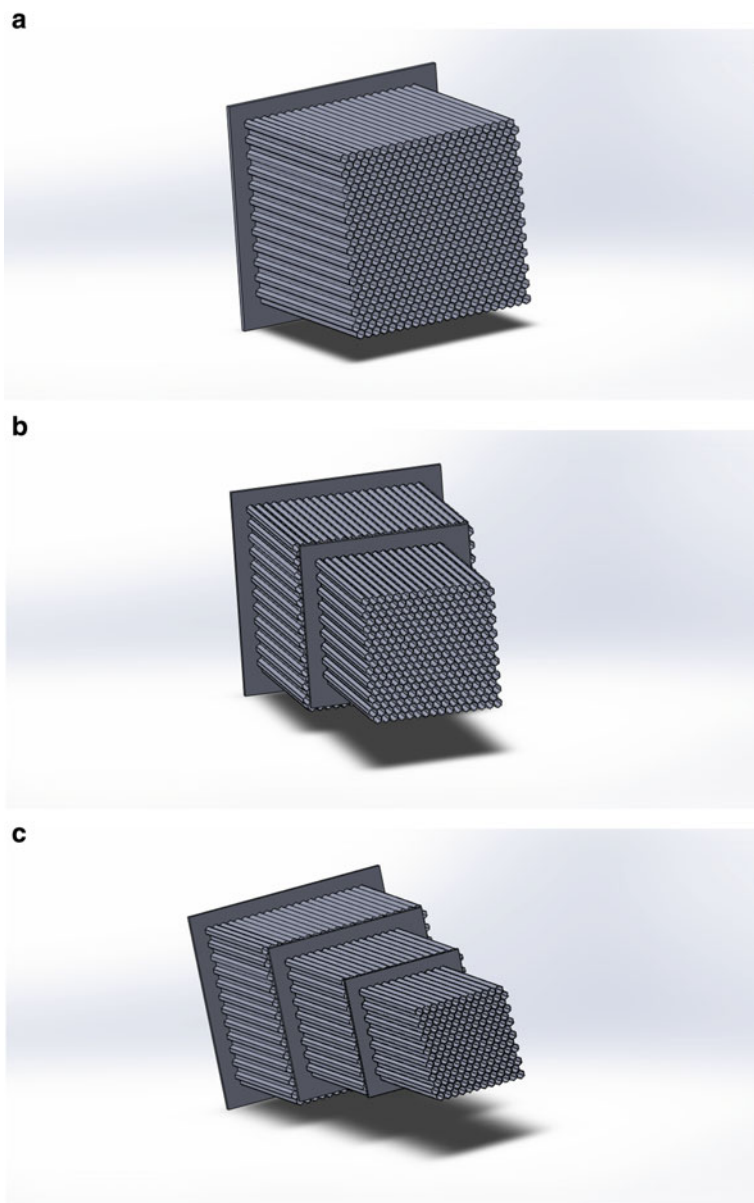


Fig. 1 a Single layer honeycomb impact attenuator, b two layered honeycomb impact attenuator, c three layered honeycomb impact attenuator

3.4 Simulation and Analysis

Drop test simulation was performed for a relatively simple geometry on SolidWorks software. In this simulation the impact attenuator was dropped from a certain height while in actual practice a heavy mass is dropped on the stationary impact attenuator.

For simulation purposes, the drop height was calculated using the mass of impact attenuator (1.1 kg), taken from CAD model.

$$\text{Drop in potential energy}(P_e) = \text{Energy to be absorbed} = 7350 \text{ J}$$

So, the drop height comes out to be 681.1 m.

The calculated height, direction of gravity and direction of impact was mentioned in the analysis, with the small face of the impact attenuator being crashed into the rigid wall. Total deformation, deformation in the direction of impact and crushing behavior were observed.

4 Drop Test Simulation

SolidWorks drop test was used to obtain a rough estimation of the real crash test. Although the deformations obtained from the drop test were significant, they still don't represent the real case scenario of a crash. A highly dynamic testing simulator would create better results. SolidWorks does not provide the necessary tools for an accurate test in this situation.

The results obtained from the SolidWorks drop test simulation shows a maximum deflection of 60.85 mm as shown in Fig. 2a. This value of maximum deflection is observed on the rear of the impact attenuator, with it being dropped small side down. The obtained value is not very close to the realistic deformation that would have been observed, but it gives us a clear and good understanding of the stresses and crushing behavior of the impact attenuator.

The maximum value of von Mises stress was observed to be $6.207 \times 10^9 \text{ N/m}^2$ shown in Fig. 2b, which is greater than the yield strength of used aluminium. This stress was observed in a relatively small area along the edge of the impact attenuator. This value is to be expected as the impact attenuator is supposed to crash into itself.

5 Dynamic Simulation

The next step was to simulate the real-life crash test of the honeycomb structure. To execute the finite element calculations Ansys Workbench was used as there were dynamic effects which needed to be taken into account. Of all the available packages, Explicit Dynamics package was used to take care of the nonlinear calculations. This

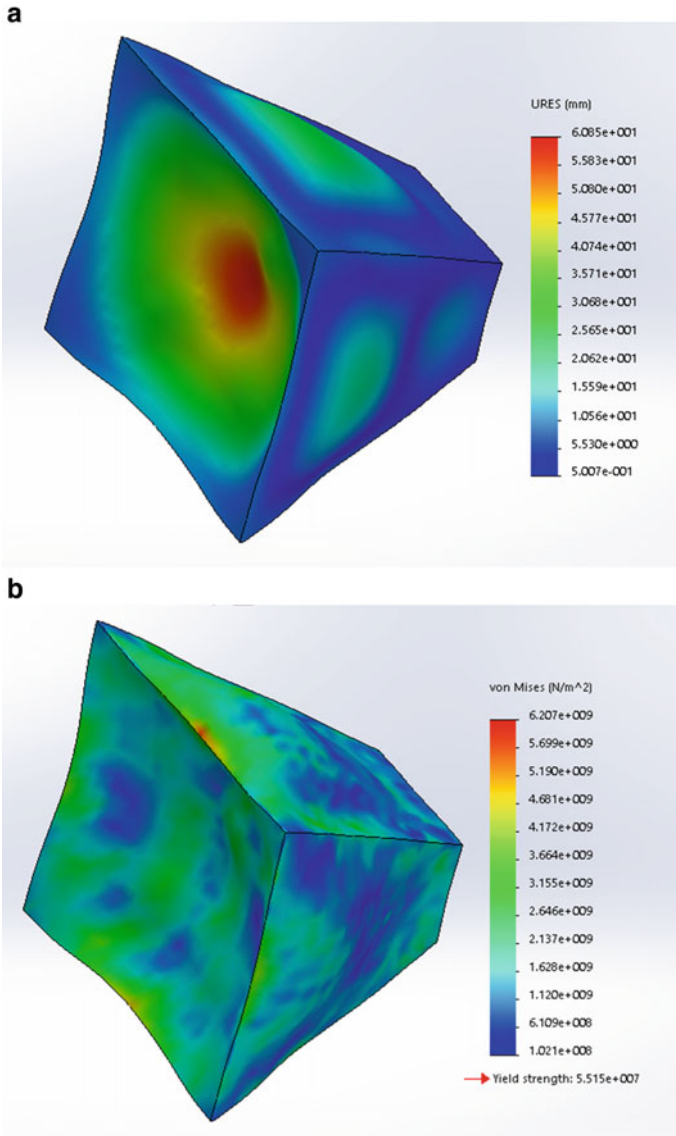


Fig. 2 a Resultant deformation of the impact attenuator, **b** stress generated in the impact attenuator

simulation was required because drop test simulations did not account for the real case. Moreover, the drop test was done on the sheet metal aluminium structure and failed the test. Hence honeycomb structure was the next choice.

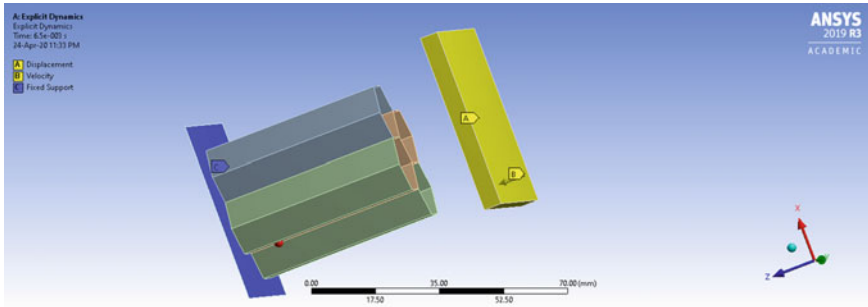


Fig. 3 Constraints applied on four cell honeycomb

5.1 Constraints

In this simulation, a rigid wall was made to strike the impact attenuator and its panel with a certain velocity. The simulation was carried on for some time until the deformation in the structure did not vary significantly with time. However, in real cases,

the structure is made to strike the rigid wall. Following are the constraints that were applied as shown in Fig. 3:

- The striking velocity of the wall was used based on the rules prescribed in the FS rulebook which was numerically equivalent to 7 m/s.
- The honeycomb cells were fixed to the panel by using bonded contact between them.
- The panel was fixed by providing fixed support, thereby restricting its motion.
- The striking wall was also restricted to move in one direction only.
- Bonded body interaction was used between the honeycomb cell and wall.

5.2 Problems Faced

- One of the major issues was the complexity of the problem. It was not possible to simulate the entire 3D structure with hundreds of cells because that would require very fine mesh size, resulting in excess CPU time and storage. So, to make it feasible, the 3D structure was converted to 2D by using only the mid-surfaces of the cells. But the model still couldn't be simulated because of the high number of cells. So, to simplify the problem, an interpolation method was used. The simulations were performed only for 1 cell, 2 cells and 4 cells structures and then the results were interpolated for the entire structure.
- Since the simulation involves crashing of structures, proper body interactions between honeycomb cell, panel and wall had to be incorporated. Bonded body

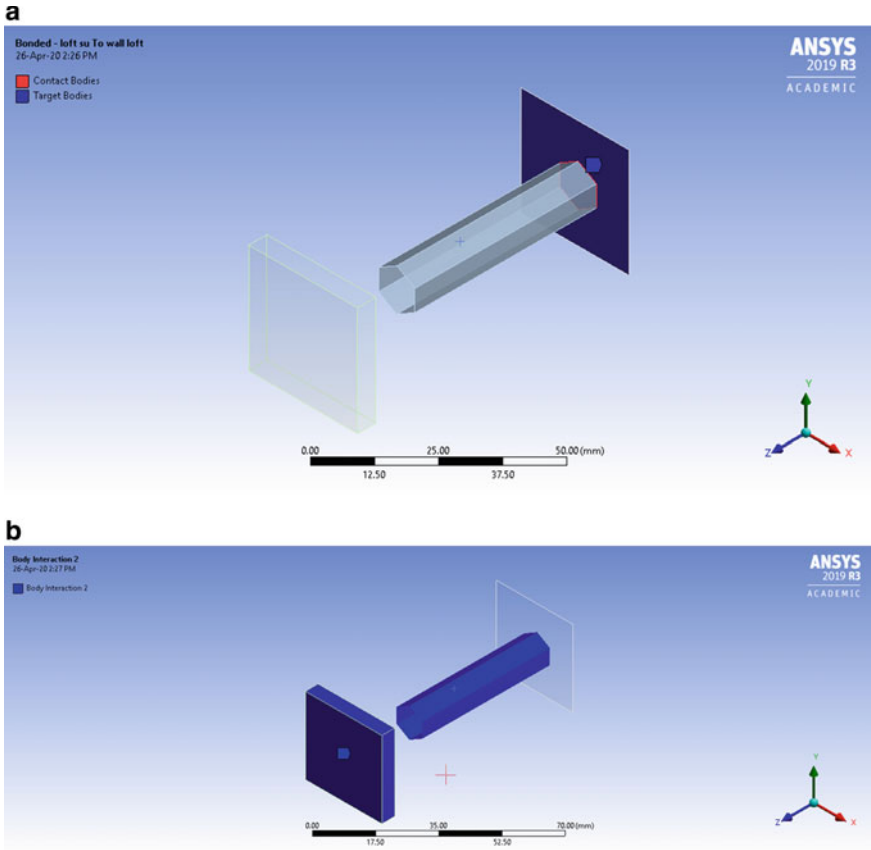


Fig. 4 a Body interaction between panel and cell, b body interaction between wall and cell

interaction was used between the honeycomb cells and striking wall to make sure that they always remain in contact shown in Fig. 4a, b.

- Suitable boundary conditions (supports, displacement and velocity) to simulate the crash test had to be studied and researched extensively.
- There were some issues in interpreting the energy plots as Ansys Workbench provides a lot of output data.

6 Results

The simulations were performed as per the mentioned constraints and boundary conditions. The results obtained were further analyzed to calculate the number of cells required and hence design the impact attenuator.

6.1 Single Cell Honeycomb

The simulation was first performed on a single celled honeycomb structure. The energy absorbed by the cell, which is equal to the change in internal energy, was found out to be 15 J as shown in Fig. 6. The maximum deformation of the cell was 37.19 mm shown in Fig. 5, (the deformation shown in the figure includes the distance traveled by the wall).

The kinetic energy of the striking wall decreases during the crash which eventually gets absorbed by the structure. The energy vs time graph shows that the energy absorbed by the structure leads to the proportional increase in the internal energy which is 15 J for single cell honeycomb structure. This energy is absorbed by crushing of the structure which can be seen in Figs. 5 and 6.

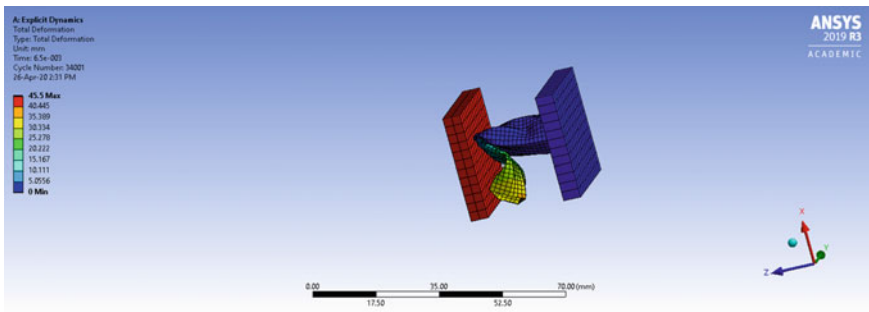


Fig. 5 Deformation of single cell

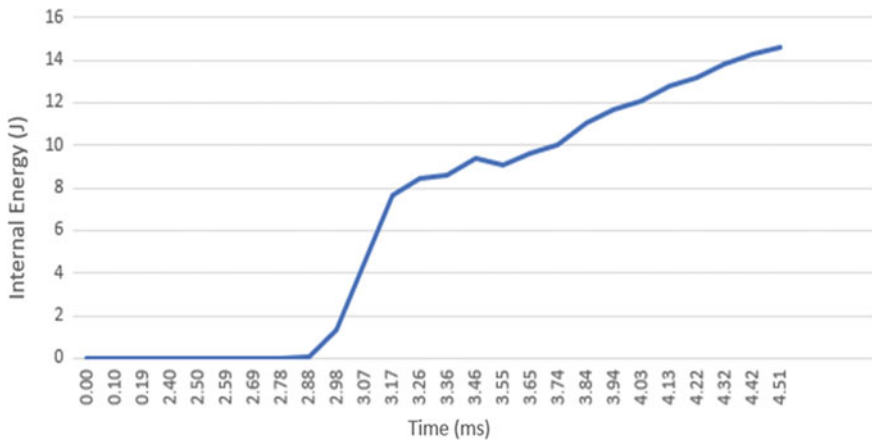


Fig. 6 Energy absorbed by single cell

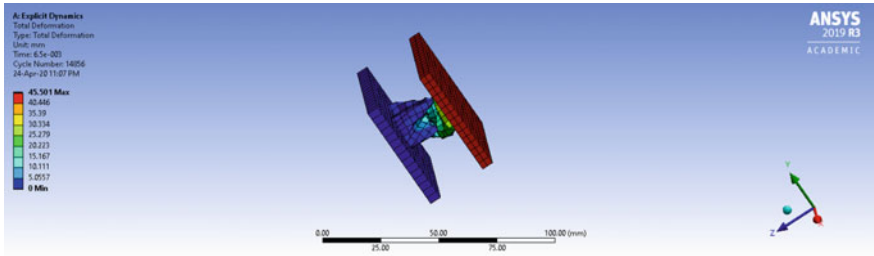


Fig. 7 Deformation of two cells

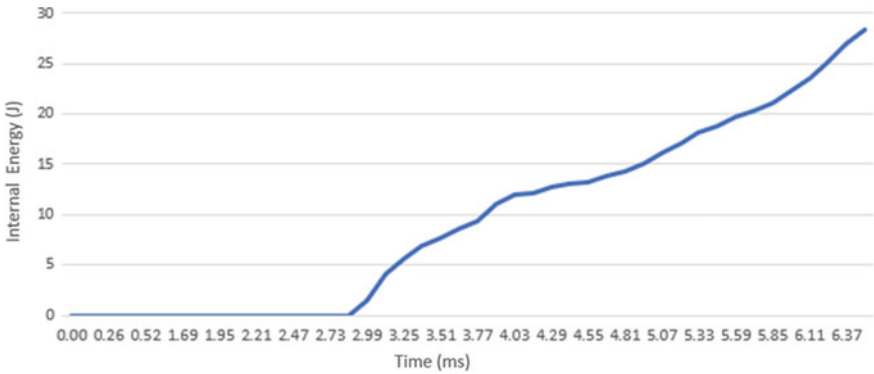


Fig. 8 Energy absorbed by two cells

6.2 Double Cell Honeycomb

The simulation was then performed on a double celled honeycomb structure. The energy absorbed by the cell was found to be 27.5 J. The maximum deformation of the cell was 30.26 mm. shown in Fig. 7, (the deformation shown in the figure includes the distance traveled by the wall).

The energy vs time graph shows that the increase in the internal energy is 27.5 J for two cell honeycomb structure. This energy is absorbed by crushing of the structure which can be seen in Figs. 7 and 8.

6.3 Four Cell Honeycomb

The simulation was then performed on a four celled honeycomb structure. The energy absorbed by the cell was found to be 55 J. The maximum deformation of the cell was 35.36 mm. shown in Fig. 9, (the deformation shown in the figure includes the distance travelled by the wall).

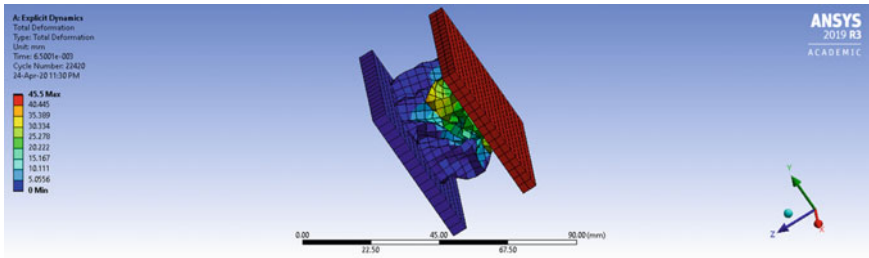


Fig. 9 Deformation of four cells

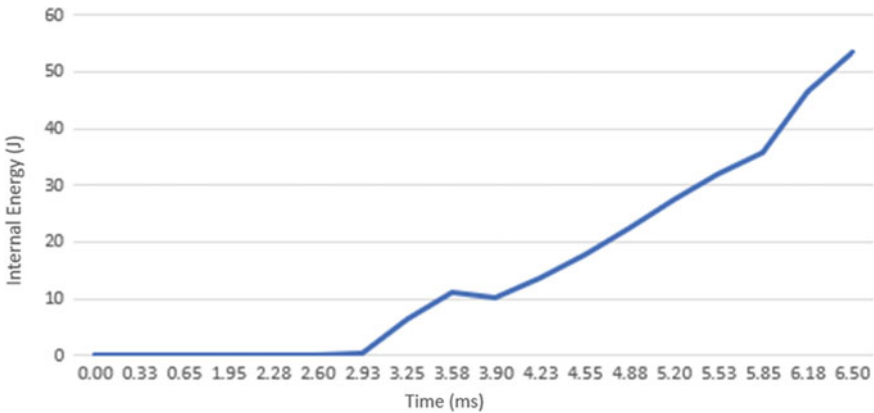


Fig. 10 Energy absorbed by four cells

The energy vs time graph shows that the increase in the internal energy is 55 J for four cell honeycomb structure. This energy is absorbed by crushing of the structure which can be seen in Figs. 9 and 10.

7 Conclusion

Two major structures were considered for the impact attenuator initially viz sheet metal steel, aluminium structures and aluminium honeycomb.

- After thoroughly studying the materials and constructing a decision matrix, it was decided that simulations would be performed on aluminium structures.
- Drop test of sheet metal aluminium structure showed that it was not suitable for our intended workload, and hence it was discarded.
- Next, dynamic simulations were performed on the aluminium honeycomb structure.

- After performing dynamic simulations for three cases, it was found out that the energy absorbed increases linearly with the number of cells.

Then the number of cells required was calculated by using the interpolation method.

Energy absorbed per cell is 15 J

So, the number of cells required to absorb 7350 J is 490.

Accounting for the errors in simulation and other unknown factors, a Factor of Safety 1.5 was decided.

So, the final number of cells is 735.

- Since the number of cells is 735, to optimize the dimension of the impact attenuator and front of the frame of the car, it was decided to proceed with the two layered honeycomb structure.
- The first layer of the IA is 270 mm × 270 mm and contains 625 cells in a 25 × 25 configuration. The second layer is 130 mm × 120 mm and contains 110 cells in a 11 × 10 configuration, with the core size of 10 mm and core height of 50 mm.

The proposed design fulfills the design requirements in terms of energy absorption as well as dimension.

References

1. Munusamy, R., Barton, D.C.: Lightweight impact crash attenuators for a small formula SAE race car. *Int. J. Crashworthiness* **15**(2), 223–234 (2010)
2. Abrahamson, C., Bruns, B., Hammond, J.W., Lutter, J.: Formula SAE impact attenuator testing (2010)
3. Kumar, D., Kumar, S., Singh, G., Khanna, N.: Drop test analysis of impact attenuator for formula SAE car (2012)
4. Lalith Sharavan, C., Joshuaraj Immanuel, K., Varun, A.K., Sudir, C., Krishna, S.: Design and experimental analysis of an impact attenuator. *Int. J. Mech. Prod. Eng.* **2**(10), 56–60 (2014)
5. Williams, T.D., Pennington, A., Barton, D.C.: The frontal impact response of a space frame chassis sports car. *Proc. Inst. Mech. Eng. J. Auto. Eng. UK: Univ. Leeds* **214**, 865–873 (2000)
6. Obradović, J., Boria, S., Belingardi, G.: Lightweight design and crash analysis of composite frontal impact energy absorbing structures (2012)
7. Heimbs, S., Strobl, F., Middendorf, P., Gardner, S., Eddington, B., Key J.: Crash simulation of an F1 racing car front impact structure (2009)
8. Jain, M., Kalia, A.V.: Study and design of impact attenuator for passenger vehicle (2014)
9. Sengupta, A., Sharma, A., Chakraborty, A.: Manufacturing an impact attenuator for formula prototype cars. *IPASJ Int. J. Mech. Eng.* **2**(11), 11–13 (2014)
10. Hiroshi, E., Yusuke, M., Hiroshi, M., Eiji, H., Satoshi, K., Koetsu, Y., Naoki, U.: Development of CFRP monocoque front impact attenuator for FSAE with VaRTM, In: SAE Technical Paper Kanazawa, University, KADO Corporation, pp. 01–08 (2007)
11. Supakit, R., Pornporm, B., Worawat, P.: Design and analysis of impact attenuator for student formula. SAE Technical Paper (2015)

Design Optimization and Static Force Analysis of L-Type Rotary Tiller Blade



Deepanshu Pandey, Dheeraj Rangera, Divyansh Bhatia, Ghanvir Singh, and Rajiv Chaudhary

Abstract Rotary tillers are sort of soil-working tools which are used to mix soil and operate by spinning the rotary blades. Due to its simple structure and high efficiency, the potential for their use nowadays is increasing day by day. The life of these blades depends upon the soil in which they are used and is around 80 h. Excessive loads and stresses cause wear of the blade tip or the cutting edges. Although the material used in the blade has sufficient wear resistance properties, the wear takes place because of geometry/profile of the blade. In this study, a mathematical model for optimization of design parameters of a rotary tiller blade in terms of specific energy consumption is used. A rotary tiller blade design was created in SolidWorks 2018 and static force and fatigue analysis for the designed blade was done in Ansys 2019.

Keywords Tiller blade · Design optimization · CAD-CAM · FEA

1 Introduction

Indian Agriculture has been the foundation of the country's economy for thousands of years and it still continues to be. Agriculture plays a pivotal role in the Indian economy. It is the way of livelihood for 43.21% of the working class in India and

D. Pandey (✉) · D. Rangera · D. Bhatia · G. Singh · R. Chaudhary
Mechanical Engineering Department, Delhi Technological University, New Delhi, India
e-mail: deepanshupandey195@gmail.com

D. Rangera
e-mail: dheerajrangera70@gmail.com

D. Bhatia
e-mail: divyanshbhatia007@gmail.com

G. Singh
e-mail: sghanvir@gmail.com

R. Chaudhary
e-mail: rajivchaudhary@dce.ac.in

has acquired 15.4% of India's GDP. Agriculture thus leads to the overall economic growth of the country and hence, it is the economy's most inclusive growth sector [1, 2]. In recent decades, the application of machinery in Indian agriculture has gained prominence in increasing agricultural productivity and optimizing production of inputs through efficient and proper use. The requirement of power for operations like seedbed preparation and harvesting has also grown at an exponential rate and its requirement has become so large that the existing human and animal power is inadequate [3].

The rotary power tiller holds promise for overcoming these problems. A rotary power tiller is a mechanical tool which consists of a number of blades that are used to plough the land and to mix and swirl up the soil. Rotary tiller helps in soil preparation, sowing, planting, fertilizer adding and spraying herbicides and watering. Hence, it is an energy consuming activity in agriculture cycle [4, 5]. The design characteristics of rotary blades are the biggest determinants of power consumption [6].

The problems that limits the persistence of rotary power tiller are high stresses and the wear of the blades. On the blade tip or blade critical edges, high stresses are developed due to the continuous fluctuating impact of soil crust/clods/stone. These blades have usage life of 40–200 h depending upon the type of the soil and they need to be replaced after that. Suitable design of the blades and optimization through total specific energy requirement can lead to lower energy consumption in rotary tillage [6].

The blade wear has its own characteristics, since they interact with various types of soil textures, moistures and other unpredictable conditions in the field. The rotary tiller blades are vulnerable to fatigue and abrasive damage under loads. This leads to shortening of service life by wear of machine parts working in soil [4]. A suitable geometric shape of the tiller blade will ensure easy cutting of soil by reducing the maximum loads and stresses. Reducing the load and stress induced, will result in low wear and thus longer life [7].

There are different types of rotary power tiller blades available, 'L' shape, 'J' shape, 'H' shape and 'C' shape, to suit and perform in different operating conditions. A comparison between these blades shows that deformations and stresses are minimum for the 'L' shape blade. The 'L' shape blades are most commonly used in India. Also, a right hand blade has lower deformation than a left hand blade [3, 8].

Mandal et al. [3] worked on the optimization of the design constraints of a rotary tiller blade using total specific energy requirements. Tafesse et al. [4] focused their study on fuel consumption optimization of different types of rotary blades under sandy clay loam environment. Mandal et al. [6] designed a rotary tiller blade using specific work method. Caslli et al. [7] research was performed by comparing H-shaped blades from two different manufacturers of blades that are used in rotary tillers. Mandal and Mukherjee [8] designed and compared 'C', 'J' and 'L' type blades using SolidWorks and Ansys and concluded that under the same operating conditions and material of the blade, 'L'-type blade produces less stress and deformation. Selvi and Kabas [9] focused on the design of a rotary tiller and its blades as a part of a larger project on agricultural machines. Tafesse et al. [10] developed a mathematical model to figure out the optimum design values in terms of the overall specific energy

requirements of rotary blades in the form of a 'Pick', a 'C', a 'I', a 'L' and a 'J'. Vegad and Yadav [11] focused their study on the structural optimization of tiller blades by means of CAD and they compared C, L and hatched type blades and optimization was done in Ansys Design Xplorer. Asl and Singh [12] created three types of rotary blades (i.e. C-type, L-type and RC-type). The validity of their model for estimation of power requirements was checked through experiments in indoor soil bin by calculating the electrical power needed to rotate the blades. Matani and Bhishnurkar [13] experimented with 37 and 45 HP power tractor and calculated soil-tool interface forces. Then the resulting effect of Von-Mises stress, maximum main stress, tensile stress and shear stress distribution plots on rotary tiller's blade was obtained.

The research work mentioned in literature review did not consider the optimization of all the geometric parameters of the blade. The purpose of this research was, therefore, to design an effective rotary power tiller blade by changing the blade parameters according to the mean values corresponding to longer life conditions as opposed to lower cost conditions and to tackle the problem of an optimal design for low stress, low power requirements and long life of the blade. A dataset was created for the different possible values of different parameters and optimal design parameters were selected on the basis of total energy requirement. This optimization method will reduce induced stresses, therefore increasing its strength and consequently reducing wear. Hence an increase in the working life of the tiller blade.

2 Materials and Methods

It has been observed from literature study that the blade starts to worn out after 25–60 h of in field operation depending upon the soil type and the total life of the rotary tiller blade is around 80–200 h depending upon the soil type and they need to be replaced after that [3, 6]. The reason for this is unnecessary loading or surface stress on the blade when it was used in the field. Interaction of these blades with soil is different from conventional ploughs and they are subjected to high friction and impact which ultimately creates non-uniform forces on these blades which results in wearing of the blades.

Many times wear is the reason behind the low self-life of the blade because there are many stones, gravel and sand present in the soil which are harder than the steel of the blades and therefore, a blade that experiences a severe wear often ends with breaking, fracture or failure. The continuous impact of stones/gravel/sand crust on the blades develops high stress areas on the blade. The geometric parameters of the blade not only determine the quality of tillage but it also determines whether it will provide easy soil cutting or not which can reduce the maximum loads and high stresses, which consequently reduces the blade wear. Therefore, it is necessary to optimize the blade geometric parameters so that blade experiences less stress and wear [7, 8].

2.1 Selection of Material

Reduction in stress and wear can be achieved by a suitable design and choosing a suitable material for the blade. Many of the researches have used structural steel, cast iron, stainless steel, mild steel, etc. as material for rotary tiller blade [14, 15]. Mild steel is the most common material for commercially available rotary tiller blades. It was observed by Kang et al. [16] that hard-facing of normal tiller blades reduced their wear, and hard-facing alloys showed clear superiority in abrasive wear resistance in contrast to un-hardfaced steel.

Therefore, to counter the problem of wear, a blade of higher hardness is required. It is known that the presence of boron, B, increases the hardening of low alloy steels and it provides wear resistant properties [7].

Hence, Boron steel (SAE-AISI 51B60) is used for blade material in this research because of its excellent hardness and its properties are illustrated in Table 1.

2.2 Optimization of Design Parameters

This research focuses on ‘L’ shaped blade because it is the most commonly used type of blade in India and for same material of the blade and loading conditions the stress developed and deformation in a L-type blade is minimum as compared to other blades [8].

Tafesse et al. [10] optimization of design parameters subjected to constraints was done by putting them in an optimization function in Lingo software which gave only one value for each parameter but practically is not feasible to design. Taking into consideration the feasibility to manufacture these blades, in this study all the parameters are varied by fixed steps so that each value of an attribute is possible to attain in manufacturing or operating the tiller. A Cartesian product of all these attributes was done to generate all possible combinations of the parameters where each row or tuple would represent a possible blade design.

This dataset is used to calculate the different power requirements, volume of soiled tilled and specific energy of each possible blade. Since, different farms have different types of soils, therefore, based on the type of the soil of the agriculture land

Table 1 Mechanical properties of Boron Steel (SAE-AISI 51B60)

Young's modulus, Pa	190×10^9
Poisson's ratio	0.29
Brinell hardness	200
Density, Kg m^{-3}	7800
Tensile strength: Yield, Pa	400×10^6
Ultimate tensile strength, Pa	660×10^6

Table 2 Instance of the dataset generated by Cartesian product; total rows = 622,080

S. No.	α (°)	φ (°)	B_w (mm)	R (mm)	L_d (mm)	V_f (m/s)	N (rpm)
1	37	10	50	235	120	0.8	150
2	37	10	50	235	120	0.8	180
3	37	10	50	235	120	0.8	210
622,078	42	15	85	260	210	2.8	240
622,079	42	15	85	260	210	2.8	270
622,080	42	15	85	260	210	2.8	300

taken under consideration for tilling by the user, the values for soil bulk density and specific soil resistance can be added accordingly.

The next section will explain all this in detail. These attributes resulted in the creation of a dataset with 622,080 different rows for optimization. The beginning and ending of the dataset is shown in Table 2 which is an instance of the dataset created (by Cartesian product) in excel, first and last 10 rows of the dataset are presented in the below table.

3 Calculation of Specific Energy

The energy requirement is of major importance in current agricultural operations. Energy requirements can be reduced by optimizing the design parameters. Energy requirements affects the cutting forces experienced by the blades which in turn decides the stresses produced in the blade. The wear of the blade is decided by the stresses and hence its life. Therefore, optimization of design is absolutely crucial because it is responsible for both energy requirements and the life of the blade. The design features of a rotavator are the main energy consumption variables. The total power required is the sum of the pushing power, the cutting and loosening of the soil slice, the overcoming of soil-metal friction between the soil and the knife of the rotary blades, and the centrifugal action of the rotary blade throwing the cut soil slice given in Eq. (1). Energy requirement can be represented in terms of the total specific energy required per unit volume of soil tilled by dividing the total power with volume of soil tilled per second. An optimization technique has been put forward for the total specific energy requirement of various blades [3, 10].

This theory was put in numerical form by Dalin and Pavlov [17]:

$$P_{\text{Total}} = P_{\text{Cut}} + P_{\text{Throw}} + P_{\text{Loss}} + P_{\text{mf}} + P_{\text{Push}}$$

$$E_{\text{TSP}} = \frac{P_{\text{Push}} + P_{\text{Cut}} + P_{\text{mf}} + P_{\text{Throw}}}{V_{\text{ST}}}$$

3.1 Calculation of Powers and Mathematical Modelling

$$P_{\text{push}} = \frac{7161.96 V_f P_e \eta_c \eta_Z}{RN \cos(\varphi)} \times [\sin(\alpha) \cos(\varphi) + \cos(\alpha) \sin(\varphi)]$$

$$P_{\text{Cut}} = K_{\text{SP}} \times B_W \times L_d \times V_f \quad P_{\text{mf}} = L_d \times RV_f \times B_w \times S_{\text{PW}} \times \mu_K$$

$$\mu_K = \frac{1.09}{\sqrt{0.105 \times R \times N}}, \quad P_{\text{Throw}} = \frac{0.219 RNL_d V_f B_W S_{\text{PW}} (3R - L_d)}{GZ},$$

$$V_{\text{ST}} = B_W \times L_d \times V_f$$

where:

P_{Total}	total power requirement, kW
φ	the angle of periphery
P_e	engine power, hp (12 hp)
P_{Loss}	Power loss in the power train, kW
L_d	depth of soil cut, m
P_{Push}	pushing power requirement, kW
V_f	Machine forward velocity, m/s
P_{Throw}	throwing the cut soil slice torque
η_c	prime mover's efficiency (0.9)
η_Z	coefficient (0.75) [3]
R	rotor radius, m
E_{TSP}	Total specific power/energy, KJ/m ³
N	rotational speed, rpm
α	the angle of direction
P_{Cut}	Cutting power requirement, kW
K_{SP}	specific soil resistance (7000 Kgm ⁻²) [18]
B_W	width of oil cut, m
P_{mf}	overcoming soil-metal friction power
S_{PW}	Dry soil bulk density (1700 Kgm ⁻³) [3]
μ_K	kinetic coefficient of soil-metal friction
Z	number of blades on the drum (3 blades)
G	acceleration due to gravity
V_{ST}	volume of soil tilled per second

Values for bulk densities (S_{PW}) and specific soil resistance (K_{SP}) are different for different types of soil textures. Based on the field soil, a suitable value for both S_{PW} and K_{SP} can be taken from [3, 18] and put into the model in excel. For reference, soil texture of loam soil and P_e (engine power) as 12 HP is taken in this research, any other value could also be used in the model based on user's choice or requirement.

On substituting Eqs. (3–8), Eq. (2) i.e. E_{TSP} becomes:

$$E_{TSP} = \left\{ \left(\frac{4834.323(V_f P_e) \sin(\alpha + \varphi)}{RN \cos(\varphi)} \right) + B_W L_d S_{PW} V_f \left(\frac{K_{SP}}{S_{PW}} + \frac{1.09R}{\sqrt{0.0105 RN}} + \frac{0.219 RN(3R - L_d)}{G} \right) \right\} / V_{ST} \quad (9)$$

Thus, a smaller effective specific energy requirement will mean a highly efficient blade, generating large amounts of backfill with low energy expenditure, hence, to optimize blade design parameters, E_{TSP} needs to be minimized.

3.2 Mathematical Optimization

$$\text{Minimum } E_{TSP} = \left\{ \left(\frac{4834.323(V_f P_e) \sin(\alpha + \varphi)}{RN \cos(\varphi)} \right) + B_W L_d S_{PW} V_f \left(\frac{K_{SP}}{S_{PW}} + \frac{1.09 R}{\sqrt{0.0105 RN}} \frac{0.219 RN(3R - L_d)}{G} \right) \right\} / V_{ST}$$

with subject to inequality constraints:

$$\begin{aligned} 150 &\leq N \leq 300 \text{ in steps of } 30; \quad 37 \leq \alpha \leq 42 \text{ in steps of } 1; \\ 10 &\leq \varphi \leq 15 \text{ in steps of } 1; \quad 50 \leq B_w \leq 85 \text{ in steps of } 5; \\ 235 &\leq R \leq 260 \text{ in steps of } 5; \quad 120 \leq L_d \leq 210 \text{ in steps of } 10; \\ 0.8 &\leq V_f \leq 2.8 \text{ in steps of } 0.4. \end{aligned}$$

As mentioned previously, a dataset of 622,080 rows was created by Cartesian product of the design parameters which are mentioned above in their respective ranges and steps. Each row combination (entire row) represented a unique set of values i.e. each row had design parameter combination different from any other row in the entire dataset.

Therefore, the dataset had 622,080 possible different blade geometries (parameters), E_{TSP} was calculated for every blade (Eq. 9) and the blades for which the value of E_{TSP} was minimum were filtered out. The function was optimized at values shown in Table 3. For effective vertical length (L_d) of 210 mm, radius of rotation i.e. the distance from axis of rotation of blade to blade tip (R) of 260 mm, blade cutting width or effective horizontal length (B_w) of 85 mm, rotational speed (N) of 300 rpm, E_{TSP} was minimum and its value was 38.640 kJ/m³.

These values were taken to design the L-type blade which is discussed in next section. The dataset contains all the power requirements (P_{push} , P_{Cut} , P_{Throw} and P_{mf}) volume of soil tilled and total specific energy/power for each blade design. Therefore, this dataset can also be used to find the suitable blade design parameters based on the power available at a field or based on how much volume of soil is required to be

Table 3 Design parameters for the minimum value of E_{TSP} from the dataset

Blade No.	Design parameters						Operational parameters				Output	
	α (°)	φ (°)	B_W (mm)	R (mm)	L_d (mm)	V_f (m/s)	N (rpm)	P_e (HP)	$V_{st} \times 10^{-6}$ m ³	E_{TSP} KJ/m ³		
17,250	37	10	85	260	210	0.8	300	12	14280	38.640		
17,256	37	10	85	260	210	1.2	300	12	21420	38.640		
17,262	37	10	85	260	210	1.6	300	12	28560	38.640		
17,268	37	10	85	260	210	2	300	12	35700	38.640		
17,274	37	10	85	260	210	2.4	300	12	42840	38.640		
17,280	37	10	85	260	210	2.8	300	12	49980	38.640		

tilled per second. This will help in efficient blade designs and effective tilling of the land could be achieved.

Figures 1 and 2 show the variation of E_{TSP} with L_d and B_w in the dataset at two different rpms i.e. at 300 and 150 rpm; and with $\alpha = 37^\circ, \varphi = 10^\circ, R = 260$ mm and $V_f = 2$ m/s kept constant for both the speeds.

As it can be seen from the plot in Figs. 3 and 4 that with increasing L_d and B_w , E_{TSP} decreases and from Table 3 it is noted that E_{TSP} is independent of V_f .

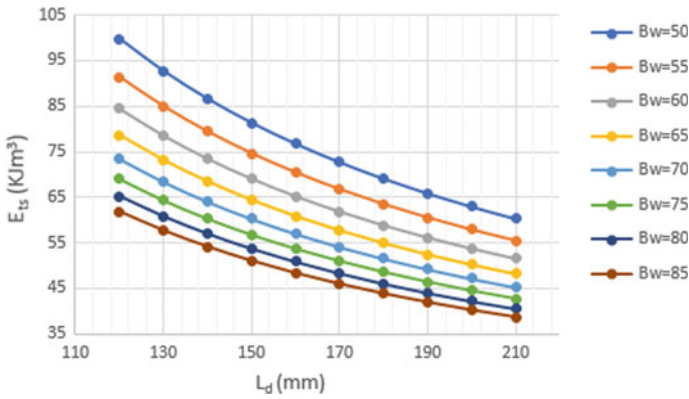


Fig. 1 Variation of E_{tsp} with L_d and B_w for $N = 300$ rpm

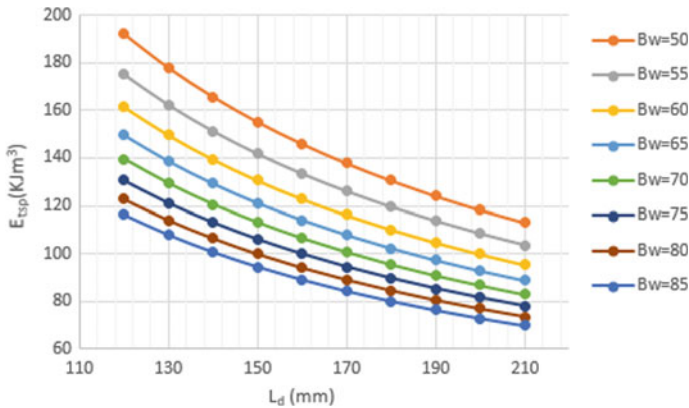
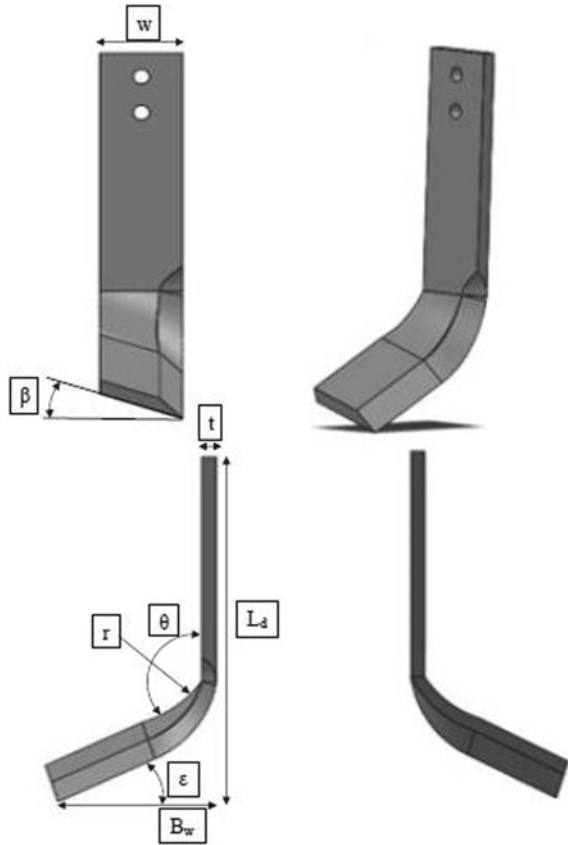


Fig. 2 Variation of E_{tsp} with L_d and B_w for $N = 150$ rpm

Fig. 3 Design of L-blade (front view, isometric view, right view, left view)



4 Design and Analysis

The design of the blade was made in SolidWorks (Fig. 3) according to the optimized geometric parameters (Table 4). Other parameters were taken similar to previous studies so that an easy comparison of the optimized parameters could be done, these were:

Blade width: $w = 40$ mm, Blade angle: $\theta = 108^\circ$, Clearance angle: $\beta = 20^\circ$,
Blade thickness: $t = 8$ mm, Curvature between L_d and B_w : $r = 40$ mm.

4.1 Static Force Analysis

The static analysis of this blade was then done on ANSYS 19 to check total deformation, Von-Mises stress and equivalent elastic strain at three different values of N i.e. 150, 240 and 300 rpm. The total number of nodes in the default mesh generated

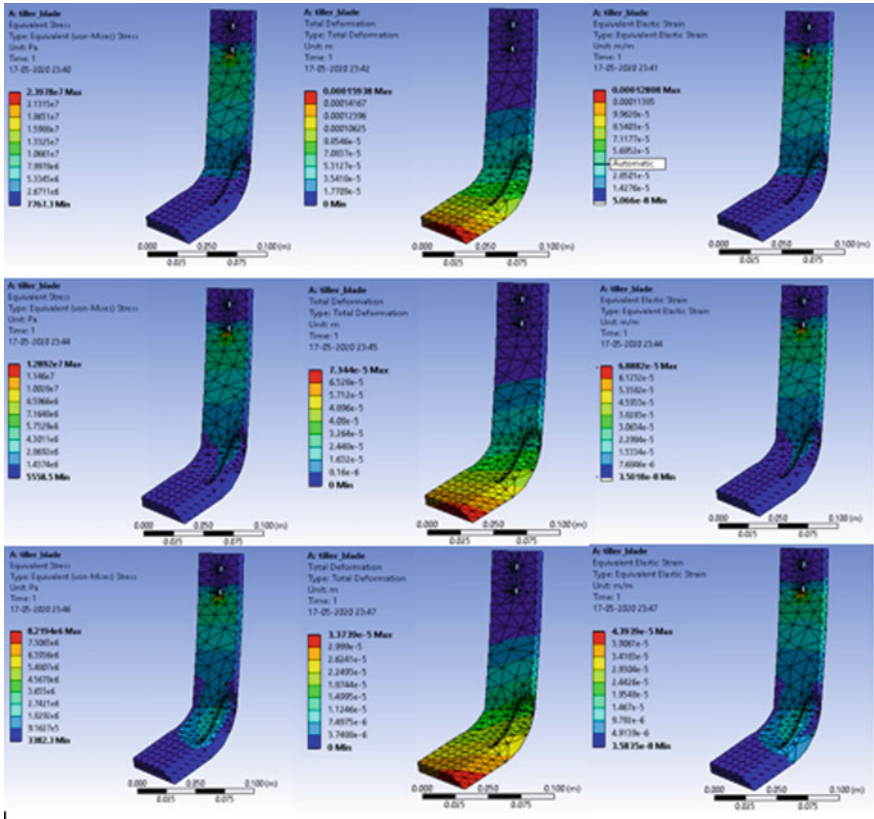


Fig. 4 Equivalent stress, total deformation and equivalent strain Ansys results for 150, 240 and 300 RPM (respectively)

Table 4 Geometrical parameters of L-blade

Parameters	Notations
w	Blade span, mm
L_d	Effective vertical length, mm
B_w	Blade cutting width, mm
r	Curvature between L_d and B_w , mm
θ	Blade angle, degree
β	Clearance angle, degree
t	Blade thickness, mm
ε_i	Bending angle, degree

for designed blade (Fig. 4) in Ansys were 4506 and total number of elements were 2360.

Steps followed in ANSYS for analysis were: import of the design, selection of fixed points, meshing, putting the parameters (rotation velocity and force) and generation of the final solution (Fig. 4).

Three rotational velocities are taken, 150, 240 and 300 rpm. For calculation of force, there are two major forces which act on rotating blade used for tilling or digging operations. Tangential force, P_o , acts at the tip of the blade through tangent of blade cutting edge [19]. Soil force, R_T , acts perpendicular to cutting edge of the blade. For analysis, soil force for is considered as uniformly distributed load acting along the cutting edge.

$$P_o = C_s \frac{75N\eta_z\eta_c}{U_{\min}} \quad R_T = \frac{P_o C_p}{i Z_e N_e}$$

where,

- P_o Maximum tangential force (kg)
- N_c Prime mover tractor power (HP)
- η_c Traction efficiency (0.9)
- η_z Coefficient of reservation of tractor power (0.75)
- C_s Reliability factor that is equal to 1.5 for non-rocky soils and 2 for rocky soils
- U_{\min} Peripheral Velocity (m/s) ($2\pi NR/60$)
- R_T soil force acting perpendicularly on the cutting edges of each of the blades
- C_p coefficient of tangential force (1.5)
- i number of flanges
- Z_e number of blades on each side of the flanges
- N_e number of blades which action jointly on the soil.

Therefore, for calculation of R_T i.e. soil force, $N_c = 12$ HP, $C_s = 1.5$ (non-rocky soil), U_{\min} was calculated for 150, 240 and 300 rpm. Number of flanges, $i = 6$, $Z_e = 3$ and $N_e = 6$. Soil force on blade were found out to be 488, 305 and 244 N for 150, 240 and 300 rpm, respectively. These three force values were used to perform the static force analysis of the rotary tiller blade in Ansys and results are shown in Fig. 4.

4.2 Fatigue Analysis

To calculate the fatigue life or number of cycles for the designed blade, maximum load needs to be applied on the cutting edge of the blade. Maximum stress of 24 MPa was obtained for rotational speed of 150 RPM (Fig. 4), but this was for engine power of 12 HP. Considering different tractor powers available and used in farms, for fatigue

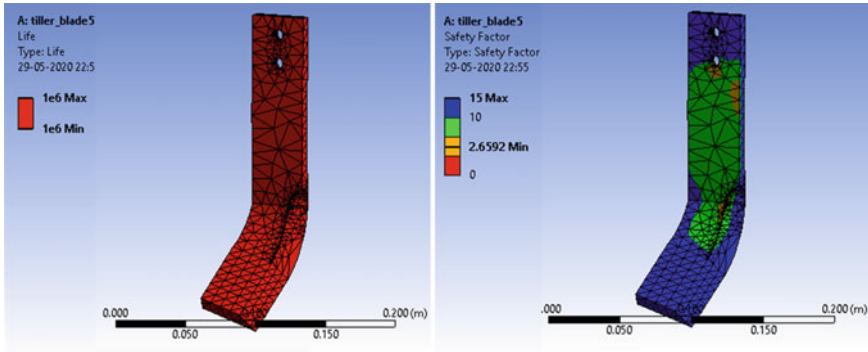


Fig. 5 Fatigue analysis result for blade life and factor of safety

analysis engine power of 40 HP is taken and force on blade for this engine power is calculated to be 1626.67 N from Eq. 10 and 11.

It was observed from various field data and surveys that the life of L-type blade in red soil is about 40–50 h [8]. Red soil is found suitable for important crops like rice, wheat, cotton, sugarcane, etc. and it is present in India in large tracts in western Karnataka, Telangana, Tamil Nadu, Andhra Pradesh, southern Maharashtra, Chhattisgarh, Jharkhand and Odisha and in scattered patches in West Bengal, Uttar Pradesh, Rajasthan [20]. Red soil texture is mainly loamy with traces of clay and sand [21]; and the optimization of blade design in this study was done for loamy soil.

On performing the fatigue analysis for the life of the blade in Ansys (Fig. 5), blade life of 10^6 cycles was obtained. For a speed of 150 rpm, life of 10^6 cycles in terms of hours is approximately 110 h and the Factor of Safety (minimum) of 2.65 was obtained.

5 Results and Discussion

The optimal design parameters corresponding to minimum E_{TSP} (38.64 kJ/m^3) were used to design the blade in SolidWorks 2018 and Boron Steel (SAE-AISI 51B60) was selected as material for the L-type rotary tiller blade. Stress analysis was performed in Ansys 2019 for three different rpm, 150, 240 and 300 to observe the stresses developed in blade under load (Fig. 4), Fig. 6 and Table 5 show the results of this analysis in terms of a plot of stress versus strain for all three different rotational speeds (top 135 node stresses from the blade were taken in each case). Also, the fatigue life of the blade was improved to 110 h.

Mandal [8], Vegad [11], Patil [14] and Shinde [18] also designed a L-type blade and performed its static force analysis. Mandal [8], used engine power of 40 HP and a force of 3800 N was applied on a L-blade and material chosen was structural steel; on applying the same force and rotational speed on blade developed in this study in

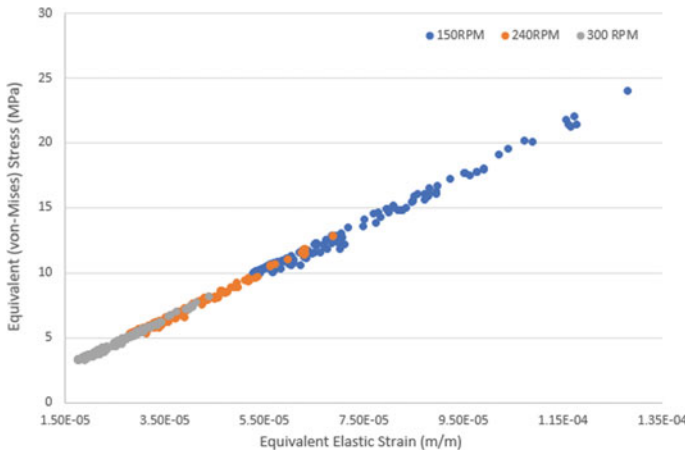


Fig. 6 Stress versus strain plot for result obtained from Ansys static force analysis

Table 5 Maximum values of stress, deformation and strain

N (rpm)	Max. von-mises stress (MPa)	Max. deformation (mm)	Max strain (m/m)
150	24	0.1593	12.8 E-5
240	12.9	0.0734	6.88 E-5
300	8.2	0.0337	4.39 E-5

Ansys, a reduction of 19.6% in maximum stress from 156.54 MPa in Mandal [8] to 125.72 MPa was obtained (Fig. 7). Aniruddha Patil et al. [14] conducted static force analysis for L-blade using various materials (structural steel, cast iron, stainless steel, etc.) On comparing results in Table 6, it can be seen that there is a significant reduction in maximum stress and maximum deformation for a force of 488 N.

Fig. 7 Stress results on applying 3800 N force on blade

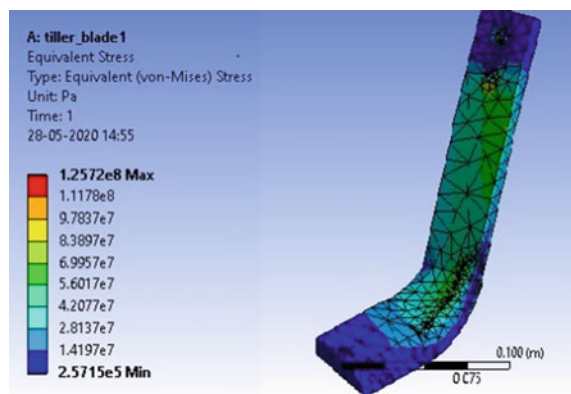


Table 6 Comparison of maximum stresses with Mandal [8] and Patil [14]

Load <i>N</i>	Material	Maximum stress (MPa)
3800	Structural dteel [8]	156.54
	Boron Steel (SAE-AISI 51B60)	125.72
363.3	Stainless steel [14]	62.84
488	Boron Steel (SAE-AISI 51B60)	24

The dataset created in this study can also be used to find blade design parameters based on the cost that needs to be spent on the blades. The optimal design was developed for minimum specific energy, whereas higher the specific energy requirement the lower volume of soil tilled and the most effective and optimum soil tillage operational cost is achieved [3, 10].

Therefore, based on the choice of the user a decision has to be made for the cost trade-off where whether the blade life and power requirements should be optimized or operational cost should be optimized. Hence, this dataset can be used to assess any case or to get an intermediate solution considering a balance of both costs. Further, any soil type or engine (tractor) power can be taken to perform studies.

6 Conclusion

A rotary tiller L-type blade was designed by optimizing its geometrical parameters and cutting angles on the basis of total specific energy requirement. A dataset was created by Cartesian product of 7 design parameters and a total of 622,080 results were obtained where each row is a possible blade design. Optimal design parameters was chosen from this dataset corresponding to minimum E_{TSP} (total specific power/energy requirement). Fatigue life analysis of the blade for red type (loam) soil (Fig. 5) predicted a life of 110 h and a minimum factor of safety of 2.65, which was more than the current life of 50 h.

Therefore, we can conclude that the optimization of rotary tiller blade by minimizing the total specific energy requirement and using Boron Steel (SAE-AISI 51B60) as blade material reduced the maximum stress and deformation produced in the blade significantly, and since high stresses (and wear) is the main reason for the low life of rotary tiller blades, the life of the blade with less stresses will increase notably which was verified by the fatigue analysis which predicted a life of 110 h for the optimized blade. The results of this study should be verified by practical tests on rotary tillers according to the results offered in this paper.

References

1. <https://tradingeconomics.com/india/agricultural-land-percent-of-land-area-wb-data.html>
2. https://www.domain-b.com/economy/agriculture/20200219_foodgrain.html
3. Mandal, S.K., Bhattacharyya, B., Mukherjee, S., Prasad, A.K.: Design optimization of rotary tiller blade using specific energy requirement (2016)
4. Tafesse, M., Intaravichai, S., Saitthiti, B., Kiatiwat, T.: Regression modeling of fuel consumption optimization of rotary blades of power tiller under sandy clay loam condition (2007)
5. Ramulu, C.: Some studies on wear characteristics of Rotavator blade (2016)
6. Mandal, S.K., Bhattacharyya, B., Mukherjee, S. Design of rotary tiller's blade using specific work method (2015)
7. Caslli, Sh., Hasanaj, A., Dimo, Dh.: Optimization of tribological parameters in the design of rotary tiller blades (2017)
8. Mandal, S.K., Mukherjee, S.: Optimization of design parameters for rotary tiller's blade. In: 1st International and 16th National Conference on Machines and Mechanisms (iNaCoMM2013), IIT Roorkee, India, 18-20 December 2013 (2013)
9. Selvi, K.Ç., Kabas, Ö.: Use of SolidWorks in designing agricultural machines (2018)
10. Tafesse, M., Intaravichai, S., Saitthiti, B., Kiatiwat, T.: The optimum design parameters in terms of total specific energy (2007)
11. Vegad, G.M., Yadav, R.: Design analysis and optimization of rotary tiller blades using computer software (2018)
12. Asl, J.H., Singh, S.: Optimization and evaluation of rotary tiller blades: computer solution of mathematical relations (2009)
13. Matani, A.G., Bhishnurkar, A.D.: Use of cad tool for design, analysis and development of rotary tillage tool (2013)
14. Patil, A., Desai, A.: Analysis of Rotavator blade performance through material selection and fatigue analysis through ANSYS simulations. In: National Conference on Progresses and Research in Mechanical Engineering, At Dharwad, India (2017)
15. Ramesh Kumar, D., Mohanraj, P.: Design and analysis of Rotavator blades for its enhanced performance in tractors. Asian J. Appl. Sci. Technol. (AJAST) (2017)
16. Kang, A.S., Cheema, G.S., Singla: Wear behavior of hardfacings on rotary tiller blades. In: 12th Global Congress on Manufacturing and Management, GCMM 2014 (2014)
17. Dalin, A.D., Pavlov, P.V.: Rotary Soil Working and Earth Moving Machines (1950)
18. Shinde, G.U., Kajale, S.R.: Design optimization in rotary tillage tool system components by computer aided engineering analysis. Int. J. Environ. Sci. Dev. 3(3) (2012)
19. Shurdha, Y.: Agricultural Mechanic. Textbook, pp 235-268 (1996)
20. https://en.wikipedia.org/wiki/Red_soil
21. <https://www.pmfias.com/indian-soil-types-red-soils-laterite-lateritic-soils-forest-mountain-soils-arid-desert-soils-saline-alkaline-soils-peaty-marshy-soils/>

Influence of Vegetable Oil Based Lubricants with Nano Particles on Surface Roughness of AISI 1020 and AA 2024 Alloy



T. Ramya, M. Venu, K. T. Sunil Kumar, and K. Anupama Francy

Abstract The present work focuses on performance of nano cutting fluids on vegetable oil in turning of AISI 1020 grade alloy steel and AA 2024 grade aluminum alloy using high speed steel tool inserts. Nano cutting fluids are particularized by dispersing Al_2O_3 nano particles in coconut oil and distilled water separately. After particularization the nano cutting fluids were tested on behalf of elementary properties to estimate its machining activity at different input parameters. Experiments were designed using L_9 orthogonal array. At the time of machining metal removal rate and temperatures at cutting was assessed. The ruggedness of the machined part surface was calculated by using Mitutoyo surf machining. The performance of components was compared by considering dry condition, pure coconut oil, and coconut oil with Al_2O_3 nano particle dispersion. The application of coconut oil based Al_2O_3 resulted in minimum cutting temperatures and surface roughness observed from the experimentation.

Keywords Nano particles · Surface roughness · Cutting fluids

T. Ramya · M. Venu · K. Anupama Francy (✉)

Department of Mechanical Engineering, Vishnu Institute of Technology, Bhimavaram,
West Godavari, Andhra Pradesh, India

e-mail: anupamafrancy.k@vishnu.edu.in

T. Ramya

e-mail: ramyatetali09@gmail.com

M. Venu

e-mail: venu.m@vishnu.edu.in

K. T. Sunil Kumar

Department of Pharmaceutics, Shri Vishnu College of Pharmacy, Bhimavaram, West Godavari,
Andhra Pradesh, India

e-mail: sunil@svcp.edu.in

1 Introduction

In industrial sectors, during the machining process, cutting fluids can perform major role because it can act as both coolant and lubricant. Nowadays, green cutting fluids are used in manufacturing industries to reduce the occurrence of major problems with conventional cutting fluids. Green cutting fluids were found to be environmental friendly.

A complete work was carried out to optimize the cutting parameters when turning of mild steel. Neeraj Saraswat [1] stated the depth of cut, feed rate, and spindle speed for optimization in turning operations of mild steel. D. Philip Selvaraj [2] investigated the turning of AISI 304 austenitic steel using Tics and Tics coated tungsten carbide cutting tool and the input parameters such as cutting speed, feed rate, and depth of cut through cutting speed are the optimal parameters for optimizing surface roughness. Krishna Pal Singh Chauhan [3] has studied the usage of Taguchi's method to maximize the rate of material removal in machining Al6061 alloy by using CNC lathe machine. The experimental results revealed that the $N_3 = 104, f_3 = 0.1, d_3 = 1.2$ gives the maximum material removal rate. For optimization of machining parameters in CNC Turning of Al6063-T₆ using Taguchi-grey analysis was adopted by Sateesh [4]. Puneet Saini [5] investigated the effect on surface roughness of machining parameters in high speed CNC Turning of EN-24 alloy steel using response surface methodology. The optimal surface roughness attained while the feed rate and depth of cut were fixed as low as possible at high cutting speed the low surface finish was achieved. Sodavadia [6] investigated on the performance of coconut oil based nano fluid as lubricants during turning of AISI 304. The experimental results revealed that the cutting temperatures, tool flank wear and surface roughness were decreased significantly with nano lubricants as compared to base oil, due to the better lubricating properties. Investigational surveys were performed out by using Al₂O₃, TiO₂ and SiO₂ as nano particles dispersed in distilled water separately were used as cutting fluids in end milling of mild steel. Finally it is observed that Al₂O₃ distilled water based nano coolant gets least mean temperature compared to other two forms of fluids [7] Okok Pujie. Poorna Chandra [8], the parameters machining can affect the cutting force and surface roughness of EN 24, HcHcr grade steel alloy jobs were the cutting speed, feed, and the machining parameters. The test results showed that the Ra was low at 350 m/min cutting speed, and 0.15 mm/rev feed. The HcHcr grade steel alloy has high hardness compared to EN24 grade alloy steel. Vamsi Krishna [9] conducted wet turning experiments to identify the 0.5% nano boric acid suspensions in SAE-40 and coconut oil to get best results. Agrawal [10] carried out experiments on M2 steel with conventional cutting fluid and aloe vera oil. From the observations it was concluded that mild steel has 6.7% lower surface roughness by using aloe vera oil compared with conventional cutting fluids. And also mild steel gets 0.14% lower tool wear by using aloe vera oil when compared with conventional cutting fluids.

From a sample of above literature, it is evident that no experimental work was conducted on conventional lathe machine by using HSS tool as a cutting tool AISI 1020, AA 2024 material. This experimental work aims to increase the performance

Table 1 Chemical composition of AISI 1020 steel alloy

Element	C	Fe	Mn	P	S
% of Content	0.17–0.23	99.08–99.53	0.30–0.60	0.04	0.05

Table 2 Chemical composition of AA 2024 aluminum alloy

Element	Al	Si	Fe	Cu	Mn	Mg	Cr	Zn	Ti	Others
% of Content	Balance	0.5	0.5	3.80–4.9	0.30–0.9	1.20–1.8	0.1	0.25	0.15	0.05

of conventional lathe machine on response parameters by applying a different type of process parameters and cutting fluids. To get the desired value, Taguchi L_9 orthogonal array was used to find the experimental values and the grey relational analysis.

2 Details of Experimental Work

2.1 Materials

The materials used for this experimental were AISI 1020, AA 2024, specimens HSS Cutting Tool, Distilled water, Pure coconut oil, Al_2O_3 nano particles, By using conventional lathe machine the machining work was carried out. Tachometer, Infrared thermometer, Vernier caliper, Steel rule, beakers, Electronic weighing scale, ultrasonic machine, Magnetic stir bar, were used in this experimental work (Tables 1 and 2).

2.2 Input Parameters and Their Levels

The spindle speed, feed, and depth were considered as input variables in the existing work. The Input variables with their coded levels were listed in Table 3:

Table 3 Levels of the input variables spindle speed, feed, and depth of cut

S. No	Input variables	Level 1	Level 2	Level 3
1	Spindle speed (rpm)	380	480	880
2	Feed (mm/rev)	1	1	1
3	Depth of cut (mm)	0.5	0.75	1

Fig. 1 Lathe machine

2.3 Preparation Technique for Nano Cutting Fluid

For this experiment a two-step nano cutting fluids preparation technique was employed. The Al_2O_3 (as nano particles) was weighed carefully by using electrical precision balance and then dispersed with pure coconut oil in a measured amount of based fluid. A corresponding mixture was achieved by using ultrasonic probe (for 15 mixtures). A single mass concentration of 0.5 gms/100 ml of coconut oil and same technique was used for distilled water nano cutting fluid. The properties of cutting fluids were checked in lab.

2.4 Set up for Experimentation Work

See Fig. 1.

2.5 Experimentation Process

The machined turning experiments were initially performed on all modern lathe machines under constant cutting conditions and in all conditions with nano particle inclusion. The performance of nano cutting fluids was compared with that of dry machine condition, coconut oil condition, and coconut oil with Al_2O_3 nano particles condition. During machining the spindle speed was measured by using Tachometer. With the help of Infrared thermometer the cutting temperatures were measured. In machined component surface ruggedness was assessed by using Mitutoyo SJ-210 surf tester. The L_9 orthogonal array was used to design the experiments in the current work.

Fig. 2 Hardness test on AISI 1020 and AA 2024



Table 4 Hardness values of the work materials

S. No	Material	Type of indicator	Scale	Load	Hardness in RHS
1	AISI 1020	1/16 Ball	B (Red)	100kgf	74.66
2	AA 2024	1/16 Ball	B (Red)	100kgf	70.166

2.6 The Hardness Test on AISI 1020 and AA 2024 Work-Material

The Rock well hardness tests were carried out in accord with the rock well hardness scale standard on RAB 250 model SAROJ hardness tester. The hardness of the AISI 1020 and AA 2024 was measured using 1.58 mm steel ball indenter diameter at normal load of 100 Kgf. The hardness measurement on the work pieces was as shown in Fig. 2 and respective hardness readings were given in Table 4.

3 Results and Discussion

Experimental results are illustrated in Tables 5–10 at various levels of oil condition.

3.1 Material Removal Rate

Graphs of metal removal rate for AISI 1020 and AA 2024 measured under various machining and lubrication conditions with spindle speed and depth of cut are plotted as shown in Fig. 3. MRR is gradually increased with increased depth of cut and spindle speed because the higher the spindle speed, work piece can rotate fast between 380 and 580 rpm. MRR is increased moderately and beyond 580–880 rpm the MRR increased very sharply. So, higher the spindle speed higher the metal removal rate. Means of MRR with depth of cut graph is plotted in Fig. 4 and MRR was observed to increase with increased depth of cut.

Table 5 Experimentation for AISI 1020 in dry condition

Experiment No.	Spindle speed (N) (rpm)	Feed (f) mm/rev	Depth of cut (d) (Mm)	MRR (mm ³ /min)	Cutting temperature (°C)	Ra (μ)
1	380	1	0.5	14928.571	33.8	2.218
2	380	1	0.75	22392.857	32.1	3.946
3	380	1	1	29857.142	35.5	4.537
4	580	1	0.5	34178.571	33.6	4.694
5	580	1	0.75	45571.428	33.4	4.851
6	580	1	1	22785.714	35.2	5.149
7	880	1	0.5	69142.857	35.3	5.496
8	880	1	0.75	34571.42	36.2	6.504
9	880	1	1	51857.142	38.0	6.801

Table 6 Experimentation for AISI 1020 in coconut oil condition

Experiment No.	Spindle speed (N) (rpm)	Feed (f) mm/rev	Depth of cut (d) (Mm)	MRR (mm ³ /min)	Cutting temperature (°C)	Ra (μ)
1	380	1	0.5	14928.571	30.6	2.006
2	380	1	0.75	22392.857	32.2	3.158
3	380	1	1	29857.142	33.4	4.100
4	580	1	0.5	34178.571	31.2	3.164
5	580	1	0.75	45571.428	33.1	4.047
6	580	1	1	22785.714	34.1	4.156
7	880	1	0.5	69142.857	34.9	4.095
8	880	1	0.75	34571.42	35.1	4.205
9	880	1	1	51857.142	37.6	4.567

Table 7 Experimentation for AISI 1020 in coconut oil +Al₂O₃

Experiment No.	Spindle speed (N) (rpm)	Feed (f) mm/rev	Depth of cut (d) (Mm)	MRR (mm ³ /min)	Cutting temperature (°C)	Ra (μ)
1	380	1	0.5	14928.571	30	2.106
2	380	1	0.75	22392.857	30.6	2.222
3	380	1	1	29857.142	32	2.371
4	580	1	0.5	34178.571	30.3	2.531
5	580	1	0.75	45571.428	31.7	3.005
6	580	1	1	22785.714	32.5	3.131
7	880	1	0.5	69142.857	33.7	3.115
8	880	1	0.75	34571.42	33.3	3.512
9	880	1	1	51857.142	36.1	3.885

Table 8 Experimentation for AISI 1020 in distilled water +Al₂O₃

Experiment No.	Spindle speed (N) (rpm)	Feed (f) mm/rev	Depth of cut (d) (Mm)	MRR (mm ³ /min)	Cutting temperature (°C)	Ra (μ)
1	380	1	0.5	14928.571	29.8	2.146
2	380	1	0.75	22392.857	30	3.058
3	380	1	1	29857.142	31.6	4.351
4	580	1	0.5	34178.571	30.2	3.041
5	580	1	0.75	45571.428	31	4.112
6	580	1	1	22785.714	31.8	4.016
7	880	1	0.5	69142.857	33	4.005
8	880	1	0.75	34571.42	32.8	4.116
9	880	1	1	51857.142	35.6	4.725

Table 9 Experimentation for AA 2024 in coconut condition

Experiment No.	Spindle speed (N) (rpm)	Feed (f) mm/rev	Depth of cut (d) (Mm)	MRR (mm ³ /min)	Cutting temperature (°C)	Ra (μ)
1	380	1	0.5	14928.571	34	2.727
2	380	1	0.75	22392.857	35.3	2.408
3	380	1	1	29857.142	36.3	3.435
4	580	1	0.5	34178.571	34.7	2.427
5	580	1	0.75	45571.428	36.2	1.868
6	580	1	1	22785.714	37.4	4.288
7	880	1	0.5	69142.857	36.8	1.605
8	880	1	0.75	34571.42	38.3	1.530
9	880	1	1	51857.142	40.2	1.743

Table 10 Experimentation for AA 2024 in coconut +Al₂O₃

Experiment No.	Spindle speed (N) (rpm)	Feed (f) mm/rev	Depth of cut (d) (Mm)	MRR (mm ³ /min)	Cutting temperature (°C)	Ra (μ)
1	380	1	0.5	14928.571	32.0	1.998
2	380	1	0.75	22392.857	32.2	2.346
3	380	1	1	29857.142	32.9	3.052
4	580	1	0.5	34178.571	33.2	1.580
5	580	1	0.75	45571.428	34.4	1.529
6	580	1	1	22785.714	33	1.619
7	880	1	0.5	69142.857	34.6	1.565
8	880	1	0.75	34571.42	35.8	1.510
9	880	1	1	51857.142	34.5	1.635

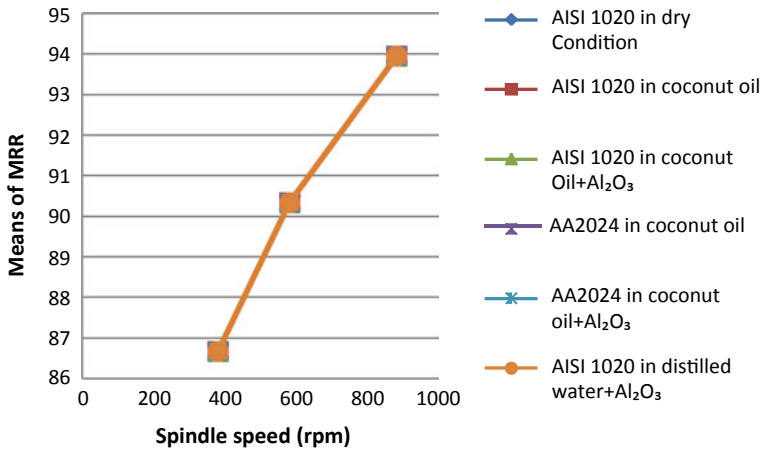


Fig. 3 Means of MRR with spindle speed

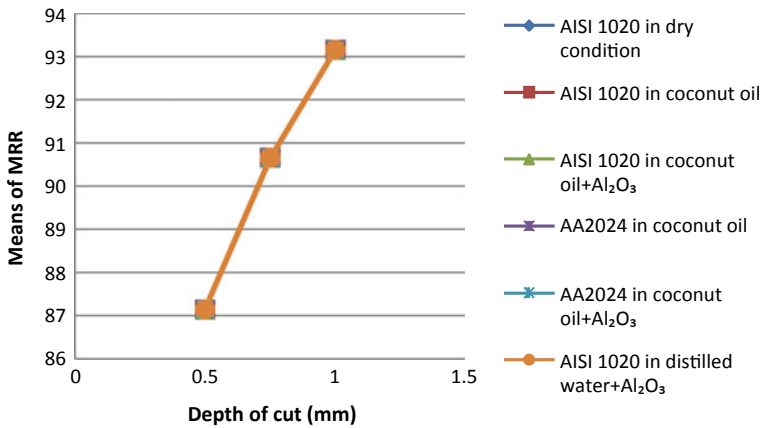


Fig. 4 Means of MRR with depth of cut

3.2 Cutting Tool Temperature

From the measurement of cutting tool temperature for AISI 1020 and AA 2024 materials, the cooling action of lubricants with nano solid lubricants suspensions was clearly evident. Means of cutting temperature with spindle speed was plotted in graph as shown in Fig. 5. Cutting temperatures increased with spindle speed at all the machining conditions. And also cutting temperature increased with increase in depth of cut (Fig. 6). The lowest cutting tool temperature obtained at the combination of coconut oil with Al₂O₃ nano particles was due to the best lubricating properties

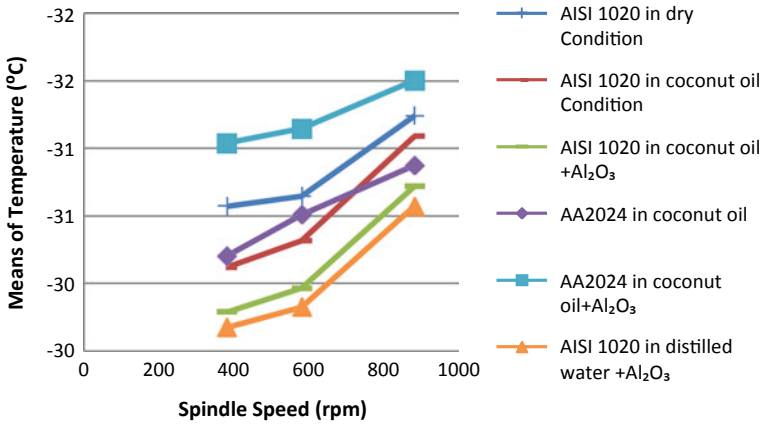


Fig. 5 Means of cutting tool temperature with spindle speed

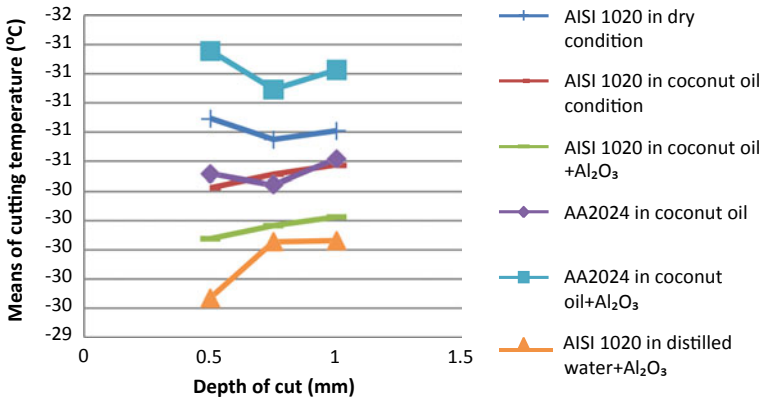


Fig. 6 Means of cutting tool temperature with depth of cut

of coconut oil, and further, the nano particles increase the heat transfer capacity of cutting fluids.

3.3 Surface Roughness

For AISI 1020 grade steel alloy and AA 2024 grade aluminum initially have the minimum surface roughness which increased with increase in spindle speed at all the machining conditions. It can be clearly observed from the graph in Fig. 7. The means of surface roughness versus depth of cut were plotted in the Fig. 8. As a consequence of selected cutting fluid conditions, surface roughness increased with

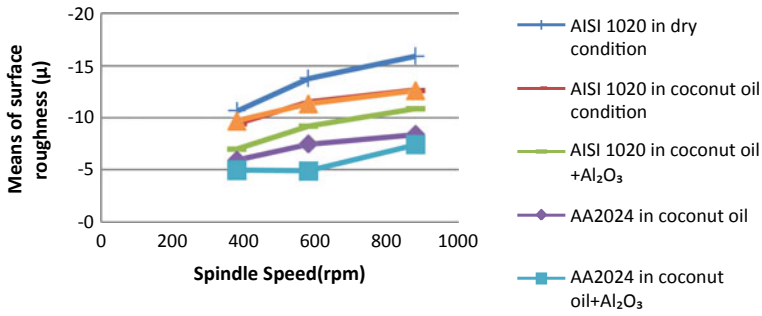


Fig. 7 Means of surface roughness with spindle speed

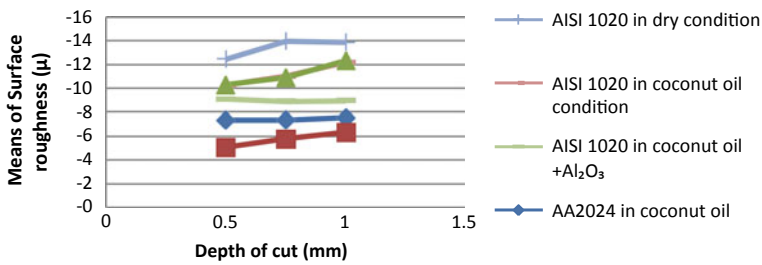


Fig. 8 Means of surface roughness with depth of cut

increased cutting depth. The minimum surface roughness was obtained by using 0.5% of Al₂O₃ Nano particles dispersed in coconut oil, since it has good lubricating properties which reduced the frictional forces between the tool and work piece; hence lower temperatures developed and eventually preventing tool wear, consequently extended tool life, which can be attributed to the surface quality enhancement.

4 Conclusion

The Nano cutting fluids were prepared by using nano particles of Al₂O₃ in coconut oil. The pH value, density, and viscosity values decreased with 0.5% w/w Al₂O₃ nano particles. Cutting temperature and surface roughness were reduced significantly with nano cutting fluids as compared to coconut oil alone. Coconut oil with 0.5% w/w Al₂O₃ nano particles showed good performance compared to other cutting fluids in terms of material removal rate, cutting temperature, and surface roughness.

References

1. Saraswat, N., Yadav, A., Kumar, A., Srivastava, B.P.: Optimization of cutting parameters in turning operation of mild steel. *Int. Rev. Appl. Eng. Res.* **4**(3), 251–256 (2014)
2. Selvaraj, D.P., Chandramohan, P.: Optimization of surface roughness of AISI 304 austenitic stainless steel in dry turning operation using Taguchi design method. *J. Eng. Sci. Technol.* **5**(3), 293–301 (2010)
3. Chauhan, K.P.S.: Experimental investigation to optimize machining parameters of Al 6061 alloy. *Int. J. Eng. Res. Technol.* **6**, 419–424 (2017)
4. Sateesh, N., Satyanarayana, K., Karthikeyan, R.: Optimization of machining parameters in turning of Al6063A-T6 using Taguchi-Grey analysis. *Mater. Today Proc.* **5**(9), 19374–19379 (2018)
5. Saini, P., Parkash, S., Choudhary, D.: Experimental investigation of machining parameters for surface roughness in high speed CNC turning of EN-24 alloy steel using response surface methodology. *Int. J. Eng. Res. Appl.* **4**(5), 153–160 (2014)
6. Sodavadia, K.P., Makwana, A.H.: Experimental investigation on the performance of coconut oil based nano fluid as lubricants during turning of AISI 304 austenitic stainless steel. *Int. J. Adv. Mech. Eng.* **4**(1), 55–60 (2014)
7. Okokpujie, I.P., Ohunakin, O.S., Adelekan, D.S., Bolu, C.A., Gill, J., Atiba, O.E., Aghedo, O.A.: Experimental investigation of nano-lubricants effects on temperature distribution of mild steel machining. *Proc. Manuf.* **35**, 1061–1066 (2019)
8. Chandra, P., Prakash Rao, C.R., Kiran, R.: Influence of machining parameter on cutting force and surface roughness while turning alloy steel. *Mater. Today Proc.* **5**(5), 11794–11801 (2018)
9. Krishna, P., Vamsi, R., Srikanth, R.R., Rao, N.: Experimental investigation on the performance of nanoboric acid suspensions in SAE-40 and coconut oil during turning of AISI 1040 Steel. *Int. J. Mach. Tools Manuf.* **50**(10), 911–916 (2010)
10. Agarwal, S.M., Patil, N.G.: Experimental study of non edible vegetable oil as a cutting fluid in machining of M2 Steel using MQL. *Proc. Manuf.* **20**, 2017–212 (2018)

Experimental Investigation, Parametric Optimization, and Cost Analysis in EDM of Aluminium-Silicon Carbide Metal Matrix Composite



Subhashree Naik, Soumyashree Sabat, Sudhansu Ranjan Das,
Debabrata Dhupal, and Bijoy Kumar Nanda

Abstract The objectives of this investigation were to find out the optimal cutting parameters and to predict the tool wear rate using a brass electrode in electrical discharge machining process for aluminium-silicon carbide metal matrix composite. The cutting parameters investigated in this research included discharge current, gap voltage, pulse-on time, pulse-off time and flushing pressure with vegetable oil-based dielectric fluid. Additionally, the response surface methodology (RSM) and analysis of variance (ANOVA) are employed, respectively, for experimental analysis, predictive modeling, and process optimization based on the Box-Behnken design of Experiments (BBDs). Then, the most appropriate optimal solution is used for cost-effective analysis. Subsequently, the performance of suggested RSM optimization method is estimated from the confirmation test. Finally, the economic analysis has been performed using a novel approach to evaluate the total machining cost for each part of rupees Rs. 151.69 during machining of aluminium-silicon carbide metal matrix composite under optimal machining conditions. Results were further analyzed using SEM study to investigate the cause of discharge current on topographical features of the machined surface.

Keywords EDM · Al-SiC MMC · TWR · Optimization · Cost analysis

1 Introduction

Owing to the advancement in the material science and technology, newer material with striking material characteristics are produced in today's world. From day to day, metal matrix composites (MMC) have extensively used in production industries like

S. Naik (✉) · S. Sabat · S. R. Das · D. Dhupal
Department of Production Engineering, Veer Surendra Sai University of Technology, Burla
768018, Odisha, India
e-mail: subhashree728@gmail.com

B. K. Nanda
Department of Mechanical Engineering, NIT, Rourkela, Odisha, India

© The Author(s), under exclusive license to Springer Nature Singapore Pte Ltd. 2021
B. Deepak et al. (eds.), *Advanced Manufacturing Systems and Innovative Product Design*,
Lecture Notes in Mechanical Engineering,
https://doi.org/10.1007/978-981-15-9853-1_15

175

aerospace, electronics, nuclear, defense, automobile, and manufacturing sectors due to their favorable characteristics like lightweight, excellent wear and high temperature resistance and high strength compared to conventional materials [1]. However, there are some problems in machining of such aforesaid advanced materials, namely Al-SiC metal matrix composite by the conventional machining processes. Its high hardness, strength, and less weight creates a serious issue of surface integrity and electrode wear. Therefore, an effective, sustainable, and reasonable technology, namely electrical discharge machining (called, EDM) helps overcoming these problems due to the excessive temperature produced by electric spark which mostly creates negligible cutting force with lowest amount of stress on the workpiece surface for removal of material with flexibility of production. However, because of the complicated and dynamic performance of EDM technique and its secure connection with a variety of parameters, large production can be obtained from the economic point of views. Many parameters affect the cutting performance in EDM like flushing pressure of dielectric [2], dielectric fluids [3], spark variables (pulse time, current, voltage, frequency) [4], electrode materials [5], etc. As well, for successful application of EDM technique as the replacement of traditional machining of several hard to cut materials can be advanced in terms of machining cost, quality, efficiency, and productivity with the most suitable and optimum input factors, which mostly waste valuable time and attempt. Under such conditions, to satisfy many typical and conflicting objectives, there is efficient use of optimization technique, modeling, and experimentation which can make EDM technique to be the most significant choice for cutting of advanced MMCs by using a recent solution. Many approaches like computational, statistical such as RSM [6], ANN [7] have been applied for predictive modeling, PSO [8], ANFIS [9], GA [10], PCA [11], and TOPSIS [12] have been used for parametric along with input parameter optimization in EDM technique. Extensive investigation has been performed with several design of experiments, modeling methods, and optimization techniques to study the machinability [13], to determine the several process outputs, and to control the process parameters during machining of various work materials (MDN 300, AISI D6, D3, D2, stainless steel, AISI 316L, grey cast iron, A2 tool steel, Inconel 601, 825, 718, Ni alloy, Al-6063, Al-6061, Al-7075 alloy, Al/SiC MMC, WC, Al-Mg₂Si, Si₃N₄/TiN MMC, poly-crystalline diamond). Though many trials have been made by researchers, the process characteristics have been found out with their related input parameters to manage the necessities of electrical discharge machining process. To enhance the material effectiveness, further analysis is required to study the effects of different machining parameters. Depending on the literature study, it is found that no likely investigations were achieved on machining hard to cut material, as aluminium-silicon carbide metal matrix composite, using EDM technique. Moreover, it was observed that maximum literature investigated on MRR, over cut, and surface quality of the machined part but the main intension is to estimate the machining performance i.e., tool wear rate and surface cracking which were not emphasized broadly. Comparatively, until now almost no researcher has performed any economic study to enable a cost-effective production with EDM. So far, to the best knowledge of the researchers, the research has not explored the safer and cleaner environment, which becomes an ideal worthy research in the current

study. Consider the recent study where the main aim is to investigate the machining efficiency in EDM of aluminium-silicon carbide metal matrix composite regarding tool wear rate, also dealing with the process factors such as gap voltage, discharge current, flushing pressure, pulse-off time, and pulse-on time. Experimentations based on Box-Behnken’s design (BBDoEs), response surface methodology (RSM) with analysis of variance (ANOVA) are consecutively applied for experimental study, predictive modeling with process optimization. The best optimal result is adopted for cost-effective analysis to justify the effectiveness of EDM technique for hard to cut materials. Results were analyzed to a greater extent using SEM micrograph to study the cause of discharge current on topographical features of the machined surface in terms of crack width and morphology of the surface formed after machining.

2 Materials and Methods

To carry out a series of experimental runs, a highly accurate CNC EDM machine tool (MAKE: ECOWIN, MODEL: MIC 432CS) has been used with highest effective current of 60 amp produced in Taiwan. At the time of machining of Al-SiC MMCs, tool wear rate (TWR) is measured by applying the equation $(T_B - T_A)/T$ that is, the weight variation of the tool material is calculated between previous to and after the EDMing with time period of ‘T’ obtained with digital weighing machine. Scanning electron microscope is used for the morphological study of the EDMed surface to improve the machinability as well as for the better understanding of EDMing technique. The experimental setup is presented in Fig. 1.

The various levels of EDMing parameters are selected from literature overview [14] and the workpiece has been gone through a throughout hole of satisfactory quality after examining. Table 1 reports the detailed EDMing parameters with their consequent levels used for the experimentation in actual along with coded values.

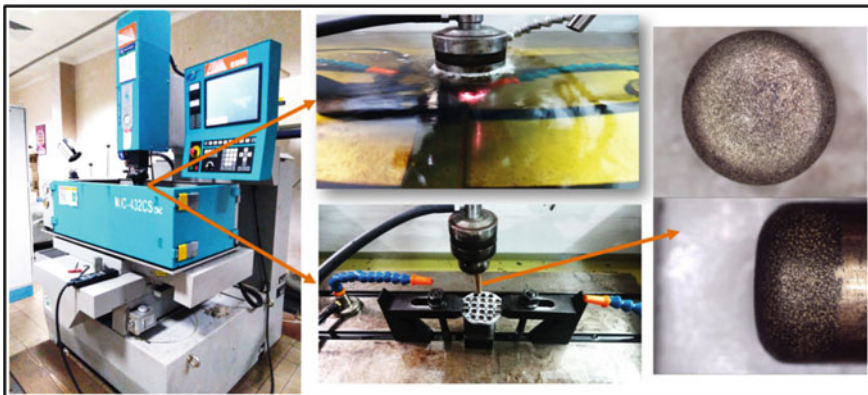


Fig. 1 Experimental unit

Table 1 Machining process factors with their corresponding levels

Process parameters	Levels		
	-1	0	1
discharge current (DC) in amp	5	10	15
gap voltage (GV) in V	1	1.5	2
pulse-on time (T _{ON}) in μ s	100	200	300
pulse-off time (T _{OFF}) in μ s	10	20	30
flushing pressure (FP) in kgf/cm ²	0.2	0.4	0.6

The suggested design of experimentation associates with the five process factors (GV, DC, T_{ON}, T_{OFF}, FP) at three different levels. The forty-six numbers of experimental runs are performed which is completely based on Box-Behnken design of experimentations (BBDos). Table 2 reports the experimental design layout with machining results after trials.

3 Results and Discussion

3.1 Response Surface Methodology Based Predictive Model

The outcomes based on the response characteristics achieved in accordance with experimentations using Box-Behnken's design (BBDos) were studied in Minitab17 by response surface methodology and the empirical model was developed for the technological response characteristics i.e., tool wear rate during machining by the stated EDMing parameters such as GV, DC, T_{ON}, T_{OFF}, FP). The developed model used for the response which is found out using regression analysis is presented below:

$$\begin{aligned}
 \text{TWR} = & 0.00104 - 0.000139 \text{ DC} + 0.000217 \text{ GV} + 0.000003 \text{ T}_{\text{ON}} \\
 & - 0.000032 \text{ T}_{\text{OFF}} + 0.00073 \text{ FP} + 0.000011 \text{ DC} \times \text{DC} \\
 & + 0.000253 \text{ GV} \times \text{GV} - 0.000000 \text{ T}_{\text{ON}} \times \text{T}_{\text{ON}} + 0.000001 \text{ T}_{\text{OFF}} \times \text{T}_{\text{OFF}} \\
 & - 0.00262 \text{ FP} \times \text{FP} - 0.000045 \text{ DC} \times \text{GV} + 0.000000 \text{ DC} \times \text{T}_{\text{ON}} \\
 & - 0.000001 \text{ DC} \times \text{T}_{\text{OFF}} + 0.000231 \text{ DC} \times \text{FP} - 0.000001 \text{ GV} \times \text{T}_{\text{ON}} \\
 & - 0.000009 \text{ GV} \times \text{T}_{\text{OFF}} - 0.000140 \text{ GV} \times \text{FP} + 0.000000 \text{ T}_{\text{ON}} \times \text{T}_{\text{OFF}} \\
 & - 0.000003 \text{ T}_{\text{ON}} \times \text{FP} - 0.000005 \text{ T}_{\text{OFF}} \times \text{FP}
 \end{aligned}$$

$$R^2 = 93.94\%, R^2(\text{adj.}) = 89.09\% \quad (1)$$

The results of tool wear rate achieved through experimentation, used to obtain a comprehensive statistical test using analysis of variance (ANOVA) which represents a

Table 2 Layout of the experimental design with results

Run order	Coded values					Actual settings					
	DC	GV	T _{ON}	T _{OFF}	FP	DC	GV	T _{ON}	T _{OFF}	FP	TWR (gm/s)
1	-1	-1	0	0	0	5	1.0	200	20	0.4	0.0008390
2	1	-1	0	0	0	15	1.0	200	20	0.4	0.0025681
3	-1	1	0	0	0	5	2.0	200	20	0.4	0.0013163
4	1	1	0	0	0	15	2.0	200	20	0.4	0.0026000
5	0	0	-1	-1	0	10	1.5	100	10	0.4	0.0017020
6	0	0	1	-1	0	10	1.5	300	10	0.4	0.0013380
7	0	0	-1	1	0	10	1.5	100	30	0.4	0.0013870
8	0	0	1	1	0	10	1.5	300	30	0.4	0.0013370
9	0	-1	0	0	-1	10	1.0	200	20	0.2	0.0014540
10	0	1	0	0	-1	10	2.0	200	20	0.2	0.0014910
11	0	-1	0	0	1	10	1.0	200	20	0.6	0.0013770
12	0	1	0	0	1	10	2.0	200	20	0.6	0.0013580
13	-1	0	-1	0	0	5	1.5	100	20	0.4	0.0009310
14	1	0	-1	0	0	15	1.5	100	20	0.4	0.0019910
15	-1	0	1	0	0	5	1.5	300	20	0.4	0.0007910
16	1	0	1	0	0	15	1.5	300	20	0.4	0.0025318
17	0	0	0	-1	-1	10	1.5	200	10	0.2	0.0015930
18	0	0	0	1	-1	10	1.5	200	30	0.2	0.0014260
19	0	0	0	-1	1	10	1.5	200	10	0.6	0.0015790
20	0	0	0	1	1	10	1.5	200	30	0.6	0.0013750
21	0	-1	-1	0	0	10	1.0	100	20	0.4	0.0012510
22	0	1	-1	0	0	10	2.0	100	20	0.4	0.0014860
23	0	-1	1	0	0	10	1.0	300	20	0.4	0.0012350
24	0	1	1	0	0	10	2.0	300	20	0.4	0.0013070
25	-1	0	0	-1	0	5	1.5	200	10	0.4	0.0009070
26	1	0	0	-1	0	15	1.5	200	10	0.4	0.0027030
27	-1	0	0	1	0	5	1.5	200	30	0.4	0.0008070
28	1	0	0	1	0	15	1.5	200	30	0.4	0.0023900
29	0	0	-1	0	-1	10	1.5	100	20	0.2	0.0009270
30	0	0	1	0	-1	10	1.5	300	20	0.2	0.0012380
31	0	0	-1	0	1	10	1.5	100	20	0.6	0.0009820
32	0	0	1	0	1	10	1.5	300	20	0.6	0.0010200
33	-1	0	0	0	-1	5	1.5	200	20	0.2	0.0008670
34	1	0	0	0	-1	15	1.5	200	20	0.2	0.0019250

(continued)

Table 2 (continued)

Run order	Coded values					Actual settings					
	DC	GV	T _{ON}	T _{OFF}	FP	DC	GV	T _{ON}	T _{OFF}	FP	TWR (gm/s)
35	-1	0	0	0	1	5	1.5	200	20	0.6	0.0005520
36	1	0	0	0	1	15	1.5	200	20	0.6	0.0025360
37	0	-1	0	-1	0	10	1.0	200	10	0.4	0.0013300
38	0	1	0	-1	0	10	2.0	200	10	0.4	0.0015090
39	0	-1	0	1	0	10	1.0	200	30	0.4	0.0013030
40	0	1	0	1	0	10	2.0	200	30	0.4	0.0012950
41	0	0	0	0	0	10	1.5	200	20	0.4	0.0014440
42	0	0	0	0	0	10	1.5	200	20	0.4	0.0011810
43	0	0	0	0	0	10	1.5	200	20	0.4	0.0012270
44	0	0	0	0	0	10	1.5	200	20	0.4	0.0014880
45	0	0	0	0	0	10	1.5	200	20	0.4	0.0014690
46	0	0	0	0	0	10	1.5	200	20	0.4	0.0015120

table having degrees of freedom, mean and sum of squares (MS with SS), probability and Fisher's values (P with F). The validity and the significance of the developed regression model for the EDMing output characteristic (TWR) have been checked as well as determined using ANOVA table, also used to determine the interaction with individual effects of different EDMing parameters on the stated output. Usually, the statistical significance is taken at 95% confidence level where P value is below 0.05, with F value is higher than the standardized Fisher's value. Table 3 shows that the model developed for tool wear rate in electrical discharge machining is significant. After carrying out the investigation, it was found that among the various input factors that have been taken during machining of Al-SiC MMC, the significant terms at 95% confidence level are DC, DC * DC, T_{ON} * T_{ON} with DC * FP. As well it is seen that DC is the main affecting factor with 75.00% contribution following the square terms T_{ON} * T_{ON}, DC * DC with interaction effect DC * FP with 7.04%, 0.91%, and 1.18%, respectively. Also the above mentioned parameters are significant because its F and P values validate the statistical significance criterion. On the other hand, the factors that is to say, gap voltage, pulse-off and pulse-on time, flushing pressure and interactions such as DC * GV, DC * T_{OFF}, DC * T_{ON}, GV * T_{OFF}, GV * T_{ON}, GV * FP, T_{ON} * FP, T_{ON} * T_{OFF}, T_{OFF} * FP found insignificant effect on TWR, due to their contributions which are very negligible.

A number of diagnostic tests like effectiveness, adequacy, and goodness-of fit were executed for the obtained regression model (TWR) to avoid the misleading result for the suggested model. The goodness-of-fit for the model is statistically significant as the determined coefficient of determination, R^2 value (0.939 for TWR) approaches to one.

Table 3 ANOVA outcomes for process response predictive models

Model for tool wear rate (TWR)						
Source	DF	SS	Contr. %	MS	F value	P value
Model	20	0.000011	91.67	0.000001	19.37	<0.000010
Linear	05	0.000010	80.46	0.000002	65.43	<0.000010
DC	01	0.000009	75.00	0.000009	321.02	<0.000010
GV	01	0.000000	1.78	0.000000	2.17	0.153
T _{ON}	01	0.000000	1.84	0.000000	0.04	0.838
T _{OFF}	01	0.000000	0.92	0.000000	3.86	0.061
FP	01	0.000000	0.91	0.000000	0.04	0.837
Square	05	0.000001	8.33	0.000000	8.94	<0.000010
DC * DC	01	0.000001	7.04	0.000001	22.58	<0.000010
GV * GV	01	0.000000	0.03	0.000000	1.20	0.284
T _{ON} * T _{ON}	01	0.000000	0.91	0.000000	4.71	0.040
T _{OFF} * T _{OFF}	01	0.000000	0.18	0.000000	2.17	0.153
FP * FP	01	0.000000	0.16	0.000000	3.30	0.081
2-way interaction	10	0.000000	02.49	0.000000	1.55	0.181
DC * GV	01	0.000000	0.09	0.000000	1.70	0.204
DC * T _{ON}	01	0.000000	0.00	0.000000	3.98	0.057
DC * T _{OFF}	01	0.000000	0.32	0.000000	0.39	0.538
DC * FP	01	0.000000	1.18	0.000000	7.36	0.012
GV * T _{ON}	01	0.000000	0.00	0.000000	0.23	0.637
GV * T _{OFF}	01	0.000000	0.31	0.000000	0.30	0.589
GV * FP	01	0.000000	0.00	0.000000	0.03	0.871
T _{ON} * T _{OFF}	01	0.000000	0.50	0.000000	0.85	0.367
T _{ON} * FP	01	0.000000	0.08	0.000000	0.64	0.431
T _{OFF} * FP	01	0.000000	0.00	0.000000	0.01	0.915
Error	25	0.000001	8.71	0.000000		
Lack-of-fit	20	0.000001	8.18	0.000000	1.50	0.346
Pure error	05	0.000000	0.53	0.000000		
Total	45	0.000012	100			

3.2 Parametric Effect on Process Response

The effect of input factors (gap voltage, discharge current, pulse-off time, pulse-on time, and flushing pressure) on performance characteristic (TWR) is graphically studied by 3D surface plot. Figure 2a gives an idea about the tool wear rate which increases with rise in discharge current. The actual reason is the production of high discharge energy, which generates maximum heat at the machining surface where melting and vaporization of MMC material caused by energy transfer and enormous

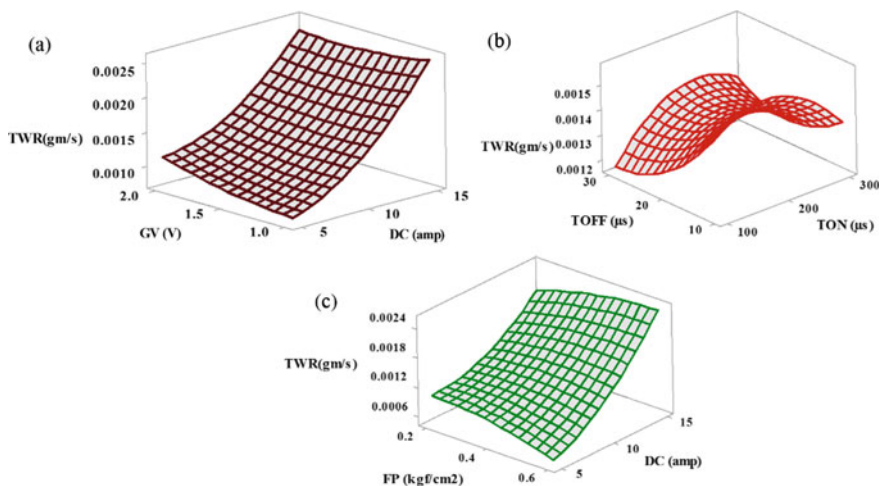


Fig. 2 Surface plots to illustrate the EDMing parameters effect on tool wear rate

amount of heat produced due to the spark resulting in an increased TWR. It is clearly observed from Fig. 2b that rise in pulse-on time increases the TWR to some extent, after that TWR falls with rise of T_{ON} beyond $200 \mu\text{s}$. From the 3D plot between the discharge current and flushing pressure Fig. 2c shows that increase in flushing pressure raises the tool wear rate. This is due to the reason that increasing flushing pressure restricts the accumulation of erosion products in between the cut of MMC workpiece and brass electrode surface, because the short circuit pulses are becoming rarer, and there is increase in working efficiency and tool wear rate. Figure 3 presents the SEM micrograph of EDMed surface containing crater (produced due to various types of interaction between the circulations of dielectric, debris, and electrical spark), debris in the form of globular modules (because of cohesion effect in the machined surface due to cold welding effects, molten material, and deficiency of flushing by dielectric fluid in between the cut), micro crack (due to overreach of the stress that induced over the tensile strength of MMC material produced by fast heating and cooling issue), micro voids (because of formation of gas during discharge process), and micro pores (because of low thermal shock resistance and fracture toughness of Al/SiC MMC).

3.3 Response Surface Methodology Based Optimization

The current research contains desirability based single-objective optimization approach of RSM to remain the tool wear rate to the minimum during EDMing. The most effective way to improve the process efficiency and product quality is design of parameter. The single-objective optimization problems can be solved by applying

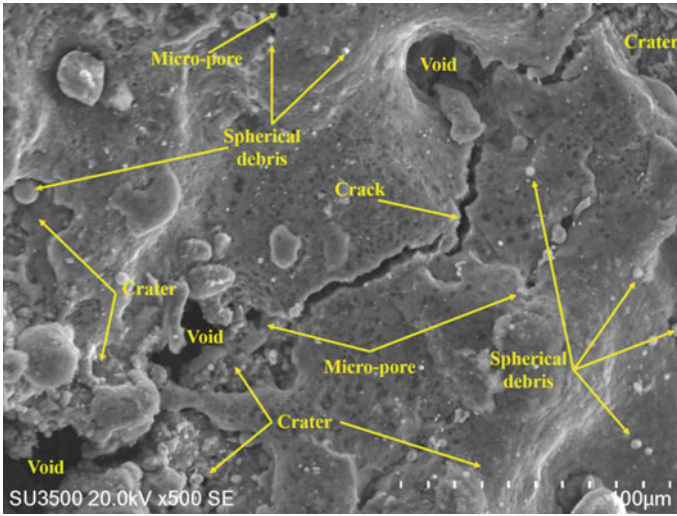


Fig. 3 SEM image of machined component having poor surface quality at $GV = 1.5$ V, $DC = 15$ amp, $TON = 200 \mu s$, $TOFF = 20 \mu s$, and $FP = 0.6 \text{ kgf/cm}^2$

the statistical based desirability function approach. The optimization outcome is calculated depending on the overall desirability i.e., weighted-geometric mean of corresponding desirability for the stated output measure considered within the range of 0–1. If the desirability value approaches to 0, then the response will be totally rejected or undesirable and if the value is near or equal to 1, then the response will be highly desirable or accepted.

The parameter design problems can be solved by using desirability function approach where the objective function $F(x)$ is stated as [15, 16]:

$$F(x) = -DF \tag{2}$$

The composite desirability function is as follows:

$$DF = \left(\prod_{i=1}^n d_i^{w_i} \right)^{1/\sum_{j=1}^n w_j} \tag{3}$$

The DF evaluates the optimal setting by minimizing $F(x)$ (maximization of DF is more preferable), d_i represents the desirability for the i th targeted performance measure, and w_i represents the weighting of d_i . The main aim is, minimization of technological parameters, so individual desirability can be defined as:

$$d_i = 1 \text{ if } Y_i \leq L_i.$$

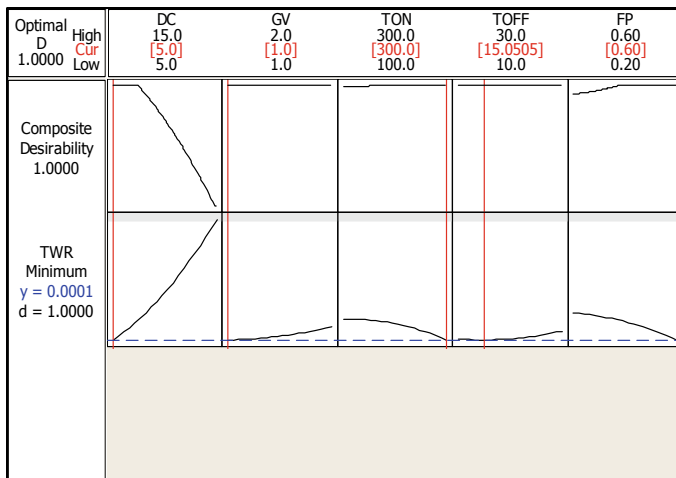


Fig. 4 Optimization plot for minimum tool wear rate using desirability function approach

$$d_i = \left[\frac{H_i - Y_i}{H_i - L_i} \right] \text{ if } L_i \leq Y_i \leq H_i \tag{4}$$

$$d_i = 0 \text{ if } Y_i \geq H_i$$

Here H_i and L_i are the most and least suitable value of Y for the i th technological characteristic, respectively. Figure 4 represents the optimization plot showing the optimal manufacturing conditions with desirability function approach for the process response of EDMing of Al/SiC MMC with discharge current (DC) of 5 amp, gap voltage (GV) of 1 V, pulse-on time (T_{ON}) of 300 μ s, pulse-off time (T_{OFF}) of 15 μ s, and flushing pressure (FP) of 0.6 kgf/cm². Finally, the optimal value that is being estimated for the pre-cited technological response is 0.0001 gm/s for TWR.

3.4 Confirmation Test

To avoid the confusing result obtained from the RSM optimization technique, the conclusion was validated by conducting a confirmation test. The experimental and optimal values of technological characteristic (TWR) were compared under the machining condition obtained by RSM technique as shown in Table 4. The error percentage obtained from RSM is 5.66%.

Table 4 Overview of confirmation test with corresponding error

Method	Optimum EDM parametric setting					Tool wear rate, MRR (gm/s)		Error (%)
	DC	GV	T _{ON}	T _{OFF}	FP	Predicted	Experimental	
RSM	5	1	300	15.05	0.6	0.0001	0.000106	5.66

Table 5 Cost evaluations in EDMed drilled hole of Al/SiC MMC

Variables	In min.	Cost	In indian Rs.
Tool positioning and zeroing time, T _p	1	machining cost per min., C _{mach/min}	Rs. 8.33
Work-piece clamping with positioning time, T _{clamp}	5	operator cost per min., C _{op/min}	Rs. 5.83
Hole drilling time at optimized cutting conditions, T _d	4.37	single tool cost, C _{elcd}	Rs. 15
Tool drawing out time, T _{edr}	1	total cutting cost per part, C _{tot} = {(C _{elcd}) + (T _{tot} *C _{mach/min}) + [(T _{clamp} + T _{edr})*1.2*C _{op/min}]}	Rs. 151.69
Total cutting time per part, T _{tot} = (T _{clamp} + T _p + T _{edr} + T _d)	11.37		

3.5 Cost Analysis

Cost awareness becomes the basic venture during EDMing in competent production system. So as to determine the production cost, essential criteria are chosen depending on product shape, accuracy, and tooling method. These days the pressure is more on cost and profit management, so the total machining cost becomes standardized by the company to establish consistency and cost benchmarks for subsequent time. The machining operations are analyzed to obtain the optimum economic conditions to avoid involvement of large expenditure. The production cost and production rate are definitely influenced by the selection of technological parameters. The total EDMing cost per part has been obtained by performing cost analysis, by considering the best optimum machining conditions proposed by RSM [17], presented in Table 5. It is observed that the total EDM cutting cost per part at optimum parameter setting is considerably lesser around Rs. 151.69. Here the cost estimation ensures that there is sudden gain in productivity. The most cost-effective solution to machine Al-SiC MMC is obtained by using brass as tool material.

4 Conclusions

In the presented case of machining of Al-SiC MMC using electrical discharge machining, several conclusions are obtained as follows:

- ANOVA analysis with 3D surface plot described that, pulse-on time and discharge current are the most influencing parameters which affect the tool wear rate (TWR) to the maximum.
- From the result it was found that discharge current has maximum contribution of 75.00% in dimensional deviation of tool wear rate.
- Surface morphology of machined surface of Al/SiC MMC is very unsatisfying (due to globules of debris, craters, micro-cracks, and voids).
- Carbide layer deposition takes place at the bottom of electrode due to dielectric cracking. And this carbide layer becomes the reason of electrode wear and affects the retention capability of electrode shape as well as machining accuracy.
- The total estimated machining cost is no more than Rs. 151.69, which is beneficial from economical point of view.

In future work, the investigation can be continued to study the effect of surface quality with different type of dielectric fluids to reduce the TWR. Moreover, future research requires for sustainability performance of electrical discharge machining process.

References

1. Mohan, B., Rajadurai, A., Satyanarayana, K.G.: Electric discharge machining of Al-SiC metal matrix composites using rotary tube electrode. *J. Mater. Process. Technol.* **153–154**, 978–985 (2004)
2. Gohil, V., Puri, Y.M.: Statistical analysis of material removal rate and surface roughness in electrical discharge turning of titanium alloy (Ti-6Al-4 V). *Proc. Inst. Mech. Eng. Part B J. Eng. Manuf.* **232**(9), 1603–1614 (2016)
3. Li, C., Xu, X., Li, Y., Tong, H., Ding, S., Kong, Q., Zhao, L., Ding, J.: Effects of dielectric fluids on surface integrity for the recast layer in high speed EDM drilling of nickel alloy. *J. Alloy. Compd.* **783**, 95–102 (2019)
4. Rahul, Mishra, D. K., Datta, S., Masanta, M.: Effects of tool electrode on EDM performance of Ti-6Al-4 V. *Silicon* **10**(5), 2263–2277 (2018)
5. Mohanty, C.P., Satpathy, M.P., Mahapatra, S.S., Singh, M.R.: Optimization of cryo-treated EDM variables using TOPSIS-based TLBO algorithm. *Sadhana* **43**(4), 51 (2018)
6. Chiang, K.-T., Chang, F.-P., Tsai, D.-C.: Modeling and analysis of the rapidly resolidified layer of SG cast iron in the EDM process through the response surface methodology. *J. Mater. Process. Technol.* **182**(1–3), 525–533 (2007)
7. Sidhu, S.S., Batish, A., Kumar, S.: Neural network-based modeling to predict residual stresses during electric discharge machining of Al/SiC metal matrix composites. *Proc. Inst. Mech. Eng. J. Eng. Manuf.* **227**(11), 1679–1692 (2013)
8. Moghaddam, M.A., Kolahan, F.: Modeling and optimization of the electrical discharge machining process based on a combined artificial neural network and particle swarm optimization algorithm. *Scientia Iranica* **27**(3), 1206–1217 (2019)
9. Nguyen, T.-T., Tran, V.-T., Mia, M.: Multi-response optimization of electrical discharge drilling process of SS304 for energy efficiency, product quality, and productivity. *Materials* **13**(13), 2897 (2020)
10. Padhee, S., Nayak, N., Panda, S.K., Dhal, P.R., Mahapatra, S.S.: Multi-objective parametric optimization of powder mixed electro-discharge machining using response surface methodology and non-dominated sorting genetic algorithm. *Sadhana* **37**(2), 223–240 (2012)

11. Sahu, S.N., Nayak, N.C.: Multi-criteria decision making with PCA in EDM of A2 tool steel. *Mater. Today Proc.* **5**(9), 18641–18648 (2018)
12. Tripathy, S., Tripathy, D.K.: Multi-attribute optimization of machining process parameters in powder mixed electro-discharge machining using TOPSIS and grey relational analysis. *Eng. Sci. Technol. Int. J.* **19**(1), 62–70 (2016)
13. Rahul, Datta, S., Biswal, B.B., Mahapatra, S.S.: Machinability analysis of Inconel 601, 625, 718 and 825 during electro-discharge machining: on evaluation of optimal parameters setting. *Measurement* **137**, 382–400 (2019)
14. Gopalakannan, S., Senthilvelan, T.: Application of response surface method on machining of Al–SiC nano-composites. *Measurement* **46**(8), 2705–2715 (2013)
15. Naik, S., Das, S.R., Dhupal, D.: Experimental investigation, predictive modeling, parametric optimization and cost analysis in electrical discharge machining of Al-SiC metal matrix composite. *Silicon* (2020). <https://doi.org/10.1007/s12633-020-00482-6>
16. Costa, N.R., Lourenço, J., Pereira, Z.L.: Desirability function approach: a review and performance evaluation in adverse conditions. *Chemometr. Intell. Lab. Syst.* **107**(2), 234–244 (2011)
17. Skrabalak, G.: Influence of electrode tool length on the micro EDM drilling performance. *Procedia CIRP* **68**, 594–598 (2018)

Optimum Design and Analysis of Bell Crank Lever for an Automobile



Ch. Sowjanya, V. Nagabhushana Rao, and B. Pavani Sri Kavya

Abstract Bell crank lever plays a vital role in the automotive manufacturing process plant in which they are installed. An attempt has been made to design and analyze the bell crank lever using CATIA and ANSYS Simulation software. The analysis is made under static loading condition for different angles such as 60, 90, 135°. The bell crank lever with different materials such as Cast iron, Low carbon steel, Magnesium alloy, and Aluminum silicon carbide have been selected for similar operating conditions. It has been analyzed by varying lever angles for the different materials and comparison is made on the basis of Von mises stresses, strains, and deformations. The shape optimization process is applied to bell crank lever. Shape optimization process helps to remove unwanted material to ensure light weight of the component. In the shape optimization process different slots such as Tapered slot, Rectangle slot, and curved slots are considered by removing the unnecessary material from component. This technique of shape optimization reduces the mass and can make the component lighter so that it can withstand higher loading conditions.

Keywords Bell crank lever · ANSYS simulation · Stress analysis · Shape optimization

Ch. Sowjanya (✉) · V. Nagabhushana Rao
Department of Mechanical Engineering, Raghu Institute of Technology and Management,
Vizianagaram 531162, India
e-mail: chandu.sowjanya21@gmail.com

V. Nagabhushana Rao
e-mail: vnbrao24ster@gmail.com

B. Pavani Sri Kavya
Vignan Institute of Information Technology, Visakhapatnam, India

1 Introduction

A bell crank resembles a capital letter L, has two arms with a pivot position at the 90° angle. This thesis contains designing and Analysis of bell crank lever using CATIA and ANSYS simulation software. It has been analyzed by varying lever angles for the different materials and comparison is made. Materials such as Cast iron, Low carbon steel, Magnesium alloy and a composite material aluminum silicon carbide is used. In modern days light weight of the components plays an important role in automobile industry. The best material and angle is considered and undergoes shape optimization process to obtain light weight material.

The objectives of this study is to analyze the bell crank lever using finite element method.

1. Analyzing the bell crank lever using finite element method.
2. Determine stresses on bell crank lever.
3. Determine Shape optimization process
4. Determine different slots by shape optimization process

Bell crank lever has great worth in automotive manufacturing process. In automobile industry weight plays significant role in cars and hence attempts are being made by engineers to bring down the weight of the car without compromising at the material strength and engine performance. This can be achieved by selecting the best suitable material and choosing the optimal shape of bell crank lever. In this thesis an attempt is made to design and analyze different materials and different angles to obtain optimum material and angle. Shape optimization technique is also considered to reduce the mass in order to obtain light weight of the component. The novelty of this thesis work is that the shape optimization has been utilized which can reduce the weight of the component by removing unwanted material and thus make the component lighter without compromising the performance.

2 Previous Work

Mr M M Dange, Prof S R Zaveri [1] Author says the stress pattern in Bell Crank Lever is studied in analytical, numerical, and photo elasticity methods. For numerical analysis bell crank lever is prepared using ANSYS where stress analysis is done by using FEM. Finite element analysis is performed on various models of varying fillet radius, optimization for volume and reduction of materials from bell crank lever and by using photo elasticity. Comparison between numerical, FEM, and experimentally are observed and that results obtained are in close agreement with each other with minimum percentage of error.

Lucas V. Fornace, San Diego [2] Author analyzed and optimized bell crank lever used in 2005 formula one car race. In this study static structural analysis of bell crank lever is done using the boundary conditions observed in the working conditions of

suspension system of a formula race car. In ANSYS stress and deformation plot has been produced for the given working conditions. After preparing an optimized design of bell crank lever, stress and deformation plot has been prepared for the same operating conditions. A considerable reduction in mass and peak load has been observed. This work better explains the way of optimization of a component.

Aman Sharma [3] Use of bell crank lever in commercial vehicles as well as racing vehicles makes it a good selection for research work. In this research work, study comprises of three parts. Initially it comprises a static analysis of bell crank lever which has been taken as a reference model from an international research paper. After that, it involves developing some improved models after observing the static analysis of reference model. Finally, comparison of the reference and improved models has been done based on ANSYS stress and deformation plots. At last the best optimized model has an appreciable amount of reduction in stress as well as weight. Some of the previous studies analyzed the bell crank lever in various directions i.e. fillet radius optimization [5], stress analysis [6–8], Finite element models [9], topology optimization [10] and fatigue analysis [11] etc.

3 Analytical Estimation of Stresses

In this thesis, analysis of bell crank lever with varying angles and materials is considered and optimization of mass of bell crank lever undergoes static loading condition of 1000 N. Properties of materials used for bell crank lever are given in Table 1.

Considering 2D design of bell crank lever with 90° angle and cast iron material is considered and are as follows (Fig. 1):

- Length of load arm $L_1 = 155$ mm
- Length of effort arm $L_2 = 135$ mm
- Inner Diameter of fulcrum, $r_i = 35$ mm
- Outer Diameter of Fulcrum $r_o = 50$ mm
- Calculation for bell crank lever for angle $\theta = 90^\circ$

Take moments about a point O

$$F \times 155 = P \times 135$$

$$P = 1148.148 \text{ N}$$

Table 1 Properties of different materials

Materials	Young's modulus (GPa)	Yield strength (MPa)	Tensile strength (MPa)	Poisson ratio	Density (kg/m ³)
CI	168	276	700	0.29	7250
LCS	207	233	365	0.27	7800
MA	45	193	230	0.29	1800
ALSIC	100	324	365	0.29	2790

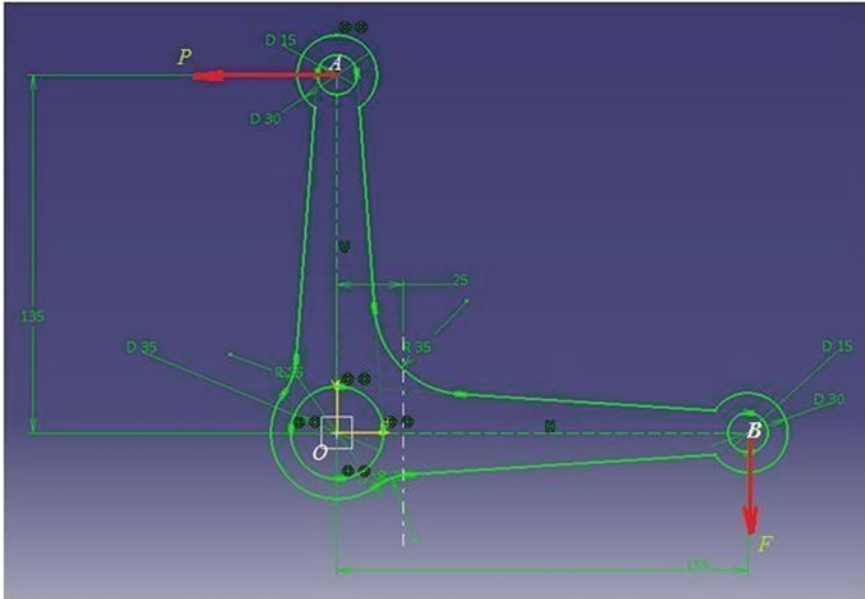


Fig. 1 Bell crank lever 2D design

Resultant force acting at the fulcrum

Substituting values of F and P in R

$$\begin{aligned} R &= \sqrt{F^2 + P^2} \\ &= 1522.57 \text{ N} \end{aligned} \quad (\text{i})$$

Design of fulcrum pin:

Bending Moment at the fulcrum

$$\begin{aligned} M &= F \times 155 \\ &= 155,000 \text{ N mm} \end{aligned}$$

Section Modulus, t = Thickness of the lever, b = Width of the lever

$$\begin{aligned} Z &= \frac{1}{6}tb^2 \\ &= 2730.67 \text{ mm}^3 \end{aligned} \quad (\text{ii})$$

Bending Stress, substituting values of M and Z from Eq. (ii)

$$\begin{aligned}\sigma_f &= \frac{M}{Z} \\ &= 56.76 \text{ N/mm}^2\end{aligned}\quad (\text{iii})$$

Design for pin at B

Bending moment at $x-x$

$$M = 1000(155 - 25) = 130,000 \text{ N mm}$$

Bending Stress,

$$\begin{aligned}\sigma_x &= \frac{M}{Z} \\ &= 47.60 \text{ N/mm}^2\end{aligned}\quad (\text{iv})$$

Design for pin at A

Taking distance from the centre of the fulcrum to $y-y$ axis as 25 mm,

Bending moment at $y-y$

$$\begin{aligned}M &= 1000(135 - 25) \\ &= 110,000 \text{ N mm}\end{aligned}$$

Bending Stress,

$$\begin{aligned}\sigma_y &= \frac{M}{Z} \\ &= 40.28 \text{ N/mm}^2\end{aligned}\quad (\text{v})$$

Von-Mises Stress:

Substituting values of σ_x and σ_y from Eqs. (iv) and (v)

$$\begin{aligned}\sigma &= \sqrt{\sigma_x^2 + \sigma_y^2 - \sigma_x \sigma_y + 4\tau_{xy}^2} \\ &= 4.7 \times 10^7 \text{ Pa}\end{aligned}\quad (\text{vi})$$

Von-Mises Strain:

$$\begin{aligned}\varepsilon &= \frac{1}{1 + \nu} \sqrt{\frac{1}{2}(\varepsilon_1 - \varepsilon_2)^2 + (\varepsilon_2 - \varepsilon_3)^2 + (\varepsilon_3 - \varepsilon_1)^2} \\ \varepsilon_1 &= \frac{1}{E} [\sigma_x - \nu(\sigma_y + \sigma_z)] \\ &= 0.211\end{aligned}$$

$$\begin{aligned}\varepsilon_2 &= \frac{1}{E}[\sigma_y - \nu(\sigma_z + \sigma_x)] \\ &= 0.155 \\ \varepsilon_3 &= \frac{1}{E}[\sigma_z - \nu(\sigma_x + \sigma_y)] \\ &= -0.149\end{aligned}$$

$$\begin{aligned}\varepsilon &= \frac{1}{1 + \nu} \sqrt{\frac{1}{2}(\varepsilon_1 - \varepsilon_2)^2 + (\varepsilon_2 - \varepsilon_3)^2 + (\varepsilon_3 - \varepsilon_1)^2} \\ \varepsilon &= 0.000294\end{aligned}\tag{vii}$$

Maximum Principal Stress

$$\begin{aligned}\sigma &= \frac{\sigma_x + \sigma_y}{2} + \frac{1}{2} \sqrt{(\sigma_x - \sigma_y)^2 + 4(\tau_{xy})^2} \\ &= 4.7 \times 10^7 \text{ Pa}\end{aligned}\tag{viii}$$

Minimum Principal Stress

Substituting values of σ_x and σ_y from Eqs. (iv) and (v)

$$\begin{aligned}\sigma &= \frac{\sigma_x + \sigma_y}{2} - \frac{1}{2} \sqrt{(\sigma_x - \sigma_y)^2 + 4(\tau_{xy})^2} \\ &= 4.01 \times 10^7 \text{ Pa}\end{aligned}\tag{ix}$$

Moment of inertia for rectangular section

$$\begin{aligned}I &= \frac{bd^3}{12} \\ &= \frac{16 \times 32^3}{12} \\ &= 43,690.66 \text{ mm}^4\end{aligned}$$

Deformation

$$\begin{aligned}\delta &= \frac{PL^3}{3EI} \\ &= 0.000167 \text{ m}\end{aligned}\tag{x}$$

Factor of safety

$$\begin{aligned}
 (FOS)_{CI} &= \frac{\text{yield strength}}{\text{working stress}} \\
 &= 4.86
 \end{aligned}
 \tag{ix}$$

4 Preparation of Model of Bell Crank Lever for 90°

A sketch of bell crank lever for different angles is created in 2D and converted to 3D solid model by using CATIA software. Bell crank lever is designed in 2D as shown in Fig. 2 and then modeled in 3D as shown in Fig. 3, the angle between the arms of the bell crank lever is 90°. By using these solid models, analysis is done for cast iron at an angle 90° with ANSYS software, and the results are shown below.

4.1 Analysis for 90° Angle Model

Cast iron

Comparing results of analytical and simulated values of bell crank lever for 90° (Table 2).

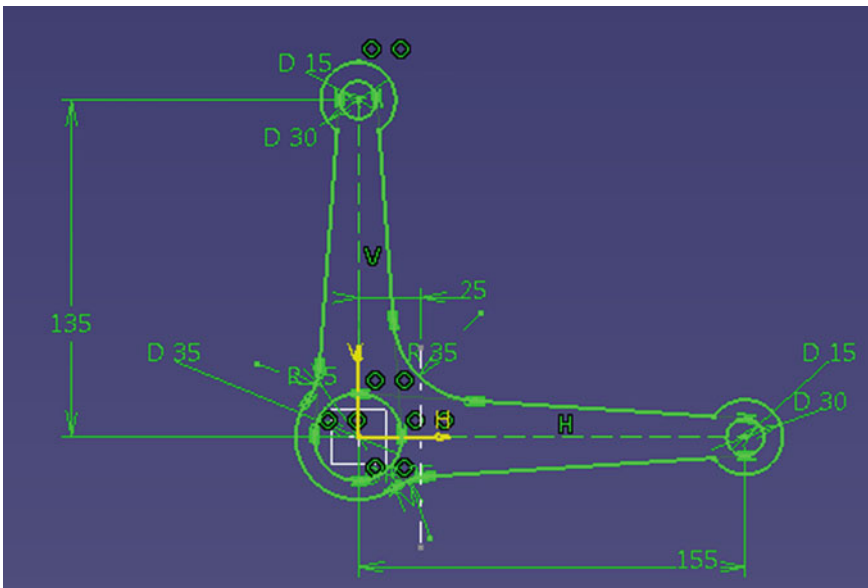


Fig. 2 2D model of bell crank lever

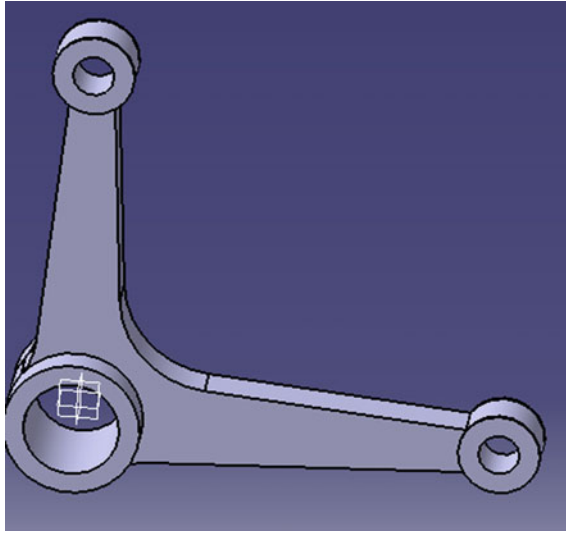


Fig. 3 3D model of bell crank lever

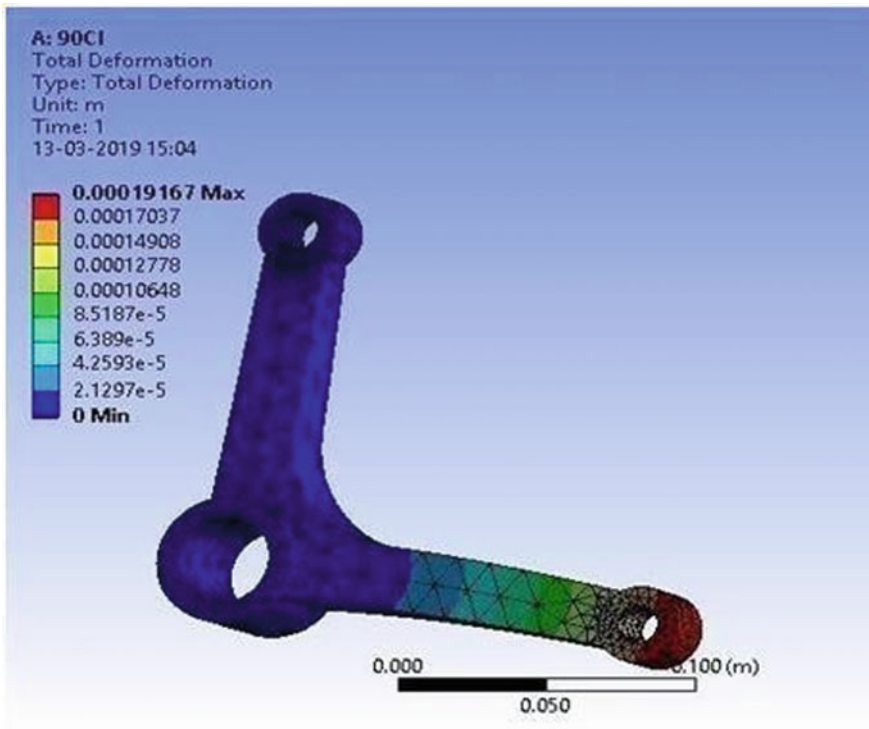


Fig. 4 Total deformation

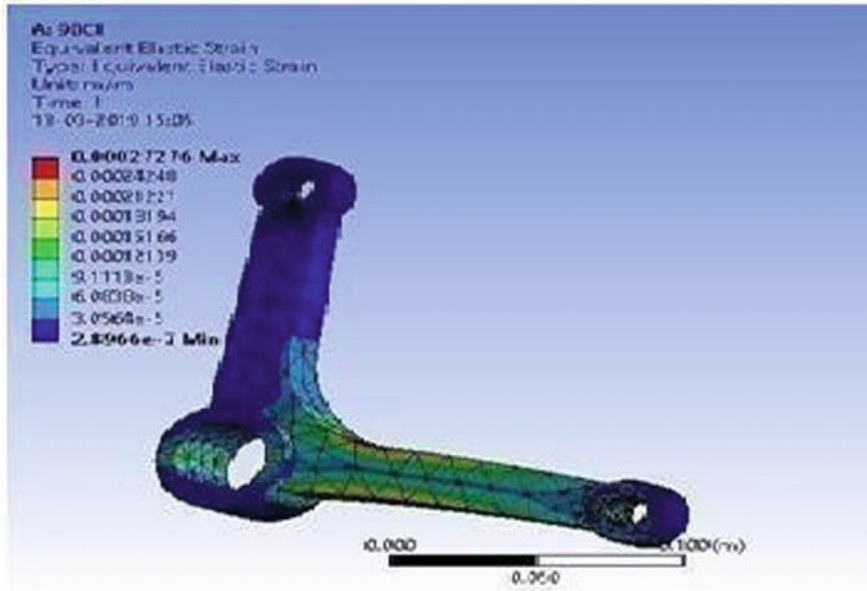


Fig. 5 Von-mises strain

- Cast iron with 90° model is considered and analytical values with simulated values of bell crank lever are compared, as they are almost equal further for different angles and different materials are considered and simulated by using ANSYS simulation software.
- Bell crank is a variety of crank that permits changes in movement at angles such as 90, 180, and 360°. The wider the angle extended by the crank, the more non linear the direction of motion which increases high stresses at angles over a period of time. In this thesis an attempt is made only for angles 60, 90, 135 because at 155° angle simulated stress values observed are high therefore we have considered only three angles.
- Comparing different materials and angles out of which 135° angle with aluminum silicon carbide material contains less stress values as shown below.

4.2 Aluminum Silicon Carbide

Bell crank lever 135° angle with aluminum silicon carbide contains less von mises stress as shown in Fig. 10, Factor of safety in Fig. 11, less von mises strain from Fig. 12, less max principal stress from Fig. 13, Minimum deformation in Fig. 14 and min. principal stress as shown in Fig. 15.

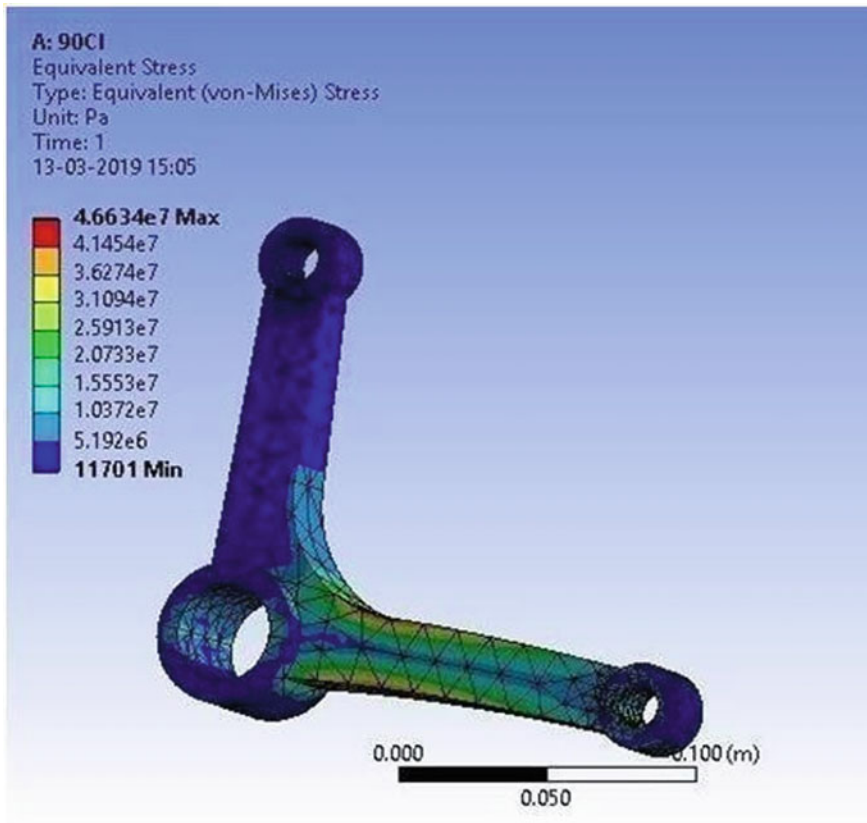


Fig. 6 Von mises stress

5 Shape Optimization

Shape optimization is part of field of best control theory and used to find the optimal while fulfilling the given constraints. Shape optimization is a process which is used to reduce the mass where the minimum stresses acted on a required object, at the same time it can bear the same loading conditions. Using finite element models, the shape is defined by the grid point locations. Applying the shape optimization for 135° angle bell crank lever since the above results obtained in the previous chapter shows that the best results are obtained for 135° angle. Hence applying the shape finder to the 3D object of the bell crank lever, the following results are found (Fig. 16).

Red colour on the object indicates the extra material in the object and it can be removed. Therefore different slots such as tapered slot, curved, slot and rectangular slots are considered and material is removed from the object. After considering the slots, the object undergoes simulation process with same loading conditions, to check whether it can withstand or not.

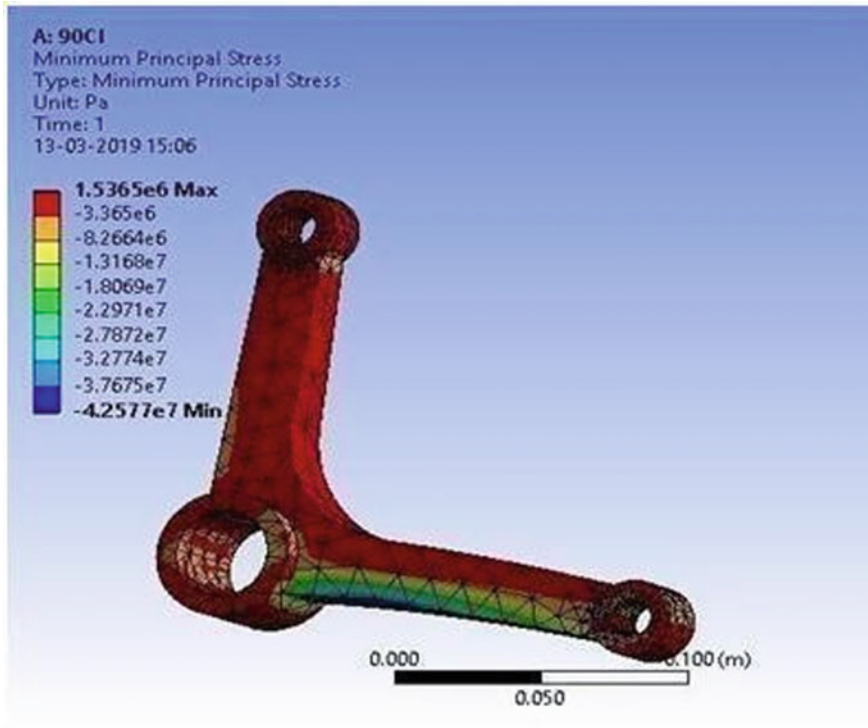


Fig. 7 Min principal stress

5.1 3D Objects Created in CATIA for Different Slots

The following figure shows the stress distribution of the bell crank lever for 1350 angle after undergone shape optimization (Figs. 17, 18, 19, 20, 21, 22, 23, 24 and 25).

Analyzing various design parameters induced in lever before and after Shape optimization of the bell crank lever by using ANSYS (Table 3).

- From the simulated results obtained from FEM, material and angle with less stress is considered. Bell crank lever for 1350 with aluminum silicon carbide is considered a light weight material weighs 403.5 g before optimization with a static load of 1KN. For the same component three different slots i.e., tapered slot, rectangle slot, and curved slot is considered and optimized at the place where stress is not acting.
- This can be known by using shape finder. After optimization weight of tapered slot is 350.0 g, rectangle slot is grams, curved slot is 357.6 g.
- From the comparison of results stresses acting for different slots are as follows; for tapered slot $9.3938e7$, for rectangle slot $8.3806e7$, for curved slot $9.48e7$. Even

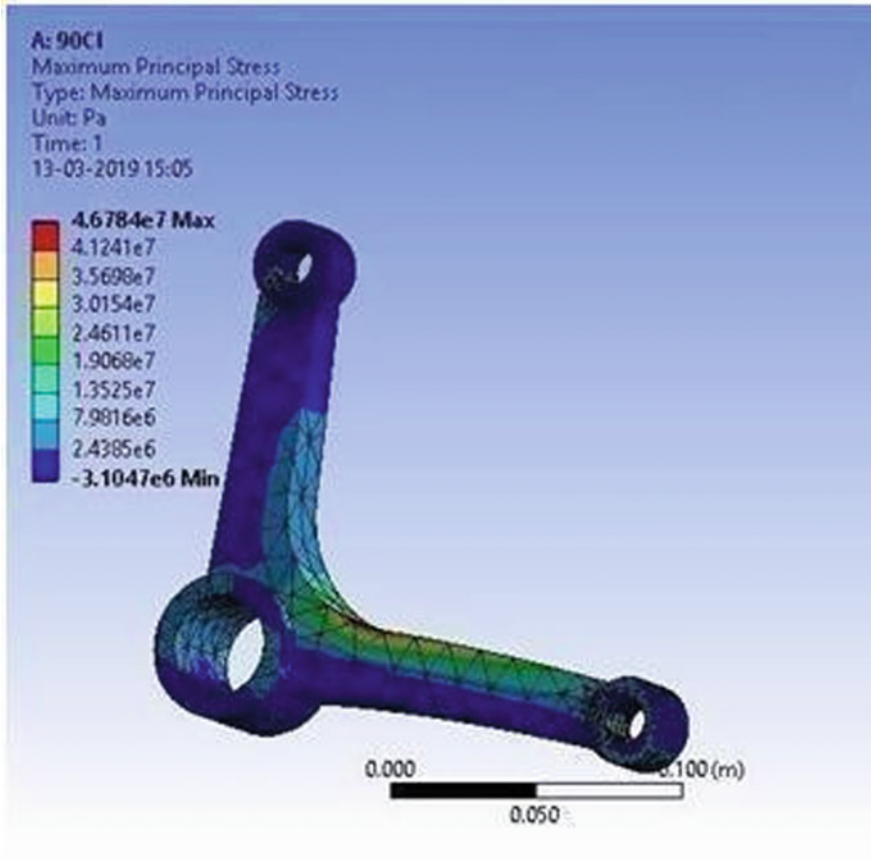


Fig. 8 Max principal stress

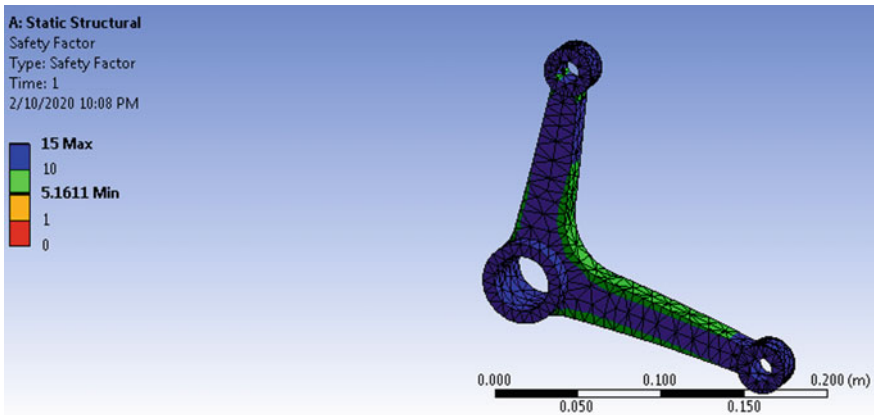


Fig. 9 Factor of safety

Table 2 Results for 90° bell crank lever

Parameters	Analytical values	FEA values	Corresponding fig
Total deformation	0.000167	0.000192	Figure 4
Von mises strain	0.000294	0.000273	Figure 5
Von mises stress	4.7E+07	4.66E+07	Figure 6
Min principal stress	4.01E+07	1.54E+06	Figure 7
Max principal stress	4.7E+07	4.68E+07	Figure 8
Factor of safety	4.86	5.161	Figure 9

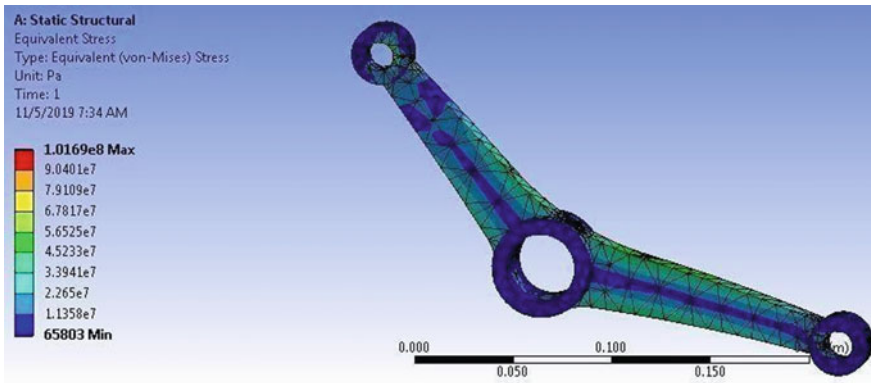


Fig. 10 Von-mises stress

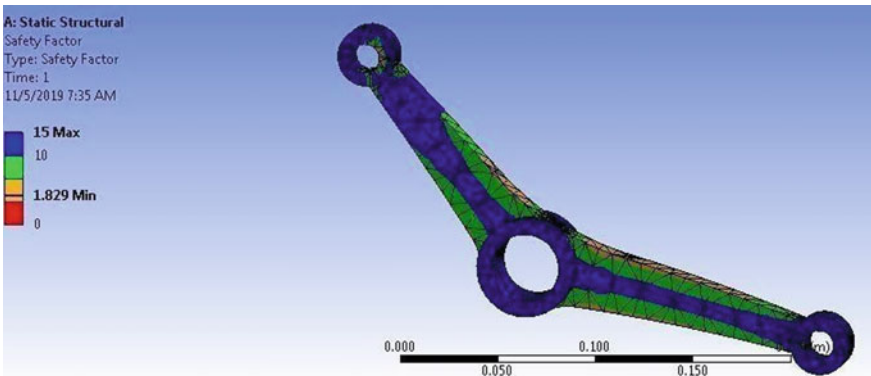


Fig. 11 Factor of safety

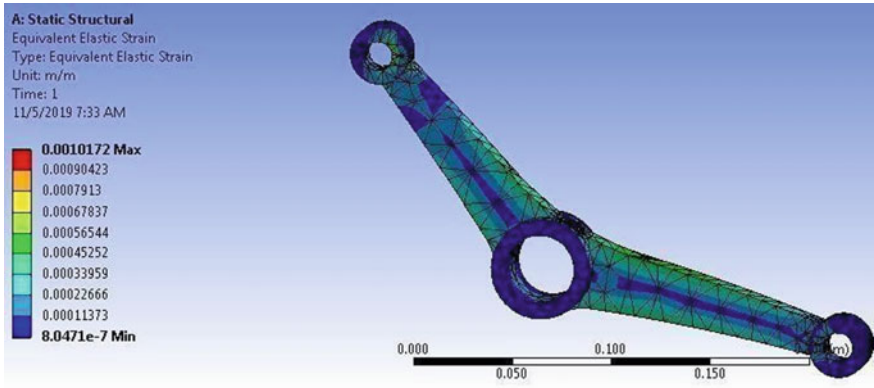


Fig. 12 Von-mises strain

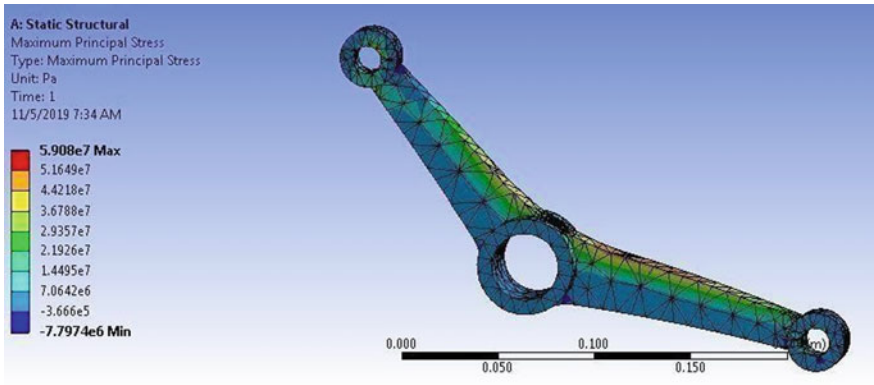


Fig. 13 Max. principal stress

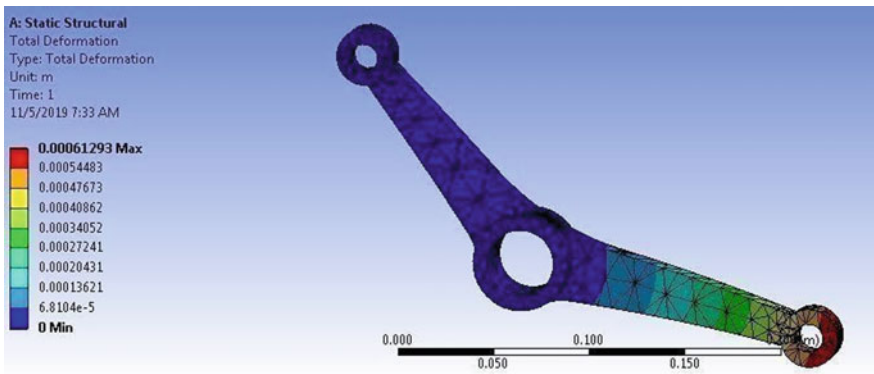


Fig. 14 Total deformation

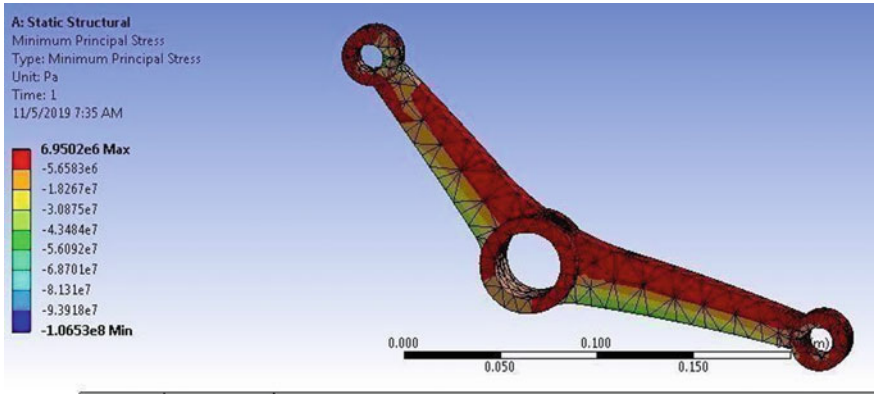


Fig. 15 Min. principal stress

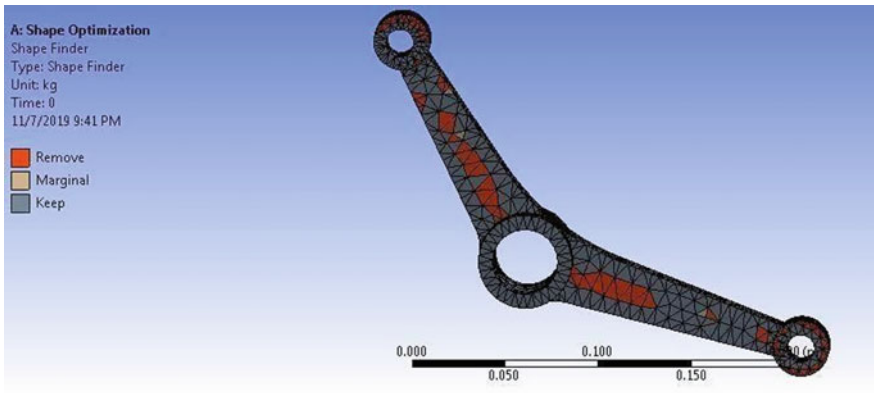
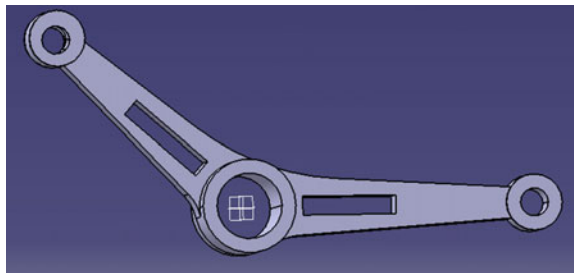


Fig. 16 Shape finder image of bell crank lever for 135°

Fig. 17 Rectangular slot



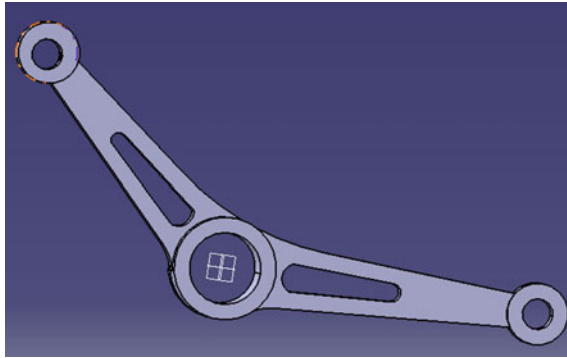


Fig. 18 Taper slot

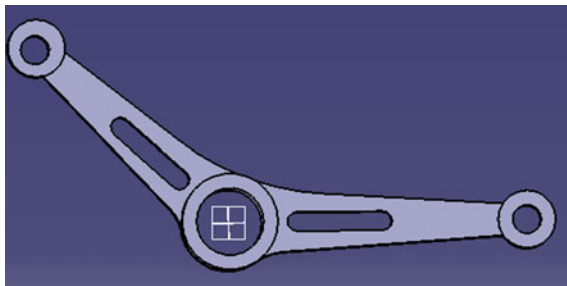


Fig. 19 Curved slot

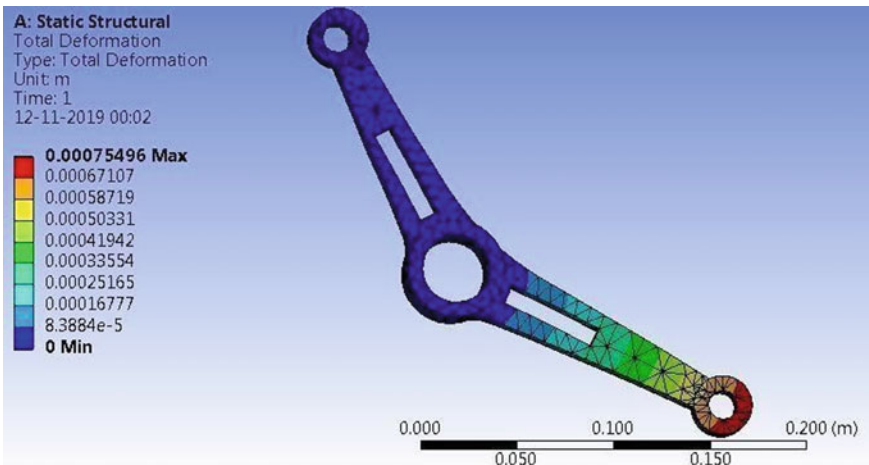


Fig. 20 Total deformation by ANSYS

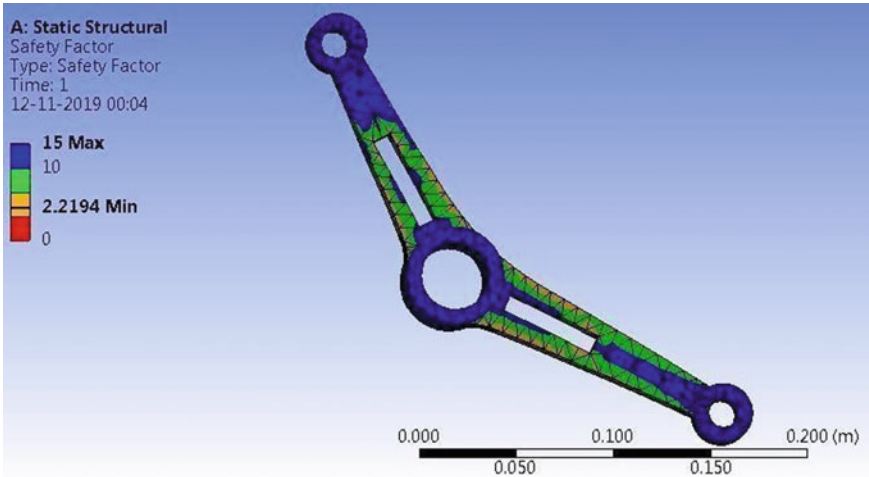


Fig. 21 Safety factor analysis by ANSYS

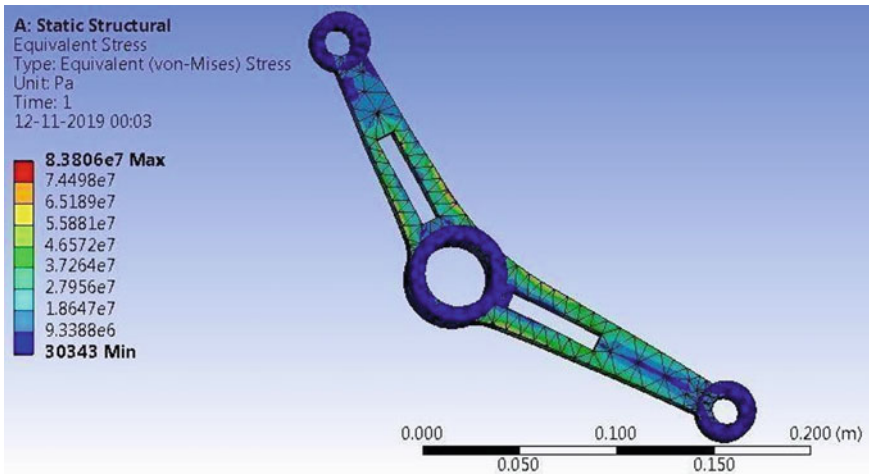


Fig. 22 Equivalent stress analysis by ANSYS

though there is less mass for tapered slot, less stress is observed for rectangle slot. Therefore bell crank lever for aluminum silicon carbide with 135° rectangle slot is considered to be optimum.

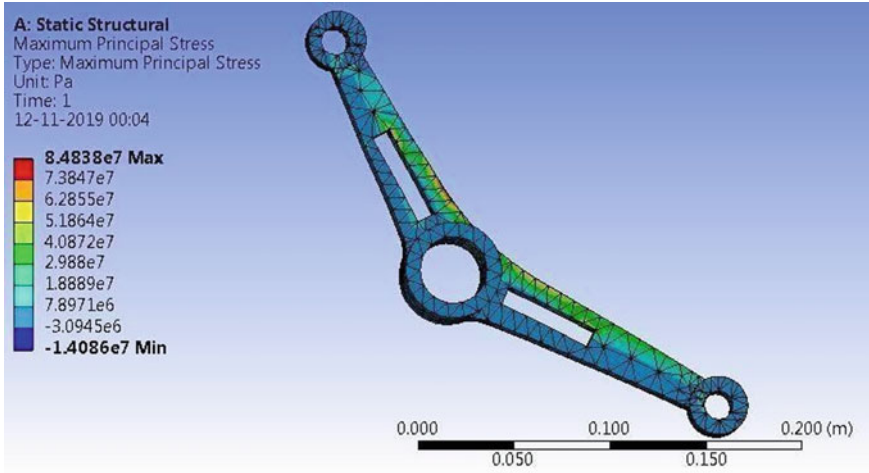


Fig. 23 Max principal stress analysis by ANSYS

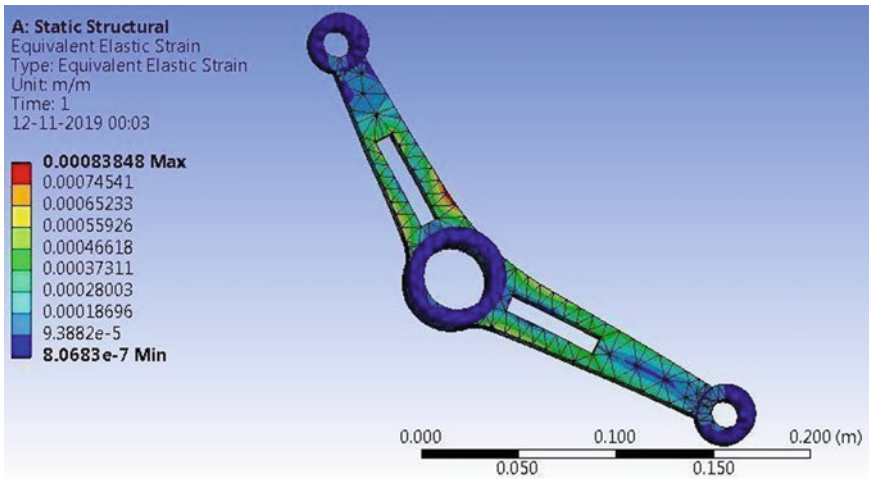


Fig. 24 Von mises strain analysis by ANSYS

6 Conclusion

In this thesis, an attempt has been made to design and analyze the bell crank lever using CATIA and ANSYS Simulation software. The analysis is carried out under static loading condition at varying different angles such as 60, 90, 135°. The bell crank lever with different materials such as cast iron, Low carbon steel, magnesium alloy, and Aluminum silicon carbide have been selected and tested under similar operating conditions. An attempt has also been made to use shape optimization technique to

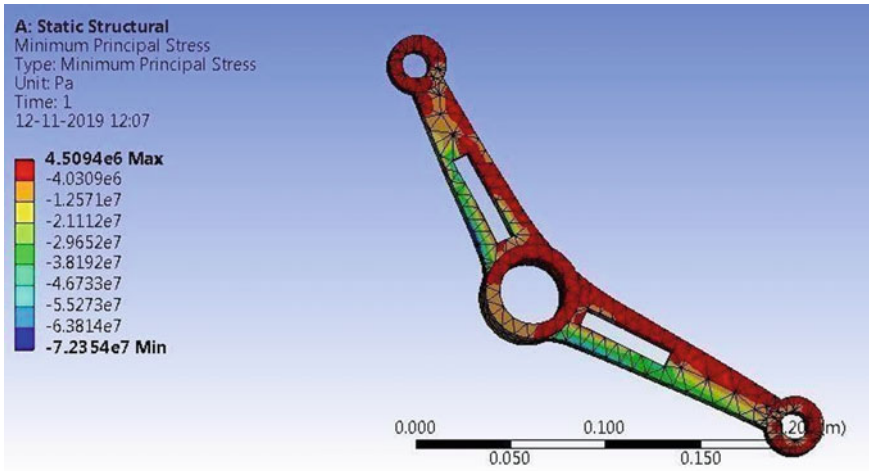


Fig. 25 Min principal stress analysis by ANSYS

Table 3 135° bell crank lever result data for various slots

Properties	Before optimization	After optimization (Curved slot)	After Optimization (Rectangular slot)	After Optimization (Tapered slot)
Mass (kg)	0.40335	0.35768	0.35871	0.35009
Volume (m ³)	1.446E-04	1.2820E-04	1.2857E-04	1.2548E-04
Total deformation (m)	0.000613	0.00074076	7.55E-04	7.51E-04
Von stress (Pa)	1.017E+08	9.485E+07	8.381E+07	9.394E+07
Von strain	1.017E-03	9.544E-04	8.385E-04	9.58E-04
F.O.S	1.829	1.961	2.2194	1.98

get the better performance by making the component lighter. The analysis revealed the following results:

1. It is observed that results obtained are in close to each other and the bell crank lever made of Aluminum silicon carbide with 1350 angle has less Von mises stress (1.02e8 Pa), less Von mises strain (0.00102 Pa), and less Minimum Principal stress (6.95e6 Pa) when compared to the other materials and angles of the bell crank lever.
2. From the results of shape optimization technique, it is observed that around 11.3% weight is reduced for the bell crank lever with rectangular slot when compared before and after optimization.
3. The von-mises stress acting on the bell crank lever is very less when compared to before and after optimization for rectangular slot.

4. Thus, the results revealed that the bell crank lever with rectangular slot got better results and can also be used further in automotive parts for withstanding the stresses and also reduction in material cost in any industry.

Finally, from the results of analysis it can be concluded that the Aluminum silicon carbide material is the best material for bell crank lever and bell crank lever with the lever angle 135° was yielding the better performance. The shape optimization technique can be utilized to make the bell crank lever component lighter to achieve the better performance.

7 Scope for Future Work

1. Static and fatigue analysis can also be performed for different models of the Bell Crank Lever which are generated in this thesis.
2. Dynamic analysis can also be done using the software like CREO, ANSYS, Hyper mesh, etc.
3. Topology Optimization technology can be done, as the ANSYS gives the tools need to design durable, light weight component for any application.
4. Photo elasticity method can be done for the same design.

References

1. Masood, M.R.: Design optimization of bell crank lever. *Int. J. Sci. Eng. Technol. Res. (IJSETR)* **8(3)** (2019). ISSN 2278-7798
2. Hasan, A.: Study the performance of the bell crank lever apparatus. *Int. J. Res. Appl. Sci. Eng. Technol.* **6(III)** (2018). ISSN 2321-9653; IC Value: 45.98; SJ Impact Factor: 6.887
3. Fornace, L.V.: *Weight Reduction Techniques Applied to Formula SAE Vehicle Design: An Investigation in Topology Optimization*. University of California, San Diego
4. Sharma, A.: Optimization of design parameters of a bell-crank lever using CAE tools. National Institute of Technology Kurukshetra, Haryana, July 2013
5. Zende, S.R.: Fillet radius optimization of bell crank lever. *Int. J. Mod. Trends Eng. Res.* (2015). e-ISSN 2349-9745
6. Dange, M.M., Zaveri, S.R.: Stress analysis of bell crank lever. *Int. J. Recent Innov. Trends Comput. Commun.* **2(8)** (2014)
7. Patil, R.: Stress analysis of bell crank lever in sewing machine. *Int. J. Innov. Sci. Eng. Technol.* **4(6)** (2017)
8. Sampat, M.V., Khatr, R.T.: An efficient product using modeling, simulation and optimization. *Int. J. Sci. Eng. Res.* **8(2)** (2017). ISSN 2229-5518
9. Essienubong, I.A., Ikechukwu, O., Ebunilo, P.O.: Determining the accuracy of finite element analysis when compared to experimental approach for measuring stress and strain on a connecting rod subjected to variable loads. *J. Robot. Comput. Vis. Graph.* **1(1)**, 12–20 (2016)
10. Javed, A.: Performance investigation of topologically optimized manipulator link. *Asian J. Eng. Appl. Technol.* **3(2)**, 47–50 (2014). ISSN 2249-068X. © The Research Publication
11. Dasu, P., Abhilash, L.: Fatigue analysis of aluminum alloy wheel. *IJRMET* **7(1)** (Nov 2016–April 2017). ISSN 2249-5762 (Online) | ISSN 2249-5770

Evaluation of Compressive Strength of Thermoplastic Materials Prepared Using 3D Printer with Different in-Fill Structures



Srinivas Kona , K. Ch. Sekhar, A. Lakshumu Naidu,
and V. V. Rama Reddy

Abstract The additive manufacturing has been proven as an auspicious technology over last one decade, material cost allied with the fabricated part is still present as a barrier for the widespread application of this technology. In this regard, cellular edifices have received substantial attention due to their high strength to weight ratio properties. In this current investigation, the specimen with square cross-section filled with different in-fill or cellular structures like fast honeycomb, wiggle, triangle, and rectilinear structures is designed using CATIA software. The specimen is prepared by using 3D printer. It is named as desktop fabrication. 3D design of a prototype was developed in CAD, this 3D model was stored in as a STL (stereolithography) format and this design was forwarded to a 3D printer. Composites, ABS, and PLA materials are generally used for 3D printing. Specimens are prepared by 3D printer use STL file developed in CAD design layer by layer. In this present work, PLA is used for preparation of the specimens. After the preparation of the specimen, compressive strength of the prepared specimen is determined, by doing a compression test using a UTM (universal testing machine). In the present work, it is observed that the compressive strength of fast honeycomb structure is superior compared to wiggle, triangle, and rectilinear cellular structures for the same quantity of material and in-fill density.

Keywords 3D printing · Additive manufacturing · PLA · Mechanical properties · Compressive strength

S. Kona (✉) · K. Ch. Sekhar · V. V. Rama Reddy
Department of Mechanical Engineering, Lendi Institute of Engineering and Technology,
Vizianagaram, India
e-mail: sri.vas028@gmail.com

A. Lakshumu Naidu
Department of Mechanical Engineering, Centurion University of Technology and Management,
R.Sitapur, Odisha, India

© The Author(s), under exclusive license to Springer Nature Singapore Pte Ltd. 2021
B. Deepak et al. (eds.), *Advanced Manufacturing Systems and Innovative Product Design*,
Lecture Notes in Mechanical Engineering,
https://doi.org/10.1007/978-981-15-9853-1_17

209

1 Introduction

In early 1980s 3D printing technology was developed for the study of photography, landscape design, and sculpting in America. Since mid-1980s 3D printing technology not much developed, in this period 3D printing is named as “RAPIDPROTOTYPING.” This technology was improved rapidly since the end of 80s and 1990s, Selective Laser Sintering (SLS) and UV light were used for developing the 3D printing. Till twentieth-century 3D printing is expensive also limited to few products only, in this period printers were utilized for research only. However, progressions in the area of 3D printing have acceptable for the design of products to no longer be limited by complex shapes or colors [1–3].

3D printing is named as additive manufacturing, which produces the 3D object layer by layer by using of the design developed in CAD. Any type of geometry and shapes were produced by additive manufacturing. Incorporation of CAD model into manufacturing leads to reduction in the parts count and build time. By using of 3D printing matting and fitting problem could be avoided. Additive manufacturing has many advantages over subtractive manufacturing, reduction in building time, wastage of material should be minimized and dimensional accuracy is maintained [1, 4–6]. However, there have some disadvantages with the additive manufacturing. Object produced by the additive manufacturing exhibit anisotropic behavior. 3D printing mainly influences the automobile and medical industries. ABS, PLA, and composites are used as the materials in the additive manufacturing. 3D object is designed in CAD packages like Catia, Pro-E, etc., after completion of designing CAD file is stored in .stl file. A computer program is used for slice the STL file into several layers from 0.1 to 0.7 mm to minimize the build time and cost of the 3D printable object. A FDM (Fused deposition modeling) was used in this research for producing the 3D object. Sliced STL file is transfer to printer to build the 3D object as per CAD model [7, 8]. The basic steps involved in the additive manufacturing are shown in the Fig. 1.

Russell A. Giordano et al. [9] have manufactured low molecular and high molecular weight Polylactic acid (PLA) components to investigate tensile strength. They observed that low molecular weight PLA component obtains higher tensile strength than the high molecular weight PLA component. Past studies observed that incorporation of carbon and glass fiber into 3D printed polymer components enhances the mechanical properties [10, 11], but the incorporation of synthetic fibers into the polymer composites results in decreases it's biodegradable quality [12]. Kalsoom et al. [13] manufactured heat sink by 3D printing with a material of 30 vol.% of micro-diamond particles/70 vol.% acrylate resins material. They reported that powder-filled composites are resisted the higher temperature than the pure polymer composites.

Past literature are analyses of different materials and their properties of 3D printed objects. The present study explains about different in-fill structures of objects. We compare the compressive strength of different in-fill structures (Fast Honeycomb,

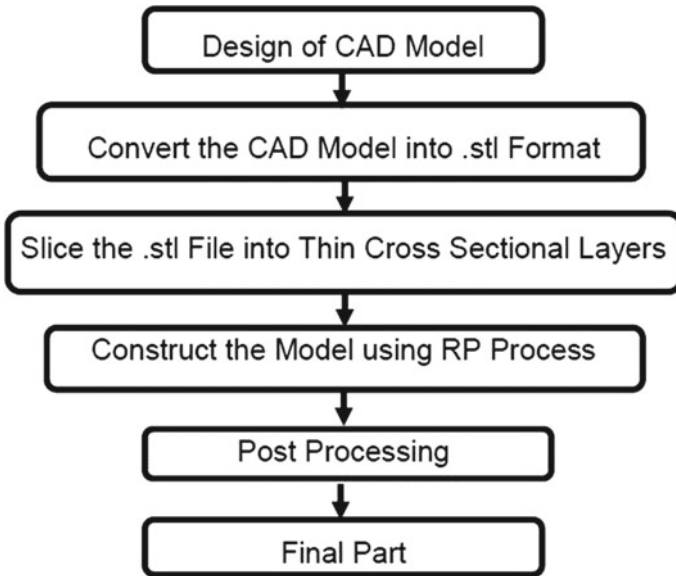


Fig. 1 Steps involved in the additive manufacturing

Triangular, Rectilinear, Wiggle) components. Among the all honeycomb infilled structured components obtained the superior compressive strength.

2 Experimental Procedure

Present investigation PLA (Polylactic acid) was used as the material for the 3D printable object. Kentstrapper zero 3D printer was used for preparing the 3D object. This printer working is based on FFF (Fused Filament Fabrication) technique. Specifications of the 3D printer were shown in the Table 1. Four different cellular structures like fast honeycomb, wiggle, triangle, and rectilinear structures were prepared for testing of the compressive strength.

CATIA V5 software was used for the design of the 3D printable objects and design was exported to into STL file. STL file is feed into the Kentstrapper zero 3D printer. Four cellular structures were shown in the Fig. 2. FDM (Fused deposition modeling) was used for developing the 3D object. In FDM process semi-molten plastic materials were used, plastic material and supporting materials were deposited in the building surface with two different nozzles. After completion of the printing supporting material was removed. Universal testing machine was used for the testing of compressive strength of the specimens. Specimens are prepared according to the ASTM standards. Specimens are in square and circular shapes with dimension of 50 mm × 50 mm × 50 mm in X, Y, and Z directions. The outer shell thickness of

Table 1 Specifications of the 3D printer

S. No.		
1	Printing are	250 × 250 × 260
2	Layer thickness	0.040–0.320 mm
3	Temperature of extruder	180–260 °C
4	Supported materials	1.75 mm, ABS, PLA, Lay wood, Lay bricks, Nylon, PET, XT, XT-carbon, and other thermoplastic materials compatible
5	Temperature of print bed	50–100 °C
6	Nozzle diameter (mm)	0.406 mm
7	Max print and movement speed	10–300 mm/s
8	Power supply	12 V, 5 A–230 V AC
9	Dimensions	560 × 430 × 420 mm
10	X, Y and Z resolution	1.2–5 μ
11	H boot	X Y Z movement
12	Extruder with interchangeable Nozzles	0.4–0.8 mm

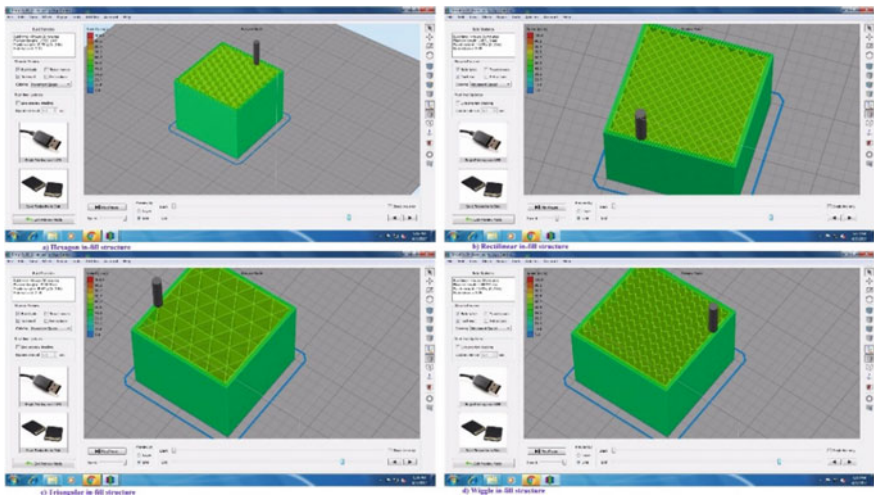


Fig. 2 Design of the cellular structures of fast honeycomb, Rectilinear, triangular, and wiggle in-fill structures

the object is 2 mm of each object. Care should be taken that the loaded ends of the specimen are parallel to each other and perpendicular to the sides.

3 Results and Discussion

Among the four specimen’s rectilinear in-fill structure has the low building time of 4 h 26 min, triangular in-fill structure has the high build time of 4 h 36 min. Wiggle in-fill structure utilizes low amount of PLA material, triangular in-fill material utilizes high amount of PLA material among the other materials. Build time of the all the specimens are nearer to each other, just 10 min difference for rectilinear to triangular. Material utilization also very nearer to the all the objects. Build time and material utilization are tabulated in Table 2.

Among four specimens fast honeycomb in-fill structure obtained the high compressive strength of 55.72 MPa, wiggle in-fill structure obtained the lowest compressive strength of 39.62 MPa. Variation in the compressive strength of specimens is shown in the Fig. 3. Results are tabulated in the Table 3. Interlayer porosity and residual stress caused by volumetric shrinkage are the main factors for the lowest compressive strength. Wiggle in-fill structure has the highest interlayer porosity which effects the compressive strength. Interlayer porosity results in weak bonding between the layers. Weak bonding between the layers causes the residual stress caused by volume shrinkage. Lower molecular diffusion and low cross-linking between the layers of polymers are happen, these factors are influencing the material behavior.

Table 2 Material utilization and build time of the specimens

S. No.	Material	In-fill structures	Build time (h min)	Material required (mm)	Mass (g)
1	PLA	Fast Honeycomb	4 h 31 min	14851.9	44.65
2	PLA	Triangular	4 h 36 min	15190.5	45.67
3	PLA	Rectilinear	4 h 26 min	14807.1	44.52
4	PLA	Wiggle	4 h 28 min	14502.9	43.78

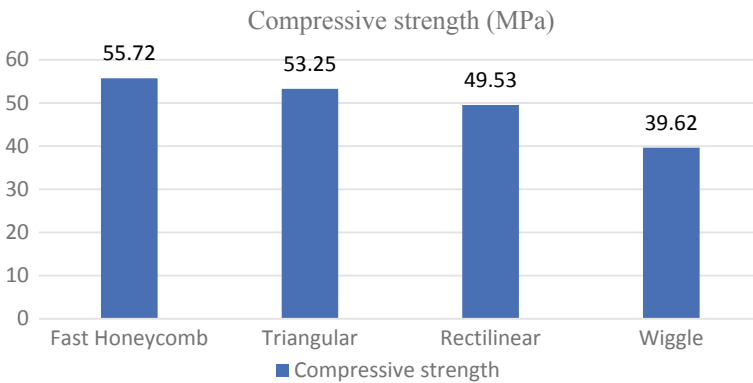


Fig. 3 Variation in compressive strength of the specimens

Table 3 Material utilization and build time of the specimens

S. No.	Material	In-fill structures	Cross-sectional area of specimen (mm ²)	Load at failure occurs (N)	Compressive strength (MPa)
1	PLA	Fast Honeycomb	807.5	45,000	55.72
2	PLA	Triangular	807.5	43,000	53.25
3	PLA	Rectilinear	807.5	40,000	49.53
4	PLA	Wiggle	807.5	32,000	39.62

Sophie C. Cox et al. [14] have manufactured 3D printed hydroxyapatite scaffolds which obtain the maximum compressive strength of 0.88 MPa. As compared to this literature we got better results. Ming Xia et al. [15] fabricated fly ash/geopolymers composites. They reported that 10% vol of fly ash/90% geopolymer composite obtained the maximum compressive strength of 29.6 MPa. Hongshi Ma et al. [16] manufactured the different composition of Fe-CaSiO₃ 3D printed scaffolds. They stated that the compressive strength of the CaSiO₃ scaffolds obtained 14.9 MPa and 30 vol.% of CaSiO₃/70 vol.% Fe scaffold obtained 126 MPa. C.S. Lee et al. [17, 18] studied the anisotropic composites. They compare the different manufacturing methods, among the all fused deposition method (FDM) method obtain the maximum tensile strength of 41.26 MPa. As compared to the previous studies, we attained better compressive strength.

4 Conclusion

The actual capabilities of additive manufacturing processes have influenced most people to maximize the performance of the designs, while minimizing their weight. In this regard, a CAD-based cellular structure building making approach is presented in this paper. Many DFAM examples along with their basic design guidelines can also be explained. Results from the honeycomb filled specimen show that our proposed design approach can save expensive build material without having to sacrifice the functional application. However, the design is not the optimal one, rather it is just an application. Therefore, in near future, this design can be optimized with the help of structural analysis tools for better performance of the conformal honeycomb in-fill or cellular structures.

References

1. Yan, C., et al.: Evaluations of cellular lattice structures manufactured using selective laser melting. *Int. J. Mach. Tools Manuf.* **62**, 32–38 (2012)

2. Chang, P.S., Rosen, D.W.: The size matching and scaling method: a synthesis method for the design of mesoscale cellular structures. *Int. J. Comput. Integr. Manuf.* **26**(10), 907–927 (2013)
3. ASTM Standard: D 1621–04 Standard Test Method for Compressive Properties of Rigid Cellular Plastics
4. Ajioka, M., et al.: Basic properties of polylactic acid produced by the direct condensation polymerization of lactic acid. *Bull. Chem. Soc. Japan* **68**(8), 2125–2131 (1995)
5. Perez, A.R.T., Roberson, D.A., Wicker, R.B.: Fracture surface analysis of 3D-printed tensile specimens of novel ABS-based materials. *J. Failure Anal. Prev.* **14**(3), 343–353 (2014)
6. Torrado, A.R., et al.: Characterizing the effect of additives to ABS on the mechanical property anisotropy of specimens fabricated by material extrusion 3D printing. *Addit. Manuf.* **6**, 16–29 (2015)
7. Conner, B.P., et al.: Making sense of 3-D printing: creating a map of additive manufacturing products and services. *Addit. Manuf.* **1**, 64–76 (2014)
8. Chia, H.N., Benjamin, M.W.: Recent advances in 3D printing of biomaterials. *J. Biol. Eng.* **9**(1), 4 (2015)
9. Giordano, R.A., et al.: Mechanical properties of dense polylactic acid structures fabricated by three dimensional printing. *J. Biomater. Sci. Polym. Ed.* **8**(1), 63–75 (1997)
10. Tekinalp, H.L., et al.: Highly oriented carbon fiber–polymer composites via additive manufacturing. *Compos. Sci. Technol.* **105**, 144–150 (2014)
11. Griffini, G., et al.: 3D-printable CFR polymer composites with dual-cure sequential IPNs. *Polymer* **91**, 174–179 (2016)
12. Srinivas, K., Lakshumu Naidu, A., Raju Bahubalendruni, M.V.A.: A review on chemical and mechanical properties of natural fiber reinforced polymer composites. *Int. J. Performability Eng.* **13**(2) (2017)
13. Kalsoom, U., et al.: A 3D printable diamond polymer composite: a novel material for fabrication of low cost thermally conducting devices. *RSC Adv.* **6**(44), 38140–38147 (2016)
14. Cox, S.C., et al.: 3D printing of porous hydroxyapatite scaffolds intended for use in bone tissue engineering applications. *Mater. Sci. Eng. C* **47**, 237–247 (2015)
15. Xia, M., Nematollahi, B., Sanjayan, J.: Printability, accuracy and strength of geopolymer made using powder-based 3D printing for construction applications. *Autom. Constr.* **101**, 179–189 (2019)
16. Ma, H., et al.: 3D printing of high-strength bioscaffolds for the synergistic treatment of bone cancer. *NPG Asia Mater.* **10**(4), 31–44 (2018)
17. Lee, B.H., Abdullah, J., Khan, Z.A.: Optimization of rapid prototyping parameters for production of flexible ABS object. *J. Mat. Proc. Technol.* **169**(1), 54–61 (2005)
18. Lee, C.S., Kim, S.G., Kim, H.J., Ahn, S.H.: Measurement of anisotropic compressive strength of rapid prototyping parts. *J. Mat. Proc. Technol.* **187**, 627–630 (2007)

Fabrication of Low Temperature Stage for Atomic Force Microscope



P. H. J. Venkatesh, M. S. R. Viswanath, Asit Kumar Meher,
and Rohan Shilwant

Abstract The AFM is been used in imaging materials. Operating at low temperatures with some advantages of low thermal noise and drift, used for high resolution measurements. The study of physical phenomenon which occurs at low temperature is possible, for example superconductivity, phase transition, etc., can be studied. Due to all these benefits developing Low temperature AFM appears to be an interesting subject of study. In this thesis, development of a compact design for low temperature stage is done which includes cooling system and temperature controlling system. The main component of cooling system is a low temperature sample stage capable of archiving up to 86 °K. Four different sample stages are designed and fabricated. Experiment was performed on these four different sample stages, which gave the temperature variation with respect to time. By observing these temperature variation optimum sample stage is chosen. These cooling was done in vacuum of order 10^{-3} mbar vacuum. To achieve this order of vacuum roots pump and sorption was used in series. Roots pump used to create vacuum of 10^{-1} mbar of vacuum both in Atomic force microscope (AFM) and then AFM is evacuated with sorption pump to achieve vacuum of order 10^{-3} mbar. AFM scan at low temperatures has been performed.

Keywords AFM (Atomicforcemicroscope) · Thermal drift · Thermal noise · Temperature · Superconductivity · Roots pump

P. H. J. Venkatesh (✉) · M. S. R. Viswanath · A. K. Meher
Department of Mechanical Engineering, Vignan's Institute of Information Technology (A),
Visakhapatnam, Andhra Pradesh, India
e-mail: Venky61788@gmail.com

M. S. R. Viswanath
e-mail: viswanath.msr@gmail.com

A. K. Meher
e-mail: asitmeher2@gmail.com

R. Shilwant
Department of Cryogenic Engineering, Indian Institute of Technology Kharagpur, Kharagpur,
India
e-mail: shilwantrb1313@gmail.com

1 Introduction

The operating atomic force microscopy (AFM) at low temperature is primary related to greater stability in tip, cantilever, and sample characteristics. Low temperature AFM with an advantage of low thermal drift, improved signal to noise ratio (low thermal noise), and eliminates mechanical drift which are used in high resolution measurement. Low temperature AFM also gives the opportunity to see properties at low temperature and in some cases change in crystal structure. Low temperature AFM also plays an important role in biological microscopy by suppressing the thermal motion of sample and keeping the sample rigid enough to withstand force of AFM stylus. AFM using in ultra-high vacuum at 4.2 K opens with a new field of research on insulator on individual molecules absorbed on substrate. Both lateral diffusion across substrate and desorption of molecule are strongly reduced at low temperature [6, 8].

Working of an AFM

The AFM works by the principle of scanning the AFM probe with a surface. The probe consists of a sharp tip end with a flexible cantilever. The tip is 4 to 5 μ in height with a apex diameter of 10-20 nm, and it is situated at the end of a cantilever 100-200 μ m long (Figs. 1 and 2).

Contact mode

See Figs. 3, 4, 5 and 6.

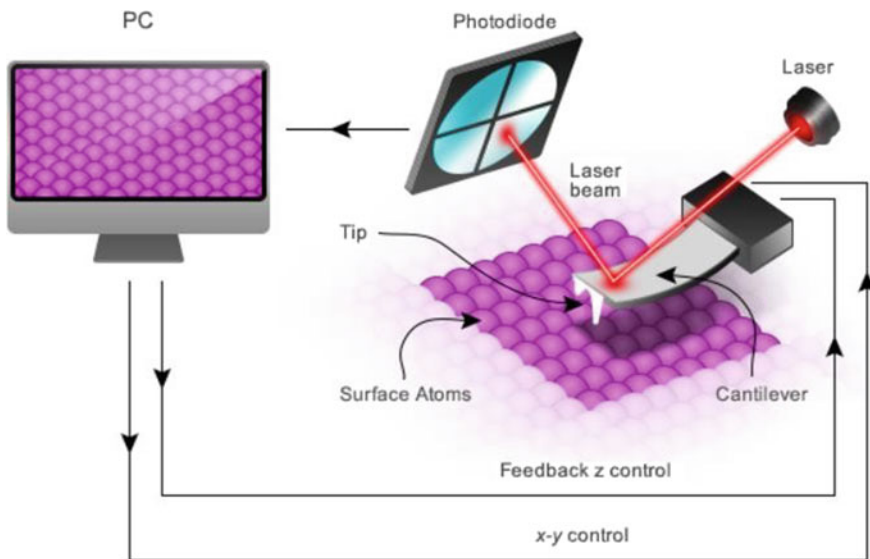


Fig. 1 Atomic force microscope

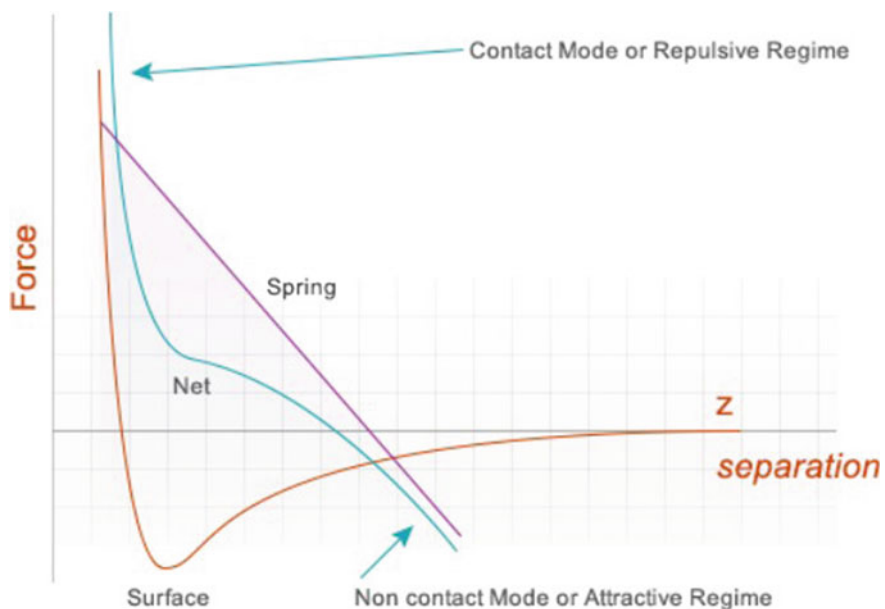
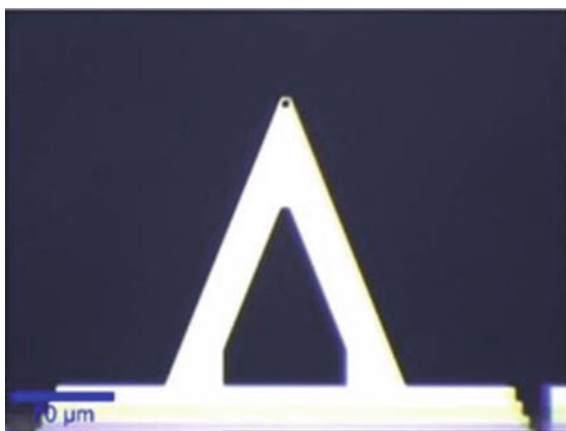


Fig. 2 Force curve diagram

Fig. 3 Cantilever tapping mode

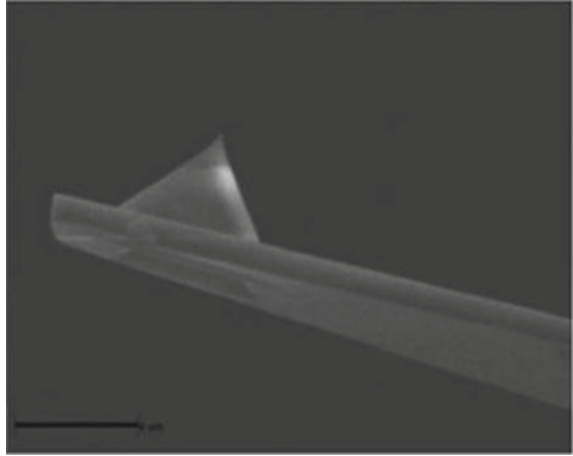
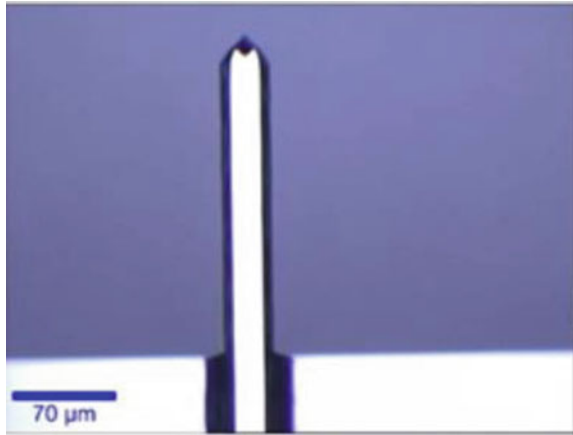


Magnetic Force Microscopy

Magnetic force microscopy (MFM) is special mode of operation of the AFM (Fig. 7).

Low temperature AFM

The low-temperature AFM required a method to detect the deflection of cantilever for high sensitivity. With the help of this instrument, the study of physical phenomenon that occurs at low temperature is possible (Fig. 8) [8, 9].

Fig. 4 Tip SEM image**Fig. 5** Tapping mode cantilever

The development of a compact design for low temperature stage is done which includes cooling system and temperature controlling system. Four different sample stages are designed and fabricated. The experiment was performed on these four different sample stages, which gave the temperature variation with respect to time. By observing these temperature variation optimum sample stage is chosen. These cooling was done in vacuum of order 10^{-3} mbar vacuum. To achieve this order of vacuum roots pump and sorption was used in series. Roots pump used to create vacuum of 10^{-1} mbar of vacuum both in Atomic force microscope (AFM) and then AFM is evacuated with sorption pump to achieve vacuum of order 10^{-3} mbar. AFM scan at low temperatures has been performed. The fabrication when it is compared to any other experiment is highly expensive compared to other fabrication methods.

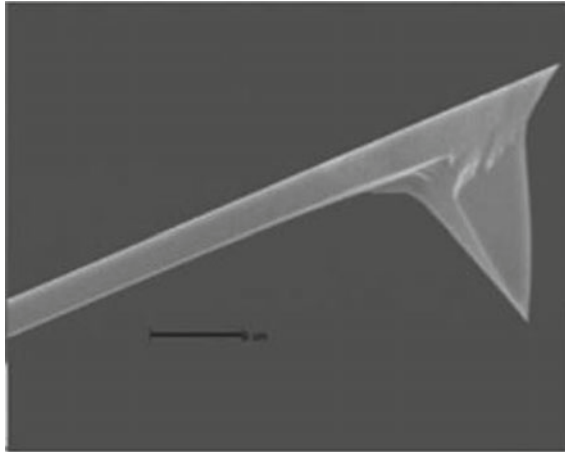


Fig. 6 Tip SEM image in downward direction

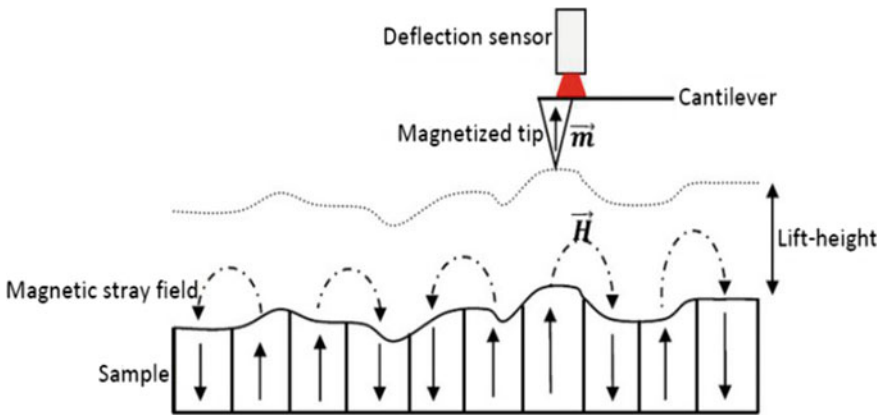


Fig. 7 Schematic principles of magnetic force microscopy

2 Literature Review

To the present day low temperature in AFM is achieved by several ways. The method followed is been disused. Both 4.2 K-based and 78 K-based cooling system are available.

Helium-based

Wintjes et al. [1] developed compact design with the tuning fork AFM is operated at variable temperatures in between room temperature and 7 K. Here cryostat is used to

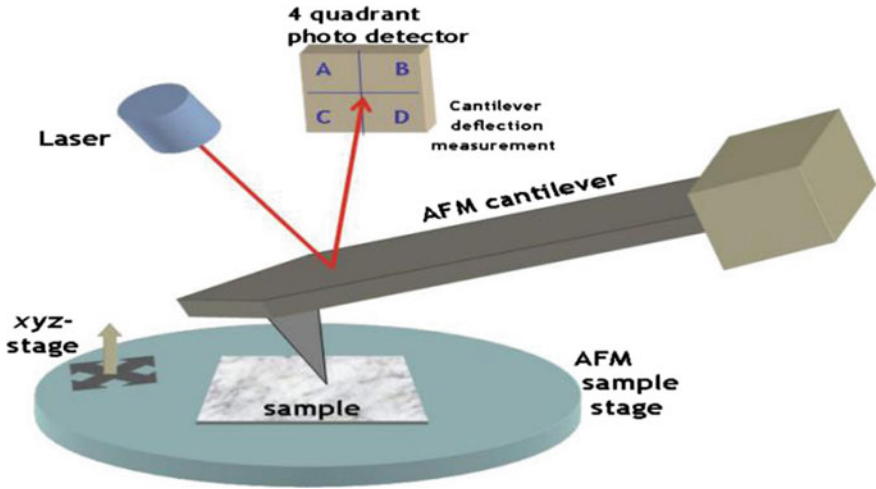


Fig. 8 Sample measurement of magnetic force microscopy

achieve low temperature, which used either nitrogen or helium as its working fluid. The results for an Ag (111) single crystal surface is determined (Fig. 9).

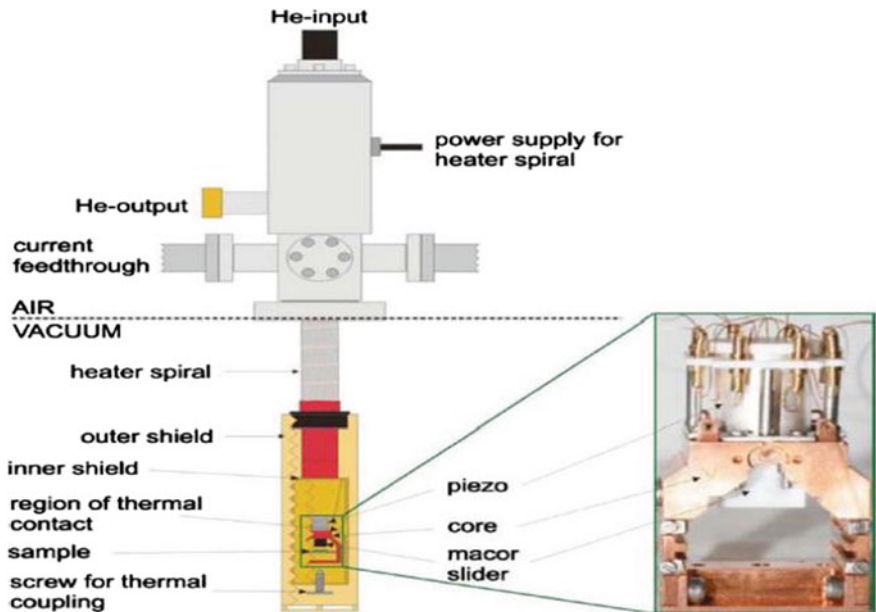


Fig. 9 Tuning fork AFM

Pan et al. [2] designed a ^3He refrigerator-based low temperature STM, can operate at temperatures down to 250 mK. This refrigerator housed in a vacuum and the liquid helium inside the super-insulated Dewar (Fig. 10).

Liquid nitrogen-based

Nakamoto et al. [3] are interested in imaging biological samples in AFM because of its extremely high resolution. Author was able to develop a less temperature, high vacuum AFM that can freeze The sample cooled with a Cu foil heat conductor, is connected to a liquid nitrogen Dewar, which also helped to eliminate the vibration due

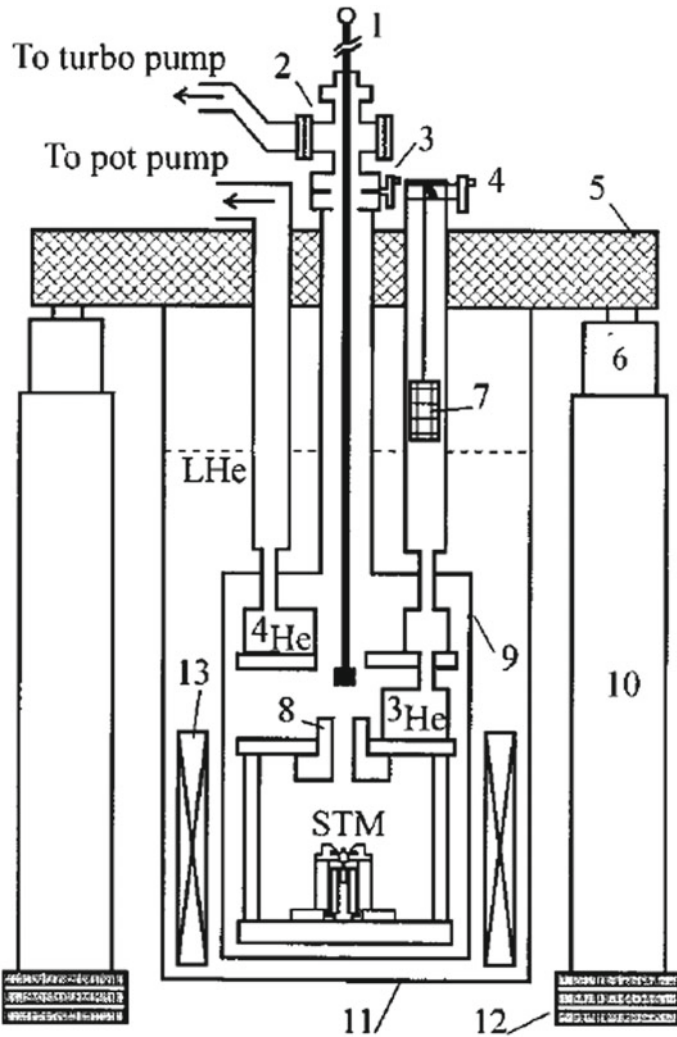


Fig. 10 Experimental diagram of He refrigerator

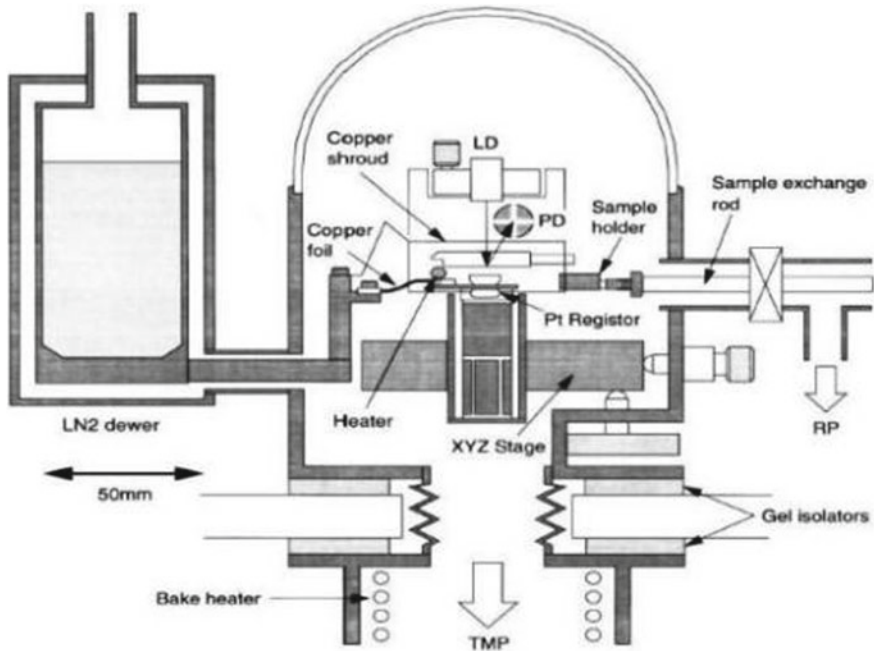


Fig. 11 Cross-section of setup

to LN2 boiling. The Freeze fracture is a two step process in which 1st is the rapid cooling of the sample and 2nd is fracture which means cracked on plane through tissue. The fracture was done by two methods 1st is with hook which is attached to sample exchanges rod and another with cooled knife (Fig. 11).

Dai et al. [4] constructed a varying temperature ultra-high vacuum AFM. The sample is fixed at particular position by using spring clamps, AFM cantilever and deflection sensor scan the sample. Here author used the cold finger technique, one end is given connection to sample holder and other end connected to the liquid nitrogen reservoir. This allows the temperature achieve to 100 K and operate to room temperature (Fig. 12).

This whole experiment is done in the ultra-high vacuum. Following diagram represents the vacuum system for setup (Fig. 13).

The temperature vs time plot for different material is as shown in Fig. 14.

From this curve, we can conclude that copper is suitable for low temperature purpose.

Allers et al. [5] the application of AFM and AFM-IR in polymer science and the principle of AFM-IR and the recent improvements to enhance its resolution and also latest progress in the use of AFM-IR as a super-resolution correlated scanned-probe infrared spectroscopy for the chemical characterization of polymer materials dealing with polymer composites, polymer blends, multi layers, and bio polymers. Finally, this novel technique can be used to determine phase separation, spherulitic structure,

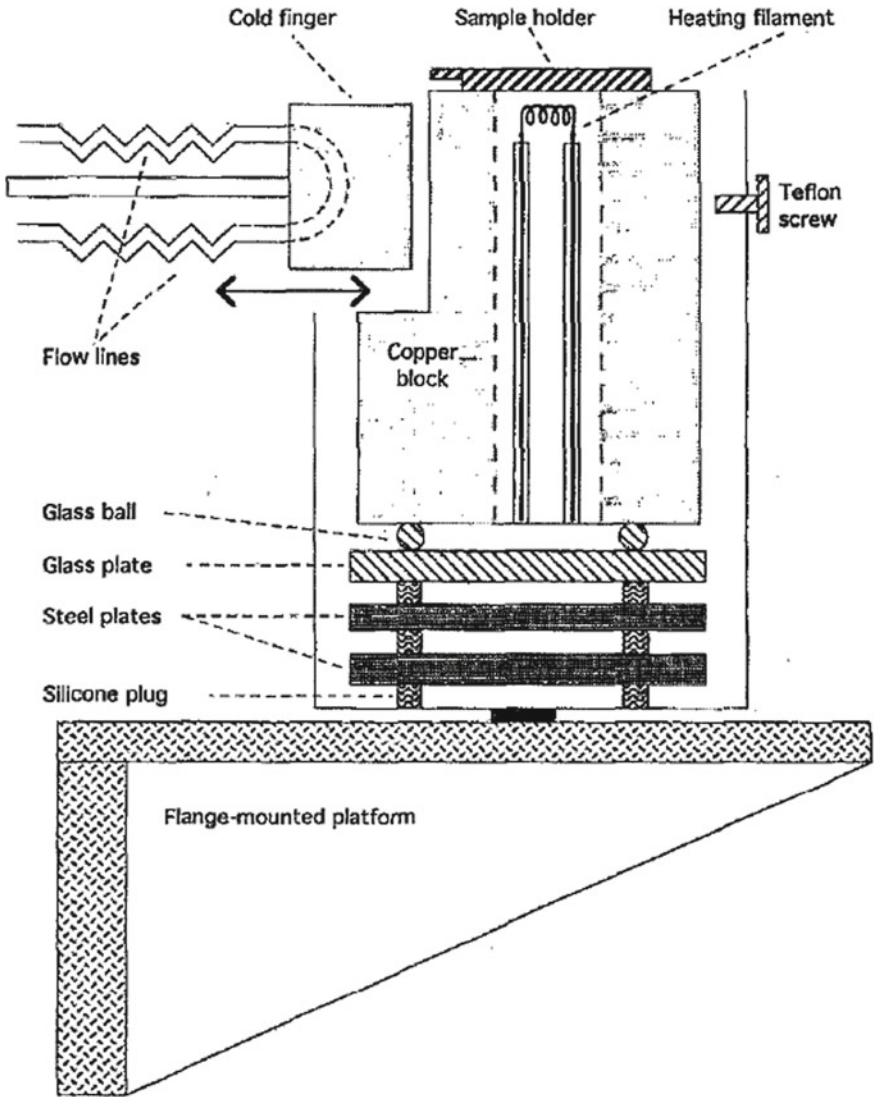


Fig. 12 Cooling system

and crystallization mechanisms at nanoscales, which has never been achieved before. The review also discusses future trends in the use of AFM-IR in polymer materials, especially in polymer thin film investigation (Fig. 15).

From these literatures conclusion is made that design of AFM head mainly depends on various parameters of the head. As per literature components of AFM

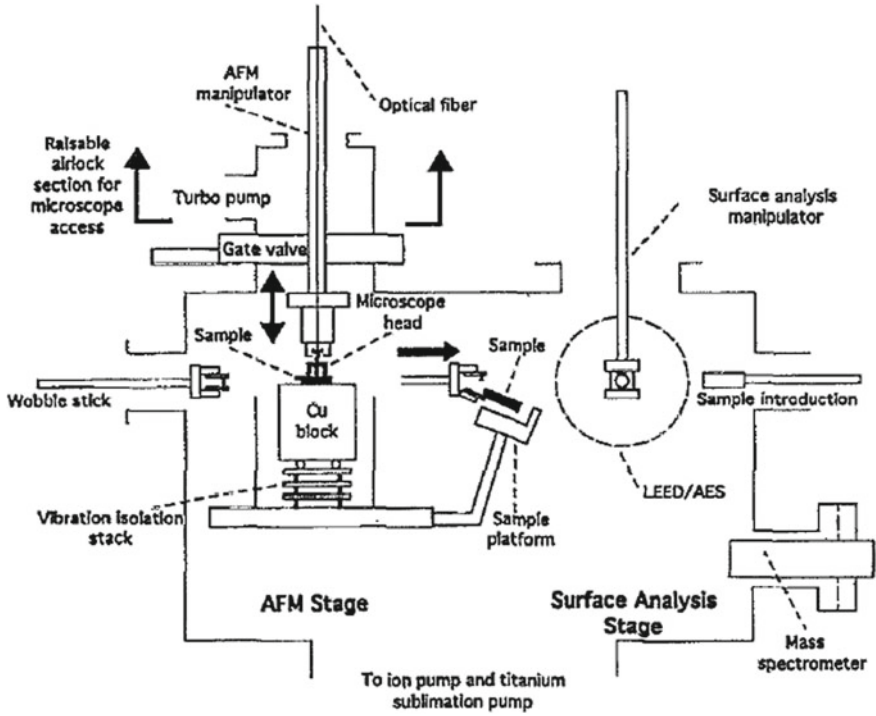


Fig. 13 Vacuum system for setup

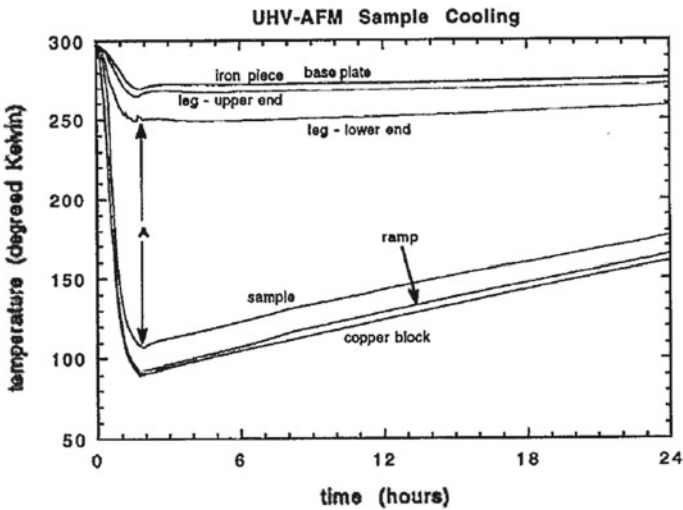


Fig. 14 Temperature versus time for different material

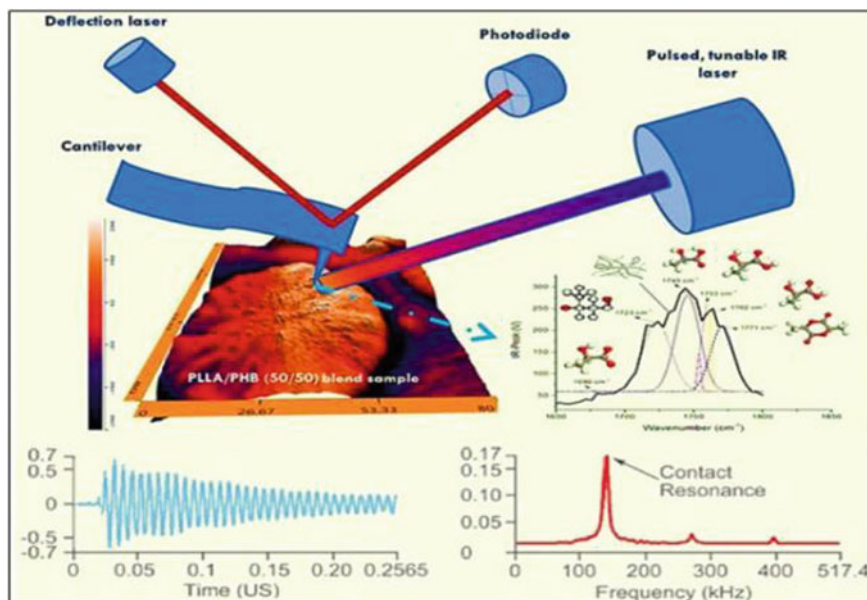


Fig. 15 AFM scanner with AFM-IR Process

where exposed to liquid helium or nitrogen which is not desirable in this case. Decision is made to adopt a design to only the sample and not the surrounding environment. As per the designs mentioned above long cooling path to connect cold finger of cooling system and the sample, that will increase the time required to cool down the sample. Taking this into account we consider including cooling stage as a part of the sample stage. There is a possibility of vibration from cryostat and this shall be eliminated in design of the stage [11–13].

Development and fabrication of cooling system for sample stage of AFM

See Figs. 16, 17, 18, 19 and 20.

Liquid nitrogen transfer device

See Fig. 21.

3 Experimental Details

The main aim of the experiment is to design and fabricate a non-magnetic stage for magnetic force microscopy (MFM) by eliminating stray fields and to design of vacuum hood adapter to maintain a vacuum of 10^{-4} mbar and to develop a cooling system for the sample stage of atomic force microscopy vacuum by using liquid

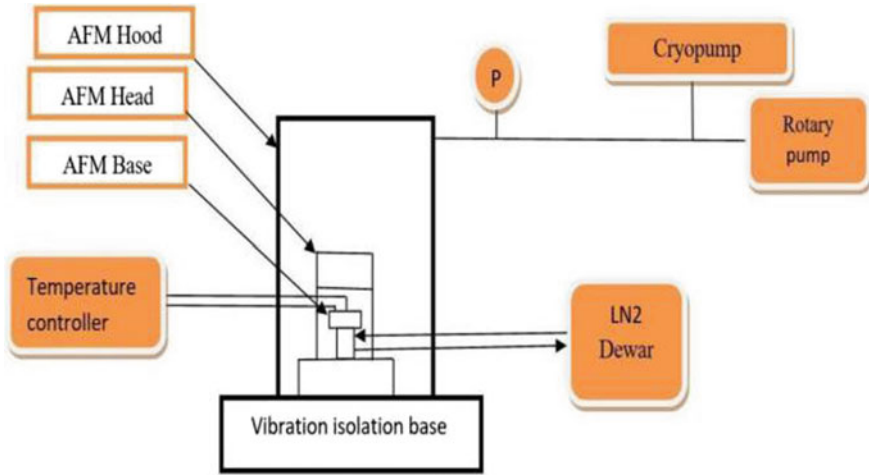


Fig. 16 Cooling system process



Fig. 17 Experimental setup for creating vacuum

nitrogen. The design of new MFM base is discussed in order to eliminate stray fields which appears in previous stage. In the old base, the sample holder houses a magnet. This magnetic base delivers constant magnetic field to tip and that causes the error due to stray fields while performing magnetic force microscopy scan. For accurate MFM scan, magnetic field other than the tip should be as minimum as possible or possibly zero. Design of new base is done to avoid magnetic fields with consideration of the complexity of AFM. It has a constraint of weight. Old assembly has a weight of 74.36 gm and new assembly is about 76.65 gm. This research is to provide cooling system to AFM. This is done by using the liquid nitrogen. If pressure in AFM is atmospheric pressure means sample stage is surrounded by air which contains moisture. As liquid nitrogen flow through sample stage, ice formation takes place.

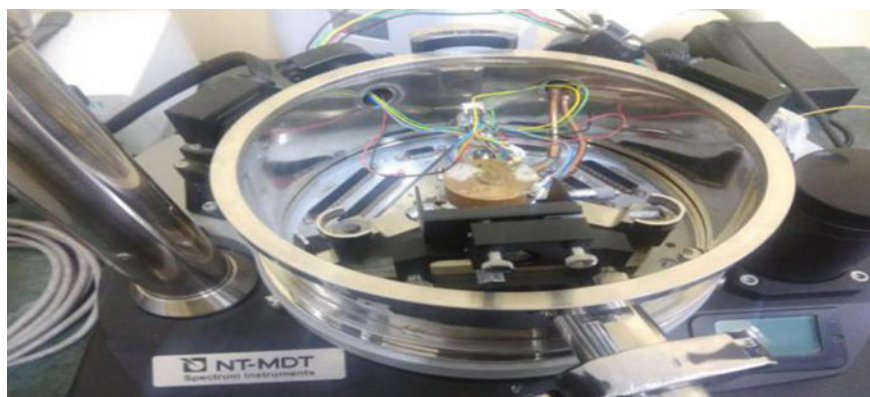


Fig. 18 New cylindrical hood with electric connection and liquid inlet and outlet

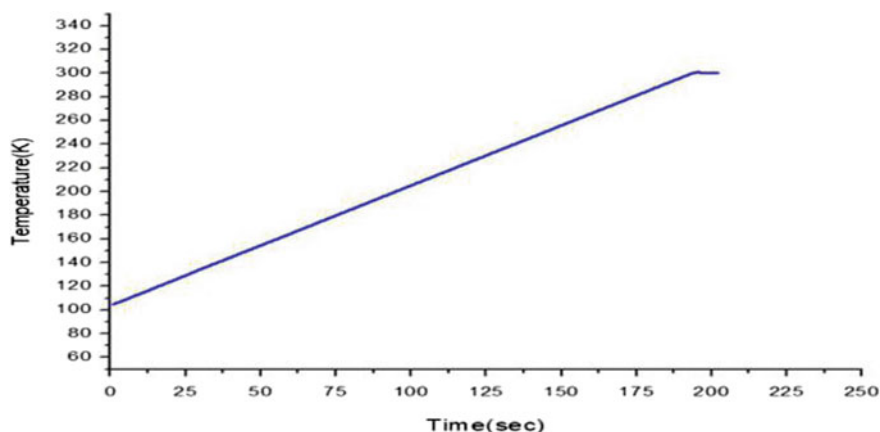


Fig. 19 Results of ramping operation performed on heater

To avoid this ice formation, vacuum system introduced in this system. So this system divides into two systems. First vacuum system and other is cooling system. One litre of liquid nitrogen converts into 162 L of gaseous of nitrogen. In this case, volume of system is almost constant. If something went wrong like at somewhere flow blocked, that will exert tremendous amount of pressure. That may cause busting the liquid nitrogen pipes inside AFM. It causes serious problem to AFM like spilling liquid nitrogen in AFM or it may damage the AFM head. Because of this reasons, a different arrangement is made with perplex to observe the issues while performing the experiment and to resolve them. Different thing was observed while performing experiment in perplex like possibility of frosting at different pressure level (Figs. 22, 23 and 24) [15–17].

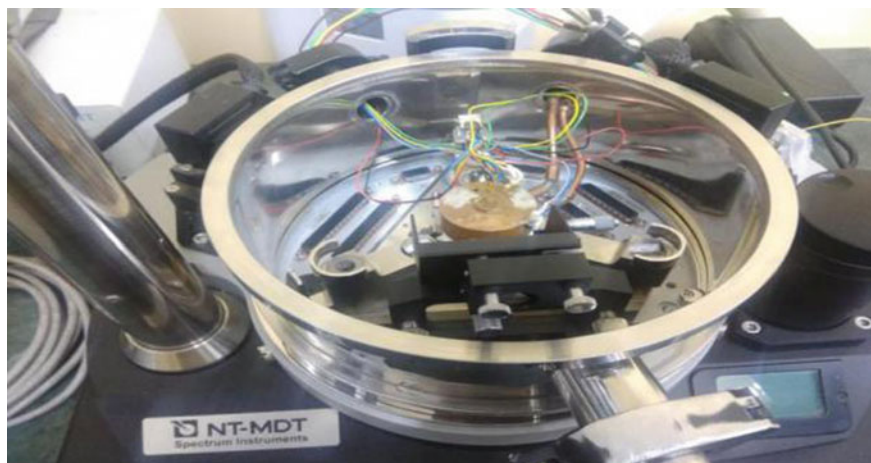


Fig. 20 Fabricated cylindrical hood



Fig. 21 Transfer device connected to perflex setup

Vacuum system

Vacuum system is consisting of roots pump and sorption pump. Roots pump is to create pressure of order 10^{-1} mbar this backing pressure for sorption pump and it also evacuate AFM chamber to approximate same pressure as sorption pump. Sorption is designed to develop pressure of order 10^{-3} mbar. Schematic diagram for vacuum system is shown in Figs. 25 and 26 [12, 13].

Cooling system

Cooling system consists of Dewar, transfer device, KF16 connector, and base. Liquid nitrogen stored in Dewar and it closed with transfer device. In self-pressurising, time take to achieve pressure transfer is huge. Least gauge pressure required to transfer

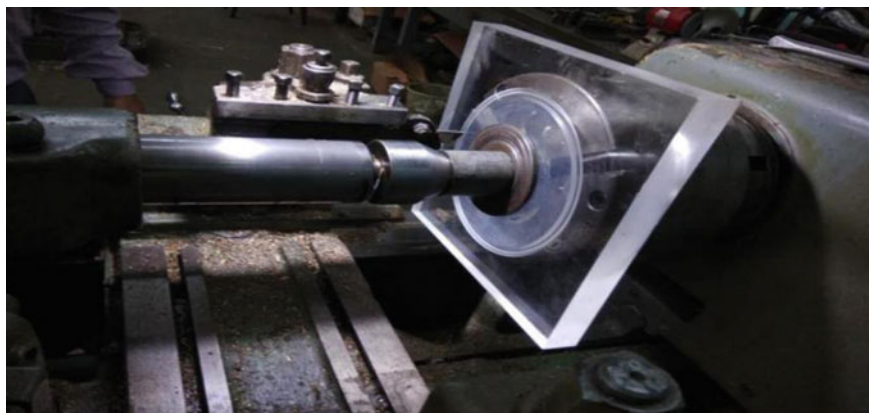


Fig. 22 Working on lathe with perplex

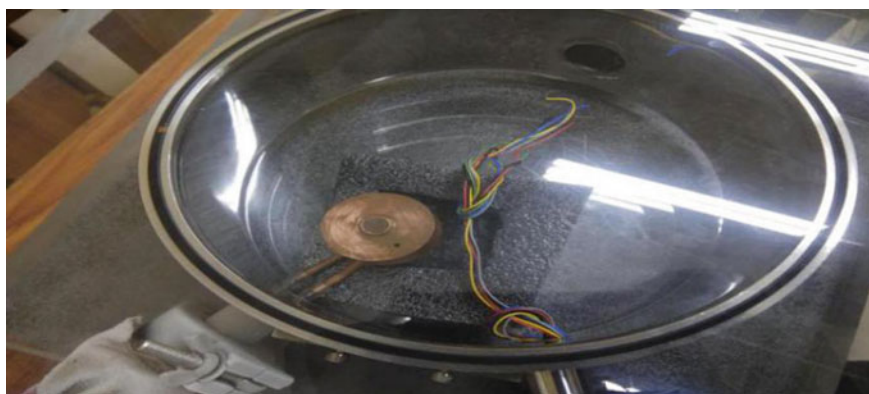


Fig. 23 Base 1 in perplex

LN₂ is 0.2 kg/cm². KF16 connector is used to connect evacuated space to atmosphere through copper pipes which are joined to connector. Base is where liquid nitrogen stays in hollow cylindrical portion of base. Take heat from copper base. Main aim in this is to cool down upper part. This heat transfer takes place in mainly in conduction mode. There is heat in leak through radiation into base. This decreases the efficiency. So insulation is provided to reduce heat in leak. Insulation consists of double layer of miler sheet then glass wool and then again miler sheet which held together by using Teflon tape (Figs. 27 and 28).



Fig. 24 Experiment with base 1 with manual LN2 filling



Fig. 25 Vacuum system connected to cylindrical hood through KF25

4 Results

MFM Base

MFM scan is done with new base and old base to observe improvement in MFM scan. As old base has magnet to hold sample. This was the issue with old base. In new base, there is no any magnetic material to exert external force other than sample (Figs. 29 and 30) [11, 12].



Fig. 26 Vacuum system connected to main AFM



Fig. 27 Base 3 connected to KF16 connector in perplex setup

With above figures, observation is made that new MFM base gives good result as compared to old base as domains of ferromagnetic material are more clearly visible with new base as compared to old base.

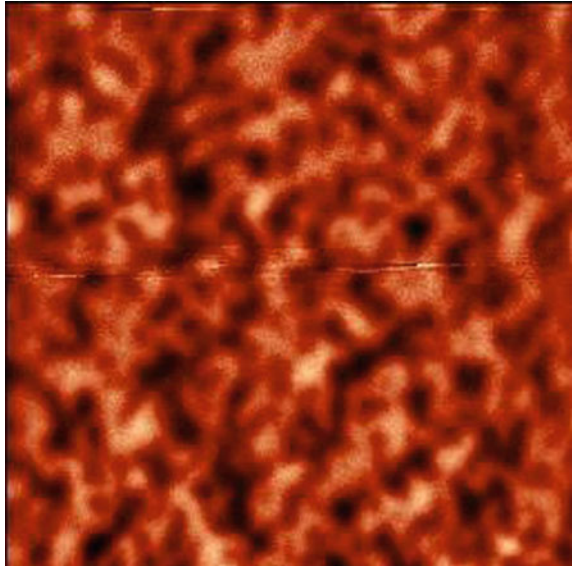
Cooling system

In cooling system, main concern is the variation of temperature with time. In this section, temperature variation with time is observed with different bases.



Fig. 28 Cooling system connected to peplex setup

Fig. 29 MFM images with old base



Base 1

Base 1 is one with having contact with upper part to bottom part through the threads. These threads are providing major thermal resistance to heat transfer. Because of this reason minimum temperature achieved with base 1 is 170 K in 1 h 30 min. Temperature vs time variation is shown in following graph (Fig. 31).

Base 2

Main objective of base 2 is to avoid tread contact to improve heat transfer. This base made with short diameter. Heat transfer is through the wall of hollow cylinder. Minimum temperature achieved with base 2 is 126 K in 12 min (Fig. 32).

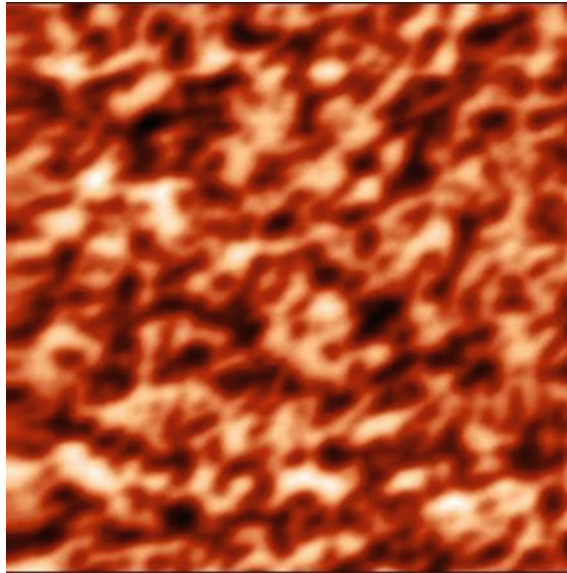


Fig. 30 MFM images with new base

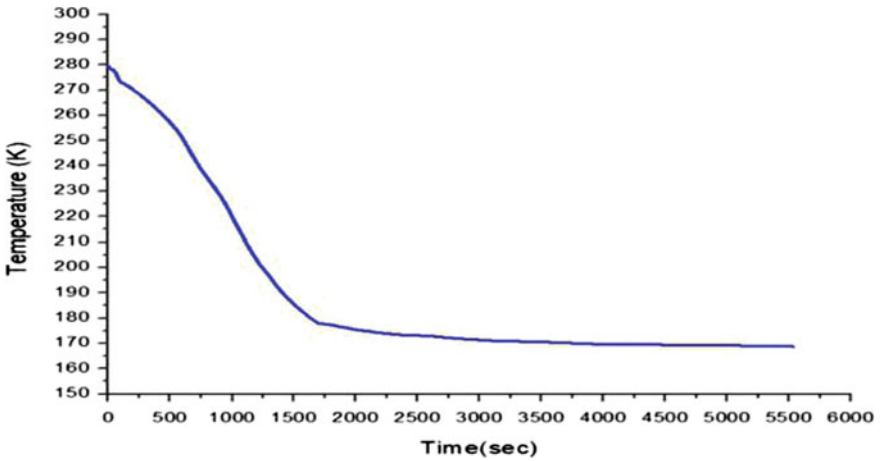


Fig. 31 Temperature versus time

Base 3

In base 3, cold finer technique is used to transfer the heat. As upper part directly coming in contact with liquid nitrogen, heat transfer is improved in very high amount. Minimum temperature achieved with base 3 is 86.8 K in 1 h 20 min. The temperature variation with time is shown in Fig. 33.

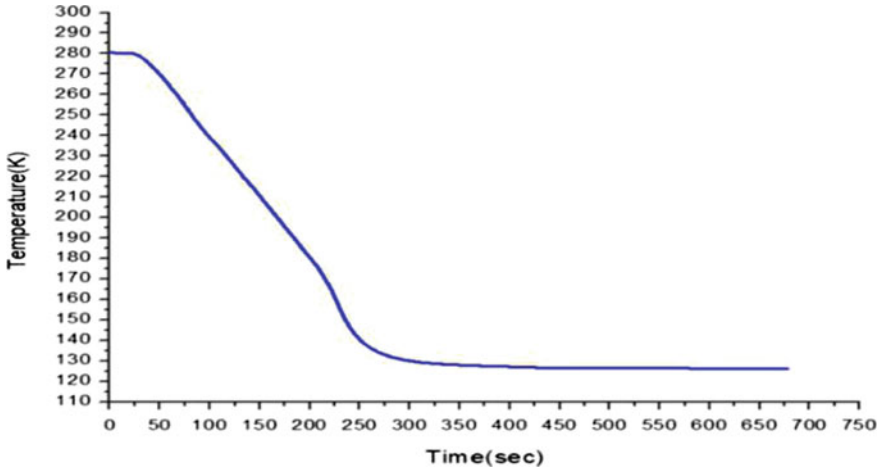


Fig. 32 Temperature versus time

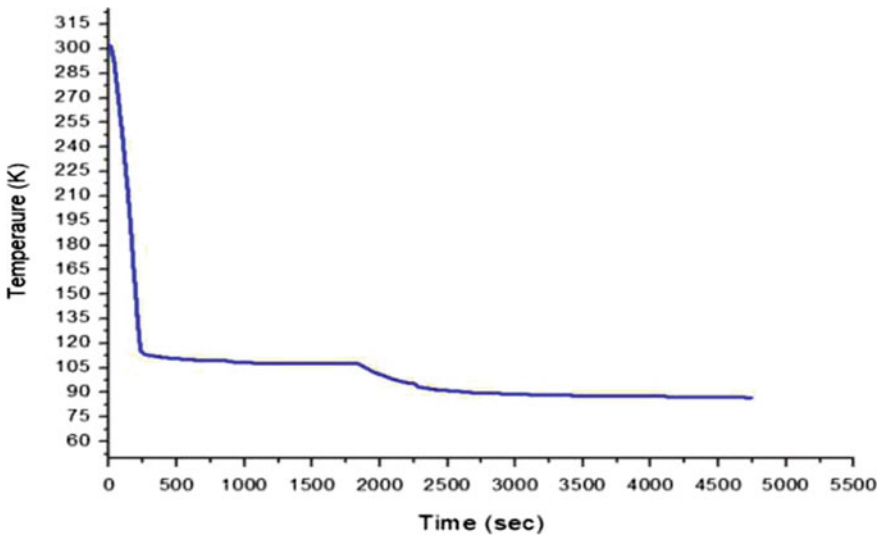


Fig. 33 Temperature versus time

Author [4] Dai et al. achieved 90 K of temperature in 2 h by using cold finger technique and here in this project 86.8 K temperature achieved within 1 h 2 min.

AFM images with base 3

AFM images of HOPG sample in different environment are shown in figures. Those shows that up to certain temperature image quality is increasing as temperature is

Fig. 34 AFM image room temperature and atmospheric pressure of HOPG sample



falling, after that suspicious noise is coming which causes the lowering image quality (Figs. 34, 35, 36 and 37).

Fig. 35 AFM image room temperature and in vacuum of HOPG sample

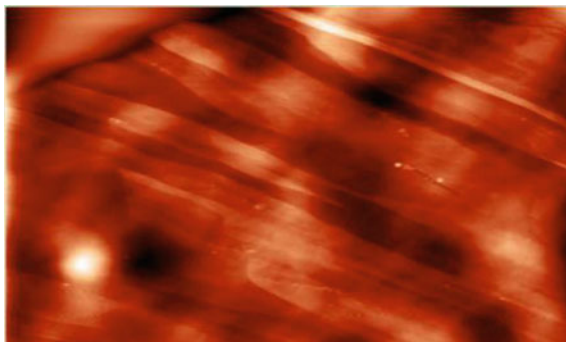


Fig. 36 AFM image at 280 K and in vacuum of HOPG sample

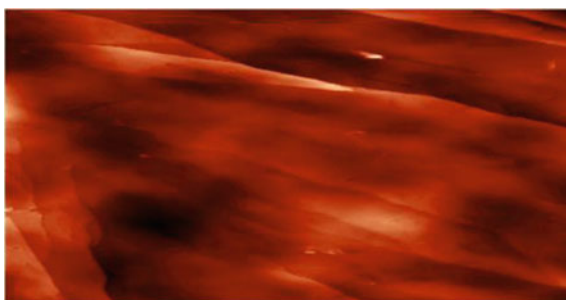
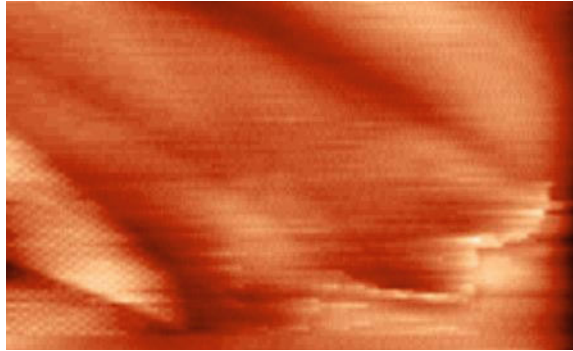


Fig. 37 AFM image at 230 K and in vacuum of HOPG sample



5 Conclusion

The development of LN₂ cooling stage we have developed three design of base. It is observed that with base 1 minimum temperature achieved is 170 K. The main constrain hear is the inadequate thermal conduction at contact with threads and large thermal mass. Hence we adopted base 2. With this base the minimum temperature achieved was 126 K. In this design brazing different copper sections imposes thermal resistance to heat transfer and since heat transfer is mainly through wall of cylinder that appears as the problem. Finally, we introduced cold finger inside the LN₂ containing cylinder which showed a drastic improvement in lowering of temperature up to 86.8 K. For further AFM scans base 3 was used to achieve low temperature. Also heater was tested to maintain desired temperature. Once low temperature was achieved, AFM scans were performing at ambient conditions, vacuum and low temperatures. Low temperature drifts the instrumental parameters drastically. By modifying the instrumental parameter, surface features started to appear at 280 K as shown in Fig. 36. Upon decrease in temperature to 230 K (Fig. 37). Suspicious noise does appear while scan and it is difficult to eliminate them at current situation. But we have captured few images which do need to be improved upon better understanding to eliminate instrumental errors which occur at low temperature. Upon further cooling at current situation it is not possible to obtain desired quality of image and eliminating the stray magnetic field has been successful and verified.

References

1. Wintjes, N., Lange, M., van Vörden, D., Karacuban, H., Utzat, D., Möllera Very, R.: Compact design for a low-temperature tuning fork atomic force. Microscope American Vacuum Society. pp. C4E21–C4E24 (2010)
2. Pan, S.H., Hudson, E.W., Davis, J.C.: 3He refrigerator based very low temperature scanning tunnelling microscope. **70-2**, 1459–1463 (1999)
3. Nakamoto, K., Mooney, C.B., Iwatsuki, M.: Development of low-temperature and high vacuum atomic force microscope with freeze–fracture function. **72-2**, 1445–1448 (2001)

4. Dai, Q., Vollmer, R., Carpick, R.W., Ogletree, D.F., Salmeron, M.: A variable temperature ultrahigh vacuum atomic force microscope. *Am. Inst. Phys.* **66**(11), 5266–5271 (1998)
5. Stylianou, A., Kontomaris, S.-V., Grant, C.: Atomic force microscopy on biological materials related to pathological conditions. **2019**:25 (2019). Article ID 8452851
6. Kirk, M.D., Albrecht, T.R., Quate, C.F.: Low-temperature atomic force microscopy. pp. 833–836 (1988)
7. Workman, R.K., Manne, S.: Variable temperature fluid stage for AFM. **71**(2), 431–439 (1999)
8. Mamin, H.J., Rugar: Sub-atto newton force detection at mill kelvin temperatures. **79**(20), 3385–3360 (2001)
9. Saito, H., Sunahara, R., Rheem, Y., Ishio, S.: Low-noise magnetic force microscopy with high resolution by tip cooling. *IEEE Trans. Magn.* **41**(12), 4394–4396 (2005)
10. Mortazavi, P., Shu, D.: Thermal conductance of metallic interface in vacuum. *EEE Trans. Nucl. Sci.* **NS-32**(5), 1891–1892 (1986)
11. Prater, C.B., Wilson, M.R., Garnaes, J., Massie, J., Elings, V.B., Hansma, P.K.: Atomic force microscopy of biological samples at low temperature. *Am. Vac. Soc.* **30**, 989–991 (1990)
12. Giessibl, F.J., Gerber, Ch., Binnig, G.: A low temperature atomic force/scanning tunnelling microscope for ultrahigh vacuum. pp. 984–988 (1990)
13. Allers, W., Schwarz, A., Schwarz, U.D., Wiesendanger, R.: A scanning force microscope with atomic resolution in ultrahigh vacuum and at low temperatures. **69**(1), 221–225 (1998)
14. Arima, E., Wen, H., Naitoh, Y., Li, Y.J., Sugawara, Y.: Development of low temperature atomic force microscopy with an optical beam deflection system capable of simultaneously detecting the lateral and vertical forces. pp. 093113-1–093113-6 (2016)
15. Radenovic, A., Bystrenova, E., Libioulle, L., Valle, F., Shubeita, G.T., Kasas, S., Dietler, G.: Characterization of atomic force microscope probes at low temperatures. **94**(6), 4210–4214 (2003)
16. Chen, H., Qin, Z., He, M., Liu, Y., Wu, Z.: Application of electrochemical atomic force microscopy (EC-AFM) in the corrosion study of metallic materials. *Materials* **13**(3), 668 (2020)
17. Nguyen-Tri, P., Ghassemi, P., Carriere, P., Nanda, S., Assadi, A.A., Nguyen, D.D.: Recent applications of advanced atomic force microscopy in polymer science: a review. **12**(5), 1142 (2020). Published online 2020 May 17

Fabrication and Testing of Magnetic Plate Handling Truck



P. H. J. Venkatesh, Sai Kumar Amda, B. Taraji Naik, Kandukuri Srinivas, and D. Thulasi Ram

Abstract The thick metallic plates are used in manufacturing industries like construction, Boiler manufacturing, Crane manufacturing, Wagons manufacturing, Heat exchangers etc. It is the one of the difficult task to handle these thick and large plates as they are heavy in weight and need to be lifted from one end manually before attaching to the crane slings. These plates are to be transported to various places in the factory for processing them to make into the final product, lifting and tying of the plates with the crane slings has to be performed many times during all kind of manufacturing process, which leads to the wastage of time, power consuming and risky process. In this paper a load carrying capacity of mild steel plate handling truck with magnetic lifting arrangement was designed using a SOLIDWORKS and fabricated the prototype model and tested.

Keywords Handling · Crane slings · Magnetic lifting · SOLIDWORKS · Mild steel plate · Fabricated

P. H. J. Venkatesh (✉)

Department of Mechanical Engineering, Vignan's Institute of Information and Technology (A),
Visakhapatnam, Andhra Pradesh, India
e-mail: Venky61788@gmail.com

S. K. Amda

Department of Mechanical Engineering, St Martin's Engineering College, Dhulapally,
Secunderabad, Telangana, India
e-mail: 108saikumar@gmail.com

B. Taraji Naik · K. Srinivas · D. Thulasi Ram

Department of Mechanical Engineering, J B Institute of Engineering and Technology, Hyderabad,
Telangana, India
e-mail: btnaik96@gmail.com

K. Srinivas

e-mail: srinivask005@gmail.com

D. Thulasi Ram

e-mail: Thulasiramdeepavath@gmail.com

1 Introduction

Material handling care is a significant undertaking in structure of the creation framework. The progression of the raw material to taking care of is done. The various kinds of dealing with hardware can be grouped into four significant classes like vehicle, lifting and situating, stacking and unit arrangement and capacity equipment. Various sorts of material taking care of frameworks have advanced yet the most well-known is for transport, lifting and situating, stacking of materials along the crude material stage to completed items and furthermore for conveying the wrapped items in advertise up to shopper points. Material taking care of gear is accessible from easy to complex frameworks for material taking care of relying upon type, size, weight and volume in a unit or one part of material. Transport gear like truck, to trucks with lifting and stacking handles are used to move materials [1, 2].

Industrial trucks and trolleys

These are utilized to move materials over factor ways and when there are inadequate or irregular stream volumes. They furnish greater adaptability in development and they might be worked with vertical lifting development or stage. Hand trucks including trucks and carts are the least complex sort of mechanical truck, are non-fueled. It might be given manual or controlled lifting handles to lift and stack beds. Various kinds of modern trucks with Fork lifting and offset are accessible for taking care of bed unit loads gave thought process and lifting power (Fig. 1).

Cranes and hoists

Electromagnets utilize power to charge the magnet and hold the material to the magnet face. Electromagnets utilize an invigorated electrical loop folded over a steel centre to situate particles inside ferrous materials a typical way, therefore making an attractive field (Fig. 2).



Fig. 1 Industrial trucks and trolley



Fig. 2 Cranes and hoists

The heavy in weight plates are need to be lifted from one end manually before attaching to the crane slings. These plates are to be transported to various places in the factory for processing them to make into the final product, lifting and tying of the plates with the crane slings has to be performed many times during all kind of manufacturing process, which leads to the wastage of time, power consuming and risky process. In this paper a load carrying capacity of mild steel plate handling truck with magnetic lifting arrangement was designed and fabricated. Compared to any other design or fabrication the investment and maintenance is more.

2 Methodology

The requirement for drilling and tapping gaps in parts so eye bolts can be connected to move them as a rule, these gaps should be filled and the surface should be revamped, adding cost to the item. Lifting the load may required two or more people in present work. Gripping and grasping action is less in the material handling equipments. More time consumption while loading/unloading especially blocking and slinging. If labours are unfocused during their working hours this may cause damage to material or injuries to operator, to avoid the above disadvantages the Magnetic truck is designed and prototype is developed and material handling efficiency can be improved [1, 3, 4].

2.1 Design and Fabrication

Solidworks

See Figs. 3, 4 and 5.

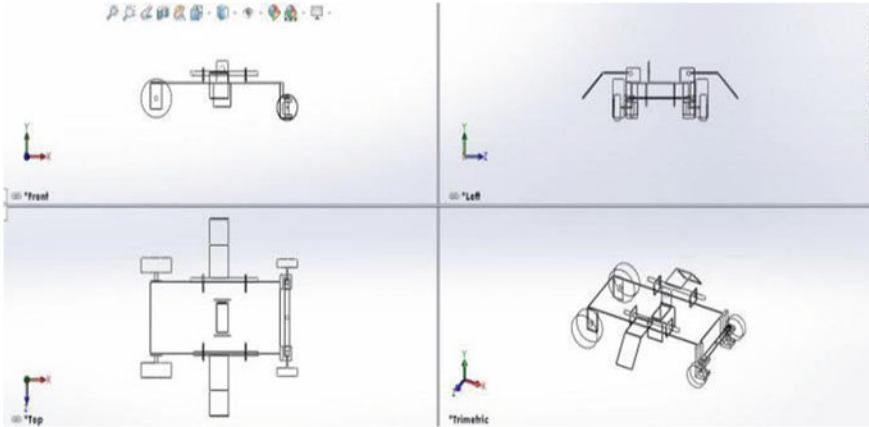


Fig. 3 Wire frame model of magnetic plate handling truck parts and assembly

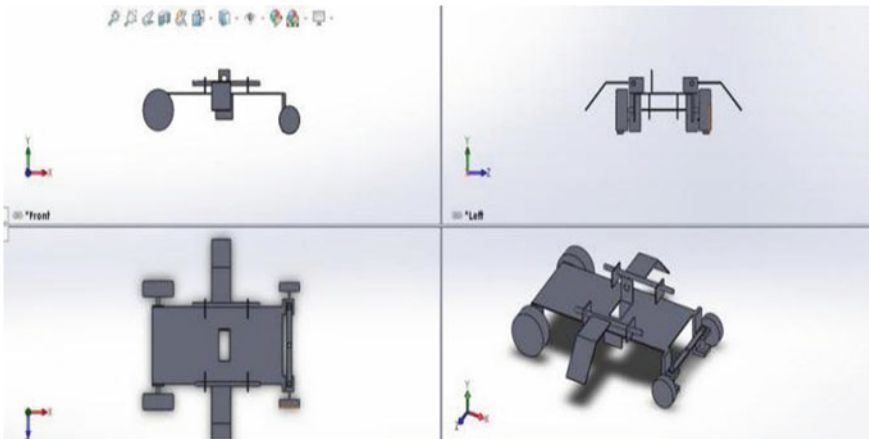


Fig. 4 3D modelling of magnetic plate handling truck parts and assembly

Fabrication

The parts and quantity required for the manufacturing of magnetic plate handling truck are mentioned in the Table 1.

The truck is fabricated by means of various operations like cutting, machining, welding, drilling, boring and milling.

Fabrication of chasis

A plate of 2.5 mm thickness is taken, and marking is performed for 150 × 70 mm. Cutting is performed as per the marking and then, grinding is performed to achieve good surface finish (Fig. 6).

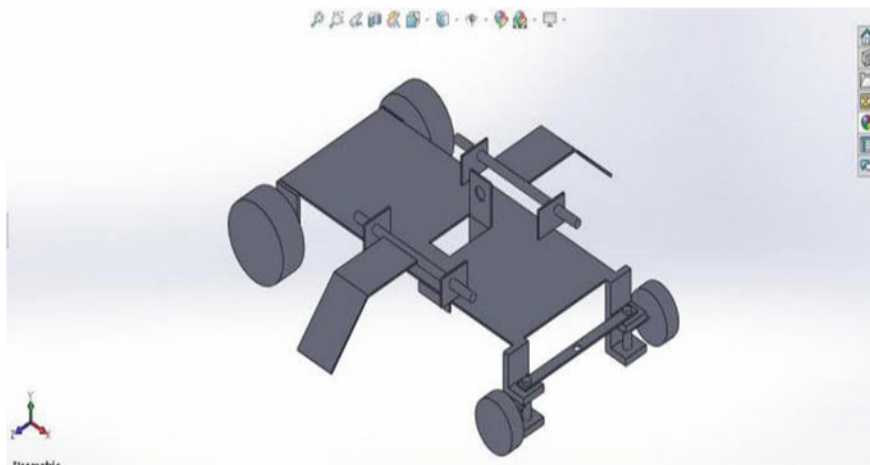


Fig. 5 3D modelling of magnetic plate handling truck

Table 1 Parts required for magnetic plate handling truck

Part	Material	Quantity
Chassis	MS plate	1
Holding arms	MS Plate	2
Obstacle plates	MS Plate	2
Magnetic lever	MS Plate	1
Supporting plates	MS Plate	4



Fig. 6 Fabrication of chassis

Fabrication of holding arms

A MS plate of 2.5 mm thickness is taken, and marking is performed for 70×150 mm. Cutting is performed as per markings and then, grinding is performed to achieve good surface finish. A notch is done using cutting machine at 50 mm distance from one end and bending is performed for 45° . A pipe of 12 mm outer diameter and 6 mm inner diameter is taken, marking is done for length 100 mm. Cutting is done for the pipe and grinding is performed to achieve good surface finish. Drilling of 3 mm diameter is performed on the pipe for fixing with motor and pipe and arm are welded using arc welding machine (Fig. 7).

Fabrication of obstacle plates

A MS plate of 2.5 mm thickness is taken, and marking is performed for 65×65 mm and then cutting is done by cutting machine. Grinding is performed to achieve good surface finish. Two plates are required. Then these plates are welded on the chassis (Fig. 8).

Fabrication of magnetic lever

A MS plate of 2.5 mm thickness is taken, and marking is performed for 70×150 mm and Cutting is performed as per markings and then, grinding is performed to achieve good surface finish. A notch is done using cutting machine at 50 mm distance from one end and bending is performed for 45° . Then two plates of dimensions 50×50 having hole of diameter 6 mm welded on bended portion at equal distance and then a hinge is welded on the other end of the plate which is having 100 mm length. A plate of 2.5 mm thickness is taken, and marking is performed for 70×50 mm and Grinding is performed to achieve good surface finish. Also, two plates of dimensions 50×50 having hole of diameter 6 mm at equal distance to fix with the lifting plate is welded on the base plate leaving equal distance from both sides (ends). The magnets are stick on the base plate with araldite. This set up is then bolted with the lifting plate.



Fig. 7 Fabrication of holding arms



Fig. 8 Fabrication of obstacle plates

Fabrication of rear wheel and front wheel

A plate of 2.5 mm thickness is taken and cutting is performed for dimension of 70×40 mm. Then grinding is performed to achieve good surface finish. A hole of diameter 12 mm is made on the plate at a distance of 15 mm from one side to fix with the motor shaft. The rear wheels having diameter 108 mm are used and a motor of capacity 10 rpm used for this wheel. A plate of 2.5 mm thickness is taken and cutting is done for 60×40 mm and grinding is performed to achieve good surface finish. A plate of 2.5 mm thickness and 120 mm length is taken and bent 90° at 40 mm from the two sides. Two quantities are made for two front wheels. A plate of 2.5 mm thickness and cutting is done for 215×20 mm and three holes of 6 mm diameter are made. And all the supporting parts are welded and the front wheel arrangement (Fig. 9).

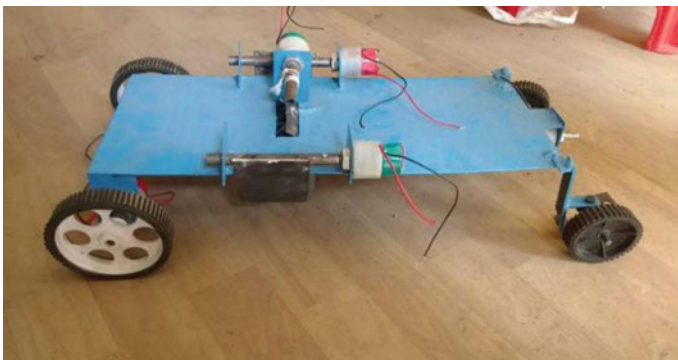


Fig. 9 Magnetic plate Handling truck model

3 Results

Holding arm calculation for Prototype model

Mass of holding arm = 300 g

Mass of material to be handled = 0.5 kg

Mass of holding arms including

Mass material handle = $0.3 + 0.5 = 0.8$ kg

Radius of holding arm $r = 0.095$ M

Force = 9.81×0.8 $F = 7.848$ N

$$\text{Torque } (T = r \times F) T = 0.095 \times 7.848 = 0.7455N - M \quad (1)$$

Speed of motor $M = 10$ rpm.

Power = $2 \times 3.14 \times 10 \times 0.74556/60 = 0.78$ W

Mass of the plate to be lifted = 1 kg

Type of the magnet considered = Ferrite

Outer radius of Magnet = 25 mm = 0.025 m

Inner radius of Magnet = 15 mm = 0.015 m

Area of Magnet $A_m = 3.14 \times (0.025 \times 0.025 - 0.015 \times 0.015) = 0.001256$ m²

Magnetic Flux $D_m = 0.2$ T

$$\begin{aligned} \text{Force } F &= D_m^2 \times A_m / 8 \times \pi \times 10^{-7} \\ &= 0.2 \times 0.2 \times 0.001256 / (8 \times 3.14 \times 10^{-7}) \\ &= 20 \text{ N's} \\ &= 20/9.81 \text{ kgs} \\ &= 2 \text{ kgs} \end{aligned} \quad (2)$$

As actual mass of the plate to be lifted is 1 kg and magnet selected is suitable to lift 2 kgs it is acceptable.

Magnetic lifting power calculations

Mass to be lifted = 1 kg

Mass of magnetic arrangement = 0.5 kg

Radius of pulley/Shaft = 0.003 m

Force $F = mg = 1.5 \times 9.81 = 14.71$ N

Torque $T = 14.71 \times 0.003 = 0.044$ N-M

Speed $N = 3.5$ rpm.

$$\text{Power} = 2 \times 3.14 \times 0.044 \times 3.5/60 = 0.016 \text{ W} \quad (3)$$

The mass of material handled found to be 0.8 kg and force required is 7.484 N. The magnetic flux required is 0.2 T. Power required to lift the plate is 0.016 W

Results and calculations for actual machine

Holding arm calculation

Mass of holding arm = 3000 kg
 Mass of material to be handled = 5000 kg
 Mass of holding arms including
 Mass material handle = 3000 + 5000 = 8000 kg
 Radius of holding arm = 0.9 M
 Force = 9.81×8000 F = 78,480 N
 Torque ($T = r \times F$) $T = 0.9 \times 78,480 = 70,632$ N-M
 Speed of motor $M = 3000$ rpm.
 Power = $2 \times 3.14 \times 3000 \times 70,632/60 = 22.17$ MW
 Magnetic strength calculation
 Maximum size of the plate to be handled 8 m × 4 m and 20 mm thick
 Mass of the plate to be lifted = $8 \times 4 \times 0.02 \times 7630 = 4883$ kg
 Approximately 5000 kg = 5 T
 Type of the magnet considered—Lifting Magnet Rectangle
 Length = 600 mm = 0.6 m
 Width = 430 mm = 0.43 m
 Area of Magnet $A_m = 0.6 \times 0.43 = 0.258$ m²
 Magnetic Flux $D_m = 0.8$ T (Neodymium max 1.4 T) (Tables 2 and 3).

$$\begin{aligned}
 \text{Force } F &= D_m^2 \times A_m / 8 \times \pi \times 10^{-7} = 0.8 \times 0.8 \times 0.258 / (8 \times 3.14 \times 10^{-7}) \\
 &= 65,732 \text{ N's} \\
 &= 65,732 / 9.81 \text{ kgs} = 6700 \text{ kgs}
 \end{aligned}
 \tag{4}$$

As actual mass of the plate to be lifted is 5000 kg and magnet selected is suitable to lift 6700 kg it is acceptable.

Magnetic lifting power calculations
 Mass to be lifted = 5000 kg
 Mass of magnetic arrangement = 2500 kg
 Radius of pulley/Shaft = 0.15 m
 Force $F = mg = 7500 \times 9.81 = 73,575$ N

Table 2 Calculations for prototype model

S. No.	Holding arm parameters	Holding arm calculated values
1	Torque	0.7455 N-m
2	Area of magnet	0.001256 m ²
3	Force	2 kg

Table 3 Calculations for actual machine

S. No.	Parameters	Calculated values
1	Torque	70,632 N-m
2	Area of magnet	0.258 m ²
3	Force	6700 kg

$$\text{Torque } T = 73,575 \times 0.15 = 11,036 \text{ N-M}$$

$$\text{Speed } N = 3000 \text{ rpm.}$$

$$\text{Power} = 2 \times 3.14 \times 3000 \times 11,036/60 = 11,551 \text{ W} = 1.15 \text{ MW}$$

The actual machine which can handle 5 ton load. The power required to lift the plate is 22.1 MW and the magnetic lifting power required is 1 MW.

4 Conclusion

The magnetic Plate handling truck is designed and fabricated and the magnetic lifting avoids wear and tear of parts to be handled. The holding arms which provide additional safety for the parts to be handled. No slinging operations taking place. The testing is done and from that, Magnetization and demagnetization mechanisms are functioning as per requirement. The prototype machine can able to lift and handle 1 kg metal plate. Holding arms are functioning as per requirement. Drive and turning mechanisms are functioning as per requirement and these kind of trucks can be manufactured with Automation techniques can be used introducing sensors in future to the current model.

References

1. Shinde, Y., Jadhav, K.: Magnetic roller for lifting toast box case. *Int. Res. J. Eng. Technol. (IRJET)*. e-ISSN: 2395-0056 (2018)
2. Gupta, V., Bansal, R.: A review on material handling equipment and their selection for potential applications. *Int. J. Tech. Res. (IJTR)* 2(1) (2013)
3. Bahale, A.P., Deshmukh, S.S.: Improving material handling efficiency in a ginning machine manufacturing company. *Int. J. Innov. Res. Sci. Eng. Technol.* 3(3), 10180 (2018)
4. Ramachandra, C.G., Pavana, K., Shet, S., Reddy, V., Virupaxappa, B.: Design and fabrication of automotive hydraulic jack system for vehicles. *IJAER* (2013)

Design of Pico Hydro Power Plant Using an Impulse Turbine



P. H. J. Venkatesh, Vivek Viswanadha, K. Sravan Kumar,
and Koyyana Ramesh

Abstract The practical design of Pelton wheel and analysis is made to measure the flow rate of rainwater entering into a small Pond by using a V-Notch weir. It was performed in a rural area with 65 houses. Every year during rainy season the amount of water used to go waste into the ponds without any utility for the people living in the rural areas with less population, the water during the rainy season flowing into the pond from the small drains into a large single connected single drain. In this paper a practical attempt is made to utilize the rain water by measuring the total flow rate of the rain water and after measuring based on the discharge obtained a small Pico hydropower plant is constructed using Pelton wheel and the amount of power is estimated.

Keywords V-notch · Flow rate · Discharge · Pico hydro plant · Pelton wheel

1 Introduction

The V-notch is a triangular-shaped open channel section measurement [1, 2] and they are used for measurement of small flow discharge value. The upper part of the section is above the water level, and the channel is always triangular shaped, the cross-sectional area can be determined easily. V-notches is used for low discharge values (Fig. 1).

The Hydropower plant generate the electrical energy from the water. A coupling of the turbine and a generator with a shaft used for converting the mechanical energy into the electrical energy.

P. H. J. Venkatesh (✉)

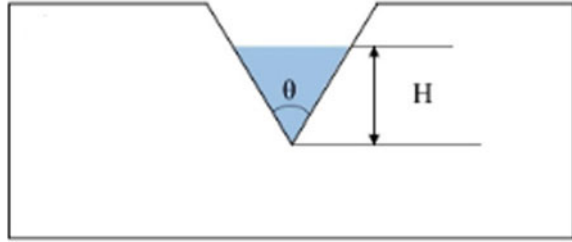
Department of Mechanical Engineering, Vignan's Institute of Information Technology (A),
Visakhapatnam, AP, India

e-mail: venky61788@gmail.com

V. Viswanadha · K. Sravan Kumar · K. Ramesh

Department of Electrical and Electronics Engineering Vignan's Institute of Information
Technology (A), Visakhapatnam, AP, India

Fig. 1 Triangle shaped Notch weir [1]



Pico hydro plants with 5 kW are suitable in remote areas for power supplies and rural isolated communities, as an economic option for extending the electricity grid. The hydropower plants are cheapest and not harmful to the environment.

1.1 Types of Hydraulic Turbines

The turbine is a rotational mechanical machine which converts fluid energy into work [3–5]. The amount of work produced by a turbine is used to generate electricity when coupled with the shaft to the generator. Turbines are divided by their principle of operation and can be divided into two types they are impulse and reactions turbine. The impulse turbine with the flow of the water to rotate the runner and discharged. Reaction turbines are pressure type turbines that depend on the pressure difference between either sides of the turbine blades. For micro-hydro, mini applications, Pelton turbines can be used effectively at head down to about 10–20 m [6, 7].

Turbine selection

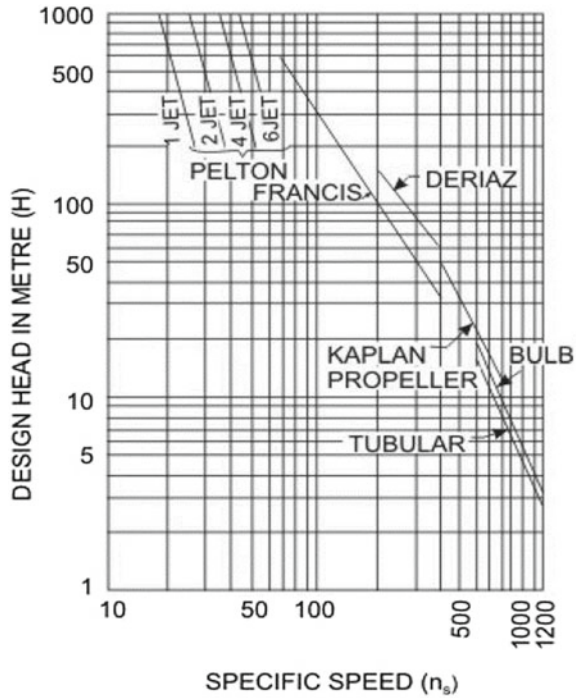
The type of turbine depends on environmental condition and depends on the total head of the water “ H ” and the Discharge “ Q ” [5, 8].

Figure 2 indicates the selection of turbine is suitable for any particular combination of Discharge and head. Pelton wheel is suitable for high head and low flow rate [5, 8].

1.2 Turbine Working Principle

The Pelton wheel is a reaction turbine which is used for a large amount of power generation is required. A micro pelton turbine is model for actual Pelton wheel which is used for the small-scale power generation. The kinetic energy formed by the water to fall on the pelton runner blades. This impact provides a necessary required torque for the rotation the runner blades by neglecting its inertia forces. The rotation of runner with blades generates a mechanical energy which is coupled with the alternator to convert into electrical energy. The water during the rainy season is a large single

Fig. 2 Specific speed versus design head [9, 10]



connected single drain. The practical attempt is made to utilize the rainwater by measuring the total flow rate of the rainwater and after measuring based on the discharge obtained a small Pico hydropower plant is constructed using Pelton wheel and the amount of power is estimated. Compare to the other power plants hydropower plant requires water resources which are available in nature plenty and investment on this plant when compared to the thermal power and nuclear power plants are less and the rainfall is the major resources for the hydropower plant (Fig. 3).

2 Methodology

2.1 Discharge Calculation Using V-Notch

The Discharge value is obtained for a simple flow of V-notch by applying Bernoulli equation or Conservation of Energy [1, 2]

$$Q = C_d \times \left(\frac{8}{15}\right) \times \sqrt{2 \times g} \times \left(\tan \frac{\theta}{2}\right) \times H^{5/2} \tag{1}$$

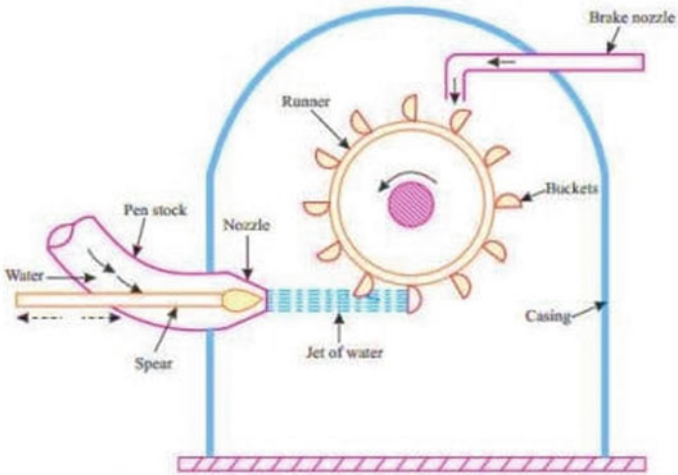


Fig. 3 Working of pelton wheel [3, 4, 6, 9, 10]

C_d : Discharge Coefficient, θ : Notch Angle, H : Height above the base V-Notches are used in seepage measurement of irrigation dams and toe drains. Discharge in V-Notches can measure from 0.006 to 0.12 m³/s.

The discharge is calculated from the following relation

$$Q = C_d \times \left(\frac{8}{15}\right) \times \sqrt{2 \times g} \times \left(\tan \frac{\theta}{2}\right) \times H^{5/2}$$

$$\theta = 60, \text{ consider } C_d = 0.62$$

$$Q = 0.467 \times \frac{8}{15} \times \sqrt{2 \times 9.81} \times \tan \frac{60}{2} \times 0.035^{5/2}$$

$$Q = 0.000193 \text{ m}^3/\text{s}.$$

Similar way the other calculations are done and tabulated in Table 1.

From the above calculations the highest value of discharge is 0.03154 m³/s is chosen as a discharge through the notch.

Table 1 Discharge values for V-notch

S. No.	Time	Head in m	Discharge Q in m ³ /s
1	12:15	0.035	0.000193
2	12:45	0.075	0.000985
3	01:15	0.300	0.03154
4	01:45	0.250	0.02000
5	02:15	0.172	0.00785

2.2 Pelton Turbine Design

The effective head available of this Pelton wheel is considered at 10 m and the discharge is [1, 11], $Q = 0.0041 \text{ m}^3/\text{s}$, $\rho = 1000 \text{ kg/m}^3$, $g = 9.81 \text{ m/s}^2$, $\eta_o = 80\%$ (Assumed).

1. Calculation for power developed by Pelton Turbine

$$P = \eta_o \times \rho \times g \times Q \times H \quad (2)$$

For, $Q = 0.03154 \text{ m}^3/\text{s}$ and 10 m of Head, $\eta_o = 80\%$.

$P = 0.8 \times 1000 \times 9.81 \times 0.03154 \times 10 = 2.475 \text{ kW}$, nearly taken as a value of 2.5 kW.

$$P = 2.5 \text{ kW.}$$

2. Calculation for Speed of the Pelton Turbine

$$N = 147.7 \times \sqrt{H} = 470 \text{ rpm} \quad (3)$$

3. Calculation of Pelton Turbine Specific Speed

$$\begin{aligned} N_s &= N \times \left(\frac{\sqrt{P}}{H^{5/4}} \right) \\ &= 470 \times \frac{\sqrt{2.5}}{10^{5/4}} = 42 \end{aligned} \quad (4)$$

4. Calculation for the absolute velocity of water at inlet of the pelton turbine

Take $C_V = 0.99$,

$$V_1 = C_V \times \sqrt{2 \times g \times H} = 3.6 \text{ m/s} \quad (5)$$

Therefore, $u = u_1 = u_2$. To achieve maximum efficiency, $u = 0.5V_1$
 $u = 6.8 \text{ m/s}$.

5. Calculation for the Mean Diameter of the Pelton turbine

$$\text{From } u = \pi \times D \times N/60 \quad (6)$$

$$D = 0.276 \text{ m.}$$

6. Calculation for the Diameter of Jet for the pelton wheel

$$\text{Diameter of Jet, } d_0 = 0.595 \times \sqrt{\frac{Q}{Z_0 \times \sqrt{H}}} = 0.034 \text{ m} \quad (7)$$

For single jet $Z_0 = 1$

7. *Jet Ratio*

$$m = \frac{D}{d_0} = 8 \quad (8)$$

8. *No. of Buckets will be*

$$Z = 15 + 0.5(8) = 19 \quad (9)$$

9. *Inlet and outlet velocity triangles for the pelton wheel*

The water Relative velocity at inlet $V_{r1} = V_1 - u_1 = 13.68 - 6.8 = 6.8 \text{ m}$, The water Whirl velocity at inlet and outlet (Fig. 4).

$$\begin{aligned} V_{w1} &= V_1, \\ V_{w2} &= V_{r2} \cos \Phi - u_2, \\ V_{r2} &= V_{r1} \\ V_{r1} &= V_{w1} - u_1 = 6.78 \text{ m/s} \\ V_{w2} &= 0.3 \text{ m/s, } V_{r2} < u_2 \end{aligned} \quad (10)$$

10. *Jet Force on the runner*

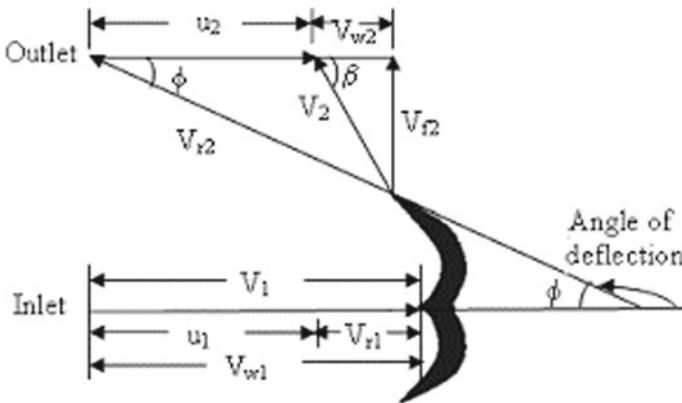


Fig. 4 Velocity Triangle of outlet and inlet of pelton wheel [6, 10]

$$F = \rho a V_1 (V_{w1} + V_{w2}), F = 56.908 \text{ N} \tag{11}$$

11. *Jet force on the bucket*

$$= \frac{\rho Q (V_1 - u)^2}{V_1} \times (1 - \cos \alpha) = 0.473 \text{ N} \tag{12}$$

12. *Bucket Design*

The dimensions of the Pelton wheel bucket are

Bucket length, $L = 3.3 d_0 = 0.1122 \text{ m}$

Bucket width, $B = 4 d_0 = 0.136 \text{ m}$

Notch depth, $S = 0.625 d_0 = 0.02125 \text{ m}$

Notch width, $M = 1.6 d_0 = 0.0544 \text{ m}$

Bucket depth, $E = 1.2 d_0 = 0.0408 \text{ m}$

Bucket height, $A = 2.5 d_0 = 0.085 \text{ m}$.

13. *Shaft diameter*

See Figs. 5, 6 and 7.

$$d_s = \sqrt[3]{\frac{1.77 \times 10^6 \times P}{N}} = 0.21 \text{ m} \tag{13}$$

Based on these dimensions the Pelton wheel is designed and the Pico hydropower plant is developed and as per the calculations the obtained power is 2.5 kW, but after

Fig. 5 Pelton wheel bucket dimensions [6]

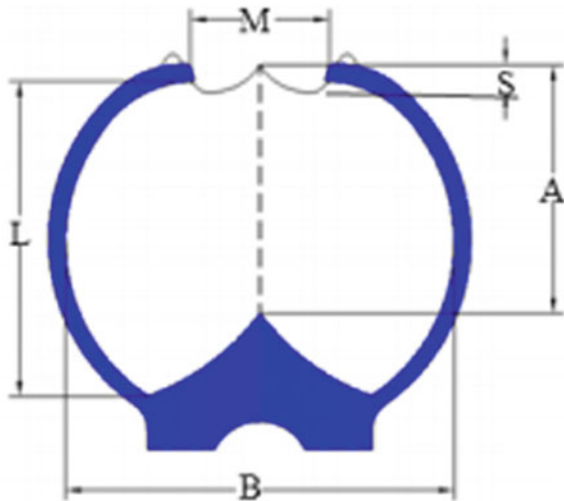


Fig. 6 Pelton wheel with runner [10]



Fig. 7 CFL bulbs [10]



performing the experiment the power obtained to a value of 2 kW there are many reasons for the loss of output power such as but For power 2.5 kW total of 85 CFL bulbs required and one single CFL consumes 0.0025 kW/h.

1. The width of the bucket is small compared to the diameter of the jet, the fluid is may not deflect on the buckets and this may lead to energy dissipated lead to the efficiency drop.
2. The placement of the Pelton wheel and the Head also important for the power output.

3 Results

The parameters calculated for the Pelton wheel indicates that the dimensional values of the Pelton wheel are based on the Discharge. The speed of the turbine depends on the Head developed. The obtained power may vary when there is variation in the

Table 2 Calculated Values of important parameters for Pelton wheel

Q , discharge	0.03154 m ³ /s
N , Speed	470 rpm
P , Power	2.5 kW
No. of buckets (Z)	22
Jet ratio, m	8
Shaft diameter	0.21 m
Absolute velocity	3.6 m/s
Specific speed	42
Mean diameter (D)	0.276 m
Wheel velocity (u)	6.8 m/s

Table 3 Pelton wheel bucket dimensions

Bucket length	0.1122 m
Bucket width	0.1360 m
Notch depth	0.0212 m
Notch width	0.0544 m
Bucket depth	0.0408 m
Bucket height	0.0850 m

discharge that depends on rainwater in order to achieve better efficiency the width of the bucket should more compared to the diameter of the jet. The Discharge is not same for every rainfall and the flow through drains are also not constant as the drains not only carry water but also solid waste due to this the flow of water is varied, the same amount of discharge cannot be maintained constant as the rainfall is not constant it changes time to time and the amount of water depends on millimeter of rainfall (Tables 2 and 3).

4 Conclusion

The Discharge value and the power value shows that the output which is obtained is depend on the amount of rainfall and the flow of water into the drain and for the power of 2.5 kW total no of 85 CFL bulbs can be used and each bulb consumes 0.025 kW/h as per calculation, but as per experiment for 2 kW, so total no of 80 CFL bulbs can be used when one CFL consumes 0.0025 kW/h as this is a practical attempt is made to develop the power plant and if the same Pelton wheel is designed for the 4 times of the existing dimensions 10 kW power can be achieved, which are used after the energy and other losses the better output power can be obtained and the designed dimensions can be used for simulation analysis and the flow variation with the different losses can be estimated properly. By establishment of these kind

of Pico hydropower plant in rural areas more amount of power can be generated and moreover the plant is not harmful to the environment and for power generation natural resources are used. The application of V-notch and pelton turbine is used to design the hydro plant.

References

1. Guru, B.G., Padhan, A., Meher, S.K., Barik, P.U.: Comparative analysis of the discharge coefficient by using V-notch and rectangular notch. *Int. J. Res. Innov. Appl. Sci. (IJRIAS)* **IV**(IX) (2019). ISSN 2454-6194
2. Bos, M.G.: *Discharge Measurement Structures*, 3rd edn. International Institute for Land Reclamation and Improvement, Wageningen, The Netherlands, pp. 40–202 (1989)
3. Oo, T.Z., Nyi, N., Khaing, C.C.: Design calculation of pelton turbine for 220 kW. *Int. J. Sci. Res. Publ.* **9**(7) (2019). ISSN 2250-3153
4. Thakur, R., Kumar, S., Kashyap, K., Kumar, A., Aggarwal, S.: Selection of erosive wear rate parameters of pelton turbine buckets using PSI and TOPSIS techniques. *Int. J. Innov. Technol. Exploring Eng. (IJITEE)* **9**(1) (2019)
5. Gupta, V., Prasad, V., Khare, R.: Effect of jet shape on flow and torque characteristics of pelton turbine runner. *Int. J. Eng. Res. Appl.* **4**(1)(Version 1), 318–323 (2014). ISSN: 2248-9622
6. Chan, Z.M.: Design calculation of penstock and nozzle for 5 kW pelton turbine micro hydropower plant. *Int. J. Trend Sci. Res. Dev. (IJTSRD)* **3**(5) (2019)
7. Prasad, V.: Numerical simulation for flow characteristics of axial flow hydraulic turbine runner. *Energy Proc.* **14**, 2060–2065 (2012). [10] Nasir, B.A.: Design of high efficiency cross-flow turbine for hydro-power plant. *IJEAT* **2**(3) (2013)
8. Sharma, A., Sharma, P., Kothari, A.: Numerical simulation for pressure distribution in pelton turbine nozzle for the different shapes of spear. *Int. J. Innov. Eng. Technol. (IJJET)* **1**(4) (2012)
9. Ishola, F.A., Kilanko, O.O., Inegbenebor, A.O., Sanni, T.F., Adedokun, A.A., Adegoke, D.D.: Design and performance analysis of a model pico size pelton wheel turbine. *Int. J. Civ. Eng. Technol. (IJCIET)* **10**(5), 727–739 (2019)
10. Mon, E.E., Khaing, C.C., zaw Lynn, A.: Design, construction and performance testing of 1 kW Pelton turbine for pico hydro power plant. *Int. J. Sci. Eng. Appl.* **8**(7), 192–196. ISSN:-2319–7560 (2019)
11. Zoppé, B., Pellone, C., Maitre, T., Leroy, P.: *Flow Analysis Inside a Pelton Turbine Bucket*, Vol. 128, p. 500 (2006) Copyright © 2006 by ASME

Experimental Analysis of Performance and Emission Characteristics of Four Stroke Single Cylinder VCR Diesel Engine Using Palm Biodiesel and Diesel Along with Comparison



Savadana Venkataramana and N. Ramanaiah

Abstract The immense importance of high energy demand with conventional fuels and the detrimental effects of pollution from fossil fuels, the focus is shifted toward the usage of alternative fuels. An initiative is considered to examine performance characteristics and magnitude of pollutants 4 strokes single cylinder VCR engine filled with diesel and palm biodiesel at a compression ratio of 18:1. Experimentation is carried out with diesel and palm biodiesel one at a time on a chosen engine at various loads. Performance evaluation contains the evaluation of brake power [BP], Brake Specific Fuel Consumption [BSFC], Brake thermal efficiency [BTE], etc. Emission analysis, the contents of CO%, NO_x (ppm), CO₂%, are measured by exhaust gas analyser. The Results reveal that the brake thermal efficiency of palm biodiesel fuelled engine is 29.01% at peak load which is more than the diesel by 20% moreover BFFC is 0.293 kg/KWH and is also less than the diesel by 30%. In the case of emission, NO_x with palm biodiesel is 415 ppm which sows 50% less than the diesel. While CO% and CO₂% are found to be 0.024 and 2.6, respectively, at maximum BP for palm biodiesel. It was observed from the carried out work, BTE was increased on par with the increase in load. It is inferred from the pragmatic condition that is considered to be a much promising substitute.

Keywords Palm biofuel · Diesel · VCR diesel engine · Exhaust gas analyser · Smoke meter

S. Venkataramana (✉)

Department of Mechanical Engineering, Vignan's Institute of Information and Technology (A), Visakhapatnam, Andhra Pradesh, India
e-mail: savyasvr@gmail.com

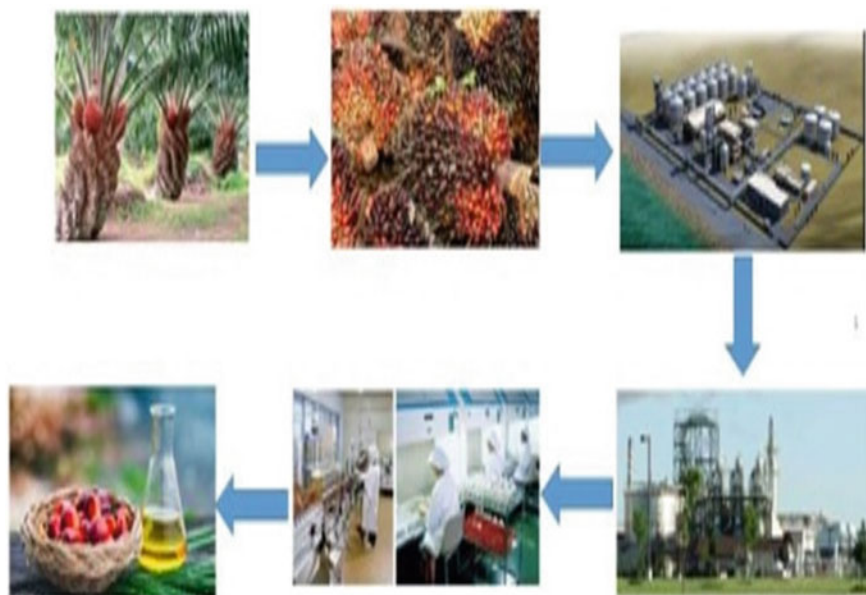
N. Ramanaiah

Department of Mechanical Engineering, Andhra University, Visakhapatnam, Andhra Pradesh, India

1 Introduction

Modern civilization worldwide promotes the automobile revolution for better living comforts and standards, which increases the importance of the transport sector. The transport sector became the highest consumer of conventional fuels. To cope up with great demand in the future and scarcity, it inevitable to go for alternative fuels [1]. Hence it is necessary to pave the way for partial replacement of diesel by biodiesels. This experimentation examines the comparison between palm biodiesel and diesel working on the VCR engine with opted specifications by choosing the choice of palm biodiesel as it is produced on an average of 4–5 tons per year, which is considerably larger than that of soybean oil [2, 3]. Pragmatism supports the choice of coconut biodiesel with many dependable results in terms of engine performance and exhaust emissions characteristics besides abundance in availability as per the highest production with 2260 kg of oil/ha [4] but it is limited in application due to edibility. In the series of considerations palm oil also became popular and is widely produced in most of the regions as supported by all tropical conditions at the rate of production around 10–35 tons per hectare. Palm trees generate palm oil from its seed and also from pulp besides edible oil [5]. Biodiesel is an alternative tool to fill the gap of scarcity in the highest demand for fuel needs in the transport sector particularly in the internal combustion engine [6]. In composition, it consists of fatty acid methyl ester and is done by the method of the transesterification from vegetables or fats [7]. At present biodiesels are used mostly with blends representing a combination of diesel and biodiesel in different proportions. The designation of the blend is represented with a volumetric percentage, where B0 represents 0% biodiesel and B100 representing 100% biodiesel [8]. Another report reported reductions in BSFC, emissions of CO, HC, smoke, and exhaust gas temperature against raise in compression ratio [CR]. It was depicted the reduction in duration of ignition while the maximum limit of pressure at maximum compression ratio results in higher NO_x emission [9]. Raheman et al. reveal that brake thermal efficiency is maximum at a maximum which was evident of the prominent influence of compression ratio at rich blends [10].

The objective of the present work is to analyze the performance and emission characteristics of both diesel and biodiesel for their comparison. It also asserted to consider palm biodiesel as much promising substitute. The experiment has been conducted on engine test rig after eight years from its installation. As the pollution and performance trend changes for the running vehicle for authorized fifteen years abide by the motor vehicle act. Therefore it also necessary to review performance at regular intervals of service life where the real problem of pollution and mileage exists besides a slight variation of treated palm biodiesel. Hence the contribution of paper reveals the characteristics of reused test rig with palm biodiesel with methanol and catalyst.



Flow Chart 1 Transesterification process

1.1 Methodology

As shown in Flow Chart 1, transesterification took place in stages for the complete transformation of basic raw form into ready to use biodiesel transformation undergone steam sterilization, stripping for separation of stalk and fruit. In the part of the secondary operation, it further has undergone digesters and then to pressers for oil extraction while discard used as fertilizer. In the part of the post-processing purification of extracted oil is done by vacuum dryer and centrifugal dryer before sending it to the boiler and finally stored in storage tanks. By-products are further produced by refining in the refinery and took shape as cooking oil. Palm oil is converted into crude oil by extraction or pressing. Crude oil might be consisting of impurities in its unrefined form which may yield troublesome problems in the engine namely poor cold flow property, increasing viscosity, coking, etc. Hence oil treatment with methanol and catalyst. Table 1 shows the properties of palm biodiesel and diesel.

1.2 Experimental Set up

The establishment of an experimental arrangement has the combination of a VCR engine and an electrical dynamometer as a loading system. The water-cooled CI engine is erected for 5.2 KW which runs at 1500 rpm. The erected set up has one

Table 1 Properties of palm biofuel and diesel

Parameters	Units	Palm bio-diesel	Diesel
Ash content	%	0.0018	0.01
Carbon residue	%	0.52	0.1
Pour point	°C	+4	-1
Flash point	°C	188	68
Kinematic viscosity at 40 °C	CST	8.40	2.75
Sediment	%	0.08	0.05
Density at 15 °C	gm/cc	0.854	0.830
Sulphur content	%	0.69	0.10
Water content	%	0.014	0.05
Gross calorific value	kcal/kg	10,100	10,000

Table 2 Specifications of VCR Engine

Engine mode	Kirloskar
Type	4-stroke, naturally aspirated and water cooled
Bore	87.5 mm
Stroke	111 mm
Cylinder volume	661 cc
Range of compression ratio	12:1 to 18:1
Injection timing	25° BTDC
Injection pressure	200 bar
Maximum power	5.2 kW at 1500 rpm
Injection nozzle	3 hole

engine panel box which consists of components like air-box, dual fuel tanks, fuel measuring arrangement, U-tube manometer, the knob for dynamometer control, etc. U-tube manometer for the observation of air supply and the amount of fuel consumed is measured with fuel measuring unit. The computerized data acquisition system for airflow rate, injection pressure, crank angle, pollutants in exhaust equipped to test rig (Table 2).

1.3 Emission Measurement System

The testing system is to meter the pollutants of the exhaust. This system consists of a Gas Analyser that reveals the number of pollutants in the exhaust gas such as CO₂, CO, NO_x, HC, O₂, and SO_x (Fig. 2; Table 3).



Fig. 2 Gas analyser

Table 3 Specifications of exhaust gas analyser

Pollutants	Carbon Monoxide(CO), Hydro Carbon(HC), Carbon Dioxide(CO), and NO _x
Mechanism	Infrared sensors for CO, CO ₂ , HC, and Electrochemical sensors for NO _x .
Data resolution	Table 1: properties of biodiesel
Time for initiation	<2 min.
Time interval for air intake	24 min time interval
Discharge of gas	500–1000 ml/min
Handling system	Particulate fine filter, S.S. Probe, PU Tubing, water separator cum filter.
Operating conditions	Temperature: 5°–45°
	Pressure: 813–1060 Mbar
	Humidity: 0–90%

2 Results

2.1 Engine Performance

Brake specific fuel consumption [BSFC] is defined as the quantity of fuel consumed to provide unit brake power. Figure 3 shows the variation of BSFC for biodiesel fuelled engine and diesel-fuelled engine against brake power. For diesel, BSFC is

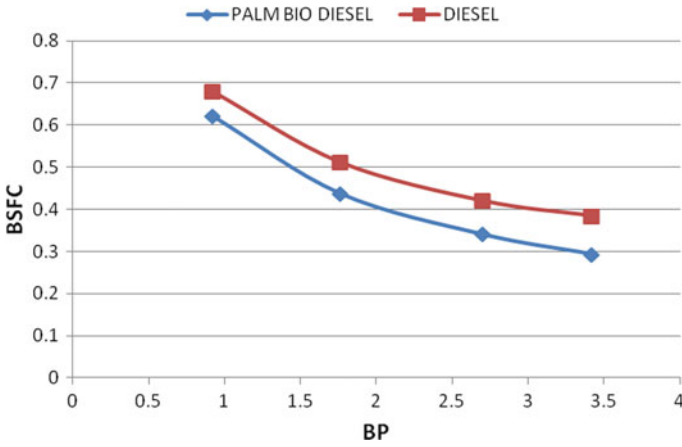


Fig. 3 BP versus BSFC

higher than palm biodiesel at all loads because of the variation of calorific value. At full load, BSFC of PBD is 23.69% less compared to plain diesel operation [8].

Brake thermal efficiency [BTE] basically defined as the ratio of brake power at crank shaft and expected energy from the complete combustion of fuel supplied to the engine. Figure 4 represents a comparison of brake thermal efficiency of palm biodiesel fuelled engine with a diesel-fuelled engine. Brake thermal efficiency for palm biodiesel is found higher than the diesel at all level of engine loads. At the maximum load, thermal efficiency for palm biodiesel is 24.8% more than the diesel [9].

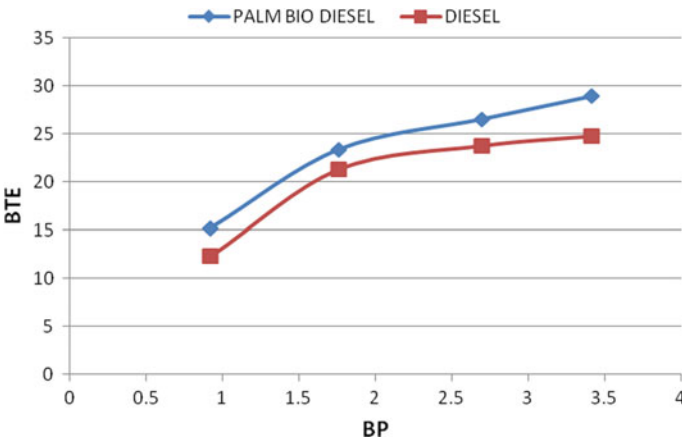


Fig. 4 BP versus BTE

2.2 Engine Emission Characteristics

Figure 5 shows the variation of CO emissions from diesel and palm biodiesel fuelled engines. Palm biodiesel emits less CO pollutants compared to diesel-fuelled engines. At the higher load palm bio, the diesel-fuelled engine emits 0.4% less than the diesel-fuelled engine. In the case of diesel, due to incomplete combustion heterogeneous mixture results in higher hydrocarbons, and carbon monoxide emissions [9].

Figure 6 BP versus NO_x the oxygen content of biodiesel is an important factor in the high NO_x formation levels because the oxygen content of biodiesel provides high local peak temperatures and a corresponding excess of air [8]. Therefore, the higher NO_x emissions can be attributed to the more complete combustion of biodiesel with the presence of more oxygen in the combustion chamber [10]. Figure 6 shows the variation of NO_x emissions from diesel and palm biodiesel fuelled engines. Palm biodiesel emits fewer NO_x pollutants compared to diesel-fuelled engines. At the

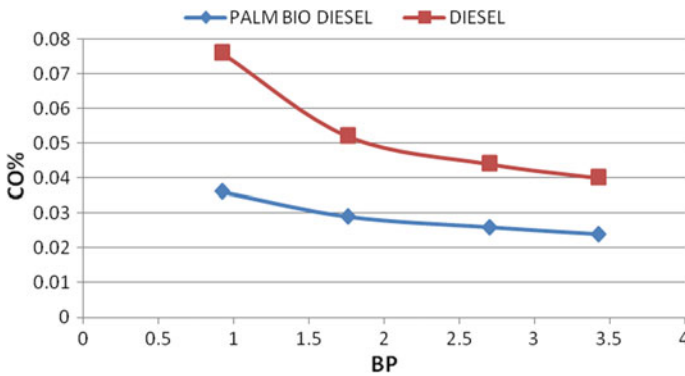


Fig. 5 BP versus CO%

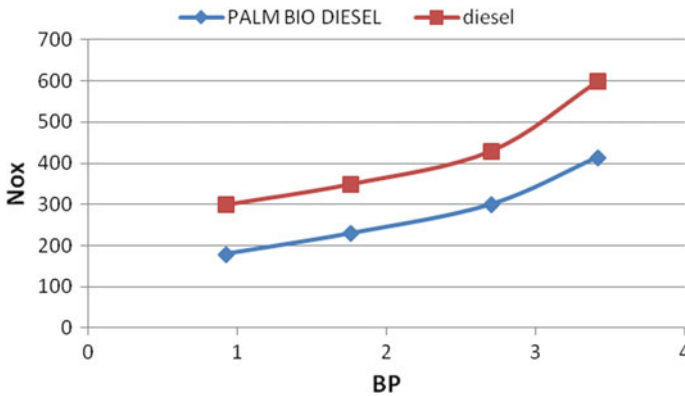


Fig. 6 BP versus NO_x

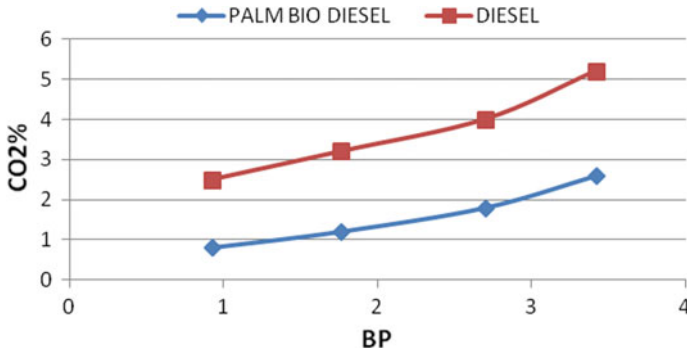


Fig. 7 BP versus CO₂%

higher load palm, biodiesel fuelled engine emits 30% less than the diesel-fuelled engine.

Figure 7 shows the variation of CO₂ emissions from diesel and palm biodiesel fuelled engines. Palm biodiesel emits less CO₂ pollutants compared to a diesel-fuelled engine. At the higher load palm, biodiesel fuelled engine emits 50% less than the diesel-fuelled engine. In case of diesel, due to incomplete combustion heterogeneous mixture results in higher hydrocarbons, and carbon monoxide emissions [9].

3 Conclusions

Based on the experimental test results from the engine testing, it can be concluded as follows Palm biodiesel fuelled engine performs less BSFC and higher BTE compared to the diesel-fuelled engine Palm biodiesel fuelled engine emits fewer pollutants of CO, CO₂, and NO_x compared to the diesel-fuelled engine. Palm biodiesel fuel is preferable as alternate to biodiesel.

References

1. Manigandan, S., Sarweswaran, R., Devi, P.B., Sohret, Y., Kondratiev, A., Venkatesh, S., et al.: Comparative study of nanoadditives TiO₂, CNT, Al₂O₃, CuO and CeO₂ on reduction of diesel engine emission operating on hydrogen fuel blends. *Fuel* **262**, 116336 (2020)
2. Balamurugan, T., Arun, A., Sathishkumar, G.B.: Biodiesel derived from corn oil—a fuel substitute for diesel. *Renew. Sustain. Energy Rev.* **94**, 772–778 (2018)
3. Dhar, A., Agarwal, A.K.: Experimental investigations of the effect of pilot injection on performance, emission and combustion characteristics of Karanja biodiesel fuelled CRDI engine. *Energy Convers. Manage.* **93**(357), 366 (2015)
4. Huang, H., Huang, R., Guo, X., Pan, M., Teng, W., Chen, Y., et al.: Effects of pine oil additive and pilot 5.injection strategies on energy distribution, combustion and emissions in a diesel engine at low-load condition. *Appl. Energy* **250**, 185–197 (2019)

5. Directive 2018/2001 of the European Parliament and of the Council of 11 December 2018 on the promotion of the use of energy from renewable sources (2018)
6. Marin-Burgos, V., Clancy, J.S.: Understanding the expansion of energy crops beyond the global biofuel boom: evidence from oil palm expansion in Colombia. *Energy Sustain. Soc.* **7**, 21 (2017)
7. Arolu, I.W., et al.: Genetic variability analysis and selection of pisifera palms for commercial production of high yielding and dwarf oil palm planting materials. *Ind. Crops Products* **90**, 135–141 (2016)
8. Samsukumar, R., Muaralidhararao, M., Gopala Krishna, A., Jayaraju, Y., Surya Sri Vatsav, P., Manikanta, V.H., Satish, S.V.V., Bhuvannaidu, S.A.C.: Performance and emission analysis on C.I. engine with palm oil biodiesel blends at different fuel injection pressures. *Int. J. Innovat. Res. Sci. Eng. Technol.* **4**(4), 2516–2527 (2015)
9. Harsono, S.S., Prochnow, A., Grundmann, P., Hansen, A., Hallmann, C.: Energy balances and greenhouse gas emissions of palm oil biodiesel in Indonesia. *Glob. Change Biol. Bioenergy* **4**, 213–228 (2012)
10. Lam, W.Y., et al.: Greenhouse gas footprints of palm oil production in Indonesia over space and time. *Sci. Total Environ.* **688**, 827–837 (2019)

Scoping Review on Composition of Non Asbestos Organic Friction Materials for Automotive Brake Pad



S. S. Shirsath  and R. N. Yerrawar 

Abstract Braking system is an important system of automobiles responsible for providing better performance and safety. The basic purpose of Braking system is to reduce the speed of moving body by providing adequate resistance, which ultimately converted into heat energy. Brake pad material plays important role in controlling the vehicle with considering input parameters like stopping distance, vehicle speed, braking force and performance parameters like coefficient of friction, noise level, fade and recovery. As speed control cannot be achieved by single-phase material so it constitutes several ingredients. Nowadays various classes of friction materials are available based on their constituents like metal, semi-metals, non-metals, ceramic and organic materials. Base composition consists of reinforcement, filler, binder, elastomer, friction modifier and abrasive. Initially asbestos material was used as filler material but worn out particle released after continuous friction pollutes the environment. Also harmful effects on human being like cancer were pointed out by many researchers. Hence, several attempts made by researchers to find an alternative friction materials. In this paper, various possible constituents of composite friction material are reviewed and evaluated their results to study their effects.

Keywords Non asbestos organic · Friction materials (FM) · Performance testing · Wear

S. S. Shirsath (✉)

G.H. Raisoni College of Engineering and Management, Pune, Maharashtra, India

e-mail: sandip.shirsath.phdme@ghrcem.raisoni.net

R. N. Yerrawar

MES College of Engineering, Wadia College Campus, Pune, Maharashtra, India

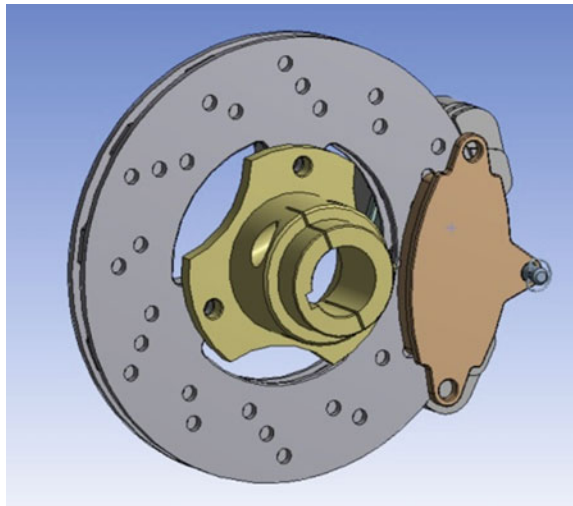
e-mail: rahul.yerrawar@gmail.com

1 Introduction

On daily basis, thousands of automobiles are manufactured and used as per different requirement. In every automobile, braking system plays a crucial role in controlling the vehicles. Nowadays, various materials are used to manufacture a brake pad like metallic, semi-metallic, ceramic-based composites and non asbestos-based organic materials. Every application of a brake friction releases wear particles in gaseous form or particulate matter. The operating condition and base constituent of friction material decide PM size. Some particles are fall on road surface and some remains as airborne matter. This airborne particulate matter enters in human body and causes harmful effect [1, 2].

The Friction materials should possess frictional coefficient with minimum possible wear rate. Since past few decades, asbestos was a filler in friction materials but its airborne particle shown harmful effect on human body [1–3]. Some researcher also moved toward copper based on the automotive brake friction material but copper-based particulate matter shown harmful effects on aquatic animals. So it becomes essential to replace Cu from Friction materials but its replacement was difficult due to unique and multifunctional properties in FMs [4, 5]. By considering all requirements, continuous developments removed the asbestos-based friction materials and the asbestos free natural fiber-based friction materials are used as a safer alternative. The actual composition of friction material is selected based on experimental trial and error method rather than fundamental understanding. Today's brake pads are consisting of more than 6–8 constituents such as reinforcement, binder, elastomer, friction modifier, abrasive and filler. Every constituent has its unique properties [6] (Fig. 1).

Fig. 1 Brake pad assembly



A friction process produces friction products like brake wear particles, friction debris and gaseous emissions. These wear debris adheres to the frictional surface and forms a friction layer. This friction layer decides the performance of brake pad [7, 8]. The surface making contact with the friction material decides tribological characteristics [9]. During operation, continuous rubbing action between the drum and friction material generates high temperature up to 350 °C [10]. Wear of friction brakes affected by many performance parameters such as braking force, pressure applied, sliding velocity, temperature, working environment, etc. There is no any relationship between performance parameters that describes the friction and wear dependence when the brakes were applied. The Rise in operating temperature reduces friction performance and leads to thermal fade. Also as temperature reduces, FM gains frictional coefficient called as recovery. The temperature on the friction surface is higher than values indicated by thermocouples because the actual friction takes place on asperities. The actual contact area while braking is less than the apparent surface area. Due to this, the performance investigation of commercial friction materials at elevated temperature is becoming key area of interest [11, 12]. During operating condition, friction materials are subjected to dry or wet conditions. The wet condition may be due to rainwater and moisture in the environment, which reduces the performance of friction material [13].

Various challenges are available in front of manufacturing of eco-friendly friction materials. Ideally, friction material should have less density, heat and water resistant, high strength, moderate hardness, low wear rate and stable frictional coefficient. Apart from this, thermal conductivity plays a crucial role in performance as lower thermal conductivity accumulates frictional heat on the working surface and leads excessive fade, similarly higher thermal conductivity results in excessive heat flow toward back-plate leads to spongy brakes [14]. It becomes essential to develop friction material which exhibits all desirable properties and manufactured from easily available materials. This method considers possible base constituents used in friction materials with tribological properties [15]. This method emphasizes on various types of wear need to consider during development of FM.

2 Material Used for Brake Pad

A homogeneous mixture of multiple ingredients considered as the reinforcing material, filler, solid lubricant, friction modifier and suitable binder, used as friction material for brake pad [16, 17]. These base constituents decide the physical, mechanical and tribological characteristics of material (Fig. 2).

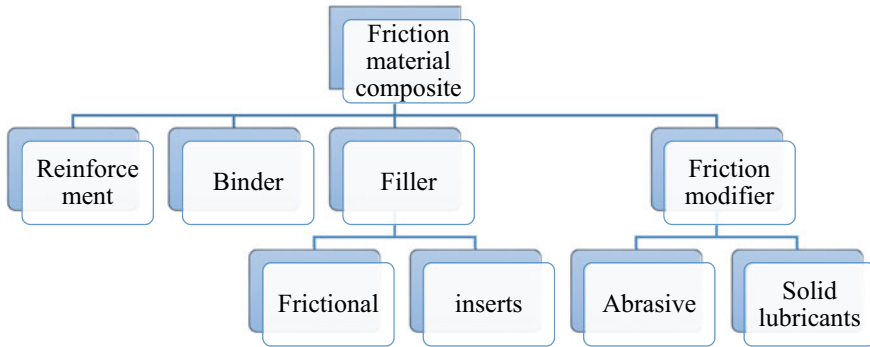


Fig. 2 Friction material composition

2.1 Fillers

The Fillers is major ingredient of friction material which improves the manufacturability. Ideally, it must be inexpensive. It fills voids. The terms form FM like metallic, semi-metallic and non-metallic material indicates filler as base material. The Fillers should be compatible with the other ingredients in terms of size and mostly nanosize is preferable. The particles of filler material should not undergo internal fracture as it is subjected to the compressive loading. The filler material selection is based on its severity with the environment. The Biodegradable fillers are preferred over nonbiodegradable, due to the less environmental impact. Some natural fillers like kenaf fibers, periwinkle shell powder, palm kernel shell powder, banana peels, etc., are available but properties induced will not be compromised [18–21].

Any materials which satisfy all these criteria are desirable. The Literature shows that the filler with crystalline structure like zinc carbonate, barite, zircon gives more strength, resistance to rupture, etc., today, the single material having desirable properties is preferred over combined materials [22, 23].

Mullite increases the density, compressive strength and decreases flexural strength of friction material. The powdered filler gives better results as compared to the fibrous material. The particle size of filler affects the properties of frictional material. Finer Periwinkle Shell increases Compressive Strength, hardness and density where as larger particle size of periwinkle shell powder imparts porosity [13, 24]. As Bagasse is eco-friendly and easily available, used as one of the ingredient in friction material [25]. The metals like waste cast iron, Cu in the powder or fiber form, increases physical and mechanical properties of the FM. Also it increases frictional coefficient up to 0.3–0.4 [26–29]. Hardness and frictional performance of the FM improved using barrite and steel wool [30]. The zircon is compatible with a friction modifier and polymer binder leads to stable frictional coefficient. The Zircon based material shoes highest frictional coefficient [31, 32]. The Palm kernel shell, banana fibers and kenaf fibers in finer powder form can replace Hazardous asbestos fillers [18–21]. As

fly ash is thermally stable, used in the friction composite material along with graphite to stabilize their friction performance [33].

2.2 Reinforcements

The reinforcement material may be in fibrous form, powder form or combination of both. The reinforcement materials are used to improve physical and mechanical properties of frictional materials. The fiber orientation decides the results of mechanical properties and improve wear resistance [34, 35]. One more requirement of reinforcing material is compatibility with other ingredients. The chemically treated fiber enhances the tribological properties of material [36, 37]. In all fibers available as reinforcement, organic fibers are most desirable, because of their less social environmental impact [38].

Jute fibers are easily available fiber used as reinforcement in the FM with average frictional coefficient of 0.50. These fibers having low strength but can be used along with the other fillers like walnut shell powder to improve properties [39, 40]. The Aramid fibers are strong synthetic fibers reduces wear rate and increases frictional coefficient of friction materials up to 0.3 [41]. The Aramid fiber also improves tribological and mechanical properties of friction material. Its combination with acrylic fibers gives highest performance [42]. Pine needle fibers can be used as reinforcement material due to its stable frictional coefficient at different operating condition and variable wear rate with temperature [43]. Kevlar is also naturally available fiber exhibits same independent properties like glass fiber with frictional coefficient of 0.39. Hence it can be considered as reinforcement material [35]. Hemp is one of the stiffest and strongest natural fiber with good mechanical properties. This having short cropping cycle and can be easily available. The experimentation shown that sample with 5 wt% hemp fiber is effective to enhance Coefficient of friction, frictional stability, fade performance, wear resistance [20]. The Brown Coconut fibers are strong and high abrasive endurance. The Friction material reinforced using coconut fiber shown comparable properties with commercial brake pads. The Bamboo fiber reinforced composites with varying percentage of natural fiber shown higher coefficient of friction and lower wear rate compared with other composites [44] (Fig. 3).

Many researches shown that Carbon fiber with some Chemical treatment is used to improve the performance characteristics of friction material. It increases the overall strength of friction material with average coefficient of friction 0.4. Glass fibers are also heat resistant, strong mechanical, thermal and tribological properties [45]. The metallic fibers like Steel wool, Copper chips are used as reinforcement which shown considerable rise in frictional coefficient and wear resistance. But main disadvantage is that it increases density of material [9, 28, 30].

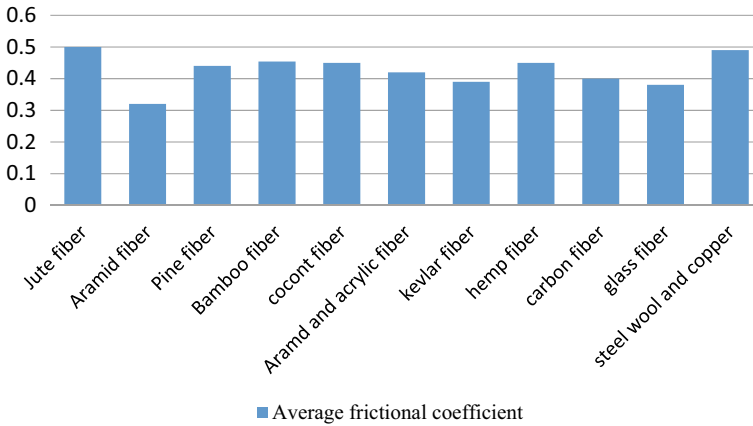


Fig. 3 frictional coefficient of reinforcement materials

2.3 Binders

Binder ensures physical integrity of the friction material. It may be in solid or viscous form. Thermosetting resins are most suitable and economical binders used as a matrix material. The capabilities of a binder to integrate the other constituents decide the overall strength of the FM [46]. Also, it has been observed that the addition of a binder enhances the frictional properties [46]. During operating conditions, it undergoes plastic deformation and creates the required frictional effect. It decides the matrix of the FM and improves its physical and chemical properties after modification. In NAO, the most commonly used binders are phenolic resin and epoxy resin. Apart from these, other binders include cashew nut shell liquid, modified resin (CR), melamine resin (MR), alkyl-modified phenolic resin, silicon-modified phenolic resin, acrylic 30%-modified phenolic resin, aromatic ring-modified phenolic resin, and straight phenolic resin [47] (Fig. 4).

2.4 Solid Lubricants

In friction material, different ingredients are combined together, which undergo internal surface friction. To manipulate this, solid lubricants are added to the base material to lubricate other constituents internally at the particle level [9, 47]. The review also states that material manufactured without a lubricant, but its performance gets degraded. Graphite is a common solid lubricant added up to 10% for the best performance in all aspects [48]. The addition of more lubricant deteriorates the internal bonding of constituents, resulting in a high wear rate. Graphite and hexagonal boron nitride also give the best frictional performance with a considerable wear rate. The addition of antimony tri-sulfide and zirconium silicate increases the frictional stability because of reduced internal friction [49, 50].

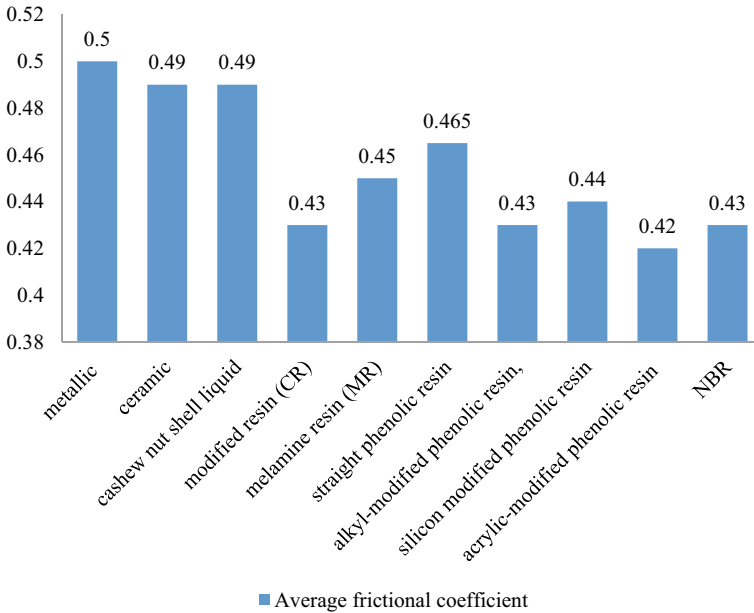


Fig. 4 frictional coefficient of binder materials

2.5 Friction Modifier

Additive stabilizes the temperature and reduces wear rate. Friction modifiers are in the form of small particles made of extremely hard material to provide the essential frictional effect. The strength of friction material increases with addition of modifier. These materials are used in low proportion due to poor compatibility with binding material. Also it helps in modifying frictional coefficient and maintaining structural integrity. The Graphite and Zirconium oxide are the most common additives used to maintain the operating coefficient of friction within feasible range [51].

3 Manufacturing of Frictional Material

As friction material is made up of different ingredients so bonding between them decides properties of composite. The proper bonding between all particles is ensured by using most suitable manufacturing process. The metal matrix-based friction material is manufactured casting and powder metallurgy route. During this proper mixing of the constituents must be ensured [52, 53]. In all manufacturing processes, the said ingredients are mixed together and blended. During mixing and blending, particle size of the fillers must be same and carefully controlled. It further decides properties

of final product. The Compression molding process is carried out at higher temperature to shape the friction material and pressure gradually increased to avoid pores [34, 42]. The naturally available materials cannot be directly applied to final application but it needs mechanical and chemical treatment to inculcate required properties [18–21]. Heat treatment can also be employed as per the requirement to refine the structure and to improve properties.

4 Types of Wear Observed

i. Outboard Pad Wear

The outboard pad side shows more wear rate as compared to inboard side. It is caused due to outer pad continuous movement of outboard pad on the rotor after the caliper release. This problem is found mainly due to Seizing guide pins, bushings and slides. Replacement of this component will remove this problem.

ii. Inboard Pad Wear

Inboard side has more wear rate compared to outboard side. It is because caliper piston does not returning to the rest position due to a worn seal, damage or corrosion. The problem of master cylinder is also responsible for this. To removes this wear, ensure working of the entire component from outboard wear problem along with the hydraulic brake system (Fig. 5).



Fig. 5 Brake pad wear

iii. Even Wear

In this type of wear, equal amounts of friction material provided on both sides of pad and spread uniformly over the surface of brake pad. It is indication of proper brake function.

iv. Tapered Pad Wear

It is caused due to improper pad installation and guide pin wear. Here material removal takes place in wedge pattern. This wear can be eliminated by checking the functioning of components like Seizing guide pins, bushings and slides.

v. Cracking, Glazing or Lifted Edges on the Pads

In this wear direct physical damage and thermal distresses to pads are observed. It is caused by over use, improper brake operation, improper functioning of hydraulic system, defective pads. Sometimes it is caused due to improper retraction of parking brake.

5 Conclusion

This review paper focused on various possible materials that can be used as friction material ingredient. The Asbestos brake pads can be replaced by best possible combination from the naturally available materials. The amount of filler and reinforcement material are a major contributor to properties of friction material. The naturally available material shows comparable properties without any harmful effects on human life and environment. From agriculture waste products also low cost easily available friction materials can be manufactured. Finer particle size increases strength of all types of friction materials. At last improper installation of brake pad and its components results in worn out brake pads. There is scope for finding out the direct relationship between mechanical and tribological properties as well as correlation between controlling parameters and wear rate is essential.

References

1. Lyu, Y., Leonardi, M., Wahlström, J., Gialanella, S., Olofsson, U.: Friction, wear and airborne particle emission from Cu-free brake materials. *Tribol. Int.* **141**, 105959 (2020). <https://doi.org/10.1016/j.triboint.2019.105959>
2. Liati, A., Schreiber, D., Lugovyy, D., Gramstat, S., Eggenschwiler, P.D.: Airborne particulate matter emissions from vehicle brakes in micro- and nano-scales: morphology and chemistry by electron microscopy. *Atmos. Environ.* **212**, 281–289 (2019). <https://doi.org/10.1016/j.atmosenv.2019.05.037>
3. Erdinc, M., Erdinc, E., Cok, G., Polatli, M.: Respiratory impairment due to asbestos exposure in brake-lining workers. *Environ. Res.* **91**, 151–156 (2003)

4. Dhir, B., Sharmila, P., Saradhi, P.P., Sharma, S., Kumar, R., Mehta, D.: Heavy metal induced physiological alterations in *Salvinia natans*. *Ecotoxicol. Environ. Saf.* **74**(6), 1678–1684 (2011). <https://doi.org/10.1016/j.ecoenv.2011.05.009>
5. Boulanger, B., Nikolaidis, N.P.: Mobility and aquatic toxicity of copper in an urban watershed. *J. Am. Water Resour. Assoc.* **39**(2), 325–336 (2003). <https://doi.org/10.1111/j.1752-1688.2003.tb04387>
6. Cho, M., Kim, S., Kim, D., Jang, H.: Effects of ingredients on tribological characteristics of a brake lining: an experimental case study. *Wear* **258**, 1682–1687 (2005)
7. Scieszka, S.: Tribological phenomena in steel-composite brake material friction Pairs. *Wear* **64**, 361–378 (1980)
8. Filip, P., Weiss, Z., Rafaja, D.: On friction layer formation in polymer matrix composite materials for brake applications. *Wear* **252**, 189–198 (2002)
9. Kim, S., Cho, M., Cho, K., Jang, H.: Complementary effects of solid lubricants in the automotive brake lining. *Tribol. Int.* **40**, 15–20 (2007)
10. Honselaar, A.C.M., de Gee, A.W.J.: Dynamic thermoanalytical test method for qualifying brake lining materials. *Tribol. Int.* **18**(1), 21–27 (1985)
11. Berry, G., Newhouse, M.L.: Mortality of workers manufacturing friction materials using asbestos. *Br. J. Ind. Med.* **40**, 1–7 (1983)
12. Verma, P., Ciudin, R., Bonfanti, A., Aswath, P., Straffellini, G., Gialanella, S.: Role of the friction layer in the high-temperature pin-on-disc study of a brake material. *Wear* **346–347**, 56–65 (2016)
13. Zhuan, L., Peng, X., Xiang, X., Su-hua, Z.: Tribological characteristics of C/C-SiC braking composites under dry and wet conditions. *Trans. Nonferrous Mater. Soc. China* **18**, 1071–1075 (2008)
14. Mahale V, Bijwe J: Role of thermal conductivity in controlling the tribo-performance of non-asbestos organic brake-pads. *J. Compos. Mater.* p. 002199832092812 (2020). <https://doi.org/10.1177/0021998320928124>
15. Rashid, B., Leman, Z., Jawaid, M., Ishak, M.R. and Al-Oqla, F.M.: Eco-friendly composites for brake pads from agro waste: a review. *Ref. Module Mater. Sci. Mater. Eng.* (2017). 10.1016/b978-0-12-803581-8.10159-6
16. Leonardia, M., Menapacea, C., Matějka, V., Gialanellaa, S., Straffelinia, G.: Pin-on-disc investigation on copper-free friction materials dry sliding against cast iron. *Tribol. Int.* **10**, 21–37 (2017)
17. Hee, K., Filip, P.: Performance of ceramic enhanced phenolic matrix brake lining materials for automotive brake linings. *Wear* **259**, 1088–1096 (2005)
18. Pujari, S., Srikanth, S.: Experimental investigations on wear properties of Palm kernel reinforced composites for brake pad applications. *Defence Technol.* **15**(3), 295–299 (2019). <https://doi.org/10.1016/j.dt.2018.11.006>
19. Sutikno, Pramujati, B., Safitri, S.D., Razitania, A.: Characteristics of natural fiber reinforced composite for brake pads material (2018). <https://doi.org/10.1063/1.5046282>
20. Kumar, N., Singh, T., Grewal, J.S., Patnaik, A., Fekete, G.: Experimental investigation on the physical, mechanical and tribological properties of hemp fiber-based non-asbestos organic brake friction composites. *Mater. Res. Express* **6**(8), 085710 (2019). <https://doi.org/10.1088/2053-1591/ab2399>
21. Madeswaran, A., Natarajasundaram, B., Ramamoorthy, B.: Reformation of eco-friendly automotive brake pad by using natural fibre composites. *SAE Tech. Paper Ser.* (2016). <https://doi.org/10.4271/2016-28-0164>
22. Balaji, S., Kalaichelvan, K.: Optimization of a semi-metallic disc brake pad formulation with respect to friction and wear. *Procedia Eng.* **38**, 1650–1657 (2012)
23. Bijwe, J., Kumar, M., Gurunath, P.V., Desplanques, Y., Degallaix, G.: Optimization of brass contents for best combination of tribo-performance and thermal conductivity of non-asbestos organic (NAO) friction composites. *Wear* **265**, 699–712 (2008)
24. Yawas, D.S., Aku, S.Y., Amaren, S.G.: Morphology and properties of periwinkle shell asbestos-free brake pad. *J. King Saud Univ. Eng. Sci.* **28**, 103–109 (2016)

25. Aigbodion, V.S., Akadike, U., Hassan, S.B., Asuke, F., Agunsoye, J.O.: Development of asbestos-free brake pad using bagasse. *Tribol. Ind.* **32**, 12–18 (2010)
26. Ficici, F., Durat, M., Kapsiz, M.: Optimization of tribological parameters for a brake pad using Taguchi design method. *J. Brazillian Soc. Mech. Sci. Eng.* **36**, 653–659 (2014)
27. Ho, S.C., Lin, J.H.C., Ju, C.P.: Effect of carbonization on mechanical and tribological behaviour of a copper-phenolic-based friction material. *Carbon* **43**, 491–502 (2005)
28. Menapace, C., Leonardi, M., Perricone, G., Bortolotti, M., Straffelini, G., Gialanella, S.: Pin-on-disc study of brake friction materials with ball-milled nanostructured components. *Mater. Des.* **115**, 287–298 (2017)
29. Straffelini, G., Ciudin, R., Ciotti, A., Gialanella, S.: Present knowledge and perspectives on the role of copper in brake materials and related environmental issues: a critical assessment. *Environ. Pollut.* **207**, 211–219 (2015)
30. Vijay, R., Janesh, M., Saibalaji, M.A., Thiyagarajan, V.: Optimization of tribological properties of nonasbestos brake pad material by using steel wool. *Adv. Tribol.* **15**, 1–9 (2013)
31. Osterle, W., Dmitriev, A.: The role of solid lubricants for brake friction materials. *Lubricant* **4**, 1–22 (2016)
32. Boz, M., Kurt, A.: Effect of ZrSiO₄ on the friction performance of automotive brake friction materials. *J. Mater. Sci. Technol.* **23**, 843–850 (2007)
33. Ozturk, B., Mutlu, T.: Effects of zinc borate and fly ash on the mechanical and tribological characteristics of brake friction materials. *Tribol. Trans.* **59**, 622–631 (2016)
34. Ma, Y., Liu, Y., Shang, W., Gao, Z., Wang, H., Guoab, L., Tong, J.: Tribological and mechanical properties of pine needle fiber reinforced friction composites under dry sliding conditions. *R. Soc. Chem. Adv.* **4**, 36777–36783 (2014)
35. Gopal, P.; Dharani, L.R.; Frank, D. Blum. Hybrid phenolic friction composites containing Kevlar pulp Part II-wear surface characteristics. *Wear*, 193 (1996) 180–185
36. Arrangnathan, N., Bijwe, J.: Fiber-surface quality enhancement to improve the performance properties of friction materials. *J. Tribol.* **139**, 1–9 (2017)
37. Xie, F., Hu, W., Ning, D., Zhuo, L., Deng, J., Lu, Z.: ZnO nanowires decoration on carbon fiber via hydrothermal synthesis for paper-based friction materials with improved friction and wear properties. *Ceram. Int.* **11**, 215–224 (2017)
38. Satapathy, B., Bijwe, J.: Composite friction materials based on organic fibres: sensitivity of friction and wear to operating variables. *Compos. Part A* **37**, 1557–1567 (2006)
39. Matejka, V., Fu, Z., Kukutschova, J., Qi, S., Jiang, S., Zhang, X., Yun, R., Vaculik, M., Heliouva, M., Lu, Y.: Jute fibers and powderized hazelnut shells as natural fillers in nonasbestos organic non-metallic friction composites. *Mater. Des.* **51**, 847–853 (2013)
40. Qi, S., Fu, Z., Yun, R., Jiang, S., Zheng, X., Lu, Y., Matejka, V., Kukutschova, J., Peknikova, V., Prikasky, M.: Effects of walnut shells on friction and wear performance of eco-friendly brake friction composites. *J. Eng. Tribol.* **228**, 511–520 (2014)
41. Kato, T., Magario, A.: The wear of aramid fiber reinforced brake pads: the role of aramid fibers. *Tribol. Trans.* **37**, 559–565 (1994)
42. Park, J., Chung, J., Kim, H.: Friction characteristics of brake pads with aramid fiber and acrylic fiber. *Ind. Lubr. Tribol.* **62**, 91–98 (2010)
43. Aranganathan, N., Bijwe, J.: Development of copper-free eco-friendly brake-friction material using novel ingredients. *Wear* **352**, 1–25 (2016)
44. Ma, Y., Shen, S., Tong, J., Ye, W., Yang, Y., Zhou, J.: Effects of bamboo fibers on friction performance of friction materials. *J. Thermoplast. Compos. Mater.* **26**(6), 845–859 (2012). <https://doi.org/10.1177/0892705712461513>
45. Österlea, W., Dörfel, I., Prielzel, C., Roocha, H., Cristol-Bulthé, A.-L., Degallaix, G., Desplanques, Y.: A comprehensive microscopic study of third body formation at the interface between a brake pad and brake disc during the final stage of a pin-on-disc test. *Wear* **267**, 781–788 (2009)
46. Shin, M.W., Cho, K.H., Lee, W.K., Jang, H.: Tribological characteristics of binder resins for brake friction materials at elevated temperatures. *Tribol. Lett.* **38**, 161–168 (2010)

47. Joo, B.S., Chang, Y.H., Seo, H.J., Jang, H.: Effects of binder resin on tribological properties and particle emission of brake linings. *Wear* **15**(434), 202995 (2019)
48. Ozturk, B., Ozturk, S.: Effects of resin type and fibre length on the mechanical and tribological properties of brake friction materials. *Tribol. Lett.* **42**, 339–350 (2011)
49. Jang, H., Kim, S.: The effects of antimony trisulfide Sb₂S₃ and zirconium silicate ZrSiO₄ in the automotive brake friction material on friction characteristics. *Wear* **239**, 229–236 (2000)
50. Aranganathan, N., Bijwe, J.: Special grade of graphite in NAO friction materials for possible replacement of copper. *Wear* 1–9 (2014)
51. Jadhav, S., Sawant, S.: A review paper: Development of novel friction material for vehicle brake pad application to minimize environmental and health issues. *Mater. Today Proc.* **19**, 209–212 (2019). <https://doi.org/10.1016/j.matpr.2019.06.703>
52. Guan, Q.F., Li, G.Y., Wang, H.Y., An, J.: Friction-wear characteristics of carbon fiber reinforced friction material. *J. Mater. Sci.* **39**, 641–643 (2004)
53. Qin, Q.D., Zhao, Y.G., Zhou, W.: Dry sliding wear behavior of Mg₂Si/Al composites against automobile friction material. *Wear* **264**, 654–661 (2008)

Investigation of Solid Particle Erosion Wear Behavior of Activated Carbon Polymer Composites



M. Sivaji Ganesh, G. Raghavendra, S. Ojha, and M. Om Prakash

Abstract The aim of these present research is to study surface topography and tribological properties of activated carbon epoxy composite for that SEM analysis was carried out for derived activated carbon and Bael shell powder then Erosion wear behavior of activated carbon epoxy composite have been investigated for that composite has been fabricated with derived activated carbon from Bael shell with hand layup technique with three different filler contents of 2, 4 and 6 wt%. To study the effect of filler content and erosion behavior of the prepared composites they are tested at different impingement angles of 30°, 45°, 60° and 90° and at three different velocities of erodent particles ($v = 86, 101$ and 119 m/s). Composites showed semi ductile nature with maximum wear resistance at 4 wt% filler.

Keywords Natural composites · Activated carbon · Erosion · Bael shell

1 Introduction

In the globalized world everyone is thinking for better material which is less or not harmful to the environment and high sustainability of material in many applications like aerospace research [1], military, automobile industries and power-producing equipment's like turbine blades [2, 3] it makes look for new material, this is achieved by the composites which are made by natural and biodegradable materials. From the past decade use of biodegradable [4] and eco-friendly material growing day by day so many natural materials like jute, coconut coir, arhar fiber, etc., are using for making natural fiber polymer composite So the natural fibers provide one way of reduced use of non-renewable energy resource in the place fibers like glass and also

M. Sivaji Ganesh · G. Raghavendra (✉)

Department of Mechanical Engineering, NIT Warangal, Warangal, Telangana 506004, India

e-mail: raghavendra.gujjala@nitw.ac.in

S. Ojha · M. Om Prakash

Department of Mechanical Engineering, Kakatiya Institute of Technology and Sciences, Warangal, Telangana 506004, India

reduces CO₂ emission. Hence glass fiber which causes health issues widely used in automobiles aerospace can be replaced by natural fibers these natural fibers are biodegradable and recyclable. The utilization of natural fiber as filler of plastics is quickly expanding; as it altogether not only improves mechanical properties but also brings down the price of composites fundamentally. Utilization of natural fiber does not have negative impact on environment and also Material cost is low and also with better properties. Composites made by appropriate selection of reinforcing material and matrix can have better or comparable strength and stiffness than available conventional metallic materials. In the current scenario natural composites have the potential not exclusively to decrease CO₂ discharge yet in addition saves non-renewable resources the particular favorable properties of common fiber are low weight, low value, and better absorption [5] and good wear resistance properties. The composite materials which are made by using polymer matrix are appropriate for non-lubricated condition so this is one of the main reason for consideration of polymer composites in applications of tribology [6].

Activated carbon can be derived generally from coal and petroleum-based products [7] which are non-renewable resources. So most of the researchers have shifted their focus to derive activated carbon from natural wastes like arhar stalks [8], coconut shells [9], rice husk [10], and so on.

Abdul Khalil [11] derived activated carbon from naturally available materials like oil, palm fruit, and bamboo stem at a carbonization temperature of 700 °C and utilized in epoxy composites as filler element. The exploratory outcome indicated that activated carbon filled epoxy composite exhibited good flexural properties over the neat epoxy.

Imoisil et al. [12] found that with increasing filler content which is activated carbon, mechanical properties of the activated carbon composite like abrasion resistance, tensile, and flexure strength increases with increasing filler content of activated carbon.

Raju [5] investigated ground nutshell particulate-based composite by distributing ground nut particles randomly in epoxy resin. The particles are modified chemically and are variable sizes and found that that moisture absorption and mechanical properties are better for composite made with ground shell particles than neat epoxy composite.

Activated carbon derived from Bael shell are mainly utilized for the treatment of waste water[13] but there is very little research work was carried out by using activated carbon derived from Bael shell in fabricating composites. So in the present investigation tribological properties of composites prepared by using activated carbon from Bael shell is studied.

2 Materials and Methods

2.1 Raw Materials

For current investigation raw materials used are

1. Activate carbon
2. Epoxy LY556
3. Hardener HY951
4. Bael shell powder.

2.2 Composite Preparation

Initially activated carbon derived from the Bael shell by two-step pyrolysis method [14]. For that washed and completely dried Bael shells are taken and grinded into powder in ball mill after that the powder was heated in crucible at a rate of $5\text{ }^{\circ}\text{C min}^{-1}$ from room temperature 28 to $800\text{ }^{\circ}\text{C}$ and kept one hour at $800\text{ }^{\circ}\text{C}$ in argon inert gas atmosphere. Three different samples of 2, 4, and 6 wt% filler content composites are prepared from Derived activated carbon composites are prepared by taking activated carbon as matrix material and epoxy as resin. The technique used for fabricating composite is hand layup process. Epoxy and hardener are mixed by taking 10:1 ratio. Epoxy mixture and filler are mixed homogenously, then the mixture is poured in $180 \times 120 \times 6\text{ mm}^3$ mould by placing a polythene release sheet kept at floor of the mould for easy removal. After that the prepared composites are cured for 48 h in room temperature after curing the samples are cut according to specific dimensions as per ASTM standards.

2.3 Scanning Electron Microscope

One of the most important physical characteristics of materials is surface morphology. Which can be studied by scanning electron microscope. In SEM image of a sample is produced by using high energetic beam of light. The sample was loaded into a circular disc and on the disc this sample is attached with the help of a particular tape. Before placing the sample in the electron chamber of microscope a platinum coating was applied on sample and also sintered. An electron beam was bombarded on the sample surface which collected surface topography in the form of backscattered electrons from which two-dimensional surface image at different magnifications can be viewed.

2.4 Erosion Test

Erosion is a type of wear which results material loss due to small solid particles repeated impact. For the current investigation the erosion test apparatus used is based on the standard of ASTM G76. Test rig of erosion schematic diagram is shown in Fig. 1 [15]. Specimens which are used for testing are cut into dimension $25 \times 25 \times 6 \text{ mm}^3$ from the prepared composite slabs the test rig consists of a feeder for particle feeding, an air compressor, an air and particle mixture unit, and a chamber for accelerating these mixtures. The dry air which was compressed is mixed with particles which are used as erodent are fed at a uniform rate by using belt-type of conveyor and feeding into the mixing chamber and after that mixture is accelerated by sending into converging nozzle which is made up of tungsten carbide of dia around 6 mm. Then the accelerated particles impact specimen which can be held at different positions with respect to particles which are impinging with the help of adjustable sample holder. For measuring velocity of the erodent particles a rotating double disc is attached with test apparatus by this set up velocity of impacting particles are measure by standard double-disc method [16].

The samples used for testing are properly cleaned in acetone, dried, and weighed after each and every test to an accuracy of 0.001 g with the help of electronic balance. Erosion test conducted under experimental conditions as shown in Table 1.

The rate of erosion (E_r) is then calculated by

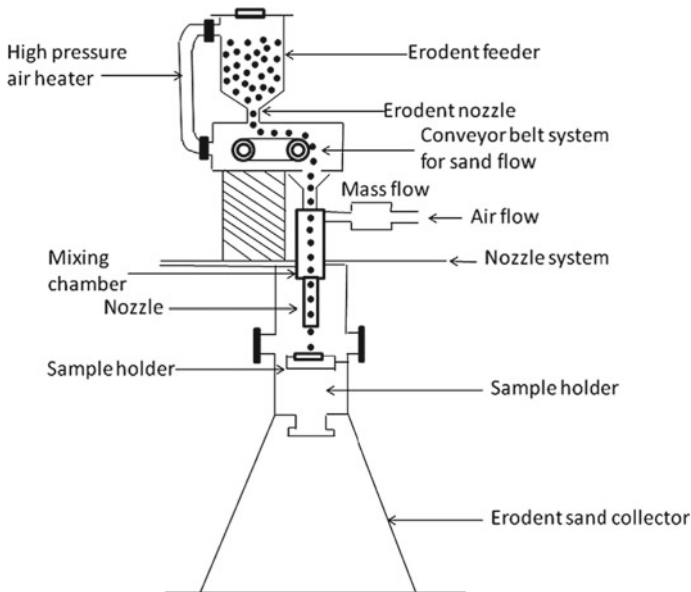


Fig. 1 Erosion test rig schematic diagram

Table 1 Conditions for the erosion test at which experimentation carried

Erodent	Silica sand
Size of erodent (μm)	200 ± 50
Shape of erodent	Angular
Feed rate of erodent (gm/min)	1.467 ± 0.02
Testing temperature	Room temperature
Distance between nozzle and sample (mm)	10
Impact velocity (m/s)	86,101,119
Angle of impingement (α°)	$30^\circ, 45^\circ, 60^\circ, 90^\circ$
Silica sand hardness (HV)	1400 ± 70

$$Er = \frac{\Delta w}{we} \quad (14)$$

Δw = Test sample weight loss(grams)

we = mass of the erodent particles (i.e., testing time \times feed rate of erodent).

3 Result and Discussion

The surface topography of Bael shell powder and activated carbon was investigated by using scanning electronic microscope analysis. Figure 2 shows Bael shell powder

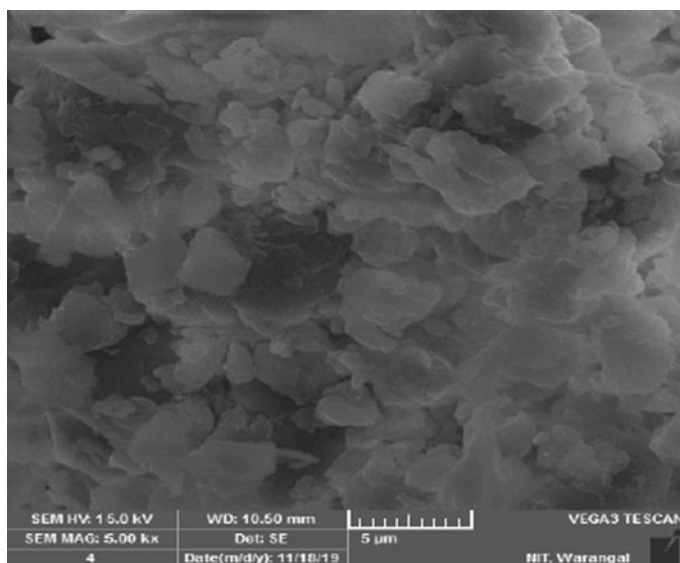


Fig. 2 SEM image of Bael shell powder

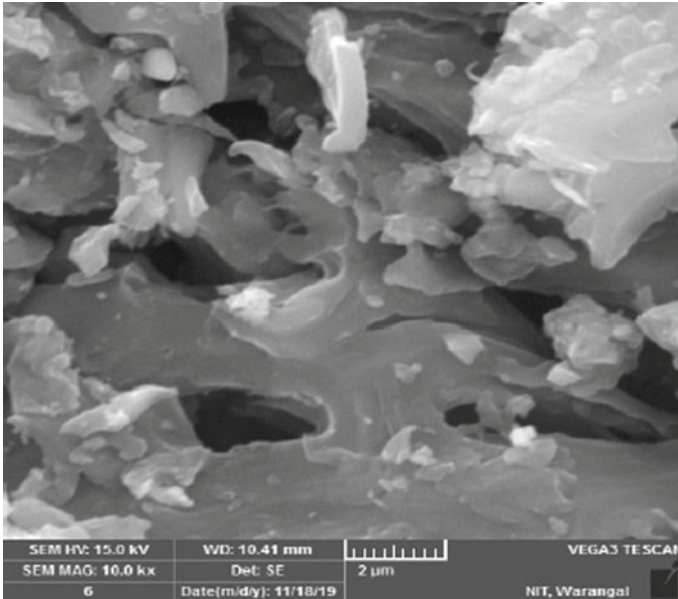


Fig. 3 SEM image of activated carbon

surface structure at $5\ \mu\text{m}$ scale. From that it can be clearly found that on the surface there was no porous structure formation. SEM image of activated carbon at $5\ \mu\text{m}$ was shown in Fig. 3. Activated carbon was derived from Bael shell at $800\ ^\circ\text{C}$ by two-step pyrolysis method from both the figures it can be observed that activated carbon surface have high porosity and void content. This is due to the Bael shell powder undergone process of pyrolysis. In the pyrolysis process powder surface was broken and volatile material gets exhausted because of activating agent penetrates into material and dehydrates [17] which leads to high porous surface. Regmi [18] also noticed similar kind of changes while preparing activated carbon.

Erosion wear behavior of prepared composite with different filler content like 2, 4, and 6 wt% at different impact velocities and also at different impingement angles are studied. Figure 4 shows the Erosion wear behavior of prepared composite at $86\ \text{m/s}$ impact velocity with different filler contents. From Fig. 4 it was observed that erosion rate decreases with increasing filler content up to 4wt% and further increase in filler content from 4 wt% leads to increase in erosion rate due to material of carbon filler wasn't hold properly by matrix phase and cause agglomeration. So bonding between epoxy and activated carbon becomes weak. So by exposing the composite to erodent particles which are impacting at high velocity causes detachment of carbon fillers which are bonded weakly. So 4 wt% is the optimum filler content used to fabricate composites to get better wear resistances.

Among the three composites of 2, 4, and 6 wt% filler contents the composite with 4 wt% filler content shows minimum erosion wear. Figures 5 and 6 show the erosion

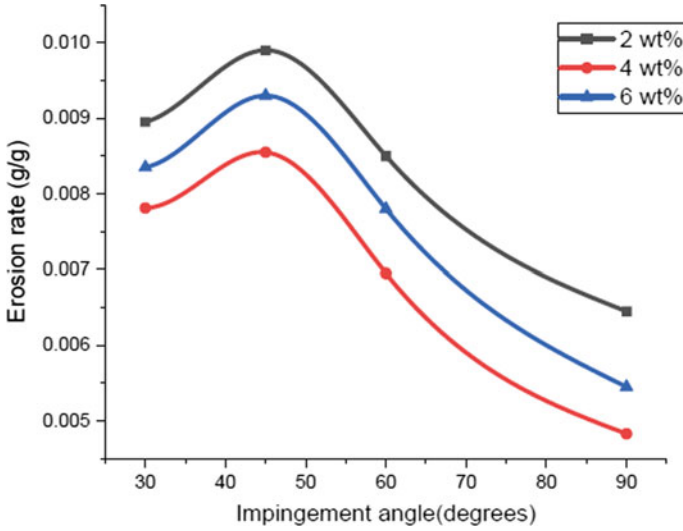


Fig. 4 Erosion wear behavior of activated carbon epoxy composite at an impact velocity 86 m/s with different filler contents

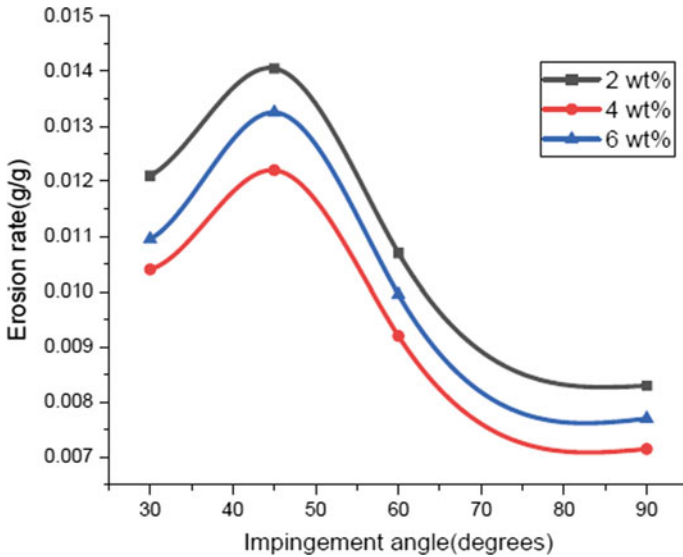


Fig. 5 Erosion wear behavior of activated carbon epoxy composite at an impact velocity 101 m/s with different filler contents

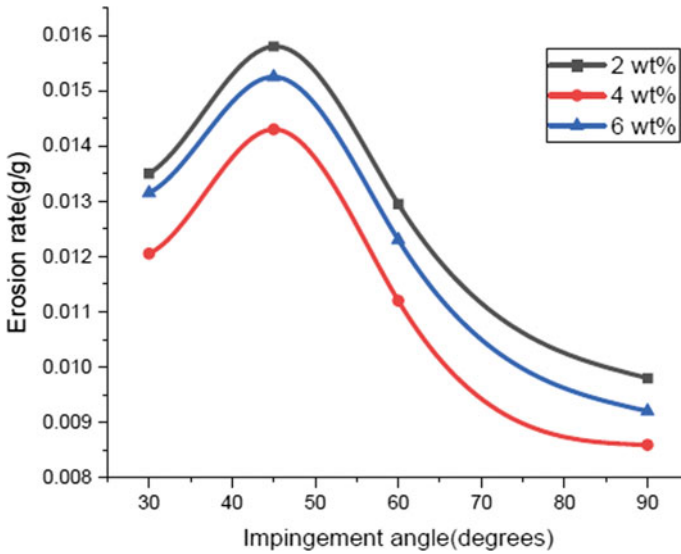


Fig. 6 Erosion wear behavior of activated carbon epoxy composite at an impact velocity 119 m/s with different filler contents

wear behavior of activated carbon epoxy composites with different filler percentages at 101 m/s impact velocity and 119 m/s impact velocity respectively which shows the similar erosion behavior as erosion behavior at impact velocity 86 m/s and also observed that erosion rate was increased with the increases of impact velocity because of increase in impact velocity erodent particle kinetic energy increases so these erodent particles strike the surface of composite with high energy leads to high loss of material. The erosion rate further increases with the increase of impact velocity to 119 m/s which can be observed from Fig. 6.

Angle of impingement has a major influence on the rate of Erosion and it is nothing but angle between the erodent particle trajectory and composite surface. When erosion rate is maximum in between 15 and 30° the composite exhibits ductile nature [19], if in between 40° and 50° exhibits semi ductile nature [20] and if at 90° [21] it exhibits brittle nature. From Figs. 4, 5 and 6 Erosion rate is maximum in between 40° and 50° angle of impingement irrespective of filler content so composite behaves as a semi ductile material. So independent of filler content all fabricated composites behave as a semi ductile material.

4 Conclusions

1. Activated carbon derived From Bael shell has high surface porosity and void content compared to Bael shell powder.

2. Activated carbon epoxy composite has maximum erosion rate in between 40° and 50° impingement angle independent of filler content under different experimental conditions which indicates the composites behaves as semi ductile material.
3. Activated carbon epoxy composite exhibits better erosion resistance better tribological properties at 4 wt% filler content among all activate carbon epoxy composites so 4 wt% filler content will be the optimum amount filler to be added.
4. In this investigation composites are prepared by hand layup technique by using other sophisticated techniques composites can be prepared so it may have better properties compared to currently fabricated composites.

References

1. Takashi, I., et al.: Aircraft wing, aircraft wing composite material, and method of manufacture. *Int. J. Innov. Eng. Technol.* **5**(1), 147–182 (2006)
2. Brøndsted, P., et al.: Composite materials for wind power turbine blades. *Annu. Rev. Mater. Res.* **35**, 505–538 (2005)
3. Vipin, V.: Analysis of turbine blade made of composite materials used in steam turbines. *Int. J. Innov. Eng. Technol.* **5**(4), 167–179 (2015)
4. Reddy, N., Yang, Y.: Bio fibres from agricultural by products for industrial applications. *Trends Biotechnol.* **23**(11), 22–27 (2005)
5. Raju, G.U., Kumarappa, S.: Experimental study on mechanical properties of groundnut shell particle-reinforced epoxy composites. *J. Reinf. Plast. Compos.* **30**(12), 1029–1037 (2011)
6. Hutchings, I.M.: *Tribology: Friction and Wear of Engineering Materials* (1992)
7. Tan, X.F., Liu, S.B., Liu, Y.G., Gu, Y.L., Zeng, G.M., Hu, X.J., Wang, X., Liu, S.H., Jiang, L.H., *Bioresour. Technol.* **227**, 359–372 (2017)
8. Om Prakash, M., Raghavendra, G., Ojha, S., Panchal, M.: Characterization of porous activated carbon prepared from arhar stalks by single step chemical activation method. *Mater. Today Proc.* (2020)
9. Shaheed, R., Azhari, C.H., Ahsan, A., Mohtar, W.H.M.W.: Production and characterisation of low-tech activated carbon from coconut shell. *J. Hydrol. Environ. Res.* **3**(1), 6–14 (2015)
10. Alvarez, J., Lopez, G., Amutio, M., Bilbao, J., Olazar, M.: Upgrading the rice husk char obtained by flash pyrolysis for the production of amorphous silica and high quality activated carbon. *Bioresour. Technol.* **170**, 132–137 (2014)
11. Khalil, H.A., Firoozian, P., Bakare, I.O., Akil, H.M., Noor, A.M.: Exploring biomass based carbon black as filler in epoxy composites: flexural and thermal properties. *Mater. Des.* **31**(7), 3419–3425 (2010)
12. Imoisili, P.E., Ukoba, K.O., Adejuge, I.T., Adgidzi, D., Olusunle, S.O.O.: Mechanical properties of rice husk/carbon black hybrid natural rubber composite. *Chem. Mater. Res.* **3**(8), 12–16 (2013)
13. Anusha, G.: The removal of iron from wastewater using wood apple shell as adsorbent. In: *Second international conference on environmental science and technology IPCBEE* (Vol. 6) (2011)
14. Bouchelta, C., Medjram, M.S., Bertrand, O., Bellat, J.P.: Preparation and characterization of activated carbon from date stones by physical activation with team. *J. Anal. Appl. Pyrol.* **82**(1), 70–77 (2008)
15. Latha, P.S. et al.: Evaluation of mechanical and tribological properties of bamboo– glass hybrid fiber reinforced polymer composite. *J. Ind. Text:* 1528083715569376 (2015)

16. Ruff, A.W., Ives, L.K.: Measurement of solid particle velocity in erosive wear. *Wear* **35**(1), 195–199 (1975)
17. Hesas, R.H., Daud, W.M.A.W., Sahu, J.N., Arami-Niya, A.: *J. Anal. Appl. Pyrol.* **100**, 1–11 (2013)
18. Regmi, P., Moscoso, J.L.G., Kumar, S., Cao, X., Mao, J., Schafran, G.: *J. Environ. Manage.* **109**, 61–69 (2012)
19. Bagci, M., Imrek, H.: Solid particle erosion behaviour of glass fibre reinforced boric acid filled epoxy resin composites. *Tribol. Int.* **44**(2011), 1704–1710 (2011)
20. Pei, Xianqiang, Friedrich, Klaus: Erosive wear properties of unidirectional carbon fiber reinforced PEEK composites. *Tribol. Int.* **55**, 135–140 (2012)
21. Rattan, R., Bijwe, J.: Influence of impingement angle on solid particle erosion of carbon fabric reinforced polyetherimide composite. *Wear* **262**, 568–574 (2006)

Computer-Aided Ergonomic Analysis for Rubber Tapping Workers



Abi Varghese  and Vinay V. Panicker 

Abstract The work-related musculoskeletal disorders (MSDs) among the rubber tapping workers are high due to awkward tapping postures and tapping at different gutter heights. In this context, a study has been carried out to conduct a posture analysis of rubber tappers using CATIA V5. For this work, three tapping heights or gutter heights of 500, 1000, and 1500 mm are considered, and the virtual environment is developed. The digital human models are created based on the anthropometric and strength data of Indian agricultural workers. The study shows that rubber workers tapping at the gutter height of 500 and 1500 mm having the maximum impact on the posture due to forward bending and stretching during tapping. The gutter height of 1000 mm between waist level and shoulder level shows the minimum impact. It is concluded that there is a correlation between the gutter height and the tapping postures among the rubber tappers.

Keywords Posture analysis · Rubber tapping · Musculoskeletal disorders · Rapid upper limb assessment (RULA)

1 Introduction

Rubber cultivation is one of the major income sources of the people in Asia. Asia produces 90% of the global natural rubber production [11]. Rubber tapping is the first and foremost step in natural rubber processing. In tapping, worker scores the bark in the downward spiral half of the trunk of the rubber tree as shown in Fig. 1, with the aid of a rubber tapping knife. In general, tapping starts on rubber trees at one meter

A. Varghese · V. V. Panicker (✉)

Department of Mechanical Engineering, National Institute of Technology Calicut,
Kozhikode, Kerala, India

e-mail: vinay@nitc.ac.in

A. Varghese

Department of Mechanical Engineering, Amal Jyothi College of Engineering,
Kottayam, Kerala, India

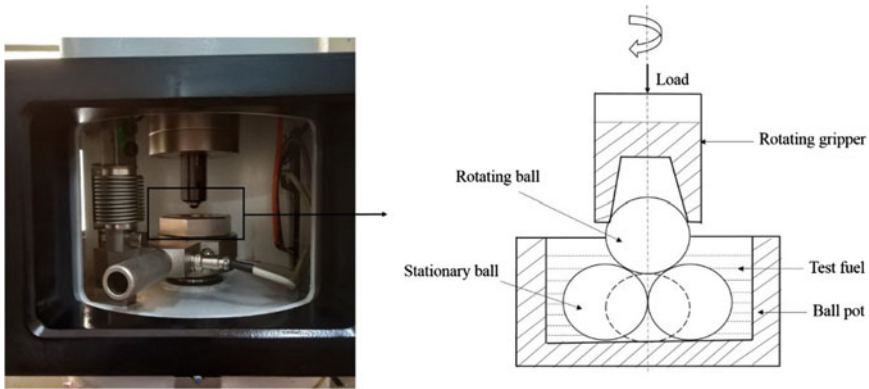


Fig. 1 Rubber tree and its tapping method

above the ground level, when the circumference of the tree trunk is about 50 cm in length. The lactiferous vessel situated between the cambium and the wood is used for collecting latex, incision of this vessel at an angle of 30° to the horizontal make the latex flow properly [3]. For tapping, two types of knife are generally used (i) Michie Golledge (ii) Jebong Knife [2]. Every worker has to tap 300–1000 rubber trees per day [1]. Due to the repetitive operation, postures like forward bending and lateral twisting, and manual workload during rubber tapping may cause musculoskeletal disorders among the rubber tappers.

The work-related musculoskeletal disorders (MSDs) among the farmworkers are very high due to heavy workload, repetitive movement during various agricultural operations, awkward posture, and the manual handling of load [4, 8]. A study conducted among the Thai rubber tapping workers reports that half of the workers (52%) have lower back pain followed by pain in legs (14.8%), upper arms (8.9%), neck (3.0%), wrists (2.3%), and lower arms (2.1%) due to awkward tapping posture and different tapping level [7]. Few researchers have found that the prevalence of low back pain among Thai rubber farmers was 55.7%, and the major factors identified as body mass index, education level and tapping level [13]. Another study was conducted among the Srilankan rubber tappers revealed that the 66% of the rubber tappers experience MSDs and the prevalence are varying in the shoulder (96.7%), back (94.4%), and neck (83.3%). The major factor associated with MSDs is a gender difference, cultural difference, age, supplementary job, and alternative hands during tapping [12]. An exploratory study was conducted among rubber tappers from Colombia reveals that tapping height, squatting, bending, and sporadic trunk rotation during tapping are the major reason for MSDs [14]. A study conducted using the Boston Carpal Tunnel Syndrome Questionnaire to evaluate Carpal Tunnel Syndrome (CTS) among Thai rubber tappers identified 133 CTS cases. The major reason was found to be the number of trees tapping per day, tapping height, hand postures during tapping and hand dominance [9]. In-line with the previous study, ergonomically designed rubber tapping knife (Jebong Knife) has been designed to

improve the wrist posture of CTS tapping workers. The result shows that there is a significant improvement in CTS symptoms and also compare the improvement with traditional knife users [10].

The review of the literature shows that most of the rubber tappers experience MSDs due to awkward tapping postures and tapping height. Therefore, it is essential to correlate the tapping height and its impact on tapping postures among the rubber tappers. In fact, this is the novelty of the present work. The objectives of this work are as follows:

- Identify the various tapping heights which are commonly used
- Apply Computer-aided Ergonomic Analysis to correlate the tapping height and its impact among the rubber tappers
- Explore the possible ergonomic intervention to improve the tapping posture.

2 Materials and Methods

2.1 Digital Human Modelling

The digital human models “Manikin” are inserted from the library in CATIA. The anthropometric data and strength data of Indian agricultural workers are adopted from [6] to design human models. As rubber tapping is predominantly seen in the state of Kerala, the anthropometric data of workers from the Southern region is applied. The various parameters considered in this work are gender, stature, weight, hip height, hip breadth, chest breadth, and waist breadth, for 95th percentile and 5th percentile population. The dimensions applied for digital human models are given in Table 1.

2.2 Work Environment Model

The rubber tapping working environment is created using CATIA V5 based on the following three types of tapping height or Gutter height, data collected during the field study.

- Tapping height below waist level (Gutter height—500 mm)
- Tapping height between waist level and shoulder level (Gutter height—1000 mm)
- Tapping height above shoulder level (Gutter height—1500 mm).

2.3 Body Posture Analysis

As an initial analysis, a posture analysis is conducted. Rapid upper limb analysis (RULA) [5] is one of the major tools to evaluate body posture analysis. It assesses

Table 1 Dimensions adopted for digital human modelling [6]

	Male					Female				
	Mean	Standard deviation	Range	5th Percentile	95th Percentile	Mean	Standard deviation	Range	5th Percentile	95th Percentile
Weight (kg)	56.1	9.7	34.0–94.0	40.2	72.1	47.2	8.3	30.0–79.0	33.5	60.9
Stature (mm)	1649	64	1490–1815	1522	1735	1508	60	1334–1676	1409	1606
Hip height (mm)	869	51	635–1030	785	954	842	42	734–939	773	911
Hip breadth (mm)	291	24	202–393	251	330	264	19	205–312	232	295
Chest breadth (mm)	278	26	191–380	234	321	241	21	204–352	206	275
Waist breadth (mm)	255	29	175–356	206	303	222	20	187–285	189	256

the muscle strain that occurs during each operation and provides the score from 1 to 7. A score value of 1 and 2, means the posture is acceptable. The score value of 3 and 4 indicates an alteration in posture. The value of 5 and 6 is poor posture and alterations are required at the earliest. Score 7 reveals a higher risk and an urgent alteration is needed.

3 Result and Discussion

3.1 Digital Human Modelling

The digital human model has been created based on the anthropometric data of the south Indian population using “Human Measurements Editor” and the proposed model is shown in Fig. 2a, b.

3.2 Work Environment Model

The working environment of rubber tapping workers has been developed in CATIA V5 using the sample dimension collected from the field and is shown in Fig. 3.

As a general practice, there are three sections in tapping with three levels of tapping height or gutter height. The initial tapping height is from 1 m from the ground level, and the score moves down nearly to the ground level. When the initial tapping area

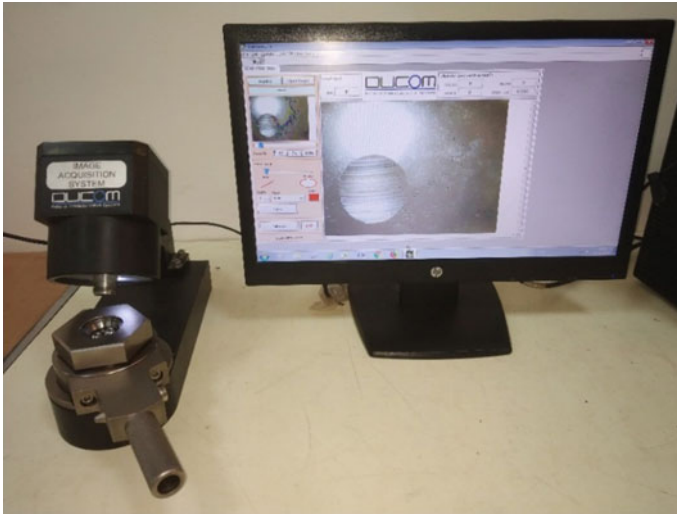
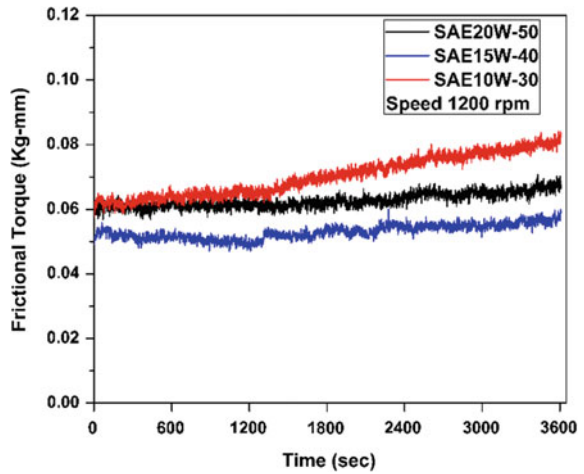


Fig. 2 a CATIA digital human model (Male), b CATIA digital human model (Female)

Fig. 3 Rubber tree and its tapping method (CATIA virtual model)



has been completed, the tapping height again starts from 1.5 m from the ground as the second section. Similarly, in the third section also consider the same procedure used as that of the second section. The three levels of gutter height are depicted in Fig. 4.

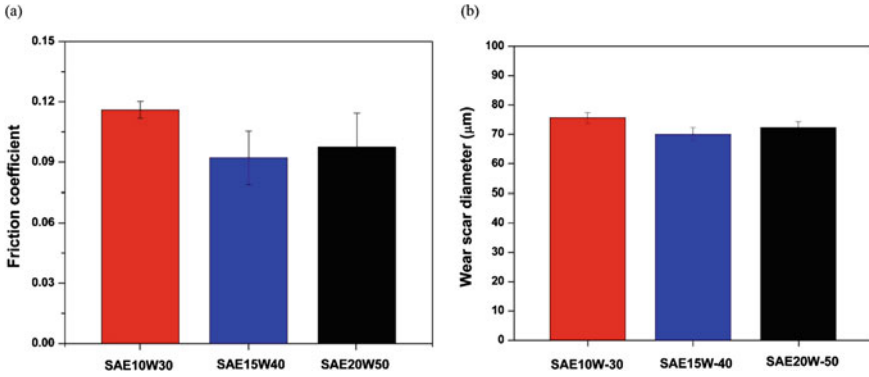


Fig. 4 Tapping height (CATIA model) **a** Below waist level, **b** between waist and shoulder level, **c** above shoulder level

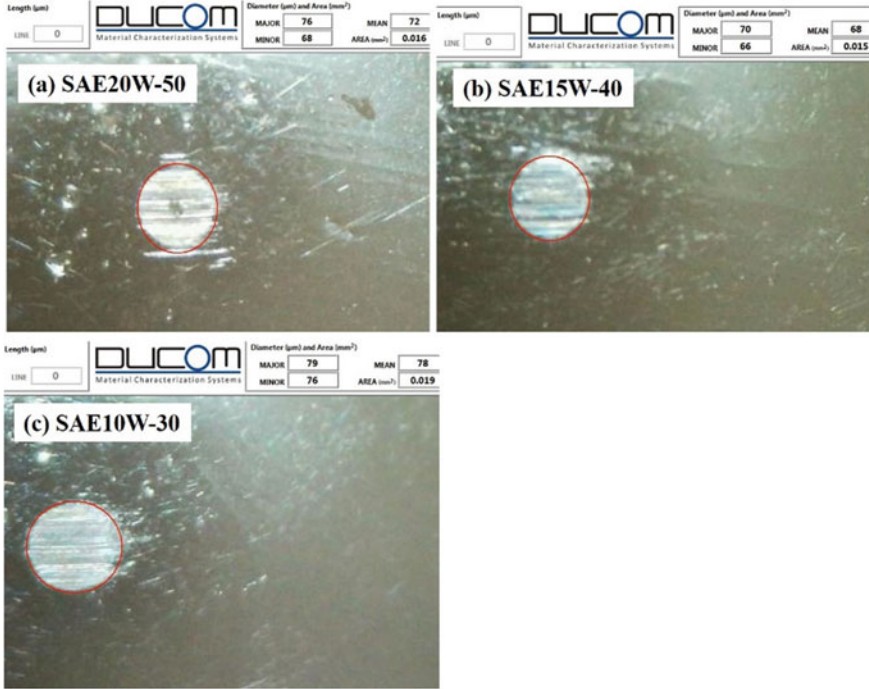


Fig. 5 RULA analysis for rubber tappers **a** Gutter height 500 mm (Female), **b** gutter height 1000 mm (Male), **c** gutter height 1500 mm (Male)

3.3 Body Posture Analysis

The RULA analysis of the male and female rubber tappers using CATIA v5 has been completed. Figure 5 shows the digital human models of rubber workers developed using CATIA.

Tables 2, 3, 4, 5 formulates the scores that are obtained from the various body parts associated with rubber tappers.

Table 2 RULA score for male rubber tappers at 95th percentile obtained from CATIA

	Male at 95th percentile					
	Gutter height (500 mm)		Gutter height (1000 mm)		Gutter height (1500 mm)	
	Left	Right	Left	Right	Left	Right
Upper arm	3	3	1	1	3	4
Fore arm	2	2	1	1	3	2
Wrist	4	3	3	4	3	4
Neck	1	1	2	2	1	1
Trunk	3	3	2	2	1	1
Leg	1	1	1	1	1	1
RULA score	6	5	3	3	4	4

Table 3 RULA score for female rubber tappers at 95th percentile obtained from CATIA

	Female at 95th percentile					
	Gutter height (500 mm)		Gutter height (1000 mm)		Gutter height (1500 mm)	
	Left	Right	Left	Right	Left	Right
Upper arm	2	3	2	2	5	5
Fore arm	2	2	2	2	3	3
Wrist	3	3	4	3	4	3
Neck	1	1	2	2	1	1
Trunk	4	4	1	1	1	1
Leg	1	1	1	1	1	1
RULA score	6	7	4	3	5	5

Table 4 RULA score for male rubber tappers at 5th percentile obtained from CATIA

	Male at 5th percentile					
	Gutter height (500 mm)		Gutter height (1000 mm)		Gutter height (1500 mm)	
	Left	Right	Left	Right	Left	Right
Upper arm	2	3	1	1	4	4
Fore arm	3	3	1	1	3	3
Wrist	3	3	3	3	3	4
Neck	1	1	2	2	1	2
Trunk	3	3	2	2	1	1
Leg	1	1	1	1	1	1
RULA score	5	5	3	3	4	5

Table 5 RULA score for female rubber tappers at 5th percentile obtained from CATIA

	Female at 5th percentile					
	Gutter height (500 mm)		Gutter height (1000 mm)		Gutter height (1500 mm)	
	Left	Right	Left	Right	Left	Right
Upper arm	2	3	2	2	5	5
Fore arm	2	2	2	2	3	3
Wrist	3	3	3	3	5	4
Neck	1	1	2	2	1	1
Trunk	3	3	1	1	1	2
Leg	1	1	1	1	1	1
RULA score	6	6	3	3	5	6

3.4 Statistical Analysis of RULA Score

Kruskal–Wallis Test is a non-parametric test used to determine the significant difference between the more than one dependent or independent variable. The summary of the Independent sample Kruskal–Wallis tests is tabulated in Table 6.

The statistical analysis reveals that the various body parts like the upper arm, forearm, neck, and trunk associated with rubber tapping operations, have a significant difference in terms of various gutter height. However, it is to be noted that the score for the wrist is found to be the same at various gutter heights.

Moreover, post hoc analyzes have been carried out and are tabulated in Table 7. The post hoc analyzes conclude that the posture with a gutter height of 1000 mm is found to have a minimum impact on the muscles due to the minimum body bending and trunk rotation.

Further, a frequency distribution of the RULA scores is done as depicted in Table 8.

Table 6 Summary of independent value of Kruskal–Wallis test

S. No.	Null Hypothesis	Significance value	Decision
1	The distribution of upper arm is the same across the gutter height	0.000	Reject the null hypothesis
2	The distribution of Fore arm is the same across the gutter height	0.080	Fail to reject the null hypothesis
3	The distribution of wrist is the same across the gutter height	0.000	Reject the null hypothesis
4	The distribution of neck is the same across the gutter height	0.000	Reject the null hypothesis
5	The distribution of Trunk is the same across the gutter height	0.000	Reject the null hypothesis
6	The distribution of RULA Score is the same across the gutter height	0.000	Reject the null hypothesis

Table 7 Post hoc analysis of RULA SCORE

Gutter height (mm)	Adjacent significance
500–1000	0.00
1000–1500	0.026
1500–500	0.337

Table 8 Frequency distribution of RULA SCORE

RULA score	Percent	Cumulative percent
4.00	16.7	45.8
5.00	29.2	75.0
6.00	20.8	95.8
7.00	4.2	100.0
Total	100.0	

The results show that about 54.2% of the RULA score is in the range between in 5 and 7, which indicates that the body posture is under risk, and appropriate alterations are needed to avoid MSDs.

4 Conclusion

The work-related musculoskeletal disorders among the rubber tapping workers are reported to be high due to the awkward tapping postures such as bending and twisting of the body during tapping and at different tapping or gutter height. The present study focuses on the computer-aided posture analysis of the rubber tapping workers

subjected to three tapping heights using RULA method. Digital human models are created using the anthropometric data of Indian agricultural workers in CATIA V5. Appropriate statistical analyses of the RULA scores have been carried out SPSS software. It is observed that the tapping or gutter height of 1000 mm have a minimum impact on postures. This may be due to the minimum body bending and trunk rotation. The scores for other body parts like the upper arm, forearm, neck, and trunk associated with rubber tapping operations have a significant difference in terms of various gutter height. The score for the wrist is found to be the same at various gutter heights. Though RULA can be used to identify risk for musculoskeletal disorders, the limitation of this method is that the duration of exposures has not been considered.

References

1. Boonphadh, P.: The perceived effects of work on health of rubber farmers in southern Thailand. Massey University, New Zealand (2008)
2. Centre for E-learning KAU Agriculture University. Plantation Crops-Rubber: KAU Agri-Infotech Portal. <http://www.celkau.in>
3. FAO Economic and Social Development Series. The Rubber Tree: Better Farming Series, ISBN 92-5-100156-1 (1977)
4. Kirkhorn, S.R., Earle-Richardson, G., Banks, R.J.: Ergonomic risks and musculoskeletal disorders in production agriculture: recommendations for effective research to practice. *J. Agromed.* **15**(3), 281–299 (2010)
5. Lynn, M., Corlett, E.N.: RULA: a survey method for the investigation of world-related upper limb disorders. *Appl. Ergon.* **24**(2), 91–99 (1993)
6. Majumder, J., Mehta, C.R., Khadatkar, A.: Anthropometric and strength data of Indian agricultural workers for farm equipment design. In: Gite, L.P. (Ed.). Central Institute of Agricultural Engineering, Bhopal, India (2009). ISBN 978-81-909305-0-5
7. Meksawi, S., Tangtrakulwanich, B., Chongsuvivatwong, V.: Musculoskeletal problems and ergonomic risk assessment in rubber tappers: A community-based study in southern Thailand. *Int. J. Ind. Ergon.* **42**(1), 129–135 (2012)
8. Momeni, Z., Choobineh, A., Razeghi, M., Ghaem, H., Azadian, F., Daneshmandi, H.: Work-related musculoskeletal symptoms among agricultural workers: a cross-sectional study in Iran. *J. Agromed.* 1–10 (2020)
9. Pramchoo, W., Geater, A.F., Tangtrakulwanich, B.: Physical ergonomic risk factors of carpal tunnel syndrome among rubber tappers. *Arch. Environ. Occup. Health* **75**(1), 1–9 (2020)
10. Pramchoo, W., Geater, A.F., Harris-Adamson, C., Tangtrakulwanich, B.: Ergonomic rubber tapping knife relieves symptoms of carpal tunnel syndrome among rubber tappers. *Int. J. Ind. Ergon.* **68**, 65–72 (2018)
11. Report of Association of Natural Rubber Producing Countries (ANRPC) (2017). www.anrpc.org
12. Stankevitz, K., Schoenfisch, A., de Silva, V., Tharindra, H., Stroo, M., Ostbye, T.: Prevalence and risk factors of musculoskeletal disorders among Sri Lankan rubber tappers. *Int. J. Occup. Environ. Health* **22**(2), 91–98 (2016)
13. Udom, C., Janwantanakul, P., Kanlayanaphotporn, R.: The prevalence of low back pain and its associated factors in Thai rubber farmers. *J. Occup. Health* **58**(6), 534–542 (2016)
14. Velásquez, S., Valderrama, S., Giraldo, D.: Ergonomic assessment of natural rubber processing in plantations and small enterprises. *Ingeniería y competitividad* **18**(2), 233–246 (2016)

User Interface/User Experience (UI/UX), Human Computer Interface (HCI)

Redesign and Assessment of Two Passenger Car Dashboard Warning Icons in India



Sourav Bhattacharya and Dhananjay Singh Bisht

Abstract Automobile instrument clusters these days are equipped with numerous warning icons for informing drivers on different critical automobile functions. In this context, abstract and complex icon designs can often be misinterpreted. Use of icons that do not reveal their functionality through their visual characteristics increases the risk of road accidents. Designers often follow relevant guidelines before designing usable warning icons. Two warning icons namely 'Brake Warning Light' (BWL) and 'Tire Pressure Monitoring System' (TPMS) were found to be the poorly usable icons in past research work by the authors and other researchers. The intent of this study is to design and evaluate usable alternative designs for these two icons in the Indian context. Standard available guidelines and Peirce's model of semiotics were adopted during this work. 50 participants volunteered in the first study to report their respective concerns with the two icons. Four alternatives each for the two icons were designed and in a second study, they were rated by 60 volunteers on the perceptual factor of 'semantic closeness'.

Keywords Automobile dashboard warning icons · Cognitive experience · User experience design · Design features · Semiotics

1 Introduction

These days, automobile warning icons are becoming increasingly complex due to the need to represent specialized automotive features. Warning icons are visual elements that guide the occupants/drivers about different operational statuses of an auto mobile. An increase in number of icons on dashboards could create more confusion among

S. Bhattacharya (✉) · D. S. Bisht
Department of Industrial Design, National Institute of Technology, Rourkela 769008, India
e-mail: souravzilla@gmail.com

D. S. Bisht
e-mail: bishtd@nitrrkl.ac.in

© The Author(s), under exclusive license to Springer Nature Singapore Pte Ltd. 2021
B. Deepak et al. (eds.), *Advanced Manufacturing Systems and Innovative Product Design*,
Lecture Notes in Mechanical Engineering,
https://doi.org/10.1007/978-981-15-9853-1_25

305

drivers in interpretation as it becomes difficult for them to remember all the functionalities associated with them and the multiple contexts of use. According to a survey conducted by British Schrader and TNS in 2014 it has been identified that 42% of drivers could not comprehend the ‘Tire Pressure Monitoring System’ (TPMS) icon due to its high degree of abstractness [1]. Survey results of Britannia Rescue (2013) also identified that 48% drivers miscomprehended the ‘Brake Warning Light’ (BWL) icon. These results indicate that most drivers failed to understand these two icons due to their poor visual characteristics [1]. It is obvious that representation of these warning icons should be clear and simple, appropriate to the true context of their usage for better interpretation. For the same, a designer should understand the basic elements that constitute an icon and how do the drivers comprehend it during driving situations.

1.1 Composition of an Icon

The study of signs and symbols is called semiotics [2]. Icons are small graphical representations used to symbolize an action, object or a concept. In cognitive research works which primarily focus on user interfaces and comprehension of signs, designers use semiotic engineering as a guidance/approach to design icons [3].

The basic elements which constitute an icon are border, background, text label, shape and colour [4]. *Borders* make an icon appear more uniform, rigid and logical. However, using borders limits the size of an image. *Background* helps in emphasizing and grouping of icons. Generally, colours applied on the background are cool and unsaturated such that the symbol can be easily recognized. *Text label* must be briefed within one or two words which increases the user’s understandability and comprehensibility for an arbitrary icon. *Shape* is probably the most important element to be considered while designing an icon—it gives distinct meaning to an icon. Correct designing of shape helps the user to distinguish within a given set of icons by reducing the time of comprehension and response. In the British Standards, warning or hazard icons are represented in triangular shape, regulatory icons in rectangular shape, prohibition icons in circular shape, etc. [5]. *Colour* plays a very important role in distinguishing the icons into their related subgroups which increases legibility and comprehension performance of users. Different factors like colour disparity, colour amalgamation and universal colours are used to design an icon which can have a significant influence on consciousness and usability of icons.

1.2 Conceptual Framework for Icon Comprehension

Developing a guideline for warning icon design needs a conceptual understanding of driver’s perception about the icons, their use and a sense of their performance in using such icons [6]. Literature on conceptual frameworks for icon comprehension

for in-vehicle information is limited [7]. One such procedure was described by [7] showing three stages of icon comprehension and its use. The *first stage* is the extraction which involves the relationship between driver, icon and surroundings and often depends on factors such as icon size, illumination, colour, stroke, width and disparity. The *second stage* is recognition which involves the relationship between the driver, icon and other visual display components depending upon the icon shape, background, level of detailing, orientation, temporal characteristics (flash rate, sequential illumination, blinking) and overlapping with other symbols or visual elements. The *third stage* is interpretation which involves a relationship between driver, icon and context/messages. It depends upon design issues like match between the icon and the context of use, cues to relative urgency, use of combined modality (e.g. auditory message is accompanied with visual alert). Therefore, an iconic message comprehension depends upon various basic factors including: semantic closeness, intricacy of message, different circumstances where the message is being used, drivers' presumptions, familiarity, driver's limitations and workload conditions. Among these factors, familiarity is found to be strongly resonating with comprehension [8].

1.3 Human Factor Guidelines for Designing Warning Icons

Various human factor design guidelines for driver-vehicle interfaces (DVI) were derived by Campbell et al. [7]. These guidelines are based on human factor concepts and as well as recent research findings documented by the US National Highway Traffic Safety Administration (NHTSA) [7]. Derived from these guidelines, design directions might be helpful to researchers, designers and automobile manufactures for designing warning icons in future considering driver limitations and capabilities.

1.4 Peirce Triangle

Numerous approaches were adopted by researchers in designing icons in the context of semiotics [2]. An important framework within this context is C. S. Peirce's triangle law of semiotics [9]. Peirce suggests that three elements namely Representamen (i.e. representation), Object (i.e. illustrated object, function or concept) and Interpretant (i.e. process of interpretation) interact with each other to form a semiotic system. For example, a tortoise (object) could be used as an icon (representamen), representing the concept of being 'slow' (interpretant). Therefore, it is not necessary that a straightforward correlation should exist between the object and representamen. At the same time, a user should be able to interpret 'a tortoise' and have a prior knowledge that tortoises are slow-moving creatures. So, its essential for a designer to understand the end users with regards to their culture, knowledge and frequency of handling an icon/sign because both designers and end users may have very different mental models [10]. Preferably speaking, the relation between the representamen and

object should be understandable to all/most users who would operate the interface [9]. Also, in terms of its implementation, an icon is said to be well-designed if it is legible [11], understandable [12], comprehensible [13] and meaningful [14].

1.5 Aim and Novelty

The aim of this study is to capture and analyze data regarding typical driver behaviours and their expectations with regards to use of warning icons for developing and testing two user-friendly warning icons. Research works in the past have focused on identification of hazardous warning lights through usability testing [1, 4] others have explored guidelines for designing warning icons [7]. This work however is novel in the sense that the authors have used factual and methodological inputs from these studies to develop their own user-centred semiotics-based icon design and evaluation process.

2 Methodology

Two existing standard automobile dashboard warning icons ‘Brake Warning Light’ (BWL) and ‘Tire Pressure Monitoring System’ (TPMS) have been found to be poorly interpreted in past research works [1]. The methodology in this paper focuses on design and assessment of these two icons.

2.1 Subjects

A total of 50 participants (31 males and 19 females), having a minimum one year driving experience, aged 22–55 years (Mean = 28.54, S.D. = 5.02) participated in the first study from West Bengal (India). Here, 20 participants (40%) were professional drivers, 12 (24%) were other jobholders, 10 (20%) were students from higher certificate programmes, and the remaining 8 (16%) were housewives.

In the second study, 60 participants (58 males and two females), aged between 22 and 58 years (Mean = 26.2, S.D. = 4.925) participated from across India. Among the 60 participants, 30 (50%) were students from higher certificate programme, 16 (26.67%) were professional drivers, 12 (20%) were professionals and the remaining 2 (3.33%) were teachers.

2.2 *Materials*

Adobe Illustrator (CS6) was used for redesigning the icons. It is a professional graphic design software which is mainly used for creating vector images of icons, logos, symbols, signs, etc. [15]. Free access Google Forms service was utilized for developing a questionnaire-based survey [16].

2.3 *Procedure*

In the first study all 50 participants were briefed about the functionalities and context of use of the two warning icons (BWL and TPMS) through an information sheet. User inputs from these 50 participants were collected regarding specific visual design features that might lead the users to misinterpret the two warning icons; also, design considerations were requested for making the icons more comprehensible.

Next, in the second study after designing four alternatives for each of the two icons, an online form was sent to other group of 60 participants for capturing participant's particulars within formation on name, age, gender and profession. Then, the participants had to rate each of the two icons on the extent of 'familiarity' with the help of a Likert scale (1 = very unfamiliar, 5 = very familiar). Thereafter, images of four alternatives for each icon were presented and the participants had to rate each alternative on the basis of the perceptual factor of 'semantic closeness' using a rating scale of 10 points (1 = very weakly related, 10 = very strongly related). Semantic closeness is defined as a measure of closeness of the relationship between what is depicted and the function it is intended to represent [8]. It was found to be the best predictor of comprehension scores among five visual design features namely 'familiarity', 'concreteness', 'semantic closeness', 'meaningfulness' and 'simplicity' [8].

All the participants were volunteers, and the study was designed in accordance with the ethical guidelines framed by the Institute Ethical Committee (NIT Rourkela).

3 *Results*

3.1 *Survey Results*

With regards to the visual evaluation of the icons, 92% participants pointed out that '!' sign in the BWL icon and the entire icon design of TPMS were problematic. The same group of participants also mentioned that replacement of '!' sign with specific visual design feature like—a 'stop sign' kind of hand gesture enclosed within a wheel or some kind of illustration like pulling the brake lever with left hand can be incorporated in the new designs for the BWL icon. In case of TPMS, 95% participants

mentioned that the icon could be replaced with a representation of a deflated tyre along with a metre gauge to represent air pressure measurement.

3.2 Warning Icon Design for Improving Driver’s Cognitive Experience

The design procedure was user-centric and based on scientific intuitions. Four alternatives icons each for BWL (BWL-1 to BWL-4) and TPMS (TPMS-1 to TPMS-4) were designed as shown in Fig. 1. Since the visual distance and visual angle were not specified, icons were designed by taking an approximate dimension but considering the requirements of standard aspect ratios. Boundaries/strokes were not provided so that the icon legibility is maintained. For achieving strong visual perception, a dark background colour was picked (Black) so that the light-coloured icons are well contrasted.

Brake Warning Light

Red colour (#FF0202) has been used here as it is the norm in representing Imminent Crash Warnings (ICWs).

In BWL-1, the ‘!’ sign enclosed within a circle is replaced by a ‘stop sign’ shaped hand which adds more immediate meaning to the icon signifying the instruction to ‘stop’ or to ‘apply brake’. The circle is symbolic of a wheel and the two arcs on represent brake pads. To improve comprehension, the word ‘BRAKE’ of typeface Segoe UI (bold/solid) has been provided at the bottom of this icon. This font style is clear and simple to understand with little excess features. Uppercase letters with equal horizontal spacing were used to increase the visibility and avoid a congested look. In BWL-2, the outer circle of the original icon remains, but the elements inside are changed—profile view of a hand pulling the brake lever is portrayed within. Equal

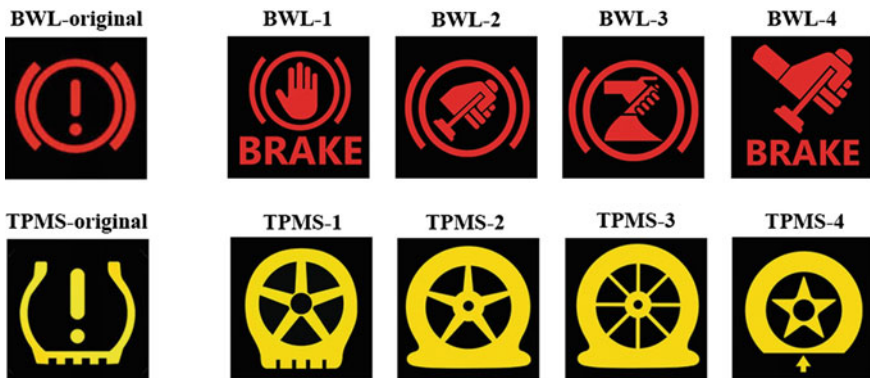


Fig. 1 Alternative design concepts for BWL and TPMS

spacing between fingers and brake lever was maintained to ensure legibility. The hand is positioned exactly in the centre of the circle at an angle of 45° with horizontal. In BWL-3, many design elements of icon remain same as in BWL-2. The difference here is that the hand pulling the brake lever was represented in a differentiation state of thumb release. Equal gaps were maintained between smaller elements to ensure legibility and distinctiveness. The internal information was centred inside the circle and placed in the middle, the arm at an angle of 90° with horizontal. Greater information of the base of the hand brake stick appears here. BWL-4 was designed by combining the visual elements of BWL-1 and BWL-2. The hand pulling the brake lever has been resized and enlarged for legibility than in BWL-2 keeping the same proportions among the internal elements. The typeface and font size of the word 'BRAKE' that was used in BWL-1 is same. The images have been resized into a larger form to increase conspicuity.

Tire Pressure Monitoring System

Flat yellow colour (#FCD800) was used as the norm to represent cautionary crash warnings (CCWs).

TPMS-1 has a resemblance with the original icon for easy interpretation by retaining its familiarity (see Fig. 1). In the icon the '!' sign enclosed within curves was changed to a clear side profile contour of a wheel consisting of five tapered, bold spokes, spaced radially at 72° angle. Here, the tyre contour is a little thinner as compared to other alternatives so as to see user's acceptance of this icon over other icons by changing different designing elements. TPMS-2 is in the shape of a side profile deflated tyre, indicating low air pressure to justify the context of icon. The wheel consists of five tapered, bold spokes spaced radially at 72° angle. Sharp corners were rounded at the junction between the inflated and deflated zones to emphasize gradual pressure release. Here a thicker tyre contour has been used than TPMS-1. TPMS-3 is very similar to TPMS-2 with the difference that the number of spokes increased from five to eight, each spaced radially at 45° angle. Thinner and straight spokes have been used in this case without any taperings to see the difference in responses and interpretation between TPMS-2 and TPMS-3. TPMS-4 is more abstract to test participant background knowledge and comprehensive skills. Here the tyre thickness is thicker as compared to other alternatives. Base of the wheel was designed flat with sharp edges. An arrow points towards this flat (upwards) emphasizing low air pressure causing the wheelbase to flatten. The alternating spokes design has been replaced in the middle with a star-shaped hub with rounded and smooth corners of the wheel.

3.3 Comprehension Score Results

To determine the best alternative for each of the two icons, a final comprehensibility testing on the basis of 'semantic closeness' was conducted. Test results showed that BWL-3 for Brake Warning Light (BWL) and TPMS-2 for Tire Pressure Monitoring

Table 1 Redesigned icons and their average comprehension scores (ref. Fig. 1)

BWL		TPMS	
Alternatives	Average rating score	Alternatives	Average rating score
BWL-1	6.77	TPMS-1	5.35
BWL-2	5.72	TPMS-2	7.4
BWL-3	8.3	TPMS-3	7.33
BWL-4	6.3	TPMS-4	6.05

System (TPMS) (see Fig. 1) received the maximum average comprehension scores of 8.3 and 7.4 respectively in a 10-point scale as shown in Table 1.

4 Discussion

Past literature [1] has indicated that many users were dissatisfied with the visual features of the BWL and TPMS warning icons. In this work, subjective perceptions of users provided insights regarding user motivations, their behaviours and pain points regarding visual designs of these two icons. These user inputs were used in making decisions while developing the alternative warning icons. Being user-centred, an expectation is that these designs would reduce driver mental workload during their use while driving and improve the overall cognitive experience.

BWL-3 for Brake Warning Light received the maximum comprehension score among the four alternatives. This is probably due to the fact that in BWL-3, the elements were designed by keeping a resemblance with reality, i.e. the manner in which we actually pull the hand brake in a car. A side profile view of a hand pulling the brake lever was used in the icon which perhaps made the icon very intuitive to the respondents who could better understand the functionality and context of its usage.

TPMS-2 for Tire Pressure Monitoring System received the maximum comprehension score among the four alternatives. This is probably due to deflated tyre representation which is more visually intuitive than the abstract exclamation sign ‘!’ in the original icon. This design also represents thicker spokes, lesser in numbers as compared to other alternatives which perhaps led to its easy interpretation than designs where there are congestions.

5 Conclusion

The key challenge of this study was to redesign two automotive warning icons by considering the user capabilities and limitations in Indian context. Human factors guidelines and Peirce’s semiotic model were adopted to develop 4 alternative designs for each icon. BWL-3 for ‘Brake Warning Light’ and TPMS-2 for ‘Tire Pressure

Monitoring System' (ref. Fig. 1) were rated as the most recommended icons by 60 participants. These two redesigned warning icons could be further tested across different societies to validate their superiority over the existing icons for BWL and TPMS signs. This research work presents contextual information, design guidelines and applied information for designing usable warning icons in automobile dashboards. Taking cues from this paper, other warning icons in automobiles, or other contexts could also be considered for redesign.

References

1. Jung, S., Choe, J.: Representation method of warning icons on automobile instrument panel for improving driver's cognitive experience. *Int. J. Control Autom.* **11**(1), 143–152 (2018)
2. Barr, P., Noble, J., Biddle, R.: Icons R icons. In: *Proceedings of the Fourth Australasian User Interface Conference on User Interface*, vol. 18, pp. 25–32
3. De Souza, C.S.: The semiotic engineering of user interface languages. *Int. J. Man-Mach. Stud.* **39**, 753–773 (1993)
4. Carney, C., Campbell, J.L., Mitchell, E.A.: *In-vehicle Display Icons and Other Information Elements: Literature Review*. Federal Highway Administration, Washington, DC (1998)
5. Ng, A.W.Y., Lo, H.W.C., Chan, A.H.S.: Measuring the usability of safety signs: a use of system usability scale (SUS). In: *Proceedings of the International Multiconference of Engineers and Computer Scientists*, vol. 2 (2011)
6. Kantowitz, B.H.: In-vehicle information systems: premises, promises, and pitfalls. *Transp. Hum. Factors* **2**(4), 359–379 (2000)
7. Campbell, J.L., Brown, J.L., Graving, J.S., Richard, C.M., Lichty, M.G., Sanquist, T., Bacon, P.L., Woods, R., Li, H., Williams, D.N., Morgan, J.F.: *Human factors design guidance for driver-vehicle interfaces*. Report No. DOT HS 812 360. National Highway Traffic Safety Administration, Washington, DC (2016)
8. Ng, A.W.Y., Chan, A.H.S.: The guessability of traffic signs: effects of prospective-user factors and sign design features. *Accid. Anal. Prev.* **39**(6), 1245–1257 (2007)
9. Isherwood, S.: Graphics and Semantics: the relationship between what is seen and what is meant in icon design. In: *International Conference on Engineering Psychology and Cognitive Ergonomics*, pp. 197–205 (2009)
10. Barker, P., Schaik, P.V.: *Icons in the mind*. In: Yazdani, M., Barker, P. (eds.) *Iconic Communication*. Intellect Books, Bristol (2000)
11. Sanders, M., McCormick, E.: Human factors in engineering and design. *Industrial Robot* **25**(2), 153 (1998)
12. Dewar, R.E.: Design and evaluation of graphic symbols. In: *Proceedings of Public Graphics*, pp. 24.1–24.18 (1994)
13. Ringseis, E.L., Caird, J.K.: The comprehensibility and legibility of twenty pharmaceutical warning pictograms. In: *Proceedings of the Human Factors and Ergonomics Society 39th Annual Meeting*, pp. 974–978 (1995)
14. Green, P.: *Development of pictographic symbols for vehicle controls and displays*. SAE Technical Paper Series, No. 790383. Society of Automotive Engineers, Warrendale, PA (1979)
15. <https://www.adobe.com/in/products/illustrator.html>. Retrieved 14 Mar 2020
16. <https://docs.google.com/forms/d/1GjpbQGFrPNqCwuyn54Fwdzi8dder1mPVRWpyT2emBs4k/edit>. Retrieved 29 Mar 2020

Designing Interface for an Online Bike Rental Service for Personified Tourism



Arvind Kumar Nishad and Anirban Chowdhury

Abstract As the world is getting toward new and better technology, they are able to manage their time and workload. Current generation uses online services to buy and sell the product and services. Through human–computer interaction (HCI) it is observed the way interaction between human and computer and through design technology, for the young generation like college students use to different social media and e-commerce site. This research work aims to design an interface for an online bike rental service. It will be easy to rent a bike by booking it online. Objectives of the study were to find what problems bike renters get to rent a bike and to improve the bike rental services through user experience and interface design strategies. The observational study was done in the bike rental shop. Then, customers and the owner were asked contextual questions and responses were recorded, in this research. It was observed that consumers find problem in this process of booking or finding bike and they are expecting a better experience. The result of this study also suggests the possibility of acceptance of novel mobile app for bike rental service where people can have better user experience, they can easily find and book the bike at any location without wasting much time and energy through the designed interface of a mobile app.

Keywords Design · Human–computer interaction (HCI) · User experience (UX) · User interface (UI) · Service design

1 Introduction

The concept of bike renting is not a new as it is available in cities like Dehradun, Goa, Delhi, Bangalore, Kerala, etc. This concept is well known in countries like Vietnam where studies have done as motorbikes embodies the very mobility and sufficient

A. K. Nishad · A. Chowdhury (✉)
School of Design (SoD), University of Petroleum and Energy Studies (UPES), Dehradun,
Uttarakhand 248007, India
e-mail: chowdhuryanirban14@gmail.com

© The Author(s), under exclusive license to Springer Nature Singapore Pte Ltd. 2021 315
B. Deepak et al. (eds.), *Advanced Manufacturing Systems and Innovative Product Design*,
Lecture Notes in Mechanical Engineering,
https://doi.org/10.1007/978-981-15-9853-1_26

and flexible to use for tourist attraction places and students studying far from home use it [1]. Everywhere people can find different posters and pamphlet for bike renting in which mobile number and picture of bikes are available which is not sufficient to the renter and the main problem arises to find the nearest place for bike renting and then calling them on phone for the detail and then thinking of booking and then discussing with partners. The process goes long again when reaching at the shop for identity, security, and cash. To reduce this finding shop here and there and reducing time of the customer an online platform can work better to find the bike rental shop and booking it at different location without wasting time. The better user experience can be implemented in bike tourism at different places [2].

2 Literature Review

As the motorbike tourism is becoming a distinctive idea to explore new places [3] the study shows how people use different social media like Facebook, Instagram, etc., for information and pictures of places to visit in vacations as it is easily available and can use them.

When people visit hill stations and traditional villages which is sometimes only possible by motorbike to reach as its mobility. Nowadays people go to different places to explore new locations with friends and partners like traditional villages and beautiful landscapes. Some studies also show how people use their weekends and small holidays with friends and partners.

The revenue of this kind of motorbike Rent is good for people working at the shop or the owner of the shop and its rental service depends on the operating of motorbike that is for how long motorbike rent is taken [4]. It is also not costly for the motorbike renter to rent a bike of their choice for some days. Minor People Riding bike illegally without driving license and bike papers is the issue which can take care of and avoid accidents which cause damage to both the owner and the person riding bike [5, 6].

2.1 *Service Design and E-commerce*

Service design is how to improve interaction between customer and service provider and make the service usable [7, 8]. E-commerce is the activity of doing online buying and selling of product or services through the internet. In e-commerce, the main objective is to sell their product or services. To improve the service on e-commerce as nowadays customers are opting for online stores as it is convenient to them [9]. To make consumer into customer the service provided before pre-purchase can be enhanced while consumer buying any product or services online. Post-purchase of any product or services, consumers should feel safe and satisfied.

2.2 *E-commerce and Rent Service*

Renting any product online is different experience from buying any product. Earlier people rent and buy the product and services directly from the shop. Now e-commerce is the latest way of buying and selling any product or service around the world. With the help of e-commerce now people can also rent the products like furniture, appliances, and electronics which is more convenient to the people who always change their location time to time. The traditional way of buying or selling product is changing in today's e-commerce world. Renting products online is the new way of business where now people can also rent products easily. Through the motorbike rental service, localities can also get monetary benefits.

Therefore, the objectives of this study are to understand the existing problems of bike rental services and provide ICT based solutions for the same.

3 Methodology

3.1 *Participants*

The customers for motorbike rent were male from college students and tourists. The age between 19 and 25 years were mostly students and tourist and 26–35 years were tourist from other countries also. The total number of users was twelve (12).

A total of 20 participants participated for User Interface evaluation. Their, age ranges from 19 to 35 years. Among them 85% were male adventure lover who know bike riding and all participants were users of mobile phones.

3.2 *Contextual Inquiry*

Contextual inquiry is the user-centered design method to take user/stakeholder responses in the live work setup [10, 11]. This method requires observational study and then some contextual questions are being asked to the person in their work environment.

The study is based on contextual inquiry at the workplace of different locations of bike rental shops (in Uttarakhand) where the owner of the shop and the bike caretaker and the customers were observed. The observational inquiry was also conducted to see the process and behavior of consumers and owner to know the problems. The owner and customers were observed during their work and then were asked for some question about their work and problems they face in the whole process of bike renting. Consumers were asked about how they feel about the bike rent service, service providers, the type of booking, and how they find about the bike shop. The

Fig. 1 Sequence model



following models were then illustrated to represent the entire data collected during contextual inquiry:

- (1) The Sequence Model (Fig. 1)
- (2) The Flow Model (Fig. 2)
- (3) The Physical Model (Fig. 3)
- (4) The Cultural Model (Fig. 4)
- (5) The Artifact Model (Fig. 5).

3.3 Tentative Design Solution

On the basis of the study of motorbike rent, it was found that the people facing problems in getting motorbike on rent, to find the place, to rent motorbike, etc. Detail findings about problems were presented in the result section. The wireframes for the

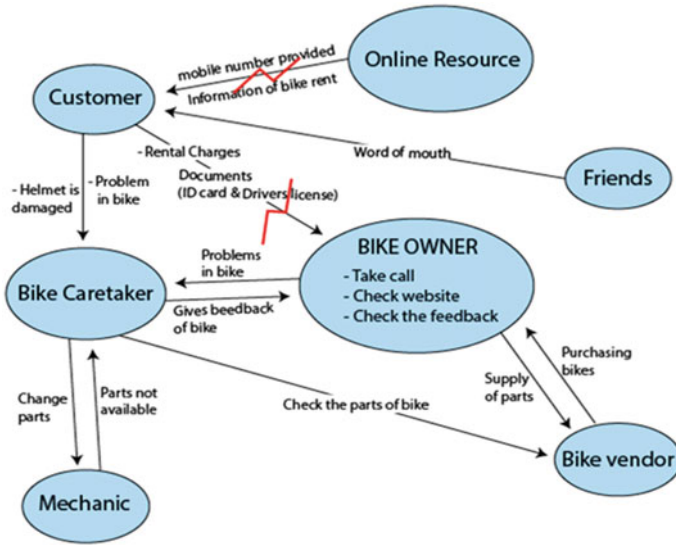


Fig. 2 Flow model

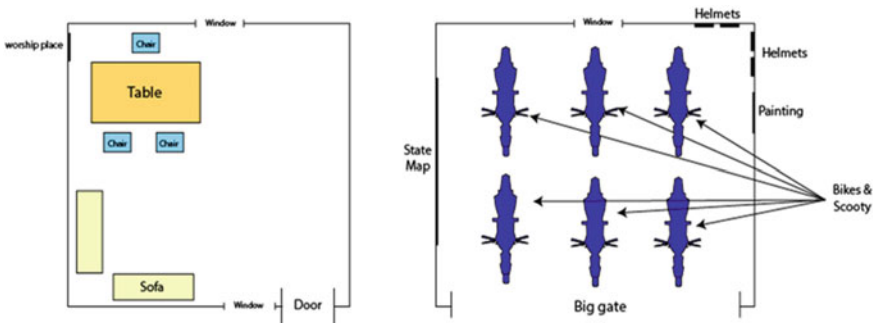


Fig. 3 Physical model (left: office; right: garage)

online platform were developed on the basis of problems tourist get during finding a motorbike shop for renting. Through this system consumers can find motorbike shop nearby to them and can also book it online. Two different wireframe(s) (Wireframe A and Wireframe B) were designed for the bake rental service mobile app keeping functionalities same but layouts and detailing were different.

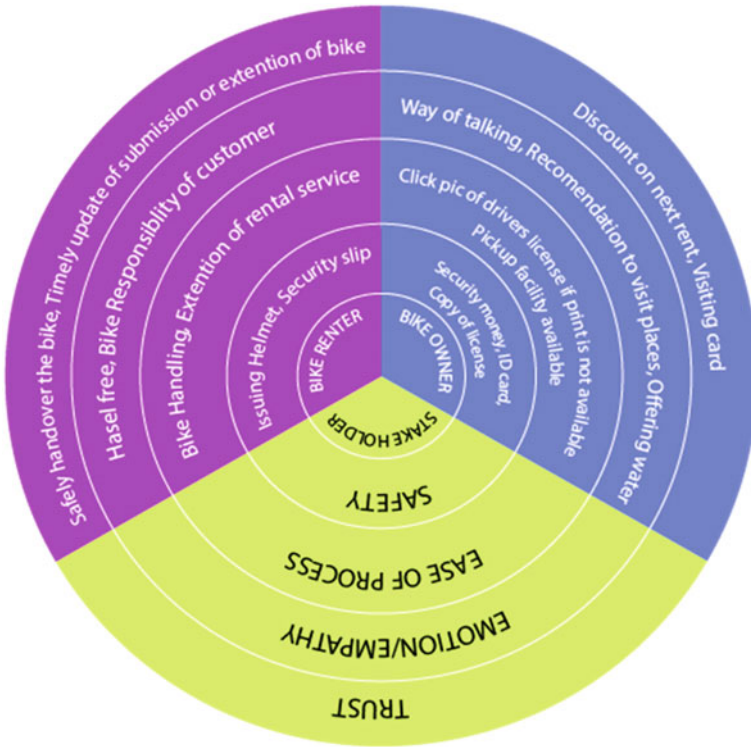


Fig. 4 Cultural model

Fig. 5 Artifact model



3.4 Usability Testing Using SUS Scale

The System Usability Scale (SUS) was adopted from Brooke (1996) [12] and applied to measure the usability of the designed wireframe (Wireframe A and Wireframe B) for the interface of the online portal for bike rental service.

4 Results

4.1 Contextual Inquiry

Through observational study, it is revealed that the target point of bike renting are the college students and tourists, the peak point of bike renting is the weekends and holidays when almost all bike is rented. The customer needs the most nearest place to reduce wastage of time according to them where they want to go and where they live or from where they are coming from to rent a bike and the availability of required bike is also important that what bike they want to rent by calling them on the phone and asking for details of the bike and the price of the bike and also it is not easy to compare bike to other available bikes. The problem comes again of finding bike shop and on reaching has to wait for the giving copy of driving license and original ID proof of both person riding bike and their partners too as every time they go to rent a bike.

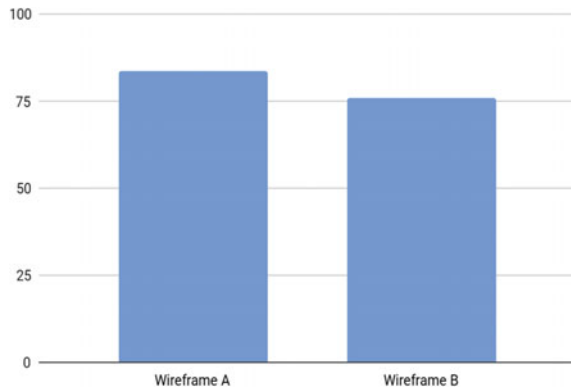
Problems related to the actions for current bike bookings are highlighted in the sequence model (Fig. 1). The information exchange related problems in the context of bike rental services were presented in the flow model (Fig. 2).

The common arrangements and layouts of the bike rental shop are presented the physical model (Fig. 3). On the basis of the contextual inquiry, the cultural model (Fig. 4) shows how trust, emotion, ease of process and safety for the customer, and bike renter works. The artifact model shows the equipment and tools used by different stakeholders and consumers during bike rental process (Fig. 5).

4.2 SUS Test Results

On comparisons between Wireframe A and Wireframe B, it was observed that the SUS score of Wireframe A (83.5) was comparatively higher than the Wireframe B (75.8) (Fig. 6). According to the Bangor et al., the SUS score greater than or equal to 70.5 is defined as “Good” and if the score is greater than the value 77.8 is defined as “Excellent” [13]. According to this study, the user interface depicted in Wireframe A falls under the excellent category and the Wireframe B falls good. Hence, Wireframe A is better than the Wireframe B.

Fig. 6 Mean variations in SUS scores



5 Discussions

From the sequence model (Fig. 1) it was observed that the availability of bike rental information at different places are limited and documentation required for bike rental was not systematic which was highlighted in flow model (Fig. 2). Today's generation is used to do everything online either it is shopping [14], reviews, bookings, food order, and for travelling. Ola and uber [15] are the cab services which is used for travelling as it is easy to book and people can get the service at their doorsteps. Buying online or from shop people generally take suggestions from the friend of any family member [16] and here for taking bike on rent people ask their friend or someone who took before bike rental which is near and of low-cost but there are only a few online services which provides bike rental and which totally works. Customer who came to shop for bike rent and came to know bikes were not available to take rent from the shop, they faced problem to find another nearby shop immediately (highlighted in Fig. 1).

It is a long process to take bike and with the help of the mobile app design it is now possible to improve the bike rental system and can make user friendly, hassle-free, and trustworthy which are expectations of target users as highlighted in Fig. 4. By focusing on college students who are away from home and tourist who comes on weekends and holidays to enjoy with a friend by easily finding bike online and booking directly without any problem. However, a similar physical infrastructure and artifacts (gadgets) were observed in the bike rental shops (Figs. 4 and 5).

It was observed in many studies that usability is the important predictor for product or interface acceptance [17–20]. The user will be satisfied if the usability of the interface is good [17, 20]. In this study, SUS score for mobile app Wireframe A (Fig. 7) was better than the Wireframe B. Hence, usability of planned mobile app (Wireframe A) might be more acceptable among target users and able to achieve the satisfaction level.



Fig. 7 Wireframes (A) of mobile app

6 Conclusion

Access to internet and using online services is the most common thing which is there in college students and tourist. Nowadays people want everything easily available to them on their phone or desktop for shopping, food delivery, Rides (Uber and Ola), and other services [14]. There are few online platforms where people can find bike rental service available to them in which some do not work properly or available only

at some places which are far. Most of the people check online for bike rent and they get random phone numbers and shop address which does not give much information about the bike rental service and the time taken during renting bike are also annoying for some people. The proposed app will resolve all these problems.

Therefore, the mobile app for bike rental service will provide the bike rental at the different locations with less time taken and without finding any other place and asking from other persons. With online bike rental service people can book bikes online anywhere according to their convenience and they can also compare bike prices and their condition of the bike.

References

1. Truitt, A.: On the back of a motorbike: middle-class mobility in Ho Chi Minh City, Vietnam. *Am. Ethnol.* **35**(1), 3–19 (2008)
2. Tripathy, A.K., Patra, M.R.: Service based system monitoring framework. *Int. J. Comput. Inf. Syst. Ind. Manag. Appl.: IJCISIM* **3**, 924–931 (2011)
3. Voda, M., Torpan, A.: Facebook and Youtube role in Transylvanian motorbike tours visualisation based on remote sensing data. *Acad. Sci. J. Geogr. Ser.* **5**, 60 (2014)
4. Diaz Olvera, L., Plat, D., Guezere, A., Pochet, P.: The motorbike taxis in Lomé: who earns what? *HAL* (2013)
5. Gillen, J.: Streets of fire: motorbike mobilities in Vietnam. *Area* **48**(1), 64–69 (2016)
6. Brammer, N., Beech, J.: Use and abuse of tourism: the Goan experience. *Tourism Culture Commun.* **5**(1), 23–35 (2004)
7. An Introduction to Service Design and a Selection of Service. Design Council, UK. <https://www.designcouncil.org.uk/sites/default/files/asset/document/Design%20methods%20for%20developing%20services.pdf>. Accessed 26 July 2020
8. Design Methods for Developing Services, Design Council, UK. <https://www.designcouncil.org.uk/resources/guide/design-methods-developing-services>. Accessed 26 July 2020
9. Surjadjaja, H., Ghosh, S., Antony, J.: Determining and assessing the determinants of e-service operations. *Manag. Serv. Qual.: Int. J.* **13**(1), 39–53 (2003)
10. Cooper, A., Reimann, R., Cronin, D., Noessel, C.: *About Face: The Essentials of Interaction Design*. Wiley, Hoboken; NJ (2014)
11. Preece, J., Sharp, H., Rogers, Y.: *Interaction design: beyond human–computer interaction*. Wiley, Hoboken; NJ (2015)
12. Brooke, J.: SUS: a ‘quick and dirty’ usability. *Usability Eval. Ind.* **11**, 189 (1996)
13. Bangor, A., Kortum, P., Miller, J.: Determining what individual SUS scores mean: adding an adjective rating scale. *J. Usability Stud.* **4**(3), 114–123 (2009)
14. Delone, W.H., Mclean, E.R.: Measuring e-commerce success: applying the DeLone & McLean information systems success model. *Int. J. Electron. Commerce* **9**(1), 31–47 (2004)
15. Kashyap, R., Bhatia, A.: Taxi drivers and taxidars: a case study of Uber and Ola in Delhi. *J. Dev. Soc.* **34**(2), 169–194 (2018)
16. Koli, A., Chowdhury, A., Dhar, D.: Requirement of new media features for enhancing online shopping experience of smartphone users. In: *Intelligent Systems Technologies and Applications*, pp. 423–435. Springer, Cham (2016)
17. Chowdhury, A., Karmakar, S., Reddy, S.M., Ghosh, S., Chakrabarti, D.: Usability is more valuable predictor than product personality for product choice in human-product physical interaction. *Int. J. Ind. Ergon.* **44**(5), 697–705 (2014)
18. Chowdhury, A., Reddy, S.M., Karmakar, S., Ghosh, S., Chakrabarti, D.: Is perception of product personality related with product usability? A cognitive ergonomics perspective. *Ergon. Enhanc. Prod.* 177–182 (2013)

19. Chowdhury, A.: Design and evaluation of user interface of a mobile application for aiding entrepreneurship. In: *Innovative Product Design and Intelligent Manufacturing Systems*, pp. 71–79. Springer, Singapore (2020)
20. Ramadas, R., Chowdhury, A.: Hypnotic computer interface (hypCI) using GEORGIE: an approach to design discrete voice user interfaces. *J. Intell. Fuzzy Syst.* **38**(5), 6507–6516 (2020) (Preprint)

Creating Awareness About Health and Hygiene During Menstrual Cycle Among Indian Adolescent Girls Using Virtual Reality



Shakti Banerjee, Anirban Chowdhury, and Anmol Srivastava

Abstract India is an especially confusing country portrayed by diversified culture, fluctuated social convictions, segment and geographic profiles with various religion. India is growing fast and moving upwardly with innovation and making a worldwide market for other people. Yet, there are various social taboos which are not talked about publicly. One such issue is the menstruation cycle in teenage girls. Menstruation cycle in teenage girls is one of the taboos which needs to be addressed in India. Numerous myths are blindly followed due to unawareness about hygiene leading to unhealthy environment and practices. As a number of individuals are shy to discuss this subject openly in the community, Virtual Reality (VR) can prove to be a beneficial medium to convey these social communication campaigns. VR can give a very personal experience to users to understand this topic. A teenage girl can see the natural changes in her body and comprehend the period cycle herself glimpsing inside the VR without taking any other individual to help. This paper aims to probe into understanding the scenario of an adolescent girl in the rural areas and come up with the proposal of effective use of VR to create better awareness on menstruation cycle management. This paper offers a perspective of the concepts and how to integrate a VR product to enhance the understanding of social awareness communication in rural areas.

Keywords Digital design · Interactivity · Rural scenario · Social awareness · Taboo · Virtual reality

S. Banerjee

MIT Institute of Design, MIT Art, Design & Technology University, Pune, Maharashtra 412201, India

A. Chowdhury (✉) · A. Srivastava

School of Design (SoD), University of Petroleum and Energy Studies (UPES), Dehradun, Uttarakhand 248007, India

e-mail: chowdhuryanirban14@gmail.com

1 Introduction

India is one of the greatest and quickest developing economies in the world. In the previous, not many years, India's monetary force has expanded. Like other creating nations, India considers trade to be the ascent of progression. Although India has its own difficulties. The second biggest populated nation is brimming with different religion, beliefs, culture, convictions, and conventions. The greater masses live in a rural area of the nation. As indicated by 2011 census, the rural areas have populace of 68.84%, while urban region has populace of 31.16% as it were. There are 40% individuals uneducated. The growing populace and the recourses are not matching to accomplish the 100% proficiency in the nation [1].

As of late with the headway of Internet, India has been advancing quickly. It is acknowledged the vast majority of the people in India steadily would be associated through computerized contraptions, an innovation where the progression of communication, exchanges would greatly occur. This change one can see that individuals have just begun feeling attributable to a smart phone, web network. This change comprehends the most extreme requirement for information for both awareness and communication for a successful win suggestion with headways and arrangements. Yet at the same time, there is a limitation concerning media infiltration to reach out to the rural places, particularly for a social awareness communication campaign in India. However simultaneously, there is a confinement concerning media invasion to connect with the rural areas, especially for a social awareness communication campaign in India.

In India as a community there are certain faith and beliefs. For the most part for making awareness campaign there are constrained media and technology utilized in the rural areas and villages. The medium like posters, wall advertisements, banners, handouts, and so on are generally used for social issues like Health and Hygiene, racism/caste, cleanliness, literacy, unawareness of diseases, etc. Radio/FM is another medium which is accessible in the villages.

India has diverse ways of communications with having 22 major languages, written in 13 different scripts and over 720 dialects [2]. Most of the time the print media and contents are not effectively used. Many cases the integration of visual media are not good enough to convey the messages. Although, in the world of technology and innovations there is opportunity to explore, to integrate them together, to get the desired impact from the target audience in the rural areas also. Effective use of visual media and technology could be the answer. Because of the penetration of Internet and mobile phone, it is easier to adapt in many villages. So far at times, films and animations are also used nowadays. These mediums are "cold" medium and they are only one-way communication to the target group. The technologies such as Augmented Reality (AR) and Virtual Reality (VR) are hot medium because these are interactive in nature. The medium which is interactive in nature is considered as "hot medium" such as recent innovations like Augmented Reality (AR) and Virtual Reality (VR). The user not only watches the visuals but actually able to interact and continuous instant feedback happens in there.

To reach out to the target group in rural and villages, the emerging media like AR, VR, and XR can be very interactive and effective to create awareness among the users.

1.1 Emerging Media for Social Awareness Communication—Immersive Media

Immersive media can be characterized as innovations that endeavor to create or mirror the physical world through computerized reproduction. It is the meeting up of innovation and reality. Virtual Reality (VR), Augmented Reality (AR), and Virtual Reality (XR) are examples of immersive technology.

VR can be characterized as a computer-generated three-dimensional world, updating in real time, and enabling human interaction through different input/output devices. Wann and Mon William explained Virtual reality (VR) is a user-centered experience, positioned instead of seeing it in a virtual world [3]. This requires the user becoming an active participant in the virtual environment and engaging with displays that require human sensation and perception to be used effectively in the research done by Moffat et al. [4].

Augmented Reality (AR) is a live, immediate or circuitous perspective on a physical, genuine condition whose physical environment, the elements of which are supplemented by computer-generated sensory information such as sound, video, graphics, or GPS data. An AR system has the following features: it integrates real and virtual objects in a real environment, runs interactively and in real time, and tracks real and 3D virtual objects. XR is described as a hybrid of AR and VR. It involves interaction between both the elements that are objects from the real world as well as the objects from the virtual world. It combines real and virtual environments according to the concept of extended reality, and concerns technologically driven interactions between humans and machines. Over the last 50 years immersive media have evolved as a term, but in recent years they have only become disruptive technologies. The AR/VR has much more advantages. Now AR/VR is largely being used commercially in Video Games but it has a gamut of applications to be used with purposeful requirements. AR/VR is being used in trainings in health domain, special needs, simulation-based army trainings, Car experience, Brand promotion, IT futuristic sectors, bigger events, assembly-line training, engineering visualization, and so forth.

Over the period of different times, various social taboos that are not discussed freely with others, but these should be tackled for improved well-being. These taboos are prevalent in Indian society, which one needs to tackle. Issues identified with well-being and cleanliness of particularly of teenagers are disregarded and neglected. One of such issue is the menstruation cycle in teenage girls. Bunches of shallow legends which adolescents tail them aimlessly. Mostly the teenage girls in the rural areas suffer

from illness because of the unawareness related to their hygiene and cleanliness. That prompts to an unhealthy environment.

1.2 Menstruation—Taboo

Menstruation is the endometrial removal—the uterine covering. Menstrual cycle is otherwise called [5, 6] “menses” is derived from the Latin menses connoting “months.” “Feminine cycle” starts from old French menstrual, which starts from Latin menstrual is, connoting “month to month,” especially of or having month to month courses. Menstruation Cycle is a typical natural wonder which a woman begins encountering once she enters her puberty. Exactly when periods come reliably, this is known as the menstrual cycle. Having standard menstrual cycles is an indication that the conceptive framework in lady’s body is working typically. The menstrual cycle gives significant body chemicals, called hormones, to keep a woman healthy. It likewise readies her body for pregnancy.

Menstruation cycle is the human body phenomenon and it’s the first step of womanhood but because of lack of awareness people generally do not talk openly. Instead of making the teenage girl understand better about our human body, the elders related to them create myths surrounded by this and that leads to taboo in the society. Many of these girls go to depressions. During the time of periods girls avoid doing their daily courses, avoid going to schools and neglect their health. Such taboo does persist not only in India but also in other third world countries, especially in the rural areas.

In any case, lamentably period and menstrual practices alongside menstrual waste removal is generally left hidden. It has been considered as a taboo and a few socio social limitations are appended to it. As a result teenager girls stay unacquainted with the logical realities and sterile well-being rehearses, which may prompt a few unfavorable well-being conditions.

1.3 Management of Menstrual Cycle

The management of menstrual cleanliness indicates legitimate cleaning and washing particularly genital zones to keep away from contamination, utilizing appropriate material for retaining menstrual blood and above all, legitimate removal of the pre-owned material for forestalling spread of disease or making harm nature. Keeping up cleanliness during periods like, changing napkin oftentimes, washing genital region after each utilization of latrine, washing, and so on are urgent strides for a young lady to manage this natural procedure with certainty and security. Lack of education may prompt absence of awareness with respect to menstrual cleanliness the executives. An investigation from UNICEF portrays that one out of three young ladies in South Asia thought nothing about feminine cycle before getting it while 48% of young

ladies in Iran and 10% of young teenage girls in India accept that monthly cycle is a disease 10.23% of juvenile young ladies in the age-bunch 12–18 drop out of school after they start bleeding. Only 35% women use sanitary pads in India [7].

Therefore it requires social communication campaign to create awareness in such rural areas. Most of the time one could notice the medium like posters, wall paintings, and leaflets are used. To improve the efficiency and effectiveness of rural health care, Government of India periodically implements programs, new techniques, and mechanisms. New strategies and components for improving the proficiency and viability of provincial medicinal services, yet no particular plan approach is utilized [8].

The Government of India propagates different Grammin (for villagers) schemes on health and cleanliness in the villages. They do put up health camp for pregnant women, for kids, or for general health. There are community health workers go to the villagers under “ASHA,” “Anganwaadi,” “Sneha,” “Saheli” programs to create awareness and give basic help like in the diets, medicine pills, etc. But still it not that effective. There is a much more prerequisite required to create an impact on awareness.

1.4 Relevance: Approach to Existing Scenario

In the exploration paper by Bhowmick, Darbar, and Sorathia, it was mentioned that the India has directed compressive examination on how VR interface utilizing HMD could help in their preparation for ASHA people group well-being laborers. Network Health Workers (CHWs), particularly Accredited Social Health Activists (ASHAs) give prosperity to Indian family units by taking care of their needs and taking care of their healthcare issues [9]. In another study, authors have primarily taken the topic on women pregnancy and childbirth. VR training modules were created and tested as third person onlooker [8]. Whereas In the proposed research paper, the emphasis given on direct empathy with the teenage girl and the interaction should be of first person. This area has not been explored. The proposed description hypothesis is the basic thinking of making the VR experience in the first person would create lots of impact on communication and able to create better impact. It has been presumed that numerous moms of pre-adult young ladies were uninformed about advising little girls about feminine cycle before their first event of period. The conversation ought to occur before the period of menarche. The accessibility of reasonable sterile packs must be there to the resident zone [10].

In the research paper, the different related issue of Menstruation has been engaged like disparity of sexual orientation. Inconsistent rights given to people bring about ladies' voices being disregarded inside families and networks. It got unthinkable and because of reluctance, fantasies, biases, and confusions irritate the worry among the women in that period [11]. In this research paper, even in the other creating nations the period considered as of girls felt that menstruation cycle was something to be embarrassed about to be viewed as a freedom of ladies, as the historical backdrop of period would recommend that cutting edge the executives of the menstrual cycle is a

substantially more helpful experience [12]. In the paper features of the respondents need appropriate information on data significant to monthly cycle. The significance of expanding mindfulness and giving exact data utilizing logical sources, for example, schools, universities, or well-being colleagues. It is prescribed that feminine cycle be talked about in courses, for example, sciences to expand the degree of information on female understudies and thusly to improve their demeanor toward this physiologic procedure [13].

1.5 Aim and Objectives

The paper's aim is to enhance understanding of the adolescent rural Indian girls for menstrual cycle using immersive media (VR). Therefore, objectives of the study are

1. To present animated information about menstrual cycle in the VR-based immersive media.
2. To present instructions about hygiene and cleanliness pertaining to menstruation.
3. To evaluate the proposed concept of immersive media using expert evaluation (heuristics based).

2 Methodology

2.1 Virtual Environment and Target User

The VR application on menstruation will be tweaked to the primary target group which is adolescent girl. The age group 14–18 years is considered for this study. Most of the users are either having primary or secondary education or ignorant from primary education. Thus, ASHA health workers are considered as secondary users of the proposed solution.

For making awareness on menstruation cycle among adolescent girls from rural areas, the Virtual Reality (VR) can be a boon to such situations where the users are shy to discuss openly. With the assistance of network community social Health workers, the teenagers can interact and view using VR Head Mount Device (HMD) and get awareness about menstruation cycle. One can watch, interact, experience in Virtual Reality and comprehend what the progressions are that occur in the human body in the adolescent years. The VR experience will guide how to maintain their cleanliness and hygiene without stressing their minds.

2.2 Interface Description

- Inside the VR, a 3D mannequin will explain the changes in the girl’s body with the user reference showing according to the ages.
- Consideration of Gaze Interaction will make it fast, natural, and effortless navigation than manual interaction.
- Explaining using animation what are the different stages of womanhood (Fig. 1).
- Inside VR, Joystick will be used for easy navigation (Fig. 2b).
- The user could see the body parts and interact with reproductive organs (Fig. 3).
- Explain the importance of Hormone and how it will help her to prepare for pregnancy.
- The menstruation period cycle will be explained in a visual way to explain the different stages. The girl can choose the calendar date, choose and interact to see the progressive differences in the ovaries and vagina.
- The voice Interactions will be in the first person. Dialogue-based narrative style would be utilized.
- Advantage with VR is that there will be constant feedback and it will help her to choose the sequence of navigation according to her wish and with comfortability.
- In India only 30% ladies are using sanitary napkins. The VR interactions also explain how to use the sanitary napkins and explain its benefits.
- One can use gestural simple command and can avoid too many texts in the Instructions.
- The hygiene practice can be visually explained. The proper use of different sanitary pads will be explained.
- Dos and Don’ts explained properly with interactive navigation. How to wear the sanitary pad. Self-examining your own body.

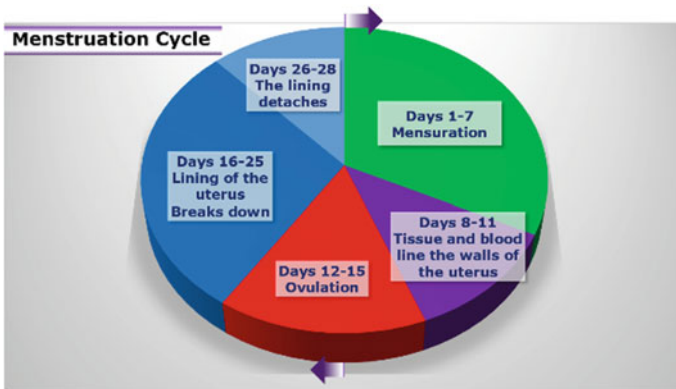


Fig. 1 Stages of menstrual cycle

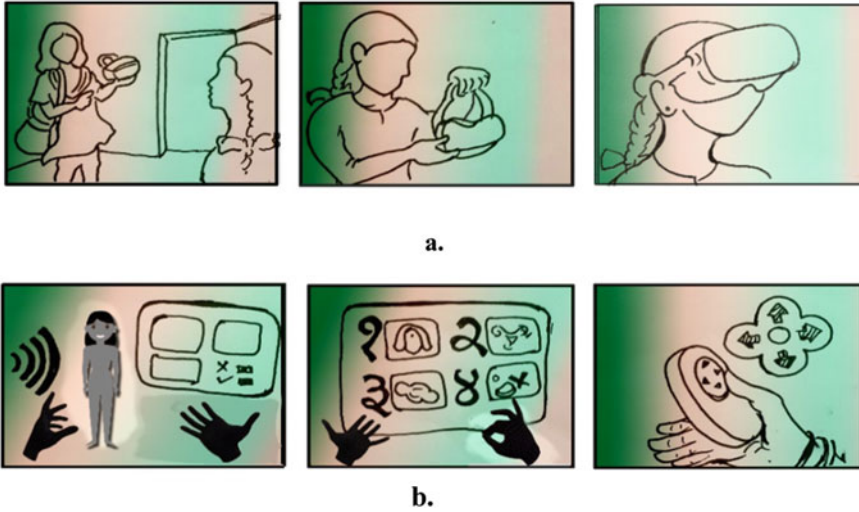


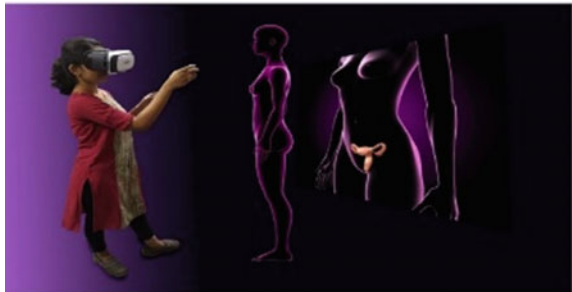
Fig. 2 **a** Initially guided by health workers how to use HMD, then the teenage girl is interacting with VR environment herself to interacting experience about the menstrual cycle; **b** voice command with the options of selecting own vernacular languages. Easy Instructions with gestures-based command and also directional easy directional jockey-based navigation. The information navigation can be controlled by the user as per their preferences

- Logical explanation of hygiene facts to create awareness against following the myths. There might be pictorial trivia to be solved by her so the whole experience could be engaging.
- Gamification could be added to create more interest.
- Advantage with VR is that there will be constant feedback and it will help her to choose the sequence of navigation according to her wish and with comfortability.
- Double Diamond Design process was applied for define and development of VR prototype (Fig. 4).

2.3 Story Simulation

- Scene 1: Welcome note to the virtual media for awareness of menstrual cycle.
- Scene 2: User Instructions to use the VR based immersive media (viewpoint control & voice instruction)
- Scene 3: Awareness of female gonadal system using animation.
- Scene 4: Awareness about female puberty and menopause.
- Scene 5: Awareness about steps in menstrual cycle
- Scene 6: Instructions for maintenance of hygiene during the menstrual cycle.
- Scene 7: Quiz about menstrual cycle and display of reward points.

Fig. 3 The teenage girl is interacting with VR environment using HTC-Vive for understanding of female gonadal system and menstrual cycle



2.4 Apparatus

- Use of HMD headset Oculus Rift/HTC Vive. In the low-cost proposal it may be Google cardboard with lesser interactions but will have VR based 3D video to view to get the experience.
- 3D software Blender, Maya for creating characters, and animation integrated in Unity3D software. SDK for VR stimulation.
- Use of optimizing size of images, model, and audio.
- The maximum the VR experience planned not more than 5 min at a stretch to avoid dizziness.

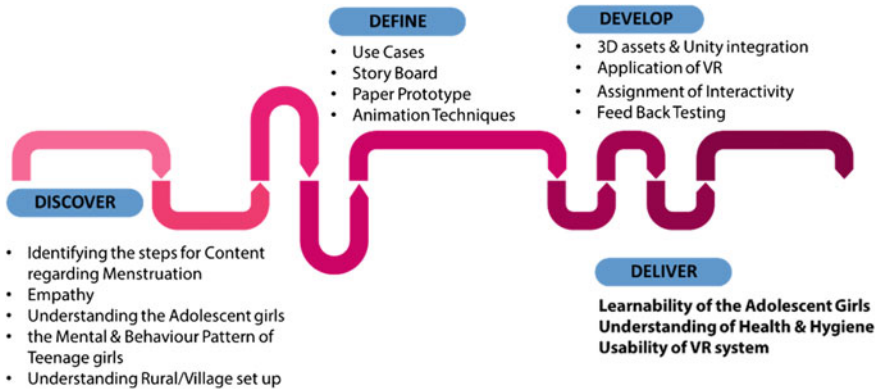


Fig. 4 Process of concept creation and development of immersive media for creating awareness of menstruation cycle among teenage girls

2.5 Heuristics Evaluation of Low Fidelity Prototype

A total of three usability experts were asked to evaluate the design low fidelity prototype using six heuristics which were adopted from Sutcliffe and Gault [14] (Table 1).

3 Results and Discussion

After heuristics evaluation it was observed that there are few problems identified by experts which are presented in Table 2. As the current prototype is low fidelity prototype, there are scopes of improvement, suggested by usability experts. They have suggested that consideration of socio cultural status of the target users for defining the realistic feedbacks using various elements of interface, integration of natural user interface (gesture-based and voice-user interfaces), presentation of more realistic human models and more visual feedback during interaction are beneficial.

4 Conclusion

In spite of the fact that the inquiry may emerge the reasonableness of VR with HMD set in the country place. The arrangement could be a pilot venture and attempt the suitability in the littler region. At that point the measured way it tends to be extended in different pieces of India. There are less expensive Headsets are coming up these days and very soon these thoughts can be actualized with minimal effort. HMD can be substitute by Google cardboard with lesser intuitive route utilizing portable system

Table 1 List of heuristics (adopted from Sutcliffe and Gault [14]) applied for expert evaluation

S. No.	Heuristics	Definition
1	Compatibility with the user’s task	Objects presented in VE and user actions should correlate as closely as possible to match the user’s understanding of artifacts from the real world; their spontaneous actions and affordances
2	Close coordination of action and representation	The portrayal of the embodied self/identity and conduct in the VE should be faithful to the actions of the user. The response time between user movement and VE display update should be less than 200 ms in order to prevent issues with motion sickness
3	Realistic feedback	The effect of the user’s actions on virtual world objects should be immediately visible and conform to the laws of physics and the user’s perceptual expectations The impact of user behavior on virtual world objects should be apparent immediately and should be consistent with the laws of physics and the perceptual expectations of users
4	Navigation and orientation support	The user ought to consistently have the option to find where they are in the VE and come back to known, preset positions. Unnatural activities, for example, fly-through surfaces may help yet these must be decided in an exchange off with instinctive nature
5	Support for learning	Active objects ought to be prompted and if vital account for themselves to advance learning of VEs
6	Sense of presence	The user’s view of engagement and being in a ‘real’ world ought to be as normal as could be expected under the circumstances

additionally, however similarly viable. Utilization of 360 video movement likewise will be valuable.

Teenage girls ought to be instructed about the realities of period, physiological ramifications, significance of monthly cycle, and appropriate clean works on during menstruation cycle. It is likewise required to bring them out of conventional convictions, restrictions, misguided judgments, and limitations. This can be accomplished with the assistance of media, sex training in school educational plan, and focused group conversations. All mothers ought to be urged to break their hindrances about examining with their girls in regards to menstruation cycle and menstrual cleanliness. Universalized utilization of clean sanitary pad can be upheld to each girl by social showcasing.

Heuristics analysis [14] suggests that there are scopes of improvement of the VR interface and an advanced immersive interface could be developed in near future

Table 2 Problems identified through heuristics evaluation and suggestions by experts

S. No.	Heuristics	Problems identified
1	Compatibility with the user's task	Moderate expression of the female reproductive organs in terms of reality. However expected level of affordances for auditory feedback and visual instructions
2	Close coordination of action and representation	Response time and user actions are perfect in the virtual environment. Although more visual feedbacks highly beneficial for few controller assisted interactions
3	Realistic feedback	It should be as per the sociocultural status of the target users. Currently the realistic feedback is limited in the prototype
4	Navigation and orientation support	Navigation through virtual environment is appropriate
5	Support for learning	Instructions were provided for use of the prototype of the immersive media
6	Sense of presence	Users are expected to be engaged with the immersive prototype moderately. Natural user interface might be integrated during development of high fidelity prototype to achieve comparatively higher sense of presence

employing the knowledge of sociocultural background of the primary and secondary users and integration of features of natural user interface. It is possible to apply the developed immersive media for educating adolescent girls about the reproductive health and hygiene. However, the perception of presence in current study is limited. Development of high-fidelity prototype with enhance features could be developed for better sense of presence [14].

References

1. Sudhira, H.S., Gururaja, K.V.: Population crunch in India: is it urban or still rural? *Curr. Sci.* **10**, 37–40 (2012)
2. Apte, M.L.: Some sociolinguistic aspects of interlingual communication in India. *Anthropol. Linguist.* **1**, 63–82 (1970)
3. Wann, J., Mon-Williams, M.: What does virtual reality NEED?: human factors issues in the design of three-dimensional computer environments. *Int. J. Hum. Comput. Stud.* **44**(6), 829–847 (1996)
4. Moffat, S.D., Hampson, E., Hatzipantelis, M.: Navigation in a “virtual” maze: sex differences and correlation with psychometric measures of spatial ability in humans. *Evol. Hum. Behav.* **19**(2), 73–87 (1998)
5. Sarkar, D.: Menstrual practice and environmental issues an exploratory study on awareness among school going adolescent girls in South Bengal

6. Dasgupta, A., Sarkar, M.: Menstrual hygiene: how hygienic is the adolescent girl? *Indian J Commun Med.* **33**(2), 77 (2008)
7. Park, K.: Park's Textbook of Preventive and Social Medicine, p. 463. Banarasidas Bhanot, Jabalpur (2011)
8. Ramachandran, D., Canny, J., Das, P.D., Cutrell, E.: Mobile-izing health workers in rural India. In: Proceedings of the SIGCHI Conference on Human Factors in Computing Systems, pp. 1889–1898 (2010)
9. Bhowmick, S., Darbar, R., Sorathia, K.: Pragati: design and evaluation of a mobile phone-based head mounted virtual reality interface to train community health workers in rural India. In: Proceedings of the 10th Nordic Conference on Human-Computer Interaction, 29 Sept 2018, pp. 299–310 (2018)
10. Devi, R.U., Sivagurunathan, C., Kumar, P.M.: Awareness about menstrual hygiene among adolescent girls in rural area of Kancheepuram District-Tamil Nadu. *Int. J. Pharm. Biol. Sci.* **7**, 267–269 (2016)
11. Kaur, R., Kaur, K., Kaur, R.: Menstrual hygiene, management, and waste disposal: practices and challenges faced by girls/women of developing countries. *J. Environ. Public Health* **20**, 2018 (2018)
12. Peberdy, E., Jones, A., Green, D.: A study into public awareness of the environmental impact of menstrual products and product choice. *Sustainability* **11**(2), 473 (2019)
13. Alharbi, K.K., Alkharan, A.A., Abukhamseen, D.A., Altassan, M.A., Alzahrani, W., Fayed, A.: Knowledge, readiness, and myths about menstruation among students at the Princess Noura University. *J. Fam. Med. Prim. Care* **7**(6), 1197 (2018)
14. Sutcliffe, A., Gault, B.: Heuristic evaluation of virtual reality applications. *Interact. Comput.* **16**(4), 831–849 (2004)

Real-Time Obstacle Proximity Warning Through Human Machine Interface and Quadrature Interpretation of a Two-Axis Robotic Inspection System



P. M. Aishwarya Priya, N. Swetha, S. Rajesh Kannan, Saji Jacob George, Joel Jose, and S. Joseph Winston

Abstract Robotic manipulators are most widely used in the inspection systems deployed to carry inspection and material handling in inaccessible and places dangerous to human operators. The Steam Generator tube inspection system of nuclear power station deploys a two Degree of Freedom (DoF) robotic arm close to the tube sheet, where the steam tube bundles end. The two robotic arm positions the inspection probe attached to its end effector at the center of each steam generation tube and pushes the probe into the steam tube to detect any tube crack. The tubes with crack will be plugged to pull out the tubes from service. Such plugged tubes will be projecting on the tube sheet surface, which hinders the robotic arm movement over the tube sheet, while reaching other tubes for inspection. In this project, we have developed PIC microcontroller-based embedded real-time obstacle (plugged tubes) proximity warning system to help the robot operator to carry inspection safely. The system reads data from the quadrature digital encoders attached on the robot's joint motors and computes the joint angles using the software written in "Embedded C" and transmits these joint angle data through serial communication to a Raspberry PI controller based Human Machine Interface (HMI) display. The joint angle data is used to calculate the inspection probe's current position using Forward Kinematic (FK) algorithm written in Python and warns the operator when the probe is close to any plugged tube location. The program also shows the pose of the robotic arm in real time on an HMI display and also indicate the proximity probe to the obstacle.

Keywords Steam generator inspection system · Robotic manipulator · Forward kinematics · Real-time embedded controller · Human machine interface

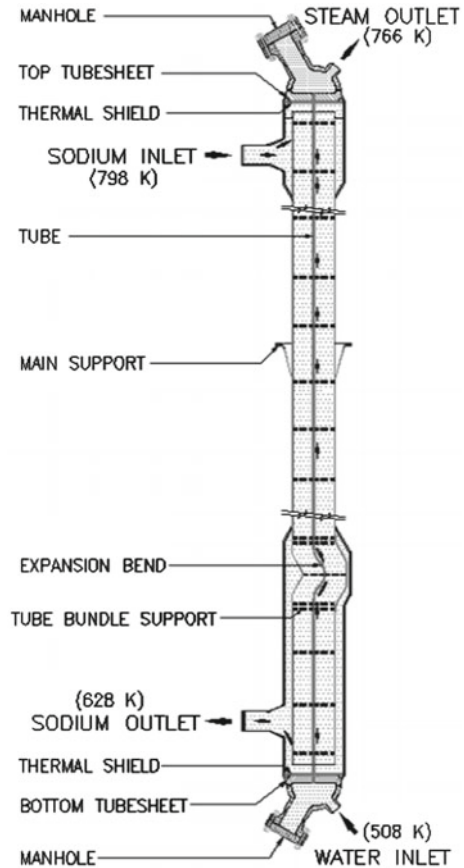
P. M. Aishwarya Priya (✉) · N. Swetha · S. Rajesh Kannan
St. Joseph's College of Engineering, Chennai, India
e-mail: aishwaryapriya1998@gmail.com

S. J. George · J. Jose · S. Joseph Winston
Indira Gandhi Centre for Atomic Research, Kalpakkam, India

1 Introduction

In thermal and nuclear power generation systems, the steam required for driving the turbine-electrical generator is produced by the Steam Generation (SG) system. The Steam Generators are heat exchangers which are used to convert the cold feed water into steam. The cold water pumped into stainless tubes of SG is heated by the hot fluid (hot air in case of coal fired thermal power plant and liquid sodium in case of nuclear power plant) that surrounds these tubes and converted into superheated steam. This superheated steam drives the steam turbine, thereby driving the coupled electrical generator to produce electrical power. In the nuclear power station, as mentioned earlier heat is produced by the reactor core. The liquid metal cooled reactor uses the heat exchanger between a secondary sodium circuit and a tertiary water circuit. The steam generator system consists long stainless steel tubes (up to 20 m (or) more in length) that are welded to the top and bottom tube sheets; and this structure is enclosed in a long cylindrical vessel (Fig. 1). The cold water pumped into these SG

Fig. 1 Steam generator of nuclear power station



stainless tubes is heated by the hot fluid liquid sodium that surrounds these tubes and is converted into superheated steam. This superheated steam drives the steam turbine, thereby driving the coupled electrical generator to produce electrical power.

The tubes of Steam Generator (SG) system requires periodic inspection [1, 2] to detect any crack induced by the thermal stress, before the cracks lead to rupture of steam tubes. The rupture of steam tubes will result in shutting down the power plant and in the case nuclear power plant, contact between the water and sodium will result in a fire accident that can lead to very serious other consequences. Hence, it is of absolute necessity to inspect the SG tubes periodically to detect any cracks in the steam tubes and seal (plug) the tubes that are defective (having cracks); thereby preventing water entering into them to avoid fire accidents and consequent serious implications. At present, most of the steam generator inspection systems are using range and proximity sensors for detecting obstacles; however, in this work, obstacle detection and avoidance is done only using existing (built-in) motor encoders and Inverse Kinematic (IK) algorithm. These SG inspection systems need to have HMI interface to avoid the exposure of human operators to hazardous environment [3].

2 Steam Generator Inspection Robot

The Steam Generator Inspection Robot is a 2-Degree-of-Freedom robotic manipulator [4] and its motion is generated by the Servo Motors attached to the two revolute joints (in shoulder and elbow joints). Figure 2 shows the prototype robotic arm installed over the tube sheet and its schematic showing link and joint coordinates and parameters. The robot has a maximum radial reach of 420 mm and payload capacity of 20 kg.

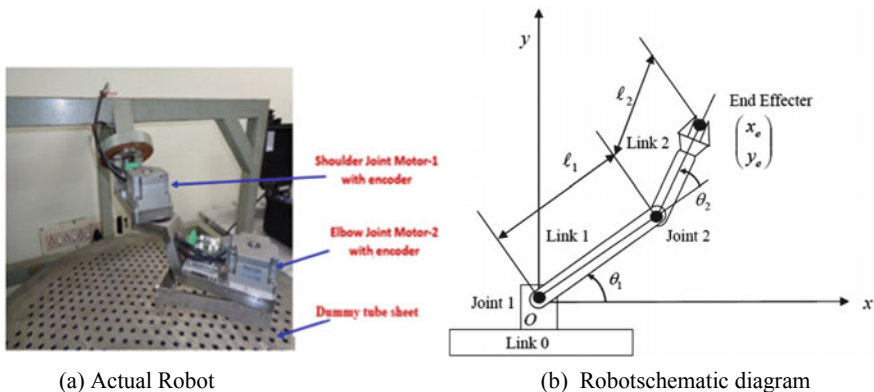


Fig. 2 Two degree of freedom (2-DoF) robotic manipulator

3 Forward Kinematics (FK) of Robot

Forward kinematic equations are used to find the end effector position of robot manipulator with respect to its reference frame (also known as the base frame). To compute robot end effector position, it is necessary to have length (link length) and joints parameters (joint angle in case revolute joint and joint displacement in case of Prismatic joint). For the two degree of freedom (2-DoF) robot manipulator used in the Steam Generator Inspection System, the position (X, Y coordinates—being a planar robot) of the end effector can be calculated using the forward kinematics (Geometric equations) given below [5, 6]. End effector position at X -axis:

$$X_e = l_1 \cos(\theta_{Sh}) + l_2 \cos(\theta_{Sh} + \theta_{El}) \tag{1}$$

End effector position at Y -axis:

$$Y_e = l_1 \sin(\theta_{Sh}) + l_2 \sin(\theta_{Sh} + \theta_{El}) \tag{2}$$

However, these geometric equations become complex to compute the end effector position, in case of higher degree robots (5–7 DoF) in many industrial applications. In such cases the DH parameters based Transformation Matrix based method [7, 8] is used for finding the end effector position with respect to Base frame. Table 1 gives DH parameters of the two degree freedom robot used in the Steam Generator tube inspection system.

In the above table, the parameters “ θ_i ” and “ d_i ” are called as joint parameters and parameters “ α_i ” and “ a_i ” are called link parameters. Using the above DH parameters and transformation matrices given below [9], we can calculate the end effector position and orientation. DH transformation for adjacent coordinate frames can be computed by applying the DH values of individual joints parameters presented in Table 1 in the equation given below:

$$\begin{bmatrix} c\theta_i & -s\theta_i c\alpha_i & s\theta_i s\alpha_i & a_i c\theta_i \\ s\theta_i & c\theta_i c\alpha_i & -c\theta_i s\alpha_i & a_i s\theta_i \\ 0 & s\alpha_i & c\alpha_i & d_i \\ 0 & 0 & 0 & 1 \end{bmatrix} \tag{3}$$

Table 1 DH parameters of prototype two degree of freedom (2-DoF) robotic arm

Joint No. (i)	Joint angle (θ_i)	Twist angle (α_i)	Link length (a_i)	Joint displacement (d_i)
1	θ_{shoulder}	0	210.0	115.0
2	θ_{elbow}	0	210.0	115.0

4 Estimation of the Shortest Distance of the Arms to the Obstacle (Plugged Tube Heads)

The next step is to calculate the shortest distance between the plugged tube heads and the robotic manipulator links. Figure 3 shows the schematic of robotic manipulator along with vectors used for calculating the shortest distance between the shoulder and elbow links of robot and nearest plugged tube heads that will obstruct the motion of robot manipulator.

Following equations are used for calculating the shortest distance between shoulder and elbow links. For the shoulder link:

$$\vec{V}_s = (x_1 - x_0, y_1 - y_0) \tag{4}$$

$$\vec{d}_{sp} = (x_q - x_0, y_q - y_0) \tag{5}$$

$$|\vec{V}_s| = \sqrt{(x_1 - x_0)^2 + (y_1 - y_0)^2} \tag{6}$$

$$|\vec{d}_{sp}| = \sqrt{(x_q - x_0)^2 + (y_q - y_0)^2} \tag{7}$$

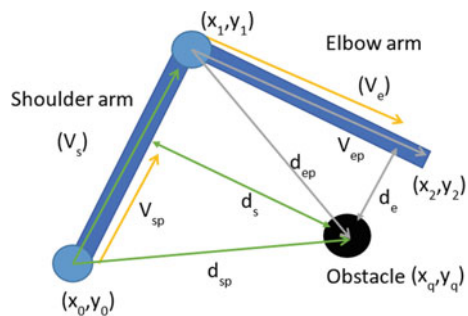
$$\vec{V}_{sp} = \frac{\vec{V}_s \cdot \vec{d}_{sp}}{|\vec{V}_s|} \tag{8}$$

$$\text{Shortest distance } (\vec{d}_s) = \vec{d}_{sp} - \vec{V}_{sp} \tag{9}$$

and for the elbow link:

$$\vec{V}_e = (x_2 - x_1, y_2 - y_1) \tag{10}$$

Fig. 3 Robotic arm and obstacle position



$$\vec{d}_{ep} = (x_q - x_1, y_q - y_1) \quad (11)$$

$$|\vec{V}_e| = \sqrt{(x_2 - x_1)^2 + (y_2 - y_1)^2} \quad (12)$$

$$|\vec{d}_{ep}| = \sqrt{(x_q - x_1)^2 + (y_q - y_1)^2} \quad (13)$$

$$\vec{V}_{ep} = \frac{\vec{V}_e \cdot \vec{d}_{ep}}{|\vec{V}_e|} \quad (14)$$

$$\text{Shortest distance } (\vec{d}_e) = \vec{d}_{ep} - \vec{V}_{ep} \quad (15)$$

5 Experimental Setup and Electronic Hardware

Figure 4 shows the schematic of the proto type steam generator inspection system. It consists of test stand over which the actual size steam generator tube sheet is kept. The 2-DoF robotic arm is mounted over the tube sheet and the robotic arm is controlled motion controller and an HMI display is provided to displace the position of the inspection probe and plugged tube heads.

The primary sensors of this obstacle proximity warning system are Quadrature encoders installed on the joint motors shaft. The system computes the robotic position based on the joint values generated by these encoders and inverse kinematics algorithms [10, 4], when the robot's joints are actuated by joint motors. These encoders are of incremental type encoders and they will generate two TTL level signals (Channels A and B) having phase difference of 90° for measuring joint angle and direction of motor rotation. The encoder produces 2000 pulses per revolution (PPR) of the joint. A third signal known as Z-signal is used for identifying reference angle (i.e.,

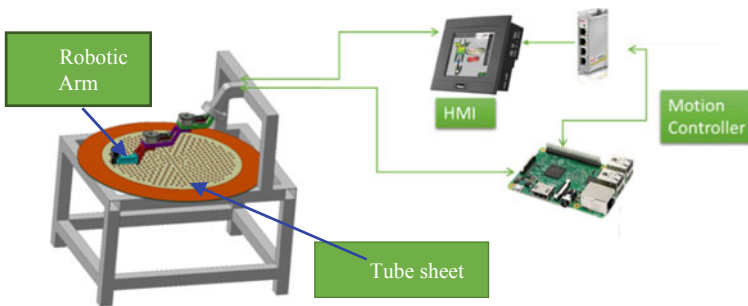


Fig. 4 Prototype steam generator inspection system

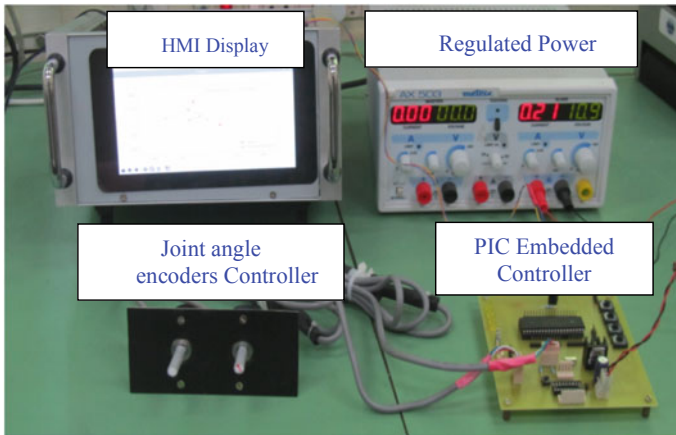


Fig. 5 Experimental facility for testing developed software modules

zero degree). The data processing device of the system is a dsPIC30F4011-High Performance Digital Signal Controller. It is a modified Harvard architecture based, 16-bit DSP chip having following features like built-in A/D Converters, Timers, etc. Apart, this DSP processor has a special feature known as “Quadrature Encoder Interface Module” that allows directly connecting the Quadrature Encoder channels (Channels A and B) and Index Pulse input (Z-signal). This feature helps in finding shaft angle and direction motion. The MAX232 device is a dual driver/receiver that includes a capacitive voltage generator to supply TIA/EIA-232-F voltage levels from a single 5 V supply. Each receiver converts ± 12 V RS232C level input signal received external device to 0–5 V TTL/CMOS levels signal for interfacing with DSP Processor. These receivers have a typical threshold of 1.3 V, a typical hysteresis of 0.5 V, and can accept up to ± 30 V inputs. Similarly, each driver converts TTL/CMOS input levels into ± 12 V RS232C level voltage (TIA/EIA-232-F levels) for transmission to external devices. Figure 5 shows the interfaced Quadrature encoders with dsPIC Microcontroller and experimental facility used for testing the developed software modules.

6 Software Algorithms Development and Results

In this project, we have developed many software modules, (1) for finding the position of Robotic Arm effector position to place at the center of Steam Tube, (2) to find the shortest path between robot link and plugged tube head, (3) To read the Quadrature sensors data to calculate the robot joint angles, and (4) Inverse kinematic algorithms to find robot end effector position to warn the robot operator to avoid plugged tube heads, while inspecting steam generator tubes to find the defective tubes. These programs were written using “Python and Embedded C” languages.

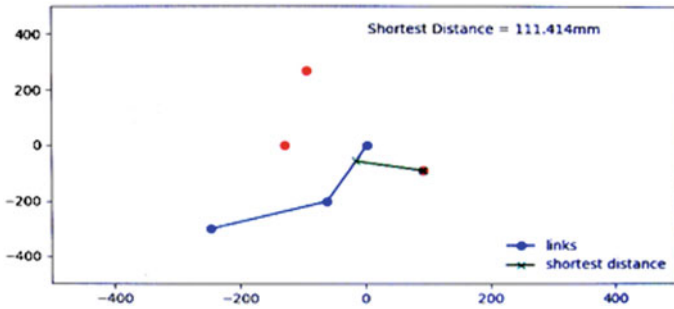


Fig. 6 HMI display showing the shortest distance between the robotic link and plugged tube head

The developed control algorithms were embedded into the dsPIC Digital Signal Processor and real-time Quadrature encoders data was fed to controller to calculate joints and thereby Robot end effector position to find the proximity of Plugged tube heads to robot operator. The data obtained was sent to the Raspberry PI based HMI Display. Figure 6 shows real-time display of the position of the plugged tubes heads (marked in RED color circles) Robot links and joints position (in BLUE lines and circles), apart from displaying shortest distance calculated by the algorithm.

7 Conclusion

In this project, we have developed PIC microcontroller-based embedded real-time obstacle (plugged tubes) proximity warning system to help the robot operator while inspecting the steam generator tubes. The system reads the quadrature channel input data from the digital encoders attached on the robot joint motors and computes the joint angles using the software written in “Embedded C.” A MAX232 IC is used to do the necessary voltage level conversion to send these joint angle data through serial communication to a PC. The joint angle data is used to calculate the robotic arm end effector’s (inspection probe) current position using Inverse Kinematic (IK) algorithm written in Python and warns the operator when the probe is close to any plugged tube location. The program also visually shows the pose of the robotic arm in real time on the operator as 2D graph indicating current inspection location along with the location of plugged tubes. It also indicates the proximity, i.e., distance to between the obstacle and probe to the robot operator.

References

1. Obrutsky, L., Renaud, J., Lakhan, R.: Steam generator inspections: faster, cheaper and better, are we there yet? In: IV Conferencia Panamericana de END, Buenos Aires—Oct 2007

2. Buckingham, R.O., Graham, A.C.: Dexterous manipulators for nuclear inspection and maintenance—case study. In: 2010 1st International Conference on Applied Robotics for the Power Industry, Delta Centre-Ville Montréal, Canada, 5–7 Oct 2010
3. Kamdi, R.P., Muthmare, A., Rathkanthiwar, A.: Human machine interface based robotic arm. *Int. J. Comput. Eng. Appl.* XII(Special Issue) (2018)
4. Joseph Winston, S., Manivannan, P.V.: Optimal damping factor for the least squares inverse kinematics for the steam generator inspection system. In: Badodkar, D.N., Dwarakanath, T.A. (eds.) *Machines, Mechanism and Robotics. Lecture Notes in Mechanical Engineering*, pp. 691–704. Springer, Singapore (2019)
5. Ghaleb, N.M., Aly, A.A.: Modeling and control of 2-DOF robot arm. *Int. J. Emerg. Eng. Res. Technol.* **6**(11), 24–31 (2018)
6. Shah, J., Rattan, S.S., Nakra, B.C.: Dynamic analysis of two link robot manipulator for control design using computed torque control. *Int. J. Res. Comput. Appl. Robotics* **3**(1), 52–59 (2015)
7. Han, K.K.K.K., Sin, A.M.T., Theingi: Kinematic and dynamic analysis of two link robot arm using PID with friction compensator. *Int. J. Sci. Eng. Res.* **8**(12), 1076–1085 (2017)
8. Kormushev Yiannis Demiris, P., Caldwell, D.G.: Kinematic-free position control of a 2-DOF planar robot arm. In: 2015 IEEE/RSJ International Conference on Intelligent Robots and Systems (IROS), Hamburg, Germany (2015)
9. Myint, K.M., Htun, Z.M.M., Tun, H.M.: Position control method for pick and place robot arm for object sorting system. *Int. J. Sci. Technol. Res.* **5**(06) (2016)
10. Ross, S.R.: Introduction to Inverse Kinematics with Jacobian Transpose, Pseudoinverse and Damped Least Squares Method. Department of Mathematics, University of California, San Diego (2009)

A New Finite Automata Approach of Right State Machine



Sarat K. Parhi

Abstract The current study deals with the development of an effective approach to solve automata problems. The proposed work addressed several theorems which make the system efficient in obtaining optimal solutions. Finally the proposed theorems have been implemented to computer automata along with the formal language for new machine in order to validate the performance of the proposed algorithms.

Keywords Automata · Theorems · Computer language · Right state machine

1 Introduction

The Right State Machine is a mathematical model [1] of a system, which has discrete inputs and outputs. The system can be in any one of the internal Configurations or “states”. The system summarizes the information concerning past inputs that are needed to determine the behavior of the system on the subsequent inputs. The control mechanism of an elevator is a good example of a Right State Machine. The major drawback of the system is that the mechanism remembers only the service request of the current floor and all the previous requests will be vanished.

In the defective machines, errors occur due to noise and same is to be avoided[2, 3]. The input data to be processed is time-consuming and requires more mathematical formulation which is very cumbersome [4, 5]. In order to avoid this, the current research work aims at development of a discrete alphabet system which can be interfaced with communication system.

S. K. Parhi (✉)

Fakir Mohan University, Vyasa Vihar, Balasore, Odisha 765019, India

e-mail: saratkumarparhi@gmail.com

2 Notations

This study considers a message which is represented with five parameters $M = (Q, \Sigma, \delta, q_0, R)$ and the message is called a Discrete Alphabet System (DAS).

Here Q = states set

Σ = alphabet set

δ = partial deterministic state transition function

q_0 = Initial state

R = right states.

Further,

$$\begin{aligned} \delta: Q \times \Sigma \\ q_0 \in Q \end{aligned} \tag{1}$$

the transmission matrix is defined as shown in Eq. (2).

$$\delta: Q \times \Sigma \rightarrow Q \times R \text{ Such that } \delta(q_1, \sigma) = (q_2, r_1) \tag{2}$$

$R(M)$ is the accepted language by the right state machine when instructions are given to machine M .

$$R(M) = \{\omega \in \Sigma^* / \delta(q_0, \omega) \text{ is the right moves and same state to itself}\} \tag{3}$$

Here Σ^* = starting sequence has zero length.

So at the initial step,

$$\text{The transition function } \delta: Q \times \Sigma^* \rightarrow Q \tag{3}$$

In general, the alphabets can be partitioned into the set of reject symbols Σ_r , and the set of acceptance symbol $\Sigma_a = \Sigma - \Sigma_r$. A set S is a map $S: R(M) \rightarrow Q^{\Sigma - \Sigma_r}$ that determines the set of alphabets $S(s) \subseteq (\Sigma - \Sigma_r)$ to occurrence of trace $S \in R(M)$.

2.1 Case Studies

2.1.1 Case Study I

Let us consider a Right State Machine (RSM) $(Q, \Sigma, \delta, q_0, R)$ where $Q = \{q_0, q_1, q_2, q_3, q_4\}$ as shown in Table 1.

$$\Sigma = \{a, b\} \text{ and } R \subseteq Q, \quad \delta: Q \times \Sigma \rightarrow (Q, R), R \subseteq Q$$

Table 1 RSM specification

States	Inputs	
	<i>a</i>	<i>b</i>
<i>q</i> ₀	<i>q</i> ₁	–
<i>q</i> ₁	<i>q</i> ₁	<i>q</i> ₂
<i>q</i> ₂	<i>q</i> ₃	–
<i>q</i> ₃	<i>q</i> ₃	<i>q</i> ₄

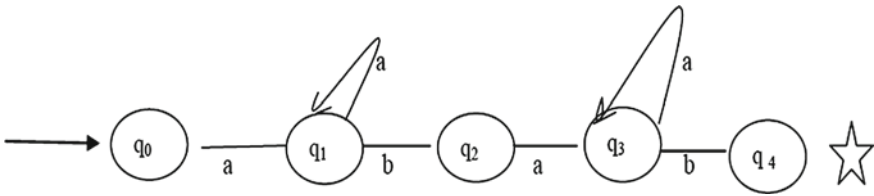


Fig. 1 Transition diagram for Table 1 case study

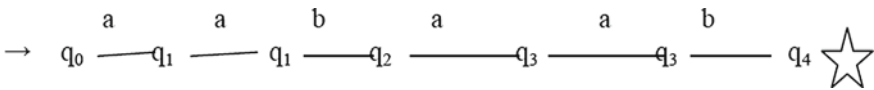


Fig. 2 Modified transmission diagram

This case the transmission diagram is obtained as represented in Fig. 1. If *a* and *b* are of even numbers, then the transitions diagram will be as per Fig. 2.

The arrow → denotes the initial state and ☆ denotes the final state.

Here, *q*₄ is the right end state.

2.1.2 Case Study II

Consider the right state machine $M = (Q, \Sigma, \delta, q_0, R)$ Where $Q = \{q_0, q_1, q_2, q_3, q_4\}$, as illustrated in Table 2

Table 2 RSM specification of case study 2

States	Inputs	
	<i>a</i>	<i>b</i>
<i>q</i> ₀	<i>q</i> ₁	–
<i>q</i> ₁	–	<i>q</i> ₂
<i>q</i> ₂	<i>q</i> ₃	<i>q</i> ₂
<i>q</i> ₃	<i>q</i> ₃	{ <i>q</i> ₃ , <i>q</i> ₄ }

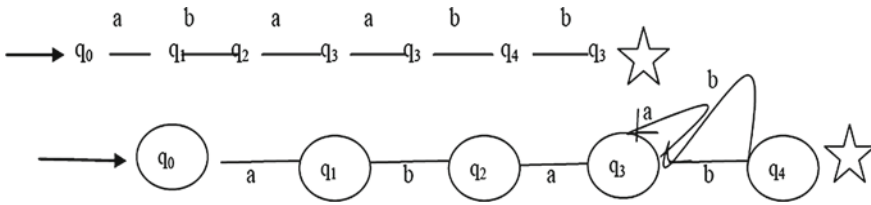


Fig. 3 Transition diagram for case study 2

$$\Sigma = \{a, b\} \text{ and } R \subseteq Q$$

Suppose the sequence is: a-b-a-b-a-b and both a's & b's are odd number and is equal to ω . Then the obtained transmission diagram is represented in Fig. 3.

3 Properties of Recursive Sets

If a set S of words over Σ to be recursive satisfies the following.

- i. The Turing machine (T^M) accepts every word in S and rejects every word in $\Sigma^* - S$.
- ii. The Right State Machine (RSM) which accepts every word in S and rejects every word in $\Sigma^* - S$.
- iii. The Finite State Machine (FSM) with two push down stores which accepts every word in S and rejects every word in $\Sigma^* - S$.

4 SKP'S Proposed Theorem

Theorem 1 *The Right State Machine is closed under complementation, That is, if S is a regular set and $S \subseteq \Sigma^*$ then $\Sigma^* - S$ is a Right State Machine.*

Proof Let S be $R(M)$ for Right State Machine $M = (Q, \Sigma, \delta, q_0, R)$ and let $S \subseteq \Sigma^*$. First let us take $\Sigma_1 = \Sigma$, for if there symbols in Σ_1 not in Σ , we can delete all transitions of M on inputs alphabets not in Σ , the fact that $S \subseteq \Sigma^*$ gives assurance that we shall not change the language of M . If there are some symbols in Σ not in Σ_1 , then none of these symbols appear in words of L . We may therefore introduce 'dead state' into M with $\delta(d, \omega) = d$ for all ω in Σ and $\delta(q, \omega) = d$ for all $q \in Q$ and $a \in \Sigma - \Sigma_1$.

Now, to accept $\Sigma^* - S$, complement the final state of M . That is let $M' = (Q, \Sigma, \delta, q_0, Q - R)$. Then M' accepts a word ω if and only if $\delta(q_0, \omega)$ is in $Q - R$, that is, ω is in $\Sigma^* - S$. Note that it is necessary to prove that M is Right State Machine and without ϵ moves.

Table 3 RSM specification

State	Inputs	
	a	b
q_0	...	q_1
q_1	q_2	...
q_2	...	q_3
q_3	q_3	...

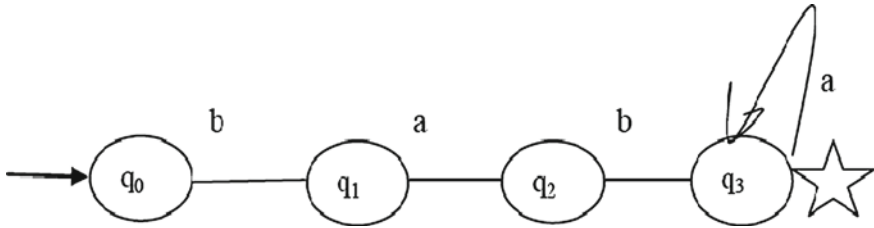


Fig. 4 Transition diagram for Example 4.1

Example 4.1 An R.S.M. that accepts string baba.

Now the R.S.M. that accepts all strings other than baba.

Here, If S is regular then there is some R.S.M. that accepts the language of S (Table 3).

The solution is represented in Fig. 4.

Suppose the even numbers of a and even number of b are in Σ^* .

The \rightarrow arrow denotes initial state and \star denotes the final state. Here q_3 is the right end state. Thus abab is in $R(M)$.

Theorem 2 The Right State Machine is Closed under the union Operation.

Proof Let us take two right state machine $M_1 = (Q_1, \Sigma, \delta_1, q_1, R_1)$ and $M_2 = (Q_2, \Sigma, \delta_2, q_2, R_2)$ that recognize sets A_1 and A_2 , respectively.

Construct M to recognize $A_1 \cup A_2$, where $M = (Q, \Sigma, \delta, q_0, R)$

(1) $Q = \{(q_1, q_2) / q_1 \in Q_1 \text{ and } q_2 \in Q_2\}$.

This set is the Cartesian product of sets a Q_1 and Q_2 . It is written $Q_1 \times Q_2$. It is the set of all pairs of states the first from Q_1 and second from Q_2 .

(2) Σ : the alphabets are same as in M_1 and M_2 . We assume that both M_1 and M_2 have the same input alphabets Σ . The theorem remains true if they have different alphabets Σ_1 and Σ_2 . We modify the proof of let $\Sigma = \Sigma_1 \cup \Sigma_2$.

(3) δ : the transition function is defined as follows for each $(q_1, q_2) \in Q$ and each $\omega \in \Sigma$, let

$$\delta((q_1, q_2), \omega) = (\delta_1(q_1, \omega), \delta_2(q_2, \omega))$$

Hence δ gets a state of M (which actually is a pair of states from M_1 and M_2), together with an input symbol and returns M 's next right state.

(4) q_0 is a pair of (q_1, q_2) .

(5) R is the set of pairs in which either member is an accept state of M_1 or M_2 , we can write it as $R = \{(q_1, q_2) | q_1 \in R_1 \text{ and } q_2 \in R_2\}$.

This expression is same as $R = \{(R_1 \times Q_2) \cup (Q_1 \times R_2)\}$.

(That is not same as $R_1 \times R_2 = R$).

This expression would define M 's accepts states to be those for which both members of the pairs are accept states.

In this case M would accept a string only both if M_1 and M_2 accept it.

This establishes the Right State Machine of M that recognizes the union of A_1 and A_2 . Thus this establishes the theorem.

Theorem 3 *The Right State Machine is closed under intersection.*

Proof $S_1 \cap S_2 = \overline{(S_1 \cap S_2)}$, where the overbar denotes complementation with respect to an alphabet including the alphabet of S_1 and S_2 . Closure under intersection then follows from closure under union and complementation. If we construct an R.S.M. for the intersection of two regular sets exist. The construction involves taking the Cartesian product of states and we sketch the construction as follows

Let $M_1 = (Q_1, \Sigma, \delta_1, q_1, R_1)$ and $M_2 = (Q_2, \Sigma, \delta_2, q_2, R_2)$ be two Right State Machines. Let $M = (Q_1 \times Q_2, \Sigma, \delta, [q_1, q_2], R_1 \times R_2)$.

Where for all $q_1 \in Q_1, q_2 \in Q_2$ and $\omega \in \Sigma$.

Then $\delta([q_1, q_2], \omega) = [\delta_1(q_1, \omega), \delta_2(q_2, \omega)]$.

It is shown that $T(R(M)) = T(R(M_1)) \cap T(R(M_2))$.

Thus this establishes the theorem.

5 Conclusion

This paper analyzed the behavior of communication system. The current study proposed theorems based on the right state machine with suitable case studies. The proposed concepts are useful to solve problems that are related to communication systems in electronics and computer science engineering fields.

Acknowledgements Thanks to Prof. Jugen Dasow for his observation of improvement of this paper.

References

1. Parhi, S.K.: A new approach of right state machine in discrete alphabet system. Int. J. Comput. Eng. Res. 5(6), 1–3 (2015)

2. Mohanty, S.R., Kumar, R.: On the synthesis of an optimal controller for a class of Discrete Event Process. In: Proceedings of First International Conference on Trends in Information Technology, CIT-98, pp. 82–86 (1998)
3. Hofcroft, J.E., Ullman, J.D.: Introduction to Automata Theory, Languages and Computation. Narosa Publishing House, New Delhi (1993)
4. Martin, J.C.: Introduction to Languages and Theory Computation. Tata Mc-Graw Hill Publishing Company, New Delhi (2005)
5. Aho, A., Ullman, J.: Principle of Compiler Design. Narosa Publishing House, New Delhi (2002)

Gleaming of Lights by Pedaling Using Arduino



T. Thirumala Rao, B. Venkateswara Rao, K. V. V. R. S. Vishnu,
and Y. Jaswanth

Abstract This paper is intended to gleam the lights and visualize the capacity of a person by his/her performance through pedaling. The idea behind this paper is the game designed for the urban community's entertainment and fitness. The performer has been given a specified count within a span to pedal and such that if he/she fails due to any cause the count display will be stopped and the performer level will be displayed through gleam of lights. The gleaming of lights works on the Arduino mega microcontroller and this is programmed using Arduino C programming. The basic working of the system is based on the pedaling by performer and this is captured by the sensor, thus resulting in the lights gleaming and matrix display displaying the level. It is designed in such a way that an average person can pedal within the program specified span.

Keywords Arduino · E-cycling · Microcontroller · Pedaling · Physical fitness

1 Introduction

Games make people enthusiastic. From past centuries games and sports have been a part of everyone's life. Starting from the Greece emperor Hercules, the founder of Olympics, who had started the competition with the intention of knowing the power and strength of a person. In the past, games and sports were meant for people who had a burning desire in them and who were passionate about their strength [1, 2]. Not more than this period it has been totally changed. The twentieth century has seen tremendous changes regarding health and workout. In the past, the people who had desire worked out hard and faced struggles in achieving the goals set by them with the available techniques [3, 4].

But by the twentieth century each sport or game is a common factor in everyone's life, this makes everyone healthier and warm minded toward their activities and in

T. Thirumala Rao · B. Venkateswara Rao (✉) · K. V. V. R. S. Vishnu · Y. Jaswanth
Department of EEE, V R Siddhartha Engineering College, Kanuru, AP, India
e-mail: bvrao.eee@gmail.com

© The Author(s), under exclusive license to Springer Nature Singapore Pte Ltd. 2021
B. Deepak et al. (eds.), *Advanced Manufacturing Systems and Innovative Product Design*,
Lecture Notes in Mechanical Engineering,
https://doi.org/10.1007/978-981-15-9853-1_30

359

this concrete jungle the only way to have peace of mind and some relief is achieved only through games and sport [5, 6]. Technology is also playing an important factor to automate these kind of activities to lure most of the people. Starting from the kids, youngsters, adults and geriatrics games are made to be easier and the goal can be achieved by just diverting their thoughts to focus on the game [7, 8].

Research Motivation

Nowadays e-fitness and entertainment plays a key role in some urban areas and metropolitan cities. Most of the people are so enthusiastic in performing these kinds of activities. The cities with places such as the malls have thrown back the throne of the parks, amusement parks, etc. Most of the people are being attracted to its fantasy and their regular service. The malls propagated such a model that kids, youngsters are finally lured by their amusements. Authors propose the fun creation in frolic activities coming with a prototype. The motif has the Arduino microcontroller in which most of the prototypes are figured. The exercise bikes are a form of indoor cycling and these are organized with a group fitness format. By using this stationary bike the performer will have the endurance of ultimate strength.

The propagated mall with this luring activity is the Trendset mall in Vijayawada. It is unique in its own way. The mall proposes the sample amusements to be performed every time and this time they have proposed an activity to be performed with the exercise bikes in order to lure many people.

2 Solution Methodologies

Various solution methodologies on e-cycling are discussed further.

2.1 Revolutions Measurement with IR Sensor

This method is achieved by fixing a black color strip on the rotary wheel such that the IR sensor is stationary and when the strip crosses the IR sensor sends the signal. The timer runs according to the code and for a specified time in seconds the count should be met, so that the count and seconds are compared with the preset values. But there are some drawbacks in this method, for instance when the rotary part over speeds then it misses the count and just skips the count to be added, the IR sensor senses the false count under some instants at overspeed and dark surfaces or spots. Such that the IR sensor makes the count even when the strip doesn't pass through it. From the above analysis the solution is not perfect. IR sensor interfaced with Arduino is shown in Fig. 1.

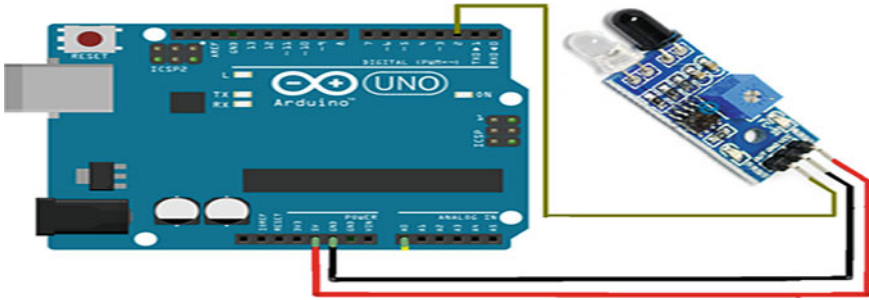


Fig. 1 IR sensor interfaced with Arduino

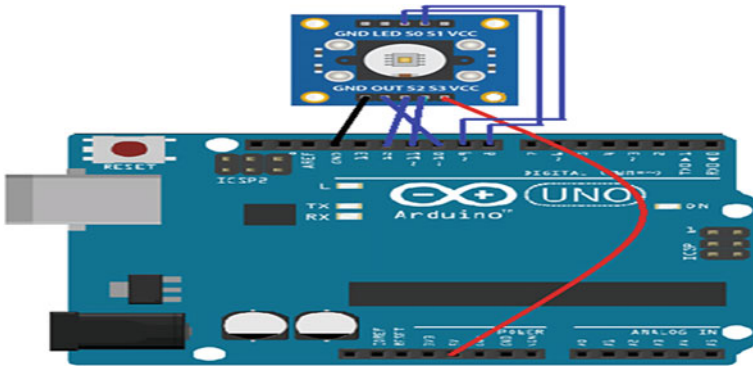


Fig. 2 Color sensor interfaced with Arduino

2.2 *Revolutions Measurement with Color Sensor*

The colored strip is placed on the rotary part such that the sensor is placed on the side and made to be stationary and the no of times the color band passes through the sensor makes the count. Drawbacks in this is the color sensor is similar to the IR sensor and it has the same drawback while at over speed it misses the count or false count may occur. Color sensor interfaced with Arduino is shown in Fig. 2.

2.3 *Revolutions Measurement with Accelerometer Sensor*

The acceleration sensor can measure the speed and the distance traveled and the sensor is placed toe to toe of the rotary element. The microcontroller performs the logic and compares with the preset speed and distance with respect to time. Such that the user or the participant will have to maintain the preset speed but not less than period of time specified which allows him to the next level. Accelerometer sensor

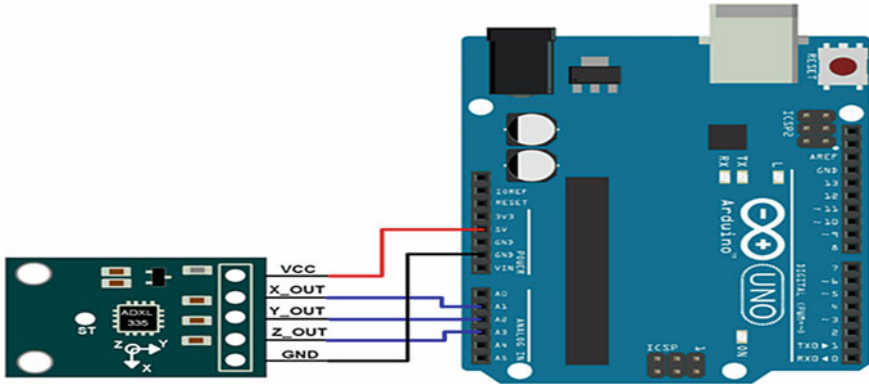


Fig. 3 Accelerometer sensor interfaced with Arduino

interfaced with Arduino is shown in Fig. 3. This sensor can be used and this makes the user assume the pedaling speed that he can make.

2.4 *Revolutions Measurement with Hall Sensor*

The hall sensor produces the pulse when the magnetic field is introduced. This sensor is chosen as per its accuracy and compatible size, compared to the remaining sensors. It has a fast response to magnetic field and there is no miss count or over count as the count exists only when the magnet cuts the sensor face. Hall sensor interfaced with Arduino is shown in Fig. 4.

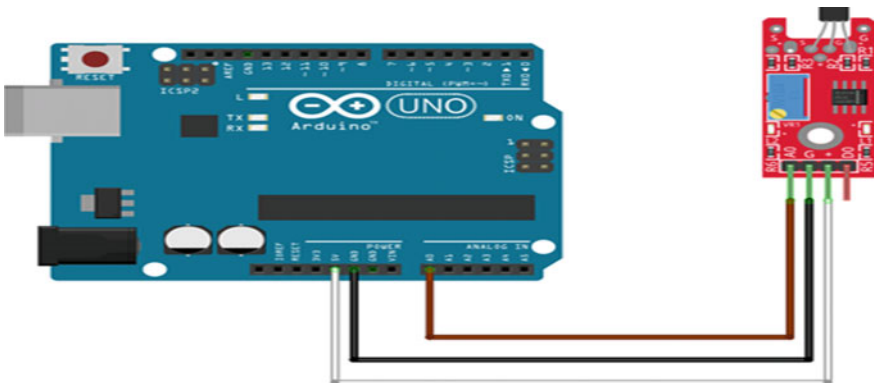


Fig. 4 Hall sensor interfaced with Arduino

3 Problem Description

Gleaming the lights and a doll to be moved after certain count of pedaling. The lights are led strips which are to be lightened up when the person crosses the certain limit of count, i.e. to indicate the next level such that he had completed the level on time and before reaching the final level successfully the doll starts clapping and cheering up indicating the final level. The counting of rotations is achieved by using the sensor and this sensor data is then generalized for the comparison in the Arduino microcontroller. Choosing the sensor is based on sensor accuracy, compact size and cost. The crisis is the power supply to the relay module to lighten up the led and the P10 display to display the level and status of the person. Here there is a distortion in the P10 display and led to blink without any interruption, and this malfunction is due to the Arduino board when it is driving both display and relay for led with Arduino. Choosing of right Arduino board to eradicate this problem manages max error.

Components required are Microcontroller, Sensor, Relay module, P10 display, Led rope, doll and Power supply. The microcontroller is the device which has a set of instructions to be performed. The microcontrollers are of multiple designs and architecture [9]. The selection of microcontroller is based on its application. The Arduino microcontroller is well suited for the motif proposed, as it has simple architecture and instruction set that everyone can understand. Arduino has several boards with different architecture. Selection of board is based on the requirements specified. Regarding the usage in the Trendset mall 13 led ropes with P10 display are interfaced such that the Arduino mega board is enough to meet the requirement. The timer is run when the user starts pedaling and this is programmed in the Arduino and at the instant user pedals the program starts executing with the logic written.

The sensor is generally based on the Hall Effect principle in which it generates a pulse when a magnet passes through it. The foremost interesting part is the connection of the sensor to the Arduino pin of an external interrupt pin and in which it counts the pulse whenever a falling edge pulse appears. The working of the sensor is simple and is described in [10]. The output module such as displays, driving circuits, memory elements, etc., are to be driven by external supply and signaling is done through the Arduino board according to the code dumped on to the board. The P10 display, doll and the relay have an external power supply module in which these are being controlled by Arduino [11, 12]. The P10 board is of 32×16 type which displays the content through different libraries available in the Arduino. The complete block diagram is shown in Fig. 5.

4 Results and Discussion

The hall sensor is energized when the magnetic flux lines passes through it, then it actuates a pulse. The magnet is fixed on the rotary part and the sensor is placed in such a way that the sensor face is just a bit gap with the magnet to be moved (in front

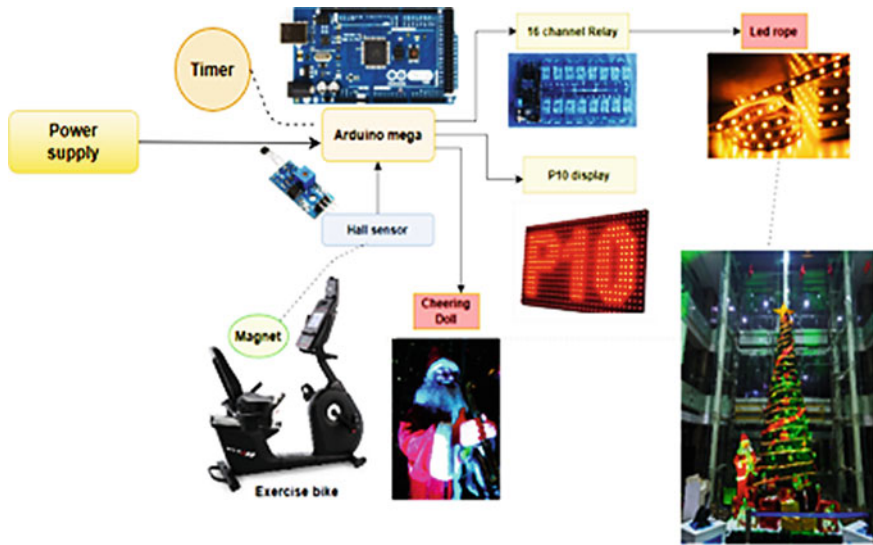


Fig. 5 Block diagram

of). The Arduino MEGA 2560 is chosen such that the P10 display board and relays (13) are controlled. The hall sensor sends the data to the Arduino microcontroller in which the preset count is to be compared. When the user starts pedaling the timer starts. According to the level of count and prefixed time the user has to achieve in a short duration than the one mentioned. Else he fails the level even though he completes the count such that the level of lights stops gleaming for a certain range. The P10 displays the level and imitates with a caption. Flow chart of the model is shown in Fig. 6.

Pedaling of exercise bike by a user and viewing of the level with gleaming of lights rolled on the tree model. Figure 7 shows the 7th level of the user.

Table 1 shows the count and revolutions with respect to the time in seconds such that the user has to complete the task. If he passes then the level will be gained and incremented to the next level by indicating through gleam of lights and level number, else indicating the past level gleam of lights and the caption to be scrolled on the display. If an average person is pedaling for 20 s continuously, his/her performance will slow down eventually, such that he/she can pedal up to 5th stage successfully.

From stage 6 it possesses the limited time for vast pedaling cycles to be done. This can be achieved by some gym person and for good cyclists, but for an average person the chances are less to achieve the full levels. The idol dances and cheers up when the user pedals to such a level.

The model is experimented in two phases

- i. The basic model, it uses the sensors such as color sensor, IR sensor and hall sensor. Although the accelerometer sensor is more accurate but for the count it

Fig. 6 Flow chart of model

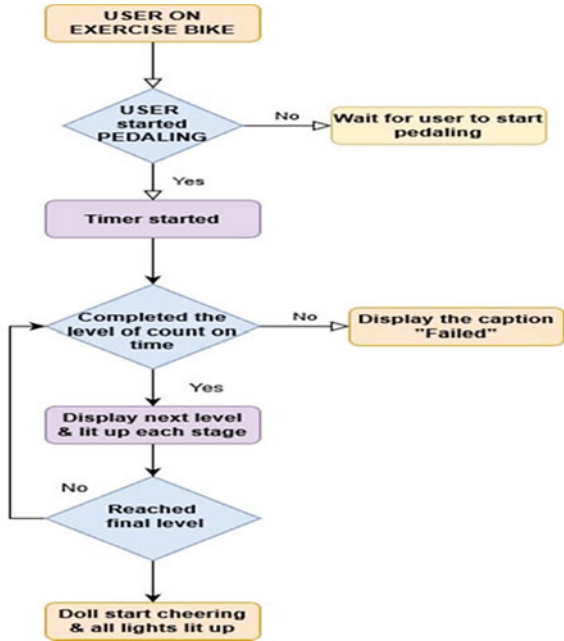


Fig. 7 Final model with display



Table 1 Time and revolution to be done by user from stage 1 to stage 13

Count/revolutions to be made	Time (s)	Captions displayed on P10 display and leds gleamed on the tree	
		If passed	If failed
10	4	1st stage 1 light gleams	U kid! No light gleams
20	8	2nd stage 2 lights gleam	Kidoo! Stage 1 lights gleams
30	12	3rd stage 3 lights gleam	Just a bit lazy! Stage 2 lights gleam
40	16	4th stage 4 lights gleam	Can do better Stage 3 lights gleam
50	20	5th stage 5 lights gleam	Stage 4 lights gleam
60	24	6th stage 6 lights gleam	Don't lose again Stage 5 lights gleam
70	28	7th stage 7 lights gleam	Good, try again Stage 6 lights gleam
80	32	8th stage 8 lights gleam	Very good, try again Stage 7 lights gleam
90	36	9th stage 9 lights gleam	Better, try again Stage 8 lights gleam
100	40	10th stage 10 lights gleam	Nice, try again Stage 9 lights gleam
110	46	11th stage 11 lights gleam	Rigid, try again Stage 10 lights gleam
120	52	12th stage doll starts 12 lights gleam	Ultimate, try again Stage 11 lights gleam
130	60	13th stage 13 lights gleam Yay you completed	Wow! try again Stage 12 lights gleam

isn't suitable. The sensors are tested in different cases such as E-bike, Cycle, gym cycle.

- ii. The final model at the Trendset mall is developed with hall sensor, because this sensor has more accuracy and sensitivity. All the work entitled including the doll, gleaming of lights took nearly 27 h continuously with trials.

5 Conclusion

The attributed gleaming of lights through pedaling has been used by most of the visitors of the Trendset mall. In such a way that the proposed model is well suited

in the urban and semi-urban areas as a part of enjoyment to the metropolitans, the citified culture is being inculcated with the new trends as the proposed model does.

Acknowledgements Authors are thankful to Dr. P. V. R. L. Narasimham, Professor & Head EEE Dept, Velagapudi Ramakrishna Siddhartha Engineering College and Sri Vamsi, Trensdet Mall, Vijayawada and Trendset mall management for their generosity and the gracious chance that they have favored to showcase our talent.

References

1. Haskell, W.L., Lee, I.M., Pate, R.R., et al.: Physical activity and public health: updated recommendation for adults from the American College of Sports Medicine and the American Heart Association. *Circulation* **116**(9), 1081–1093 (2007)
2. Consolvo, S., Klasnja, P., McDonald, D.W., et al.: Goal-setting considerations for persuasive technologies that encourage physical activity. In: 4th International Conference on Persuasive Technology, pp. 1–8. ACM (2009)
3. T Park, I Hwang, U Lee et al. (2012): ExerLink: enabling pervasive social exergames with heterogeneous exercise devices, 10th International Conference on Mobile Systems Applications and Services ACM, 15–28
4. Rajesh, M.V., Venkateswararao, B.: Conference hall automation system using Python-Kivy application. *Int. J. Innov. Technol. Expl. Eng. (IJITEE)* **8**(6S4), 446–449 (2019). ISSN: 2278-3075. <https://doi.org/10.35940/ijitee.f1092.0486s419>
5. Hafsa, B.V., Rao, G.S., Ganesh, Ch.: Modeling and Implementation of Single-Phase Z-Source Inverter using Arduino. *Int. J. Innov. Technol. Expl. Eng. (IJITEE)* **8**(2S), 35–40 (2018)
6. Foster, C., Florhaug, J.A., Franklin, J., et al.: A new approach to monitoring exercise training. *J. Strength Cond. Res.* **15**(1), 109–115 (2001)
7. Agarwal, D.: Amusement and leisure theme park: the future of Indian tourism. *Int. J. Emerg. Trends Inf. Knowl. Manag.* **1**(1) (2017)
8. Kooijman, J., Meijaard, J.P., Papadopoulos, J., Ruina, A., Schwab, A.: A bicycle can be self-stable without gyroscopic or caster effects. *Science (New York, N.Y.)*. **332**, 339–342 (2011)
9. Jones, T., Harms, L., Heinen, E.: Motives, perceptions and experiences of electric bicycle owners and implications for health, wellbeing and mobility. *J. Transp. Geogr.* **53**, 41–49 (2016). <https://doi.org/10.1016/j.jtrangeo>
10. Hartmann, F.: The relationship between the physical activity single item question and the Global Physical Activity Questionnaire (GPAQ). Master thesis, ETH Zurich (2017)
11. Jaswanth, Y., Rachana, R., Venkateswara Rao, B.: Protection of microgrids with Arduino control scheme. *J. Controller Convert. MAT J.* **4**(3), 43–49 (2019)
12. Rajesh, M.V., Venkateswararao, B.: Artificial intelligence based machine learning assistance for self-driving car using Raspberry Pi. *Int. J. Adv. Res. Sci. Eng.* **6**(11), 1718–1724 (2017)

A Vision-Based Unstructured Road Detection Algorithm for Self-driving Cars



R. Rajesh and P. V. Manivannan

Abstract Unstructured road detection is one of the difficult tasks for self-driving cars than the detection of road with proper lane markings. Also, it is an extremely difficult task to detect the highly deteriorated district and taluk roads using currently available vision-based algorithm; as the exposed gravels and grass covering on both sides (edges) of road adds more noise in the input image. To address this issue, a novel vision-based road detection technique is proposed in this research work. This new method uses noise to enhance the road edges in the image and unstructured straight road is detected using Hough Transform. This paper is divided into three parts: bird's eye view transformation of 2D road image received from the vehicle camera to correct the perspective distortion and easier identification of Region of Interest (ROI), addition of noise in the ROI of image to differentiate the valid road from the background and use of Hough Transform to identify the edges of unstructured road having no road markings. Finally, we present a simple way to find the centerline on the detected road for departure warning to reduce the additional computation. The simulation results corroborate that the proposed method detects the road successfully and can be used in real-time detection system.

Keywords Autonomous road vehicle · Unstructured road detection · Image feature enhancement

1 Introduction

The common causes for more road accidents and causalities are reckless over speeding, alcohol consumption while driving, driver fatigue, distraction, and others. In the year 2018 alone, India reported more than 467,044 road accidents resulting in

R. Rajesh (✉) · P. V. Manivannan
Indian Institute of Technology Madras, Chennai, India
e-mail: rajeshravi1396@gmail.com

P. V. Manivannan
e-mail: pvm@iitm.ac.in

© The Author(s), under exclusive license to Springer Nature Singapore Pte Ltd. 2021
B. Deepak et al. (eds.), *Advanced Manufacturing Systems and Innovative Product Design*,
Lecture Notes in Mechanical Engineering,
https://doi.org/10.1007/978-981-15-9853-1_31

369

151,417 mortalities, injuring close to 469,418 people. The majority of people (64.4%) were killed due to over speeding [1]. The major reasons for accidents are driver errors like: high speed, driving in opposite direction, not following road rules/ignoring traffic signals, driver fatigue leading to losing alertness coupled with unexpected pedestrian/animal crossing. Almost 93% of accidents are due to driver errors only [2]. Hence, the introduction of a self-driving vehicle is expected to improve the safety of the driver and passenger, increase traffic density, reduce environmental damages, and reduction road accidents due to human errors and related causalities [3]. In addition, lane detection and lane departure warning (LDW) systems are important in avoiding collisions in roads. However, the lane detection algorithms currently in use require proper lane markings on the road to be get detected and they fail (or) poorly detect the lane marking of deteriorated roads. So, there is a need for road edge detection algorithm to detect unstructured deteriorated roads without any road markings, poor road surface, indistinguishable color texture. In this research work, we have come up with a novel road edge detection algorithm that takes care of noise in the unstructured road image. The proposed method adds noise in the raw road image to enhance pixels of road edges and uses Hough Transform to identify the edges and centerline of ROI of the road without any difficulty.

2 Relevant Work

For the past few decades, a greater number of researchers are working to improve the performance of intelligent transportation systems (ITS). The notable work starts with development of LDW system that throws an alert, if the vehicle crosses the centerline of the lane [4]. The major challenges with lane detection are: missed lane markings, faded out lane lines, low light (night time), and noise in the image [5].

The main problem with lane detection is detecting both sides of the lane boundaries. To make the computationally efficient lane detection algorithm, color-based segmentation method [6], was used. However, this method is not suitable, if illumination problem is there due to reflection. A fan scanning detection [7] is used to remove interference and this approach explores the edge pixels from left to right and also from bottom to top, to calculate the line segment in detecting adjacent lane to improve the ADAS. This method is purely based on the thresholding process. The unstructured scenes are more stirred by illumination variation; hence, it is harder to incur robust appearance with offline training. To overcome this, the sample region selection is done automatically by a vanishing point and the border of the sample region is selected by projecting the imaginary rays [8]. Subsequently, graph-based segmentation is used to initialize the subregions as one pixel and based on the color difference between subregions, the neighboring subregions are unified iteratively but its computational cost is high. In [9], vanishing point-based segmentation is used to detect the lane region.

To make the efficient lane detection method, researchers [10] have proposed a Hue, Saturation, Value (HSV)-based image denoising by using Gaussian filter and

adaptive ROI. Then, the lane line segment is detected and tracked using Hough Transform and Extended Kalman filter, respectively. This method performs well for roads with proper lane markings, but not suitable for unstructured roads. An FPGA based dual-stage lane detection algorithm was proposed [11] to tackle the difficulties like shadows, occlusion, brightness variation. An adaptive threshold-based unstructured road detection method was proposed to detect the lanes under the influence of light, shadows, and other adverse factors [12]. However, it is suitable only for the lane which can be easily identified from the background.

By using Hough Transform lane marking are detected and by using Lateral Offset Ratio (LOR) [13], based framework the lane departure warning is issued, when vehicle deviates from the centerline. However, this method adds computational burden for the lane departure warning system. The lane departure prediction based on the number of frames was proposed to reduce the computation [14], but it is not accurate. All these methods are meant for the regular roads with lane marking. From the literature survey, it is ascertained that there is a need for an algorithm to detect unstructured road which could not be easily identified from the noisy background.

3 Methodology

In this work, image processing techniques: Color to Grayscale conversion, Histogram equalization, adding noise, image sharpening, edge detection, and selecting ROI have been performed on the raw image to enhance its quality, before road edges were detected using Hough Transform. The input image was captured using a mobile phone camera (having 3456×4608 resolution) and is converted into a bird's eye (top) view using inverse perspective mapping to correct the perspective distortion of road before the preprocessing steps. The road edges are detected using Hough Transform and the methodology followed in this work is shown in the Fig. 1.

3.1 *Inverse Perspective Mapping for Bird's-Eye View*

The true parallel road edges appear to converge in 3D space due to perception distortion and this can be corrected through Inverse Perspective Mapping (IPM) and its output is called bird's-eye view. Bird's-eye view gives the top view of the input front-facing image where, the parallel road edges appear parallel, a necessary condition for detecting the curved lane. In this work, the unstructured road image captured by the vehicle camera is a perspective distorted; hence, it is difficult to distinguish the valid road width at faraway point. The perspective distortion needs to be corrected before further processing video data to identify the road edges (i.e. similar to lane marks in highway). The input image is taken using a mobile phone camera at 3456×4608 resolution. As it is computationally expensive to process such high-resolution images fully, only an image section representing 10 m distance ahead of camera is

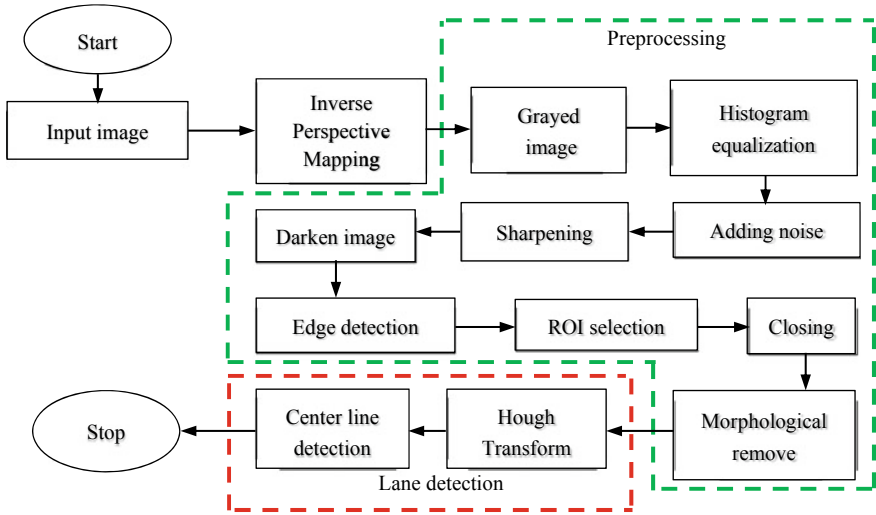


Fig. 1 The proposed methodology for unstructured road detection

converted into Bird’s-eye view image (top view image) with reduced resolution of 480×640 pixels. To perform this conversion, we need camera parameters. For that, we initially calibrated the camera using a checkerboard image of 20×20 mm size in MATLAB and the transformation is done using “birdsEyeView” MATLAB function. The camera parameters used for the bird’s-eye image are shown in Table 1. The top view image retains all the information as in the original input image.

Table 1 Parameters used for bird’s-eye view image

Parameters	Values
Focal length $[f_x, f_y]$	$[3614, 3618]$ pixels
Principal point $[cx, cy]$	$[2328, 1720]$ pixels
Input image size $[H, W]$	$[3456, 4608]$
Intrinsic matrix	$\begin{bmatrix} 3614 & 0 & 0 \\ 0 & 3618 & 0 \\ 2328 & 1720 & 1 \end{bmatrix}$
Height from ground	1.5 m
Pitch	0
The distance ahead of sensor	10 m
Space to one side	2.5 m
Bottom offset	3 m
Output image size $[H, W]$	$[480, 640]$

3.2 *Image Preprocessing*

As our input image is an unstructured street road made of red soil and basalt/granites which is in a deteriorated state and covered by grasses on each side of the road. It is impossible to segment the image based on Hue, Saturation, Value image. Hence, we convert the RGB image into a grayscale image based on the luminosity method as given in Eq. (1).

$$\text{Grayscale} = ((0.3 * R) + (0.59 * G) + (0.11 * B)) \quad (1)$$

To enhance the contrast of the image, histogram equalization is done. This will make the white as whiter and black as blacker, and easier to identify the feasible road region. The bird's-eye image is having noise because of stretching the front-facing image. So, it is difficult to reduce the noise by applying image filters instead, we added salt and pepper noise with a noise density of 0.05. Now, the added noise on the histogram equalized image gives you the distinguishable road region from the background. After that, region of interest for the feasible road is selected manually using a polygon with defined pixel coordinates. Then, sharpen the selected region of interest using the ROI filter to get the virtually segmented road region. Here, thresholding is not applicable because of the color texture of the input image. Hence, the sharpened image is added with -50 constant value to darken the image. This makes the image to be easier for the region of interest selection for lane boundary. A canny edge detector is applied to detect the edges on the darkened image, and neglect edges occupying less than 30 pixels to get rid of smaller objects.

Based on the variation between detected edges on ROI sharpened portion and background is considered as the ROI of lane boundaries. Hough transform cannot be directly applied to the ROI of lane boundary because of its open edges, it may lead to give wrong Hough peaks. Hence, the ROI of lane boundary is undergone morphological operations like closing and remove. The closing operation makes the edges as solid white lines and remove operation removes the interior pixels of the white line. With this, preprocessing steps are over.

3.3 *Lane Detection*

Hough Transform (HT) is the most familiar technique for detecting straight lines. After completing the preprocessing stage, the lane line segments are detected using Hough Transform. The standard Hough Transform uses the parametric representation of a line is given by Eq. (2).

$$\rho = x \cos \theta + y \sin \theta \quad (2)$$

Fig. 2 The relation between lane line and Hough transform

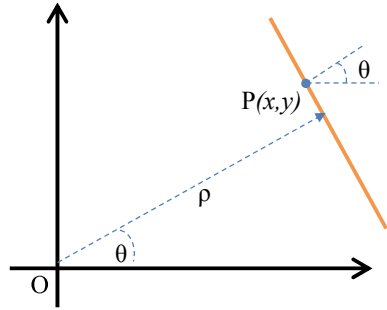
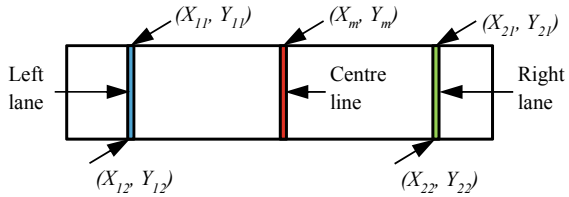


Fig. 3 Detected left and right lane along with the centerline on top view image



where, ρ is the distance from origin to the line passing through $P(x, y)$, θ is an angle in degrees between the x -axis and the ρ vector. The relation of the lane line and the Hough Transform is depicted in Fig. 2.

CenterLine Detection. The centerline between the detected lanes can be determined by Eq. (3) and Fig. 3. depicts the detected lanes with a centerline. X_m is same for all Y_m values which varies from 40th pixel to 420th pixel with an increment of 10 pixels on a bird's-eye view image. Using Eq. (3), the centerline can be determined for the lane departure with zero additional computation cost. If the centerline along the vehicle's Y-axis deviates from the detected centerline of the road, the vehicle throws departure warning.

$$\text{Center line } (X_m) = ((X_{22} - X_{12})/2) + X_{12} \tag{3}$$

4 Simulation Results

The simulation is done on MATLAB R2018a with Intel(R) Core (TM) i5-7200U CPU @ 2.50 GHz, 12 GB installed RAM, and $\times 64$ based processor. An Oneplus6 mobile phone camera is used to take the input image. The simulation results (Figs. 4, 5, 6, 7, 8, 9, 10, and 11) show that the proposed method successfully detects unstructured road lane.

During the image preprocessing steps, the noise and illumination variations due to sunlight are taken care of by adding noise, sharpening, and darkening the

Fig. 4 Input image



Fig. 5 Bird's-eye view using IPM



Fig. 6 Adding salt and pepper noise

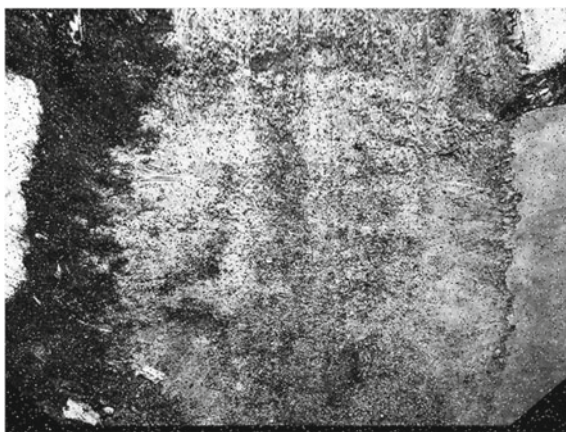


Fig. 7 Sharpened image

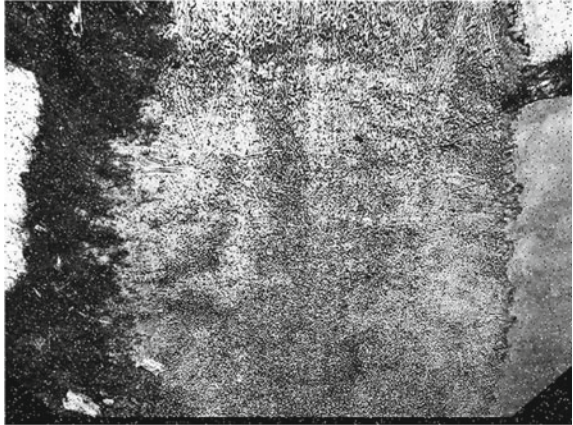


Fig. 8 Extracted left lane

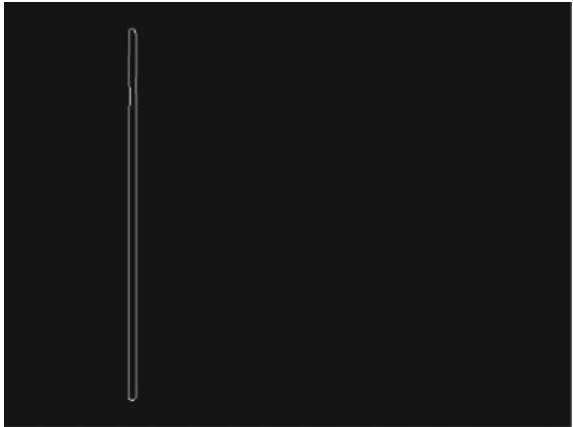


Fig. 9 Extracted right lane

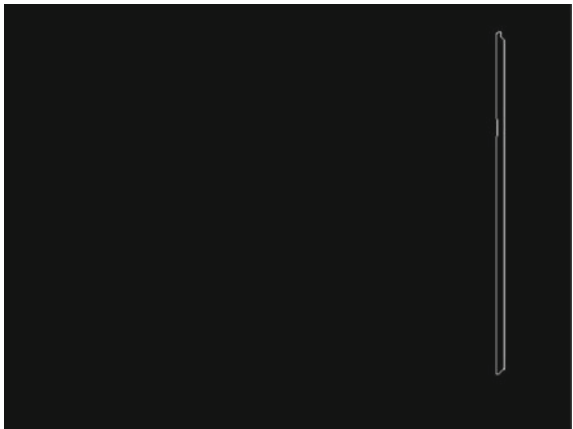


Fig. 10 HT-based detected lanes

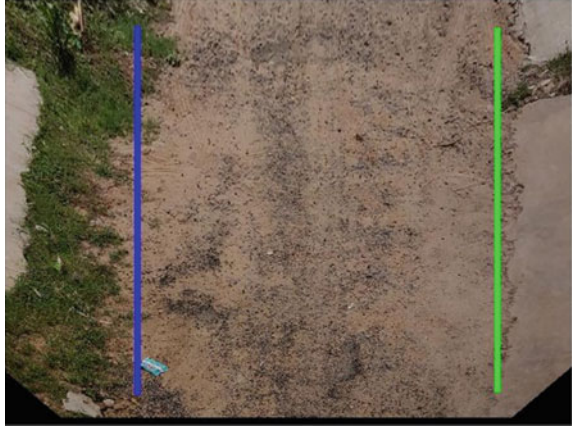


Fig. 11 Detected lane with centerline

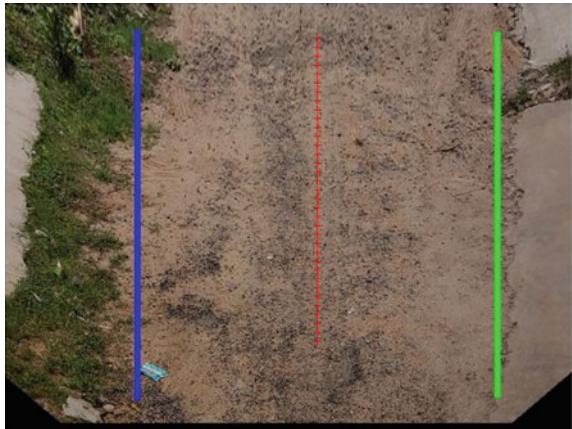


image. Hence, the proposed algorithm shows robust performance in detecting the unstructured road lanes under the influence of heavy noises and sunlight.

4.1 Comparative Study

To evaluate the performance of the developed algorithm, the algorithm was made to run for 200 iterations on the same platform used for the simulation and the average computation time achieved is 1.54 s. Also, the developed method is 1.82 and 1.97 times faster than the sample region based on vanishing point and imaginary ray method, and edge-based method, respectively. The comparative result is shown in the Table 2.

Table 2 Performance comparison

Method	Image size	Average time (s)
Kong et al. [9]	240 × 180	3.04
Phung et al. [8]	100 × 140	2.81
Proposed method	480 × 640	1.54

5 Conclusion

In this paper, we proposed a novel vision-based unstructured road detection technique uses a new method of image preprocessing steps and Hough Transform to detect lanes. First, the input image is converted into a top view image then, applied the preprocessing steps to select the ROI based on canny edge detector results. Secondly, HT-based lane detection is done along with a simple centerline detection for lane departure warning. The proposed method shows good detection results on highly deteriorated roads influenced by noise and sunlight. In this work, Region of Interest (ROI) is selected based only on the intensity difference between the sharpened area and background. In the future, it is proposed to use adaptive ROI selection to make the algorithm more robust.

References

1. Saluja, N.: Road Accidents Claimed Over 1.5 Lakh Lives in 2018, Over Speeding Major Killer. The Ministry of Road Transport, India (2019)
2. Direct, Budget: Car Accident Statistics 2019. Auto & General Services Pty Ltd, Australia (2019)
3. Atkins Ltd.: Research on the impacts of connected and autonomous vehicles (CAVs) on traffic flow, U.K. Dept. Transport, London, U.K. (2016)
4. Chen, M., Jochem, T., Pomerleau, D.: Aurora: A vision-based roadway departure warning system. In: Proceedings of IEEE RSJ Intelligent Robots and Systems, issue no. 03, pp. 243–248 (1995)
5. Nguyen, V., Kim, H., Jun, S., Boo, K.: A study on real-time detection method of lane and vehicle for lane change assistant system using vision system on highway. *Eng. Sci. Technol. Int. J.* **21**(5), 822–833 (2018)
6. Chiu, K.Y., Lin, S.F.: Lane detection using color-based segmentation. In: IEEE Proceedings. Intelligent Vehicles Symposium, pp. 706–711 (2005)
7. Wu, C.F., Lin, C.J., Lin, H.Y., Chung, H.: Adjacent lane detection and lateral vehicle distance measurement using vision-based neuro-fuzzy approaches. *J. Appl. Res. Technol.* **11**(2), 251–258 (2013)
8. Phung, S.L., Le, M.C., Bouzerdoum, A.: Pedestrian lane detection in unstructured scenes for assistive navigation. *Comput. Vis. Image Underst.* **149**, 186–196 (2016)
9. Kong, H., Audibert, J.Y., Ponce, J.: General road detection from a single image. *IEEE Trans. Image Process.* **19**(8), 2211–2220 (2010)
10. Li, M., Li, Y., Jiang, M.: Lane detection based on connection of various feature extraction methods. *Adv. Multimedia* (2018)
11. Malmir, S., Shalchian, M.: Design and FPGA implementation of dual-stage lane detection, based on Hough transform and localized stripe features. *Microprocess. Microsyst.* **64**, 12–22 (2019)

12. Wu, L., Yu, Q., Xu, T., Zhang, S.: An unstructured road detection method with multi-environmental adaptability. *Int. J. Simul. Syst. Sci. Technol.* **17**(12) (2016)
13. Em, P.P., Hossen, J., Fitriani, I., Wong, E.K.: Vision-based lane departure warning framework. In: *Heliyon*, vol. 5, issue no. 8 (2019)
14. Yi, S.C., Chen, C., Chang, C.H.: A lane detection approach based on intelligent vision. *Comput. Electr. Eng.* **42**, 23–29 (2015)

Experimental Investigation of Automatic Aeration Process and Condition of Aqua Ponds Monitoring System with the Help of Internet of Things



Mummina Vinod, M. Raghuraman, and V. Mahesh Chakravarthi

Abstract The operating cost and investment cost increases every other day in the field of aquaculture and one of the most common issues in the aquaculture is the deficiency of oxygen in the pond. To overcome this situation, the farmers are using aeration process, this process might be easier for observation but, it needs a lot of human effort and cost for maintenance. In traditional method most of the farmers are operating these aerators in the time interval bases but not on the basis of DO (Dissolved Oxygen) and weather temperature conditions, due to this the operating cost is very high and the productivity is also low. To overcome all these problems an automated aeration system is designed along with an application and it is work on the basis of Internet of things platform. In this system DO sensor, temperature sensor and some other mechatronic elements are used, according to the inputs given by sensors the aeration process is working and the farmer can monitor the system from any location without any human observation at pond. One main advantage in this system is that it can turn off the aerators automatically when there is no necessity of working in order to save the power. An experiment was conducted with this system in Bhimavaram, Andhra Pradesh and we had compared the process parameters with the traditional method.

Keywords Dissolved oxygen · Aeration · Aquaculture · Internet of things

1 Introduction

Dissolved Oxygen is very essential in aquaculture it places a major role especially in Shrimp ponds. DO indicates the quality of the pond water and health of the aqua animals. If DO concentration is very low, it will cause stress, low growth rate, poor appetite, increases of disease and leads to death in aqua animals [1]. The Fig. 1 shows the problems faced by the aqua farmers. The DO concentration in aqua pond

M. Vinod (✉) · M. Raghuraman · V. M. Chakravarthi
Vishnu Institute of Technology, Bhimavaram, Andhra Pradesh 534202, India
e-mail: vinodmummina@gmail.com

© The Author(s), under exclusive license to Springer Nature Singapore Pte Ltd. 2021
B. Deepak et al. (eds.), *Advanced Manufacturing Systems and Innovative Product Design*,
Lecture Notes in Mechanical Engineering,
https://doi.org/10.1007/978-981-15-9853-1_32

381



Fig. 1 Death of prawns due to low DO and breaking of aerators due to heavy loads

Table 1 Level of growth in international shrimp farming

Level	Providing of feed	Aeration	Yield range in kg/ha
Extensive	Not provided	Not provided	Less than 500
Semi-intensive	Provided	Not provided	500–2500
Intensive	Provided	Provided	2500–10,000
Super-intensive	Provided	Provided	Greater than 10,000

is depends on salinity and water temperature, DO level decreases with the increasing of both these parameters. The degree of pond water turbulence and degree of sunlight penetration with water also affect the DO level in the pond. Different aqua animals need different DO levels, for warm water fishes minimum 5 mg/L [5] is mandatory and for coldwater species minimum 6 mg/L [5] is mandatory. Therefore the required DO level for Shrimp cultivation is 4 to 5 mg/L or higher [2, 3], Salinity is 10–28 ppt and the temperature range is 24–34 °C [2]. So aqua farmers should maintain sufficient amount of DO in the pond otherwise they may get losses due to low growth rate or potential death of aqua animals. To avoid all these problem, farmers are using aerators in the aqua ponds. The aerators will mix the atmospheric air (oxygen) with water to increase the amount of oxygen content in water. Table 1 [2] represents the yield difference between, with aerators and without using of aerators. It is hard to maintain the required Dissolved Oxygen value and salinity of water without any mechanical aeration system.

1.1 Current Approach

In current approach to run the aerators a continuous human observation is required even at night time also because DO level decreases during the night time compared with daytime [4]. Monitoring of ponds during the night time is very risk for the farmers and also it is very tough job for them, so farmers are spending lot of money for labors to operating aerators during night time. According to DO level and weather



Fig. 2 Current approach method

conditions we should run the aerators otherwise the oxygen content in the pond will get reduced and leads to fish deaths. The majority of farmers run the aerators according to time basis only but not on the basis of DO level and temperature, due to this there is a chance to wastage of power and aerators may be damaged due to heavy loads. In case if we not run the aerators at required time then the loss will be very high. So 24 × 7 human observation is required for current approach. The Fig. 2 shows the current approach.

1.2 Empirical Relations of Aerators

The performance of the aerators is completely depending upon the Standard Aeration Efficiency (SAE) and Standard oxygen-transfer rate (SOTR). SOTR [6] is defined as the amount of the oxygen transferred to a water body in unit time under standard conditions.

$$SOTR = K_{La20} \times (C^\circ - C_0) \times V = K_{La20} \times 9.07 \times V \times 10^{-3} \quad (1)$$

where:

$$K_{La20} = \frac{(K_{La})_T}{\varnothing^{T-20}} = \text{Coefficient of overall oxygen transfer at } 20^\circ\text{C (h}^{-1}\text{)}$$

$$(K_{La})_T = \text{Coefficient of overall oxygen transfer at } T^\circ\text{C (h}^{-1}\text{)}$$

$$\varnothing = \text{correction factor for temperature} = 1.024(\text{for clean water})$$

C° DO saturation value at rest condition (mg/L)

- C_0 Concentration of initial DO (mg/L)
 9.07 Saturated dissolved oxygen level of clean water in (mg/L) at 20 °C and saturated atmospheric pressure
 V Water volume (m³)
 10^{-3} Units Converting Factor to kg

SAE [6] is defined as the amount of oxygen transferred per unit of energy input.

$$\text{SAE} \left(\frac{\text{kg O}_2}{\text{kWh}} \right) = \frac{\text{SOTR}}{P} \quad (2)$$

where:

- $P = \left(\frac{2\pi N \tau}{60} \times 10^{-3} \right)$ Power required to run the aerator shaft (kW)
 N Speed in rpm
 τ Torque.

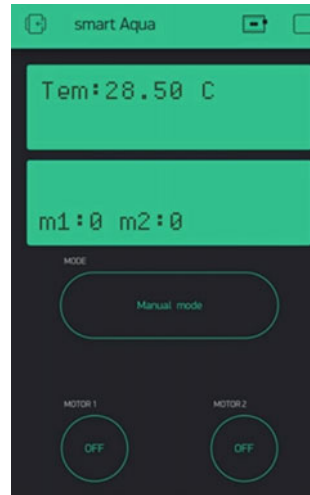
2 Proposed Approach

To overcome all the problems in the current approach we proposed a smart aqua system which is works on the Internet of things. It allows the aerators to run only when the DO level and temperature levels are not in desired range and hence no need of human monitoring. Farmers are able to know the condition of the pond like DO level, temperature of the aqua pond water and the working of the aerators with the help of monitoring application installed in their smartphone from any location. The WiFi module (ESP8266) is the only component that is responsible for the working of entire application along with DO sensor and temperature sensor. ESP8266 sends and receives the internet signal and passes the information to the relay module. Then the relay module acts as switch and works according to program. This smart system is having two different modes like Manual and Auto mode to operate the aerators.

2.1 Manual Mode

Manual means it can be controlled or operated with the aid of human from anywhere. The designed application is set with manual mode to help the farmers to control the aerators in emergency situations. Those situations include failure of DO sensor and temperature sensor and also in cases like improper working of the system. The Fig. 3 shows the working of the application in manual mode. In manual mode farmer can operate which aerator set is required.

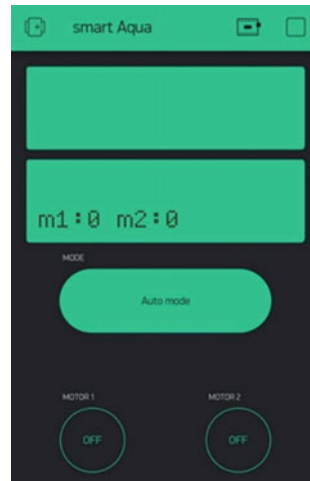
Fig. 3 Manual mode



2.2 Auto Mode

In the auto mode, the application will be working based on the coding program by itself without any human interference as shown in Fig. 4. The sensors in the system sense all the readings and works according to the code. Initially after checking the authentication, it senses the DO value and then allows the aerators to rotate if the value is not in the desired range (5 mg/L) and otherwise it will be in rest condition. Later, it senses the temperature value and runs the system only if the value is greater than the 34 °C. A human cannot operate aerators when it is set to auto mode.

Fig. 4 Auto mode

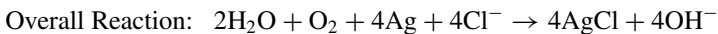
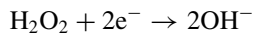
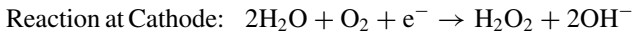


3 Experiment Setup

The proposed smart aqua system is installed in aqua field located in Bhimavaram, Andhra Pradesh. It is observed for one yield and compared with the current approach method. In this study, we cultivated shrimp. Initially we took two acres of aqua pond, in one acre smart aqua system is installed and remaining acre follows current approach as shown in Fig. 5.

3.1 Polarographic DO Sensor

The Polarographic DO sensor [7] is an electrochemical type sensor in which the anode is silver; the cathode is gold and the potassium chloride (KCl) act as an electrolyte as shown in the Fig. 6. The electrolyte solution and electrodes are isolated from the sample by a membrane. When the constant voltage is applied to the circuit the electrodes are get polarized and the following reactions are occurring at the electrodes surface.



Due to these reactions the electrical signals travel from cathode to the anode through the membrane and this electrical current is directly related to the oxygen



Fig. 5 Experiment setup is installed in the aqua field

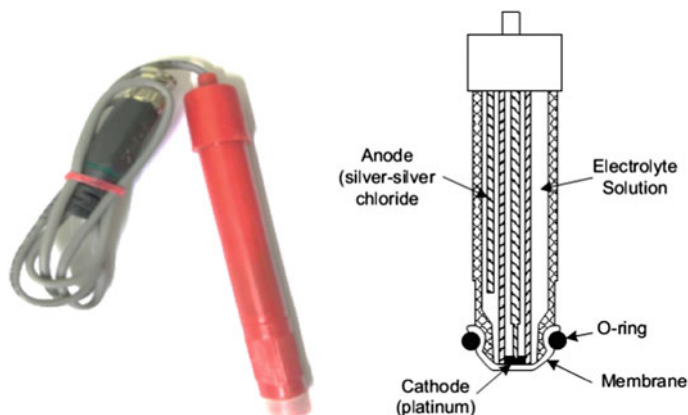


Fig. 6 Polarographic DO sensor

Table 2 Technical specifications of DO sensor

S. No.	Description	Limits
1	Range	0–20.0 ppm
2	Accuracy	± 0.2 ppm to ± 1 count
3	Resolution	0.1 ppm
4	DO sensor	Amperometric gold/silver membrane type
5	Power	9 V battery

concentration in the water. The technical specifications of Polarographic DO sensor as shown in Table 2.

4 Results and Discussion

We conducted an experiment along with aqua farmers from March-2019 to May-2019 and compared both Current approach system (CAS) and Smart Aqua system (SAS) with one another. We installed the SAS in one acre for one yield and for another one acre we followed the traditional method (CAS). We took nearly 1.7 Lakhs of shrimp seeds per acre [8] for cultivation and the cost per single seed is 0.75 Rs. [8]. The harvesting time period for shrimp is nearly 90–120 days [8, 9]. For aeration purposes we used 4 aerator sets per acre [9] for both the systems. The number of seeds, cost for seed and aerator sets are common for both the systems.

We monitored the SAS installed aqua field with the app 24×7 and we got the data like temperature of the water, DO in the water and working of aerators through the App installed in our phone. According to the environmental conditions and DO level in the water the SAS operates the aerators without need of human help but in

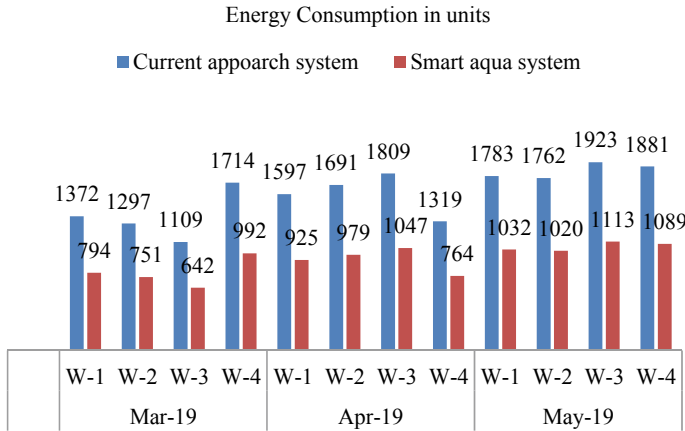


Fig. 7 Energy consumption in CAS and SAS

the current approach method farmer observation is needed for operating the aerators throughout the day. We collected the electrical consumption data to run the aerators from the energy meter on a weekly basis for both the systems as shown in the Fig. 7, by observing simple we can say that the smart aqua systems consume less power compared with the current approach method because the SAS works according to the weather conditions and DO level in the aqua pond. Depending on the size of the shrimp the market value is varying [11]. Size is nothing but kg per mean body weight of the shrimp. After completion of the yield the body weight of the shrimp is 20 g in SAS and 16.66 g in CAS.

Therefore,

$$\text{Size} = \frac{1 \text{ kg}}{\text{Mean body weight}} = \frac{1000}{20} = 50 \text{ count in SAS}$$

$$\text{Size} = \frac{1 \text{ kg}}{\text{Mean body weight}} = \frac{1000}{16.66} = 60 \text{ count in CAS}$$

Theoretical calculations for productivity of shrimp

$$\text{Tonnage harvest} = \frac{\text{Population}}{\text{Mean body weight}} = \frac{170,000}{50} = 3400 \text{ kg in SAS}$$

$$\text{Tonnage harvest} = \frac{\text{Population}}{\text{Mean body weight}} = \frac{170,000}{60} = 2833 \text{ kg in CAS}$$

From theoretical calculations we estimated the crop production as 3400 kg in SAS and 2833 kg in CAS but practically we got 3242 kg in SAS and 2618 kg in CAS. Finally we got 624 kg of shrimp more in SAS compared with CAS, because in SAS the DO level is maintained in a proper way throughout the day. The DO level shows

Table 3 Comparison of current approach system and SAS

Items	Current approach system			Smart aqua system		
	No.of units	Price in Rs./units	Total price in Rs.	No.of units	Price in Rs./units	Total price in Rs.
Time period	3 months	–	–	3 months	–	–
Cost of seed	1.7 lakhs	0.75	127,500	1.7 lakhs	0.75	127,500
Aerators used	4	35,000	140,000	4	35,000	140,000
Labor charge for feeding	3 months	7000	21,000	3 months	7000	21,000
Labor charge for operating aerators	3 months	8000	24,000	0	0	0
Current charges to operate aerators	19,257	2.00	38,500	11,150	2.00	22,300
Production of shrimp	2618 kg	–	–	3242 kg	–	–
Selling price	2618 kg	350	916,300	3242 kg	350	1,134,700
Profit in selling price	–	–	–	–	–	218,400
Total Investment	–	–	351,000	–	–	310,800
Savings in investment	–	–	–	–	–	40,200

a vital role in the growth of the shrimp [10]. The money spent for different items in both the systems was presented in Table 3. From Table 3 we can identify that the Cost of seed, number of aerators used and labor charges for feeding are same in both the systems but in SAS labor charge for operating aerators is zero and productivity is also increases compared with current approach.

5 Conclusion

To eliminate all the problems faced by the aqua farmers with the traditional method, a smart aqua system is developed which can give perfect solution to reduce the labor cost, energy consumption and human efforts. In this experimental study it has been observed that the productivity of aquatic animals increases in aquaculture and also enhances the profit up to 36% earned by aqua farmers. This proposed method is very

beneficial to the aqua farmers compared with the traditional methods, by using this method the farmer got Rs. 40,200/- savings in total investment due to omission of unnecessary running of aerators and he can able to increase his selling profits up to Rs. 218,400/- due to increased production rate.

References

1. Supriatna, Marsoedi, Hariati, A.M., Mahmudi, M.: Dissolved oxygen models in intensive culture of whiteleg shrimp, *Litopenaeus vannamei*, in East Java, Indonesia. *AAFL Bioflux* **10**(4), 768–778 (2017)
2. Robertson, C.E.: Australian prawn farming manual: Health management for profit. Queensland (2006)
3. Boyd, C.E.: Guidelines for aquaculture effluent management at the farm-level. *Aquaculture* **226**(1–4), 101–112 (2003)
4. Rahman, A., Dabrowski, J., McCulloch, J.: Dissolved oxygen prediction in prawn ponds from a group of one step predictors. *Sciencedirect* (2019)
5. Kibria, G.: Environmental update-dissolved oxygen: the facts. *Outlet* **162**, 2–4 (2004)
6. Roy, S.M., Moulick, S., Mukherjee, C.K., Mal, B.C.: Effect of rotational speeds of paddle wheel aerator on aeration cost. *Am. Res. Thoughts* **2**(1)
7. Jones, S.T., Heindel, T.J.: A review of dissolved oxygen concentration measurement methods for biological fermentations. In: *Mechanical Engineering Conference Presentations, Papers, and Proceedings*. 200 (2007)
8. <https://westgodavari.ap.gov.in/fisheries/>
9. <http://www.agritech.tnau.ac.in/>
10. Chakravarty, M.S., Ganesh, P.R.C., Amarnath, D., Shanthi Sudha, B., Babu, T.S.: Spatial variation of water quality parameters of shrimp (*Litopenaeus vannamei*) culture ponds at Narsapurapeta, Kajuluru and Kaikavolu villages of East Godavari district, Andhra Pradesh. *Int. J. Fish. Aquat. Stud.* **4**(4), 390–395 (2016)
11. Suriya, M., Shanmugasundaram, S., Mayavu, P.: Stocking density, survival rate and growth performance of *Litopenaeus vannamei*-(Boon, 1931) in different cultured shrimp farms. *Int. J. Curr. Res. Biol. Med.* **1**(5) (2016)

Modeling and Designing of Plug-in Electric Vehicle Under V2G Compatability



K. Kiran Kumar and B. Srinivasa Rao

Abstract Since last decade, the utilization of vehicles increases rapidly and these fuel engine vehicles cause environmental problems. To overcome these greenhouse effects electric vehicles play a prominent role. In electric vehicles the engines are replaced by electric motor and fuel tanks are replaced by battery banks. In these electric vehicles, plug-in vehicles providing a competitive range due to increase in power electronics and energy storage. Bidirectional converters are proposed in these plug in vehicles to control the battery system. And also a suitable controller is proposed to this converter to maintain an effective operation of vehicle. This proposed system is tested and verified using MATLAB Simulink.

Index Terms Electric vehicle · PV system · Power electronic converter · PWM technique · Battery energy system

1 Introduction

The constant ascent in gas costs alongside the expanded worries about the contaminations delivered by petroleum product motors are constraining the present vehicle market to discover new choices to decrease the non-renewable energy source use. Alongside the exploration on bio-fuel driven motors; diverse electric vehicles and crossover electric vehicles are developing as feasible choices to supplant, or possibly decrease, the flow armada of non-renewable energy source driven vehicles [1]. Albeit flow made electric/mixture vehicles are being promoted as an approach to diminish petroleum product use, a few promising advances are being exhibited that can use power hardware to charge the battery from the utility utilizing module vehicles or

K. Kiran Kumar (✉) · B. Srinivasa Rao
Department of EEE, Aditya Institute of Technology and Management, Tekkali, AP 532201, India
e-mail: kirankalyanal@gmail.com

B. Srinivasa Rao
e-mail: bsreee2013@gmail.com

go about as a disseminated asset to send power back to the utility with vehicle-to-network capacities. Right now, module vehicle topologies are portrayed to audit the force hardware required for them. The recently developing Vehicle-To-Grid V2G innovation is additionally talked about alongside financial matters and consistence necessities to permit the vehicle to be associated with the matrix [2]. Before delving into the subtleties of intensity gadgets required for the electric/crossover vehicles, the regular types of these vehicles are portrayed beside get acclimated with the wordings.

This paper proposes a concept to design an Electric vehicle operated with PV-Battery system and also have the capability to transfer energy to grid system (V2G capability).

2 Electric Vehicles

In general, the electric vehicle consists of battery storage systems in place of fuel tanks and electric motors in place of combustion engines. Here, the electric motors chosen are either synchronous motor or induction motor. A bidirectional dc-dc converter is used to control the charging capability of battery. In this paper, an alternative generation system is used to charge the battery. The main advantage of this electric vehicle is simple in construction and easy to maintenance. And also, the requirement of battery capacity for this type of electric vehicles is more which increases the economic and complexity in circuit. To overcome this difficulty plug-in electric vehicles PEV are introduced. The structure of electric vehicle is shown in Fig. 1 [3].

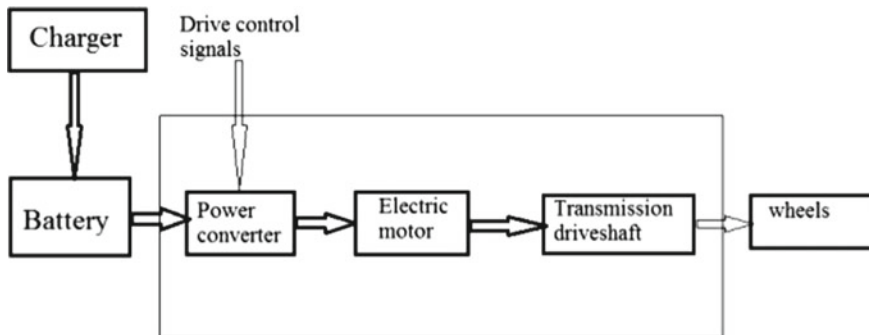


Fig. 1 Block diagram of EV

2.1 Proposed Electric Vehicle Structure

Generally, an Electric Vehicle is an automobile device and it consists of many components and more number of wires connecting them. The block diagram shown in Fig. 1 shows the minimum components required for an Electric Vehicle. In general EVs, the combustion engines are replaced by electrical motors and conventional fuel tanks are replaced by battery banks. In EVs both electric motor and batteries play a key role and occupy 50% of total weight of the vehicle. As from the diagram, battery, power converter, electric motor, charger and energy management systems are the key components.

- In electric cars batteries are fuel sources. In order to reduce the cost and weight of the battery banks a super capacitor or fuel cell and plug-in charge based devices are the alternative solutions.
- Generally, in EVs there is a possibility to use two converters. One converter is to boost the battery or dc voltage by using suitable dc/dc converter and the second converter converts the battery energy to AC, which is required to operate electric motor efficiently. In this paper a single stage three level pulse width modulation PWM based converter is proposed.
- In EVs, the batteries act like fuel tanks and similarly the electric motors act like engines [4]. There are different types of electric motors available in present market like, BLDC motor, Brushed DC motor and Induction Motors. In this paper, the induction motor is chosen as engine in EVs.

2.2 Plug-in Vehicles

Generally, in electric vehicle the capacity of battery usage is more. In order to reduce the battery capacity and maintain economic concept rechargeable batteries are proposed. This also called as plug-in charge vehicles. The structure of plug-in hybrid electrical vehicles (PHEV) is shown in Fig. 2.

2.3 Plug-in Electric Vehicle Charger Topology

Figure 3 shows the proposed structure of bidirectional converter based electric vehicle which has capable of vehicle to grid and vice versa. For this, a bidirectional inverter and dc-dc converter topologies are proposed. The advantage of these converters are that these are designed with 6 less number of switches. To improve the stability, power quality and dynamic behavior of the system, this system consists of some passive components [5]. The output of the bidirectional dc/dc converter is given to a conventional three phase inverter. The purpose of this inverter is produce required to operate the induction motor drive effectively. Here, this paper proposes a multilevel

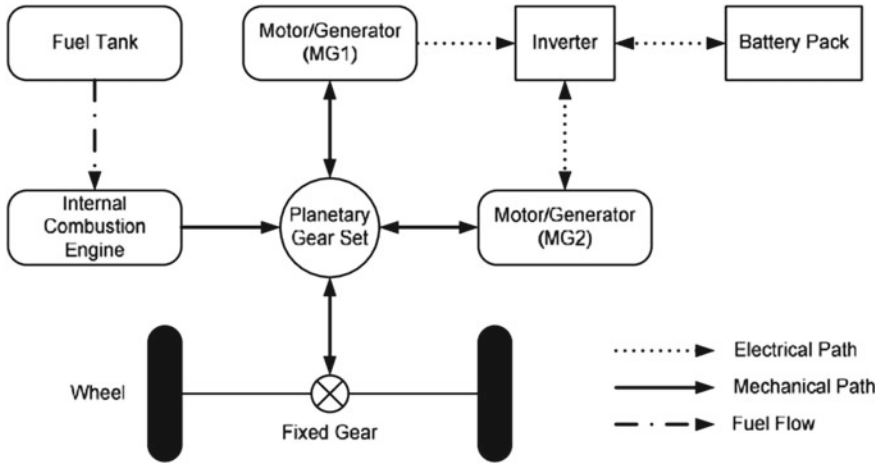


Fig. 2 Configurations converted PHEV

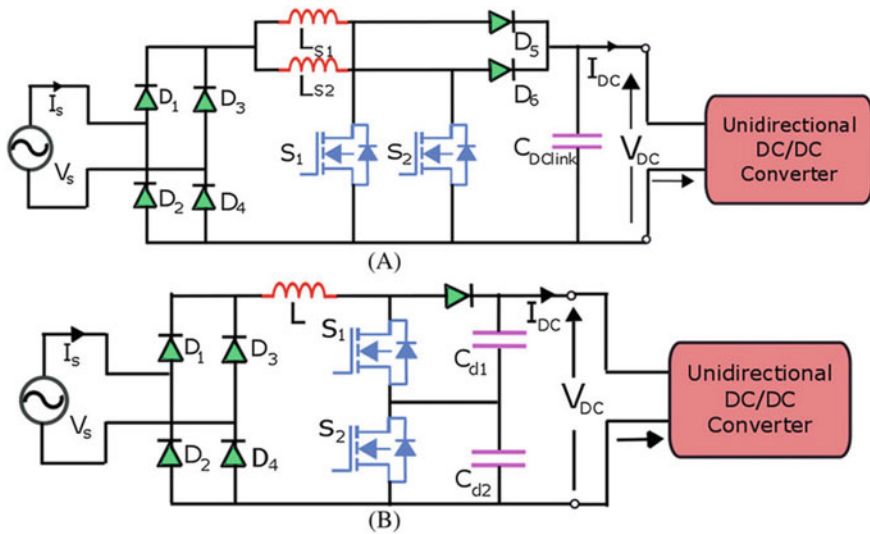


Fig. 3 PEV charger topology

inverter. The advantage of multilevel inverter is that the generated high power and high voltage have been effectively controlled. The unique nature of multilevel inverter is to generate high voltage levels [9].

V2G capabilities [6]. Firstly, the DC bus voltage is compared with reference to bus voltage and applied to PI controller. Then reference current is generated with the help of error bus voltage, battery voltage and maximum current obtained from capacity of battery, applied to PWM technique to generate required reference signals for chopper as shown in Fig. 4 [8].

Figure 5 shows the control diagram for inverter used in electric vehicle. This controller also designed for both G2V and V2G facilities. The reference signals used in this controller is based on dc bus voltages and ac voltage [7–10]. The phase required for this controller is obtained with phase locked loop PLL from ac bus voltages. And dc bus voltage is compared with reference bus voltage. The generated reference current is used to generate gate signals with the help of PWM controller.

3 Simulation Diagram and Results

The proposed plug-in electric vehicle system with PV as source is implemented and tested in MATLAB/Simulink environment. Here, the PV system is designed for 460 W panel and connected to battery system. The MATLAB diagram for proposed system with PV source is shown in Fig. 6.

Case 1: Performance results for PEV system The above Fig. 7 shows the simulation result for grid voltage and current measured after bidirectional converter. The gate signals for single phase bidirectional converter of electric vehicle is shown in Fig. 8. The dc voltage of converter is shown in Fig. 9 and the charging conditions of battery soc is shown in Fig. 10.

Case 2: Performance results for PEV system with PV Implementation See Figs. 11, 12 and 13.

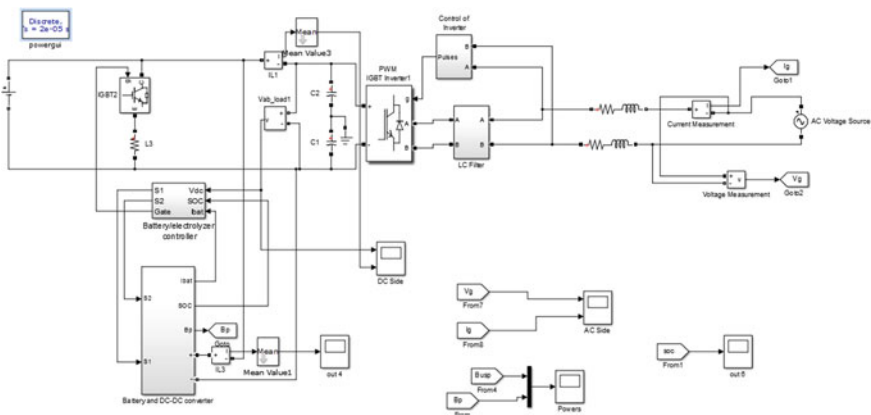


Fig. 6 Experimental diagram for Plug-in vehicle

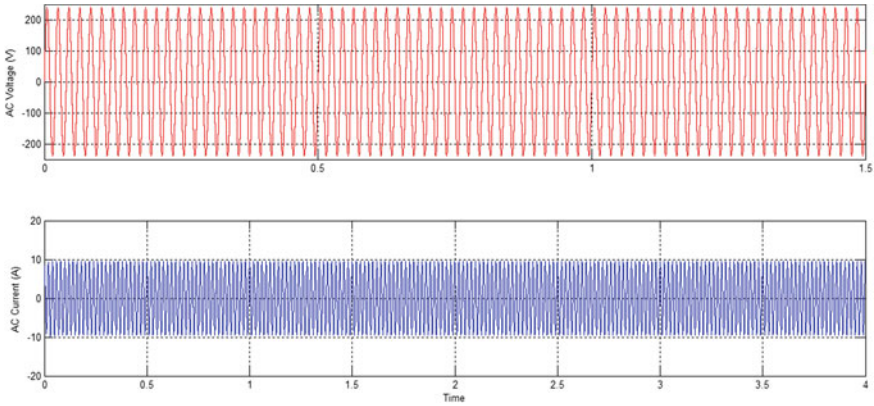


Fig. 7 Simulation result for AC side voltage and current

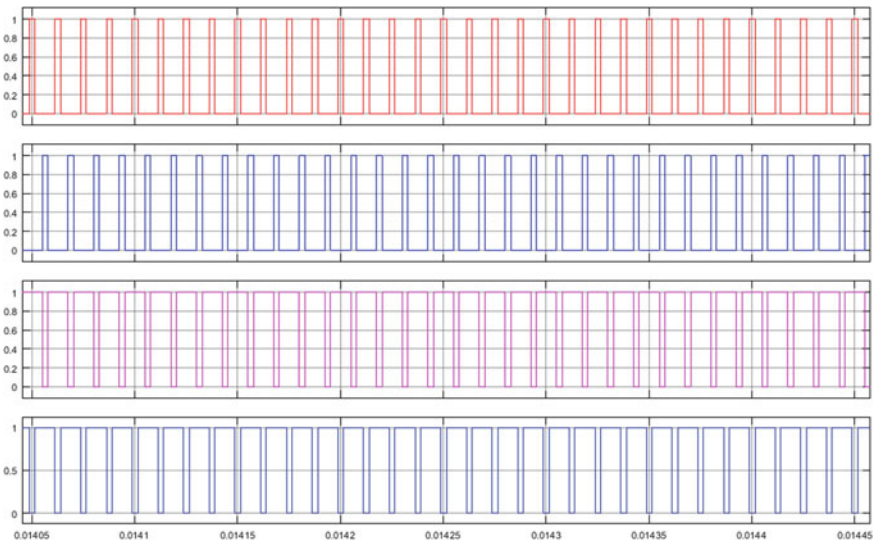


Fig. 8 Gate triggering pulses for AC/DC bidirectional converter

4 Conclusion

In this paper, a new bidirectional converter is designed for PV based Plug-in EV. A Suitable control strategy for both DC-DC chopper and DC/AC bidirectional converter is designed to control the voltage levels. The reference signals required for both converters are taken from DC and AC bus voltages, and from the energy box. This proposed system is tested in MATLAB/Simulink and verified the results. The performance of EV is better in use of PV system as compared with Plug-in model. If

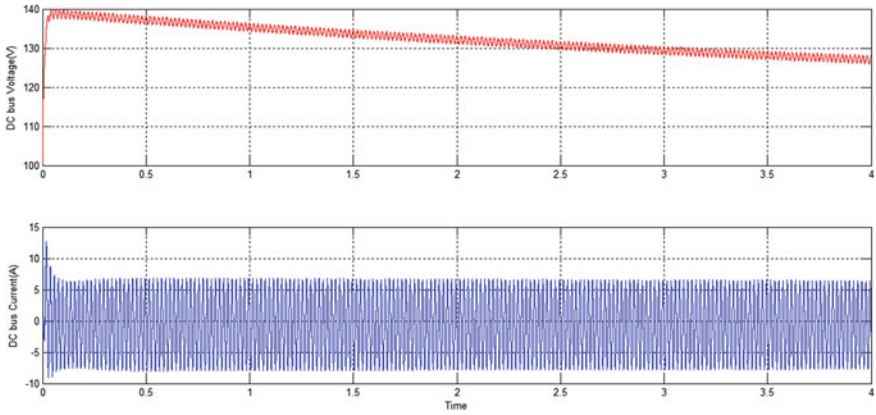


Fig. 9 Simulation result for DC-DC converter current and voltage under large change

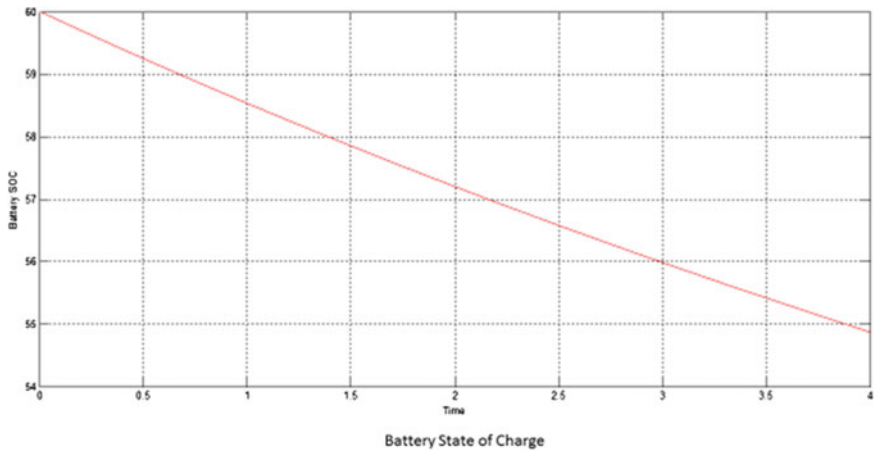


Fig. 10 Simulation result for battery SOC

the controllers for both converters are implemented using automation concept, the performance and speed of EV can be increased efficiently and it also increases the mileage.

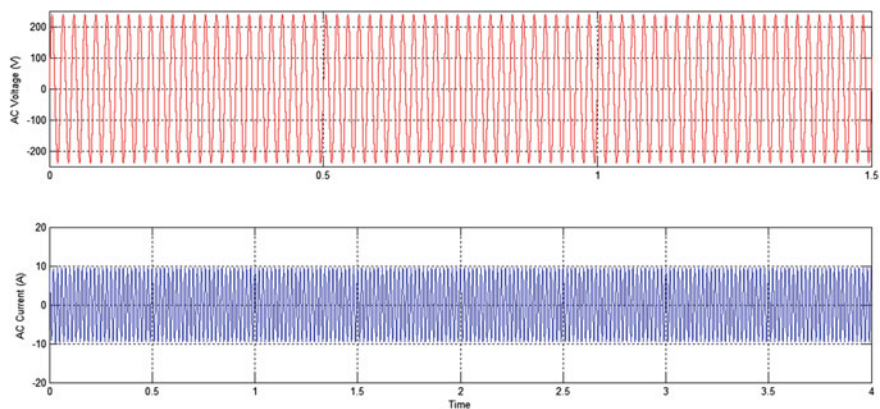


Fig. 11 Simulation result for AC side voltage and current

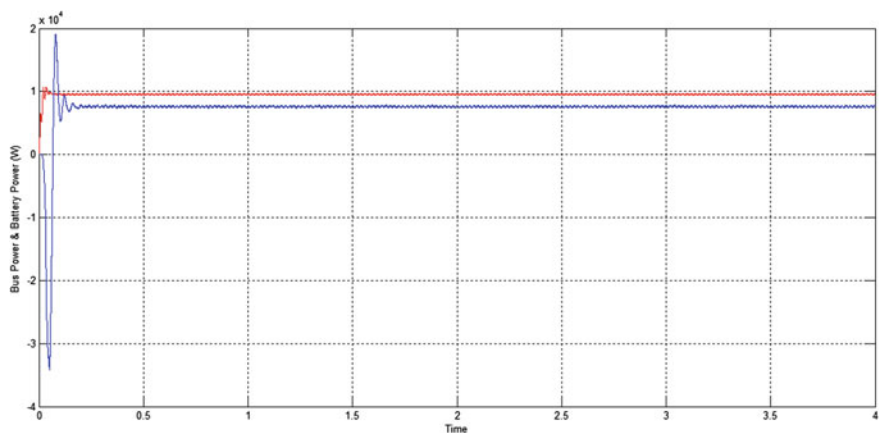


Fig. 12 Simulation result for DC and battery powers

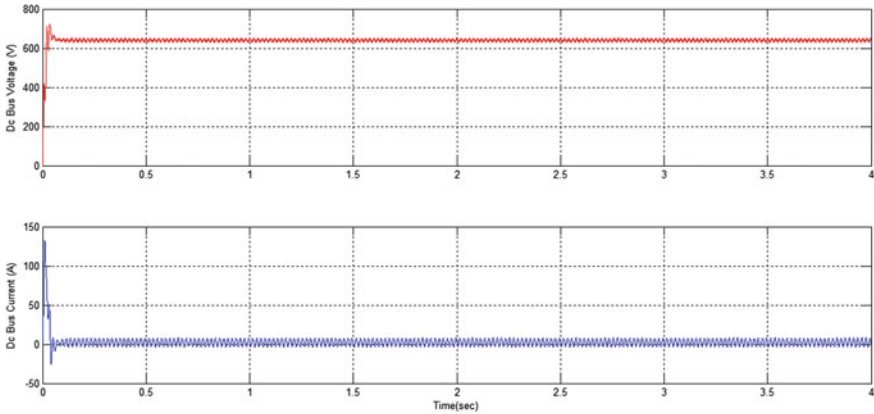


Fig. 13 Simulation result for DC–DC converter and voltage

References

1. Wang, B., Payman, D.: Electrical safety considerations in large-scale EVs charging stations. *IEEE Trans. Ind. Appl.* **55**(6) (2019)
2. Ruan, J.: A Novel Dual-Motor 2-Speed Direct Drive Battery EVs Drivetrain, vol. 7. *IEEE Access* (2019)
3. Zhang, L.: Robust lateral motion control for in-wheel-motor-drive EVs with network induced delays. *IEEE Trans. Veh. Technol.* **68**(11) (2019)
4. Xiong, R.: Li-ion battery health prognosis based on a real BMS used in EVs. *IEEE Trans. Veh. Technol.* **68**(5) (2019)
5. Ahn, J.-H.: High-efficiency adaptive-current charging strategy for EVs considering variation of internal resistance of Li-Ion battery. *IEEE Trans. Power Electron.* **34**(4) (2019)
6. Li, Y.: Deep reinforcement learning-based energy management for a series hybrid ev enabled by history cumulative trip information. *IEEE Trans. Veh. Technol.* **68**(8) (2019)
7. Zhang, S.: A Vehicle-Environment Cooperative Control Based Velocity Profile Prediction Method and Case Study in EM of Plug-in HEVs, vol. 7. *IEEE Access* (2019)
8. Laha, A.: Game theory based charging solution for networked EVs: a location-aware approach. *IEEE Trans. Veh. Technol.* **68**(7) (2019)
9. Jeong, S.: Charging automation for EVs: is a smaller battery good for the wireless charging EVs? *IEEE Trans. Autom. Sci. Eng.* **16**(1) (2019)
10. Su, Y.: Dynamic Coordinated Control During Mode Transition Process for a plug-in Hybrid Electric Vehicle, vol. 7. *IEEE Access* (2019)

Influence of Drone Rotors Over Droplet Distribution in Precision Agriculture



Umamaheswara Rao Mogili and B. B. V. L. Deepak

Abstract Countries like India, more than 70% of the people depend on rice cultivation. Based on this precision agriculture in India requires the information about the condition of cultivated plants and the response to undesirable appearances of pests. Recent technology, Unmanned Aerial Vehicle (UAV) performs the aerial spraying over rice plants to kill the pests which are harmful. But, offsite and less amount of droplet deposition over the plants is the major concern in pesticide spraying applications. The rotors of the unmanned aerial vehicle effect the deposition of the droplets over the rice plants. This study results on the impact of the UAV rotors speed on the spray deposition and spraying liquid coverage on the plant surface. The sample liquid (water) sprayed from the moving UAV over the sample plant using a flat fan nozzle with 0.2 MPa. The UAV moved with the speed of the 2 m/s. A conical shaped thick plastic foil was used as a droplet collector and fixed on sample plant in three levels such as lower level, middle level and upper level of the plants. The distance between the sample plants to the UAV is 1 m and the arms of UAV to flat fan nozzle are 0.2 m. The tests were conducted at various speeds of rotors with 0% throttle, 50% of throttle and 100% throttle given by the radio transmitter. The height from the plant surface to the nozzle of UAV is approximately 0.5 m. The impact of the propeller's rotational speeds differs from the distribution of the liquid on droplet collectors. The observations state the impact of the rotors rotational speeds are less at middle-level sample points. It shows approximately the same values in the three tests conducted at 0, 50, and 100% throttle rates are 34, 33, and 36%. The tests were conducted in an indoor environment to avoid wind speeds.

Keywords Unmanned aerial vehicle · Quad copter · Pesticide spraying · Droplet deposition · Flat-fan nozzle

U. R. Mogili (✉) · B. B. V. L. Deepak
Department of Industrail Design, National Institute of Technology Rourkela, Rourkela, India
e-mail: umajrfnit@gmail.com

B. B. V. L. Deepak
e-mail: deepak.bbvl@gmail.com

© The Author(s), under exclusive license to Springer Nature Singapore Pte Ltd. 2021
B. Deepak et al. (eds.), *Advanced Manufacturing Systems and Innovative Product Design*,
Lecture Notes in Mechanical Engineering,
https://doi.org/10.1007/978-981-15-9853-1_34

401

1 Introduction

Unmanned aerial vehicles, also called drone systems, developed for the need on security purposes. The popularity of equipment and technological progress has made them one of the mass-produced and prime uses of civilian users. At present, the cultivation fields use manually and half mechanized tools and equipment for the plant protection process in India. This leads to high labor intensity and delivery's high-cost agriculture product. It is also difficult to operate this equipment in mountain areas. Some situations like pesticide spraying over the plants manually lead to a high probability of poisoning farmer health.

The UAVs driven by brushless motors are much cheaper to buy and easy to install. These are usually multi-rotors that derive energy from the lithium-ion polymer batteries mounted on them. The time of flight depends on the weight of the UAV and various components fixed within it. Amateur introducing unmanned aerial vehicles in photography, surveillance, and remote sensing [1]. In recent years, it was adopted over precision agriculture applications such as bare soil Identification, weed identification, crop monitoring, and pesticide spraying [2, 3]. Coming to one of the above agriculture applications pesticide spraying sprays harmful pesticides and fungicides over the agriculture pests without human interaction. The UAV mounted installations that spray for spraying consist of a pesticide tank, a pressure pump driven by a motor, flat-fan nozzles, and sprays that can be mounted on the arms of the UAV. The air of the drone generated by the propeller accelerates the speed of spraying the sprayed pesticide and spreads the plant's veins to the point of reaching leaves and roots, even those that are located near the ground.

The most-variable pressure nozzles are used to spray the liquid. UAV pesticide applications picking up a possible gaining to control pests, diseases, and weeds in the field. One of the most popular drones in the world adapted for combating weeds and pests by spraying is built and released on the in 1997, by the Yamaha Motor Company, the Yamaha R-MAX model. It is an unmanned helicopter that has been designed primarily for the needs of precision agriculture and apart from spraying plant protection products; it can also be used for fertilizing liquid mineral fertilizers [4]. Due to specialized conditions and the capacity of fluid tanks, experiments with UAVs are carried out within the range. There are no flow meters and devices to consequently control the rate of the droplets. It is conceivable at that point to control it by changing the spray nozzles. The control of the pesticide dosage within the field is done by changing the UAV flight altitude and speed. The advanced installation in UAV states the pressure of the liquid is regulated by the need to change the rotational speed of the pump, and the speed of the rotors [5].

As the climate conditions, UAV rotors speed, nozzle types, properties of the pesticide, and size of droplet influence the deposition of the droplet over the plant. In the time of aerial spraying droplet deposition on the plant must be reached maximum quantity to control disease on the plant. For this reason uniform deposition of the droplets is required while spraying the pesticides. Mainly, the high speed of the rotors and its types shows a negative impact on the amount of droplets deposit. Also, the

thrust generated by the different types of rotors affects the droplet deposition on plants [6]. The droplet deposition rates at various UAV speeds, spray rates, irregular wind speeds, and its course had been investigated. The different UAV flying velocities had increasingly noticeable effects on the distribution of droplets on the water sensitive paper collector [7]. At low rotor speeds, a spray drift experiment was conducted with LURMARK-04F80 nozzle in a wind tunnel with different influencing factors such as different UAV speeds, pressure rates, spray rates, and nozzle angles to provide the optimum result to reduce the drift [8]. However, due to the weather conditions, the sprayed droplets will float to non-target areas, which comes about in poor control impact, waste of pesticide and it leads to weather pollution [9, 10]. At the same time, a UAV can be utilized for the exact application of pesticides with less hazard of over and under application completely different climate conditions. The experimenting results show that the UAV in 1.5 m height with 50, 75, 100% nozzle opening surface within the speed range of 1–5.8 m/s gives the uniform spraying results [11].

A WPH642 unmanned helicopter uses infrared thermal imagery to study the impact of spraying parameters on droplet deposition distribution over rice plants. The uniform spraying results indicates droplets distribution on the rice plants done accurately by observing the temperature changes in the infrared images while spraying process [12]. A small UAV used to conduct an experiment over the paddy field which influences spraying parameters on the deposition of droplets over the plant. The results show the UAV altitude and velocity impacts and influences the average amount deposition of the droplets [13]. A UAV electrostatic sprayer used to measure the deposition of the droplets with carbon paper collectors and defined the drift. The study indicates the electrostatic sprayer can make the consistency of deposition of the droplets, reduce the pesticide drift and increases pesticide utilization in the field [14].

Despite these above limited technical research on aerial spraying carried out over the parameters weather conditions, droplet deposition, uniformity of spraying, droplet drift, spraying, and nozzle parameters. But not provided the influenced factors of the droplet deposition over the plants in relation to pesticide spraying with the use of UAV. The aim of this study was to explore the deposition of the droplets over the collectors arranged in the plant at various positions (lower level, middle level, and upper level). At the same time, propellers throttle was increased at various levels. After spraying at different conditions the collectors were collected and the liquid was subject to droplet analysis. The results evaluate the droplet deposition was uniformity on the middle level of the plant. The findings will be first in India and it will be helpful to gain efficient spraying through the UAV to get the benefit from the advanced technology in precision agriculture.

Table 1 Specification of quad copter spraying system

Quad copter components	Specifications
Number of rotors	4
Brushless motors	4
speed	0–10 m/s
Altitude	0–20 m
Number of spraying nozzles	1
Nozzle type	Flat fan
Nozzle pressure	0.2 mPa
Rotor diameter	APC SF 10*4.7
Motor speed	920 kV
Battery	LIPO 4 s

2 Materials and Methods

2.1 Quad Copter Spraying System Specifications

The unmanned aerial vehicle used in the experiment was a quad copter UAV developed in the industrial design department, National Institute of Technology, Rourkela, India. This quad copter unmanned aerial system model having four arms and one spray nozzle for downward spray was used in this study. The four brushless motors attached on four arms of the quad copter and the propellers are fixed to it. Complete specifications of the quad copter system are provided in the Table 1. The four motor running using a 4S LIPO battery. The quad copter had a smooth take-off and landing in its autonomous mode with a flying speed of 1–10 m/s and a height of 10 m above the ground level. These heights and flying speeds, time span, autonomous modes and spraying path fixed by the UAV software interface. The quad copter controlled by a 6 channel radio transmitter (Fly Sky).

2.2 Experimental Design

The experiment setup was built in the department laboratory to avoid the effect of the weather conditions, which influences the size of the droplet coming from the quad copter UAV nozzle. The design mainly consists of four parts: the moving part, quad copter UAV, spraying part, and sample plant with a collector. The moving part is a Kawasaki 6 Degree of Freedom (DoF) robot moves in horizontal and vertical positions and is controlled manually shown in Fig. 1. To decide the trajectory of the quad copter sprayer system while spraying it is fixed to the robot and the robot moves horizontally with the speed of 2 m/s.

Fig. 1 Quad copter fixed to the Kawasaki 6 DoF robot



The spraying part connected with a vertical plastic bar between the two arms of quad copter UAV. At the downward of the vertical bar, a flat fan nozzle was fixed for spraying the liquid. The spraying part nozzle is below the arms of the quad copter with a distance of 0.2 m. The water is taken as spraying liquid delivery from the flat fan nozzle and the pressure of the liquid while reaching the nozzle is 0.2 mPa. A flowering plant, taken as a sample plant and placed on the iron table under the quad copter UAV with a distance of 1 m. The sample plant is planted in the loamy soil of a flowerpot. A conical shaped folded thick plastic foil was used as a collector to collect the sprayed liquid. Sample conical-shaped plastic foil fixed to the rice plant shown in Fig. 2. The collectors placed on the plant in three positions lower the level of the leaf area, the middle level of the plant and the upper level of the plant surface. The collectors were rigidly fixed to the plant which was not moved while increasing the propellers throttle at various speeds.

The rotational speed of the rotor is controlled by a 6 channel fly sky radio transmitter with speeds of 0, 50, and 100 throttle. The radio transmitter throttle positions are shown in Fig. 3a–c, The 6 DoF robot moved with the speed of 2 m/s and spray unit spray the liquid over the plant with 0% throttle and the collectors collect the

Fig. 2 Collectors fixed with sample rice plant

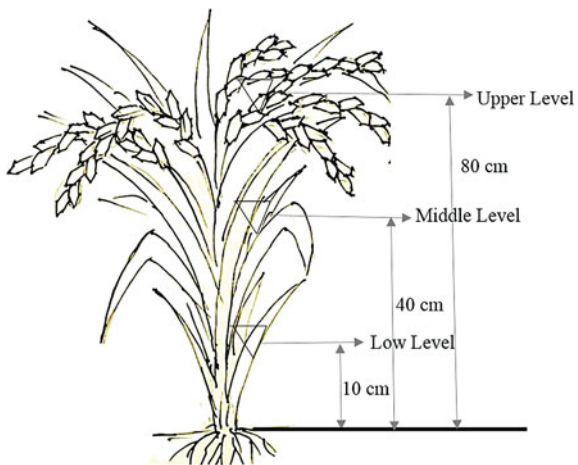




Fig. 3 a 0% throttle b 50% throttle c 100% throttle

droplets in three levels. Again the same test conducted with 50 and 100% of throttle and collectors collect the samples.

The experimental design is shown in Fig. 4. The test is conducted three times and each time three levels of samples are collected to analyze. The volume of liquid is most commonly measured with graduated cylinders, although beakers, burettes, and pipettes are also used. Each of these instruments is marked with lines and all lines are called the scale. Each line is a division or graduation and only some of the divisions are marked. Some of the instruments are more precise than others. Graduate cylinder and beakers are used for most common liquid volume measurements. Burettes and pipettes are used to measure the tasks that require the most precise measurement of liquid volume. In this study, the collected liquid was determined from the precision values of the extinction measurement using the graduate transfer pipette and individual tests are conducted for each level and the values are listed. The units of the listed liquid values are cubic meters.

Fig. 4 Experimental setup in the Robotics Lab of the National Institute of Technology lab



3 Results and Discussion

Quad copter UAV spraying is better efficacy than found controlled mechanized sprayers. However, the key issue in aerial spraying applications depends on parameters such as accuracy, mobility, efficiency, and drift of the pesticides reached to the target plants. The study carryouts a spraying test to decide the speeds of rotors, which influences the droplet deposition on test plants that could be appropriate to apply the same scenario for aerial spraying applications over rice plants. In Table 2, the descriptive statistics of deposition of the droplets on three levels on the plant at various throttle rates are demonstrated. The units of the liquid are taken in cubic centimeters.

Based on Table 2 measurements, the percentage share of the liquid settled on the collectors on all levels and individual levels are calculated using a formula. The values are shown in Table 3.

$$P_n(\%) = \frac{V_n}{\sum V_n} * 100 \tag{1}$$

where P_n is the covering percentage of the share of the liquid collected from the collectors on the nth level is in relation with liquid collected from all levels. V_n is the volume of liquid settled on the collectors on nth level. While Fig. 5 shows the means of covering percentage comparison of deposition of droplets at various throttle rates at three levels.

Figure 5 presents the percentage of droplets collected from the collectors mounted on the upper level reduced when the rotational speed of the rotors increases at 0, 50, and 100%. When talking to the collectors from the lower levels it is quite opposite to of upper level collectors and increased at various throttle rates. But no change in the liquid settled on collectors at the middle level and red dotted line in Fig. 5, shows

Table 2 Collected liquid values in three levels at various throttle rates (units: cubic centimeters)

Level	Throttle		
	0%	50%	100%
Upper level	0.0000062	0.0000057	0.0000033
Middle level	0.0000046	0.0000044	0.0000047
Lower level	0.0000024	0.0000031	0.0000052

Table 3 Covering percentage of collectors with liquid at various throttle rates

Level	Droplet coverage % at		
	0%	50%	100%
Upper level	46.97	43.18	25.00
Middle level	34.85	33.33	35.61
Lower level	18.18	23.48	39.39

Fig. 5 Spray uniformity of the liquid collected from collectors at various throttle rates

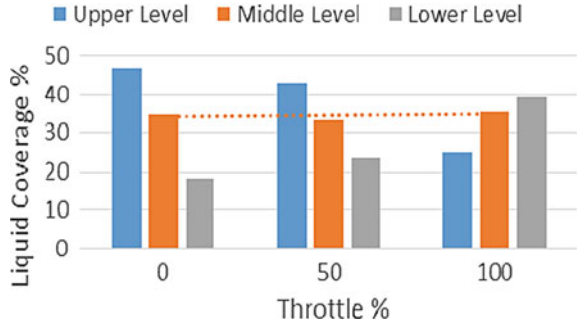
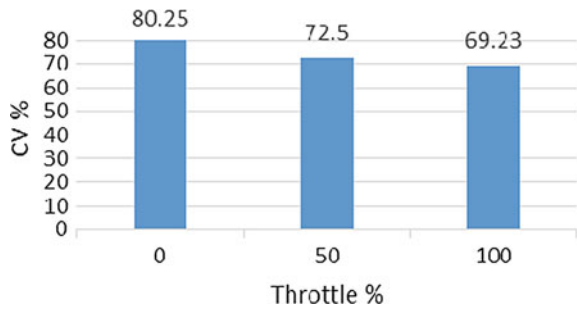


Fig. 6 The overall effect of the droplet deposition on all levels



the no change of droplet deposition over the plants. The results state that the impact of rotors always shows its influence on the droplet deposition over the plants.

The Coefficient of Variation (CV) was calculated to study the droplet distribution among the sample collectors arranged at three levels. The uniformity of droplet deposition depends on the value of the CV shown in Fig. 6. If the value is less then droplet deposition, it was calculated using the following equations:

$$CV(\%) = \frac{S}{\bar{V}} * 100 \tag{2}$$

where S is the standard deviation and \bar{V} is the average of all sampling collectors.

$$S = \sqrt{\frac{\sum_{i=1}^n (V_i - \bar{V})^2}{(n - 1)}} \tag{3}$$

where V_i is the deposition value of every sampling collector. While Fig. 6 states increasing the throttle of rotors reduces the inequality index of the droplet deposition on the collectors at three levels. At the same time, the values show the droplet deposition at the middle level of the plant is uniformity.

4 Conclusion

Mainly the utilization of quadcopter UAVs can be a great way for aerial spraying applications. In specific, they can show a high impact on diseases and weed prevention in the crop fields. Also, these UAVs can be sprayed with pesticides in some difficult conditions like remote areas where humans are difficult to reach.

In summary, the droplet deposition over the plants at various throttle rates are studied and analyzed. The rotor rotational speed affects the volume of droplet distribution on the plants at different levels. When the quadcopter UAV throttle at 0, 50 and 100%, the coefficient of variation of the droplet deposition was normal and it demonstrated better spray consistency at the middle level of the plant. The coverage rate of the liquid at three levels 80, 72, and 69%. The middle level sampling points attaining the good spray uniformity over the plants. The rotor's rotational speeds increases alternatively the distribution of the droplets is reduced on the surface of the plant canopy.

In reality, the study explores assistance to supply specialized understanding in moving forward to the quality and viability of quadcopter UAV for aerial spraying over the rice plants. In the future, efforts can be made to study the optimization of spraying parameters, nozzle types, droplet drift, and spraying spacing in between crop rows. It also helped in a speedup of aerial spraying techniques and helps near ground spraying.

Acknowledgements This work is supported by SERB, Govt. of India with the Sanction order No. ECR/2017/000140 on Dt. July 5, 2017.

References

1. Everaerts, J.: The use of unmanned aerial vehicles (UAVs) for remote sensing and mapping. *The International Archives of the Photogrammetry, Remote Sensing and Spatial Information Sciences*, 37(2008), pp. 1187–1192. Anning, R.G.: *The Automated Office: Part I. EDP Analyzer* **16**, 9 (1978)
2. Zhang, C., Kovacs, J.M.: The application of small unmanned aerial systems for precision agriculture: a review. *Precis. Agric.* **13**(6), 693–712 (2012). (Springer)
3. Mogili, U.R., Deepak, B.B.V.L.: Review on application of drone systems in precision agriculture. *Procedia Comput. Sci.* **133**, 502–509 (2018)
4. Giles, D.K., Billing, R.C.: Deployment and performance of a UAV for crop spraying. *Chem. Eng. Trans.* **44**, 307–322 (2015)
5. Huang Y., Hoffmann W.C., Lan Y., Wu W., Fritz B.K.: Development of a Spray System for an unmanned aerial vehicle platform 2009. *Appl. Eng. Agric.* **25**(6), 803–809
6. Mogili, U.R., Deepak, B.B.V.L.: Study of takeoff constraints for lifting an agriculture pesticide sprinkling multi-rotor system. In: *Advances in Materials and Manufacturing Engineering* (pp. 203–210). Springer, Singapore (2020)
7. Kharim, M.N.A., Wayayok, A., Shariff, A.R.M., Abdullah, A.F., Husin, E.M.: Droplet deposition density of organic liquid fertilizer at low altitude UAV aerial spraying in rice cultivation. *Comput. Electron. Agric.* **167**, 105045 (2019)

8. Ding, S., Xue, X., Qin, W., Gu, W., Cai, C., Cui, L.: Influencing factors research and performance experiment on droplets deposition at low wind speed. *Int. J. Precis. Agric. Aviat.* **2**(1) (2019)
9. Fritz, B.K.: Role of atmospheric stability in drift and deposition of aerially applied sprays-preliminary results. In: 2004 ASAE annual meeting ASAE paper 041031 (2004). <https://doi.org/10.13031/2013.16134>
10. Huang, Y.B., Thomson, S.J., Hoffmann, W.C., et al.: Development and the prospect of unmanned aerial vehicle technologies for agricultural production management. *Int. J. Agric. Biol. Eng.* **6**(3), 1–10 (2013). <https://doi.org/10.3965/j.ijabe.20130603.001>
11. Hussain, S., Cheema, M., Jehanzeb, M., Arshad, M., Ahmad, A., Latif, M. A., Ashraf, S., Ahmad, S.: Spray uniformity testing of unmanned aerial spraying system for precise agro-chemical applications. *Pak. J. Agric. Sci.* **56**(4) (2019). Poor, H.: An introduction to signal detection and estimation, Chap. 4. Springer, New York (1985)
12. Zhang, J., He, X.K., Song, J.L., Zeng, A., Zeng, A., Liu, Y., et al.: Influence of spraying parameters of unmanned aircraft on droplets deposition. *Trans. CSAM* **43**(12), 94–96 (2012)
13. Chen, S.D., Lan, Y.B., Li, J.Y., Zhou, Z.Y., Jin, J., Liu, A.M.: Effect of spray parameters of a small unmanned helicopter on distribution regularity of droplet deposition in hybrid rice canopy. *Trans. Chin. Soc. Agric. Eng.* **32**(17), 40–46 (2016)
14. Ru, Y., Zhou, H.P., Jia, Z.C., Wu, X.W., Fan, Q.N.: Design and application of electrostatic spraying system. *J. Nanjing Forest. Univ.Nat. Sci. Ed* **35**(1), 91–94 (2011)

CAD/CAM/CIM and Robotics

Effect of Porosity and Thermal Medium on the Vibration Characteristics of Two-Dimensional FGM Plates



I. Ramu, M. Raghuraman, and M. Venu

Abstract The present method develops the rectangular component and has four nodes owning degrees of freedom, seven per each joint formed with the author and his co-workers. It is applied to determine the vibration characteristics of porous two-dimensional functionally graded material (FGM) plates. The performance of the adopted element is evaluated by examining the present results of the fundamental frequency parameters with the published results. It followed that the performance of the present aspect is considered adequate for the temperature-dependent material porous plates under the heated conditions discussed in this investigation with supported boundary circumstances. The effect of even and uneven porous distributions on free vibration characteristics of the two-dimensional plate studied in detail. Observe the distribution of 2D properties' impact on the natural frequency of plate. Also, the influence of the rise in temperature on two-dimensional FG plates examined in the present work.

Keywords 2D FG material plates · Porosity · Thermal environment · Finite element method · Natural frequency

Nomenclature

$\delta^{(n)}$	Displacement vector
$\delta_i^{(n)}$	Node displacement vector
N_i	Shape functions
σ	Normal stress
τ	Shear stress
ε	Strain

I. Ramu (✉) · M. Raghuraman · M. Venu
Faculty of Mechanical Engineering, Vishnu Institute of Technology, Bhimavaram, Andhra Pradesh 534202, India
e-mail: ramuinala@gmail.com

γ	Shear strain
$K_b^{(e)}$	Element bending stiffness matrix
$K_s^{(e)}$	Element shear stiffness matrix
$M^{(e)}$	Element mass matrix
$i\alpha$	Temperature distribution index value
T	Effective temperature
T_a	Atmospheric temperature or Room temperature
ΔT	Temperature difference $\Delta T = T_c - T_a$
T_c	High temperature at ceramic side

1 Introduction

The advanced composite material made from ceramic and metallic constituents, the mixture is termed as functionally graded materials. These blended mixture material constituents are varying smoothly in one or more directions, respectively. First, the concept of FGM was introduced by Japanese scientist Koziwae in 1980. The two-dimensional FGM material characteristics vary smoothly along the thickness direction as well as length direction by continually changing the ratio of constituent's mixture. Numerous industrial applications of FGM, then several researchers inspired the attractive intensive research interests in this field. They implied mainly focused on static, natural oscillation and active properties of one dimensional FGM structures. In high-thermal condition applications, FGMs are used hence the structural elements like beams and plates have generated extensive applications such as aerospace industry, engine combustion chamber and nuclear reactors. The manufacturing defects and operating condition may cause deteriorate the structural properties. The degradation may be due to high thermal and localized disputes during the production process like porosities. The degradation of structural properties may source to failure. Hence, the vibration characteristics of porous 2D FGM plates considered as important in the present study.

Some of the researchers were developed with various techniques to examine the vibration characteristics of the plate with 1D FG. The structural attributes of FG thin plates were studied by Zhang and Zhou [1] with the neutral surface novel concept. Reddy and Chin [2] studied the response of the changing characteristics of FG cylinders and plates with thermomechanical circumstances. They explained a discrete element model formulation with a thermomechanical load. Yang and Shen [3] examined the FG plate transient acquiescence under thermic loads through utilizing the Galerkin approach. The finite plate element modal with the Rayleigh-Ritz method with nonlinear thermal-transfer equalization used for thermic spread within the depth by Naghdabadi and Hosseini [4]. Young-Wann [5] considered temperature-dependent material properties to investigate the FG rectangular plates in the same year. Others used Rayleigh-Ritz to obtain a frequency equation. Shahrjerdi et al. [6] used Navier's method to get vibration properties of solar FG plates following thermal loads. Talha

and Singh [7] performed a vibration investigation of FG plates applying the discrete component approach by acknowledging thermo-mechanical loads.

Currently, the effect concerning porosity toward the characteristics of FG structures like beams is considered. Ebrahimi and Jafari [8] discussed the impact of porosities in the beam for vibration analysis under thermomechanical loads. Ebrahimi et al. [9] analyzed the natural frequencies of compositionally assorted beams with various porosities in thermal circumstances. Rezaei and Saidi [10] have examined the significance of porosities on plate vibration features. Huang and Shen [11] worked on the vibration characteristics of temperature-dependent material components.

From the presented report, scholars have not extended research work considering the porosities on 2D FGM plates. The present work is to obtain a finite element approximate interpretation for natural frequencies of graded material plates with porosity. The basics formulation of the plate element has developed, applying the higher-order hypothesis. Finally, the equation of motion regarding the temperature-dependent material plate is acquired, applying Hamilton’s principle and determined with the finite element approach. The formulated solution investigates the influence of porous distribution on 2D FG plates in the thermal circumstances.

2 Formulation of the Problem

Considering the temperature-dependent mechanical properties with a nonlinear equation to analyze the thermal conditions are expressed as

$$P = P_0(P_{-1}T^{-1} + P_1T + P_2T^2 + P_3T^3 + 1) \tag{1}$$

here, T indicates temperature, P_0, P_{-1}, P_1, P_2 and P_3 are the heat-dependent material property coefficients.

2.1 Two-Dimensional (2D) FGM Plates

The 2D-FGM plate with a porous material and with various distributions of metal and ceramic along x and z directions are considered for this analysis as shown in Fig. 1a–c. The changing material attributes (\Re) mentation as modulus of rigidity and density of mass, etc., for the 2D FGM plates are determined [8] using the Voigt model as

$$\Re(x, z, P) = \Re_m(P)\left(v_m(x, z) - \frac{\xi}{2}\right) + \Re_c(P)\left(v_c(x, z) - \frac{\xi}{2}\right) \tag{2}$$

The quantity fraction of ceramic is acquired by power law as shown in below.

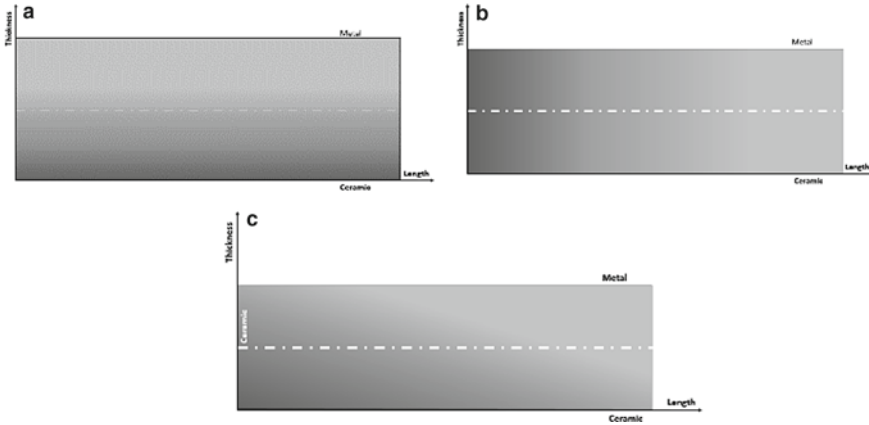


Fig. 1 a Material properties distribution along thickness direction. b Material properties distribution along axial direction. c 2D FG material distribution

$$v_c(x, z) = \left(\frac{1}{2} + \frac{z}{t}\right)^{xa} \left(\frac{x}{L}\right)^{za} \tag{3}$$

The material properties of porous FGM I denote the even distribution of porosity and FGM-II displays the irregular form of porosity as shown in Fig. 2a, b, respectively.

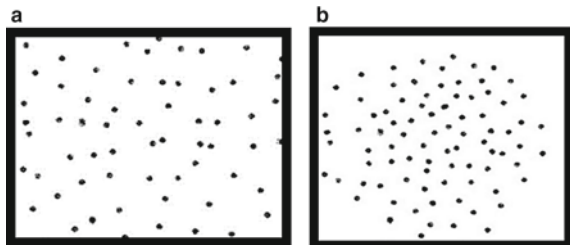
Accordingly above equation modulus of rigidity ‘E’ and Poisson’s ratio ‘ϑ’ of porous 2D FGM-I plate is applied as

$$E(x, z) = E_m(P) + (E_c(P) - E_m(P))v_c(x, z) - \frac{\xi}{2}(E_c(P) + E_m(P)) \tag{4}$$

$$\vartheta(x, z) = \vartheta_m(P) + (\vartheta_c(P) - \vartheta_m(P))v_c(x, z) - \frac{\xi}{2}(\vartheta_c(P) + \vartheta_m(P))$$

Consequently, modulus of rigidity ‘E’ and Poisson’s ratio ‘ϑ’ can be formulated for porous FGM-II as

Fig. 2 a Even distribution of porosities on 2D FG plate. b Uneven distribution of porosities on 2D FG plate



$$E(x, z) = E_m(P) + (E_c(P) - E_m(P))v_c(x, z) - \frac{\zeta}{2}(E_c(P) + E_m(P))\left[1 - \frac{2|z|}{t}\right] \quad (5)$$

$$\vartheta(x, z) = \vartheta_m(P) + (\vartheta_c(P) - \vartheta_m(P))v_c(x, z) - \frac{\zeta}{2}(\vartheta_c(P) + \vartheta_m(P))\left[1 - \frac{2|z|}{t}\right]$$

3 Mathematical Formulation

3.1 Higher Order Shear Deformation Hypothesis

Reddy's equivalences are adapted toward the basic kinematics of plate structures is described below

$$\begin{aligned} u &= u_n + z\theta_x - c_1 z^3 (\theta_x + w_{n,x}), \\ v &= v_n + z\theta_y - c_1 z^3 (\theta_y + w_{n,y}) \\ w &= w_n \end{aligned} \quad (6)$$

The constitutive law relations are generated by using strain-displacement with the neutral axis as the reference that can be formulated as

$$\{\varepsilon^{bd}\} = \begin{Bmatrix} \varepsilon_x \\ \varepsilon_y \\ \gamma_{xy} \end{Bmatrix} = \begin{Bmatrix} \varepsilon_x^{(nx)} \\ \varepsilon_y^{(n)} \\ \gamma_{xy}^{(nx)} \end{Bmatrix} + z \begin{Bmatrix} \varepsilon_x^{(1)} \\ \varepsilon_y^{(1)} \\ \gamma_{xy}^{(1)} \end{Bmatrix} - z^3 \begin{Bmatrix} \varepsilon_x^{(3)} \\ \varepsilon_y^{(3)} \\ \gamma_{xy}^{(3)} \end{Bmatrix} \quad (7)$$

$$\{\gamma^{sh}\} = \begin{Bmatrix} \gamma_{yz} \\ \gamma_{xz} \end{Bmatrix} = \begin{Bmatrix} \gamma_{yz}^{(nx)} \\ \gamma_{xz}^{(nx)} \end{Bmatrix} + z^2 \begin{Bmatrix} \gamma_{yz}^{(2)} \\ \gamma_{xz}^{(2)} \end{Bmatrix} \quad (8)$$

here $c_1 = \frac{4}{3h^2}$ and $c_2 = 3c_1$.

3.2 Finite Element Approach

In this study, a four noded quadrilateral component possessing a joint at an individual intersection with five degrees of freedom is considered. There are two in-plane displacements along the x -axis and y -axis, added one movement along with the oblique inclination—similarly, another two rotation degrees of freedom.

The element displacement vector $\delta^{(n)}$ is written as

$$\{\delta^{(n)}\} = \sum_{i=1}^n N_i \delta_i, \delta_i, \quad (9)$$

here $\{\delta^{(n)}\} = \{u, v, w, \theta_x, \theta_y\}$, the displacement vector per node of an element.

$$\{\delta^{(e)}\} = \{u_i, v_i, w_i, \theta_{xi}, \theta_{yi}\}_{i=1,2,3,4} \quad (10)$$

The matrix represented to shape functions

$$[N] = \{[N_{u_n}] [N_{v_n}] [N_{w_n}] [N_{\theta_x}] [N_{\theta_y}]\}^T \quad (11)$$

The nodal displacement vector of strain can be expressed $\{\delta^{(e)}\}$ as follows

$$\{\varepsilon^{bd}\} = [B_{bd}]\{\delta^{(e)}\} \quad (12)$$

$$\{\gamma^{ss}\} = [B_{ss}]\{\delta^{(e)}\} \quad (13)$$

Characterization of strain energy of an element can be expressed as

$$U_{PE}^{(e)} = \frac{1}{2} \int_0^l \int_0^b [\{\delta^{(e)}\}^T ([K_b^{(e)}] + [K_s^{(e)}]) \{\delta^{(e)}\}] dx dy \quad (14)$$

The component dynamic energy can be expressed as

$$V_{KE}^{(e)} = \frac{1}{2} \int_v \rho(z)(\dot{u}^2 + \dot{v}^2 + \dot{w}^2) dx dy dz \quad (15)$$

The component expressed using kinetic energy ($T^{(e)}$)

$$V_{KE}^{(e)} = \frac{1}{2} \int_0^l \int_0^b [\{\delta^{(e)}\}^T [M^{(e)}] \{\delta^{(e)}\}] dx dy \quad (16)$$

3.3 Thermal Environment Condition

Along the depth direction, the temperature gradient varies nonlinearly is to be considered for this analysis. The simple power function is assumed with a nonlinear temperature gradient along z -direction is presented as

$$T = T_a + \Delta T \left(\frac{1}{2} + \frac{z}{t} \right)^{\alpha} \tag{17}$$

Particularly, in high thermal applications, FGM work with a nonlinear variation of material properties and nonlinear thermal distribution conditions are to consider.

3.4 Governing Equation of Motion

To implement the equation of motion of an element, Hamilton’s system is adopted.

$$\delta \int_{t_1}^{t_2} \left(U_{PE}^{(e)} - V_{KE}^{(e)} \right) dt = 0 \tag{18}$$

The graded material porous plate is divided into a small number of elements, and the energies of kinetic and potential of a component are to be formulated using the displacement vector of an element.

$$U_{PE}^{(e)} = \frac{1}{2} \{ \delta^{(e)} \}^T [K^{(e)}] \{ \delta^{(e)} \} \tag{19}$$

$$V_{KE}^{(e)} = \frac{1}{2} \{ \dot{\delta}^{(e)} \}^T [M^{(e)}] \{ \dot{\delta}^{(e)} \} \tag{20}$$

The global displacement vector, mass, and stiffness matrix of the FGM plate are substituted in the above equation and obtain the governing equation of motion as follows

$$[[K] - \omega_n^2[M]]\{\delta\} = 0 \tag{21}$$

4 Numerical Results and Discussions

4.1 Comparison Study

It is necessary to confirm the validation of the derived formulation before calculating the FGM plate’s vibration characteristics in thermal atmosphere. The vibration characteristics of 2D FG plates by the power-law changes of the material attributes as studied in this work since there are few works, the fundamental frequency of 1D FG plates obtained in this work is compared with Huang and Shen [11] and represented in Table 1. The published results of the frequency parameters are observed to

Table 1 Simply supported temperature-dependent material plate (ZrO₂/Ti-6Al-4V) frequency parameter

Material		Mode				
		(1, 1)	(1, 2)	(2, 2)	(1, 3)	(2, 3)
ZrO ₂	Ref. [11]	7.868	18.659	28.203	34.015	42.045
	Present	7.909	18.669	28.169	34.685	41.564
0.5	Ref. [11]	6.876	16.264	24.578	29.651	36.664
	Present	6.941	16.376	24.701	30.409	36.347
1	Ref. [11]	6.437	15.202	22.956	27.696	34.236
	Present	6.513	15.362	23.166	28.515	34.014
2	Ref. [11]	6.101	14.372	21.653	26.113	32.239
	Present	6.099	14.384	21.688	26.695	31.821
Ti-6Al-4V	Ref. [11]	5.322	12.455	18.766	22.603	27.921
	Present	5.284	12.472	18.819	23.172	27.768

check the present method for numerical correctness. The present numerical results comprise a good agreement with literature results in Table 1.

$$\text{Frequency parameter } \Omega = \bar{\omega}(a^2/h)\sqrt{(\rho_0(1 - \nu^2)/E_0)}$$

4.2 Influence of Even and Uneven Porosities on Natural Frequencies

The axial and thickness direction distribution of two-dimensional FG plate varies from one dimensional FG plate. The geometrical characteristics of a plate with $a/h = 10$, index values are of axil $a_x = 1$, thickness $a_z = 1$ and porosity 0.2 considered for this study. Figures 3 and 4 display the difference of the first-mode frequency

Fig. 3 Variation of even porosity distribution on first mode frequency parameter

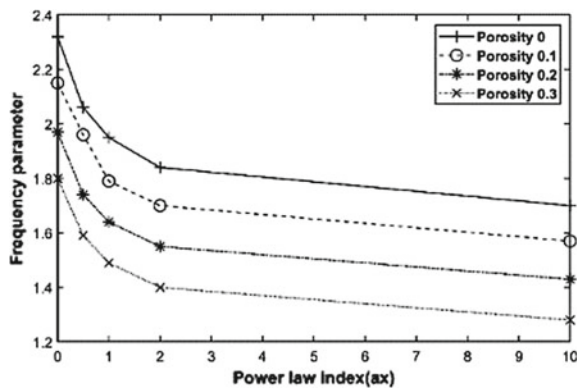
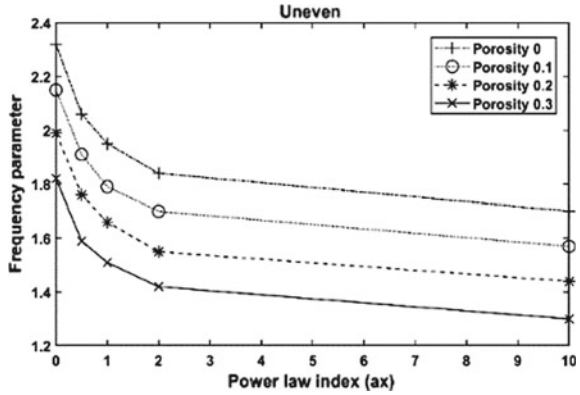


Fig. 4 Variation of uneven porosity distribution on first mode frequency parameter



parameters by the axial grading criteria for even and uneven distribution, respectively. The parameters of frequency in these figures are varied with various even and uneven porosities. The effect of the distribution of porosity on the setting of frequency inconsiderably declines by the raise in the porous value (0, 0.1, 0.2, 0.3), although the index values kept constant.

In Fig. 5, the comparison between the even and the uneven porous volume fractions of 0.2 and 0.3 is illustrated for numerous values of the axial indexes. With that same thermal circumstance, the even and uneven porous volume fractions are applied to determine the frequency parameter. The frequency parameter is varied for even and uneven porous characteristics.

Figure 6 explains the effect of temperature difference on the frequency parameter of porous 2D FG plate with even and uneven circumstances. Also, it is seen that the effect of the uneven porous condition is more frequency than the even porous condition with constant porous volume fraction. Thus, it can be said that the uneven porous condition is very important to study 2D FG plates.

Fig. 5 Comparison of even and uneven porosities distribution on frequency parameter of plate

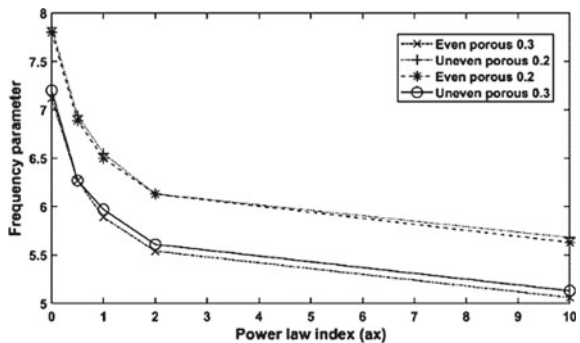
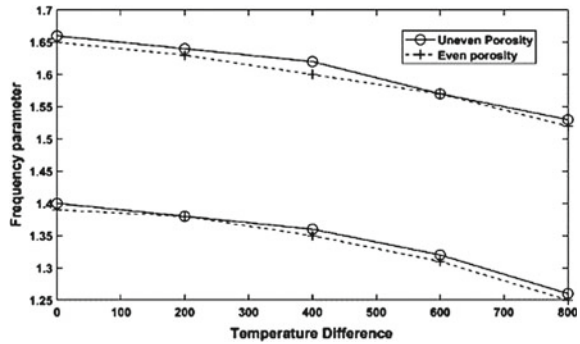


Fig. 6 Frequency parameter variation with rise of temperature of even and uneven porosities of FGM plate



5 Conclusion

The basic formulation of porous FGM plates is modeled utilizing the higher-order hypothesis, and a numerical explication has been proposed by using the finite element approach. These concepts of even and uneven porous circumstances are developed and utilized to formulate 2D FG plates. It has implied that the parameters of frequencies concerned by the present numerical method are in good compromise with the published research work. Subsequently, the uniform and nonuniform distribution of porosity, the bidirectional modification of material characteristics, and temperature on the 2D FG plates have studied. The fundamental frequency of 2D FGM plate is decreased as the porosity increase; it has observed in this study. The future scope is focused on the experimental analysis of the FGM strictures under different operating environments.

References

1. Zhang, D.G., Zhou, Y.H.: A theoretical analysis of FGM thin plates based on physical neutral surface. *Comput Mater Sci* **44**, 716–720 (2008)
2. Reddy, J.N., Chin, C.D.: Thermomechanical analysis of functionally graded cylinders and plates. *J. Therm. Stresses* **21**, 593–626 (1998)
3. Yang, Y., Shen, H.S.: Vibration characteristics and transient response of shear-deformable functionally graded plates in thermal environments. *J. Sound Vib.* **255**(3), 579–602 (2002)
4. Naghdabadi, R., Hosseini KordkheJli, S.A.: A finite element formulation for analysis of functionally graded plates and shells. *Arch. Appl. Mech.* **74**, 375–386 (2005)
5. Kim, Y.-W.: Temperature dependent vibration analysis of functionally graded rectangular plates. *J. Sound Vib.* **284**, 531–549 (2005)
6. Shahrjerdi, A., Mustapha, F., Bayat, M., Majid, D.L.A.: Free vibration analysis of solar functionally graded plates with temperature dependent material properties using second order shear deformation theory. *J. Mech. Sci. Technol.* **25**(9), 2195–2209 (2011)
7. Talha, M., Singh, B.N.: Thermo-mechanical induced vibration characteristics of shear deformable functionally graded ceramic-metal plates using the finite element method. *Proc Inst Mech Eng Part C: J Mech Eng Sci* **225**:50–65 (2011)

8. Ebrahimi, F., Ghasemi, F., Salari, E.: Investigating thermal effects on vibration behavior of temperature-dependent compositionally graded Euler beams with porosities. *Meccanica* **55**, 223–249 (2016)
9. Ebrahimi, F., Jafari, A.: A Higher-order thermomechanical vibration analysis of temperature-dependent FGM beams with porosities. *J. Eng.* 1–20 (2016)
10. Rezaei, A.S., Saidi, A.R.: Exact solution for free vibration of thick rectangular plates made of porous materials. *Compos. Struct.* **134**, 1051–1060 (2015)
11. Huang, X.-L., Shen, H.-S.: Nonlinear vibration and dynamic response of functionally graded plates in thermal environment. *Int. J. Solids Struct.* **41**, 2403–2427 (2004)

FEA Approach for Modal Analysis of an Electric Motor in Electric Vehicle Drive



Tushar Amale, Prajwal Badwaik, Sumedh Durge, Ajay Dube, and Amit Belveker

Abstract This paper represents a modal analysis of electric motor in electric drive for determining the modal vibration of electric motor by using the modeling, finite element meshing and the computation of modal vibration for electric motor. Electric motor parts are created and assembled in Catia V5 which facilitated the easy assembly of the complex parts. Discretization of electric motor is carried out in hyper mesh as it converts the domain into mesh and easily shows the failure element. Computation of modal vibration is done by using the numerical method. To avoid the resonance rigid body and natural frequencies are calculated at different mode and shown.

Keywords Catia V5 · Hypermesh · Finite element meshing · Abacus · Electric motor · Modal analysis

1 Introduction

In recent years electric motors have attracted the attention of researchers and automotive companies due to the pressing environmental issues. The vibration and noise in the electric motor are mostly generated by the electromagnetic forces due to electric

T. Amale (✉) · P. Badwaik · S. Durge · A. Dube · A. Belveker
Department of Mechanical Engineering, Savitribai Phule Pune University, Pune, Maharashtra, India
e-mail: tnamale@mitaoe.ac.in

P. Badwaik
e-mail: ppbadwaik@mitaoe.ac.in

S. Durge
e-mail: sgdurge@mitaoe.ac.in

A. Dube
e-mail: abdube@mitaoe.ac.in

A. Belveker
e-mail: abbelveker@mitaoe.ac.in

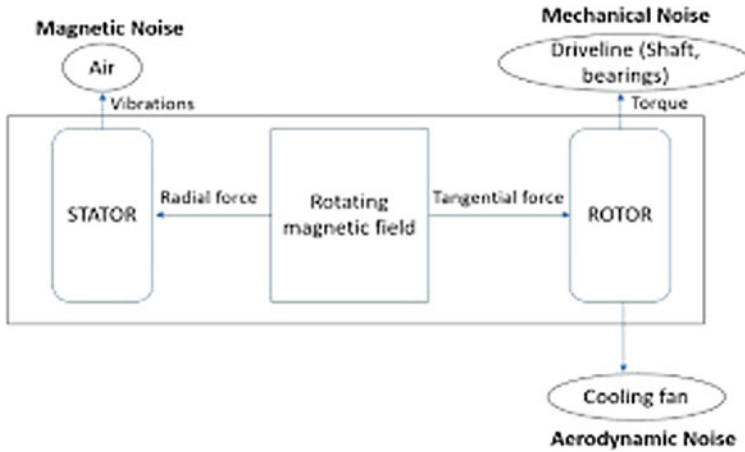


Fig. 1 Generation of noise of different origin in electric motor

energy supply to electric motor and subsequently can be amplified by the dynamic response of the motor structure. Vibrational behavior of electric motor can be found out by modal analysis. By calculation, modal analysis takes a lot of time so numerical method is used for the computation of the modal vibration in the electric motor. The vibrating noise in electric motor is phenomenon of complex nature and origin. Generation of noise of different origins in rotating electrical machine is, the first one is electromagnetic vibration in which noise is produced due to the magnetic force, the second cause of noise is mechanical which is due to the structural problem in mechanical assembly and the third one is aerodynamic noise which is due to the flow of ventilating air through or over the motor. These sources are illustrated in Fig. 1.

Energy conversion happening in the electric motor is from electric energy to vibrating energy. The electric supply to the electric motor produces magnetic field subsequently which produces magnetic forces. This magnetic force excites the stator-frame winding parts in electric motor which produces the mechanical vibration. There have been magnetic, mechanical and aerodynamic noise creation and the behavior of motor under that noise is very well explained in the paper by Sathyan et al. [1]. A detailed review on the different forms of vibration and noise in electrical motors can be found in a paper by Vijayraghavan [2].

Inspired by the studies and findings in the research paper this paper investigated the aspect of noise vibration in electric motor and formulated the most favorable approach to find out the modal vibration. Modeling, finite element meshing and computational methodology represent the successfully numerical technique for computation of modal vibration generated by electric motor. Although many studies have been carried out in this field of research, this paper contributes through fully modeling, meshing and numerically analysis of electric motor and implementation of which is explained in detail.

This FEM modeling approach of doing this project makes us very comfortable by creating the complex geometry very simple in Catia V5 then discretization of domain in hypermesh increases the quality of the result and also result of computation of the modal frequencies at the different modes gives in seconds which makes project very efficient.

2 Methodology

This section explains the methods to get the numerical computational result. Methodology involves three models: first modeling of electric motor, second one is finite element meshed model and last one is modal analysis. The results of the numerical simulations are presented in this section.

2.1 Modeling

The modeling of the electric motor parts like stator, rotor, winding, frame, front housing, end housing, mid housing, magnet, drive shaft, etc., are done in CatiaV5. There are 39 parts assembled in the assembly of the electric motor. Assembly of electric motor is shown in Fig. 2 and assembled parts are given Table 1.

2.2 Finite Element Model

Finite element meshing is performed in hyper mesh with the standard element shown in Table 2 and the operating parameter is given in Table 3. The general idea behind discretization is to break a domain into a mesh, and then replace derivatives in the governing equation with difference quotients. There are several ways in which this can be done—the most prominent being forward difference, backward difference and central difference. In the meshing of this model we have used two types of element one is hexahedral and second one is tetrahedral. One Hexahedral corresponds to six Tetrahedral. Linear hexahedral uses Gauss integration points to generate the element characteristics stiffness, mass, and tetrahedral uses exact formula without any integration to get the same characteristics. 1st order hexahedral element is used where simple of geometry and 2nd order tetrahedral element is used where the complex shape of the geometry. Refined FEM models are shown in Fig. 3.

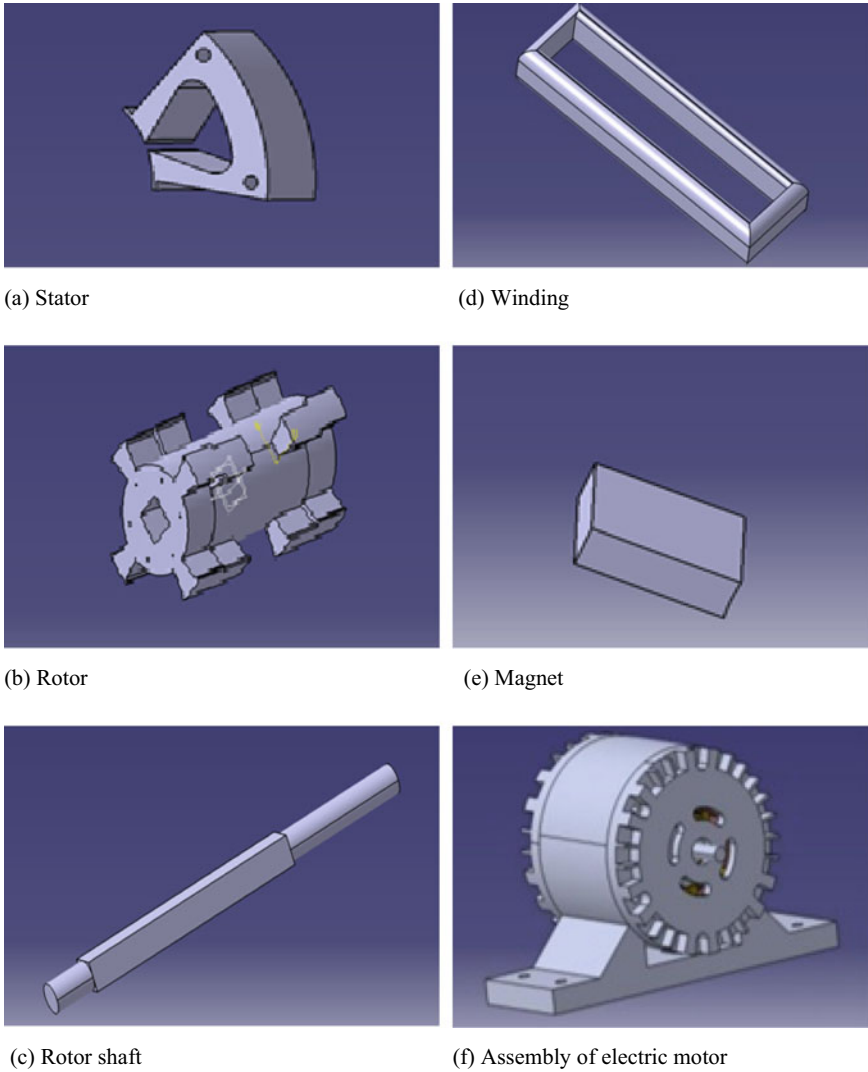


Fig. 2 Assembled parts of electric motor

3 Results and Discussion

The results of the numerical simulations are presented in this section. The Modal vibration frequency computation of electric motor is done by using Abacus software. We have calculated the rigid body and natural frequencies which are tabulated in Table 4. The mode shape frequencies along the three axial and three rotational axes are shown in Fig. 4. Along the x , y and z direction first three rigid body frequencies

Table 1 Modeling parts and repetition

S. No.	Part name	No of part
1.	Machine base plate	1
2.	Frame key LHS and RHS	2
3.	Magnet	12
4.	mid housing	1
5	Outer sleeve	1
6.	Rotor	1
7.	Shaft	1
8.	Side housing LHS, side housing RHS	2
9.	Stator blocks	12
10.	Winding	6

Table 2 Finite element meshing parameter

S. No.	Part name	Element type	Material property
1	Machine base plate	2nd order tetrahedral	Mild steel
2	Frame key lhs and rhs	1st order hex	Mild steel
3	Magnet	1st order hex	iron or nickel
4	Mid housing	2nd order tetrahedral	Mild steel
5	Outer sleeve	1st order hex	Mild steel
6	Rotor	2nd order tetrahedral	Mild steel
7	Shaft	2nd order tetrahedral	Mild steel
8	Side housing LHS, side housing RHS	2nd order tetrahedral	Mild steel
9	Stator blocks	1st order hex	Mild steel
10	Winding	2nd order tetrahedral	Copper

Table 3 Operating parameter of electric motor

S. No.	Parameter	Magnitude	Unit
1	Power	150	Watt
2	Voltage	24	Volt
3	Speed	2000	RPM

are zero which shows that it does not vibrate along the x , y and z direction and along the rotational axes it has some values which shows it deflects along the rotational axes.

Onward we have calculated the natural frequencies of vibration up to 20 modes. These frequencies should not be matched with natural frequency of car, if it did there will be a chance of resonance and that could be a very dangerous situation.

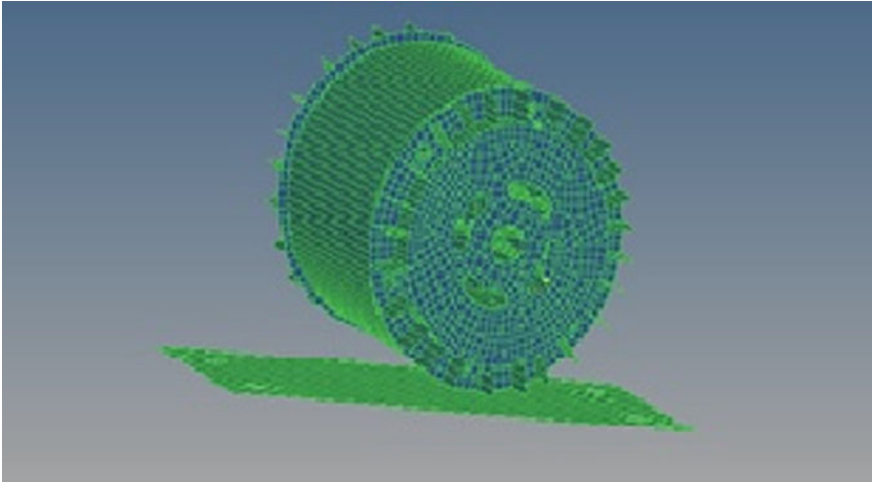
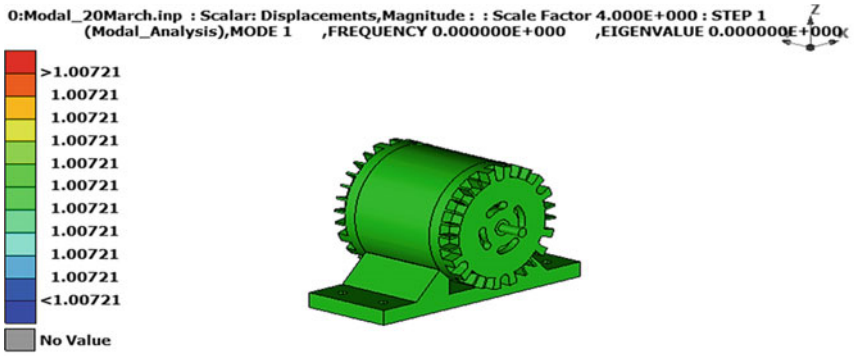


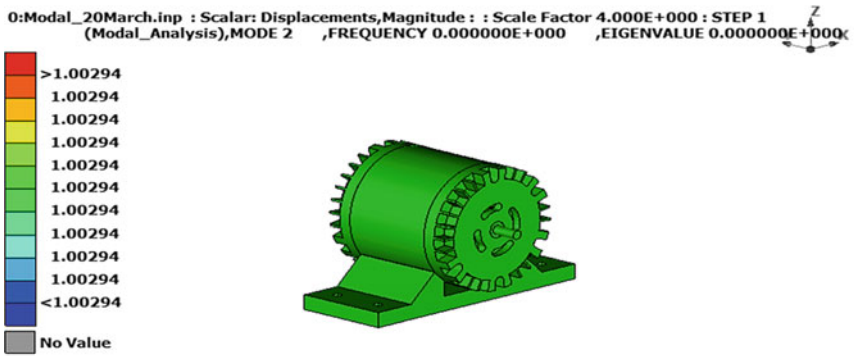
Fig. 3 Finite element meshed model

Table 4 Modal analysis results

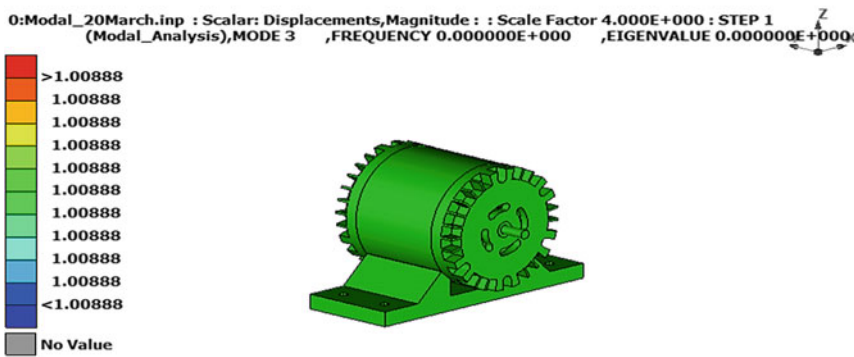
S. No.	Frequencies	Modes	Frequency (Hz)
1	Rigid body modes	1	0
2		2	0
3		3	0
4		4	32.565
5		5	33.389
6		6	39.827
7	Natural frequency	7	1164.4
8		8	1888.4
9		9	1891.4
10		10	2317.8
11		11	2515.7
12		12	2866.2
13		13	2981.6
14		14	3335.3
15		15	3514.7
16		16	3691.8
17		17	3766
18		18	4527.6
19		19	4909.3
20		20	4957.6



(a)



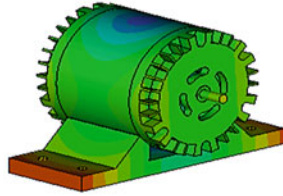
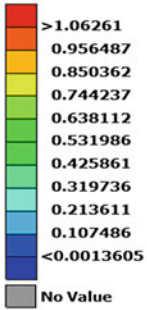
(b)



(c)

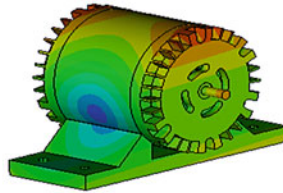
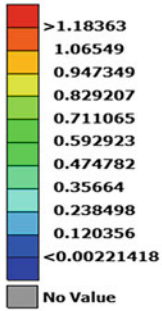
Fig. 4 Mode 1, 2, 3, 4, 5 and 6 for electric motor

0:Modal_20March.inp : Scalar: Displacements,Magnitude : : Scale Factor 4.000E+000 : STEP 1
(Modal_Analysis),MODE 4 ,FREQUENCY 3.256500E+001 ,EIGENVALUE 4.186604E+004



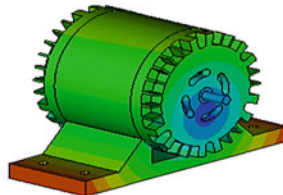
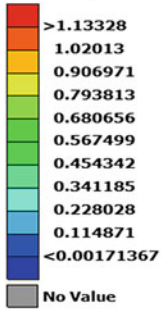
(d)

0:Modal_20March.inp : Scalar: Displacements,Magnitude : : Scale Factor 4.000E+000 : STEP 1
(Modal_Analysis),MODE 5 ,FREQUENCY 3.338900E+001 ,EIGENVALUE 4.401154E+004



(e)

0:Modal_20March.inp : Scalar: Displacements,Magnitude : : Scale Factor 4.000E+000 : STEP 1
(Modal_Analysis),MODE 6 ,FREQUENCY 3.982700E+001 ,EIGENVALUE 6.262027E+004



(f)

Fig. 4 (continued)

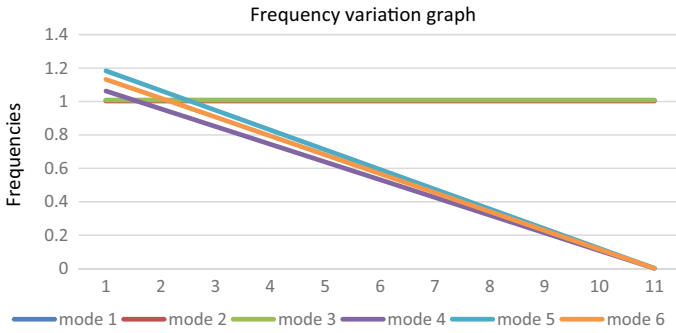


Fig. 5 Frequency variation for various mode

Table 5 Frequency variation for various mode

Frequencies	Mode 1	Mode 2	Mode 3	Mode 4	Mode 5	Mode 6
Max frequency	1.00721	1.00294	1.00888	1.06261	1.18363	1.13228
	1.00721	1.00294	1.00888	0.956487	1.06549	1.02013
	1.00721	1.00294	1.00888	0.850362	0.947349	0.906971
	1.00721	1.00294	1.00888	0.744237	0.829207	0.793813
	1.00721	1.00294	1.00888	0.638112	0.711065	0.680656
	1.00721	1.00294	1.00888	0.531986	0.592923	0.567499
	1.00721	1.00294	1.00888	0.425861	0.474782	0.454342
	1.00721	1.00294	1.00888	0.319736	0.35664	0.341185
	1.00721	1.00294	1.00888	0.213611	0.238498	0.228028
	1.00721	1.00294	1.00888	0.107486	0.120356	0.114871
Min frequency	1.00721	1.00294	1.00888	0.00136	0.002214	0.0017136

To avoid this condition we have to calculate frequency of motor so that resonance phenomenon cannot happen.

Graphical representation of the frequency variation along the translational and rotational axis is shown in graph (Fig. 5) obtained through simulation results which are also illustrated in Table 5. It shows that mode 1, 2, 3 shows no frequency variation (along translational axis) as it is a straight line whereas mode 4, 5, 6 shows frequency variation (along rotational axis) as the line is deflecting.

4 Conclusion

This paper successfully illustrated how the model is proposed, meshed and analyzed using numerical method.

The modal frequency obtained in the result (Table 4) shows that motor does not vibrate along the translation axes and it vibrates over the rotational axes.

So, the natural frequencies up to 20 modes show that it has very less chance to match up with natural frequencies of car so that it will avoid the resonance.

5 Application of This Approach

1. Modal analysis numerical approach is used in numerous application, more important are like aerospace engineering, automobiles, defence equipments, fixed and rotary wing aircrafts, machine tools and rotating equipment.
2. Vibration in electric motor creates the heat, so for the dissipation of heat we can do the experimental as well thermal analysis in future.

References

1. Sathyan, S., Aydin, U., Belahcen, A.: Acoustic noise computation of electrical motors using the boundary element method. *Energies* (2020, January 3)
2. Vijayraghavan, P.: Krishnan, R (1998), Noise in electric machines: a review. *IEEE Trans. Ind. Appl.* **35**, 1007–1013 (1998)
3. Belmans, R.J.M., D’Hondt, L., Vandenput, A., Geysen, W.: Analysis of the audible noise of three phase squirrel cage induction motors supplied by inverters. *IEEE Trans. Ind. Appl.* **23**, 842–947 (1987)
4. Besnerais, J.L., Lanfranchi, V., Hecquet, M., Brochet, P.: Characterization and reduction of audible magnetic noise due to PWM supply in induction machines. *IEEE Trans. Ind. Electron.* **57**, 1288–1295 (2010)
5. Le Besnerais, J., Lanfranchi, V., Hecquet, M., Brochet, P., Friedrich, G.: Acoustic noise of electromagnetic origin in a fractional-slot induction machine. *COMPEL-Int. J. Comput. Math. Electr. Electron. Eng.* **27**, 1033–1052 (2008)
6. Besnerais, J.L.: Fast prediction of variable-speed acoustic noise due to magnetic forces in electrical machines. In: *Proceedings of the XXII International Conference on Electrical Machines (ICEM)*, Lausanne, Switzerland, 4–7 September, pp. 2259–2265 (2016)
7. Ko, H., Kim, K.: Characterization of noise and vibration sources in interior permanent-magnet brushless DC motors. *IEEE Trans. Mag.* **40**(6)
8. Gieras, J.F., Wang, C., Lai, J., Ertugrul, N.: Analytical prediction of noise of magnetic origin produced by permanent magnet brushless motors. In: *2007 IEMDC ‘07 IEEE International Electric Machines & Drives Conference*, Hamilton Sundstrand, Rockford (2007)
9. Timar, P.L.: *Noise and Vibration of Electrical Machines*. Springer, London (1988)
10. Furlan, M., Cernigoj, A., Boltežar, M.: A coupled electromagnetic-mechanical-acoustic model of a DC electric motor. *COMPEL-Int. J. Comput. Math. Electr. Electron. Eng.* **22**, 1155–1165 (2003)

Analysis of Interference-Fit Orbital Motor Using Finite Element Analysis in ANSYS Workbench



Dinesh Kumar Ramesh, Avinash Ramakrishnan Rao,
Sai Tharun Reddy Garlapati, and Abhijit Nag

Abstract In the present work, the finite element analysis of interference-fit rotor-stator assembly of orbital motor has been carried out. The main drawback of a running-fit orbital motor is the generation of gaps between the rotor and the stator under working conditions. Gaps generated at the transition contacts lead to fluid leakages from the High-Pressure Zone to the Low-Pressure Zone. These leakages cause a reduction in pressure differential. Due to this loss in pressure, the output torque as well as the overall efficiency is affected. Therefore, in order to overcome this drawback, interference is provided in the rotor-stator assembly. In the present work, the interference is provided by increasing the radius of the rollers. The contact analysis is carried out in ANSYS Workbench. The values of stresses and deformation for two different positions of the rotor is obtained.

Keywords Rotary piston machines · Orbital motor · FEA · CAD/CAE

D. K. Ramesh · A. R. Rao (✉) · S. T. R. Garlapati · A. Nag
Department of Mechanical Engineering, Birla Institute of Technology, Mesra, Ranchi 835215,
India
e-mail: avinash.rao2998@gmail.com

D. K. Ramesh
e-mail: rdkumaar99@gmail.com

S. T. R. Garlapati
e-mail: tharunreddy1997.g@gmail.com

A. Nag
e-mail: abhijitnag@bitmesra.ac.in

1 Introduction

Orbital Motor is Low Speed High Torque (LSHT) hydrostatic motor which converts hydraulic pressure energy into rotational mechanical energy. It falls under floating-axis type Rotary Piston Machines (ROPIMA). These machines consist of epitrochoid-shaped rotor acting as the piston and an envelope acting as the stator (Fig. 1).

The first work on profiles useful for epitrochoid generated star and ring gear was developed by Ansdale and Lockley [1] while working on the rotor-stator design of Wankel engines and similar Rotatory Piston Machines (ROPIMAs). In their approach, the epicyclic motion of two centrodes was considered as the base circles of the epitrochoid and its envelope. Colbourne [2, 3] formulated a unique procedure for development of envelope of trochoidal profiles which perform planetary motion. Robinson and Lyon [4] proposed methods on modification of epitrochoidal profiles which were more useful for ROPIMAs. These modified profiles were called 'constant difference modified epitrochoid'. Due to this modification, the active envelope of this profile transforms into a circular arc. Stryczek [5, 6] and Biernacki and Stryczek [7] used cycloidal gear tooth design methods to design GEROTOR type ROPIMAs. In their approach, the epitrochoid was generated by rolling the generating circle on the outer periphery of a fixed circle. Nag and Maiti [8] unified the various geometric design approaches for profile generation of epitrochoid generated star rotor used in ROPIMA type hydrostatic units. The dissimilarity in expressions of profile geometries obtained by different methods mentioned before arises due to the differences in coordinate system considerations and pair of centrodes used to generate the profile.

Maiti and Sinha [9] established the geometric as well as kinematic relations among the different epitrochoid generated ROPIMAs. Maiti [10] also established the theoretical guidelines for the sequence of change in chamber states. As the rotor rotates, pressurized fluid enters the chambers that undergo expansion and fluid is discharged from the chambers that undergo compression. At any instant, either three or four adjacent chambers are in compression phase and the remaining chambers are in expansion phase. The phase lag of a piston which is at a dead centre, with the piston reaching the opposite dead centre is given by

Fig. 1 Cross-sectional view of orbital motor (www.orbitalmotors.net)



$$\xi_o = \pi/Z(Z - 1) = \pi/42 \quad (1)$$

The deformation and gap generated at the contacts were obtained for both epitrochoid generated rotor-stator assembly of fixed and floating axis ROPIMA type hydrostatic unit by Maiti [11, 12]. A dimensionless analytical technique based on Hertz's contact theory was used. Roy et al. [13] used FEM approach to estimate the deformation and gap generated in running fit rotor-stator assembly of orbital motors.

The main drawback of a running-fit orbital motor is the generation of gaps between the rotor and the rollers under working conditions. When these gaps are generated at the transition contacts, which separate the chambers at high pressure from those at low pressure, there is a loss in pressure differential between the High-Pressure Zone (HPZ) and Low-Pressure Zone (LPZ). Due to this loss in pressure, the output torque as well as the overall efficiency is affected. Therefore, in order to overcome this drawback, interference is provided in the rotor-stator assembly.

Interference in the rotor-stator assembly can be achieved by the following ways:

- Increasing the chordal thickness of the epitrochoid
- Decreasing the pitch circle radius
- Increasing the roller radius (Fig. 2).

Any investigation on the analysis of interference-fit type orbital motor is not available in open literature. In the present investigation we have used FEM approach to estimate the stresses and deformation generated in the rotor-stator assembly of an interference-fit orbital motor, for two different angular positions of the rotor under static and no fluid condition. Interference is provided by increasing the radius of rollers.

2 Methodology

2.1 Modelling

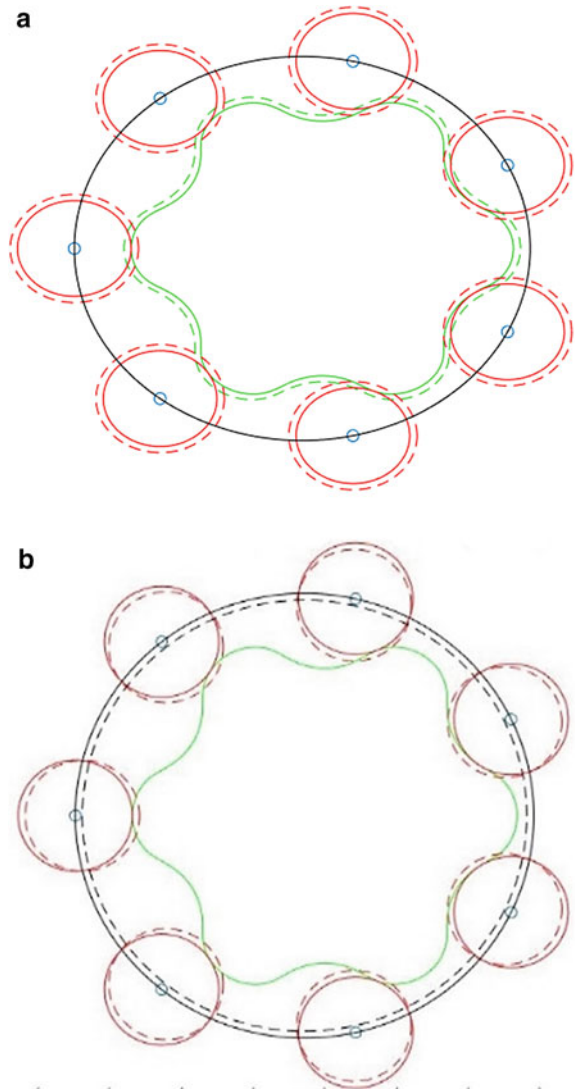
The profile for the constant difference modified epitrochoid and its active envelope is plotted in MATLAB. Lockley's approach is used to obtain the unmodified epitrochoid, which is then modified by parallelly shifting the generated curve along the direction normal to the unmodified epitrochoid. This gives the equation of modified epitrochoid as:

$$X_m = A_o \cos \psi + C_o \cos Z\psi - r_m \cos(\psi + \varphi) \quad (2)$$

$$Y_m = A_o \sin \psi + C_o \sin Z\psi - r_m \sin(\psi + \varphi) \quad (3)$$

The envelope is the outer boundary for the orbiting motion of the rotor. Due to the implementation of constant difference modification of the epitrochoidal profile, the

Fig. 2 a Introducing interference by increasing chordal thickness and roller radius. **b** Introducing interference by decreasing pitch circle radius



active envelope becomes a circular arc, which permits the placement of the rollers with their centers at the crunodes. Location of crunodes (Fig. 3; Table 1):

$$X_c = A_o \cos(\pi(2 * n - 1)/7) - C_o \tag{4}$$

$$Y_c = A_o \sin(\pi(2 * n - 1)/7) \tag{5}$$

Fig. 3 Profile of modified epitrochoid and its envelope

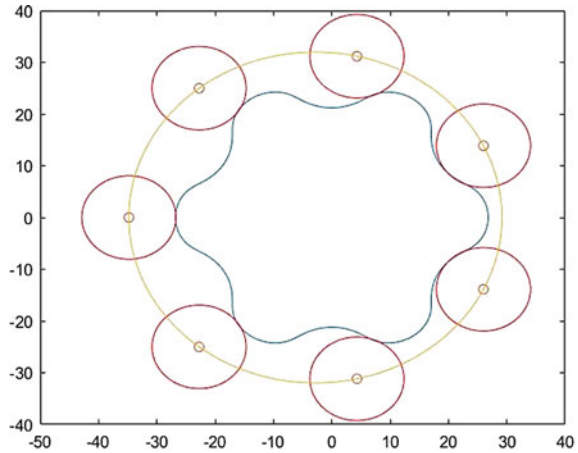


Table 1 Parameters and its values

Parameters (in mm)	Values
Diameter of the outer centrode (D)	39.361
Diameter of the inner centrode (d)	33.738
Generating point arm (A_o)	31.9808
Amount of parallel shifting of profile (r_m)	7.9706
Centre distance (C_o)	2.8115
Interference	0.004

The points obtained from MATLAB are used to generate a CAD model of the rotor-stator assembly in CATIA V5 (Fig. 4).

2.2 Analysis

The 3D CAD model generated in CATIA V5 was imported into Ansys Mechanical Static Structural in order to perform the Finite Element Analysis of the rotor-stator assembly. The assembly was modeled using AISI 4340 Alloy Steel with the following properties (Table 2).

Mesh The three-dimensional hex-dominant structured mesh is used to model the assembly. The SOLID186 element is used which is a 3D higher order 20 node (including midside nodes) solid element. Advanced size function is used to capture curvature in the assembly. A convergence study is performed and the following mesh parameters are used (Fig. 5; Table 3).

The same mesh parameters were used for the rotor position $\xi = 2.1428^\circ$.

Fig. 4 3D model of the rotor-stator assembly for $\xi = 0^\circ$

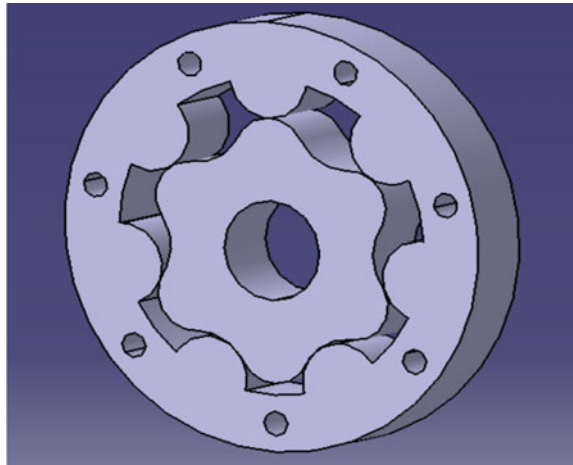


Table 2 Material properties

Properties	Values
Tensile strength	745 MPa
Yield strength	470 Mpa
Poisson's ratio	0.3

Fig. 5 Meshed model of the rotor-stator assembly for $\xi = 0^\circ$

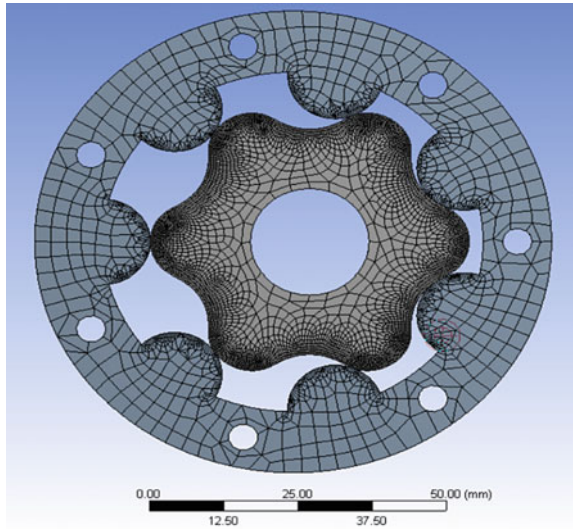


Table 3 Mesh parameters

Defaults	Physical preference	Mechanical
	Relevance	0
Sizing	Use advanced size function	On: curvature
	Relevance centre	Medium
	Smoothing	Medium
	Transition	Fast
Mesh control	Face sizing	0.2 mm on all contacting surfaces
	Behavior	Soft

Table 4 Contact parameters

Type	Frictionless
Behavior	Auto asymmetric
Formulation	Pure penalty
Detection method	Program controlled
Normal stiffness	9.87e8 N/m [14]

Contact Definition Seven different contacts were generated in the rotor-stator assembly. Hence seven different contact regions were manually added. The contact type selected for solving this problem was frictionless contact. The target surface is modeled using TARGE170 elements and the contact surface is modeled using CONTA174 elements. These are 8 node surface-to-surface contact elements. The contact behavior was set to auto-asymmetric. The contact formulation was set to Pure Penalty which is a penalty-based method mainly used to model nonlinear solid contact. This formulation was chosen as it is more sensitive to the magnitude of contact stiffness which is obtained from previously established results. The following parameters are used (Table 4):

Boundary Conditions Fixed support was given to the faces of the holes in the stator. This type of boundary condition prevents any flat or curved face from moving or deforming. It restricts all the degrees of freedom (DOFs) for any selected surface, edge or vertices.

Remote displacement was given to the face of the rotor. The motion along *X*, *Y* directions was allowed and motion along *Z* direction was restricted. The rotations about *X*, *Y* and *Z* axes were also restricted. This falls under the category of remote boundary conditions. A remote displacement can be used to apply displacements as well as rotations at any arbitrary location in space (Fig. 6).

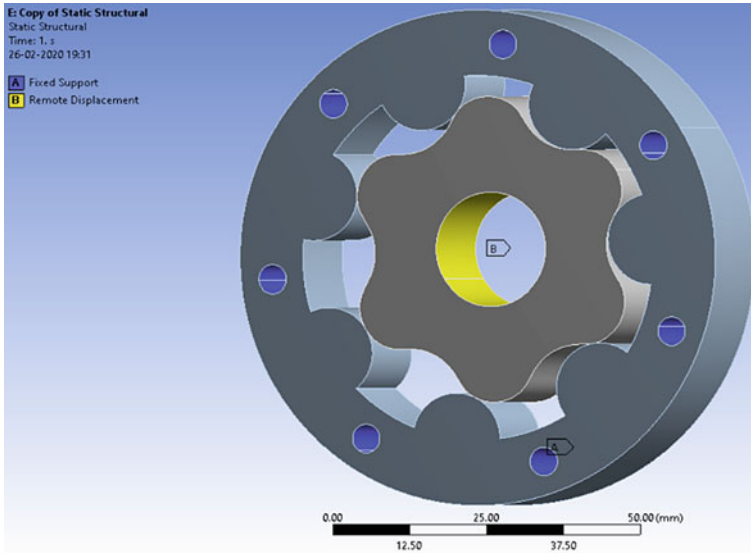


Fig. 6 Boundary conditions

3 Results and Discussion

Initial penetration of 0.004 mm is provided between the rotor and stator as shown in the Fig. 7a.

After performing contact analysis, the penetration reduces to a negligible value as shown in the Fig. 7b.

The stresses generated in rotor and stator for two different angular positions are as shown in the Fig. 8.

Deformation of rollers at each contact is obtained along the direction of contact normal by defining local coordinate system in the given directions. This direction is found by joining the point of intersection of the centrodes (i.e. instantaneous center) and the crunodes. The directional deformation at roller 1 is as shown in the Fig. 9.

The directional deformation at each roller for two different angular positions of rotor is as follows (Table 5).

The contact settings and boundary conditions assigned for the following analysis were also assigned for a similar analysis in which the rotor was considered rigid. The directional deformation at each contact, in a direction normal to the contact, was found for different angular positions of the rotor. The value of this directional deformation was plotted against angular position of rotor, for each of the seven contacts. This method is validated by comparing the plot of deformation at the contacts obtained by the present approach which is based on Finite Element Analysis with the plot of deformation obtained by minimum potential energy method as

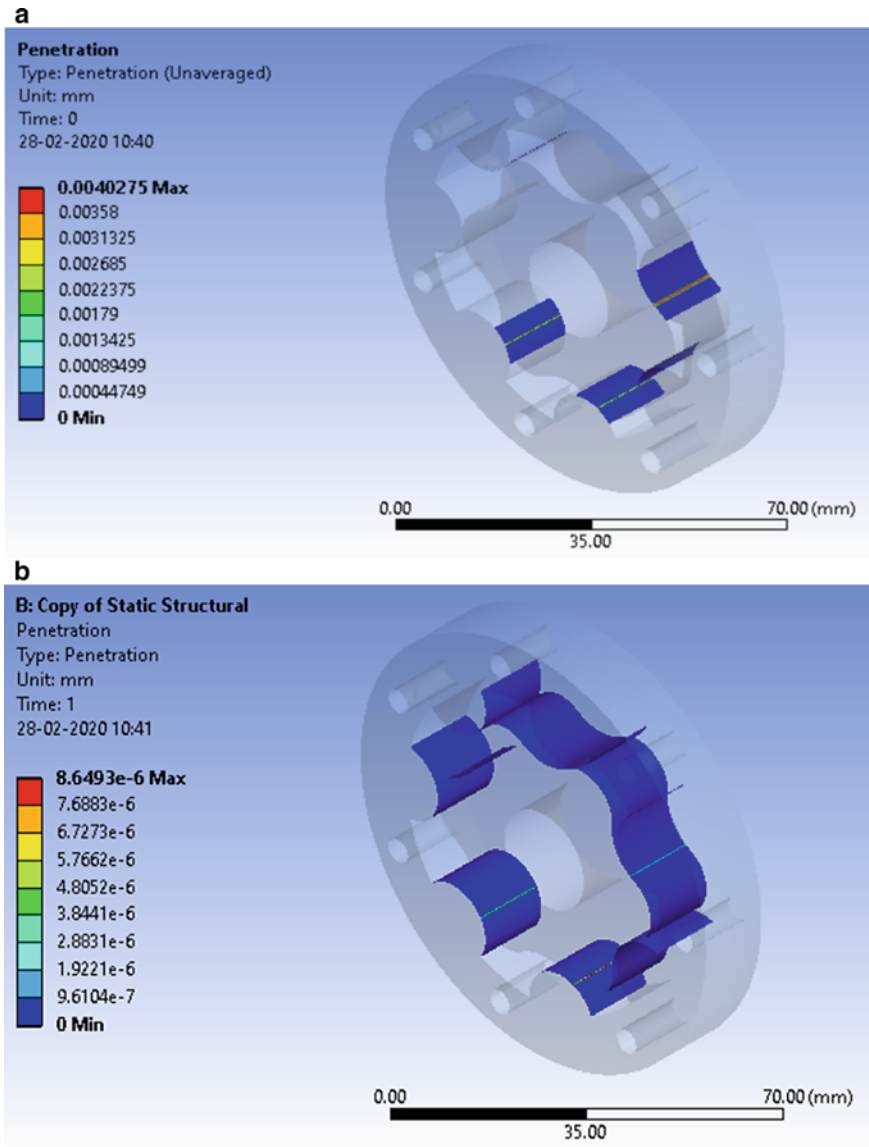


Fig. 7 a Initial penetration. b Final penetration after analysis

described by Nag et al. [15]. The difference in the value of directional deformation arises due to the difference in the chosen value of interference (Fig. 10).

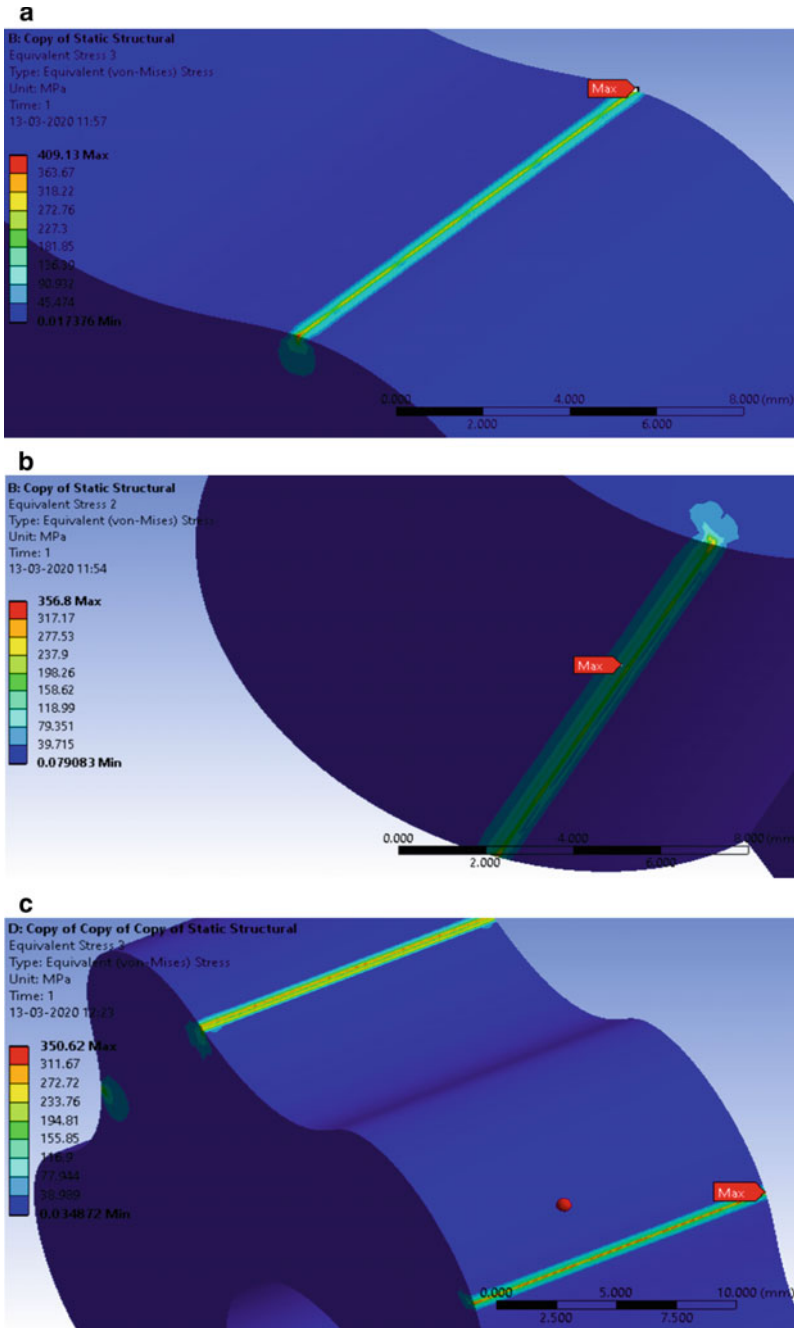


Fig. 8 a Stresses in rotor at $\xi = 0^\circ$. b Stresses in stator at $\xi = 0^\circ$. c Stresses in rotor at $\xi = 2.1428^\circ$. d Stresses in stator at $\xi = 2.1428^\circ$

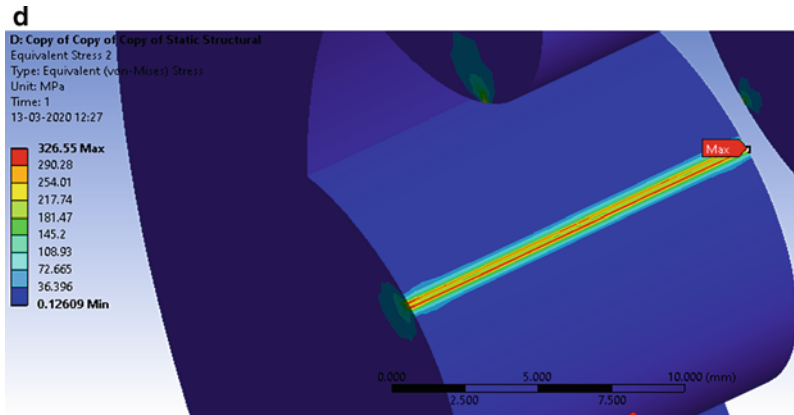


Fig. 8 (continued)

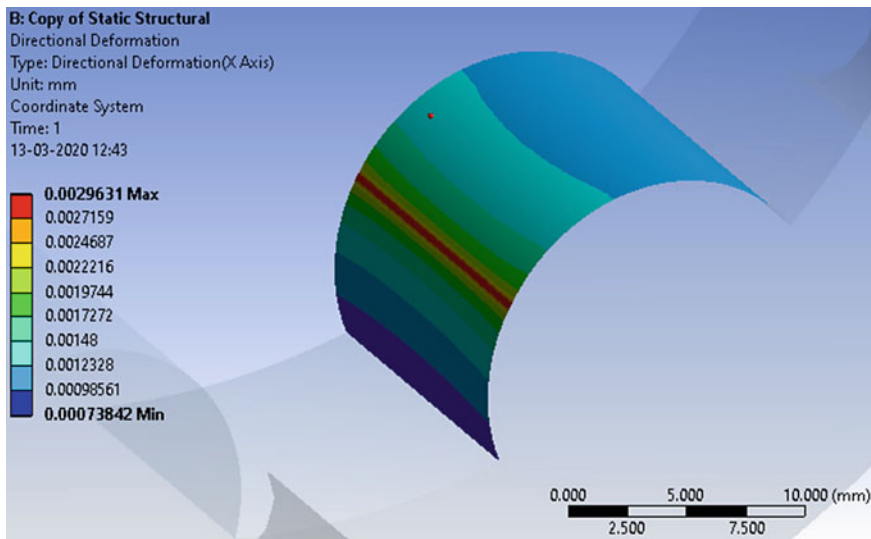


Fig. 9 Directional deformation in roller at $\xi = 0^\circ$

Table 5 Directional deformation

Contact	$\xi = 0^\circ$ (mm)	$\xi = 2.1428^\circ$ (mm)
1	0.002963	0.003056
2	0.001731	0.001768
3	0.000948	0.001214
4	0.000586	0.000728
5	0.001045	0.000728
6	0.001647	0.001629
7	0.002978	0.002671

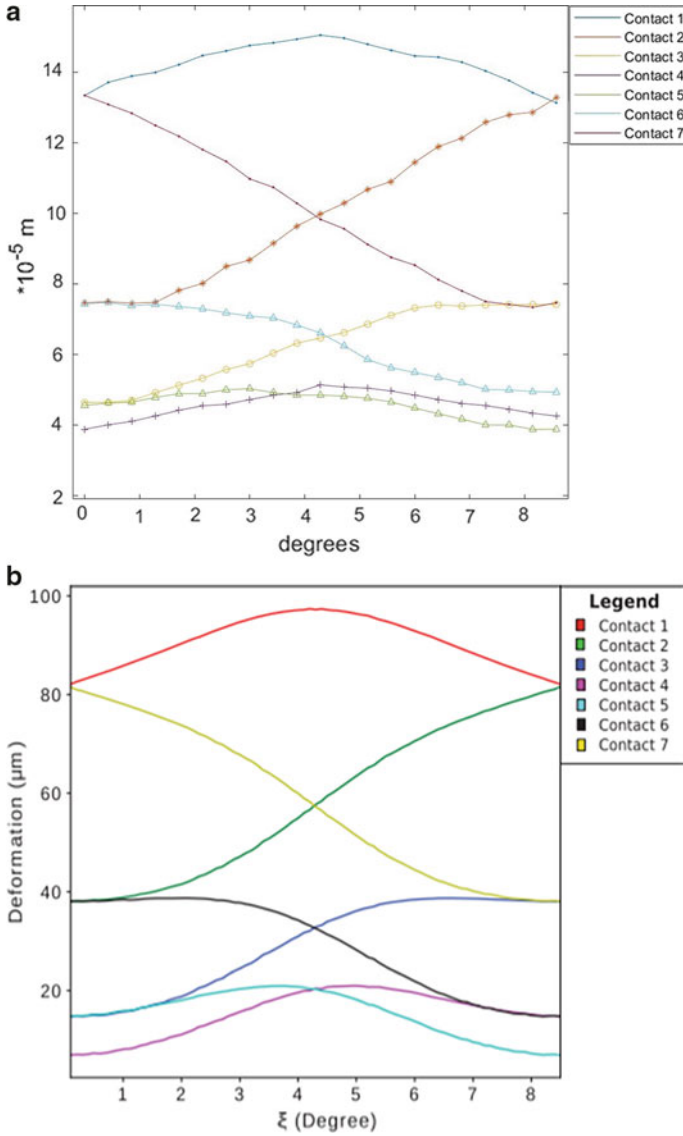


Fig. 10 **a** Plot based on finite element analysis. **b** Plot based on minimum potential energy method, Nag et al. [15]

4 Conclusion

Gap generation under working condition of running-fit orbital motor affects the torque producing capacity and the overall efficiency of the motor. Introducing interference minimizes this gap generation and therefore minimizes the fluid leakage from

high-pressure zone to low-pressure zone. However, introducing interference subjects the rotor-stator assembly to pre-stress. We have used FEA technique to accurately estimate the stresses generated in the assembly due to interference. Deformation of rollers in a direction normal to each contact, which helps in gap reduction, is also calculated.

References

1. Ansdale, R.F.: *The Wankel RC Engine*, 1st edn. Iliffe, London (1968) (Appendix: mathematical analysis of the NSU Wankel RC engine, by DJ Lockley)
2. Colbourne, J.R.: The geometry of trochoid envelopes and their application in rotary pumps. *Mech. Mach. Theory* **9**, 421–435 (1974)
3. Colbourne, J.R.: Gear shape and theoretical flow rate in internal gear pumps. *Trans. Can. Soc. Mech. Eng.* **3**(4), 215–223 (1975)
4. Robinson, F.J., Lyon, J.R.: An analysis of epitrochoidal profiles with constant difference modification suitable for rotary expanders and pumps. *J. Eng. Ind. Trans. ASME* **198**(1), 161–165 (1976)
5. Stryczek, J.: Cycloidal gears in design of gear pump and motors. *Arch. Mach. Des. Archiwum Budowy Maszyn, Tom XXXVI ZESZYT Wroclaw* **1–2**, 57–87 (1990)
6. Stryczek, J.: Principles of the design of cycloidal gears in hydraulic machinery. *Arch. Mach. Des. Archiwum Budowy Maszyn, Tom XXXVII ZESZYT Wroclaw* **3**, 201–218 (1990)
7. Biernacki, K., Stryczek, J.: Analysis of stress and deformation in plastic gears used in gerotor pumps. *J. Strain Anal. Eng. Des.* **45**(7), 465–479 (2010)
8. Nag, A., Maiti, R.: Unification of Epitrochoid origin profile design approaches for external lobed Star member used in hydrostatic and gear units. *Proc. Inst. Mech. Eng. Part C: J. Mech. Eng. Sci.* **227**(2), 299–310 (2012)
9. Maiti, R., Sinha, G.L.: Kinematics of active contact in modified epitrochoid generated rotary piston machines. *Mech. Mach. Theory* **23**(1), 39–45 (1988)
10. Maiti, R.: Distributor valve port sequences in epitrochoid generated rotary piston type hydrostatic units. *Arch. App. Mech.* **62**, 223–229 (1992)
11. Maiti, R.: Active contact stresses at epitrochoid generated ROTORSTATOR set of fixed axis or equivalent system ‘ROPIMA’ type hydrostatic units. *ASME J. Eng. Ind.* **113**(4), 465–473 (1991)
12. Maiti, R.: Active contact problems in epitrochoid generated ‘floating axis’ orbital rotary piston machines. *ASME J. Eng. Ind.* **115**(3), 337–340 (1993)
13. Roy, D., Maiti, R., Das, P.K.: Mechanics and FEM estimation of gaps generated in starring active contacts of ORBIT motor during operation. *Int. J. Mech. Mater. Des.* (2019)
14. Cornell, R.W.: Compliance and stress sensitivity of spur gear teeth. *ASME J. Mech. Des.* **103**(2), 447–459 (1981)
15. Optimization of the interference parameters of an Orbit motor using genetic algorithm. *Proc IMechE Part C: J. Mech. Eng. Sci.* 1–15 (2020)

Comparison of Mechanical Performance of the Various Stent Materials: A Finite Element Analysis (FEA) Approach



M. Raghuraman, I. Ramu, and V. Chaithanya Vinay

Abstract The objective of this research work is to study and compare the mechanical properties of different biocompatible materials used in stent implantation viz. Aluminium Alloy (AA2024), Magnesium alloy (Mg–10Al–3Zn), Stainless steel (SS316L), and Titanium alloy (Ti–6Al–4V). At present, the materials used for stentings such as Cobalt–Chromium alloy, Stainless Steel SS316L, Magnesium alloy, and Nitinol are not reasonable and cause problems to the artery. The material world is marching toward the trend of improving the strength and simultaneously reducing the weight of the material. Hence, in this work, an effort has been made to use Titanium alloy material for cardiovascular stents; this material has been preferred as an entrant material that has remarkable biocompatibility, extraordinary strength-to-weight ratio, resistance to corrosion, and also exhibits good mechanical properties and resistance to corrosion.

1 Introduction

Coronary Artery Diseases are the partial narrowing or complete obstruction of the coronary arteries and is usually brought about by atherosclerosis. At first, the reduced blood flow may not show any symptoms of this disease but with the accumulation and growth of plaque, the body tends to develop the signs and symptoms of the coronary artery disease which may comprise pain in chest, short breath, and in the long run it may result even in a heart attack.

M. Raghuraman (✉) · I. Ramu
Faculty of Mechanical Engineering, Vishnu Institute of Technology, Bhimavaram,
Andhra Pradesh 534202, India
e-mail: raghuraman262@gmail.com

V. Chaithanya Vinay
VIT Vellore, Vellore, Tamil Nadu 632014, India

1.1 Stent

A stent is a splint positioned inside the blood vessel to dismiss any obstacle caused due to the plaque. A splint is nothing but a medical device that maintains in position a movable or displaced part, which is an artery in this case. It supports the walls of the artery to lessen its blockage caused due to the accumulation of plaque.

1.2 Stent Placement

Angioplasty is frequently combined with the enduring placement of a stent which is nothing but a small wire mesh tube. The stent helps brace the artery open and reduce the occurrence of restenosis. Some stents are layered with a drug to help retain the artery open. This type of stents is known as drug-eluting stents while others that do not contain any drug are known as bare-metallic stents. Drug-eluting stents are many a time chosen over bare-metal stents for the reason that the latter conveys a greater risk of restenosis. Few works have been carried out on the titanium alloy (Ti-6Al-4V) as a stent material as discussed by Auricchio et al. [1].

Recently, various medicinal case study demonstrated that stent inserts may prompt myocardial infarction, thrombosis [2–5] restenosis [6], and unbalanced angina [7]. It was likewise detailed that stent might fail any time, which results in recurrence of stenosis, coagulation, torment, and other medical problems in patients [8, 9]. If the patients were detected with the failure of the stent [10], they need to undertake a further medical procedure such as surgery to evacuate the fizzled stent and embed another one to take care of the issue.

2 Modeling of Stent

The geometry of the stent model has been created in Solidworks 2018 software by using various 3D-geometric modeling techniques like 2D and 3D entities, Boolean operations as shown in Fig. 1.

Fig. 1 Stent model



The Mechanical properties considered for different biomaterials are tabulated below.

Material	Material properties				
	Young’s modulus, E (in MPa)	Density (in kg/m ³)	Poisson’s ratio	Tensile yield strength, y (in MPa)	Ultimate tensile strength, u (in MPa)
Aluminum alloy (AA2024)	71,000	2770	0.33	280	310
Magnesium alloy (Mg–10Al–3Zn)	45,000	1800	0.35	193	255
Stainless steel (SS316l)	193,000	7750	0.31	207	586
Titanium alloy (Ti–6Al–4V)	96,000	4620	0.36	930	1070

3 Finite Element Analysis(FEA)

After modeling the stent, it is imported as IGES file. The stent model is meshed and the boundary conditions are applied to the meshed volume. For simulation, the degrees of freedom (DOF) of one end of the stent is constrained and uniform pressure of magnitude 13.3 kPa, corresponding to the mean blood pressure of 100 mmHg is applied normal (radially) to the inner face of the stent. Static analysis is carried out to determine the displacements, stresses, strains, and forces in the stent under the given loading conditions.

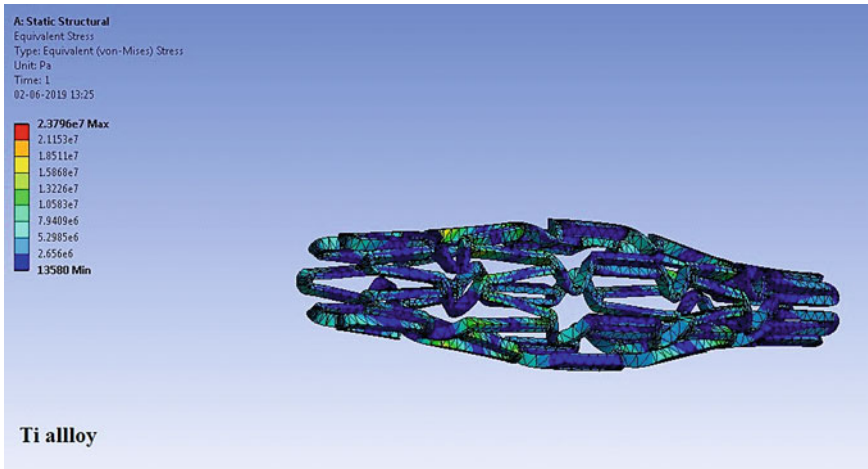


Fig. 2 Von-Mises stress of Titanium alloy (Ti-6Al-4V)

The extreme and lowest Von-Mises Stress of the stent model made of titanium alloy under the given boundary conditions was found to be 13,580 Pa and 2.3796e+007 Pa respectively as shown in Fig. 2.

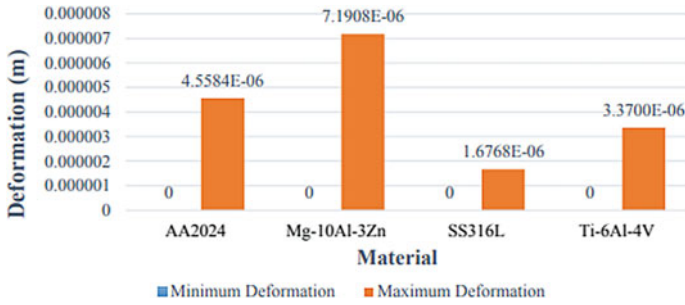
4 Results and Discussion

Three materials, AA2024, Mg-10Al-3Zn, and SS316L, which are primarily used for the fabrication of the stent were examined to study the consequence of materials on the mechanical behavior of the stent under given loading conditions. In addition, Titanium alloy Ti-6Al-4V was also assessed to study the outcome of a particular material on stent arrangement.

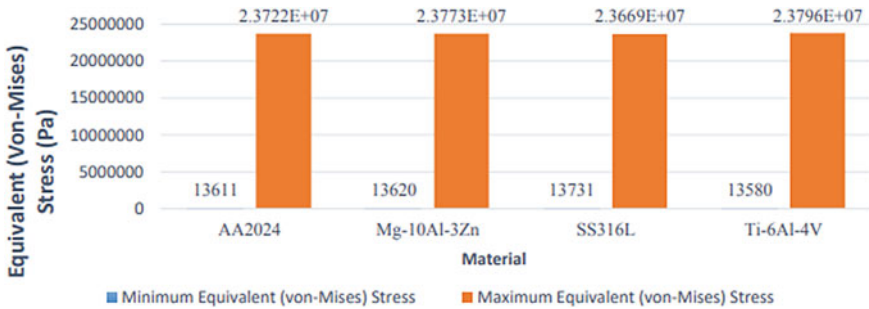
Stents made of Aluminum alloy AA2024 and Magnesium alloy Mg-10Al-3Zn have a tendency to experience greater deformation compared to that of Stainless Steel SS316 and Titanium alloy Ti-6Al-4V (Graph 1), exhibiting less radial stiffness.

Graph 2 depicts the comparison of the distribution of Von-Mises stress on stent for four diverse materials resulting from the arrangement of the stent. From the calculated outcomes, it seems that the choice of material has an impact on the magnitude of the maximum Von-Mises stress on the stent. Stents made of Mg-10Al-3Zn have the least value of maximum Von-Mises stress than that of the other three materials namely AA2024, SS316L, and Ti-6Al-4V. While the minimum Von-Mises stress was induced in Ti-6Al-4V in comparison to AA2024, SS316L, and Mg-10Al-3Zn.

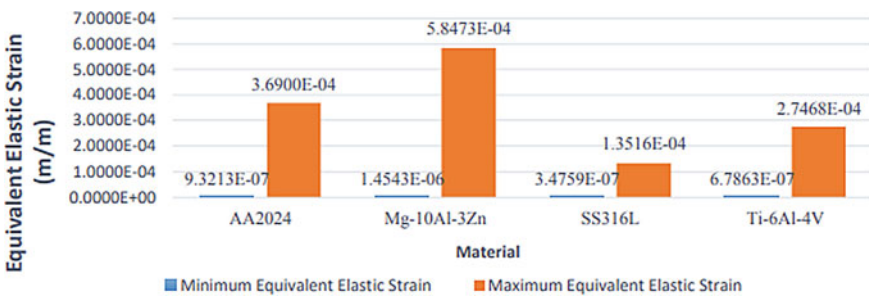
Graph 3 shows the Elastic strain induced in different materials of the stent for the same stent model and loading conditions. It can be observed that Stainless Steel (SS316L) and Titanium (Ti-6Al-4V) exhibits better elastic strain when compared



Graph 1 Total deformation of stent materials under 13.3 kPa pressure



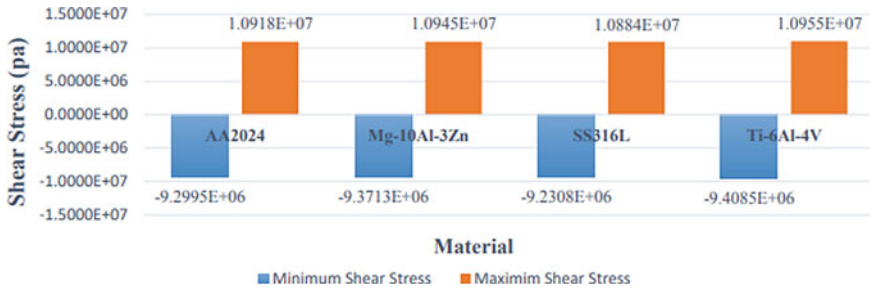
Graph 2 Equivalent stress of stent materials under 13.3 kPa pressure



Graph 3 Equivalent elastic strain of stent materials under 13.3 kPa pressure

to Al alloy AA2024 and Mg alloy Mg–10Al–3Zn. Of all the four materials, the maximum elastic strain was observed in Mg alloy Mg–10Al–3Zn while the minimum elastic strain was observed in Stainless steel SS316L.

Graph 4 depicts the comparison of the shear stress-induced in different materials for the same stent model. Stresses on the stent are affected by the material chosen. For the same design, the maximum shear stress was induced in Stainless steel SS316L and the minimum shear stress was induced in Al alloy AA2024.



Graph 4 Shear stress of stent materials under 13.3 kPa pressure

5 Conclusion

For a given loading condition, severe deformation was observed in stents made of Al alloy AA2024 and Mg alloy Mg-10Al-3Zn in comparison with Stainless Steel SS316L and Titanium alloy Ti-6Al-4V. Thus, it can be concluded that the mechanical behavior of Titanium alloy Ti-6Al-4V under a given loading condition is on par with that of the widely used stent material, i.e., Stainless Steel SS316L. Hence the Titanium alloys can be considered as an alternative material for the manufacture of stents.

Titanium is viewed as the most biocompatible metal because of its resistance to corrosion from bodily fluids, bio-inactivity, and high fatigue limit. One of the greatest favorable conditions for titanium is its strength. When comparing with von-mises and shear stresses stainless steel is better because of the low modulus. But, titanium holds as much strength as steel and is particularly lighter in weight (nearly 50% lighter) in comparison to steel, making this material perfect for its utilization as surgical implants.

6 Scope for Future Work

Depending on the results obtained from this research, in the future, the work can be extended

- To perform the fluid flow analysis (CFD) of titanium alloy (Ti-6Al-4V) stents.
- To perform topology optimization for titanium alloy stent and find an optimum shape for the stent.

References

1. Auricchio, F., Constantinescu, A., Conti, M., Scalet, G.: A computational approach for the lifetime prediction of cardiovascular balloon-expandable stents. *Int. J. Fatigue* **75**, 69–79 (2015)
2. Park, J.S., Shin, D.G., Kim, Y.J., Hong, G.R., Cho, I.H.: Acute myocardial infarction as a consequence of stent fracture and plaque rupture after sirolimus-eluting stent implantation. *Int. J. Cardiol.* **134**, e79–e81 (2009)
3. Choe, H., Hur, G., Doh, J.H., Namgung, J., Lee, S.Y., Park, K.Y., Chang, W.I., Lee, W.R.: A case of very late stent thrombosis facilitated by drug-eluting stent fracture: comparative images before and after stent fracture detected by 64-multidetector computed tomography. *Int. J. Cardiol.* **133**, e125–e128 (2009)
4. Lei, L., Qi, X., Li, S., Yang, Y., Hu, Y., Li, B., et al.: Finite element analysis for fatigue behaviour of a self-expanding Nitinol peripheral stent under physiological biomechanical conditions. *Comput. Biol. Med.* **104**, 205–214 (2018)
5. Alherz, A.I., Tanweer, O., Flamini, V.: A numerical framework for the mechanical analysis of dual-layer stents in intracranial aneurysm treatment. *J. Biomech.* **49**(12), 2420–2427 (2016)
6. Okamura, T., Hiro, T., Fujii, T., Yamada, J., Fukumoto, Y., Hashimoto, G., Fujimura, T., Yasumoto, K., Matsuzaki, M.: Late giant coronary aneurysm associated with a fracture of sirolimus-eluting stent: a case report. *J. Cardiol.* **51**, 74–79 (2008)
7. Adlakhna, S., Sheikh, M., Bruhl, S., Eltahawy, E., Pandya, U., Colyer, W., Cooper, C.: Coronary stent fracture: a cause of cardiac chest pain? *Int. J. Cardiol.* **141**, e23–e25 (2009)
8. Umeda, H., Gochi, T., Iwase, M., Izawa, H., Shimizu, T., Ishiki, R., Inagaki, H., Toyama, J., Yokota, M., Murohara, T.: Frequency, predictors, and outcome of stent fracture after sirolimus-eluting stent implantation. *Int. J. Cardiol.* **133**, 321–326 (2009)
9. Celik, T., Iyisoy, A., Dogru, M.T., Isik, E.: Coronary stent strut fracture after drug-eluting stent implantation: a newly recognized complication. *Int. J. Cardiol.* **132**, 121–122 (2009)
10. Sweeney, C., McHugh, P., McGarry, J., Leen, S.: Micromechanical methodology for fatigue in cardiovascular stents. *Int. J. Fatigue* **44**, 202–216 (2012)

Applicability of Empirical Correlations for Critical Heat Flux in Transfer Line Cool-Down Boiling



Asit Kumar Meher, P. H. J. Venkatesh, M. S. R. Viswanath, J. Naga Raju, and Ankit Kumar

Abstract The Cool down of move lines with the cryogenic liquids is a stream bubbling procedure having diverse warmth move regimes. In Cryogenic fuel move frameworks, high exactness numerical models are required for anticipating this two-stage stream bubbling procedure. The punishment of wasteful model leads into higher edge of structuring and working expenses. There has consistently been a drive to figure an all inclusive connection which can cover an expansive scope of liquids alongside the thermodynamic conditions for anticipating heat motion. These relationships anyway don't cover cryogenic liquids explicitly for transient chill off bubbling of move lines. Consequently, the expectation of this investigation is to confirm these two-stage heat move connections for anticipating basic critical heat flux (CHF) against accessible stream bubbling information for cryogenic liquids. Cryogenic quenching trial test information is looked at against accessible relationships and the mean outright deviation in anticipating most extreme warmth transition from every connection is introduced. Results obtained through this work means that

A. K. Meher (✉) · P. H. J. Venkatesh · M. S. R. Viswanath
Department of Mechanical Engineering, Vignan's Institute of Information Technology (A),
Visakhapatnam, Andhra Pradesh, India
e-mail: asitmeher2@gmail.com

P. H. J. Venkatesh
e-mail: Venky61788@gmail.com

M. S. R. Viswanath
e-mail: viswanath.msr@gmail.com

J. Naga Raju
Department of Mechanical Engineering, J B Institute of Engineering and Technology, Hyderabad,
Telangana, India
e-mail: nagaraju.jntun@gmail.com

A. Kumar
Department of Cryogenic Engineering, Indian Institute of Technology, Kharagpur, West Bengal,
India
e-mail: ankit8913@gmail.com

the current relationships are unequipped for precisely anticipating the size of warmth move during the procedure words.

Keywords Liquidnitrogen · Horizontalpipe · Flow boiling · Chill-down · Horizontal pipe · Flow boiling · Critical heat flux · Stream bubbling · Cryogenic fuel · Quenching · Warmth transition

Nomenclature

Greek symbols

μ	Viscosities
σ	Surface tension
ρ	Density
φ	Acceleration term
K	Thermal conductivity
g	Acceleration due to gravity
C_p	Specific heat capacity

Correlation parameter

H_{fg}	Latent heat of vapourisation
ΔH	Enthalpy of sub cooling
Pe	Peclet number
Fr	Fraude number
F_d	Drag force on single bubble
D	Tube diameter
D_b	Diameter of the bubble
η	Fraction of cross-section occupied
τ	Shear stress

Subscript

l	Liquid
v	Vapour
0	For zero critical vapour quality
X	Vapour quality
cr	Critical

- c Core
- b Bubble
- i Interface
- w Wall

1 Introduction

The Heat transfer systems during the cool-down procedure, The chill down of cryogenic exchange lines is a stream bubbling procedure and is appeared in Fig. 1. The chill down starts in the film bubbling system due to abrupt blazing of fluid because of huge beginning temperature distinction. As the divider temperature diminishes, the framework moves toward the purpose of least warmth move between the liquid and the exchange line divider. This point is explicitly named as Leindenfrost point (LFP). Stream at that point enters and goes through the progress bubbling system rapidly. This warmth move system is the most precarious of three bubbling systems and it closes when the fluid comes in consistent contact with the exchange line divider at the CHF. The purpose of CHF describes the fluid predominant of Nucleate bubbling system (NB). Warmth move is greatest at the CHF point because of the way that the protecting fume layer decreases and the proficient cooling process happens through both reasonable and inert warmth move process. As the cooling procedure proceeds

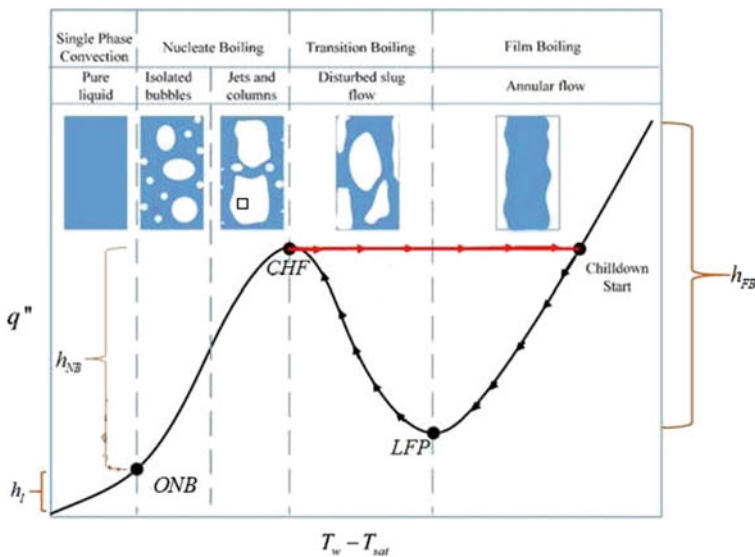


Fig. 1 Flow boiling curve at low vapour quality

with further the void portion diminishes and the framework moves toward the beginning of nucleate bubbling (ONB) point. The framework develops from the two-stage heat move procedure to the single-stage fluid convection and further chill off of the channel divider happens by the reasonable warming of the cryogenic liquid.

Cryogenic propellants provide remarkable advantages in generating higher specific impulse compared to the earth storable propellants and are the first choice for the operation of rocket engines carrying higher payload. In space flights applications, transfer lines are required to carry cryogenic propellants from tankers into the run-tank and from both tankers and run-tank to the test objects. Optimization of the cool-down process includes the use of small amount of cryogen while not exceeding the maximum allowed thermal stress. Nonetheless, the consistency of one liquid model is emphatically subject to the warmth move connections just as change rules utilized for recreating different bubbling systems, for example, film bubbling, progress bubbling, nucleate bubbling lastly constrained convection to fluid, that happen during cool-down boiling (Fig. 1). It tends to be envisioned that exact estimation of Critical heat flux (CHF) during the pipe cool down can be used to clearly demarcate the transition from pre-CHF to post-CHF conditions and is therefore imperative to mathematically model cool-down process.

In this work, by discussing the observations recorded in various publications regarding physical mechanism leading to CHF and the involved parameters affecting the magnitude, a basic understanding is developed first. Later, rigorous review of currently available literature is carried to select various correlations for checking their applicability in predicting CHF during transient forced flow boiling process. Cryogenic quenching data is selected from the experimental publications and the method of gathering data with assumptions taken to compute CHF is presented. Finally, the value of CHF obtained from each correlation is validated with collected experimental values to check the deviation.

2 Methodology

2.1 *Validation of Previously Reported Correlations*

Cool-down process is a transient phenomenon where both wall temperature and heat flux changes with time. At the very point of time the maximum heat flux that occurs is collected from the literature along with all the parameters governing the experiment. The 09 correlations stated in Chapter 02 is numerically modelled in software to obtain magnitude of CHF for various input parameters like pressure, diameter of the channel, mass flux, etc. The values which are obtained from solving mathematical formulation of correlations are then compared to the experimentally calculated values are used to validate CHF correlations [1].

Validation of Bubble crowding model

The mathematical model of bubble crowding is first formulated in EES version 9.4.4.0. The mathematical model is an iterative process which requires initial guess of heat flux. Also, the input parameters required to solve CHF through this model are length of the section, diameter of the tube, inlet mass flux, inlet saturation pressure or temperature. In the present work, initial guess value is attempted with the input parameters. After getting convergence of initial guess and the final value for a specific set of inlet conditions, the values are then validated with the previously reported experimental parameters to check for the deviation. 3.2.1 Mathematical formulation of bubble crowding model suggested by Kwon and Chang [1] (Fig. 2)

$$\frac{\partial G_b A_b}{\partial z} + G_{bc} P_i - G_{cb} P_i = 0 \tag{1}$$

$$\frac{\partial G_b(1 - x_b) A_b}{\partial z} + \frac{q_{evap} P_w}{h_f g} + G_{bc}(1 - x_b) P_i - G_{cb}(1 - x_c) P_i = 0 \tag{2}$$

The total balance of energy with the control volume yields

$$\frac{\partial G_b h_b A_b}{\partial z} + G_{bc} h_b P_i - G_{cb} h_c P_i - q_w P_w = 0 \tag{3}$$

From Eq. (1) and the finite critical void fraction rearrange Eq. (3) as (Fig. 3)

$$q_w = G_{cb}(h_b - h_c) \frac{P_i}{P_w} \tag{4}$$

$$\begin{aligned} & - \frac{\partial P}{\partial z} + \frac{\tau_i P_i}{A_b} - \frac{\beta \tau_{w,v} P_w}{A_b} - \frac{F_d}{A_b D_b^2} - \rho_b g \\ & + \frac{(G_{cb} \bar{U}_c - G_{bc} \bar{U}_b) P_i}{A_b} = \frac{1}{A_b} \frac{\partial (\rho_b A_b \bar{U}_b^2)}{\partial z} \end{aligned} \tag{5}$$

Fig. 2 The conceptual configuration for the bubbles formed on the heated wall and separated flow control volumes

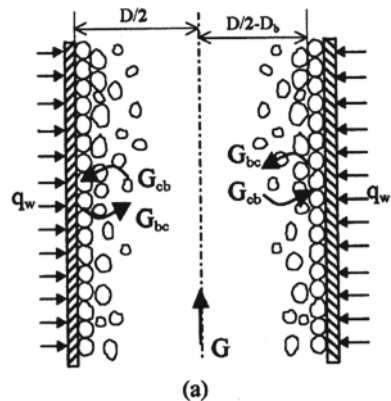
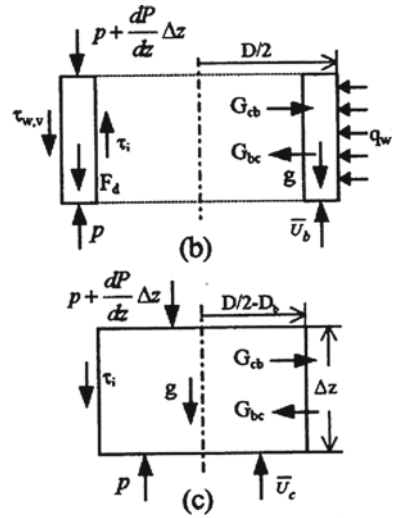


Fig. 3 Configuration of separated flow control volume for **a** wall bubbly layer **b** core



$$-\frac{\partial P}{\partial z} + \frac{\tau_i P_i}{A_c} - \rho_c g - \frac{(G_{cb}\bar{U}_c - G_{bc}\bar{U}_b)P_i}{A_c} = \frac{1}{A_c} \frac{\partial(\rho_c A_c \bar{U}_c^2)}{\partial z} \tag{6}$$

Based on the assumption, transverse mass transport for the interface is limited at the CHF condition which signifies, at the CHF

$$G_{bc} = G_{cb} = G^* \tag{7}$$

From (5), (6), (7)

$$G^* = \left[\frac{-\tau_i P_i}{\eta_c(1 - \eta_c)A} + \frac{\beta \tau_{w,v} P_w}{(1 - \eta_c)A} - (\rho_c - \rho_b)g + \frac{\pi D F_d}{D_b^2(1 - \eta_c)A} + \phi \right] * \frac{A(1 - \eta_c)\eta_c}{(\bar{U}_c - \bar{U}_b)P_i} \tag{8}$$

Neglecting insignificant terms with proper remark, from Eq. (4) and (7) relation of CHF is obtained as

$$q_{\text{chf}} = \left[-(\rho_c - \rho_b)g + \frac{\pi D F_d}{D_b^2(1 - \eta_c)A} \right] * \frac{(h_b - h_c)A\eta_c(1 - \eta_c)}{(\bar{U}_c - \bar{U}_b)P_w} \tag{9}$$

The variation in vapour quality is calculated to be 0 in axial direction due to finite critical void fraction in the bubbly layer control volume:

$$q_{\text{evap}} = G_c b(x_b - x_c) h_{fg} \frac{P_i}{P_w} \tag{10}$$

The variation in vapour quality is calculated to be 0 in axial direction due to finite critical void fraction in the bubbly layer control volume: Generalized correlations of CHF for the forced convection boiling:

Along with the internal flows, CHF in external forced convection boiling systems utilizing external flows is significant in many industrial applications and has paramount importance in acquiring the insight into the basic mechanism leading to the occurrence of CHF. The observation regarding the flow pattern made through the experiments conducted by Katto and Kurata [2] reveals that the flow regime is bubbly with the input heat flux (q) is low but as the value of q is increased coalescence of vapour takes place near the heated surface. The author used the data for water and R-113 and formalized a generalized Eq. (14) for predicting CHF (Table 1).

The observations are recorded near the critical heat flux condition for saturated liquid flow on uniformly heated plate in submerged condition at one atmospheric pressure. For water the experimental data obtained is for flow velocity ranging from 1.26 to 9.10 m/s and for R-113 velocity range from 1.26 to 6.02 m/s.

Quench test and heated tube tests

Anytime or length along the tube, the heated cylinder HTC is characterized as:

$$h_{HT} = \frac{q_{heater}}{T_i - T_{sat}} \tag{12}$$

$$q_{heater} = \frac{IV}{A_s} \tag{13}$$

From the method of Burggraf [3] T_i is the inner wall temperature can be determined

Table 1 Correlation equation of CHF at zero inlet sub cooling and for K

Regime	Q_{co}/GH_{fg}	K
L-regime	$C \left(\frac{\sigma \rho_l}{G^2 l}\right)^{0.043} \frac{1}{l/d}$	$\frac{1.043}{4C \left(\frac{\sigma \rho_l}{G^2 l}\right)^2}$
H-regime	$0.10 \left(\frac{\rho_v}{\rho_l}\right)^{0.133} \left(\frac{\sigma \rho_l}{G^2 l}\right)^{\frac{1}{3}} \frac{1}{1+0.0031 \frac{l}{d}}$	$\frac{5}{6} \frac{0.0124+d/l}{(\rho_v/\rho_l)^{0.133} \left(\frac{\sigma \rho_l}{G^2 l}\right)^{1/3}}$
N-regime	$0.098 \left(\frac{\rho_v}{\rho_l}\right)^{0.133} \left(\frac{\sigma \rho_l}{G^2 l}\right)^{0.433} \frac{(l/d)^{-27}}{1+0.0031 \frac{l}{d}}$	$0.416 \frac{(0.0221+d/l)(d/l)^{0.27}}{(\rho_v/\rho_l)^{0.133} \left(\frac{\sigma \rho_l}{G^2 l}\right)^{0.4333}}$

Table 2 Range of experimental conditions and deduced value of critical heat flux from literature [5]

Total No. of data points	Fluid	Pressure range	Mass flux range	CHF values (KW/m ²)
103	Liquid Nitrogen	150–720 kPa	6–1650 kg/m ² sec	39–270

$$T_i = T_o + \left(\frac{r_o^2}{4\alpha} \left(\left(\frac{r_i}{r_o} \right)^2 - 1 - 2 \ln \left(\frac{r_i}{r_o} \right) \right) \right) \frac{dT_o}{dt} + \left(\frac{1}{64\alpha^2} (r_i^4 - 5r_o^4) \right. \\ \left. - \frac{r_o^2 r_i^2}{8\alpha^2} \ln \left(\frac{r_i}{r_o} \right) - \frac{r_o^4}{16\alpha^2} \ln \left(\frac{r_i}{r_o} \right) + \frac{r_o^2 r_i^2}{16\alpha^2} \right) \frac{d^2 T_o}{dt^2} \quad (14)$$

$$q_c = \rho C_p \left(\frac{r_i^2 - r_o^2}{2r_i} \right) \frac{dT_o}{dt} + \frac{(\rho C_p)^2}{k} \left(\frac{r_i^3}{16} - \frac{r_o^4}{16r_i} - \frac{r_o^2 r_i}{4} \ln \left(\frac{r_i}{r_o} \right) \right) \frac{d^2 T_o}{dt^2} \\ + \frac{(\rho C_p)^3}{k^2} \left(\frac{r_i^5}{384} - \frac{3r_o^4 r_i}{128} + \frac{3r_o^2 r_i^3}{128} \right. \\ \left. - \frac{r_o^6}{384r_i} - \frac{r_o^2 r_i^3}{128} \ln \left(\frac{r_i}{r_o} \right) - \frac{r_o^4 r_i}{32} \ln \left(\frac{r_i}{r_o} \right) \right) \frac{d^3 T_o}{dt^3} \quad (15)$$

q_{axial} is the axial conduction term, assumed negligible except at the liquid quench front [4]

$$q_{\text{rad}} = \sum \epsilon_i \sigma F_{ij} (T_i^4 - T_j^4) \quad (16)$$

F_{ij} is the view factor between surface i and j , and T_i and T_j are the temperatures of the radiating surfaces,

$$q_{\text{gas conduction}} = -k_{\text{gas}} \frac{dT}{dx} \quad (17)$$

Darr et al. [5]

An enormous number of LN2 chill-down tests are driven in a parametric way over a wide extent of brutal Re, for a wide scope of stream headings for a little SS test territory. There were two test stations a distance away of 14.9 and 40.1 cm from the narrows which contains 6 thermocouples introduced to it. Preliminary course of action is showed up in the figure. Modifications were made to the test gear to stream both drenched and subcooled gulf, and along these lines a couple of data was evaluated at negative amicability attributes.

Noteworthy points from the reported test of Darr et al. [5]

Compared with high Re LH2 streams, for an identical divider superheat, the heavier nitrogen invests more energy in Film boiling and therefore the lighter hydrogen over time in nucleate boiling. Along these lines, for top mass motion and low or no subcooling, the FB stream profile relies upon the liquid and during this manner Liquid to Vapor (L/V) thickness proportion. Littler L/V proportion is sweet for blending and separation of the fume layer along the divider, consequently advancing fluid contact along the dividers prior within the chill down (Fig. 4).

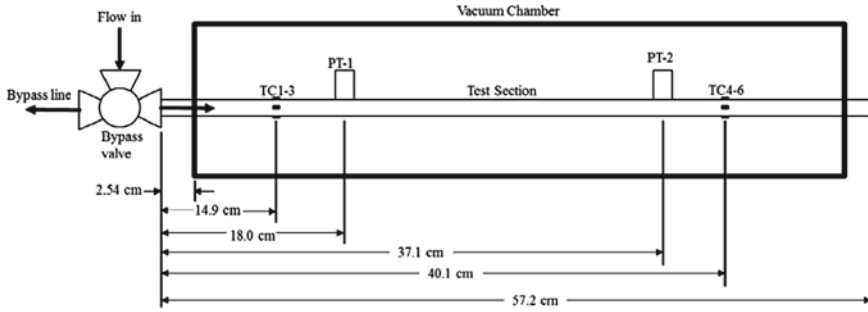


Fig. 4 System schematic test section [5]

Chi et al. [6]

Chi et al. [6] report one low flow LH2 chill-down trial for an Al test area where pressure, temperature and stream rate information was accessible at stations 2 and 5. While mass stream temperature estimations were likewise accessible, test HTC's trusted immersion temperature, and properties were registered utilizing pressure referenced at every area at the precise time of event of CHF (Fig. 5).

Jin et al. [7]

Cryogenic chill-down experiments are led on a 12.7 mm external diameter, 1.25 mm wall thickness and seven m long treated steel pipe with fluid nitrogen (LN2). The pipe is vacuum protected during the test to limit the warmth leak from temperature and to empower one to numerically recreate the procedure with none problem. The temperature and therefore the pressure profiles of the chill-down line are acquired at the area which is 5.5 m during a good ways from the channel bay. The exploratory boundaries are referenced in table. The transient narratives of temperature, weight and mass stream rate during the road chill-down procedure are checked and, and therefore the warmth move coefficient of warmth flux are figured by the converse critical thinking technique for Burggraf [3] (Fig. 6).

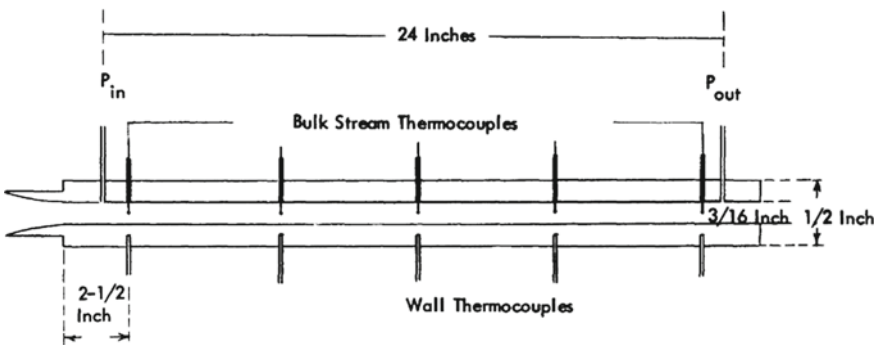


Fig. 5 Schematic of test section in chill-down experiment [6]

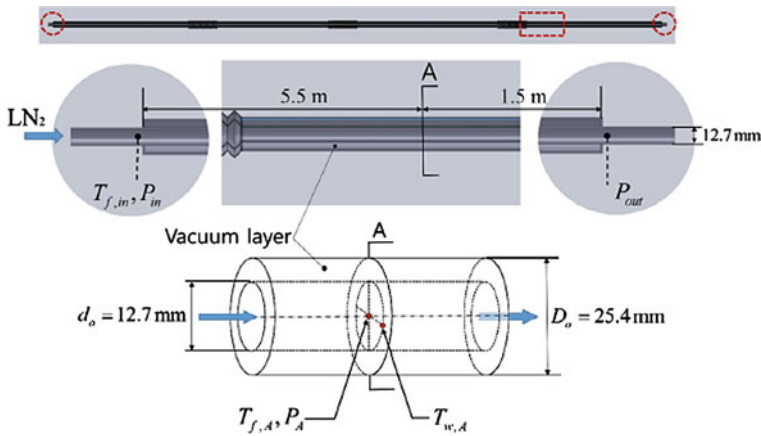


Fig. 6 Experimental test section reported in Jin et al. [7]

Repudiated experimental data

Due to inadequate information provided in previously reported experimental papers like the papers do not report the operating pressure or the length of test section to calculate the corresponding correlation value and hence are discarded during the present study. These experimental papers are mentioned below mentioning the cause of not using these correlations.

Burke et al. [8] was the first researcher to conduct LN2 chill-down experimental studies. The paper however do not report to all the parameters needed to deduce correlation value. While the pressure and stream rate information were accommodated a solitary run, insufficient data was accessible to compute correlation and normal convection heat releases, nor were areas of estimations indicated to ascertain balance quality. Moreover, separation between the outer wall estimating stations was not given, and the wall temperature follows introduced in the paper were arrived at the midpoint of more than four distinct areas. Bronson et al. [9] was the principal specialist to lead LH2 chill-down test examines, however the information couldn't be utilized to survey the relationships in light of the fact that the gulf states of the liquid were obscure, the pressure was not accessible at each external divider temperature perusing, and the stream rate time follows were not accessible. For registering exploratory CHF from the external divider follows, the paper doesn't indicate enough data about the testing office to ascertain parasitic heat leak. Hedayatpour and Antar [10] revealed a numerical model dependent on LN2 extinguishing information, however the paper is disposed of in light of the fact that solitary temperature variety information is given.

3 Results

From Table 3 it is evident that the correlation which possesses minimum mean deviation in calculating CHF is the correlation of Katto and Kurata [2] along with Katto [11]. However, there is a significant amount of error even by using these two correlations. From Graphs 4.1 to 4.12, the correlations of Katto and Ishii [12], Hall and Mudawar [13], Mudawar and Maddox [14], Nishikawa et al. [15] underpredicts the CHF value from the reported experimental data points. Moreover, the correlation of Zuber [16], Lienhard and Dhir [17], and the modified correlation of Katto and Ohno [18] are causing overprediction of CHF values (Table 2).

Various plots are drawn to check the performance of each correlation against the experimental CHF value [5] (Figs. 7, 8, 9, 10, 11, 12 and 13).

The correlation of Katto [11], Katto and Ishii [12] has shown the mean value of mean deviation compared to other correlations. The experimental condition includes horizontal flow of liquid nitrogen and the parameters governing the phenomenon of CHF during the flow boiling condition is in accord with the two correlations mentioned above. Also, it is noted that the value of mean deviation is not much

Table 3 Mean absolute deviation (MAD) of the CHF value calculated from various correlations from the experimental CHF Data points [5]

Author	Katto [11]	Zuber [16]	Katto and Ishii [12]	Hall and Mudawar [13]	Lienhard and Dhir [17]
MAD	66.534	95.909	111.395	128.214	129.18
Author	Mudawar and Maddox [14]	Katto and Kurata [2]	Y.Katto and Ohno [18]	Nishikawa et al. [15]	
MAD	89.518	60.678	578.12	74.189	

Fig. 7 Plot of CHF from the correlation of Katto [11]

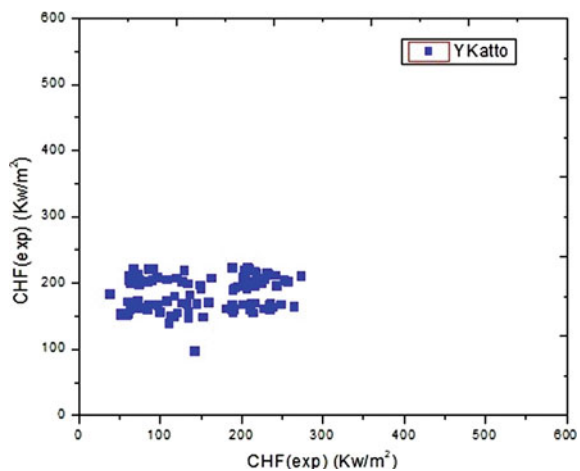


Fig. 8 Plot of CHF from the correlation of Zuber [16]

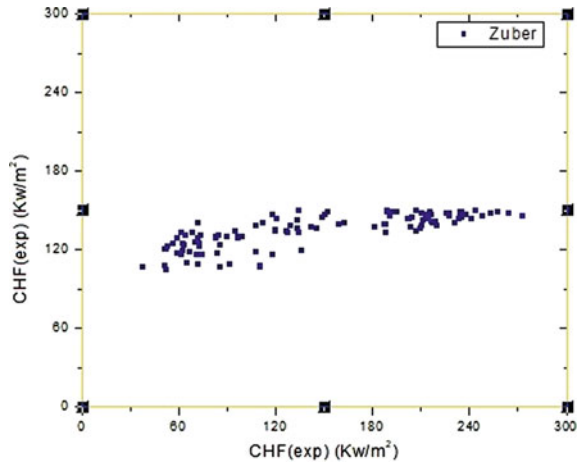
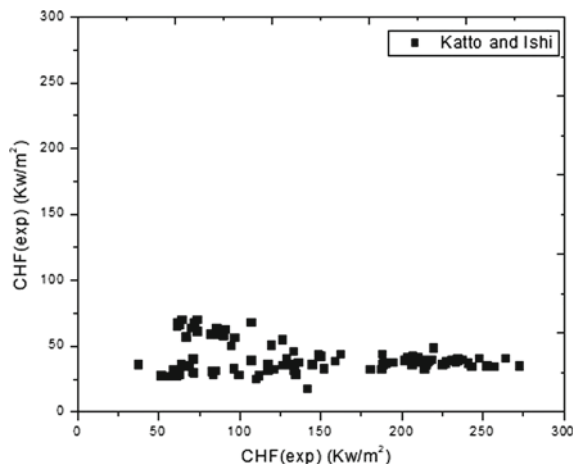


Fig. 9 Plot of CHF from the correlation of Katto and Ishii [12]



significant keeping in mind the assumptions taken during experimental calculation of heat flux (Tables 4, 5, 6 and 7).

The mean absolute deviation found is minimum from the correlation of Zuber [16]. However, the model of Lienhard and Dhir [17] shows the maximum mean deviation. It is noteworthy here that the two correlations [16, 17] are different just in a constant term. Therefore, the results obtained can be attributed to the low mass flux condition and the low L/V ratio. Other correlations are also showing less mean deviation. Moreover, the correlation of Katto [11] has also performed good as it accounts for very less deviation for two data points.

Fig. 10 Plot of CHF from the correlation of Hall and Mudawar [13]

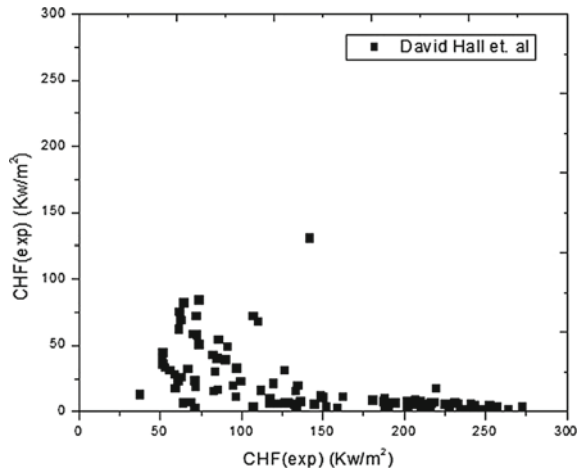
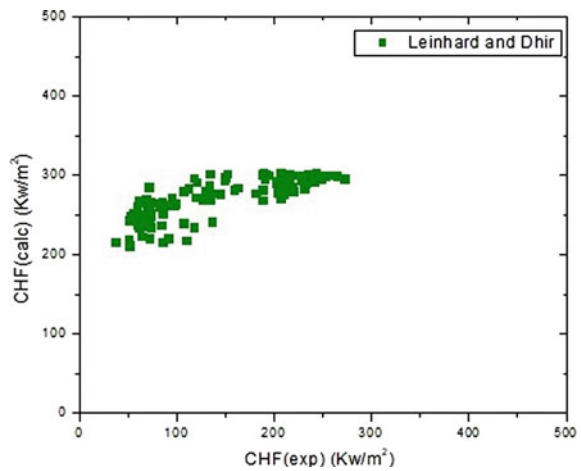


Fig. 11 Plot of CHF from the correlation of Lienhard and Dhir [17]



Probable reasons of discrepancies

The discrepancies between the two values can be significantly due to following reasons. All correlations were derived using the heated tube tests, and not transient chill-down tests. For steady state or heated tube tests, there occurs negligible thermal gradient across the pipe wall and the system is in equilibrium with known flow rate and equilibrium quality of flow, temperature, etc. while in transient cool-down process heat flux is determined through solid conduction through the pipe wall. Moreover, regarding the thermal mass of the system, the chill-down process approaches steady state when there is heavy thermal mass which results in slow cool down. The temperature versus time curve will then have very less slope approaching steady state condition. But, the pipe used in the experiments is having very less thermal mass

Fig. 12 Plot of CHF from the correlation of Mudawar and Maddox [14]

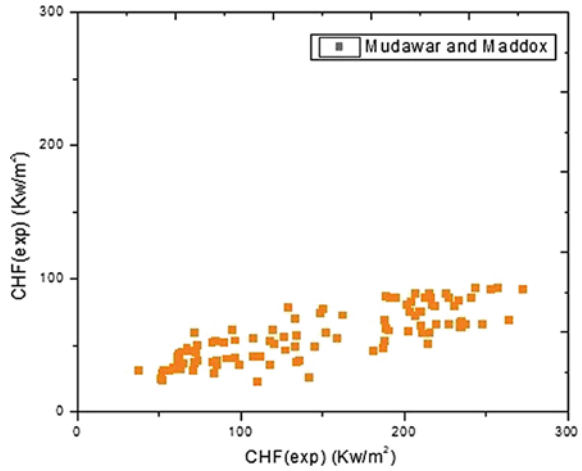


Fig. 13 Plot of CHF from the correlation of Katto and Ohno [18]

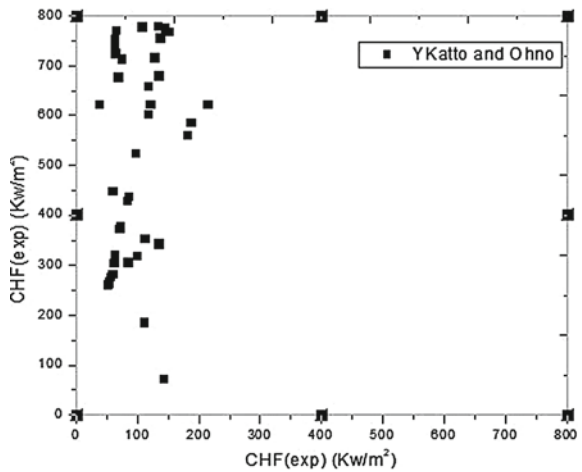


Table 4 Range of experimental conditions and deduced value of critical heat flux from literature [7]

Total No. of data points	Fluid	Pressure range	Mass flux range	CHF values (KW/m ²)
05	Liquid Nitrogen	176–433 kPa	19–51 kg/m ² sec	42–65

and is quenched with cryogenic fluids causing large temperature gradient far from steady state conditions. Also, it can be stated to address the amount of deviation between experimental CHF and correlations is that there is no method to measure all the variables like void fraction, in situ non-equilibrium quality which governs the maximum heat flux point.

Table 5 Mean absolute deviation (MAD) of the CHF value calculated from various correlations with the experimental CHF Data points [7]

Author	Katto [11]	Zuber [16]	Katto and Ishi [12]	Hall and Mudawar [13]	Lienhard and Dhir [17]
MAD	13.194	78.838	11.847	41.8	205.698
Author	Mudawar and Maddox [14]	Katto and Kurata [2]	Katto and Ohno [18]	Nishikawa et al. [15]	
MAD	38.65	27.79	44.48	36.56	

Table 6 Range of experimental conditions and deduced value of critical heat flux from literature [6]

Total no. of data points	Fluid	Pressure range	Mass flux range	CHF values (KW/m ²)
03	Liquid Hydrogen	27–30 Psi	36–45 kg/m ² sec	43–47

Table 7 Mean absolute deviation (MAD) of the CHF value calculated from various correlations with the experimental CHF Data points [6]

Author	Mudawar and Maddox [14]	Katto and Kurata [2]	Katto and Ohno [18]	Nishikawa et al. [15]	
MAD	25.09	12.46	24.512	10.512	
Author	Katto [11]	Zuber [16]	Katto and Ishii [12]	Hall and Mudawar [13]	Lienhard and Dhir [17]
MAD	29.087	4.41	30.77	Hall and Mudawar [13]	54.747

4 Conclusion

The transfer of cryogenic propellants through the transfer lines is a flow boiling process. Optimization of the cool-down process includes the use of small amount of cryogen while not exceeding the maximum allowed thermal stress. The penalty of inefficient model leads into higher margin of designing and operating costs. The disparity between the current set of correlations to predict CHF and cryogenic quenching data from the experiments is recorded. The probable reasons for the disparity are tried to address. A set of 113 experimental points are taken and 09 correlations are verified to check the applicability in that range of conditions. Although, the correlation of Katto [11] shows minimum deviation in comparison to other correlations mentioned in Tables 1 and 3 yet the discrepancy recorded is very significant to provide satisfactory results with a wide range of parameters. Thus, there is a need to develop a universal correlation which can be applied to cryogenic fluids over wider range of parameters to accurately predict CHF during flow boiling process. This work can be further extended to find a universal correlation that can be applied to a large number of fluids and conditions. To develop a correlation very large number of data

points are required and hence the foremost requirement is to consolidate a database which can contain various flow parameters and the corresponding CHF value. Also, the lack of experimental CHF values for cryogenic fluids channelizes an urge to go for experimental setup to record temperature change and further in calculating CHF values.

Appendix

The deduced experimental parameters and obtained CHF values from the previously reported paper of Darr et al. [5].

A.K. Darr [5]	Nitrogen 6-1650	12.7mm	11.8mm	Vertically upw Pressure 150-720kpa(Material SS304)
(54 Chlidown tests)				against gravity
CHF				6thermocouples
	106.000	94.000		233 Kpa
CHF	Mass flux	length		pressure(kpa)
51.212	294.034	40.1cm		154.635
36.959	630.682			165.680
109.612	217.330			168.836
50.427	294.034			173.570
117.011	673.295			217.751
70.563	404.830			220.907
58.572	477.273			224.063
83.288	340.909			225.641
135.699	767.045			238.264
51.040	298.295			246.154
52.500	306.818			266.667
82.232	357.955			269.822
84.609	473.011			277.712
55.472	315.341			279.290
71.135	417.614			315.582
82.362	468.750			320.316
58.389	323.864			321.893
95.830	562.500			328.205
98.812	362.216			336.095
83.585	758.523			347.140
60.562	349.432			361.341
133.970	387.784			361.341
68.047	715.909			364.497
126.468	754.261			367.653
132.398	822.443			400.789

Different set of parameters and test section length

Chi et al. [6]				
85.141	470.694	14.5cm		165.398
71.439	383.435			176.949
90.734	491.826			177.116
83.965	348.572			183.368
60.827	401.462			217.082
73.275	328.036			217.160
66.418	600.950			231.363
106.873	356.195			233.009
61.428	342.379			244.286
71.995	402.024			262.529
82.024	349.832			278.002
71.981	388.294			280.682
69.483	384.967			291.033
96.222	539.239			322.382
89.373	483.329			326.213
81.897	451.946			335.224
84.379	466.068			344.322
73.175	399.686			345.522
187.685	1053.702			362.071
126.058	529.380			373.207
94.314	704.205			375.526
206.345	1151.808			377.791
119.204	689.376			388.921
208.810	1179.145			408.931
203.202	1173.383			417.959
209.420	1138.435			425.792
219.374	715.546			431.064
128.497	1229.532			438.058

Report of parameters from experiment of Chi et al. [6]

Chi et al [26]	length of section	Mean temp	Mass flow rate	Mass flux(kg/m ² -sec)	CHF
ID(mm)					
0.476cm	15.24cm	127.78 k	0.000793787	44.6	47.36
0.476cm	45.72 cm	180 k	0.00088	49.45	47.27
0.476cm	60.96 cm	112.5 k	0.000644	36.189	47.22

Report of parameters from experiment of Jin et al. [7]

Lingxue et. al.[27]		ID=10.2mm		
PARAMETERS				
ID(mm)	MASS FLUX(kg/m ² -sec)	Sat pressure Kpa	Length of the test section	Critical heat flux(Kw/m ²)
10.2	19.58	176	5.5m	42
10.2	31.139	255	5.5m	38
10.2	44.414	293	5.5m	45
10.2	45.779	315	5.5m	42
10.2	50.989	433	5.5m	65

The repudiated experimental paper of Yuan et al. [19] and Shukla et al. [20]

Repudiated experiments											
Sun Yuan [33]	Fluid	Mass flux(kg/m ² -s)	length total	OD	ID	Insulation	Orientation	Remarks	section01	section3	section5
CHF[kW/m ²]	Nitrogen	3.6-10.8	254mm	15.8mm	11.1mm	Vacuum jacketed	Horizontal	Low mass flux	76.2mm	127mm	177.8mm
4.200		3.600						film boiling		127.000	
7.100		7.200						thermocouple05		127mm	
9.800		10.800						Bottom wall		127.000	
Al Shukla [31]											
	Nitrogen										
38.000		10.000	300.000		13.5(S1)		Horizontal	two thermocouples each at 5 locations at top and bottom at each section			
42.000		66.000									
		10.000	650.000								
		66.000									
105.000		10.000	1300.000								
118.000		66.000									
		10.000	300.000		21(S2)						
81.000		10.000	300.000								
102.000		66.000									
		10.000	650.000								
		66.000									
71.200		10.000	1300.000								
150.000		66.000									

The value of CHF from each individual correlation is calculated from the input parameters of experimental papers. Some figures are shown below to brief about the work with some data points

Katto and Kurata [14]									
length=40.1cm									
Pressure(kPa)	rho_0[kg/r sigma]	*10 Massflux	(rho_0 v_0)/Heat of vapourisation(kJ/kg)	intermediate terms	CHF(kW/m ²)_CALC				
154.635	786.660	0.803	294.034	6.819	194.120				
165.680	785.580	0.789	630.682	7.269	193.210				
168.836	784.730	0.785	217.330	7.398	192.950				
173.570	783.460	0.779	294.034	7.591	192.570				
217.751	772.630	0.729	673.295	9.377	189.280				
220.907	771.910	0.726	404.830	9.504	189.060				
224.063	771.200	0.723	477.273	9.631	188.840				
225.641	770.850	0.721	340.909	9.695	188.730				
238.264	768.080	0.709	767.045	10.202	187.870				
246.154	766.400	0.702	298.295	10.518	187.350				
266.667	762.170	0.683	306.818	11.339	186.020				
269.822	761.540	0.681	357.955	11.465	185.820				
277.712	759.980	0.674	473.011	11.781	185.330				
279.290	759.670	0.673	315.341	11.844	185.240				
315.581	752.840	0.644	417.614	13.292	183.090				
320.316	751.990	0.640	468.750	13.480	182.760				
321.893	751.700	0.639	323.864	13.543	182.670				
328.205	750.580	0.634	562.500	13.795	182.300				
336.095	749.190	0.628	362.216	14.109	181.850				
347.140	747.280	0.621	758.523	14.549	181.230				
361.341	744.880	0.611	349.432	15.114	180.440				
361.341	744.880	0.611	387.784	15.114	180.440				
364.497	744.350	0.609	715.909	15.240	180.260				
367.653	743.820	0.606	754.261	15.366	180.090				

Lienhard and Dhir [8]									
Pressure(kPa)	rho_0[kg/r sigma]	*10 Massflux	(rho_0 v_0)/Heat of vapourisation(kJ/kg)	intermediate terms	CHF				
154.635	786.660	0.803	294.034	6.8186	194.1200				
165.680	785.580	0.7888	630.6818	7.2694	193.2100				
168.836	784.730	0.7848	217.3295	7.3980	192.9500				
173.570	783.460	0.7789	294.0341	7.5906	192.5700				
217.751	772.630	0.7294	673.2955	9.3773	189.2800				
220.907	771.910	0.7262	404.8295	9.5043	189.0600				
224.063	771.200	0.7230	477.2727	9.6312	188.8400				
225.641	770.850	0.7214	340.9091	9.6946	188.7300				
238.264	768.080	0.7091	767.0455	10.2020	187.8700				
246.158	766.400	0.7017	298.2955	10.5180	187.3500				
266.667	762.170	0.6833	306.8182	11.3390	186.0200				
269.822	761.540	0.6806	357.9545	11.4650	185.8200				
277.712	759.980	0.6738	473.0114	11.7810	185.3200				
279.289	759.670	0.6725	315.3409	11.8440	185.2300				
315.581	752.840	0.6436	417.6136	13.2920	183.0400				
320.316	751.990	0.6400	468.7500	13.4800	182.7600				
321.893	751.700	0.6388	323.8636	13.5430	182.6700				
328.205	750.580	0.6341	562.5000	13.7950	182.3000				
336.097	749.190	0.6284	362.2159	14.1090	181.8500				
347.140	747.280	0.6205	758.5227	14.5490	181.2300				

Mudewar and Maddox [19]		length=40.1cms				dia=11.8mm					
Pressure(kPa)	rho_1(kg/m ³)	sigma*10	Massflux(kg/m ² s)	rho_2(v/kg)	Heat of vapourisation(kJ/kg)	Intermediate terms				CHF calc	
154.6351	786.6600	0.8033	294.0341	6.8186	194.1200	415.3855	5486.3780	0.0500	1.1657	24.2330	
165.6805	785.5800	0.7888	630.6818	7.2694	193.2100	925.4311	25740.6012	0.0292	1.1657	31.5350	
168.8363	784.7300	0.7848	217.3295	7.3980	192.9500	322.3607	3075.4859	0.0612	1.1657	23.0002	
173.5700	783.4600	0.7789	294.0341	7.5906	192.5700	443.1013	5681.2148	0.0494	1.1657	25.5380	
217.7515	772.6300	0.7294	673.2955	9.3773	189.2800	1155.1553	32256.5868	0.0270	1.1657	36.9317	
220.9073	771.9100	0.7262	404.8295	9.5043	189.0600	700.2870	11724.0544	0.0384	1.1657	31.3705	
224.0631	771.2000	0.7230	477.2727	9.6312	188.8400	832.3044	16381.9760	0.0342	1.1657	33.1889	
225.6410	770.8500	0.7214	340.9091	9.6946	188.7300	596.8214	8380.2594	0.0432	1.1657	30.0506	
238.2643	768.0800	0.7091	767.0455	10.2020	187.8700	1385.3383	43115.9790	0.0244	1.1657	39.3899	
246.1538	766.4000	0.7017	298.2955	10.5180	187.3500	548.8299	6634.7488	0.0468	1.1657	29.9698	
266.6667	762.1700	0.6833	306.8182	11.3390	186.0200	590.7908	7248.6311	0.0454	1.1657	31.2833	
269.8225	761.5400	0.6806	357.9545	11.4650	185.8200	693.8691	9913.9649	0.0407	1.1657	32.9500	
277.7120	759.9800	0.6738	473.0114	11.7810	185.3200	932.0362	17520.0369	0.0334	1.1657	36.3076	
279.2899	759.6700	0.6725	315.3409	11.8440	185.2300	623.3855	7805.2665	0.0443	1.1657	32.1706	
315.5819	752.8400	0.6436	417.6136	13.2920	183.0400	884.7334	14434.5080	0.0357	1.1657	36.8672	
320.3156	751.9900	0.6400	468.7500	13.4800	182.7600	1001.4104	18308.3188	0.0329	1.1657	38.4174	
321.8935	751.7000	0.6388	323.8636	13.5430	182.6700	693.8235	8759.0961	0.0425	1.1657	34.3982	
328.2051	750.5800	0.6341	562.5000	13.7950	182.3000	1218.3534	26657.5963	0.0289	1.1657	41.0141	
336.0947	749.1900	0.6284	362.2159	14.1090	181.8500	795.1412	11175.6296	0.0391	1.1657	36.2182	

Katto and Ishii [16]		length=40.1cm				dia=1.8cm					
Pressure(kPa)	rho_1(kg/m ³)	sigma*10	Massflux(kg/m ² s)	rho_2(v/kg)	Heat of vapourisation(kJ/kg)	Intermediate terms				u	CHF
154.6351	786.6600	0.8033	294.0341	6.8186	194.1200	21.7075	0.3738	61.3527	0.0567	18.2244	
165.6805	785.5800	0.7888	630.6818	7.2694	193.2100	23.0341	0.8028	57.9710	0.0339	36.3075	
168.8363	784.7300	0.7848	217.3295	7.3980	192.9500	23.4101	0.2769	57.0427	0.0688	25.4310	
173.5700	783.4600	0.7789	294.0341	7.5906	192.5700	23.9722	0.3753	55.7074	0.0560	28.0881	
217.7515	772.6300	0.7294	673.2955	9.3773	189.2800	29.1089	0.8714	45.8226	0.0314	36.5147	
220.9073	771.9100	0.7262	404.8295	9.5043	189.0600	29.4689	0.5245	45.2547	0.0440	30.7874	
224.0631	771.2000	0.7230	477.2727	9.6312	188.8400	29.8276	0.6189	44.7016	0.0394	32.4902	
225.6410	770.8500	0.7214	340.9091	9.6946	188.7300	30.0065	0.4423	44.4305	0.0492	29.0277	
238.2643	768.0800	0.7091	767.0455	10.2020	187.8700	31.4331	0.9987	42.3757	0.0285	37.8764	
246.1538	766.4000	0.7017	298.2955	10.5180	187.3500	32.3170	0.3892	41.1914	0.0532	27.5732	
266.6667	762.1700	0.6833	306.8182	11.3390	186.0200	34.5922	0.4026	38.4081	0.0517	27.6362	
269.8225	761.5400	0.6806	357.9545	11.4650	185.8200	34.9390	0.4700	38.0146	0.0465	29.0612	
277.7120	759.9800	0.6738	473.0114	11.7810	185.3200	35.8054	0.6224	37.0630	0.0385	31.8014	
279.2899	759.6700	0.6725	315.3409	11.8440	185.2300	35.9794	0.4151	36.8790	0.0504	27.7668	
315.5819	752.8400	0.6436	417.6136	13.2920	183.0400	39.9007	0.5547	33.1092	0.0411	30.0977	
320.3156	751.9900	0.6400	468.7500	13.4800	182.7600	40.4031	0.6233	32.6764	0.0379	31.2245	
321.8935	751.7000	0.6388	323.8636	13.5430	182.6700	40.5720	0.4308	32.5337	0.0485	27.5883	
328.2051	750.5800	0.6341	562.5000	13.7950	182.3000	41.2432	0.7494	31.9765	0.0335	33.0853	
336.0947	749.1900	0.6284	362.2159	14.1090	181.8500	42.0778	0.4835	31.3082	0.0447	28.4881	

David D. Hall [17]		length=40.1				dia=1.8cm							
Pressure(kPa)	rho_1(kg/m ³)	sigma*10	Massflux(kg/m ² s)	rho_2(v/kg)	Heat of vapourisation(kJ/kg)	Intermedi weber nu i deno.				zero inlet subcooling	CHF calc		
154.6351	786.6600	0.8033	294.0341	6.8186	194.1200	12.91426	1.614445	21.84936	0.002922	166.7688	7.632661	807.9004	44.60859
165.6805	785.5800	0.7888	630.6818	7.2694	193.2100	12.84687	7.574541	98.30916	0.001881	229.2558	2.331988	1059.258	13.10676
168.8363	784.7300	0.7848	217.3295	7.3980	192.9500	12.82775	0.905006	12.60919	0.003695	154.9299	12.28706	706.2568	68.29834
173.5700	783.4600	0.7789	294.0341	7.5906	192.5700	12.79975	1.671779	22.39834	0.003105	175.8096	7.849225	785.7413	42.92955
217.7515	772.6300	0.7294	673.2955	9.3773	189.2800	12.57111	9.491963	120.3245	0.002088	266.1196	2.211683	1100.352	10.60858
220.9073	771.9100	0.7262	404.8295	9.5043	189.0600	12.55665	3.449971	44.32008	0.00289	221.2067	4.991117	831.1338	23.7441
224.0631	771.2000	0.7230	477.2727	9.6312	188.8400	12.54241	4.820631	61.46233	0.002628	236.8231	3.853141	880.7181	18.18254
225.6410	770.8500	0.7214	340.9091	9.6946	188.7300	12.53537	2.466012	31.91237	0.003254	209.3297	6.559516	774.5297	8.83003
238.2643	768.0800	0.7091	767.0455	10.2020	187.8700	12.48072	12.74635	160.0836	0.002019	290.8888	1.817105	1034.574	8.279816
246.1538	766.4000	0.7017	298.2955	10.5180	187.3500	12.44812	1.95237	25.30334	0.003702	260.8796	8.175982	718.5757	36.57444
266.6667	762.1700	0.6833	306.8182	11.3390	186.0200	12.36802	2.133014	27.38116	0.003793	216.4894	7.90651	709.2816	33.81051
269.8225	761.5400	0.6806	357.9545	11.4650	185.8200	12.35627	2.917326	37.04729	0.003466	230.5793	6.223757	748.956	26.43998
277.7120	759.9800	0.6738	473.0114	11.7810	185.3200	12.3274	5.155522	64.55421	0.002957	259.2428	4.015893	824.4422	16.78721
279.2899	759.6700	0.6725	315.3409	11.8440	185.2300	12.32174	2.296812	29.30073	0.00382	223.1353	7.615349	760.6697	31.73317
315.5819	752.8400	0.6436	417.6136	13.2920	183.0400	12.19975	4.247561	52.8192	0.003416	261.1403	4.944042	755.8157	19.25353
320.3156	751.9900	0.6400	468.7500	13.4800	182.7600	12.18495	5.387485	66.64625	0.003203	274.4144	4.117477	785.5567	15.90444
321.8935	751.7000	0.6388	323.8636	13.5430	182.6700	12.18003	2.57749	32.39391	0.004045	239.2902	7.386888	682.5086	28.45593
328.2051	750.5800	0.6341	562.5000	13.7950	182.3000	12.16063	7.84438	96.3926	0.002895	296.872	3.078821	834.6161	11.73833
336.0947	749.1900	0.6284	362.2159	14.1090	181.8500	12.13695	3.288589	40.91346	0.003857	254.0676	6.209879	701.7902	23.36292

Zuber [15]						dia=1.18cms		
Pressure	rho_l(kg/r	sigma(*10	Massflux(kg/r	rho_v(kg/	Heat of vapourisation(kj/kg)	Intermediate terms	CHF calc	CHF exp
154.6351	786.6600	0.8033	294.0341	6.8186	194.1200	0.6058578	105.0528	51.2115
165.6805	785.5800	0.7888	630.6818	7.2694	193.2100	0.583818598	107.4181	36.9586
168.8363	784.7300	0.7848	217.3295	7.3980	192.9500	0.577805212	108.0468	109.6119
173.5700	783.4600	0.7789	294.0341	7.5906	192.5700	0.569088132	108.9722	50.4270
217.7515	772.6300	0.7294	673.2955	9.3773	189.2800	0.501613969	116.6335	117.0109
220.9073	771.9100	0.7262	404.8295	9.5043	189.0600	0.49756238	117.122	70.5631
224.0631	771.2000	0.7230	477.2727	9.6312	188.8400	0.493597738	117.6031	58.5721
225.6410	770.8500	0.7214	340.9091	9.6946	188.7300	0.491645349	117.8404	83.2883
238.2643	768.0800	0.7091	767.0455	10.2020	187.8700	0.476694522	119.689	135.6991
246.1538	766.4000	0.7017	298.2955	10.5180	187.3500	0.467935866	120.7938	51.0401
266.6667	762.1700	0.6833	306.8182	11.3390	186.0200	0.446938584	123.4962	52.4998
269.8225	761.5400	0.6806	357.9545	11.4650	185.8200	0.443919429	123.8916	62.2318
277.7120	759.9800	0.6738	473.0114	11.7810	185.3200	0.436566883	124.8609	84.6889
279.2899	759.6700	0.6725	315.3409	11.8440	185.2300	0.435134996	125.0561	55.4724
315.5819	752.8400	0.6436	417.6136	13.2920	183.0400	0.40512933	129.1223	71.1348
320.3156	751.9900	0.6400	468.7500	13.4800	182.7600	0.401592644	129.6069	82.3619
321.8935	751.7000	0.6388	323.8636	13.5430	182.6700	0.400424805	129.77	58.3889
328.2051	750.5800	0.6341	562.5000	13.7950	182.3000	0.395837745	130.4058	95.8303
336.0947	749.1900	0.6284	362.2159	14.1090	181.8500	0.390291905	131.1808	98.8118

Nishikama et. al						corr01			CHF01
Pressure(kPa)	rho_l(kg/r	sigma(*10	Massflux(kg/r	rho_v(kg/	Heat of vapourisation(kj/kg)	int terms			
154.6351	786.6600	0.8033	294.0341	6.8186	194.1200	0.061386		0.05173 181.349	
165.6805	785.5800	0.7888	630.6818	7.2694	193.2100	0.048535		0.05173 305.9358	
168.8363	784.7300	0.7848	217.3295	7.3980	192.9500	0.068426		0.05173 148.4305	
173.5700	783.4600	0.7789	294.0341	7.5906	192.5700	0.062349		0.05173 182.6232	
217.7515	772.6300	0.7294	673.2955	9.3773	189.2800	0.049289		0.05173 324.9395	
220.9073	771.9100	0.7262	404.8295	9.5043	189.0600	0.058112		0.05173 230.0792	
224.0631	771.2000	0.7230	477.2727	9.6312	188.8400	0.055232		0.05173 257.5078	
225.6410	770.8500	0.7214	340.9091	9.6946	188.7300	0.061567		0.05173 204.9112	
238.2643	768.0800	0.7091	767.0455	10.2020	187.8700	0.047831		0.05173 356.5568	
246.1538	766.4000	0.7017	298.2955	10.5180	187.3500	0.06498		0.05173 187.8538	
266.6667	762.1700	0.6833	306.8182	11.3390	186.0200	0.065056		0.05173 192.0746	
269.8225	761.5400	0.6806	357.9545	11.4650	185.8200	0.062017		0.05173 213.3885	
277.7120	759.9800	0.6738	473.0114	11.7810	185.3200	0.056932		0.05173 258.1614	
279.2899	759.6700	0.6725	315.3409	11.8440	185.2300	0.064866		0.05173 195.9956	
315.5819	752.8400	0.6436	417.6136	13.2920	183.0400	0.060194		0.05173 238.0213	
320.3156	751.9900	0.6400	468.7500	13.4800	182.7600	0.058115		0.05173 257.5433	
321.8935	751.7000	0.6388	323.8636	13.5430	182.6700	0.065454		0.05173 200.3107	
328.2051	750.5800	0.6341	562.5000	13.7950	182.3000	0.054985		0.05173 291.6691	
336.0947	749.1900	0.6284	362.2159	14.1090	181.8500	0.063483		0.05173 216.3117	

CHF02	corr03		CHF03
31.56663	55.93634	4.31985	12.94868
32.95533	119.417	4.167163	28.65665
33.35166	41.09506	4.12499	9.962464
33.94047	55.4897	4.064119	13.65356
39.08937	124.8925	3.605289	34.64148
39.43555	75.00633	3.578445	20.96059
39.77894	88.32562	3.552247	24.86472
39.94915	63.05298	3.539388	17.81465
41.2937	141.2227	3.441471	41.03557
42.11263	54.76794	3.384671	16.18117
44.17503	55.93283	3.250069	17.20974
44.48362	65.18481	3.230909	20.17538
45.24855	85.9053	3.184433	26.97664
45.40151	57.24238	3.175422	18.0267
48.7444	74.9112	2.989085	25.06159
49.15895	83.95538	2.967471	28.2919
49.29849	57.97697	2.960332	19.58461
49.84807	100.4929	2.932407	34.26976
50.52479	64.55158	2.898809	22.26831

Y Katto and Ohno [20]		length=40.1cms		Y KATTO[13]		dia=1.18cms		C=0.25			
Pressure(kPa)	rho_l(kg/m ³)	sigma*10	Massflux(kg/m ² s)	rho_v(kg/m ³)	Heat of vapourisation	L/d	corr01	CHF01			
154.6351	786.6600	0.8033	294.0341	6.8186	194.1200	33.98305	0.172643695	289.9722			
165.6805	785.5800	0.7888	630.6818	7.2694	193.2100	33.98305	0.161541237	579.2432			
168.8363	784.7300	0.7848	217.3295	7.3980	192.9500	33.98305	0.176994478	218.4042			
173.5700	783.4600	0.7789	294.0341	7.5906	192.5700	33.98305	0.172384827	287.2255			
217.7515	772.6300	0.7294	673.2955	9.3773	189.2800	33.98305	0.159981372	599.9533			
220.9073	771.9100	0.7262	404.8295	9.5043	189.0600	33.98305	0.167097388	376.3389			
224.0631	771.2000	0.7230	477.2727	9.6312	188.8400	33.98305	0.164710869	436.8381			
225.6410	770.8500	0.7214	340.9091	9.6946	188.7300	33.98305	0.169527414	320.9646			
238.2643	768.0800	0.7091	767.0455	10.2020	187.8700	33.98305	0.157966188	669.8542			
246.1538	766.4000	0.7017	298.2955	10.5180	187.3500	33.98305	0.171238556	281.6045			
266.6667	762.1700	0.6833	306.8182	11.3390	186.0200	33.98305	0.170588206	286.5018			
269.8225	761.5400	0.6806	357.9545	11.4650	185.8200	33.98305	0.168306687	329.4271			
277.7120	759.9800	0.6738	473.0114	11.7810	185.3200	33.98305	0.164235865	423.6425			
279.2899	759.6700	0.6725	315.3409	11.8440	185.2300	33.98305	0.170046358	292.2783			
315.5819	752.8400	0.6436	417.6136	13.2920	183.0400	33.98305	0.165609682	372.5152			
320.3156	751.9900	0.6400	468.7500	13.4800	182.7600	33.98305	0.163925352	413.2437			
321.8935	751.7000	0.6388	323.8636	13.5430	182.6700	33.98305	0.169205416	294.5651			
328.2051	750.5800	0.6341	562.5000	13.7950	182.3000	33.98305	0.161298269	486.717			
336.0947	749.1900	0.6284	362.2159	14.1090	181.8500	33.98305	0.167441965	324.5509			



References

1. Kwon, Y.M., Chang, S.H.: A mechanistic critical heat flux model for wide range of subcooled and low quality flow boiling. *Nucl. Eng. Des.* **188**(1), 27–47 (1999)
2. Katto, Y., Kurata, C.: Critical heat flux of saturated convective boiling on uniformly heated plates in a parallel flow. *Int. J. Multiph. flow* **6**, 575–582 (1980)
3. Burggraf, O.R.: An exact solution of the inverse problem in heat conduction theory and applications. *ASME J. Heat Transfer* **86**, 373–380 (1964)
4. Kawanami, O., Nishida, T., Honda, I., Kawashima, Y., Ohta, H.: Flow and heat transfer on cryogenic flow boiling during tube quenching under upward and downward flow. *Microgravity Sci. Technol.* **9**(3–4), 137–138 (2007)
5. Darr, S.R., Hu, H., Schaeffer, R., Chung, J., Hartwig, J.W., Majumdar, A.: Numerical simulation of liquid nitrogen chill down of a vertical tube. In: 2015 SciTech Conference, Orlando, FL, January 5–9, 2015
6. Chi, J.W.H., Edmiston, J.M., Hansen, O.R.: Effect of vertical flow at low flow rates on transient two-phase flow and boiling heat transfer. In: WANL-TME-795, May 1964
7. Jin, L., et al.: Experimental investigation on chill-down process of cryogenic flow line. *Cryogenics* **79**, 96–105 (2016)
8. Burke, J.C., Byrnes, W.R., Post, A.H., Ruccia, F.E.: Pressurized cooldown of cryogenic transfer lines. *Adv. Cryogenic. Eng.* **4**, 378–394 (1960)
9. Bronson, J.C., Edeskuty, F.J., Fretwell, J.H., Hammel, E.F., Keller, W.E., Meier, K.L., Schuch, A.F., Willis, W.L.: Problems in cool-down of cryogenic systems. *Adv. Cryog. Eng.* **7**, 198–205 (1961)
10. Hedayatpour, A., Antar, B.: Analytical and numerical investigation of cryogenic transfer line chilldown. In: AIAA-90-2373, 26th Joint Propulsion Conference, Orlando, FL, July 16–18 1990
11. Katto, Y.: A generalized correlation of critical heat flux for the forced convection boiling in vertical uniformly heated round tubes. *Int. J. Heat Mass Transf.* **21**, 1527–1542 (1978)
12. Katto, Y., Ishii, K.: Burnout m a high heat flux boiling system with a forced supply of liquid through a plane jet. In: 6th International Heat Transfer Conference, vol. 1, p. 435. National Research Council of Canada (1978)
13. Hall, D.D., Mudawar, I., Critical heat flux (CHF) for water flow in tubes—II. Subcooled CHF correlations. *Int. J. Heat Mass Transf.* **43**, 2605–2640 (2000)

14. Mudawar, I., Maddox, D.E.: Enhancement of critical heat flux from high power micro electric heat sources in a flow channel. *J. Electron. Package*. **112**, 241–248 (1990)
15. Nishikawa, K., Yoshida, S., Yamada, A., Ohno, M.: Experimental investigation of critical heat flux in forced convection boiling of Freon in a tube at high subcritical pressure. In: *Proceedings of the 7th International Heat Transfer Conference*, vol. 4, pp. 21–326 (1982)
16. Zuber, N.: Hydrodynamic aspects of boiling heat transfer, AEC report no. AECU-4439 (1959)
17. Lienhard, J.H., Dhir, V.K.: Hydrodynamic prediction of peak pool boiling heat fluxes from finite bodies. *J. Heat Transfer* **95**, 152–158 (1973)
18. Katto, Y., Ohno, H.: An improved version of the generalized correlation of critical heat flux for the forced convection boiling in uniformly heated vertical tubes. *Int. J. Heat Mass Transf.* **27**(9), 1641–1648 (1984)
19. Yuan, K., Ji, Y., Chung, J.N., Shyy, W.: Cryogenic boiling and two-phase flow during pipe chilldown in earth and reduced gravity. *J. Low Temp. Phys.* **150**, 101–122 (2008)
20. Shukla, A.K., et al. *IOP Conf. Ser.: Material Science Eng.* 278 012035 2017

Virtual Design Optimization of Motorbike Rear Sprocket Based on ANSYS and Hybrid MOORA-Fuzzy Inference System



Abhishek Barua , Dilip Kumar Bagal , Siddharth Jeet , Swastik Pradhan , Dulu Patnaik, and Ajit Kumar Pattanaik

Abstract Sprockets are most commonly employed as a part of vehicle segment and in machineries to transfer rotating movement among two shafts wherever adapts are contrary or to convey firm movement to a path and so on. They are present in different measurements, teeth number and are prepared of various materials. Being very vital it is very important these sprockets are designed properly and right material is used. There is a need for an improved material so that it can sustain more forced frequency and so that more fruitful results can be achieved in shorter time. In this study, the current sprocket of Mild steel is distinguished with the sprocket of Chromoly steel. CAD modelling of sprocket has been made through Reverse Engineering approach and analysed using Finite Element Analysis. In light of the outcomes, sprocket's design has been optimized for weight reduction which can achieve better result under different torque condition keeping same constrictions using MOORA technique and MOORA coupled Fuzzy Inference System respectively. In this study, weight reduction of sprocket is done by introducing pockets on the ribs. The dimensions of the pocket have been taken as input parameters and analysis has been conducted using the L9 orthogonal array in ANSYS 17.2 version. This practice assists as a different tactic for sprocket design evaluation and its behaviour in chain drives which is desired in the automobile industries.

Keywords Sprocket · ANSYS · CAD · Chromoly steel · MOORA · Fuzzy inference system

A. Barua · S. Jeet

Centre for Advanced Post Graduate Studies, BPUT, Rourkela, Odisha 769004, India

D. K. Bagal (✉) · D. Patnaik · A. K. Pattanaik

Government College of Engineering, Kalahandi, Bhawanipatna, Odisha 766002, India

e-mail: dilipbagal90@gmail.com

S. Pradhan

Lovely Professional University, Phagwara, Punjab 144411, India

1 Introduction

A chain sprocket is a profiled toothed cog which works with track belt, chain or other indented object for transmission of turning effort between 2 shafts. Inside worldwide principles sprockets are reasonably essential mechanical gadgets. Be that as it may, their adaptability prompts numerous differentiating styles. Sprockets can be provided in different materials and styles, contingent on the application and seriousness of administration prerequisites [1]. The sprocket's teeth work inside a roller chain, in this way exchanging rotational vitality between parallel shafts over separations. Sprockets have a few purposes of high-grinding contact with a roller chain, which is imperative to proficient pivot, yet in addition wears the sprocket and roller chain rapidly. This is battled with greased up bushings around the stick that the sprocket handles, and additionally between the plates that hold the chain together [2].

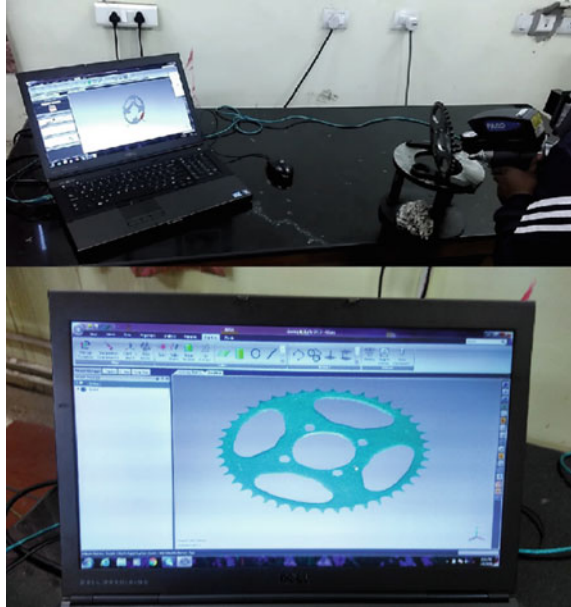
Sprockets are designed in such a means that they will mesh correctly if they get fitted to a chain drive system. It is the most efficient sprocket to deliver a constant and positive speed drive. Generally, different types of steels or aluminium alloys are used to make sprockets according to their mode of operations. The materials used in the sprocket are one of the chief criteria for designing. The material can resolve the amount of vibration it is able to take or whether the input speed will basis resonance or not. These all be contingent on the natural frequencies it will generate and produce deformation and stress. The composite materials are chosen over the conventional materials used now for the reason that of their strength even at light weight [1–9].

In this paper, FEM modelling and simulation is figured using the CATIA and ANSYS. Computer Aided Modelling (CAD) of sprocket has been made through Reverse Engineering approach and analysed using Finite Element Analysis. In light of the outcomes, sprocket's design has been optimized for weight reduction for better performance under different torque condition keeping the same restraints using MOORA technique and MOORA coupled Fuzzy Inference System respectively. In this study, weight reduction of sprocket is done by introducing pockets on the ribs. The dimensions of the pocket have been taken as input parameters and analysis has been conducted using the L9 orthogonal array in ANSYS 17.2 version.

2 CAD Modelling of Sprocket Through Reverse Engineering

Reverse Engineering is a practice of reproducing an existing section, subassembly, or object, without guide of documentation, drawings or computer model. For some product development processes reverse engineering is utilized to create surface models by 3D-examining strategy, and thus this system grants to fabricate distinctive parts for automobiles, machineries, moulds, dies, press tools in a short development period. Here, FaroArm scanner is utilized for producing 3D model of the sprocket which is preminent portable coordinate measuring machine (PCMM). The design

Fig. 1 Sprocket specimen scanned using FaroArm scanner



of the sprocket was taken from rear wheel conventional sprocket model of Hero Xtreme having 43 teeth. The specimen was cleaned, coated with developer liquid and then scanned by using FaroArm Fusion scanner. The scanned model was generated in Geomagic studio software which is used for transforming 3D scanned data into highly accurate native CAD models. After generating, the model was imported in CATIA V5 R21 for more accurate development [8]. Figure 1 Shows the sprocket specimen scanned using FaroArm scanner.

After scanning the specimen and generating a CAD model in Geomagic Studio, the “.stl” file is imported to CATIA V5 R21 for further development. Since the teeth profile of original sprocket specimen is worn out, it is needed to be re-designed in the software.

The thickness of the sprocket is 7.2 mm. Certain formulae are taken for sprocket teeth profile generation. The specimen is having 43 teeth on the surface. The calculations are done using formulae show in Table 1 and the teeth profile is generated [8]. Figure 2 shows the sprocket tooth geometry. Figure 3 shows CAD model generated by scanning imported in CATIA V5 R21. Figure 4 depicts sprocket tooth geometry generated in CATIA while Fig. 5 shows the final CAD model of sprocket generated in CATIA.

Previously, many researchers have carried out their research in development of the sprocket. Some have tried to replace the conventional material with other alternative material which can show similar mechanical behaviour when subjected to similar loading condition like that of conventional material [4, 5]. Some have also tried to optimize the design of the sprocket based on the values of stress, strain or deformation at particular area [3]. They have achieved the optimized design by introducing a

Table 1 Formulae for the development of sprocket tooth form [1]

Formulae	Value		
	(in)	(mm)	–
$P = \text{chain pitch}$	0.5	12.7	–
$N = \text{No. of teeth}$	–	–	43
$Dr = \text{chain roller Dia.}$	0.335	8.51	–
$Ds = 1.0005 Dr + 0.003$ (seating curve dia.)	0.340	8.628	–
$R = Ds/2 = 0.5025Dr + 0.0015$	0.170	4.314	–
$A = 350 + \frac{60^\circ}{N}$	–	–	36.4°
$B = 180 - \frac{56^\circ}{N}$	–	–	16.7°
$ac = 0.8 \times Dr$	0.268	6.807	–
$M = 0.8 \times Dr \cos\left(350 + \frac{60^\circ}{N}\right)$	0.216	5.479	–
$T = 0.8 \times Dr \sin\left(350 + \frac{60^\circ}{N}\right)$	0.159	4.039	–
$E = 1.3025 Dr + 0.0015$	0.438	11.121	–
Chordal Length of Arc. $xy = (2.605 Dr + 0.003) \sin\left(90 - \frac{28^\circ}{N}\right)$	0.127	3.230	–
$yz = Dr\left[1.4 \sin\left(17^\circ - \frac{64^\circ}{N}\right) - 0.8 \sin\left(18^\circ - \frac{56^\circ}{N}\right)\right]$	0.048	1.230	–
$ab = 1.4Dr$	0.469	11.913	–
$W = 1.4Dr \cos \frac{180^\circ}{N}$	0.468	11.881	–
$V = 1.4Dr \sin \frac{180^\circ}{N}$	0.034	0.870	–
$F = Dr\left[0.8 \cos\left(18^\circ - \frac{56^\circ}{N}\right) + 1.4 \cos\left(17^\circ - \frac{64^\circ}{N}\right) - 1.3025\right] - 0.0015$	0.271	6.878	–
$H = \sqrt{F^2 - \left(1.4Dr - \frac{P}{2}\right)^2}$	0.159	4.045	–
$S = \frac{P}{2} \cos \frac{180^\circ}{N} + H \sin \frac{180^\circ}{N}$	0.261	6.628	–
$PD = \frac{P}{180^\circ/N}$	6.850	173.984	–

pocket or removing the material from that particular area thus making the sprocket lighter than the original design. In this study also after designing the sprocket, taking previous studies as a reference, pockets have been added on each ribs of the sprocket for design optimization. Weight of the original sprocket was found out to be 712 g approx. Figure 6 shows the dimensioning of pockets in sprocket by using ANSYS Space Claim.

Taking input parameters shown in Table 2 and according to the L9 orthogonal array designed to conduct experiment, all the output responses are recorded for every different design of the sprocket which is discussed in the later section.

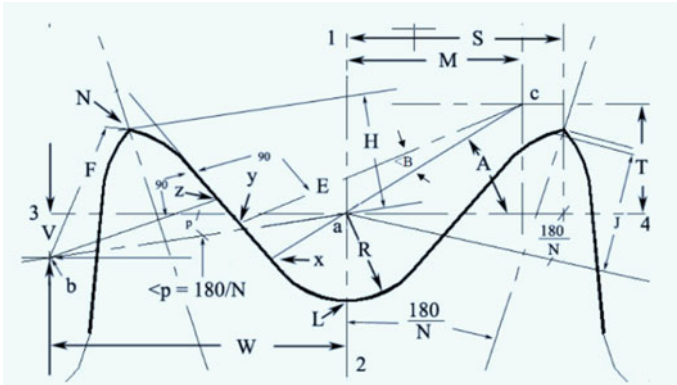


Fig. 2 Sprocket tooth geometry [1-3]

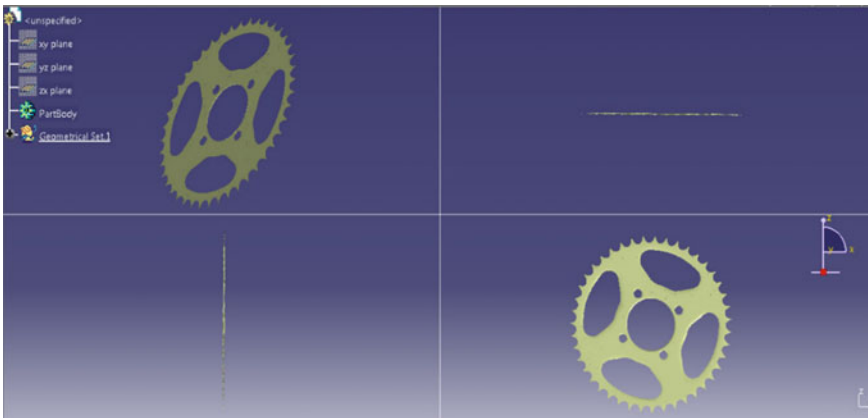


Fig. 3 CAD model generated by scanning imported in CATIA V5 R21

3 Material for Motorcycle Sprocket

The material choice for sprocket manufacturing relies on strength and operating circumstances like noise, wear, load, etc. including cost and in addition the material execution. They might be fabricated from any material in accordance to the service and area of requirement. Carbon steel is generally utilized for sprocket manufacturing because of its great wearing possessions, magnificent machinability and simplicity of creating muddled shapes by machining. Alloy steels are additionally used in a few spots for substantial working condition or aluminium alloy is used for high speed operation like motorcycle racing. In this study, Chromoly steel (AISI 4140) which is also known as high tensile alloy steel has been used for designing the sprocket. Alloying components incorporate Chromium and Molybdenum. Thus, it is called

Fig. 6 Dimensioning of pockets in sprocket by using ANSYS space claim

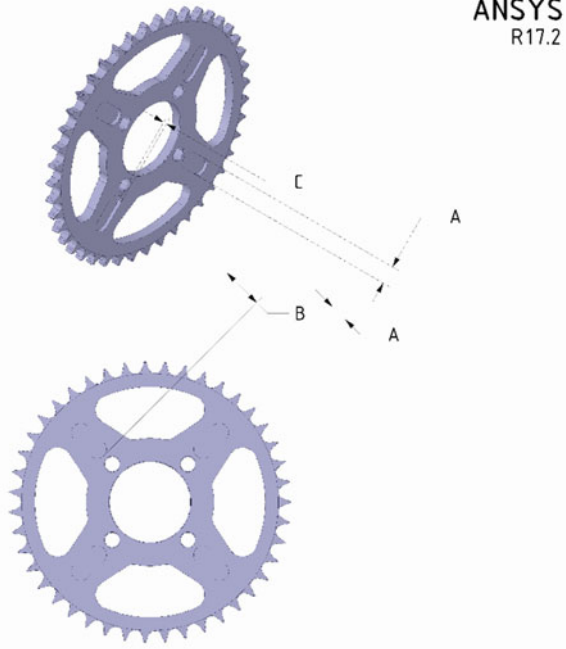


Table 2 Input parameters of pocket dimension

Factors	Symbol	Level 1	Level 2	Level 3
Width (mm)	A	8	10	12
Length (mm)	B	21	24	27
Thickness (mm)	C	2.5	3	3.5

Table 3 Mechanical properties of chromoly steel (Approx.)

Properties	AISI 4140
Elastic modulus	210 GPa
Density	7870 kg/m ³
Ultimate tensile stress	650 MPa
Poisson's ratio	0.28
Yield strength	400 MPa

4 Finite Element Analysis (FEA) of Sprocket

It is an onscreen way for envisaging a product's behaviour to practical forces, illustrates whether a product behaviour. Here, Static Analysis is done by using ANSYS 17.2 and boundary conditions are fitted to get desired solution [1–9].

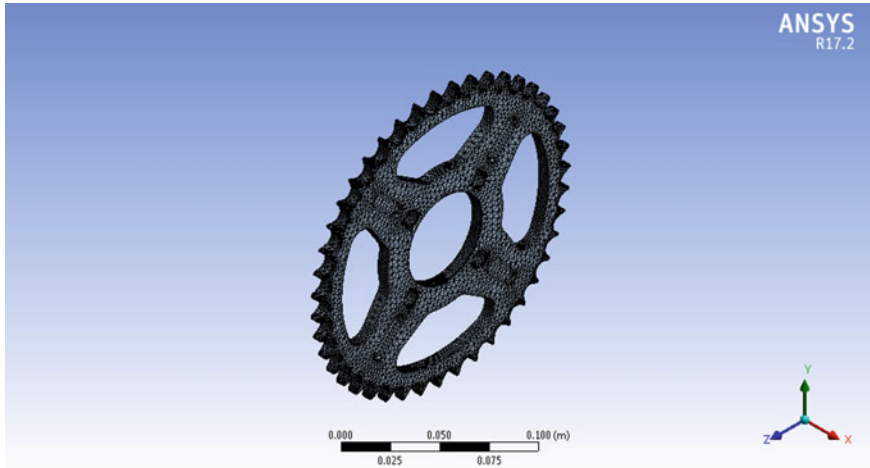


Fig. 7 Meshed model of sprocket

4.1 Meshing

For meshing, CATPART file of the CAD model of sprocket was imported to ANSYS 17.2. Tetrahedral element was used for meshing. Meshing tool in ANSYS workbench was used for creation of fine mesh with element size 2 mm after convergence. Figure 7 demonstrates the meshed model of sprocket in ANSYS Workbench [8].

4.2 Boundary Conditions

Subsequently meshing is accomplished, after which boundary conditions were applied which are reference points for calculation of analysis results [8]. Forces acting on sprocket-Torque at the rear sprocket and Gravitational force which is neglected in this case.

Calculation for Torque at rear sprocket [7, 8]:

1. Maximum Power from engine: 11.6 kW at 8500 rpm
2. Maximum torque by Engine (T_e): 13.5 Nm @ 6500 rpm
3. Primary Gear Reduction (i_x): 3.35
4. Final Gear Reduction (i_o): 3.0714
5. Torque at rear sprocket = $(i_x) \times (i_o) \times (T_e) = 3.35 \times 3.0714 \times 13.5 = 138.9$ Nm.

The CAD model has been restraint at the boundary and maximum torque 138.9 Nm was applied at centre. Boundary conditions applied on the sprocket are shown in Fig. 8.

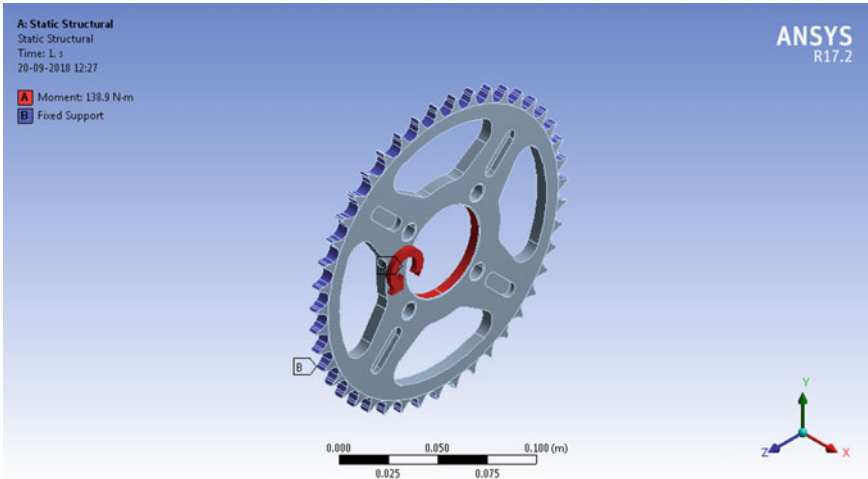


Fig. 8 Boundary conditions applied on sprocket

4.3 Solution

After meshing and boundary condition applied on the CAD model, analysis process was done in ANSYS 17.2 version. It computed the deflection in the model with respect to boundary conditions applied over it and calculated the stress. Results were observed and consequently changes were planned according to higher stress region acquired.

5 MOORA Technique (Multi-objective Optimization on the Basis of Ratio Analysis)

In MOORA technique, output responses are set in decision matrix as stated in Eq. (1) [10–17].

$$X = \begin{bmatrix} x_{11} & x_{12} & \dots & x_{1n} \\ x_{21} & x_{22} & \dots & x_{2n} \\ \vdots & \vdots & \dots & \vdots \\ x_{m1} & x_{m1} & \dots & x_{mn} \end{bmatrix} \tag{1}$$

Normalizing the data of the formed matrix using the Eq. (2).

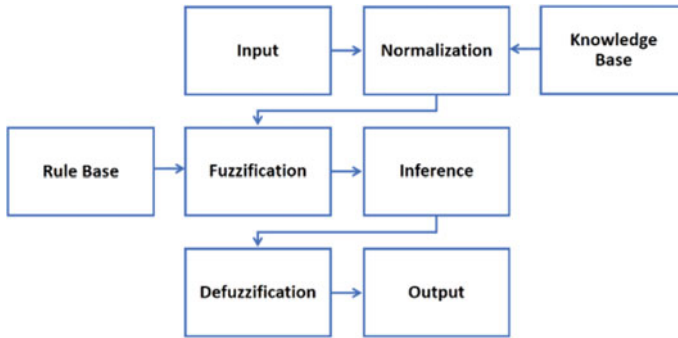


Fig. 9 Layout of fuzzy editors on fuzzy inference system

$$x_{ij}^* = x_{ij} / \left[\sum_{i=1}^m x_{ij}^2 \right]^{\frac{1}{2}} \quad (j = 1, 2, \dots, n) \tag{2}$$

A normalized assessment value is calculated after the consideration of weight using Eq. (3) and ranked from higher to lower value [10–13]:

$$y_i = \sum_{j=1}^g w_j x_{ij}^* - \sum_{j=g+1}^g w_j x_{ij}^* \tag{3}$$

6 Fuzzy Inference System

It organizes four representations; fuzzification interface, decision-making unit, rule base and database, and defuzzification interface. Fuzzy rule base uses “if-then” controller rules with minimum 2 inputs and single output. The layout of Fuzzy editors on Fuzzy inference system is shown in Fig. 9.

7 Results and Discussion

The experimental layout was made conferring to Taguchi’s method. The factors and their levels for the experiment are tabulated in Table 2. According to the factors and levels, the suitable minimum numbers of experimental run that can be done with to Taguchi array is L9. The L9 layout of the experiment is presented in Table 4. The finite element analysis was conducted under static loading conditions to find maximum stress, deformation and weight of each design.

Table 4 L9 orthogonal array of experimental runs with output results

Run No.	A	B	C
1	8	21	2.5
2	8	24	3
3	8	27	3.5
4	10	21	3
5	10	24	3.5
6	10	27	2.5
7	12	21	3.5
8	12	24	2.5
9	12	27	3

Now, MOORA method was used to find out the optimum dimension for the pocket. The normalization of output responses was done using Eq. (2). Overall assessment values were calculated and their ranking according to the highest value of the MOORA index. Table 5 shows the normalized assessment values, Overall assessment values and ranks of the responses.

From the ranking of Overall assessment value, experiment no. 8 shows the highest value among all experiments. Hence, the optimal dimension for pocket for sprocket using MOORA based method is found to be at length of 24 mm, width of 12 mm and thickness of 2.5 mm respectively.

The fuzzy logic method was implemented to single Fuzzy-MOORA overall assessment value than considering complicated multiple outputs. Mamdani’s inference technique was chosen for finding membership function values and centroid method is used for defuzzification approach. For formulation of statement for prediction fuzzy logic, If-Then rule statements were employed, which have three weighted normalized assessment value such as maximum stress, deformation and weight obtained with one output as a Fuzzy-MOORA overall assessment value. Fuzzy logic

Table 5 Normalized assessment values of responses

Run No.	Maximum stress	Maximum deformation	Weight obtained	Y_i	Rank
1	0.3374	0.3141	0.3374	-0.1070	2
2	0.3226	0.3271	0.3351	-0.1154	7
3	0.3498	0.3429	0.3325	-0.1108	3
4	0.3285	0.3273	0.3346	-0.1134	5
5	0.3386	0.3455	0.3316	-0.1150	6
6	0.3288	0.3261	0.3338	-0.1126	4
7	0.3200	0.3438	0.3315	-0.1205	8
8	0.3466	0.3271	0.3335	-0.1069	1
9	0.3263	0.3446	0.3299	-0.1182	7

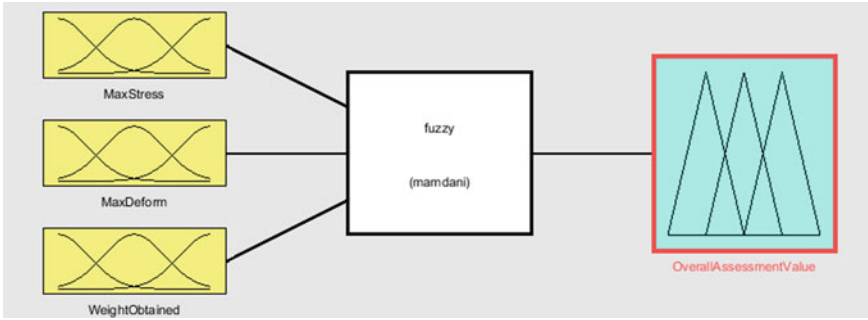


Fig. 10 Fuzzy inference system fuzzy editor

tool of MATLAB (R2018a) software was used. Figure 10 shows the Fuzzy inference system fuzzy editor. Figure 11 shows Fuzzy environment rule editors for prediction of Fuzzy-MOORA overall assessment value, for a given input value of weighted normalized assessment value of maximum stress, deformation and weight obtained.

From the ranking of Fuzzy-MOORA overall assessment value is shown in Table 6, experiment no. 8 shows the highest value among all experiments. Hence, the optimal dimension for pocket for sprocket using Fuzzy based MOORA method is found to be at width of 12 mm, length of 24 mm and thickness of 2.5 mm respectively. Hence by using the optimal pocket dimensions obtained from both the methods, the pockets

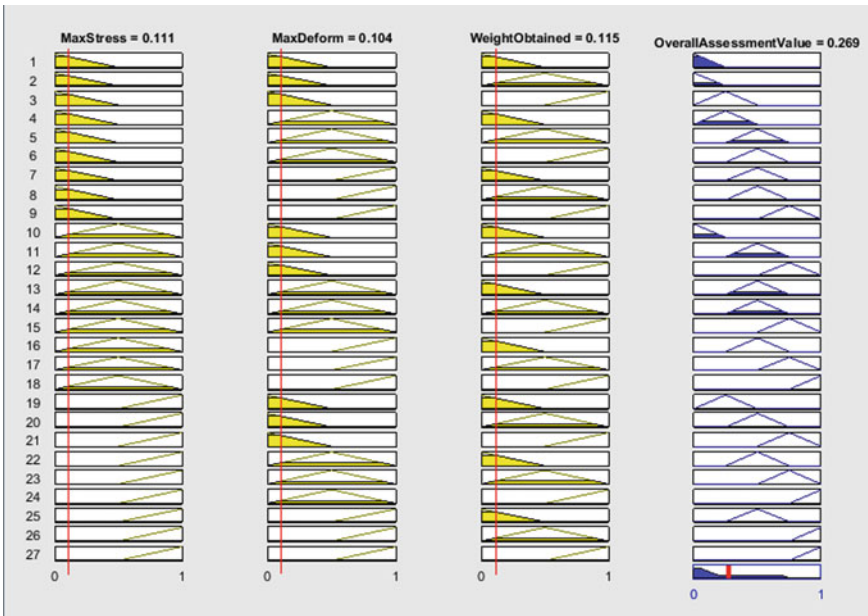


Fig. 11 Fuzzy environment rule editors

Table 6 Fuzzy-MOORA overall assessment value

S. No.	Fuzzy-MOORA overall assessment value	Rank
1	0.2690	6
2	0.2660	9
3	0.2700	2
4	0.2670	7
5	0.2700	3
6	0.2670	8
7	0.2700	4
8	0.2710	1
9	0.2700	5

Table 7 Original and optimum parameter

Optimization techniques	Optimal pocket dimension			Output responses			% Weight reduction
	A (mm)	B (mm)	C (mm)	Maximum stress (MPa)	Maximum deformation (mm)	Weight obtained (g)	
MOORA	12	24	2.5	30.315	0.0017197	692.59	2.72
Fuzzy-MOORA	12	24	2.5	30.315	0.0017197	692.59	2.72

have been redesigned and analysed under same boundary conditions as done before. Table 7 shows original and optimum parameter.

8 Conclusions

A statistical and a combination of statistical with heuristical optimization approach has been adapted for design optimization of chain sprocket. Subsequently weight optimization has been achieved by employing two different approach. From outcomes of finite element analysis, all the combination of pocket dimension has stress values are in reduced amount than their corresponding tolerable yield stress was analysed. Hence, the design was safe. According to the MOORA technique, the optimal dimension of pocket for sprocket is found to be at length of 21 mm, width of 12 mm, and thickness of 3.5 mm respectively. It gives a subsequent weight reduction after employing both MOORA and Fuzzy-MOORA technique to 692.59 g from 712 g i.e., 2.72% reduction. More optimal results can be achieved by considering some more design factors like different loading condition, different materials or by employing different optimization techniques. According to survey after approx. 20,000 km of motorcycle drive chain sprocket assembly needs to be replaced. But, after proper

designing, chain sprocket can run longer. Researchers are also searching for more alternative materials to replace the conventional mild steel. Cost of material is another factor which restricts the use of alternate materials in place of existing materials for sprocket manufacturing for motorcycles. So, these can be used for further development of chain sprocket and more efficiency can be achieved during power transmission.

Acknowledgements The authors would like to acknowledge Dr. M. R. Khan, Department of Industrial Design, NIT, Rourkela for scanning and development of the CAD model of specimen.

References

1. Ambole, N.P., Kale, P.R.: Finite element analysis carbon fiber sprocket using ANSYS. *Int. J. Sci. Res. Dev.* **4**(5), 310–314 (2016)
2. Ebhota, W.S., Ademola, E., Oghenekaro, P.: Fundamentals of sprocket design and reverse engineering of rear sprocket of a Yamaha CY80 motorcycle. *Int. J. Eng. Technol.* **4**(4), 170–179 (2014)
3. Nikam, P., Tanpure, R.: Design optimization of chain sprocket using finite element analysis. *Int. J. Eng. Res. Appl.* **6**(9), 66–69 (2016)
4. Barua, A., Jeet, S., Kar, S.: An overview of concurrent engineering and virtual manufacturing application in motorcycle sprocket production. *Int. J. Sci. Eng. Res.* **9**(4), 42–45 (2018)
5. Barua, A., Mishra, S.P., Rout, S.P., Paul, S., Naik, B., Bagal, D.K.: Comparative structural analysis of cross drilled motorcycle petal disc brake rotor based on fea using different composite materials. *Int. J. Sci. Res. Rev.* **8**(6), 419–429 (2019)
6. Saxena, A., Parey, A., Chouksey, M.: Study of modal characteristics of a geared rotor system. *Procedia Technol.* **23**, 225–231 (2016)
7. Goharimanesh, M., Akbari, A., Tootoonchi, A.A.: More efficiency in fuel consumption using gearbox optimization based on Taguchi method. *J. Ind. Eng. Int.* **10**(61) (2018). <https://doi.org/10.1007/s40092-014-0061-y>
8. Barua, A., Jeet, S., Parida, B., Sahoo, B.B., Bagal, D.K., Samantray, A.: Virtual optimization of motorcycle sprocket material by using FEA and Taguchi coupled TOPSIS-GA-SA. *Int. J. Adv. Sci. Res. Manag.* **3**(9), 54–63 (2018)
9. Barua, A., Kar, S.: Review on design optimization of sprocket wheel using different techniques. *Int. J. Adv. Mech. Eng.* **8**(1), 55–62 (2018)
10. Panda, S.N., Bagal, D.K., Pattanaik, A.K., Patnaik, D., Barua, A., Jeet, S., Parida, B., Naik, B.: Comparative evaluation for studying the parametric influences on quality of electrode using Taguchi method coupled with MOORA, DFA, and TOPSIS method for electrochemical machining. In: Parwani, A., Ramkumar, P. (eds.) *Recent Advances in Mechanical Infrastructure. Lecture Notes in Intelligent Transportation and Infrastructure*, pp. 115–129. Springer, Singapore (2020). https://doi.org/10.1007/978-981-32-9971-9_13
11. Sahoo, B.B., Barua, A., Jeet, S., Bagal, D.K.: Multi objective optimization of WEDM process parameters using hybrid RSM-GRA-FIS, GA and SA approach. *Int. J. Res. Advent Technol.* **6**(7), 1752–1761 (2018)
12. Parida, B., Barua, A., Jeet, S., Bagal, D.K.: Fabrication and mechanical characterization of jute-glass-silk fiber polymer composites based on hybrid RSM-GRA-FIS and RSM-TOPSIS approach. *Int. J. Res. Eng. Appl. Manag.* **4**(5), 25–33 (2018)
13. Barua, A., Jeet, S., Parida, B., Samantray, A., Bagal, D.K.: Comparative evaluation and optimization of 4-cylinder CI engine camshaft material using finite element analysis: a hybrid MOORA technique and Taguchi based desirability function analysis approach. *Int. J. Tech. Innov. Mod. Eng. Sci.* **4**(11), 105–114 (2018)

14. Jeet, S., Barua, A., Parida, B., Sahoo, B.B., Bagal, D.K.: Multi-objective optimization of welding parameters in GMAW for stainless steel and low carbon steel using hybrid RSM-TOPSIS-GA-SA approach. *Int. J. Tech. Innov. Mod. Eng. Sci.* **4**(8), 683–692 (2018)
15. Barua, A., Jeet, S., Cherkia, H., Bagal, D.K., Sahoo, B.B.: Parametric optimization of FDM processed part for improving surface finish using MOORA technique and desirability function analysis. *Int. J. Appl. Eng. Res.* **14**(13), 1–7 (2019)
16. Barua, A., Jeet, S., Bagal, D.K., Agrawal, P.K., Pattanaik, A.K.: Comparative analysis based on MCDM optimization of printing parameters affecting compressive and tensile strength of fused deposition modelling processed parts. *Int. J. Tech. Innov. Mod. Eng. Sci.* **5**(2), 383–392 (2019)
17. Jeet, S., Barua, A., Cherkia, H., Bagal, D.K.: Comparative investigation based on MOORA, GRA and TOPSIS method of turning of nickel-chromium-molybdenum steel under the influence of low cost oil mist lubrication system. *Int. J. Appl. Eng. Res.* **14**(13), 8–20 (2019)

Fused Filament Fabrication (FFF) Based 3D Printer and Its Design: A Review



Krishnanand and Mohammad Taufik

Abstract A digital fabrication technology, which fabricates a part using the 3D CAD model by layer over layer material deposition, is termed as additive manufacturing (AM) or 3D printing. There are various additive manufacturing techniques but the Fused Filament Fabrication (FFF) technique is more popular among them. The popularity of FFF is because of low cost and easy construction of a 3D printer and the availability of various feed materials. In this paper, various applications and materials used in additive manufacturing are discussed. The complete process of 3D printing is discussed along with a detailed discussion of FFF based 3D printing. At the end of the paper, an overview of the design of an FFF based 3D printer is provided.

Keywords Fused filament fabrication · FFF · Fused deposition modeling · FDM · 3D printing · Design of 3D printer

1 Introduction

Additive Manufacturing (AM) is included in the list of the most emerging and prominent technologies of the current era, i.e., industrial revolution 4.0 [1]. In contrast to the conventional subtractive manufacturing processes like turning, milling, drilling, etc. In Additive Manufacturing a digital 3D solid model is converted into a real-world physical product by deposition of material in the layer by layer fashion. According to ISO/ASTM 52900 [2] standard, Additive Manufacturing can be described as a “Process of deposition of material in layer by layer fashion to build a product from solid CAD model.” Initially, this method of manufacturing was used mainly for the development of prototypes that is why it is also called Rapid prototyping. Another name of Additive Manufacturing is 3D Printing. This technology can be utilized

Krishnanand · M. Taufik (✉)

Department of Mechanical Engineering, Maulana Azad National Institute of Technology (MANIT), Bhopal 462003, India
e-mail: taufikmohd86@gmail.com

© The Author(s), under exclusive license to Springer Nature Singapore Pte Ltd. 2021
B. Deepak et al. (eds.), *Advanced Manufacturing Systems and Innovative Product Design*,
Lecture Notes in Mechanical Engineering,
https://doi.org/10.1007/978-981-15-9853-1_41

497

for product design as well as customization of products [3]. There is “design freedom” in 3D printing technology. It is a big supporting tool for researchers to develop innovative products that can be economically manufactured [4]. In 1990, Stratasys invented a new layer by layer production manufacturing technology that is known by name of Fused Deposition Modelling (FDM). Nowadays this technology is termed as Fused Filament Fabrication (FFF) and whenever someone hears the term “3D printing” this is the first technology that comes in mind. Since 1984, when the first 3D printer was developed, the technology reached at new levels and 3D printing systems gained wider scope of applications and became more affordable [5]. The most common use is rapid prototyping. Apart from rapid prototyping, it can be used in numerous industries—the medical industry, automobile sector, aerospace and aviation, food industry, heavy engineering industry, construction and architectural model, toy industry, jewelry, and fashion industry are some of them [6].

Polymers like—ABS and PLA are well-known materials for FFF type 3D printing but materials like ceramics, metals, composites, and other smart materials are also used in 3D printing. Blok et al. [7] used carbon fiber/nylon composite as print material. They found good mechanical properties of fiber/nylon composite printed part [7]. Dul et al. found improved thermal, mechanical, and electrical properties of the FFF printed part using a composition of 6 wt% fraction of CNT in ABS [8]. With biopolymer options, most developments are essentially research initiatives, targeting mainly the applications in scaffold printing tissue engineering [9]. Recent trends show that metals and alloys are also being used in 3D printing on a wider scale. Alloys of Aluminum [10], cobalt [11], nickel [12], stainless steel [13], titanium [14] are most preferred alloys among them. These are used in dental applications, aerospace industry, and biomedical industry [3]. 3D printing is used in construction to make Building components of metals and concrete with well-developed techniques [15]. Kim et al. made some clothes, garments, and other fashion stuffs under different conditions, and find some parameters that are hindering the use of FFF technology in the fashion industry [16]. 3D printing is also helping in teaching methods to enhance student’s knowledge by seeing the 3D printed prototypes [17]. 3D printing is helping the medical students to perform the experiment on 3D printed part. Students can get practical knowledge and live demonstration with the help of 3D printed parts.

3D printing provides increased productivity and reduced cost, flexible and responsive manufacturing, greater quality control, reduction in need of transportation—saves energy and time [3]. 3D printing allows ideas to develop faster, one can believe on the design of product before expending money in tool designing by examining the prototype developed with the help of 3D printing [5]. 3D printing is environmentally and ecologically promising [4]. Shape complexity, material complexity, part consolidation, design freedom, and customization are distinctive features of additive manufacturing. 3D printing is good for customized products, but it is not good for mass production. Intellectual property issues, limitation of size [5], the strength of the product, surface quality, accuracy are some challenges in 3D printing. As per the authors knowledge this is the novel effort to put the combined study of FDM process as well as detailed design of FDM-based 3D printer and discussion on the electronics components used in 3D Printers.

2 Types of 3D Printing

As per ASTM standard F2797 [18], 3D printing methods are categorized into seven groups—extrusion-based processes, material jetting, powder fusion-based processes, vat polymerization, sheet lamination, directed energy deposition, and Binding jetting. Each of these technologies has its application in numerous industries. These are now not limited to just prototyping, but also used to manufacture various types of products. Out of all these technologies material extrusion-based technology is most common and affordable. An example of material extrusion-based additive manufacturing technique is Fused Filament Fabrication (FFF). This study presents design overview of FFF technology dependent 3D printers.

2.1 Fused Filament Fabrication

This technology was patented by Stratasys. After the expiration of the patent, it has emerged as an open-source development community. As a result, this technology becomes more affordable compare to other technologies [5]. In this method, a wire form feed material (ABS, PLA, etc.) also called filament is pushed into a heating nozzle with the help of an auto-loading carrier. In the nozzle, this material is heated up to the semi-liquid state and then extruded out of extrusion nozzle along the deposition path. Generally, the printing head is having movement horizontal plane ($x-y$) while the build plate or fabrication platform moves in the vertical direction (z) (see Fig. 1a).

Like that layer by layer deposition takes place to form a product. FFF technology is very flexible, it can handle with the small overhangs. FFF can't produce undercut without support material. For FFF technology we have many choices for printing materials among which ABS and PLA are the most preferred. Materials are selected according to need by trading off between strength and temperature properties [20].

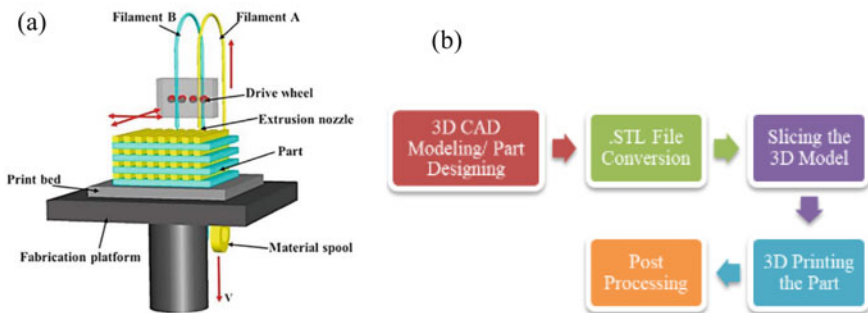


Fig. 1 a Fused filament fabrication process [19], b process of 3D printing

3 Process of 3D Printing

A sequence of steps is followed to get the final 3D printed part. 3D Solid modeling is the first step of 3D printing. Then 3D solid model is converted into STL format after that some slicing software is used to slice the model and then it is sent into the 3D printer to print. After printing, post-processes are performed to remove support material, improve the finishing, etc. (see Fig. 1b).

The 3D solid model design of the part to be printed is prepared using some computer-aided design software packages like SolidWorks, CATIA, etc. If CAD drawing of the part to be 3D printed is not available in that case reverse engineering can be applied [20]. Through 3D scanning of the part to be reproduced, we can obtain its 3D model and that 3D model can be used to 3D print that part.

CAD software packages provide the flexibility of saving the designed solid model in number of file formats. But, for maintaining the consistency, the stereolithography format (STL) has been standardized as the file format in the additive manufacturing industry. STL is also called Standard Tessellation Language. 3D CAD model is tessellated, and its surface is represented by triangles.

STL file only contains the surface geometry of the 3D objects. It does not represent color, texture, material, or other CAD model attributes. However, there in the market, a new file format is also being used that is Additive Manufacturing File (AMF). Which can handle many other features along with surface geometry [21]. This STL file is transported to 3D printing system using some CAM software system [22].

STL file is imported to some slicing software like Cura, KISSlicer, Slic3r, etc. In that software, some pre-processing parameters like—build orientation [23], support structures, layer thickness, are defined and this STL file is sliced in many layers. Every slice is like a 2D image [24]. After slicing, the data of the file is converted into a G-code that decides the movement of the extrusion nozzle of 3D printer [5].

In this step, actual part fabrication is done by a 3D printer. G-code file obtained after slicing solid CAD model is utilized to generate the motion of the tool to deposit the melted filament as layer over layer fashion. The printing time of the model is variable, and it depends on parameters used in slicing software [5].

In this step removal of the support structure, post-curing, and finishing of the printed part is done. Poor surface quality is one of the major drawbacks of the 3D printed part, especially of FFF printed part. A stepped rough surface is inbuilt characteristic of part made by the FFF process [25].

There are two major approaches to improve the surface quality in post-processing—one is chemical smoothing, and another is mechanical smoothing of the surface [26, 27, 30]. Taufik et al. [23, 28, 29, 31] used a laser-based finishing process, they developed an important method for complete removal of the inbuilt rough surface of FFF printed part.

4 Result and Discussion

4.1 Design of FFF Based Open-Source 3D Printer

Expiration of Stratasys patent on the FDM technology, economical availability, simple design, cheap fabrication, and easy assembly are the main reasons for the popularity of open-source FFF 3D printers [25]. There is an open-source FFF 3D printer design called RepRap; many projects are made using this open-source design [32]. The continuous growth of FFF is ensured by consistent performance enhancement, cost reduction of the manufacturing system, and development of new feedstock materials. Understanding the relationship between processing condition which determines the properties of the finished part and acceptable feed material properties will have a significant contribution to enhance the design and quality standard of FFF-based 3D printers [25]. Key elements of FFF based 3D printer are—filament feeding mechanism, material melting assembly, extrusion nozzle, gantry, printing bed, and environment. To fabricate all these key elements for open-source FFF-based 3D printer various mechanical and electronic components are needed like—pulley, belt, bearing, stepper motor, microcontroller, print bed, structure to hold all components, etc.

4.2 Material Feed Mechanism

Screw type extruder is a traditional extruder in which granular or pelletized feed material is used, but this mechanism is not used commercially. Commercially used feed material is polymer filament with a diameter up to 3 mm [25]. To feed this filament inside liquefier a roller machine is used. This mechanism is consisting of two rollers (see Fig. 2a).

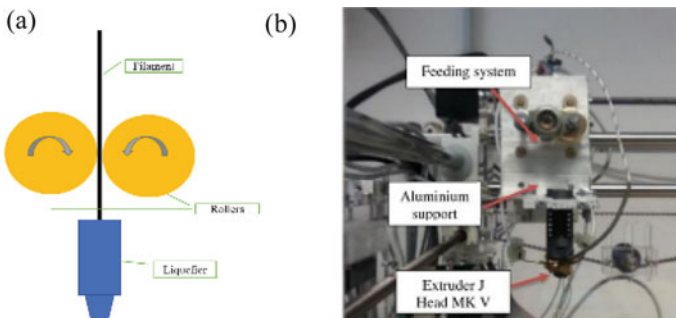


Fig. 2 a Material feed mechanism for FFF based 3D printer, b assembly of liquefier, print head, and gantry [33]

At least one roller should have a grooved surface to provide minimum friction to hold the wire from feed material and push it in the material melting channel [34]. Electric motor with precise rotation is used to rotate the roller, so that it can push the feed material in melt forming channel.

4.3 Material Melting Channel, Extrusion Nozzle, and Gantry

The feed material melting channel or liquefier is one of the main parts of the FFF based 3D printer [25]. Liquefier is consisting of a channel in a metallic block. This channel is used for the flow of filament or melted material to the nozzle. Liquefier chamber is heated by resistive heating principle. Generally, there are two ways of heating, either liquefier channel is surrounded by a coiled heating element or liquefier assembly is embedded with cartridge heaters. It is necessary to maintain a uniform temperature throughout the channel [25]. To maintain the uniform temperature a controller and thermocouple system is used [26]. The amount of melted feed material is dependent on the heat flux and filament feeding rate. Therefore, there should be enough heat flux and rate of material feeding because the higher temperature may degrade the polymer and lower temperatures will cause poor adhesion of layers [26].

The print head consists of a nozzle which extrudes the material to deposit in layers. It may be fixed with a heating chamber or replaceable. The push force imparted by filament feeding mechanism on filament is decided by the geometrical features of the extrusion nozzle and the viscous force exerted by the melted filament. The opening of the nozzle also determines the resolution of the printed part. Generally, the nozzle opening varies from 0.2 to 0.5 mm [25].

The print head and liquefier assembly are integrated into a gantry that provides the motion to the whole assembly in x and y -directions (see Fig. 2b). Stepper motor, gear, and timing belt are used to provide the motion to the gantry. The speed of the gantry movement will decide the speed of the fabrication of the part.

4.4 Build Surface and Environment

The print head and liquefier assembly have movement in horizontal plane, while a build surface or print bed on which material is extruded, moves vertically or in the z -direction. These two motions are responsible for the 3D structure to be printed. This build surface is an important element of FFF-based 3D printer system design. This surface should provide favorable conditions to extruded material to adhere to it. In the case of PLA and ABS as the build material, Kepton films are used on build surface to better adhesion between build surface and extruded materials. It also offers easy removal of the fabricated 3D part. If there is a large thermal gradient between the depositing layers, then it leads to warps and distorted shape of the final 3D printed part [35]. A turbofan on the extruder assembly pushes the air to cool

the part and maintain the temperature distribution. To reduce the non-uniformity of temperature heated build surface is used that also provides better adhesion for the extruded material. This method is economical, but it limits the build size of the part to be printed. However advanced system provides a temperature-controlled environment to tackle this problem [25].

5 Conclusion

In this paper review study of additive manufacturing with an emphasis on the Fused Filament Fabrication (FFF) process is done. Detailed introduction of AM methods along with its merits and demerits is given. Additive manufacturing processes are material specific so various AM materials along with their application are discussed. Research for advanced materials for AM technologies is one of the main future scopes. FFF based 3D printing is more popular because of the low cost and simple design of an FFF based 3D printer. In this paper key elements of an FFF-based 3D printer are discussed. These key elements provide an overview of the design of the FFF-based 3D printer. One can easily develop this type of 3D printer for personal use or research purpose.

6 Future Scope

Future scope lies in the development of such an open-source hybrid 3D printer to print a part with better finish. In this hybrid form of FDM 3D printer filament as well as pellets form of materials can be used. New material can be developed which are compatible with these printers and offer improved mechanical, thermal, and electric properties.

Acknowledgements This work was supported by the Science and Engineering Research Board (SERB)—DST under its Start-up Research Grant (SRG) scheme [Grant number: SRG/2019/000943].

References

1. Dilberoglu, U.M., Gharehpapagh, B., Yaman, U., Dolen, M.: The role of additive manufacturing in the era of industry 4.0. *Procedia Manuf.* **11**(June), 545–554 (2017)
2. 52900:2015, A.: Standard terminology for additive manufacturing—general principles—terminology. ASTM Int. (2015)
3. Shahrubudin, N., Lee, T.C., Ramlan, R.: An overview on 3D printing technology: technological, materials, and applications. *Procedia Manuf.* **35**, 1286–1296 (2019)

4. Bikas, H., Stavropoulos, P., Chryssolouris, G.: Additive manufacturing methods and modeling approaches: a critical review. *Int. J. Adv. Manuf. Technol.* (2016)
5. Gokhare, V.G., Raut, D.N., Shinde, D.K.: A review paper on 3D-printing aspects and various processes used in the 3D-printing. *Int. J. Eng. Res. Technol.* **6**(06), 953–958 (2017)
6. Sharma, S., Goel, S.A.: Three-dimensional printing and its future in medical world. *J. Med. Res. Innov.* **3**(1), 1–8 (2018)
7. Blok, L.G., Longana, M.L., Yu, H., Woods, B.K.S.: An investigation into 3D printing of fibre reinforced thermoplastic composites. *Addit. Manuf.* **22**, 176–186 (2018)
8. Dul, S., Fambri, L., Pegoretti, A.: Filaments production and fused deposition modelling of ABS/carbon nanotubes composites. *Nanomaterials* **8**(1) (2018)
9. Singamneni, S., Warnakula, A., Smith, D.A., Le Guen, M.J.: Biopolymer alternatives in pellet form for 3D printing by extrusion. *3D Print. Addit. Manuf.* **6**(4), 217–226 (2019)
10. Martin, J.H., Yahata, B.D., Hundley, J.M., Mayer, J.A., Schaedler, T.A., Pollock, T.M.: 3D printing of high-strength aluminium alloys. *Nature* **549**(7672), 365–369 (2017)
11. Hitzler, L., Alifui-Segbaya, F., Williams, P., Heine, B., Heitzmann, M., Hall, W., Merkel, M., Öchsner, A.: Additive manufacturing of cobalt-based dental alloys: analysis of micro-structure and physicomechanical properties. *Adv. Mater. Sci. Eng.* (2018)
12. Murr, L.E.: *Frontiers of 3D printing/additive manufacturing: from human organs to air-craft fabrication* (2016)
13. DebRoy, T., Wei, H.L., Zuback, J.S., Mukherjee, T., Elmer, J.W., Milewski, J.O., Beese, A.M., Wilson-Heid, A., De, A., Zhang, W.: Additive manufacturing of metallic components—process, structure and properties (2018)
14. Uhlmann, E., Kersting, R., Klein, T.B., Cruz, M.F., Borille, A.V.: Additive manufacturing of titanium alloy for aircraft components. *Procedia CIRP* (2015)
15. Paolini, A., Kollmannsberger, S., Rank, E.: Additive manufacturing in construction: a review on processes, applications, and digital planning methods. *Addit. Manuf.* **30**(October), 100894 (2019)
16. Kim, S., Seong, H., Her, Y., Chun, J.: A study of the development and improvement of fashion products using a FDM type 3D printer. *Fash. Text.* **6**(1) (2019)
17. Verner, I., Merksamer, A.: Digital design and 3D printing in technology teacher education. *Procedia CIRP* **36**, 182–186 (2015)
18. ASTM F2792-12: Standard terminology for additive manufacturing technologies (2012)
19. Ngo, T.D., Kashani, A., Imbalzano, G., Nguyen, K.T.Q., Hui, D.: Additive manufacturing (3D printing): a review of materials, methods, applications and challenges (2018)
20. Kun, K.: Reconstruction and development of a 3D printer using FDM technology. *Procedia Eng.* **149**(June), 203–211 (2016)
21. Hiller, J.D., Lipson, H.: STL 2.0: a proposal for a universal multi-material additive manufacturing file format. In: 20th Annual International Solid Freeform Fabrication Symposium, SFF (2009)
22. Zwier, M.P., Wits, W.W.: Design for additive manufacturing: automated build orientation selection and optimization. *Procedia CIRP* 128–133 (2016) (Elsevier B.V.)
23. Taufik, M., Jain, P.K.: Orientation techniques in layered manufacturing: a review. In: *Proceedings of International Conference on Innovations in Design and Manufacturing* (2012)
24. Sharma, A.: Utility and challenges of 3D printing. *IOSR J. Mech. Civ. Eng.* **02**(02), 49–53 (2016)
25. Turner, B.N., Strong, R., Gold, S.A.: A review of melt extrusion additive manufacturing processes: I. Process design and modeling. *Rapid Prototyp. J.* **20**(3), 192–204 (2014)
26. Gibson, I., Rosen, D.W., Stucker, B.: *Additive manufacturing technologies: rapid prototyping to direct digital manufacturing* (2010)
27. Taufik, M., Jain, P.K.: Part surface quality improvement studies in fused deposition modelling process: a review (2020)
28. Taufik, M., Jain, P.K.: Laser assisted finishing process for improved surface finish of fused deposition modelled parts. *J. Manuf. Process.* **30**(October), 161–177 (2017)

29. Taufik, M., Jain, P.K.: Development and analysis of accurate and adaptive FDM post-finishing approach. In: *3D Printing and Additive Manufacturing Technologies*, pp. 59–71 (2018)
30. Taufik, M., Jain, P.K.: Surface finish of PC-ABS parts fabricated by fused deposition modelling. In: *Proceedings of the National Conference on Futuristics in Mechanical Engineering (FME)*, pp. 20–6. MMMUT Gorakhpur (2014)
31. Taufik, M., Jain, P.K.: Estimation and simulation of shape deviation for additive manufacturing prototypes. In: *ASME 2016 International Design Engineering Technical Conferences and Computers and Information in Engineering Conference*. ASME (2016)
32. Jones, R., Haufe, P., Sells, E., Iravani, P., Olliver, V., Palmer, C., Bowyer, A.: Reprap—the replicating rapid prototyper. *Robotica* (2011)
33. Galantucci, L.M., Bodi, I., Kacani, J., Lavecchia, F.: Analysis of dimensional performance for a 3D open-source printer based on fused deposition modeling technique. *Procedia CIRP* **28**, 82–87 (2015)
34. Agarwala, M.K., Jamalabad, V.R., Langrana, N.A., Safari, A., Whalen, P.J., Danforth, S.C.: Structural quality of parts processed by fused deposition. *Rapid Prototyp. J.* (1996)
35. Wang, T.M., Xi, J.T., Jin, Y.: A model research for prototype warp deformation in the FDM process. *Int. J. Adv. Manuf. Technol* (2007)

Determination of Optimal Ordering Policy Using Genetic Algorithm for a Multi-stage Serial Supply Chain



Rachit Kumar, Richard Johnson, Ritvik Mohandas, Pranav Pramod, Dony S. Kurian, and V. Madhusudanan Pillai

Abstract The main goal of every business operation is to achieve minimum inventory costs. One way of doing this is by reducing the supply chain inventory distribution related costs. This is accomplished by optimizing the replenishment order decisions made by the supply chain members. This paper aims to determine the optimal ordering policy for each member of a four-stage serial supply chain using an artificial agent based on Genetic Algorithm (GA). Unlike the previous works reported in the literature, this paper focuses on a supply chain that works in a lost sales environment, and has a stochastic demand of large size. Additionally, performance of the supply chain employing GA policy is compared against industrially adopted Order-Up-To (OUT) policy and theoretically researched 1-1 policy. The results from the study show that GA policy gives much better results compared to OUT and 1-1 policies.

Keywords Supply chain · Genetic algorithm · Ordering policy · Inventory management

1 Introduction

The management of Supply Chains (SC) is becoming a matter of critical importance for today's businesses. The SC related inventory distribution costs account a significant impact on the total product cost and hence, it is necessary to improve the inventory distribution process within the SC [1].

SC consists of numerous decision-making processes of which inventory ordering decisions are critical for performance improvement. The agents of the SC at each stage are responsible for making inventory replenishment decisions based on their interacting environment. The main aim of these agents is to minimize the total inventory cost by considering the entire SC. Besides, the order size determination is complex when faced with uncertain customer demand and lead time that causes a

R. Kumar · R. Johnson · R. Mohandas · P. Pramod · D. S. Kurian · V. Madhusudanan Pillai (✉)
Department of Mechanical Engineering, National Institute of Technology Calicut, Kozhikode
673601, India
e-mail: vmpp@nitc.ac.in

© The Author(s), under exclusive license to Springer Nature Singapore Pte Ltd. 2021
B. Deepak et al. (eds.), *Advanced Manufacturing Systems and Innovative Product Design*,
Lecture Notes in Mechanical Engineering,
https://doi.org/10.1007/978-981-15-9853-1_42

507

phenomenon called bullwhip effect [2] in SCs. In addition, ordering decisions made by the human agents are met with biases that lead to non-optimal SC performances [3].

In recent years, Genetic Algorithm (GA) has been employed effectively in various SC fields like forecasting, economic lot-size scheduling, job-shop scheduling, inventory replenishment system, etc. [4]. It is one of the powerful stochastic search and optimization techniques created on the principles of natural selection and evolution [5]. Kimbrough et al. [6] were the first to study the application of artificial agents using GA to determine the ordering decisions in SCs under a backorder shortage management environment. They have proved that the artificial agents were successful in finding optimal ordering policy, and outperformed humans in decision-making. Later, O'Donnell et al. [7] accomplished to reduce the bullwhip effect that occurred in the SCs by the application of GA.

Lately, a lot of studies are on-going that employ Reinforcement Learning (RL) methods for determining the optimal ordering policy. van Tongeren et al. [8], Chaharsooghi et al. [9] and Bharti et al. [10] solved an RL system for order management based on Q -learning algorithm. Oroojlooyjadi et al. [11] has used a Deep Q -Network for inventory optimization, and obtained a near-optimal SC performance better than the base stock policy.

Although GA and other methods have been used for solving SC ordering management problems previously, it hasn't been applied for large demand size problems. The ability of GA to perform searches in large state space is hence not addressed in the literature. In addition, determination of optimal ordering policy for a multi-stage serial SC operated with a lost sales environment has not been considered by the previous researchers. Hence, in this paper, we address the above-mentioned gaps and further, a comparative analysis of the SC performance obtained by GA with other well-known policies is also carried out.

The organization of the paper is as follows: Sect. 2 provides a brief description about the SC adopted in this paper. Section 3 gives information about the GA implementation. Section 4 describes the comparative analysis of results obtained by GA with other policies. Section 5 provides a conclusion and also discusses the scope of future works.

2 Supply Chain Description

This paper considers a four-stage serial SC where each stage is managed by four different decision-making agents. The agents of the SC include a Retailer, a Wholesaler, a Distributor and a Factory. Figure 1 demonstrates flow of orders and shipments occurring in the assumed SC. Here, the Retailer agent faces a stochastic customer demand generated from a normal distribution that has a mean of 100 and standard deviation 15. The demand size considered make the proposed work an application to large space problem, unlike the previous works [6, 7, 9] that experimented on small demand size [for example, $U(1, 15)$]. The Factory agent is assumed to have unlimited

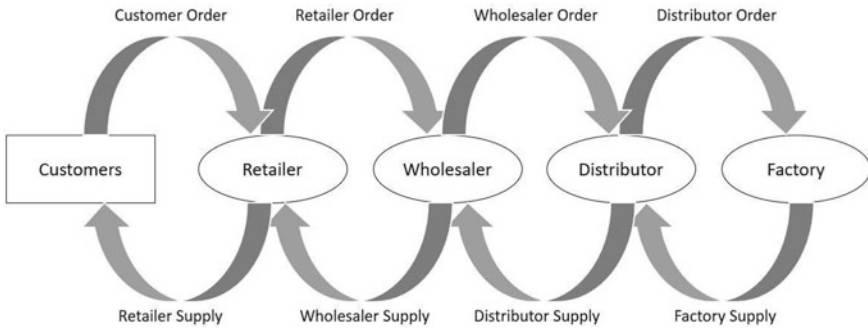


Fig. 1 Order and shipment flows in the supply chain

production capacity and therefore, production order issued by the Factory agent is released after production without any shortage.

Each SC agent (i) allocates an incoming order received from the downstream agent ($i - 1$) based on the beginning inventory of the period t , where $t = 1, 2, 3, \dots, T$. If the beginning inventory is available enough to meet the incoming order, then the agent (i) allocates an amount equal to the order size. On the contrary, if available inventory is less than the order received, then the agent (i) allocates only the available inventory on-hand. The orders not met are then considered as lost sales.

Each stage is managed independently by the respective agents, and they are responsible for placing orders to the upstream agent ($i + 1$). The proposed work assumes that the agent (i) places an order at the end of the period (t) and it reaches the upstream agent ($i + 1$) at the beginning of ($t + 1$)th period without any information lead time. However, the order allocated by the agent (i) reaches the downstream agent ($i - 1$) after a delivery lead time of two weeks. The ultimate aim of the agents is to minimize the Total Supply Chain inventory Cost (TSCC) which comprises holding cost and lost sales cost [see Eq. (1)].

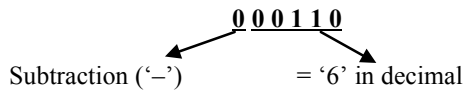
$$TSCC = \sum_{i=1}^4 \sum_{t=1}^T [C_i^h \times I_i^+(t) + C_i^s \times I_i^-(t)] \tag{1}$$

where, C_i^h is the holding cost per unit and C_i^s is the lost sales cost per unit. The unit holding cost considered in the proposed study is 5 for the Retailer, 4 for Wholesaler, 3 for Distributor and 1 for the Factory. Similarly, the unit lost sales costs are 10, 8, 6, and 2 for the Retailer, Wholesaler, Distributor and the Factory respectively. The end period inventory is denoted as $I_i^+(t)$, and $I_i^-(t)$ is the corresponding lost sales.

3 Genetic Algorithm Implementation

3.1 Rule Depiction

Genetic Algorithm (GA) consists of a certain number of chromosomes in each generation. The chromosomes represent a rule which is used to determine the ordering policy. Each rule has six bits to determine an ordering policy. The five bits from the right represent a value in base 2 (binary), and the bit at extreme left determines the addition or subtraction of that value from the downstream demand. For example, the rule 000110 can be inferred as $X - 6$:



This suggests that if the downstream demand is X , then the order placed will be ' $X - 6$ '. In case, if the value of $(X - 6)$ is negative, it is taken as zero because orders less than zero are unrealistic.

3.2 GA Design

Initially, a pool of 60 chromosomes is generated randomly as the first generation. The policy of each of these chromosomes is implemented, and they are sorted in decreasing order of their fitness value. The best half of the chromosomes, i.e., 30 chromosomes are selected using rank selection operator and is added to the next generation. These selected chromosomes then go through single-point crossover followed by bitwise mutation. The crossover and mutation rates are fixed as 0.8 and 0.3 respectively. Half of these are then selected randomly and added to the next generation. In other words, 15 chromosomes are added to the next generation after crossover and mutation. The remaining 15 chromosomes of the new generation are furnished using random addition. The above sequence of operations is iterated until a specified number of generations is reached (number of generations = 500). The best chromosome of each generation is identified to determine the optimal ordering policy.

4 Problem Instances and Results

Initially, GA is applied to the four-stage serial SC to determine the best ordering policy in a lost sales environment. The simulation was coded in Python 3.7 and ran on a machine with 3.70 GHz Intel Xeon CPU and 32 GB memory. The number of

Table 1 Input demand data

	Customer demand data (Normal (100, 15)) for 25 weeks
Test problem 1	[120, 97, 128, 99, 107, 119, 108, 111, 126, 91, 109, 95, 107, 93, 85, 115, 86, 127, 97, 89, 100, 90, 122, 98, 101]
Test problem 2	[96, 129, 94, 91, 105, 119, 103, 131, 94, 96, 100, 92, 119, 97, 85, 81, 101, 90, 79, 100, 84, 77, 49, 97, 76]
Test problem 3	[87, 119, 95, 116, 119, 92, 91, 115, 104, 96, 90, 91, 112, 123, 85, 112, 114, 102, 84, 97, 111, 99, 111, 95, 88]
Test problem 4	[72, 108, 104, 100, 110, 111, 86, 129, 77, 136, 94, 122, 129, 84, 97, 98, 90, 86, 120, 74, 97, 107, 105, 90, 99]
Test problem 5	[100, 120, 92, 125, 131, 92, 93, 113, 97, 95, 107, 102, 101, 87, 92, 94, 90, 124, 84, 103, 108, 105, 109, 84, 81]

Table 2 Results of the GA

Test problem	TSCC	Policy
Test problem 1	6608	[-3, -6, -9, -10]
Test problem 2	7353	[-4, -9, -9, -10]
Test problem 3	9046	[-4, -5, -6, -9]
Test problem 4	8355	[-3, -5, -7, -11]
Test problem 5	7994	[-5, -7, -9, -11]

periods of operation considered is 25 weeks, of which performance was evaluated from 4th week to 22nd week to avoid the warm-up and end game effects. Moreover, the effectiveness of GA is investigated against five test problems whose customer demand is as given in Table 1. The ordering policy determined and the corresponding TSCC obtained by the application of GA is provided in Table 2.

4.1 Comparative Analysis

The proposed work also aims to compare the performance of the SC operated by GA with other well-known policies. The same order management problem is simulated for two other inventory ordering policies: (i) Order-Up-To (OUT) policy and (ii) 1-1 policy.

OUT policy is the most widely adopted industrial ordering policy where an order is placed at each review period by subtracting the current inventory position from a desired target inventory level [12]. 1-1 policy is widely discussed in the literature in which an order is placed by a SC agent which is equal to the incoming downstream demand [6]. The performance of the two policies with respect to TSCC is determined by simulating the operations of SC in Microsoft Excel and a comparison of TSCC is illustrated as shown in Fig. 2.

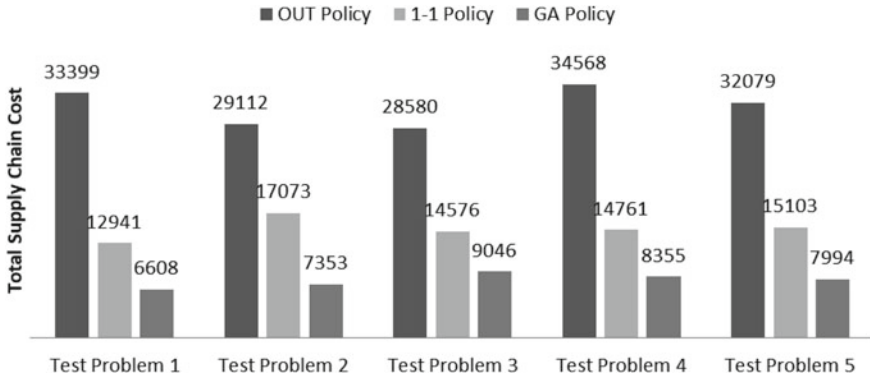


Fig. 2 Comparative analysis

From Fig. 2, it can be clearly observed that the performance of the SC is enhanced by employing GA compared to the other two policies. The minimum cost achieved is the least for the SC where GA is applied in all the test problems. Furthermore, the average performance improvement with respect to TSCC by using GA policy is 75% as compared to OUT policy, and more than 47% for 1-1 policy. Additionally, for test problem 1, a line graph illustrating cumulative of the SC cost incurred during the period of evaluation is plotted for the three policies and it is shown in Fig. 3.

Figure 3 clearly depicts that as the number of periods increases the policy derived through GA becomes increasingly beneficial as compared to the other two policies. This analysis proves the efficiency of the GA in deriving the optimal ordering policies in stochastic demand scenarios when the other policies fail to provide any substantial result.

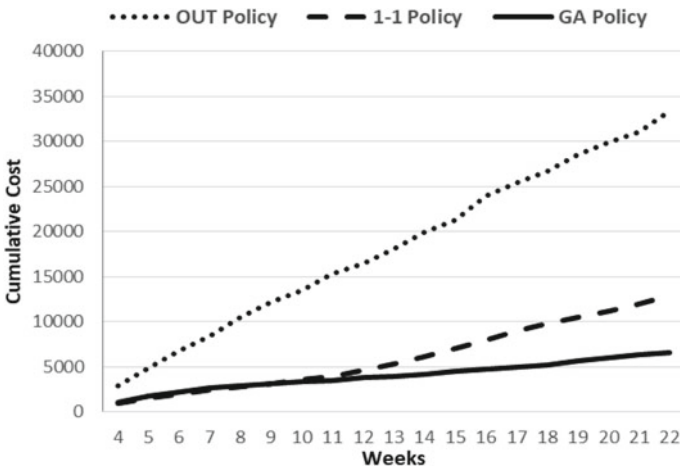


Fig. 3 Accumulated cost of the policies

5 Conclusion

This paper has focused on implementing a widely accepted GA to SC ordering management problem. For this, a four-stage serial SC was considered that is consistent to the literature. The present study addressed a lost sales shortage environment unlike the previous works reported in the literature that focused on backorder environments. Additionally, this paper takes care of the large state-space problem as well.

The ordering policies discussed in this paper are analytically proven for deterministic scenarios. In real-time business conditions, it is challenging to exactly forecast the demand for a certain period, and hence, these policies do not provide the best results in such situations. Therefore, the objective of this paper to utilize the GA as an artificial agent to derive enhanced ordering policies in stochastic demand scenarios is effectively delivered. The comparative analysis of the SC performances clearly indicates that the ordering policies obtained through GA outperformed the results of the well-known policies by a high margin. Hence, this work also adds to the flexibility and robustness of artificial agents, like GA, in assessing and determining the optimal inventory ordering decisions of an SC.

Further work can be done by utilizing stochastic lead time to supplement the results obtained in this paper. Research can also be done for nonlinear SCs to establish the flexibility of the artificial agents.

References

1. Lapinskaitė, I., Kuckailytė, J.: The impact of supply chain cost on the price of the final product. *Bus. Manage. Educ* **12**(1), 109–126 (2014)
2. Lee, H.L., Padmanabhan, V., Whang, S.: Information distortion in a supply chain: The bullwhip effect. *Manage. Sci.* **43**(4), 546–558 (1997)
3. Serman, J.D.: Modeling managerial behavior: Misperceptions of feedback in a dynamic decision making experiment. *Manage. Sci.* **35**(3), 321–339 (1989)
4. Jauhar, S.K., Pant, M.: Genetic algorithms in supply chain management: a critical analysis of the literature. *Sādhanā* **41**(9), 993–1017 (2016)
5. Goldberg, D.E., Holland, J.H.: Genetic algorithms and machine learning. *Mach. Learn.* **3**, 95–99 (1988)
6. Kimbrough, S.O., Wu, D.J., Zhong, F.: Computers play the beer game: can artificial agents manage supply chains? *Decis. Support Syst.* **33**(3), 323–333 (2002)
7. O'donnell T., Maguire, L., McIvor, R., Humphreys, P.: Minimizing the bullwhip effect in a supply chain using genetic algorithms. *Int. J. Prod. Res.* **44**(8), 1523–1543 (2006)
8. van Tongeren, T., Kaymak, U., Naso, D., van Asperen, E.: Q-learning in a competitive supply chain. In: *Proceedings of the IEEE International Conference on Systems, Man and Cybernetics*, pp. 1211–1216, Montreal (2007)
9. Chaharsooghi, S.K., Heydari, J., Zegordi, S.H.: A reinforcement learning model for supply chain ordering management: an application to the beer game. *Decis. Support Syst.* **45**(4), 949–959 (2008)
10. Bharti, S., Kurian, D.S., Pillai, V.M.: Reinforcement learning for inventory management. In: Deepak, B., Parhi, D., Jena, P. (eds.) *Innovative Product Design and Intelligent Manufacturing Systems. Lecture Notes in Mechanical Engineering*. Springer, Singapore (2020)

11. Oroojlooyjadid, A., Nazari, M., Snyder, L., Takáč, M.: A deep Q -network for the beer game: a reinforcement learning algorithm to solve inventory optimization problems. arXiv preprint [arXiv:1708.05924](https://arxiv.org/abs/1708.05924) [cs. LG] (2017)
12. Daniel, J.S.R., Rajendran, C.: A simulation-based genetic algorithm for inventory optimization in a serial supply chain. *Int. Trans. Oper. Res.* **12**(1), 101–127 (2005)

Comparative Investigation of CNC Turning of Nickel-Chromoly Steel Under Different Cutting Environment with a Fabricated Portable Mist Lubricator: A Super Hybrid Taguchi-WASPAS-GA-SA-PSO Approach



Siddharth Jeet , Abhishek Barua , Dilip Kumar Bagal , Swastik Pradhan , Dulu Patnaik, and Ajit Kumar Pattanaik

Abstract A quick rise in the improvement of some radical high performance application materials has been witnessed in last decade poses substantial contest in machining. Many strategic processes have been concocted, where green machining practices have been agreed foremost stress and minimum quantity lubrication (MQL) technique or oil mist lubrication (OML) technique is one of them. In latest spell, oil mist lubrication system has been advanced for serving the machining process more capably in the manufacturing industries but cost comes as a snag for its widespread area of use. To tackle this problematic situation, the present study contracts with the fabrication of a portable OML system which can contest the class and efficacy of machining of the existing OML system. To check the quality of the fabricated setup, turning of Nickel-Chromoly Steel (AISI 4340) with different machining backgrounds has been done. The effect of addition of around 1 μm size Aluminium oxide (Al_2O_3) and Carbon nanotubes (CNT) powder has been probed during turning with the help Taguchi-based design of experiment. A super hybrid optimization technique, i.e., Taguchi coupled WASPAS with Genetic Algorithm, Simulated Annealing and Particle Swarm Optimization has been used to determine optimal cutting condition. The study, therefore, not only shows the efficiency of the fabricated OML setup but also shows that by using CNT as lubricant, the output responses are very minimum as per the requirement in comparison to other lubricants while machining AISI 4340 steel. This study also shows the use of multiple meta-heuristic optimization shows more accurate result as compared to statistical approach.

S. Jeet · A. Barua

Centre for Advanced Post Graduate Studies, BPUT, Rourkela, Odisha 769004, India

D. K. Bagal (✉) · D. Patnaik · A. K. Pattanaik

Government College of Engineering, Kalahandi, Bhawanipatna, Odisha 766002, India

e-mail: dilipbagal90@gmail.com

S. Pradhan

Lovely Professional University, Phagwara, Punjab 144411, India

Keywords AISI 4340 · Al_2O_3 · CNT · Fabricated OML system · GA · Minimum quantity lubrication · PSO · SA · WASPAS

1 Introduction

Dry machining is acknowledged as elective arrangement ready toward ensuring higher manageability with inferior conservative effect of assembling procedure. A fascinating innovation, these days progressively utilized additionally in mechanical uses, is Minimum Quantity Lubrication (MQL). A few exploration works have exhibited its advantages in improvement of the machining exhibitions regarding both device wear obstruction and surface honesty as for dry cutting [1–3] just as in maintaining a strategic distance from not just the expenses related with the cutting liquid transfer yet in addition the costs identified with the machine device cleaning [4–7]. Solid Lubricant (SL) helped MQL procedure, is accepting more extensive consideration these days since it permits an uncommon enhancement of liquid exhibitions by regulating both warmth age and rubbing between device and work piece lacking noteworthy increment of procedure overheads, and, in the meantime, it additionally keeps away from those issues identified with the utilization of cryogenic temperatures as happens when utilizing the previously mentioned half and half systems. The exhibitions of SL-helped MQL were tried [8–10], demonstrating the improvement of grease film made between contact surfaces over the option of different added substances described by different capacities, for example, hostile to wear, against rubbing and hostile to consumption capacities. The utilization of lamellar powders, for example, boron nitride or graphite, which would in general hold fast to apparatus faces decided development of defensive layer proficient to limit erosion, in this way diminishing the cutting powers, the produced temperatures and, thusly, likewise the instrument wear [11–14]. So, for improving constrained cooling limit of MQL method, the utilization of liquids advanced through nanometer-sized strong particles or strands, to be specific metallic or fired added substances, was tried, which demonstrated to assume an imperative job in cooling and lubrication [15–21].

A lot of work has been done on both low and medium carbon steels, Aluminium alloy and metal matrix composites, but less attention has been given in the investigation of Nickel Chromium Molybdenum steels concerning different Nano-lubricants especially Al_2O_3 (Aluminium oxide) and CNT (Carbon nanotubes) Nano-particle along with different conventional cutting oil, vegetative oil and emulsified oils. The present study contracts with novel approach of fabrication of a portable mist lubricator system which can contest the class and efficiency of machining of the existing oil mist lubrication (OML) system. To check the quality of the fabricated setup, turning of Nickel-Chromoly Steel (AISI 4340) with different machining backgrounds has been done. The effect of addition of around $1\ \mu\text{m}$ size Aluminium oxide (Al_2O_3) and Carbon nanotubes (CNT) powder has been probed during turning with the help of Taguchi-based design of experiment. A super hybrid optimization technique, i.e., Taguchi coupled WASPAS with Genetic Algorithm, Simulated Annealing

and Particle Swarm Optimization has been used to determine optimum cutting condition for machining of AISI 4340 Nickel-Chromium-Molybdenum steel in different lubricating environments after comparing the machining constraints.

2 Fabrication of Portable Mist Lubricator Setup

A portable mist lubricator setup was cast off for creation of required oil-mist on the cutting zone. The fabricated OML setup and its block diagram is shown in Figs. 1 and 2 respectively.

Fig. 1 Fabricated portable mist lubricator setup (PMLS)

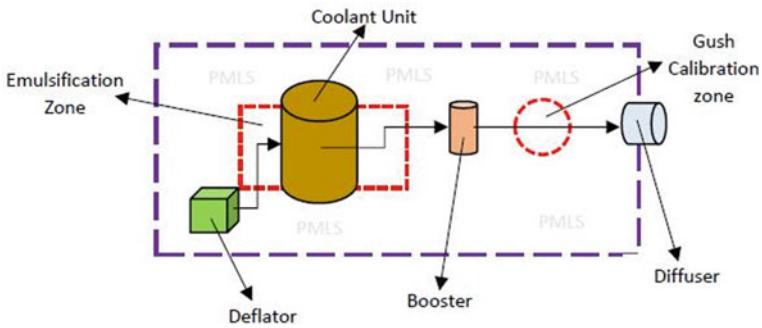


Fig. 2 Block-diagram of fabricated PMLS

2.1 Components for PMLS (*Portable Mist Lubricator Setup*)

MLS Envelope/Case

The laminates of Polypropylene are fabricated into a case for serving the envelope of PMLS components. PIM is used for the synthesis of designed envelope.

Micro-Deflator and Micro-Booster

LDPE micro deflator intensifies the air to stir-up the fluid and Nano-particles whereas the LDPE micro booster engages the resultant mixture with the diffusing unit.

Pressure Gauge and Flow-indicator

Pressure gauge drafted to the deflator unit for measuring the air pressure and the flow-meter which scales the rate of flow is delineated after the fluid boosting unit.

ABS fluid mixing chamber

Light weight ABS fluid mixing chamber is the ultra-mixing unit of fluids and particle inducted.

Connecting Accessories and Valves

- PVC Pipes/Hose—Round tubular PVC hoses/pipes connect the pump output to nozzle and output from compressor to nozzle.
- Hose Connectors—PVC hose fittings (i.e., female 90° elbows) serves the purpose of connecting the hoses arranged in the setup.
- Brass Ball Valves—Brass Ball valves with the two-piece inline lever handle acts as the check post in the fabricated setup.

Fine-mesh Nozzle/Spray Diffuser

- Exit Diameter—0.5 mm, Operating pressure—4 bar
- Controls directional fluid flow (i.e., increased velocity)
- Superior spray pattern (adjustable ratchets)
- Fine atomization and high transfer efficiency.

Coolant tank/unit

It is attached to PMLS, inside of which lubricant/coolant is stored. It is having capacity of 1.25 litres with dimension of radius 6 inches and height 8 inches.

2.2 Working

Mist lubrication is always supplied at high speed and high pressure through diffuser at the cutting zone. In the fabricated system, a Micro-deflator supplies air pressure ranging around 4 bar-6 bar. This high pressure air after deflator enters inside the fluid

mixture chamber to which Coolant tank is attached. Nanoparticles are inducted at controlled measures. Mixing chamber maintains itself at optimum pressure which also restricts the reverse flow of fluid. The mixture then entrails to Micro-booster where the mixture is boosted through hose and is impinged at a high speed from the diffuser at chip tool interface [21].

3 Experiment Methodology

A tubular job of AISI 4340 steel with 20 mm diameter and 40 mm length was used for the experiment on a CNC lathe machine (Brand: MTAB Ltd., Bangalore, India; Model: Flexturn), revealed in Fig. 3. AISI 4340 Nickel-Chromium-Molybdenum steel having chemical composition and physical characteristics as shown in Tables 1 and 2 respectively. The machining is done using uncoated cemented carbide tool inserts (P30 grade) with VNMG 120408 insert and ISO SSBK 2020K12 tool holder.

Fig. 3 CNC turning machine fitted with fabricated cheap portable mist lubricator



Table 1 AISI 4340 steel’s chemical composition

Elements	Fe	Si	Ni	P	S	Mn	C	Mo	Cr
wt%	>61.9	2.0	14.0	0.03	0.05	0.75	>0.4	3.0	18.0

Table 2 Mechanical properties of AISI 4340

Density, Kg/m ³	7850	Yield strength, MPa	480
Poisson's ratio	>0.30	Tensile strength, MPa	745
Elastic modulus, GPa	210	Vickers hardness	228

Table 3 Aluminium oxide (Al₂O₃) properties

Formula	Al ₂ O ₃
Appearance	White solid
Molar mass, g/mol	101.96
Crystal structure	Various
Density, g/cm ³	3.95
Solubility in water	Insoluble
Melting point, °C	2072
Particle size, nm	Less than 50 (avg. size)

The experiments are executed in three different oil-mist lubrication (OML) environment with variant in nanoparticles varieties. Conventional cutting oil was employed as the base liquid for three conditions. Aluminium oxide and Carbon nanotubes were used to formulate nanofluids for delivering on cutting zone during turning. Al₂O₃ particles is mixed with the water soluble cutting oil with Dimethyl formamide as a dispersing agent whereas the CNT particle is mixed with conventional cutting fluid with Phenyl-ethyl alcohol as dispersing agent thoroughly with the help of stirrer machine for maintaining proper suspension behavior avoiding particle settlement at the base [22]. Three dissimilar types of environments are:

1. Flood mist Lubrication.
2. Conventional cutting fluid + Al₂O₃ nanoparticles (5% volume), OML assisted.
3. Conventional cutting fluid + CNT nanoparticles (5% volume), OML assisted.

During the experimental trials careful considerations were undertaken during the inductance of emulsifiers, dispersing agent and wetting agent. Similarly, cutting factors and their levels have been chosen for performing the trials. In this case cutting speed, depth of cut and feed with suitable levels of operation was chosen. Tables 3 and 4 give the properties of Aluminium oxide and Carbon Nanotubes, respectively. Table 5 shows input cutting parameters and their levels.

4 Optimization Methods

4.1 WASPAS Method (Weighted Aggregated Sum Product Assessment)

The paramount practice of this method are [23].

Table 4 Carbon Nanotubes properties

Formula	C (Linear)
Molar mass, g/mol	12.01
Appearance	Black powder
Density, g/cm ³	2.26
Particle size, nm	Less than 50 (avg. size)
Melting point, °C	3550
Crystal structure	Hexagonal honeycomb cylinder
Solubility in water	Yes (under certain conditions)

Table 5 Operating factors with levels

Factors	Code	Lvl 1	Lvl 2	Lvl 3
Cutting speed in m/min	A	50	60	90
Feed in mm/rev	B	0.06	0.09	0.12
Depth of cut in mm	C	0.25	0.50	0.75

1. Preliminary decision matrix setting.
2. Decision matrix normalizing using Eq. (1) [maximization] and Eq. (2) [minimization]:

$$\bar{x}_{ij} = x_{ij} / \max_i x_{ij} \quad (1)$$

$$\bar{x}_{ij} = \min_i x_{ij} / x_{ij} \quad (2)$$

3. Total comparative significance calculation with weighted sum method by Eq. (3):

$$Q_i^{(1)} = \sum_{j=1}^n \bar{x}_{ij} \cdot w_j \quad (3)$$

4. Total comparative significance calculation with weighted product method by Eq. (4):

$$Q_i^{(2)} = \prod_{j=1}^n \bar{x}_{ij}^{w_j} \quad (4)$$

5. Total relative significance by Eq. (5) and ranking them from greater to lesser value:

$$Q_i = \lambda \cdot Q_i^{(1)} + (1 - \lambda) \cdot Q_i^{(2)} \quad (5)$$

4.2 Genetic Algorithm

Genetic Algorithm is based on the natural encroachment manner which is applied to advance responses for complex upgrade issues. Here, the wellbeing work reestablishes a single numerical health which is comparative with the utility or the limit of the individual which that chromosome addresses. Two guardians are picked and their chromosomes are recombined, usually using the instruments of half and half and change. Hybrid is progressively significant for quickly investigating a hunt space. Transformation gives just a modest quantity of arbitrary pursuit [24–30].

4.3 Simulated Annealing

Simulated Annealing is a probabilistic method which reflects the path toward hardening (moderate cooling of fluid metal) with a particular ultimate objective to achieve least unguent regard in a minimization issue. The cooling wonder is surrendered out by administering a temperature like boundary gave the idea of the Boltzmann likelihood circulation [24–30].

4.4 Particle Swarm Optimization

Particle swarm optimization (PSO) is a populace based stochastic enhancement method. The insight of multitude depends on the guideline of social and mental conduct of the multitude. The optimization method is instated with a populace of irregular arrangements and looks for optima by refreshing ages. The potential arrangements called particles fly through the issue space by following the current ideal particles. There is just one bit of food in the region being looked. All the feathered creatures don't have the foggiest idea where the food is. In any case, they know how far the food is in their inquiry. So the best procedure to achieve the food is to just follow the fowl, which is closest to the food. In improvement issues, each feathered creature in the hunt space is referred to as molecule. All the particles are assessed by the wellness capacity to be optimized and have speeds for the particles. The particles fly through the issue space by following the current ideal particles [30]. The issue is instated with a gathering of irregular particles and afterward looks for optima by refreshing ages.

5 Results and Considerations

Trials are done using Taguchi's experimental design as shown in Table 6. Accord-

Table 6 DOE used for different lubrication condition

Run no.	A	B	C
1	50	0.06	0.25
2	50	0.09	0.50
3	50	0.12	0.75
4	60	0.06	0.50
5	60	0.09	0.75
6	60	0.12	0.25
7	90	0.06	0.75
8	90	0.09	0.25
9	90	0.12	0.50

ingly, 9 experiments are performed under three diverse cutting conditions, i.e., flood mist lubrication, OML enriched Al₂O₃ particles and MQL enriched CNT particles and surface finish, chip thickness and temperature of the work piece.

5.1 Optimization Using WASPAS Method

Since semantic terms, used to express the responses, have already been converted into crisp (real) values, normalization of the decision matrix by applying Eq. (2) for surface roughness, chip thickness and temperature is done with respect to their minimization. Consequently, total relative significance of alternatives based on WSM and WPM is designed by using Eqs. (3) and (4), respectively. Lastly, combined condition of optimality of WASPAS method is calculated by using Eq. (5). Table 7

Table 7 Total relative importance with their rank of WASPAS method for different lubricating environment

Run no.	Flood mist		OML + Al ₂ O ₃		OML + CNT	
	Q_i	Rank	Q_i	Rank	Q_i	Rank
1	0.6857	9	0.5432	8	0.4597	9
2	0.7528	5	0.5925	5	0.5695	6
3	0.7344	6	0.6190	4	0.5893	4
4	0.7303	7	0.5539	7	0.5409	8
5	0.8017	4	0.5240	9	0.5761	5
6	0.7247	8	0.7010	3	0.7074	2
7	0.8710	2	0.5786	6	0.5438	7
8	0.9211	1	0.7147	2	0.6870	3
9	0.8519	3	0.9903	1	1.0000	1

shows total relative importance with their rank of WASPAS method for different lubricating environment.

5.2 Best Experimental Run

In Table 7, from total relative importance values of alternatives, it was detected that investigational results obtained in experiment no. 8 for flood mist lubrication, experiment no. 9 for both OML + Al₂O₃ and OML + CNT are the best result according to the ranking. Now the total relative importance of alternatives was used to plot mean effect for SN ratios. Based on this study, selection of mixture of the levels will be done in accordance to the smaller average response. In Fig. 4, the arrangement of A3 B2 C3 displays the least value of the SN ratio plot for machining of AISI 4340 steel using flood mist lubrication. Similarly, A3 B3 C2 is the lowest value of SN ratio plot for machining of AISI 4340 steel using OML + Al₂O₃ and OML + CNT lubrication respectively.

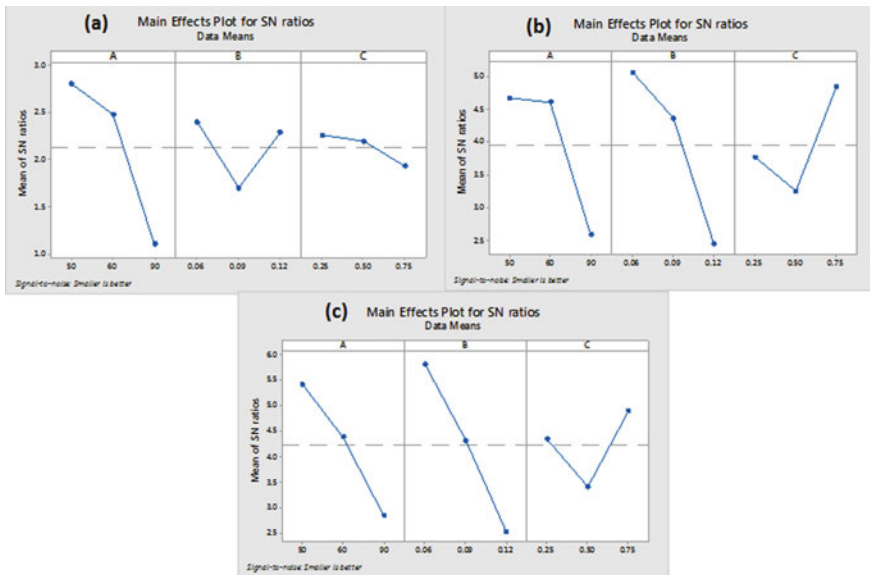


Fig. 4 SN ratio main-effect plot for of total relative importance of **a** Flood mist lubrication, **b** OML + Al₂O₃ lubrication, **c** OML + CNT lubrication

5.3 Optimization Using Genetic Algorithm, Simulated Annealing and Particle Swarm Optimization

Consequently, designing constraints are distinct in normal optimal format and deciphered using Genetic Algorithm, Simulated Annealing and Particle Swarm Optimization. The minimization problem expressed in mathematical form using the total relative significance of WASPAS method for different cutting environment is as below:

For Flood mist lubrication
Minimize

$$ab/(2.44188 - 0.0355996a + 1.21842b + 0.0039937ac) \quad (6)$$

For OML + Al₂O₃ lubrication
Minimize:

$$ab/(4.37495 - 0.00666129a + 0.729547ab + 0.02076ac) \quad (7)$$

For OML + CNT lubrication
Minimize

$$ab/(5.27231 + 0.0111547a + 0.512368ab + 0.00520095ac) \quad (8)$$

all equations are subjected to constraints:

$$\begin{aligned} 50 &\leq a \leq 90 \\ 0.06 &\leq b \leq 0.12 \\ 0.25 &\leq c \leq 0.75 \end{aligned}$$

For GA, finest solution was achieved after 51, 67, 53 generations for flood mist, OML + Al₂O₃ and OML + CNT respectively. For Simulated Annealing, finest solution was achieved after 1500, 2291, 2258 generations for Flood mist, OML + Al₂O₃ and OML + CNT respectively. Optimum parameters obtained by GA, SA and PSO for all cutting conditions are shown in Table 8. Figure 5 shows best fitness value with generations for flood mist lubrication using GA, SA and PSO. Figure 6 shows best fitness value with generations for OML + Al₂O₃ lubrication using GA, SA and PSO. Figure 7 shows best fitness value with generations for OML + CNT lubrication using GA, SA and PSO.

5.4 Most Influential Factor

Figure 8 gives analysis of variance (ANOVA) result calculated values from the total

Table 8 Optimal parameter setting and fitness value obtained using GA, SA and PSO

Algorithm	Flood mist		OML + Al ₂ O ₃		OML + CNT	
	Factor setting	Fitness value	Factor setting	Fitness value	Factor setting	Fitness value
Genetic algorithm	A1 B1 C1	0.70303	A1 B1 C3	0.42801	A1 B1 C3	0.39671
Particle swarm optimization		0.70303		0.42801		0.39671
Simulated annealing		0.70303		0.42820		0.39674

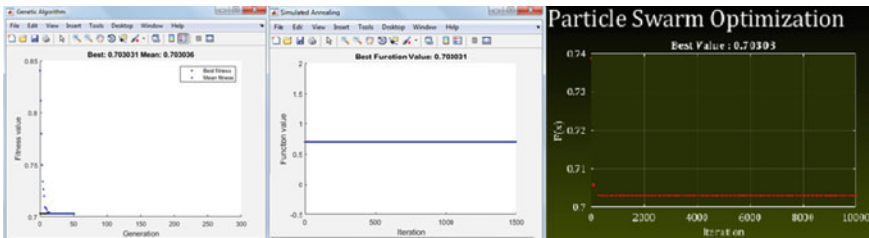


Fig. 5 Best fitness value with generations for flood mist lubrication using GA, SA and PSO

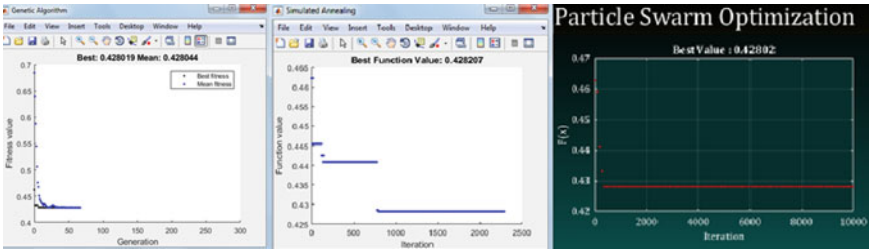


Fig. 6 Best fitness value with generations for OML + Al₂O₃ lubrication using GA, SA and PSO

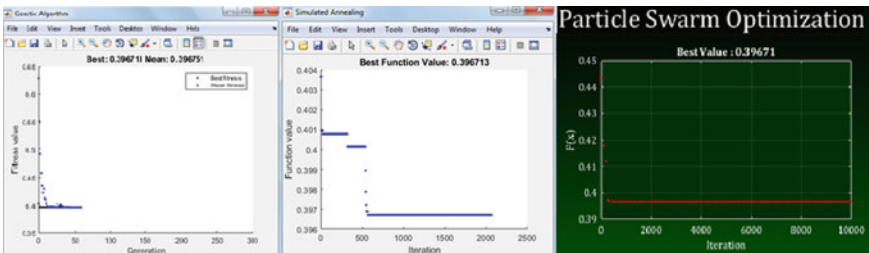
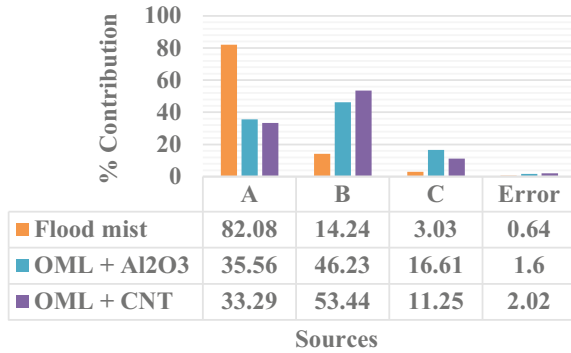


Fig. 7 Best fitness value with generations for OML + CNT lubrication using GA, SA and PSO

Fig. 8 ANOVA result for total relative significance of different lubricating environment



relative significance of flood mist, OML + Al₂O₃ and OML + CNT lubrication respectively. According to Fig. 8, factor A (cutting speed) is peak important parameter for flood mist lubrication technique followed by factor B, feed and factor C, depth of cut if the minimization of surface roughness, chip thickness and temperature are simultaneously considered. Similarly, factor B, is the most significant controlled parameters for OML + Al₂O₃ and OML + CNT lubrication followed by factor A, cutting speed and factor C, depth of cut.

5.5 Confirmation Experiment

The confirmation experiments were led to different lubricating environment [31–33]. Table 9 shows result of confirmatory test of different lubricating environment with different optimizing method.

6 Conclusions

This exploration exertion was done to study the effect of cutting parameters on the surface roughness, chip thickness and temperature for AISI 4340 steel under different lubricating condition using a fabricated PMLS. It can be concluded that the fabricated PMLS works perfectly unlike the mist lubricator which is readily available in the market. The following results found after using MLS setup and listed below:

- This type of mist lubricator setup is portable in nature and easy to operate.
- Hard polymeric envelope imparts restraint toward scratch resistant.
- Individual polymeric surface/cover/body of setup equipment’s (i.e., ABS Coolant mixture chamber, connecting accessories and of both Deflator and Aerator) imbibes the property of low weight in portable designed setup.

Table 9 Result of confirmatory test

Lubrication type	Technique	Optimal setting	Predicted value	Experimental value
Flood mist	Taguchi-WASPAS	A3 B2 C3	0.47401	0.44812
	Genetic algorithm		0.70303	0.68792
	Simulated Annealing	A1 B1 C1	0.70303	0.68792
	Particle swarm optimization		0.70303	0.68792
OML + Al ₂ O ₃	Taguchi-WASPAS	A3 B3 C2	0.37365	0.35881
	Genetic algorithm		0.42801	0.40759
	Simulated annealing	A1 B1 C3	0.42820	0.40759
	Particle swarm optimization		0.42801	0.40759
OML + CNT	Taguchi-WASPAS	A3 B3 C2	0.36672	0.32667
	Genetic algorithm		0.39671	0.35916
	Simulated annealing	A1 B1 C3	0.39674	0.35916
	Particle swarm optimization		0.39671	0.35916

- Imparts the Mach ability of the present designed portable setup using mist lubrication principles reveals notable improvements over conventional flood mist cutting fluid supply.

A comparative analysis has been done based on Taguchi's approach with WASPAS method along with Genetic Algorithm, Particle Swarm Optimization and Simulated Annealing which was used to define the optimal. Based on the experiments performed on CNC turning machine the subsequent conclusions are made:

1. The optimal setting of input parameters for turning using different optimization is shown in Table 10.
2. The percentage contributions of each parameter for turning process using Taguchi-WASPAS method under different lubrication condition is stated in Fig. 8 where cutting speed is the most substantial parameter for flood mist lubrication technique followed by feed and depth of cut if the minimization of surface roughness, chip thickness and temperature are simultaneously considered. Similarly, feed is the most substantial parameters for OML + Al₂O₃ and OML + CNT lubrication followed by cutting speed and depth of cut.
3. It can be seen that by using CNT as lubricant, the output responses are very minimum as per the requirement in comparison to other lubricants.
4. From results, it was clinched that use of the super hybrid Taguchi based WASPAS, GA, SA, and PSO algorithm can proficiently pursuit the optimum process parameters for machining conditions. All the meta-heuristic approaches give

Table 10 Optimal cut parameters using three optimization methods

Lubrication type	Optimization technique	Optimal setting	Cutting speed (m/min)	Feed (mm/rev)	Depth of cut (mm)
Flood mist	Taguchi-WASPAS method	A3 B2 C3	90	0.09	0.75
	Simulated annealing				
	Genetic algorithm	A1 B1 C1	50	0.06	0.25
	Particle swarm optimization				
OML + Al ₂ O ₃	Taguchi-WASPAS method	A3 B3 C2	90	0.12	0.50
	Simulated annealing				
	Genetic algorithm	A1 B1 C3	50	0.06	0.75
	Particle swarm optimization				
OML + CNT	Taguchi-WASPAS method	A3 B3 C2	90	0.12	0.50
	Simulated annealing				
	Genetic algorithm	A1 B1 C3	50	0.06	0.75
	Particle swarm optimization				

same factor setting and predicted value, leading to establishment of economical resolution for commercial machining of AISI 4340 steel in CNC turning.

References

1. Chinchankar, S., Choudhury, S.K.: Hard turning using HiPIMS-coated carbide tools: wear behavior under dry and minimum quantity lubrication (MQL). *Measurement* **55**, 536–548 (2014)
2. Leppert, T.: Effect of cooling and lubrication conditions on surface topography and turning process of C45 steel. *Int. J. Mach. Tools Manuf* **51**(2), 120–126 (2011)
3. Attanasio, A., Gelfi, M., Giardini, C., Remino, C.: Minimal quantity lubrication in turning: effect on tool wear. *Wear* **260**(3), 333–338 (2006)
4. Weinert, K., Inasaki, I., Sutherland, J.W., Wakabayashi, T.: Dry machining and minimum quantity lubrication. *CIRP Ann. Manuf. Technol.* **53**(2), 511–537 (2004)
5. Bagal, D.K., Parida, B., Barua, A., Jeet, S., Sahoo, B.B.: Multi-parametric optimization in CNC dry turning of chromoly steel using taguchi coupled desirability function analysis and utility concept. *Int. J. Appl. Eng. Res.* **14**(13), 21–26 (2019)
6. Diniz, A.E., Ferreira, J.R., Filho, F.T.: Influence of refrigeration/lubrication condition on SAE 52100 hardened steel turning at several cutting speeds. *Int. J. Mach. Tools Manuf.* **43**(3), 317–326 (2003)

7. Maruda, R.W., Krolczyk, G.M., Feldshtein, E., Nieslony, P., Tyliczszak, B., Pusavec, F.: Tool wear characterizations in finish turning of AISI 1045 carbon steel for MQCL conditions. *Wear* **372–373**, 54–67 (2017)
8. Reddy, N.S.K., Rao, P.V.: Experimental investigation to study the effect of solid lubricants on cutting forces and surface quality in end milling. *Int. J. Mach. Tools Manuf.* **46**, 189–198 (2006)
9. Francis J. Clauss.: *Solid Lubricants and Self-Lubricating Solids*. 1st edn. Academic Press Inc (1972)
10. Moura, R.R., Silva, M.B., Machado, Á.R., Sales, W.F.: The effect of application of cutting fluid with solid lubricant in suspension during cutting of Ti-6Al-4V alloy. *Wear* **332–333**, 762–771 (2015)
11. Reeves, C.J., Menezes, P.L., Lovell, M.R., Jen, T.C.: The size effect of boron nitride particles on the tribological performance of bio lubricants for energy conservation and sustainability. *Tribol. Lett.* **51**(3), 437–452 (2013)
12. Dilbag, S., Rao, P.V.: Performance improvement of hard turning with solid lubricants. *Int. J. Adv. Manuf. Technol.* **38**(5–6), 529–535 (2008)
13. Essa, F.A., Zhang, Q., Huang, X.: Investigation of the effects of mixtures of WS₂ and ZnO solid lubricants on the sliding friction and wear of M50 steel against silicon nitride at elevated temperatures. *Wear* **374–375**, 128–141 (2017)
14. Yang, J.F., Jiang, Y., Hardell, J., Prakash, B., Fang, Q.F.: Influence of service temperature on tribological characteristics of self-lubricant coatings: A review. *Frontiers Mater. Sci.* **7**(1), 28–39 (2013)
15. Azwadi, N., Sidik, C., Samion, S., Ghaderian, J., Yazid, M.N.A.W.M.: Recent progress on the application of nanofluids in minimum quantity lubrication machining: a review. *Int. J. Heat Mass Transfer* **108**, 79–89 (2017)
16. Sharma, A.K., Tiwari, A.K., Dixit, A.R.: Progress of nanofluid application in machining: a review. *Mater. Manuf. Processes* **30**(7), 813–828 (2015)
17. Vajjha, R.S., Das, D.K.: Experimental determination of thermal conductivity of three nanofluids and development of new correlations. *Int. J. Heat Mass Transf.* **52**(21–22), 4675–4682 (2009)
18. Mao, C., Huang, Y., Zhou, X., Gan, H., Zhang, J., Zhou, Z.: The tribological properties of nanofluid used in minimum quantity lubrication grinding. *Int. J. Adv. Manuf. Technol.* **71**, 1221–1228 (2014)
19. Najjha, M.S., Rahman, M.M., Kadirgama, K.: Performance of water-based TiO₂ nano fluid during the minimum quantity lubrication machining of aluminium alloy, AA6061-T6. *J. Clean. Prod.* **135**, 1623–1636 (2016)
20. Kumar, M., Bijwe, J., Ramakumar, S.S.V.: PTFE based nano-lubricants. *Wear* **306**(1–2), 80–88 (2013)
21. Jeet, S., Barua, A., Cherkia, H., Bagal, D.K.: Comparative investigation based on MOORA, GRA and TOPSIS method of turning of nickel-chromium-molybdenum steel under the influence of low cost oil mist lubrication system. *Int. J. Appl. Eng. Res.* **14**(13), 8–20 (2019)
22. Jeet, S., Barua, A., Samantray, A., Bagal, D.K.: Sustainable implementation of MQL technique in metal grinding operation employing conventional and nano-particles enriched metal-working fluids: a conceptual approach. *Int. J. Res. Eng. Appl. Manage.* **4**(4), 550–554 (2018)
23. Naik, B., Paul, S., Barua, A., Jeet, S., Bagal, D.K.: Fabrication and strength analysis of hybrid jute-glass-silk fiber polymer composites based on hybrid Taguchi-WASPAS method. *Int. J. Manage. Technol. Eng.* **IX**(IV), 3472–3479 (2019)
24. Jeet, S., Barua, A., Bagal, D.K., Pattanaik, A.K., Agrawal, P.K., Panda, S.N.: Multi-parametric optimization during drilling of aerospace alloy (UNS A97068) using hybrid RSM-GRA, GA and SA. *Int. J. Manage. Technol. Eng.* **IX**(II), 2501–2509 (2019)
25. Maity, K.P., Bagal, D.K.: Effect of process parameters on cut quality of stainless steel of plasma arc cutting using hybrid approach. *Int. J. Adv. Manuf. Technol.* **78**(1–4), 161–175 (2015)
26. Barua, A., Jeet, S., Parida, B., Sahoo, B.B., Bagal, D.K., Samantray, A.: Virtual optimization of motorcycle sprocket material by using FEA and Taguchi coupled TOPSIS-GA-SA. *Int. J. Adv. Scientific Res. Manage.* **3**, 54–63 (2018)

27. Jeet, S., Barua, A., Parida, B., Sahoo, B.B., Bagal, D.K.: Multi-objective optimization of welding parameters in GMAW for stainless steel and low carbon steel using hybrid RSM-TOPSIS-GA-SA approach. *Int. J. Tech. Innov. Mod. Eng. Sci.* **4**, 683–692 (2018)
28. Bagal, D.K., Barua, A., Jeet, S., Satapathy, P., Patnaik, D.: MCDM optimization of parameters for wire-EDM machined stainless steel using hybrid RSM-TOPSIS, genetic algorithm and simulated annealing. *Int. J. Eng. Adv. Technol.* **9**(1), 366–371 (2019)
29. Sahoo, B.B., Barua, A., Jeet, S., Bagal, D.K.: Multi objective optimization of WEDM process parameters using hybrid RSM-GRA-FIS, GA and SA approach. *Int. J. Res. Advent Technol.* **6**(7), 1752–1761 (2018)
30. Bagal, D.K.: Experimental investigation and optimization of cutting parameters in plasma arc cutting. *NIT Rourkela Ethesis* **1**(2), 1–452 (2015)
31. Barua, A., Jeet, S., Bagal, D.K., Satapathy, P., Agrawal, P.K.: Evaluation of mechanical behavior of hybrid natural fiber reinforced nano sic particles composite using hybrid Taguchi-Cocoso Method. *Int. J. Innov. Technol. Exploring Eng.* **8**(10), 3341–3345 (2019)
32. Bagal, D.K., Barua, A., Pattanaik, A.K., Jeet, S., Patnaik, D.: Parametric optimization based on mechanical characterization of fused deposition modelling fabricated part using utility concept. In: Singh, S., Prakash, C., Ramakrishna, S., Krolczyk, G. (eds.) *Advances in Materials Processing. Lecture Notes in Mechanical Engineering*, pp. 313–325. Singapore, Springer (2020)
33. Panda, S.N., Bagal, D.K., Pattanaik, A.K., Patnaik, D., Barua, A., Jeet, S., Parida, B., Naik, B.: Comparative evaluation for studying the parametric influences on quality of electrode using taguchi method coupled with MOORA, DFA, and TOPSIS method for electrochemical machining. In: Parwani, A., Ramkumar, P. (eds.) *Recent Advances in Mechanical Infrastructure. Lecture Notes in Intelligent Transportation and Infrastructure*, pp. 115–129. Springer, Singapore (2020)

Computational Analysis of Composite MoS₂-TiO₂-ZrO₂ Soft Coating on Tribological Performance in Dry Sliding Contact



Avinash Borgaonkar and Ismail Syed

Keywords Archard equation · Composite coating · MoS₂ · TiO₂ · Tribological properties · ZrO₂

1 Introduction

Martins et al. [1] performed FZG gear efficiency tests and FZG gear scuffing tests of composite MoS₂/Ti coating. They observed that composite MoS₂/Ti coating applied on the gear surfaces promotes a remarkable decrease in the friction coefficient and operating temperature. The coating also helps to enhance the scuffing load carrying capacity of FZG gears. Celiktas et al. [2] prepared four different Cu-based brake lining samples using powder metallurgy method. The frictional wear and behavior of prepared samples are analyzed experimentally. Among these four samples, sample II having 5% MoS₂ addition exhibits excellent frictional and wear properties. The compression test was also performed experimentally for all the prepared samples. A simulation model was developed using ANSYS to find out the structural reaction under compression. The experimental and numerical results obtained for the compression tests were observed to be in close agreement. In order to investigate the effect of application of thin film of MoS₂ solid lubricant Doshi et al. [3] developed a 3D model of superconducting magnet system of SST-1. They performed nonlinear structural analysis, employing ANSYS software. They have considered different loading conditions such as in-plane and out-of-plane electromagnetic loads, gravity load, and loads developed due to coil quench events. In order to minimize the computational time axisymmetric model has been taken into consideration. They observed

A. Borgaonkar · I. Syed (✉)

Department of Mechanical Engineering, National Institute of Technology Warangal, Warangal, Telangana 506004, India

e-mail: syedismail7@nitw.ac.in

that application of MoS₂ film leads to significant improvement in frictional and wear properties as compared to unlubricated conditions. Yan et al. [4] formulated a theoretical model to predict wear characteristic of a ball-on-disc test rig. The model is based on plain strain theory. Cai et al. [5] simulated a disc-on-flat model using ANSYS software. In this the disc is coated with different coating thickness. In order to reduce computation time axisymmetric model is used. Sivitski et al. [6] developed a simulation model in ANSYS assuming material is elastic and the shape at the contacting surface is elliptical and contact is frictionless. The transient analysis is performed to acquire the load step data. Khot et al. [7] performed analysis of pin-on-disc test rig employing ABACUS software to find out the developed contact stresses. The obtained simulation results compared with the theoretical Hertzian contact stress values. For high stiffness and elastic-plastic deformation Galarkin's approach is used to achieve faster convergence. In order to simulate the behavior of contacting surfaces in brake and clutch system where excess frictional heat is generated; Abdullah et al. [8] developed a pin-on-disc model using ANSYS software. For pin CONTRA 174 (structural-thermal) whereas for disc SOLID226 (structural) elements were used. Suresh et al. [9] formulated a simulation model on ANSYS by employing a deformable aluminium pin and rigid disc considering frictional contact. The rotational velocity is kept constant by varying the load. The wear depth assumed to be negligible to maintain constant contact pressure in case of linear Archad wear law. The Archad wear coefficient is calculated from the iterative experiments.

From the available literature, there is no trace related to frictional and wear analysis of the composite MoS₂-TiO₂-ZrO₂ (80:10:10% contribution) coating material. In the present work, a computational 3D model of pin-on-disc has been developed using ANSYS 15.0 software. The different parameters such as material properties, load, speed, etc., provided as input to the software and investigated the developed contact stresses. The wear volume is investigated for respective load and speed condition and compared with the experimental values reported in literature [10].

2 Materials and Methodology

The contact between pin and disc defined as a frictional contact. For nonlinear iterative convergence, Newton-Rhapson method is used considering ramped effect so that load will act gradually on the contact faces. The top layer on the pin modeled with composite coating with required coating thickness and material properties [10]. The counter disc is assigned with structural steel material.

A 3D model of pin and disc is developed in CREO PARAMETRIC 2.0 as shown in Fig. 1. Initially both pin and disc modeled individually and then assembled. The dimension of the pin is 12 mm diameter and 10 mm height whereas disc (wear track) diameter of 80 mm with 10 mm thickness. These dimensions are directly taken from the experimental analysis. The developed 3D pin-on-disc model using CREO software has been imported into ANSYS through.igs file interface.

The developed 3D model has been discretized as shown in Fig. 2. The meshing is

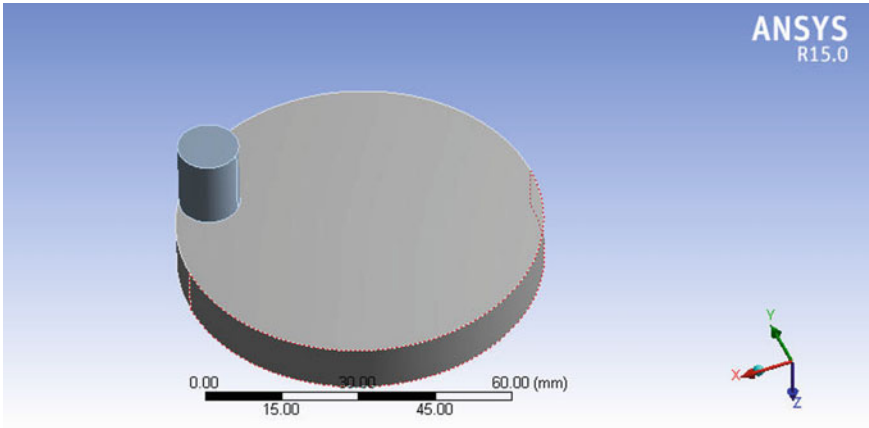


Fig. 1 Simulation model for pin-on-disc test rig

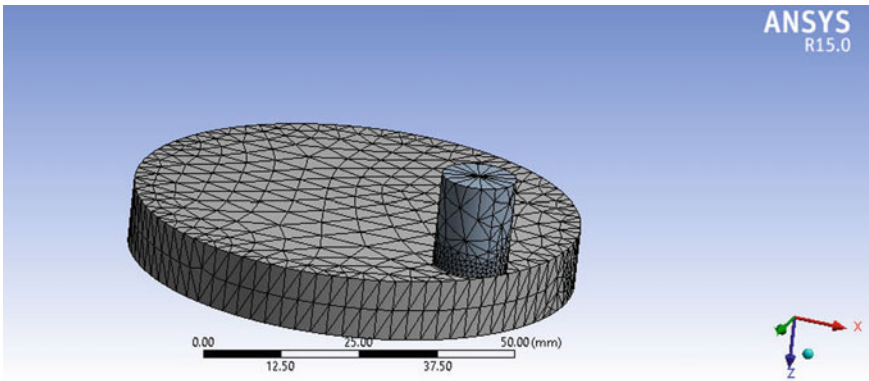


Fig. 2 Discretization of the model

constructed tetrahedron elements. At the contact, the stresses are concentrated and high value of stress is generated; so there is requirement of more numbers of nodes near to contact. For increasing the number of nodes refinement is done which makes the meshing more compact and convergence takes place at faster rate.

In order to simulate sliding contact condition in the present work the disc is rotating about Z-axis and rotation of disc about X-axis and Y-axis defined as zero, whereas the pin is stationary at one place. For achieving this either the face of pin is to be fixed or the lower face of the disc is to be fixed. In the present work, the lower face of the disc is fixed so that it will directly restrict the translation motion in all three axes and two rotational motions about X-axis and Y-axis as depicted in Fig. 3. The applied normal load is acting on the top face of the pin and the rotational velocity is acting about Z-axis on the disc, both the inputs acting simultaneously.

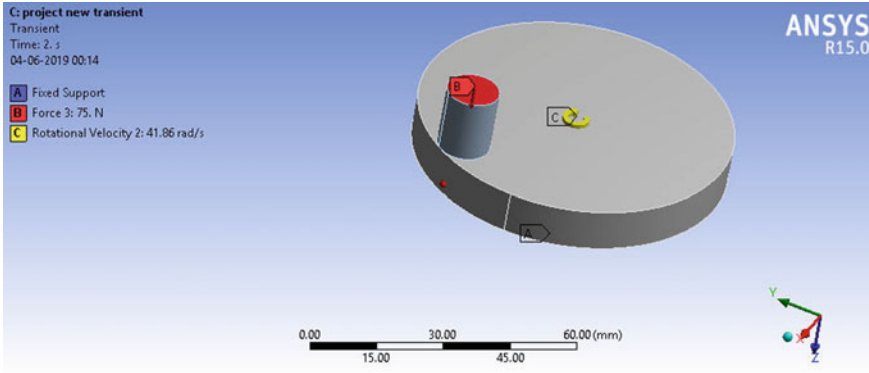


Fig. 3 Boundary conditions

3 Results and Discussion

3.1 Estimation of Wear

The Archard wear equation is function of wear coefficient, sliding distance, and hardness of the material.

$$Q = \frac{K * W * L}{H} \tag{1}$$

where, Q is the total volumetric wear,

K is an Archard wear coefficient,

W is the applied normal load,

L is the total sliding distance,

H is the material hardness.

In order to investigate the volumetric wear, the Archard wear coefficient is taken equal to 6.67×10^{-6} (mm^3/Nm) [11]. Subsequently the contact stress values obtained from the computational study converted into normal load and evaluated the wear volume as below,

$$Q = \sigma * K * A * D \tag{2}$$

The contact stresses at different normal loads 25 N, 50 N, and 75 N at 400 rpm speeds are obtained from the computational analysis are shown in Fig. 5a, b, c. From the obtained contact stress values, the wear volume is predicted for each condition. The experimental and computational results are compared and represented in Table 1.

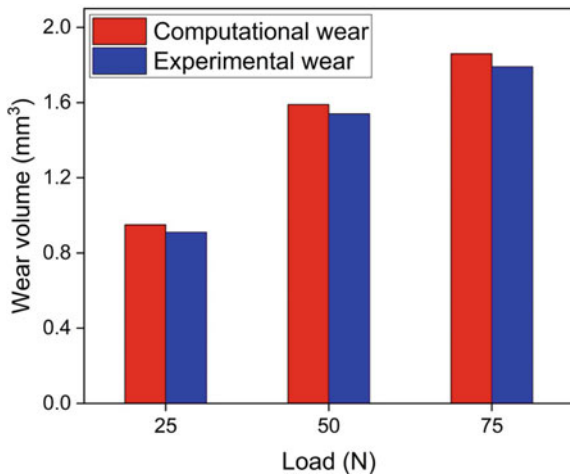
The obtained results from both computational and experimental methods have been compared and depicted in Fig. 4 (Fig. 5).

Table 1 Wear volume estimation

Normal load (N)	COF	Experimental wear volume W_e (mm ³)	Contact stress from ANSYS (σ) (MPa)	Computational wear volume (mm ³) $W_c = \sigma * K * A * D$	Error (%)
25	0.29	0.91	0.42	0.95	4.2
50	0.32	1.54	0.703	1.59	3.1
75	0.262	1.79	0.82	1.86	3.7

A is cross sectional area of coated pin sample
 D is the total sliding distance

Fig. 4 Comparison of computational and experimental wear at load 25 N, 50 N, 75 N with speed 400 rpm



In order to verify the accuracy of the model, by keeping same loads 25 N, 50 N, and 75 N the speed is changed from 400 to 200 rpm. The simulation is carried out for the above load and speed conditions to obtain the contact stress values. From the obtained contact stress values, the wear volume is predicted for each condition. The experimental and computational results are compared and represented in Table 2.

The obtained results from both computational and experimental methods have been compared and depicted in Fig. 6.

From the comparison of wear volume obtained by computational and experimental methods, it is observed that, the results are in close agreement to each other. The % error shows the deviation in the results obtained by both the methods which is less than 10%, so that the developed model can be used to predict the results for other load and speed conditions. These obtained computational results are in line with previously reported literature [9, 10].

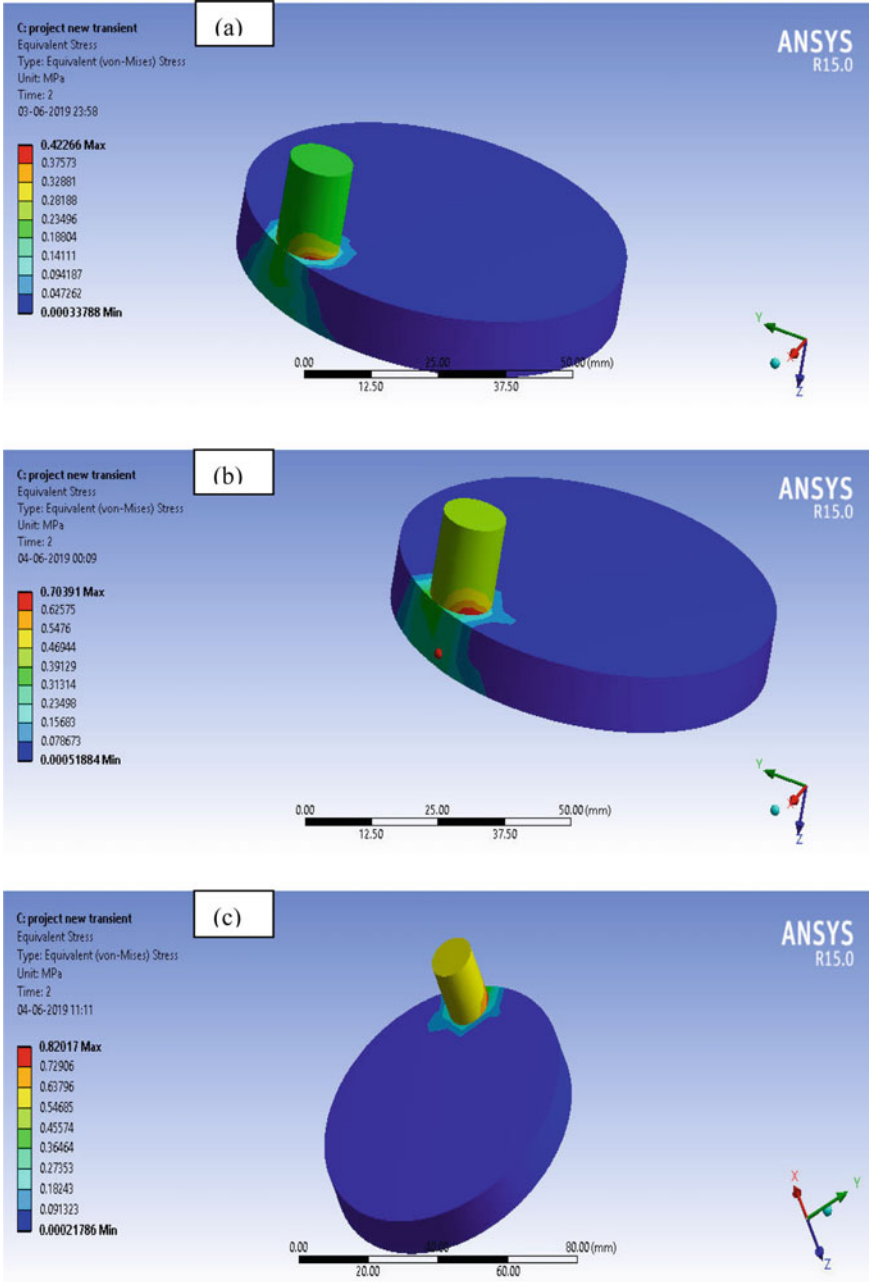
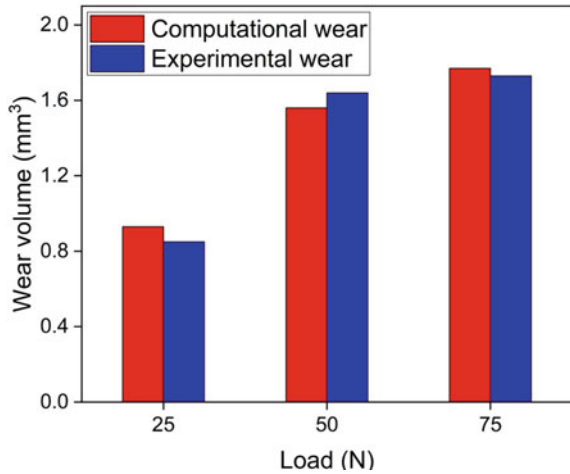


Fig. 5 Contact stress a 25 N, b 50 N and c 75 N with speed 400 rpm

Table 2 Wear volume estimation

Normal load (N)	COF	Experimental wear volume W_e (mm ³)	Contact stress from ANSYS (σ) (MPa)	Computational wear volume (mm ³) $W_c = \sigma * K * A * D$	Error (%)
25	0.3	0.85	0.41	0.93	8.6
50	0.35	1.64	0.69	1.56	4.8
75	0.31	1.73	0.78	1.77	2.2

Fig. 6 Comparison of computational and experimental wear at load 25 N, 50 N, 75 N with speed 200 rpm



4 Conclusion

This study demonstrates a 3D FEM model for the solution of composite MoS₂-TiO₂-ZrO₂ coated pin-on-disc dry sliding contact problem. The solution for the developed computational model is obtained by using ANSYS 15.0 software. The results obtained from the computational model for different load and speed conditions are compared with experimental results. The computational and experimental results are in close agreement. It is observed that with the increase in load the contact stress and wear volume increases proportionally. The maximum wear is 1.86 mm³, 1.77 mm³ took place at 75 N load with developed contact stresses of 0.82 MPa, 0.78 MPa at 400 rpm and 200 rpm speed respectively.

References

1. Martins, R.C., Moura, P.S., Seabra, J.O.: MoS₂/Ti low-friction coating for gears. Tribol. Int. **39**(12), 1686–1697 (2006)

2. Celiktas, E., Topuz, A., Kazanci, Z.: Friction and wear behaviors of aircraft brake linings material. *Aircraft Eng. Aerosp. Technol.* **84**(5), 279–286 (2012)
3. Doshi, B., Sarkar, B., Sharma, R., Sahu, A.K., Rewatkar, P., Sonara, D., Saxena, Y.C., Bhaskar, V.R., Kumar, S., Nagbhushanam, S.: Design requirement, qualification tests and integration of a thin solid lubricant film of MoS₂ for the cold mass support structure of the steady state superconducting tokamak SST-1. *Nucl. Fusion* **46**(3), 100–105 (2006)
4. Yan, W., O'Dowd, N.P., Busso, E.P.: Numerical study of sliding wear caused by a loaded pin on a rotating disc. *J. Mech. Phys. Solids* **50**(3), 449–470 (2002)
5. Cai, J., Xu Y.M., Lin, H.B.: A study of contact stress on coatings of wheel-slide using ANSYS. *Adv. Mater. Res.* **452**(1), 175–179 (2012)
6. Sivitski, A., Podra, P.: Finite element method and its usable applications in wear models design. In: 9th International DAAAM Baltic Conference, Industrial Engineering, pp. 24–26 (2014)
7. Khot, S., Borah, U.: Finite element analysis of pin-on-disc tribology test. *Int. J. Sci. Res.* **4**(4), 2319–7064 (2015)
8. Abdullah, O.I., Schlattmann, J.: Temperature analysis of a pin-on-disc tribology test using experimental and numerical approaches. *Friction* **4**(2), 135–143 (2016)
9. Suresh, R., Prasanna Kumar, M., Basavarajappa, S. Kiran, T.S., Yeole, M., Katare, N.: Numerical simulation & experimental study of wear depth and contact pressure distribution of aluminum MMC pin on disc tribometer. *Mater. Today Proc.* **4**(10), 11218–11228 (2017)
10. Borgaonkar, A.V., Rai, D., Ismail, S.: Development and investigation of the tribological performance of pure MoS₂ and composite MoS₂-TiO₂-ZrO₂ coating material. In: 10th International Conference on Industrial Tribology (IndiaTrib-2019), IISc Bangalore (2019)
11. Barman, K., Shipway, P.H., Voisey, K.T., Pattinson, G.: Evolution of damage in MoS₂-based dry film lubricants (DFLs) in fretting wear-the effect of DFL thickness and contact geometry. *Prog. Org. Coat.* **105**(1), 67–80 (2017)

Optimal Path Planning of Steam Generator Tube Inspection System's Robotic Manipulator Using Genetic Algorithm



S. Joseph Winston and P. V. Manivannan

Abstract Prototype Fast Breeder Reactor (PFBR) has eight Steam Generators (SG) that transfers the heat from molten sodium to the water and converts the water into super-heated steam. SG is a shell and tube type counter flow heat exchanger, which has 547 steam tubes connecting the top and bottom headers of the SG. These steam tubes are surrounded by Sodium and water/steam will be flowing in the tubes. (i.e. sodium is present in the shell side and water/steam in the tube side). The water/steam pressure will be 172 bar and any breach in one of the tubes (due to crack) will eventually result in water coming in contact with sodium and leading to violent reaction. Hence, all mitigation efforts are to be taken proactively to isolate a degrading tube(s) through proper Pre-Service inspection (PSI) and In-Service inspections (ISI) using Remote Field Eddy Current technique (RFEC). Though PSI is a comprehensive inspection, ISI is generally carried out on 10% of the total heat transfer area, i.e. about 54 tubes, through periodic inspections. A two-axis robotic system called PFBR SG Inspection System (PSGIS) is used to position the probe/cable pusher end effector system to perform the tube inspection with RFEC probe. Since there is no straight forward scheme available to optimally choose the inspection sequence, Genetic Algorithm (GA) is used to optimize the tube inspection order to reduce the duty cycle and total inspection time. In this work, we have developed a genetically evolved optimal inspection algorithm to reduce overall inspection time and the results of the investigations are presented.

Keywords Steam generator · Robotic manipulator · Genetic algorithm · Path planning

S. Joseph Winston (✉)

Indira Gandhi Centre for Atomic Research, Kalpakkam, India
e-mail: winston@igcar.gov.in

P. V. Manivannan

Indian Institute of Technology Madras, Chennai, India
e-mail: pvm@iitm.ac.in

1 Steam Generator Inspection System

1.1 Introduction

Prototype Fast Breeder Reactor (PFBR) has 8 Steam Generators (SG) to transfer the reactor heat to water and convert the water to high pressure steam to run the steam turbine-electrical generator combination to generate electrical power. PFBR is a 500 MWe nuclear power plant. There are 547 tubes in SG connecting the bottom header and top header, which supplies the water through all tubes for heat transfer from the sodium in the shell side. The top header collects the steam and sends it to the steam turbine to drive electrical power generator. The Remote Field Eddy Current (RFEC) technique-based probe is used to carry out the tube inspections through Pre-Service Inspection (PSI) and In-Service Inspection (ISI) of the SG for the safe operation of the system. A two-axis robotic manipulator called as PFBR SG Inspection System (PSGIS) is used for remotely pushing/pulling the RFEC probe into the SG tubes for inspection. There has been a constant effort all over the world [1] for the development of SG inspection systems, as the plant down times are mainly due to the outage of SGs. The SG inspection system will be fixed to the top header manhole and the robotic system descends down into the header to carry out the tube inspection. As, there is no straight forward scheme available to optimally choose the inspection sequence, in this work a Genetic Algorithm (GA) is used to optimize the tube inspection order to reduce the duty cycle and total inspection time and the results of the investigations are presented.

1.2 PFBR SG Inspection System

PSGIS system has 7 modules to perform various tasks. The Device Deployment Module (DDM) deploys a two-axis precision robotic system called the Tube Locator Module (TLM) close to the tube sheet for inspecting the tubes. TLM positions & orients the Remote Field Eddy Current (RFEC) probe over any one of the desired tubes that needs to be inspected and pushes the probe into tube along with the cable using the Cable Pusher Module (CPM) which forms the end-effector of the robotic system. A Comprehensive Control Module (CCM) controls the overall system. Figure 1a shows the PSGIS system and the precision robotic arm is shown in Fig. 1b. Unlike the conventional robotic system which has the base as the fixed reference coordinate frame, this system while deployment may have errors in aligning with the tube sheet plane which is corrected in the Inverse kinematics through a three-point calibration method [2, 3].

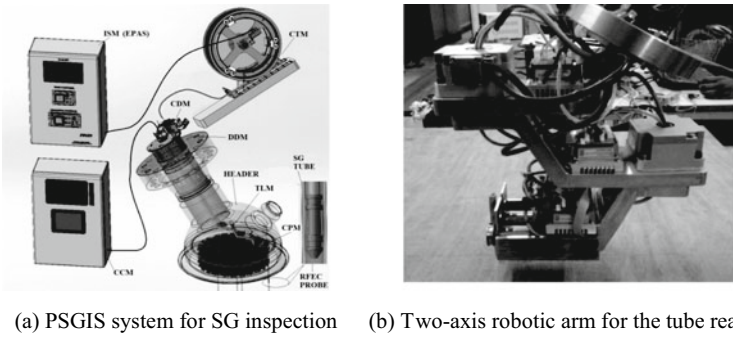


Fig. 1 a PSGIS system for SG inspection. b Two-axis robotic arm for the tube reach

1.3 Steam Generator Tube Sheet and Numbering Scheme

The Steam Generator top and bottom headers are connected with 547 tubes (ending in top and bottom tube sheets). The water pumped in these tubes will be converted to steam by the high temperature liquid sodium surrounding them. This steam is collected at the top header and sent to drive the steam turbine for electrical power generation. The 2-DoF robotic manipulator end effector along with cable management system pushes the RFEC probe into the steam tube (entire length of 23 m)—i.e. up to the bottom weld zone for inspection. Figure 2a shows the SG Tube Sheet surface and the tube numbering scheme for all the 547 tubes. The inner most tube at the centre of Tube Sheet (marked as RED circle) is numbered as (0, 0). The steam tubes have an Inner Diameter (ID) of $\phi 12.6$ mm and a pitch of 32.2 mm. The tube array pattern is a triangular pitch. Such a triangular pitch can be well represented as hexagonal rows of tubes with a centre single tube. Hence, in order to mathematically represent the tube array pattern, the following equations are deduced from the geometry.

The total number of tubes in each row goes in a multiple of 6. There are 14 rows of tubes and the hexagonal array pattern is modified beyond 11th row tubes to make it circular to fit the tube bundle inside the cylindrical shell. 12th, 13th and 14th rows

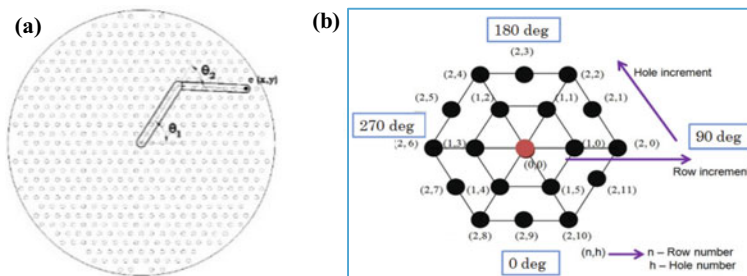


Fig. 2 a Steam Generator (SG) Tube sheet. b Tube numbering scheme

have missing tubes which are appropriately coded in PYTHON program to represent the actual pattern of tubes in SG tube sheet

$$(r, \theta) = \left(a\sqrt{n^2 + h^2 - nh}, \cos^{-1}\left(\frac{a(2n - h)}{2r}\right) \right) \quad (1)$$

$$\begin{bmatrix} x \\ y \end{bmatrix} = \begin{bmatrix} r \cos \theta \\ r \sin \theta \end{bmatrix} \quad (2)$$

In Eqs. (1) and (2), the ‘ r ’ and θ are polar coordinates of the tube centres, ‘ a ’ is tube pitch, ‘ n ’ is row number, ‘ h ’ is tube number in the row as seen from Fig. 2b. In the tube sheet, the outermost tubes are located at a maximum radial distance of 397 mm. However, the robot arm’s maximum radial reach of 420 mm, which covers all the tubes.

2 Optimal Path Planning for Reduced Inspection Time

It becomes important to plan the inspection path starting from the first tube to the last tube, in a particular order during the inspection campaign. In case of PSI, all the 547 tubes have to be inspected and this requires a proper sequencing of tubes in appropriate order to reduce the total inspection time for a SG. Inspecting 547 tubes means the robotic end effector has to visit all the 547 tubes. A random user choice will lead to enormous inspection time by increased total travelled path, giving rise to more duty cycle to the actuators used in the robotic system. During the ISI campaign 10% of the tubes need to be inspected in a randomly selected set of tubes from the total 547 tubes. Typically, the random tubes will be widely distributed over the entire tube sheet plane. Unless a proper tube inspection order is evaluated, the total inspection time will be more due to too many random paths between the tubes. The following are the commonly used evolutionary algorithms for planning random movement of robotic manipulator (in shortest path), where there is no straight forward mathematical scheme available. Some of the commonly used evolutionary algorithms [4] are; (a) Genetic Algorithm, (b) Particle swarm Algorithm, (c) Ant colony d) Simulated Annealing. Genetic Algorithm [5, 6] is widely used in path planning applications due to its simplicity in representing the problem. A good optimizer is needed to solve a problem heuristically and search for a good solution in a set of possible solution, where there is no other straight forward way to solve. The GA uses selection of a population to do crossover and mutation to form child chromosomes and the fitness tested. The better fit individual will be retained for more reproduction, whereas the weak individuals are discarded. The following sequence shows the abstraction of the GA. Following steps are involved in the GA process flow:

Step 1: Generate random population of ‘ n ’ chromosomes
(Tube inspection path sequence)



Fig. 3 Inspection sequence as a chromosome containing tube information as genes

Step 2: Evaluate the fitness $f(x)$ of each chromosome ‘ x ’ in the population (Find out the path distance connecting all the tube points)

Step 3: Create a new population by repeating following steps until the new population is complete

Step 3.1: Select two parent chromosomes from the population according to their fitness (the better fitness, the bigger chance to be selected).

Step 3.2: With a crossover probability cross over the parents to form a new offspring (children). If no crossover was performed, offspring is an exact copy of parents.

Step 3.3: With a mutation probability mutate new offspring at each locus (position in chromosome).

Step 3.4: Place new offspring in a new population (New tube order sequence).

Step 4: Use new generated population for a further run of algorithm

Step 5: If the end condition is satisfied, stop, and return the best solution in current population

Step 6: Go to Step-2.

The set of tubes selected for an inspection campaign are from the total 547 tubes in a random fashion. Typically, 10% of the total tubes are about 54 tubes out of 547 tubes are chosen for inspection. The tubes are selected by its position which is typically the tube number. The tube number/position represents the gene which carries the information of the position of the tube which is the cartesian information on the tube sheet. The tubes put in certain order, i.e. tubes as genes packed in a particular order constitutes the chromosome. Just as in the genetics, the tubes as genes packed in a particular inspection sequence describes the chromosome. Figure 3 shows the tube order.

If there are ‘ k ’ number of selected tubes for inspection and the inspection sequence in an array of the tube centre point coordinates, the interconnected distance can be expressed as follows;

$$\text{Min Total distance} = \sum_{n=1}^k \sqrt{(x_{n+1} - x_n)^2 + (y_{n+1} - y_n)^2} \tag{3}$$

The tube order is represented by the term ‘ n ’ and hence summing up all the interconnected distances is the total path distance visiting all tubes by the robotic manipulator using inverse kinematic algorithm [7–9]. Lesser the distance, lesser is the inspection time and lesser the duty cycle of the actuator and also it has direct implication on the down time of the plant for inspection. In order to save cost and time, it is required to choose the correct order of tube paths that the total inspection

distance is minimal. Hence the fitness function is written such that the total distance is computed and the score for the chromosome that has a tube order which gives less distance is offered high. The cross over and mutation are the important parameters in Genetic Algorithm where the chromosome is divided into two or multiple at different locations to swap the part of the chromosome with the parent’s fitness studied.

3 Hardware and Software Development and Testing

Figure 4 shows the Steam Generator Inspection Robotic Manipulator Control system. The developed Genetic Algorithm-based robot control program (PYTHON program) is ported on a ‘Raspberry Pi’ embedded controller, which is interfaced with main motion controller through the communication protocol TCP/IP as shown in Fig. 4.

The GA generates inspection tube sequence and feeds to the motion controller and suggests the user to proceed in the best optimal tube inspection order to reduce the overall inspection time. In order to understand the performance of the evolutionary algorithm, Genetic Algorithm, the problem is coded in the scripting language PYTHON. The GA engine, PYEVOLVE [10] is used for the GA functions. However, the tube numbering algorithm also is coded in such a way to truly represent the actual tube array of the tube sheet in the PFBR SG. In order to test the performance of the path planning algorithm, different set of case studies were carried out. During the study, the robotic arm was operated at a linear speed of 20 mm/s (while evaluating the Random and GA optimized paths). In one of the case studies, inspection of four rows of tubes are considered for simulation. Figure 5a shows the result of this study and it can be noticed that how the random sequence of tube testing will take up more inspection time, compared to the path planned, Fig. 5b with Genetic Algorithm in a structured sequence. In other case study, of 547 tubes in 14-Rows, 10% tubes were selected for inspection at random sequence which represents the actual scenario. Figure 6a shows path followed by Robot manipulator to inspect all these 10% tubes at the same random way; while Fig. 6b shows the path followed using GA algorithm that is time optimal.

Fig. 4 The steam generator inspection robotic manipulator control system

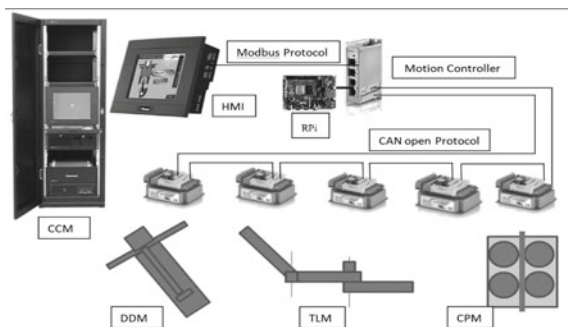


Fig. 5 **a** Random path, (4-Rows). **b** GA evolved path (4-rows)

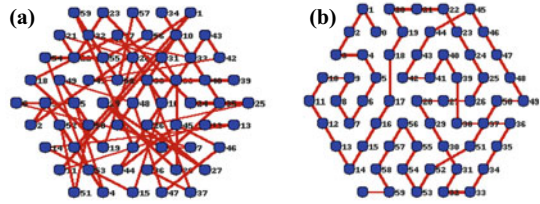


Fig. 6 **a** Random path, (14-Rows). **b** GA evolved path (14-rows)

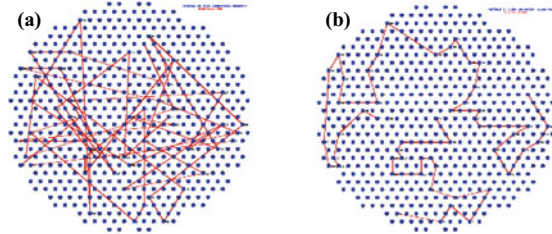


Figure 7 shows the raw score, that is the total distance connecting all the tube centres in a particular sequence. The figure shows a very quick way the evolution takes place minimizing the total distance. The crossover considered is 0.9 and the mutation 0.001 which shows a very good evolution of best optimal solution in all the cases.

Due to the circular symmetry of the tube sheet, repeated runs though not the same tube order was obtained but the raw score, i.e. the path distances obtained are almost the same which also gives the confidence on the GA evolved output. Table 1 shows the tubes considered for the inspection campaign and minimum path distance travelled by the inspection probe (for random and GA algorithms). It may be noted that with GA algorithm the total distance travelled is always less and this helps to

Fig. 7 The max, min and average raw scores during the evolution of the optimal path

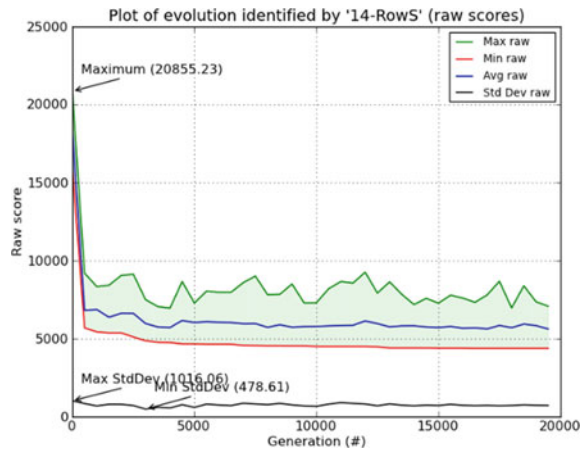


Table 1 Minimized total distance in the complete path of an inspection campaign

S. No.	Row No of tubes	Total tubes	Tubes inspected (%)	No. of tubes for inspection	Total distance (mm)		Improvement in Inspection time (%)
					Random	GA	
1	2	19	100	19	1500	577	62
2	3	37	100	37	4110	1091	74
3	4	61	100	61	8718	2035	77
4	5	91	100	91	15,892	3334	79
5	14	547	10	54	235,085	4374	98

reduce the overall inspection time (as high as, 98% in case inspecting all 547 tubes) and also the cost.

3.1 Conclusion

Periodic inspection of the PFBR Steam Generator tubes for detecting flaw in the tube is very important for the safe operations of the system. The RFEC inspection probe is commonly used for SG tubes inspection. However, during inspection, it is necessary to locate every steam tube location as per inspection procedure, and position the robotic end effector (i.e. REFC probe) at tube centre accurately using shortest path. Typically, 10% of the total 547 tubes randomly are chosen for inspection during In-Service campaigns and that amounts to 54 tubes. Hence, it is imperative to sequence the inspection through proper tube order to have overall minimized path distance to reduce inspection time. Since there is no direct scheme to reduce the distance explicitly, evolutionary algorithms are must to minimize the total distance of the path sequenced for inspection of the selected tubes. Hence, Genetic Algorithm was used in this study and the PYEVOLVE [5] GA engine has been used to represent the GA functions. The program has been made in the scripting language PYTHON and it has been tested under various cases: 2-Rows,3-Rows, 4-Rows of tubes, 5-Rows of tubes and finally for 14 Rows of tubes with 10% tubes randomly considered. The results show that the developed GA algorithm is able to optimally control robotic manipulator path (i.e. shorted path) during inspection of SG tubes, which reduces inspection time and cost. In the future, the developed algorithm will be fine-tuned for sequencing all 547 tubes for inspection.

References

1. Obrutsky, L., Renaud, J., Lakhan, R.: Steam generator inspections: faster, cheaper and better, are we there yet? In: IV Conferencia Panamericana de END, Buenos Aires—Octubre 2007

2. Joseph Winston, S., Jose, J., Subramanian, A., Murugan, S., Bhaduri, A.K.: Rigid Body Transformations for Calibration of Prototype Fast Breeder Reactor, Steam Generator Inspection Device. *Advancements in Automation, Robotics and Sensing*. Springer, Berlin, pp. 23–40 (2016)
3. Joseph Winston, S., Jose, J., Jagadishan, D., Sakthivel, S., Visweswaran, P., Murugan, S., Amarendra, G., Manivannan, P.V.: Degenerated degree of freedom sensing without loss of accuracy while estimating the rigid body parameters for the calibration of a 2 axis robotic arm for prototype fast breeder reactor, steam generator inspection system. In: *Machines, Mechanism and Robotics: Proceedings of iNaCoMM 2017, Lecture Notes in Mechanical engineering*, Springer
4. Sivanandam, S., Deepa, S.: Introduction to particle swarm optimization and ant colony optimization. In: *Introduction to Genetic Algorithms*. Springer, Berlin (2008)
5. Gad, A.: Introduction to Optimization with Genetic Algorithm. <https://towardsdatascience.com/introduction-to-optimization-with-genetic-algorithm-2f5001d9964b>
6. Xin, J., Zhong, J., Yang, F., Cui, Y., Sheng, J.: An improved genetic algorithm for path-planning of unmanned surface vehicle. *Sens. Open Access J.* (2019)
7. Joseph Winston, S., Manivannan, P.V.: Optimal damping factor for the least squares inverse kinematics for the steam generator inspection system. In: *Machines, Mechanism and Robotics: Proceedings of iNaCoMM 2017, Lecture Notes in Mechanical engineering*, Springer
8. Jazar, R.N.: *Theory of Applied Robotics-Kinematics, Dynamics, and Control*, 2nd edn. Springer, Berlin
9. Peter, C.: *Robotics vision and control*. In: *Fundamental Algorithms in MATLAB*. Springer, Berlin
10. Perone, C.S.: *Pyevolve Documentation*. <http://pyevolve.sourceforge.net/index.html>

Kinematic Simulation of Dual Arm Agricultural Mobile Robot



A. Sridhar Reddy, V. V. S. Kesava Rao, and B. B. V. L. Deepak

Abstract From the last few decades, more than 60% of Earth's population was engaged in agriculture, but now there is decline in population who are engaged in agriculture. The population engaged in agriculture decreases by the time. India is the world's second largest producer of sugarcane. During production, planting, tending and harvesting sugar cane is labour intensive process. Cane cutting is a tough physical operation and requires large skilled labour. In India currently available sugarcane harvesters are very expensive, which is not feasible for small scale farmers, and not available throughout the country. To overcome the problem, we proposed dual arm mobile robot, so that it can able to hold the sugarcane stalk after that it can place cane at rare side of the robot. To transmit the cane stalk in required path, we have to generate a trajectory for end-effector. We define the end-effector position by calculating the joint angles, treating as Inverse Kinematics problem. And also generated the velocity and acceleration diagrams for the joints.

Keywords Agricultural robot · Forward kinematics · Inverse kinematics · RoboAnalyzer

1 Introduction

For the last few decades, more than 60% of Earth's population was engaged in agriculture, but now there is decline in population who are engaged in agriculture. In overall population, the total workforce is distributed mainly in three economic sectors, i.e., Agriculture sector, Industry sector and Service sector. Agriculture sector is still the main employer in India with 211.3 mn engaged in 2015–2016, which is nearly 16.5%

A. Sridhar Reddy (✉) · V. V. S. Kesava Rao
Department of Mechanical Engineering, Andhra University, Visakhapatnam 530003, India
e-mail: asridhreddy@gmail.com

B. B. V. L. Deepak
Department of Industrial Design, National Institute of Technology, Rourkela 769008, India

lower compared with previous decade [1] and followed by Service sector and Industrial sector. Nowadays, around 43% of the population engaged in agriculture keeps on falling. The reasons are: the age of individuals in farming households is increasing as well as the population involved in agriculture has been reducing and moving towards other sectors.

India is the second largest producer of rice, wheat, sugarcane [2]. During sugarcane production, planting, tending and harvesting sugar cane is labour intensive process. Cane cutting is a tough physical operation and requires large skilled labour. Due to shortage of labour during harvesting, farmers lose their profit, since cutting and transfer of cane stalk to sugar mill is time dependent process. In India currently available sugarcane harvesters are very expensive, which is not feasible for small scale farmers, and these are not available throughout India. So the crop area decreases by the time.

To develop fully agricultural farm, robot is only first step. So there is a need to develop an agricultural robot which is useful for small scale harvesting, which can reduce strenuous, monotonous, physical work of labour. In this we focused mainly in modelling of sugarcane harvesting robot. A dual arm robotic manipulator holds the cane stalk during cutting and then it can place cane at rare side of the robot.

2 Sugarcane Harvesting Robot

2.1 CAD Modelling

The robot consists of moving base and two arms. The two arms are placed at different heights from the ground. Each arm is having 3 rotary joints, at the end, each arm is equipped with plier (end-effector) having 1 dof (degree of freedom) for holding cane stalk. One cutter wheel is placed at bottom of the mobile robot to cut the sugar cane. The model is designed in SolidWorks software, shown in Fig. 1.

2.2 Kinematics Modelling

For trajectory planning and control, Kinematics modelling is the basis. To analyse the robot structure, Denavit–Hartenberg method is used [3]. Based on the space position and orientation, parameters are listed to establish the coordinate relationship between adjacent joints. Based on the $D-H$ parameters, we solve the problem for joint angles by using Forward Kinematics or Inverse Kinematics. Configuration of proposed dual arm serial manipulators with revolute joints is shown in Fig. 2.

The robot with two serial manipulators each has 3 dof. The two manipulators need to establish coordinate systems. In $D-H$ coordinate system, robot can be viewed as a series of linkages [5], shown in Fig. 3.

Fig. 1 Agricultural mobile robot having two arms and cane cutter

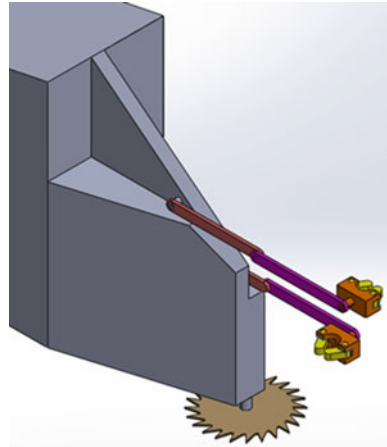


Fig. 2 Configuration of proposed dual arm manipulator

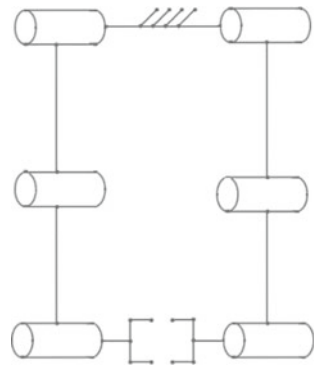


Fig. 3 Frame assignment for dual arm manipulator

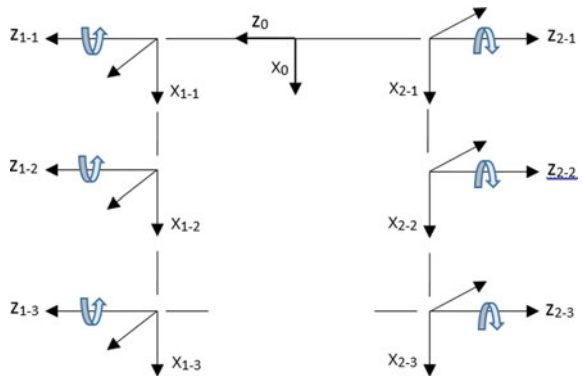


Table 1 DH parameters for the dual arm

Link $i-j$	$\alpha_{i(j-1)}$	$a_{i(j-1)}$	d_{ij}	θ_{ij}
1-1	0	0	d_{11}	θ_{11}
1-2	l_{11}	0	0	θ_{12}
1-3	l_{12}	0	d_{12}	θ_{13}
2-1	0	π	d_{21}	θ_{21}
2-2	l_{21}	0	0	θ_{22}
2-3	l_{22}	0	d_{22}	θ_{23}

$D-H$ parameters are shown in Table 1, where $\alpha_{i(j-1)}$, $a_{i(j-1)}$, d_{ij} and θ_{ij} ($i = 1, 2$ arm number; $j = 1, 2, 3$ number of joints) are parameters related to the link and joint. Which represent the link twist, link length, link offset, and joint angels respectively.

For solving the transformation matrix, kinematics model is established for final homogeneous transformation matrix, coordinate system of transformation between the links is performed as given in Eqs. 1 and 2.

$${}^0T_{12} = {}^0T_{11} \times {}^1T_{12} \times {}^2T_{13} \quad (1)$$

$${}^0T_{22} = {}^0T_{21} \times {}^1T_{22} \times {}^2T_{13} \quad (2)$$

Based on the equation above the transformation matrix are given in Eq. 3.

$${}^{i-1}T_i = \begin{bmatrix} C\theta_i & -S\theta_i & 0 & a_{i-1} \\ S\theta_i C\alpha_{i-1} & C\theta_i C\alpha_{i-1} & -S\alpha_{i-1} & -S\alpha_{i-1}d_i \\ S\theta_i S\alpha_{i-1} & C\theta_i S\alpha_{i-1} & C\alpha_{i-1} & C\alpha_{i-1}d_i \\ 0 & 0 & 0 & 1 \end{bmatrix} \quad (3)$$

where,

$$C_i = \text{Cos}\theta_i, \quad S_i = \text{Sin}\theta_i$$

By substituting the DH parameters in Eq. (3), the final transformation matrix is given in Eq. (4).

$${}^0T_3 = \begin{bmatrix} n_x & o_x & a_x & p_x \\ n_y & o_y & a_y & p_y \\ n_z & o_z & a_z & p_z \\ 0 & 0 & 0 & 1 \end{bmatrix} \quad (4)$$

The elements in the above matrix Eq. (4), are shown in following Eqs. (5) to (16)

$$n_x = C_3 \times (C_1 \times C_2 - S_1 \times S_2) - S_3 \times (C_1 \times S_2 + C_2 \times S_1) \quad (5)$$

$$n_y = C_3 \times (C_1 \times S_2 + C_2 \times S_1) + S_3 \times (C_1 \times C_2 - S_1 \times S_2) \quad (6)$$

$$n_z = 0 \quad (7)$$

$$o_x = -C_3 \times (C_1 \times S_2 + C_2 \times S_1) - S_3 \times (C_1 \times C_2 - S_1 \times S_2) \quad (8)$$

$$o_y = C_3 \times (C_1 \times C_2 - S_1 \times S_2) - S_3 \times (C_1 \times S_2 + C_2 \times S_1) \quad (9)$$

$$o_z = 0 \quad (10)$$

$$a_x = 0 \quad (11)$$

$$a_y = 0 \quad (12)$$

$$a_z = 1 \quad (13)$$

$$p_x = C_1 \times l_1 + l_2 \times (C_1 \times C_2 - S_1 \times S_2) \quad (14)$$

$$p_y = l_1 \times S_1 + l_2 \times (C_1 \times S_2 + C_2 \times S_1) \quad (15)$$

$$p_z = d_1 + d_2 \quad (16)$$

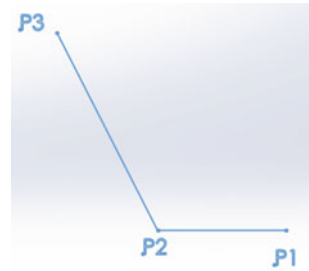
Equations (5)–(16) will determine the position and orientation of the end-effector which are obtained from the given link parameters and joint angles this approach is called as the forward kinematics. In opposition to this, the joint angles and the different configuration of the manipulator are resulting from the position as well as orientation of the end-effector, which is termed the Reverse Kinematics problem.

Sugarcane grows in the range of 1500 to 2100 mm in height and with 20 to 50 mm diameter. The function of end effector is to hold the sugarcane during cutting. By using the vision sensors [6], position of the sugarcane can be estimated.

We assumed the cane stalk being in vertical position, then the mobile robot will reach to the cane. This is the initial position (P1) that end-effector to hold the cane. During the advancement of the robot in forward direction, cutting will be taken place by the cane cutter which is placed at bottom of the robot (shown in Fig. 1).

The position at which cutting is completed is taken as point 2 (P2) of the end-effector. From position 1 to position 2, the end-effector moves horizontally in opposite direction to the robot movement. Then the end-effector will move the stalk to rare side of the robot for loading (P3) as shown in Fig. 4.

Fig. 4 Intermediate positions of the robot arm



During holding of the sugarcane, for stability purpose we added other manipulators to the robot left side and this is placed at 10 cm above the first arm.

First of all the cane stalk should cut by the cutting wheel, which is placed at bottom of the robot. During the cutting, the robot is moving towards the stalk, so the end-effector holds the stalk in the same orientation but position keeps on changing. Based on this, the path of end-effector is defined. This leads to inverse kinematics problem.

3 Results and Discussions

This problem is solved by RoboAnalyzer software [7], by selecting the 3R-Planar manipulator by giving the different positions of the end-effector as input, the joint angles are calculated by the software. As this is a inverse Kinematics problem, we get two different solutions for each joint angles at all positions except at first position of the manipulator. Because the first position is achieved by full extension of the manipulator (Table 2).

For the arm 1, the position of the end-effector is selected from Table 3 as: for P2-solution 2, and for P3-solution 1. And orientation of the arm for these solutions is shown in Fig. 5.

Similarly for Arm 2 also the joint angles at different positions obtained are shown in Table 3.

For Arm 2; the joint angles for selected are: for position 1: Sol.1 is taken, for position 2: Sol. 2 is taken, for position 3: Sol.1 is taken.

Table 2 Joint variables for Arm 1 by inverse kinematics

Joint variables	Position 1		Position 2		Position 3	
	Sol. 1	Sol. 2	Sol. 1	Sol. 2	Sol. 1	Sol. 2
θ_1	0	0	-28.955	28.955	57.3681	100.0121
θ_2	0	0	104.478	-104.478	67.9757	-67.9757
θ_3	0	90	14.4775	165.5225	-35.344	57.9336

Table 3 Joint variables for Arm 2 by inverse kinematics

Joint variables	Position 1		Position 2		Position 3	
	Sol. 1	Sol. 2	Sol. 1	Sol. 2	Sol. 1	Sol. 2
θ_1	0	0	-28.955	28.955	47.5088	104.4188
θ_2	0	0	104.478	-104.478	100.807	-100.807
θ_3	0	90	14.4775	165.5225	-58.316	86.3882

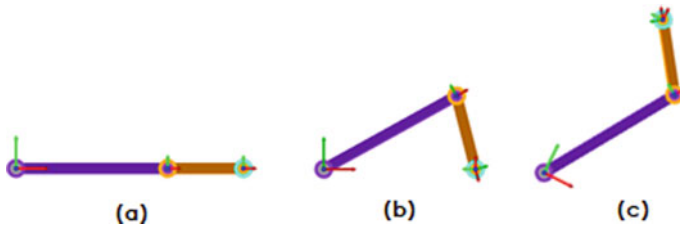


Fig. 5 Arm 1 position at a P1, b P2 and c P3 locations

The available solutions from the Inverse Kinematics are taken as input values for generating path, joint velocity, and joint accelerations by using the Forward Kinematics, generated by RoboAnalyzer

The joint value (angular displacement) velocity and acceleration for the Arm 1 from position P1 to P2 is shown in Fig. 6.

The joint value (angular displacement) velocity and acceleration for the Arm 1 from position P2 to P3 shown in Fig. 7.

4 Conclusions

1. Using Denavit–Hartenberg method, the Direct Kinematics model for the dual arm mobile robot has been successfully approached.
2. Based on Denavit–Hartenberg method, the Inverse Kinematics model for the dual arm mobile robot has been successfully approached.
3. Joint velocities and acceleration observed for all links at all positions.

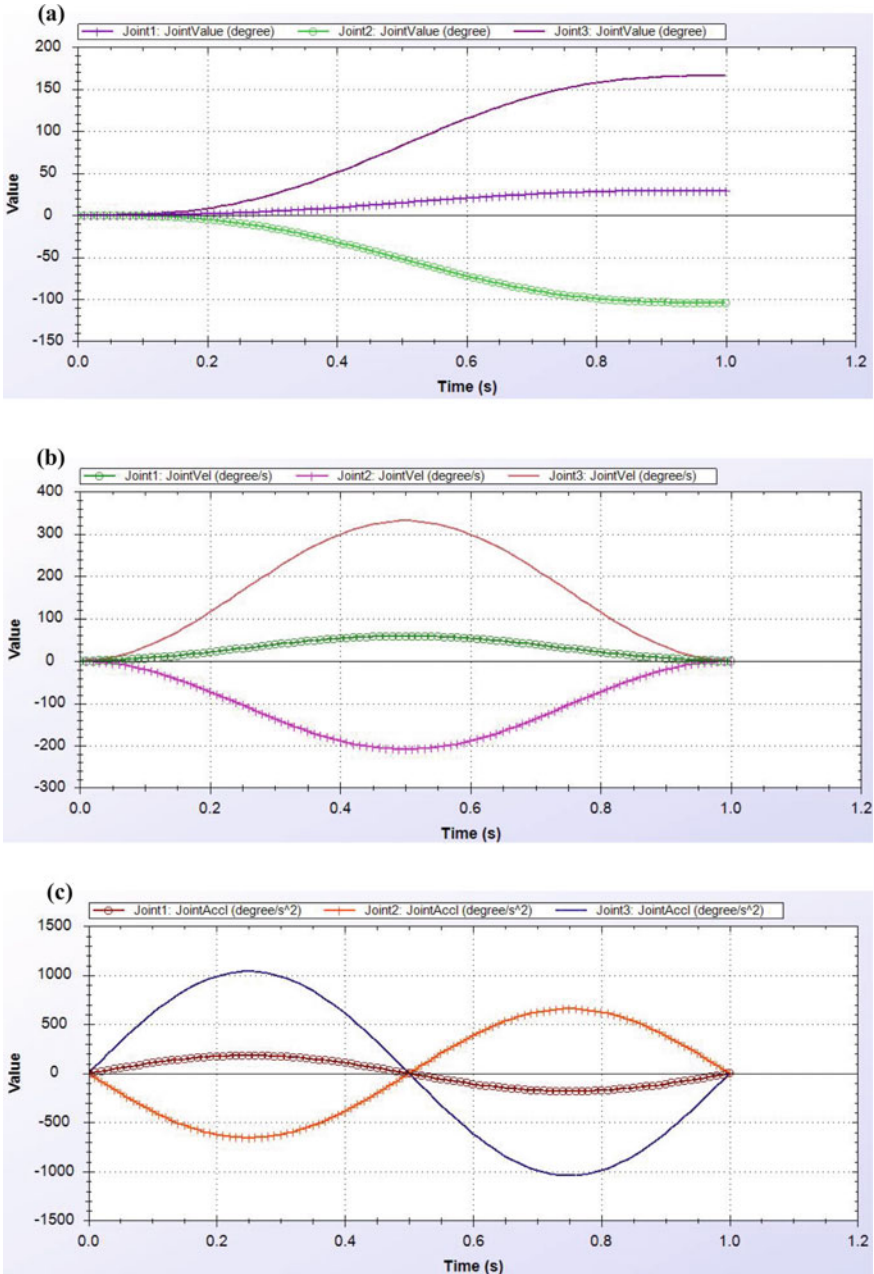


Fig. 6 a Joint values for Arm 1: P1 to P2. b Joint velocities for Arm 1: P1 to P2. c Joint accelerations for arm 1: P1 to P2

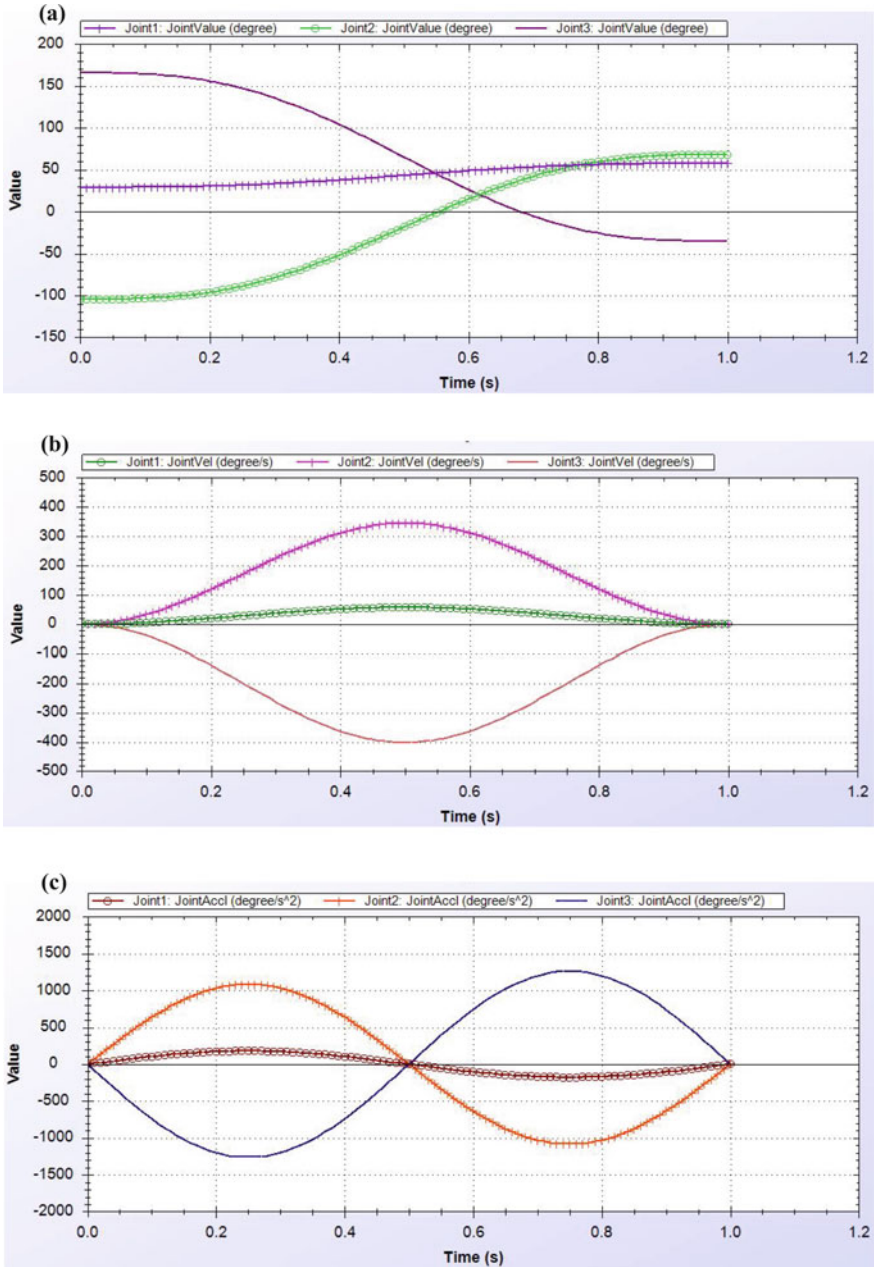


Fig. 7 a Joint values for Arm 1: P2 to P3. b Joint velocities for Arm 1: P2 to P3. c Joint accelerations for Arm 1: P2 to P3

References

1. Source: IMA India (2017)
2. Food and Agriculture Organization for United Nations home page. <http://www.fao.org/india/fao-in-india/india-at-a-glance/en/>. Last accessed 13 May 2020
3. Feng Ding., Cong Liu.: Applying coordinate fixed Denavit– Hartenberg method to solve the workspace of drilling robot arm. *International Journal of Advanced Robotic Systems* (2018)
4. John, J., Craig, T.: *Introduction to Robotics Mechanics and Control*, 3rd edn. Pearson Education International, NJ (2005)
5. Lin, X., Qiu, C., Zeng, Q., Li, A.: Kinematics analysis and trajectory planning of collaborative welding robot with multiple manipulators. In: *52nd CIRP Conference on Manufacturing Systems*, pp 1034 –1039. Elsevier
6. Mukesh Kumar, T., Dhananjay, D., Makteda.: A role of computer vision in fruits and vegetables among various horticulture products of agriculture fields: A survey. *Information Processing in Agriculture* 7, 183– 203 (2020)
7. RoboAnalyzer home page. <http://www.roboanalyzer.com>. Last accessed 6 May 2020